



The
University
Of
Sheffield.

The Impact of Hydraulic Regime upon Biofilms in Drinking Water Distribution Systems

Katherine Emma Fish

Department of Civil and Structural Engineering,
The University of Sheffield

Thesis submitted for the degree of Doctor of Philosophy

Submitted: September 2013

I dedicate this thesis to my Mum, Sarah

Abstract

Within Drinking Water Distribution Systems (DWDS) microbial biofilms form on pipe walls, adhered via extracellular polymeric substances (EPS; primarily carbohydrates and proteins) and may adversely affect water quality if mobilised. Biofilms may be conditioned to resist the hydraulic forces experienced during development and EPS characteristics may exist which promote a stable biofilm structure. However, the EPS of real drinking water biofilms has yet to be characterised and interactions between hydraulics, EPS and the microbial community have received little attention.

This study determined the impact of Steady State (SS), Low Varied Flow (LVF) and High Varied Flow (HVF) hydraulic regimes upon drinking water biofilms and their subsequent responses to elevated shear stress (via flushing). Multi-species biofilms were developed within a full scale DWDS experimental facility replicating the environmental conditions of real systems. A fluorescent microscopy approach was developed to concurrently visualise and quantify biofilm physical structure, specifically characterising the cells, carbohydrates and, unusually, proteins. Bacterial, fungal and archaeal community structures were evaluated via DNA based fingerprinting analyses.

Bacteria, fungi and archaea were abundant within biofilms conditioned to SS, but LVF and HVF biofilms were dominated by similar bacterial communities, less diverse than those within SS biofilms. Despite a similar community structure, LVF biofilms were distinguishable from HVF by (proportionally) more extensive EPS, with greater protein content; SS and HVF biofilms had a similar EPS and cell content. Post-flushing, biofilms remained attached, commonly carbohydrate with a reduced diversity of embedded microorganisms. However, the elevated shear increased the concentration of iron and manganese (particles indicative of discolouration) in the bulk water and removed protein from the biofilms; these changes were least pronounced for LVF biofilms. Overall, hydraulic regime conditioned different biofilm structures, which responded differently to increased shear stress; therefore, it may be possible to manage the hydraulics of DWDS to create biofilms that present less risk to water quality.

Acknowledgments

The work presented herein was supported by a Natural Environment Research Council sponsored PhD studentship (NE/H52489X/1). All the research undertaken during this PhD was part of the multidisciplinary project “Pipe Dreams” which is funded by the U.K. Engineering and Physical Sciences Research Council (Challenging Engineering: EP/G029946/1). Molecular analysis was supported by a NERC Biomolecular Facility “Small Project Grant” (see Appendix 1).

Many people have helped me during the course of my PhD and I’d like to extend my thanks and gratitude to all who have made this thesis possible. In particular I wish to thank my supervisors Prof. Joby Boxall and Prof. Mark Osborn for their academic guidance, personal support, challenging questions and sense of humour - especially the puns! I’d like to specifically thank Joby for his patience in explaining many an engineering term or equation, his suggestions regarding water quality and digital image analysis and, most of all, for answering all my excited or exasperated knocks on his door. In a similar vein, I’d like to thank Mark for his molecular microbiology guidance, be it in person or over the phone, fastidious editing skills and for introducing me to the fascinating world of microbial ecology, for which I am particularly grateful. Thank you both for giving me the opportunity to work on such a rewarding project, I appreciate you allowing me the freedom to drive my work and am grateful for all the discussions, constructive critique and encouragement you provided along the way.

Sample collection was greatly assisted by Isabel Douterelo and Rebecca Sharpe to whom I would like to offer special thanks, not only for their invaluable lab assistance but for all the useful discussions over cake and coffee, all the encouragement and all the laughs throughout my PhD, the lab would have been a lonely place without you both. I’m truly indebted to Rich Collins who provided intensive support regarding the digital image analysis and who should share the credit of the script writing, without his generous assistance this process would have been much more stressful. Aimeric Blaud has been an invaluable help with the molecular analysis of fungal communities and multivariate statistics, for this, his encouragement and his friendship I am very thankful. My grateful thanks are also extended to all the technical and support staff at Sheffield, particularly: Nicola Green (CLSM experimental officer), Chris Hill (SEM technician), Maggi Killion, Andy Krupa and Lindsay Hopcroft. I have been fortunate to work within a great supportive atmosphere during my PhD and for that, in addition to those already named, I would like to thank: Will Furnass, Ant Leeder and all the members of Pipe

Dreams; Prof. Catherine Biggs and the members of her lab; Jesse Harrison, Cindy Smith and other C51 members; all those within the Sheffield NBAF; and everyone in the PWG offices.

I am privileged to have the support of my family (a particular thanks to my Dad and Gran) and my friends who have been extremely understanding of my commitments during my PhD and ensured that I maintain a social life regardless! Specifically, for their endless encouragement, their interest every time I have gone off on a biofilm related tangent and their comments on this thesis, I'd like to thank: Louise Fish, Emily Hounslow (thank you both for keeping me sane), Katie Woodley, Luke Marshall (thank you both for the tinfoil help and wine), Daniel Green, Drew Murphy and Mike Rhodes (thank you each for the humorous escapes from science). I'd like to say a very special thank you to Alex Williams for his multitude of support and encouragement; always being prepared for me to bounce my ideas off him, keeping me calm before my first international conference presentation, understanding when I turned into a hermit during the writing of this thesis and always believing I could do it, I am truly lucky to have you as a co-pilot. Finally, I wish to thank my Mum, to whom this thesis is dedicated, I am extremely appreciative of the hours spent proof reading over the years, the many evenings spent listening to my practice talks and I will forever be grateful for her unfailing support, understanding and encouragement, thank you.

Table of Contents

Abbreviations and Nomenclature	xi
List of Figures	xiii
List of Tables	xvi
Chapter 1: Introduction and Literature Review	1
1.1 Introduction	1
1.2 Why Care About Microbial Drinking Water Quality?	3
1.2.1 Public health	3
1.2.2 Discolouration	5
1.3 The DWDS Environment	7
1.3.1 Infrastructure	7
1.3.2 Hydrodynamics	9
1.3.3 Water quality: organics/inorganics	10
1.3.4 Microbial management	12
1.3.5 Environmental parameters	14
1.4 DWDS Microbiology and the Biofilm System	14
1.4.1 Microbiota of the pipeline	14
1.4.1.1 Bacteria	17
1.4.1.2 Fungi	19
1.4.1.3 Archaea	21
1.4.1.4 Protozoa	21
1.4.1.5 Viruses	22
1.4.2 Sources of contamination	22
1.4.3 Planktonic state vs. biofilm state	23
1.4.4 The biofilm cycle	25
1.4.4.1 Primary adhesion (initial attachment)	25
1.4.4.2 Secondary adhesion and mature biofilm development	26
1.4.4.3 Biofilm detachment	28
1.4.5 Biofilm architecture and composition	29
1.4.5.1 The EPS matrix	30
1.4.5.2 Influence of detachment	32
1.4.5.3 Sessile microbial community: interactions and processes	32
1.5 Ecological/Engineering Effects and Biofilm Response	33
1.5.1 Pipeline surface	34
1.5.2 Hydraulic conditions	37
1.5.3 Biodegradable matter and inorganic nutrients	41
1.5.4 Disinfection	45
1.5.5 Environmental parameters	49
1.6 Investigating DWDS Biofilms: A Methodological Aside	50
1.6.1 DWDS simulation and biofilm samples	51
1.7 Conclusions	54
Chapter 2: Aims and Objectives	56

Chapter 3: Methodology	58
3.1 Experimental System	58
3.1.1 DWDS experimental facility	60
3.1.2 Coupons	62
3.1.3 Online instrumentation	63
3.2 Experimental Programme and Sampling Regime	64
3.2.1 Growth phase.....	65
3.2.1.1 Duration	65
3.2.1.2 Hydraulic regimes and environmental conditions	66
3.2.1.3 Sampling during the growth phase	67
3.2.2 Mobilization phase.....	68
3.2.2.1 Flushing steps.....	68
3.2.2.2 Flushing protocol and sampling regime	69
3.3 Water Quality Samples.....	70
3.3.1 Physicochemical parameters and instrumentation	70
3.3.2 Water physicochemistry: methods.....	71
3.3.3 Water physicochemistry: data analysis	72
3.3.3.1 Turbidity	72
3.3.3.2 Discrete water quality samples	74
3.4 Biofilm Samples – Community Structure Analysis	75
3.4.1 Biofilm removal and filtering	76
3.4.2 DNA extraction.....	76
3.4.3 Gel electrophoresis.....	77
3.4.4 PCR amplification and purification	77
3.4.4.1 PCR reaction mixes and cycle conditions	79
3.4.4.2 PCR purification.....	79
3.4.5 Community fingerprinting	80
3.4.5.1 T-RFLP: bacteria and archaea.....	80
3.4.5.2 ARISA: fungi.....	81
3.4.6 Community composition data analysis.....	81
3.4.6.1 Electropherograms and alignment of profiles	81
3.4.6.2 Diversity indices and multivariate statistics.....	82
3.5 Biofilm Samples - Scanning Electron Microscopy.....	83
3.5.1 SEM samples	84
3.5.2 SEM analysis method.....	84
3.6 Summary of Samples.....	84
Chapter 4: Evaluating Biofilm Physical Structure – Method Development	86
4.1 Introduction.....	86
4.2 Chapter Aim and Objectives.....	88
4.3 Preliminary Biofilm Samples.....	89
4.4 Method Development and Optimisation: EPS Physical Extraction Analysis	90
4.4.1 Extraction techniques and associated methods.....	90
4.4.2 Extraction trials with standard solutions	90
4.4.2.1 Materials and methods	90
4.4.2.2 Results and discussion.....	91

4.4.3	Extraction trials with drinking water biofilms.....	93
4.4.3.1	Materials and methods	93
4.4.3.2	Results and discussion.....	94
4.5	Method Development and Optimisation: Fluorescent Microscopy Imaging of EPS.....	95
4.5.1	Fluorophores and biofilm staining protocols.....	95
4.5.2	Confocal Laser Scanning Microscopy (CLSM) imaging methods	98
4.5.2.1	Optimising settings.....	98
4.5.2.2	Imaging and unmixing samples	99
4.5.3	Results and discussion: fluorophore combinations.....	100
4.5.3.1	Autofluorescence of controls.....	100
4.5.3.2	Individual fluorophores.....	101
4.5.3.3	Dual fluorophore combinations	101
4.5.3.4	Triple fluorophore combinations	103
4.5.3.5	Summary	103
4.6	Digital Image Analysis (DIA) of Triple Stained Samples.....	104
4.6.1	Median filters.....	104
4.6.2	Thresholding	104
4.6.3	Biofilm physical structure: quantification analysis	106
4.6.3.1	Calculating area fraction	106
4.6.3.2	Area distribution throughout the biofilm	106
4.6.3.3	Calculating relative volume.....	108
4.6.3.4	Calculating the spread.....	108
4.6.3.5	Analysis of peak location.....	109
4.6.3.6	Analysis summary of the physical structure parameters.....	109
4.6.3.7	Replication of three vs. five inserts.....	109
4.6.4	Biofilm physical structure: qualitative analysis.....	111
4.7	Conclusions and Outlook.....	113
4.7.1	Summary of the final EPS analysis method	114
Chapter 5: Characterising the Community and Physical Structure of a Steady State Biofilm 116		
5.1	Introduction and Aims.....	116
5.2	Results	118
5.2.1	Bulk water quality	118
5.2.2	Biofilm physical structure	118
5.2.2.1	Visualization and qualitative analysis of area distribution	119
5.2.2.2	Quantitative analysis of volume, spread and peak location	122
5.2.2.2.1	Position effects.....	123
5.2.2.2.2	Day 0 vs. Day 28	126
5.2.3	Biofilm community structure	129
5.2.3.1	PCR amplification of 16S rRNA genes and ITS regions.....	129
5.2.3.2	Microbial community analysis.....	130
5.2.3.2.1	Variation in relative taxon richness, evenness and diversity.....	130
5.2.3.2.2	Variation in bacterial, archaeal and fungal community structure	132
5.3	Discussion	137
5.3.1	Summary	141

Chapter 6: The Influence of Conditioning Hydraulic Regimes upon Biofilm Physical and Community Structure	142
6.1 Introduction and Aims	142
6.2 Results	145
6.2.1 Bulk water quality	145
6.2.2 Biofilm physical structure	145
6.2.2.1 Visualization and qualitative analysis of area distribution	147
6.2.2.2 Quantitative analysis of volume, spread and peak location	151
6.2.2.2.1 Hydraulic effect (SS vs. LVF vs. HVF)	151
6.2.3 Biofilm community structure	157
6.2.3.1 PCR amplification of 16S rRNA genes and ITS regions	157
6.2.3.3 Effect of hydraulic regime upon relative taxon richness, evenness and diversity	159
6.2.3.4 Effect of hydraulic regime upon bacterial and fungal community structure.....	161
6.3 Discussion	165
6.3.1 Summary	171
Chapter 7: Assessing the Response of Biofilms Developed under Different Hydraulic Regimes to an Elevation in Shear Stress	173
7.1 Introduction and Aims	173
7.2 Results of Hydraulic and Stagnation Effects upon Pre-flush Biofilms	174
7.2.1 Biofilm physical structure Pre-flush	174
7.2.1.1 Visualization and qualitative analysis of area distribution	176
7.2.1.2 Quantitative analysis of volume, spread and peak location	178
7.2.2 Biofilm community structure Pre-flush	182
7.2.2.1 Relative taxon richness, evenness and diversity	183
7.2.2.2 Microbial community structure	184
7.2.2.2.1 Stagnation effect on biofilm structure	184
7.2.2.2.2 Hydraulic effect on Pre-flush biofilm structure	187
7.2.3 Discussion	190
7.2.4 Summary of stagnation and hydraulic effects Pre-flush.....	191
7.3 Results Concerning the Effect of hydraulic regime upon Post-flush samples.....	192
7.3.1 Biofilm physical structure Post-flush	194
7.3.1.1 Visualization and qualitative analysis of area distribution	194
7.3.1.2 Quantitative analysis of volume, spread and peak location	197
7.3.2 Biofilm community structure Post-flush.....	200
7.3.2.1 PCR amplification of 16S rRNA genes and ITS regions	200
7.3.2.2 Relative taxon richness, evenness and diversity	200
7.3.2.3 Community structure	202
7.3.3 Summary of hydraulic effects Post-flush.....	204
7.4 Results Concerning Variations in Water Quality and Biofilm Structure in Response to Elevated Shear Stress	205
7.4.1 Bulk water quality	206
7.4.2 Biofilm physical structure response.....	208
7.4.2.1 Quantitative analysis of volume, spread and peak location	208
7.4.3 Community structure response	213
7.4.3.1 Variation in relative taxon richness, evenness and diversity	213

7.4.3.2 Variation in microbial community structure	214
7.4.4 Summary of responses to elevated shear stress	218
7.5 Discussion	220
Chapter 8: Concluding Comments	226
8.1 Summary of Findings	226
8.1.1 A robust EPS analysis approach was developed (Objective 1)	226
8.1.2 Hydraulics influenced biofilm structure (Objectives 2 and 3)	227
8.1.3 Variation in biofilm structure leads to different responses to elevated shear stress (Objective 4).....	230
8.2 Future Work	232
8.2.1 Different environmental conditions	232
8.2.2 Improvements to the DWDS experimental facility.....	233
8.2.3 Further analysis of the biofilm structure	234
8.2.4 Improved characterisation of the bulk phase.....	235
8.2.5 Field studies	235
8.3 Outlook	236
Reference List	237
Appendices	264
Appendix 1 Grant Bids, Scientific Dissemination and Awards	264
Appendix 2 Supporting data for turbidity analysis.....	267
Appendix 3 Buffers and Solutions	267
Appendix 4 Internal Size Standards.....	268
Appendix 5 Review of extraction, quantification and chemical composition techniques	270
Appendix 6 Optimised physical protocols for EPS analysis	272
Appendix 7 Supporting information for optimising the fluorescent staining and imaging method	273
Appendix 8 Statistical Analysis of Bulk Water Quality	275
Appendix 9 Supporting information for comparisons between biofilms from the growth phase of different hydraulic regimes.....	276
Appendix 10 Supporting information for comparisons between biofilms from the mobilization phase of different hydraulic regimes	280

Abbreviations and Nomenclature

-1	per
%	percentage
°C	degrees Celsius
μ (as prefix)	micro
μm	micrometre
μs	microsecond
χ ²	chi-square, statistical output from Kruskal Wallis test
2D	2 dimensions
3D	3 dimensions
6-FAM	6' carboxyfluorescein
AFM	atomic force microscopy
ANOSIM	analysis of similarity, used for multivariate data
ANOVA	analysis of variance
AOA	ammonia oxidising archaea
AOB	ammonia oxidising bacteria
AOC	assimilable organic carbon
AQC	analytical quality control
ARISA	Automated Ribosomal Intergenic Spacer Analysis
ATP	adenosine triphosphate
AU	arbitrary unit
BDOC	bio-available dissolved organic carbon
BFP	biofilm forming potential
BOM	biodegradable organic matter
BSA	bovine serum albumin
CER	cation exchange resin
CFU	colony forming unit
CLSM	confocal laser scanning microscopy
Cl	chlorine
Con A Rho	concanavalin A tetramethylrhodamine
CTAB	hexadecyltrimethyl ammonium bromide
DAPI	4',6-diamidino-2-phenylindole
df	degrees of freedom
DIA	digital image analysis
DMA	district management areas
DNA	deoxyribonucleic acid
dNTP	deoxyribonucleoside triphosphate
DOMs	Distribution Operation and Management Strategies
DPD	n,n-diethyl-p-phenylenediamine
DWDS	drinking water distribution system
DWI	Drinking Water Inspectorate
EDTA	ethylenediaminetetraacetic acid
EM	environmental mycobacteria
EPA	Environmental Protection Agency
EPS	extracellular polymeric substances
<i>et al.</i>	and others
FD+EtOH	freeze drying with ethanol precipitation
FITC	fluorescein-5-isothiocyanate
Fe	iron
FOV	fields of view
g	gram

G6PDH	glucose-6-phosphate Dehydrogenase
global R	statistic from ANOSIM (value 0-1, 0=no difference, 1=completely different)
HDPE	high density polyethylene
HVF	High Varied Flow (test condition)
ICPOES	Inductively Coupled Plasma Optical Emission Spectroscopy
ID	internal diameter
ITS	internal transcribed spacer, region of fungal DNA
kPa	kilopascal
kV	kilovolts
l	litre
LOD	limit of detection
LVF	Low Varied Flow (test condition)
m	metre
mm	millimetre
M	molar
m (as a prefix)	milli
MAC	<i>Mycobacteria avium</i> complex
MAP	microbially available phosphorous
max	maximum (abbreviation used in Tables and Figures)
MDPE	medium density polyethylene
min	minimum (abbreviation used Tables and Figures)
mV	milli volts
Mn	manganese
N	Newtons
n =	indicates replication
n (as prefix)	nano
nm	nanometres (wavelength)
nMDS	non-metric multi-dimensional scaling
nt	nucleotide
NTU	nephelometric turbidity units
ORP	oxidising redox potential
p	p value from statistical tests, followed by one of "<", ">" or "="
pa	pascal
PBS	phosphate buffer solution
PCR	polymerase chain reaction
pH	measure of acidity/alkalinity of a solution, based on a log scale (1 -14)
PODDS	Prediction Of Discolouration in Distribution Systems (model)
PSM	Particle Settling Model (of discolouration)
PVC	polyvinyl chloride
PWG	Pennine Water Group
R ²	linear regression - co-efficient of determination
RC DC	reducing agent, detergent compatible
RCF	relative centrifugal force
RM	Raman microscopy
RNA	ribonucleic acid
RPM	revolutions per minute
rRNA	ribosomal ribonucleic acid
SDS	sodium dodecyl sulfate
SEM	scanning electron microscopy
SIMPER	similarity percentages, statistical test used with multivariate data
SIMPROF	similarity profile test, used with multivariate data
SS	Steady State (test condition)

TAE	Tris acetate ethylenediaminetetraacetic acid
TOC	total organic carbon
T-RF	terminal-restriction fragment
T-RFLP	Terminal-restriction Fragment Length Polymorphism
U	unit
UK	United Kingdom
uPVC	unplasticised PVC
USA	United States of America
V	volts
VBNC	viable but not culturable
W	W-value, statistical output from Wilcoxon test
w/v	weight/volume
WHO	World Health Organisation
WSPs	Water Safety Plans

List of Figures

Figure 1.1 Schematic example of a drinking water system.	8
Figure 1.2 Diversity of ages and materials of pipelines within the DWDS.....	8
Figure 1.3 Schematic example of diurnal variation in flow rate.	9
Figure 1.4 An example of temporal variation in water quality properties.	10
Figure 1.5 Processes involved in biofilm development	25
Figure 1.6 Schematic representation of biofilm adhesion.....	26
Figure 3.1 Drinking Water Distribution System (DWDS) simulation pipe rig.....	59
Figure 3.2 Schematic diagram of the DWDS experimental facility (not to scale).....	61
Figure 3.3 PWG Coupon dimensions (A) and positions (B).....	62
Figure 3.4 Calibration curve of turbidity standard solutions.	64
Figure 3.5 Daily flow patterns of the hydraulic regimes used in this study.....	67
Figure 3.6 Mobilization phase schematic showing the flushing steps and sampling regime.	68
Figure 3.7 Standard curve used to determine boundary shear stress values.	69
Figure 3.8 Turbidity data during the mobilization phase before and after wavelet analysis.	73
Figure 3.9 Turbidity response during the mobilization phase	74
Figure 4.1 SEM image of a drinking water biofilm.....	89
Figure 4.2 Experimental design for EPS analysis of drinking water biofilm samples.....	94
Figure 4.3 Auto-fluorescence of the unstained controls, imaged at 488 nm.	100
Figure 4.4 Emission spectra of protein fluorophores.	102
Figure 4.5 Reference spectra for the triple stain combination.....	103
Figure 4.6 Example of the normalised data at different threshold values.	105
Figure 4.7 Area distribution of cells, carbohydrate and proteins throughout Day 28 biofilms developed under SS hydraulic conditions.....	108
Figure 4.8 Schematic representation of three different hypothetical area distributions and their spread	109
Figure 4.9 Relative volume of cells, carbohydrates and proteins from Day 28 biofilms when imaged at five and seven FOV.	110
Figure 4.10 Unmixed and thresholded 2D images of a drinking water biofilm	111
Figure 4.11 Z-stack gallery of a Day 28 biofilm	112

Figure 4.12 Example of a 3D projection of a Day 28 biofilm Z-stack.	113
Figure 5.1 Area distribution plots for biofilms from Day 0 and Day 28 of the SS condition.....	120
Figure 5.2 The area distribution and an example of the 3D arrangement of cells, carbohydrates and proteins of biofilms from Day 0 and Day 28 of the SS condition.....	121
Figure 5.3 Relative volume of each of the stained biofilm components (cells, carbohydrates and proteins) for samples from Day 0 and Day 28.	124
Figure 5.4 Relative volume of stained biofilm components within samples from Day 0 and Day 28.	126
Figure 5.5 Spread of each of the stained biofilm components for Day 0 and Day 28 biofilms.	128
Figure 5.6 Carbohydrate and protein peak locations in relation to the cell peak location	128
Figure 5.7 Agarose gel electrophoresis images of purified PCR products	129
Figure 5.8 Representative T-RFLP or ARISA electropherograms of drinking water biofilm communities at Day 0 and Day 28, from the SS experiment.	131
Figure 5.9 Cluster analysis using T-RFLP profiles to show the similarity between biofilm bacterial communities.	133
Figure 5.10 nMDS plots of archaeal and fungal community structures at Day 0 and Day 28. .	134
Figure 5.11 Results from SIMPER analysis comparison of microbial communities in drinking water biofilms at Day 0 and Day 28.	136
Figure 6.1 Representative SEM images of a cleaned insert (A) and Day 28 biofilm samples (B to H) developed under different hydraulic regimes.	144
Figure 6.2 The area distribution of cells, carbohydrates and proteins within biofilms developed for 28 days	148
Figure 6.3 A representative example of the 3D arrangement of cells, carbohydrates and proteins within Day 28 biofilms	150
Figure 6.4 Relative volumes of stained biofilm components within Day 28 biofilms developed under SS, LVF or HVF hydraulic conditions.	154
Figure 6.5 Spread of each of the stained biofilm components for Day 28 biofilms developed under SS, LVF or HVF regimes.....	156
Figure 6.6 Peak location of carbohydrates and proteins, in relation to the cell peak location (indicated by the dotted line), for Day 28 biofilms from SS, LVF and HVF experiments.	156
Figure 6.7 Agarose gel electrophoresis images of archaeal PCR products from biofilms developed under LVF conditions.	158
Figure 6.8 Representative T-RFLP or ARISA electropherograms of drinking water biofilm communities after 28 days of development under SS, LVF or HVF conditions.	160
Figure 6.9 nMDS plot of bacterial community structures from biofilms developed under the SS, LVF or HVF hydraulic conditions for 28 days.	162
Figure 6.10 Results from SIMPER analysis comparison of bacterial communities sampled at Day 28 from different hydraulic regimes.....	164
Figure 6.11 Comparison of the fungal communities within Day 28 biofilms from SS and LVF hydraulic conditions.....	165
Figure 6.12 Summary of some of the patterns in biofilm structure parameters seen between the biofilms from SS, LVF and HVF conditions after 28 days of development.	167
Figure 7.1 Area distribution of cells, carbohydrates and proteins within Pre-flush biofilms developed under SS, LVF and HVF conditions.	175
Figure 7.2 A representative example of the 3D arrangement of cells, carbohydrates and proteins within Pre-flush biofilms from A) SS; B) LVF and C) HVF conditions.	177

Figure 7.3 Relative volumes of stained biofilm components within Pre-flush biofilms developed under SS, LVF or HVF hydraulic conditions.	180
Figure 7.4 Carbohydrate and protein peak locations within Pre-flush biofilms from SS, LVF and HVF conditions.	182
Figure 7.5 Representative T-RFLP or ARISA electropherograms of Pre-flush biofilm communities from the SS, LVF or HVF experiments.	184
Figure 7.6 Dendrograms showing the similarity between biofilm communities from Day 28 and Pre-flush sample points of the SS condition.	186
Figure 7.7 Dendrograms showing the similarity between biofilm communities from Day 28 and Pre-flush sample points of the LVF condition.	187
Figure 7.8 Dendrogram showing the similarity between bacterial biofilm communities from Day 28 and Pre-flush sample points of the HVF condition.	187
Figure 7.9 Comparison of bacterial community structures from Pre-flush biofilms developed under the SS, LVF and HVF hydraulic conditions.	189
Figure 7.10 Comparison of the fungal community structure of Pre-flush biofilms from SS and LVF conditions.	190
Figure 7.11 Summary of some of the patterns in biofilm structure parameters seen between the Pre-flush biofilms from SS, LVF and HVF conditions.	192
Figure 7.12 Representative SEM images of a cleaned insert (A) and Post-flush biofilm samples (B to H) developed under different hydraulic regimes.	193
Figure 7.13 The area distribution of cells, carbohydrates and proteins within Post-flush.	195
Figure 7.14 A representative example of the 3D arrangement of cells, carbohydrates and proteins within a Post-flush biofilm from A) SS; B) LVF; C) HVF conditions.	196
Figure 7.15 Relative volumes of stained biofilm components within Post-flush biofilms previously developed under SS, LVF or HVF conditions.	197
Figure 7.16 Spread of each of the stained biofilm components throughout Post-flush biofilms previously developed under SS, LVF or HVF regimes.	199
Figure 7.17 Representative T-RFLP or ARISA electropherograms of Post-flush biofilm communities from the SS, LVF or HVF experiments.	201
Figure 7.18 Comparison of the bacterial communities of Post-flush biofilms from SS, LVF or HVF conditions.	203
Figure 7.19 Comparison of the fungal communities within Post-flush biofilms from SS and HVF hydraulic conditions.	204
Figure 7.20 Summary of some of the patterns in biofilm structure parameters seen between the Post-flush biofilms from SS, LVF and HVF conditions.	205
Figure 7.21 Concentrations of iron (in red) and manganese (in blue) during the flushing phase of biofilms developed under SS, LVF and HVF conditions.	207
Figure 7.22 Comparison of the relative volume and spread of cells, carbohydrates and proteins in SS conditioned biofilms, Pre-flush and Post-flush.	209
Figure 7.23 Comparison of the relative volume and spread of cells, carbohydrates and proteins in LVF conditioned biofilms, Pre-flush and Post-flush.	210
Figure 7.24 Comparison of the relative volume and spread of cells, carbohydrates and proteins in HVF conditioned biofilms, at Day 28, Pre-flush and Post-flush.	212
Figure 7.25 Comparison of the bacterial communities of Pre and Post-flush biofilms conditioned to the SS hydraulic regime.	215

Figure 7.26 Comparison of the fungal communities of Pre and Post-flush biofilms conditioned to the SS hydraulic regime.	216
Figure 7.27 Comparison of the archaeal communities of Pre and Post-flush biofilms conditioned to the SS hydraulic regime.	217
Figure 7.28 Comparison of the bacterial communities of Pre and Post-flush biofilms conditioned to the LVF hydraulic regime.	218
Figure 7.29 Comparison of the bacterial communities of Day 28, Pre and Post-flush biofilms conditioned to the HVF hydraulic regime.	218
Figure 7.30 Summary of some of the patterns in biofilm physical and community structure between Pre-flush and Post-flush biofilms previously developed under SS, LVF or HVF conditions.	219

Within the Appendices

Figure A 4.1 Electropherogram of the ROX™ GeneScan™ 500 size standard.	268
Figure A 4.2 Electropherograms showing the profile of ROX™ GeneScan™ 2500.	269
Figure A 7.1 CLSM image demonstrating the detrimental effect of the multiphoton laser on a dual stained sample.	273
Figure A 7.2 Example of a single FOV imaged at the six scan speeds (μs)	275
Figure A 9.1 The area distribution of cells, carbohydrates and proteins of A) LVF Day 0 biofilms (n=25) and B) HVF Day 0 biofilms (n=24).	277

List of Tables

Table 1.1 Examples of drinking water guidelines stated by various governing bodies.	12
Table 1.2 Examples of microorganisms isolated and identified in the course of drinking water research.	15
Table 1.3 Breakdown of biofilm features/components.	24
Table 1.4 Examples of experimental systems used in studying pipeline biofilms	53
Table 3.1. Specifications of online instrumentation.	64
Table 3.2 Overview of the hydraulic regime experiments completed in the DWDS experimental facility.	65
Table 3.3 Flow rate, velocity and boundary shear stress at each of the flushing steps comprising the mobilization phase.	70
Table 3.4 Bulk water quality parameters and the instrumentation used for their assessment.	71
Table 3.5 Oligonucleotide primer pairs used to amplify 16S rRNA genes and ITS regions, PCR cycling conditions used in each case are indicated.	78
Table 3.6 Summary of samples analysed across all experiments	85
Table 4.1 The EPS physical extraction, quantification and biochemical analysis techniques evaluated in this study.	87
Table 4.2 Mean observed values of known protein concentrations generated by RC DC and Bradford assays (\pm confidence interval).	92
Table 4.3 Mean observed values of known glucose concentrations generated using the phenol-sulfuric method (\pm confidence interval).	92

Table 4.4 Concentration of protein in EPS extracted from 1070.80 mm ² of drinking water biofilms using the CER and EDTA methods (\pm confidence interval).	95
Table 4.5 Fluorophores (fluorescent stains) evaluated in this study, including the staining and imaging details.	97
Table 4.6 Fluorophore combinations applied to the biofilm samples in this study.	102
Table 4.7 Final details of the optimised image settings.....	115
Table 5.1 Water quality of the bulk water during the formation of biofilms under SS conditions	118
Table 5.2 Results from the Kruskal Wallis tests (and Wilcoxon if stated) to determine significant differences (in bold) between the samples within the position and loop datasets.	125
Table 5.3 Relative volumes of the stained biofilm components at Day 0 and Day 28.	127
Table 5.4 Range and median of various ratios of relative volumes of different components within biofilms from Day 0 and Day 28.	127
Table 5.5 Richness, evenness and diversity indices of the bacterial, archaeal and fungal communities from SS drinking water biofilm sampled at Day 0 and Day 28.	131
Table 6.1 Bulk water quality during the formation of biofilms during the SS, LVF and HVF experiments	146
Table 6.2 Comparison of the relative volumes of the stained biofilm components of Day 28 biofilms developed under SS, LVF and HVF conditions.	153
Table 6.3 Comparison of relative volume ratios of different components within Day 28 biofilms from SS, LVF or HVF hydraulic conditions.....	154
Table 6.4 Statistical comparisons of the spread of the stained biofilm components in biofilms developed under SS, LVF or HVF conditions for 28 days.	156
Table 6.5 Relative richness, evenness and diversity indices of the bacterial and fungal communities from biofilms sampled at Day 28 from the SS, LVF or HVF condition.	161
Table 7.1 Median relative volumes (μm^3) of the stained biofilm components in Day 28 and Pre-flush biofilms developed under SS, LVF and HVF conditions. Data for the individual stained components is provided in (A) and for combinations, as indicated, in (B).....	179
Table 7.2 Median ratios of various different components within Day 28 and Pre-flush biofilms from SS, LVF and HVF conditions.	179
Table 7.3 Median spreads of the different components within Day 28 and Pre-flush biofilms from SS, LVF and HVF conditions.	179
Table 7.4 Results from the statistical comparisons of the relative volume of the stained biofilm components within Pre-flush biofilms developed under SS, LVF and HVF conditions.....	181
Table 7.5 Results from the statistical comparisons of the various ratios of the stained biofilm components within Pre-flush biofilms developed under SS, LVF and HVF conditions.....	181
Table 7.6 Number of DNA extractions for which bacteria, archaea or fungi were detected... ..	182
Table 7.7 Relative richness, evenness and diversity indices of the bacterial and fungal communities from Pre-flush biofilms sampled from the SS, LVF or HVF experiments.	184
Table 7.8 Comparison of the relative volumes of the stained biofilm components of Post-flush biofilms, previously developed under SS, LVF or HVF conditions.	198
Table 7.9 Comparison of the values of the various ratios of relative volumes of different components within Post-flush biofilms from SS, LVF or HVF hydraulic conditions.....	198
Table 7.10 Results from statistical comparisons of the spread of each of the stained biofilm components in Post-flush biofilms developed under SS, LVF or HVF conditions.	199

Table 7.11 Relative richness, evenness and diversity indices of the bacterial and fungal communities with Post-flush biofilms	202
Table 7.12 Regression analysis results for iron and manganese during the flushing phase of each hydraulic experiment as indicated. Significant results are shown in bold.....	208
Table 7.13 Relative volume ratios of Pre-flush and Post-flush biofilms from SS.....	209
Table 7.14 Relative volume ratios of Pre-flush and Post-flush biofilms from LVF.....	210
Table 7.15 Relative volume ratios of Pre-flush and Post-flush biofilms from HVF.....	211
Table 7.16 Loss of biofilm volume from SS, LVF and HVF biofilms as a response to elevated shear stress.....	220

Within the Appendices

Table A 2.1 Comparison of turbidity in "Pre-Flush" water samples during the mobilization phase of the SS experiment.	267
Table A 5.1 Summary of the extraction, quantification and chemical assay approaches used in the literature.....	270
Table A 7.1 Z-stack imaging times for different scan speeds and optical thicknesses.	274
Table A 7.2 Imaging times for 5 slice lambda-Z-stacks imaged under different scan speeds. .	275
Table A 8.1 Kruskal Wallis p values for water quality parameter comparisons	276
Table A 9.1 Results from the Wilcoxon test to determine any position or loop effect upon the relative volumes of the stained components of biofilms from the LVF or HVF regimes.....	276
Table A 9.2 Results from the Wilcoxon test to determine any effect of position or loop upon the spread of the stained components of biofilms from the LVF or HVF regimes.....	277
Table A 9.3 Results from the Wilcoxon test to determine any effect of position or loop upon the peak location of carbohydrates or proteins of biofilms from the LVF or HVF regimes.	277
Table A 9.4 Comparison of the relative volume of the stained components within Day 0 and Day 28 biofilms, developed under LVF conditions.	278
Table A 9.5 Comparison of the relative volume of the stained components within Day 0 and Day 28 biofilms, developed under HVF conditions.....	278
Table A 9.6 Comparison of the spread of the stained biofilm components within Day 0 and Day 28 biofilms, developed under LVF conditions.....	278
Table A 9.7 Comparison of the spread of the stained biofilm components within Day 0 and Day 28 biofilms, developed under HVF conditions.....	279
Table A 9.8 Comparison of the relative volumes of the stained biofilm components within Day 0 biofilms developed under SS, LVF or HVF conditions.	279
Table A 9.9 Comparison of the spread of the stained biofilm components within Day 0 biofilms developed under SS, LVF or HVF conditions.....	280
Table A 9.10 Relative richness, evenness and diversity indices of the bacterial communities from Day 0 of the different hydraulic conditions.	280
Table A 10.1 Statistical comparisons of biofilm physical structure parameters to determine any effect of position or loop upon the Pre-flush biofilms from the SS, LVF or HVF regimes. .	281
Table A 10.2 Statistical comparisons of biofilm physical structure parameters to determine any effect of position or loop upon the Post-flush biofilms from the SS, LVF or HVF regimes..	281

Chapter 1: Introduction and Literature Review

1.1 Introduction

Drinking water is a fundamental human resource, the insufficient supply and inadequate safety of which remains one of the main causes of mortality worldwide (WHO, 2002; WHO & OECD, 2003). Consequently, drinking water quality is a global concern, primarily because of the potential for contaminated water to rapidly transmit, potentially fatal, microbial diseases to vast numbers of people, in a short space of time (Szewzyk *et al.*, 2000). Impacts of microbial contamination upon public health have highlighted the need for water protection and, ultimately, driven science and engineering to develop various infrastructures and approaches to facilitate the production and distribution of safe drinking water (Berry *et al.*, 2006). These systems have been introduced, developed and improved since the mid-19th century, leading to the sophisticated water treatment processes and Drinking Water Distribution Systems (DWDS) that modern day engineering has made possible (Szewzyk *et al.*, 2000).

Some form of water treatment and/or protected supply is now common place across many areas; it has been reported that 86% of the world's population had access to an "improved" water source (defined as protected from outside contamination) in 2010, compared to 76% in 1990 (WHO & UNICEF, 2012). Furthermore, the percentage of people in less economically developed countries with safe water is on the rise, from 30% in 1970 to 80% in 2000 (Lomborg, 2001). The majority of those with access to an "improved" source are now supplied via piped water – the DWDS (54% in 2010, compared to 45% in 1990; WHO & UNICEF, 2012).

Focusing solely on the initial implementation of these systems is not, however, enough to ensure the provision of safe water. DWDS are evolving systems, with a piecemeal design and construction, that experience ever changing demands with variation in water chemistry and quality (Covert *et al.*, 1999; Vreeburg & Boxall, 2007; Machell *et al.*, 2009). Moreover, DWDS are an aging infrastructure, experiencing deterioration while simultaneously facing greater customer demands. Therefore, constant maintenance, monitoring and protection are integral to sustaining the DWDS infrastructure and a high quality water supply. Thus, in the UK, since 1990, many DWDS have been renovated and, according to the Drinking Water Inspectorate (DWI) guidelines, water suppliers are now required to develop Distribution Operation and Management Strategies (DOMs). Within the DOMs, suppliers outline their plans regarding

continued operation assessment, maintenance of the network and preservation, or advancement, of water quality (DWI, 2002). A water quality management framework was also set out in the Bonn Charter Report (IWA, 2004), which encompassed the development of Water Safety Plans (WSPs), complementary to the WHO drinking water quality guidelines (WHO, 2011). WSPs are based upon the hazard and critical point analysis approach of risk assessment and combine system design evaluation, operational monitoring and management plans to help maintain the DWDS infrastructure and the quality of drinking water.

Although disease outbreaks initially drove DWDS implementation, new pressures are emerging which will drive the future development of our pipe networks and, in particular, changes in population density and distribution (Defra, 2011) will lead to variations in the public demand regarding drinking water quantity and quality. Thus, in an era where climate change and population increases are reported to be causing water shortages (Karanja *et al.*, 2011; Hunter, 2011; WHO & UNICEF, 2012), the water industry is faced with providing continually higher volumes of potable water at a maintained or improved quality (WHO & OECD, 2003; Defra, 2011), all with diverse, aging infrastructure (UKWIR, 2003). The reality is that treated drinking water is a perishable resource and deterioration of the quality during distribution remains an important issue for suppliers, consumers and governing bodies alike. Therefore, research at the pipeline level is essential to further understand the processes occurring within DWDS, in order to develop effective, maintainable management strategies that will sustain both the distribution infrastructure and a high quality water supply into the future.

Drinking water quality is determined by a multitude of chemical, physical and microbiological parameters and their interactions. Research is becoming increasingly focussed on exploring an array of these water quality parameters at the pipe level, especially discolouration, but the incorporation of an appreciation of the microbiology of DWDS has generally been limited to the role of planktonic cells. Microorganisms are found not only in a free-living planktonic state but also, more commonly, in a sessile, surface-bound state termed the biofilm (Costerton *et al.*, 1987, 1995; Dunne, 2002; Wright *et al.*, 2004). Biofilms are heterogenic microbial assemblages, embedded within a self-produced matrix of extracellular polymeric substances (EPS), with which inorganic particles may be associated (Costerton *et al.*, 1987; 1995; Dunne, 2002; and others). Various abiotic and biotic properties of the pipe network may influence the presence, architecture and microbial composition of biofilms (van der Wende *et al.*, 1989; Jenkinson & Lappin-Scott, 2001), which then in turn effect various characteristics of the DWDS. Within the context of DWDS, biofilms may be described as a reservoir of cells within the

pipeline, which place a chlorine demand upon the system, mediate processes that contribute to aesthetic degradation and inoculate attached assemblages downstream. Moreover, the mobilization of biofilm bound material into the bulk phase may adversely affect water quality and safety. Hence, while microorganisms no longer pose as great a public health risk as they once did, their continued presence and activity within the DWDS, particularly as biofilms, could potentially have a substantial impact upon the infrastructure and management of the distribution system and, arguably more importantly, the quality of water distributed. Therefore, it is proposed that understanding the environmental influences on the dynamics of the biofilm is paramount to continuing to provide safe, high quality drinking water.

The scope of this review is to highlight the importance of understanding the microbial ecology of our pipelines, particularly the interactions between the physico-chemical environment and the biofilms of the DWDS. An outline of the current understanding, and its limitations, with respect to water quality, along with various abiotic and biotic aspects of DWDS will be presented. A comprehensive review of the microbiota associated with drinking water will be provided, along with an overview of the current understanding of biofilm development. Consideration will be given to what is known about the way the DWDS environment shapes biofilms and how, in turn, biofilms affect the pipeline environment. Throughout this review the merits and limitations of the model systems or methodological approaches applied to investigate the DWDS and biofilms will be considered; various knowledge gaps will be highlighted and the potential direction for future research outlined.

1.2 Why Care About Microbial Drinking Water Quality?

1.2.1 Public health

The relationship between a microbial presence in drinking water and reduced water quality began to be recognised following epidemiological studies of London (UK) water supplies in the 1800's, which identified *Vibrio cholera* as the cause of more than 10,000 deaths (Szewzyk *et al.*, 2000). Research has since irrefutably established the presence of various pathogens within drinking water and controls are now in place that act to minimise the level of microbial contamination, thus reducing public health problems and water quality degradation (Williams & Braun-Howland, 2003; Ratnayaka *et al.*, 2009). Indeed outbreaks of waterborne illness have been reduced by water improvements in the past few decades. For example, the occurrence of diarrhoea (which affects 4 billion and kills 2.2 million people a year) has reduced by 25-33%.

Similarly, the incidence of trachoma (a bacterial infection), to which approximately 500 million people are at risk, has decreased by 25% (based on medians) and the future expansion of water distribution systems has the potential to prevent 1.4 million deaths a year in children alone (Esrey *et al.*, 1991; WHO, 2000; WHO & UNICEF, 2000; 2012). It could be argued that water supply and sanitation improvements in the last century have done more to protect and ensure public health than anything else, including medical developments.

Nevertheless, even with modern systems, outbreaks occasionally occur. For example, drinking water contamination with *Campylobacter spp.* and *Escherichia coli* O517 during 2000, in Walkerton, Canada, caused serious illness in over 2,000 people and seven deaths (WHO & UNICEF, 2000). Similarly in 2005, and again in 2008, between 66,000 and 70,000 people were exposed to the protozoan *Cryptosporidium* via contaminated water in North Gwynedd, Wales (DWI, 2005; 2008). Several authors have reported that quality degradation during distribution accounts for a significant proportion of documented waterborne disease outbreaks (Ainsworth, 2002; Craun & Calderon, 2001). However, small-scale water quality issues, which may go undetected, also occur during distribution. These could occur due to contaminant ingress, from cross-connections or non-sterilised construction materials, via back-pressure (due to a component external to the DWDS exceeding the pressure of the network) or back-siphonage (due to a pressure drop within DWDS; Craun & Calderon, 2001; US EPA, 2004; Ratnayaka *et al.*, 2009). Another possible cause is that cells are eroded from biofilms at concentrations that may go undetected but still result in a low-level continuous presence of microorganisms (Tinker *et al.*, 2009). Whilst such contamination does not violate drinking water standards, it has the potential to increase the discolouration or turbidity of water (a monitored water quality parameter). Moreover, depending upon the particular species and cell concentration, such contamination may lead to endemic disease transmission, particularly of gastrointestinal illnesses or cryptosporidiosis (Tinker *et al.*, 2009). Although this low level contamination may not cause fatalities, it has been suggested that if 10% of infected adults miss a day of work due to their gastro-illness, this background contamination can have substantial economic consequences (Payment, 1997; Payment *et al.*, 1997); Roberts *et al.* (2003) stated that the cost of diarrheal disease in the UK is ~ £743 million per annum. However, in many cases the cause of infection is unclear. In a questionnaire based study, which asked participants about various aspects of their life over the two week period prior to receiving the questions, including the occurrence of cryptosporidiosis (gastro illness), Hunter *et al.* (2005) discovered an unexpected positive relationship between the occurrence of cryptosporidiosis and a loss of water pressure ($p < 0.001$) in the drinking water supply. These

two factors were more strongly correlated than the occurrence of illness and interactions with an infected individual ($p=0.001$). It is important to note that symptoms were self-reported and the correlative results do not necessarily imply causation. The study did not set out to investigate a relationship between drinking water and diarrhoea; therefore the questions were not designed to specifically identify events occurring before the onset of the illness. Nevertheless, a pattern between a disrupted water supply (mainly the result of a burst) and gastro illness was observed. Therefore, although water quality is having fewer fatal impacts upon public health it remains influential in the distribution of systematic infections, which can subsequently have wider impacts upon socio-economics.

1.2.2 Discolouration

Discolouration has been commonly observed to be due to dissolved or suspended particulate materials of a fine size, the accumulation and subsequent mobilization of which causes water quality issues at the tap (Seth *et al.*, 2003; Polychronopolous *et al.*, 2003; Boxall *et al.*, 2003). Turbidity (unit NTU) is a measurement of water “clarity” obtained by determining the degree of light scattering due to suspended material (Russell, 1994). It is a commonly monitored water quality parameter used as an indicator of discolouration. In the UK turbidity is regulated such that “finished” water, leaving the treatment plant, should be ≤ 1 NTU and “endpoint” water (i.e. the consumers tap) should be ≤ 4 NTU. There are incidents however, where “finished” water complies with regulations but “endpoint” water does not (Bristol Water, 2008), indicating the role of DWDS as biological and chemical reactors which interact with bulk water and alter its quality (Gauthier *et al.*, 2001; Boxall *et al.*, 2003; Seth *et al.*, 2003; Husband *et al.*, 2008). These problems have yet to take precedence in developing areas of the world where DWDS are being newly implemented but, as customer expectations change, it is expected these areas will face the same problems currently experienced in countries with long standing DWDS. In many countries, water supply is seen as a “service industry”, where customer confidence and satisfaction are paramount and the public demand and expects very high levels of service. Consequently, in places such as Australia (Ginige *et al.*, 2011) or Holland (Vreeburg & Boxall, 2007) which are a very “water aware” countries, or the UK (DWI, 2001; Scottish Executive, 2009), where water supply is privatised, the majority of water quality related consumer contacts with water suppliers are a consequence of discolouration. Therefore further understanding of interactions within the DWDS with respect to turbidity is important in improving compliance with standards and to limit customer complaints.

Causes of discolouration have been attributed to corrosion, chemical reactions and biological interactions (LeChevallier *et al.*, 1987; Kirmeyer & AWWA, 2000). Several studies into modelling discolouration have assumed this process is governed by sedimentation of particles, (controlled by gravitational settling) and their subsequent mobilization; this forms the basis of the Particle Settling Model (PSM; Wu *et al.*, 2003). However, settlement of particles of sizes and densities of those responsible for discolouration has been demonstrated to occur at 10^{-6} ms^{-1} , therefore, even low hydraulic forces within the DWDS would be sufficient to maintain the suspension (Boxall *et al.*, 2001). Consequently, it is unlikely that gravity driven sedimentation processes and remobilization are the main drivers of increased turbidity during distribution in live DWDS. It is more feasible that interactions at the pipe-water interface lead to particle attachment, consequently concentrating the previously suspended or precipitating material, which would then cause turbidity if re-mobilised - the “cohesive layer” theory. An alternative modelling approach – Prediction of Discolouration in Distribution Systems (PODDS) has been developed using this theory and states that particle attachment is characterized by “layers” of different attachment strengths which are determined by the hydraulic regime within the pipeline (Boxall *et al.*, 2001). Mobilization of the attached material then occurs when hydraulic forces exceed those experienced during conditioning (Boxall *et al.*, 2001). This theory has been validated by both field and laboratory studies, which established that pipelines that had previously experienced low flow rates/shear stresses had a greater risk of discolouration (Boxall & Saul, 2005; Cook, 2007; Husband & Boxall, 2010; and others). Moreover, it is in line with the concept of biofilms - which are, by definition, material adhered to a surface - playing a significant role in discolouration events. However, PODDS is an empirical tool and, while useful, it has limited understanding of the interactions driving discolouration.

Microbially-mediated processes occurring within the biofilms of DWDS can contribute to aesthetic degradation affecting water colour, taste and odour. For instance “red”, “black” or “blue” water problems can occur as a result of iron, sulphate or copper reducing bacteria, respectively, which cause bio-corrosion and leach substances from the pipe surface into the water column (LeChevallier, 1999; Flemming *et al.*, 2002; Boe-Hansen *et al.*, 2002). The mobilization of biofilm microorganisms and associated material into the bulk water, following a change in DWDS hydrodynamics (Stoodley *et al.*, 2001a; 2002), may also lead to discoloration as a result of elevated turbidity levels (Boxall *et al.*, 2001; Husband *et al.*, 2008; Husband & Boxall, 2010). Increases in turbidity have been correlated with occurrences of gastro illness (MacKenzie *et al.*, 1995; Morris *et al.*, 1996; Schwartz *et al.*, 1997; 2000), in this respect, discolouration can mask health issues (Mann *et al.*, 2007). The mobilization of biofilm bound

material may also lead to an increase in the concentration of inorganics (e.g. iron or manganese) and planktonic microbial numbers, potentially causing regulatory quality failures at the tap (Jenkinson & Lappin-Scott, 2001; Dunne, 2002) and impacting upon the management of the pipe network by affecting the efficiency of disinfectants (Levy *et al.*, 1998). Mobilization of the biofilm material may also, potentially, engender periodic contamination and health risks if pathogenic species are present. Reducing the incidence of discolouration is of paramount importance but in order to do so we need to better understand the processes behind discolouration, in which microbial ecology is emerging as an important driver.

1.3 The DWDS Environment

In some areas DWDS may be a relatively simple standpipe system, however, in many they are an extensive pressurised network of pipes combined with pumps, valves and storage tanks or service reservoirs (Figure 1.1), to assist the management of water distribution (Ratnayaka *et al.*, 2009). DWDS are heterogenic with respect to infrastructure, system management and water composition and are now recognised as more than inert transport systems (Gauthier *et al.*, 1999). Various characteristics such as the fabric of the network, hydrodynamics, organic/inorganic concentrations, type and concentration of disinfectant, or environmental parameters, interact in a complex manner, placing a multitude of constraints on the microbiota present (Chandy & Angles, 2001; Lehtola *et al.*, 2002; Keinanen *et al.*, 2004).

1.3.1 Infrastructure

DWDS are typically supplied with treated water from either a surface or ground water source. The exact treatments employed vary but generally include filtration and disinfection steps. Following treatment, the “finished” water is often pumped to a service reservoir from which it is distributed through a pipe network. In the UK, the two main sections of the DWDS infrastructure are the trunk mains and district management areas (DMAs; Figure 1.1). Trunk mains run between “facilities” of the network, e.g. from the treatment works to the service reservoir, but have no direct customer connections. DMAs are integrated networks of distribution pipes, which can be isolated from the rest of the DWDS by valves (Figure 1.1); they deliver water from local storage or trunk mains to the consumer (Ratnayaka *et al.*, 2009).

Distribution systems are constantly evolving; during expansion or maintenance, pipelines may be repaired, replaced or redirected, hence the system is composed of pipes of diverse age,

material, diameter (from centimetres to metres), length and, arguably, efficiency (Boxall *et al.*, 2007; Ratnayaka *et al.*, 2009; Machell *et al.*, 2009). For instance, in the UK, the majority of the DWDS (69%) has been in place for at least 30 years or longer (Figure 1.2A), with maximum ages of a hundred years or more (UKWIR, 2003). A range of materials have been, and still are, used to construct distribution pipelines (Figure 1.2B) including metals, plastics and cement. Although the majority of pipelines are iron based, both within the UK and internationally, polyvinyl chloride (PVC) and high or medium density polyethylene (HDPE/MDPE) are now steadily replacing older pipes lines (Kerr *et al.*, 1999; UKWIR, 2003; Husband & Boxall, 2010). In the UK, in particular, many of the pipelines are cast iron lined; the modern approach is to line the pipes with an epoxy based resin which produces a surface with plastic like properties.

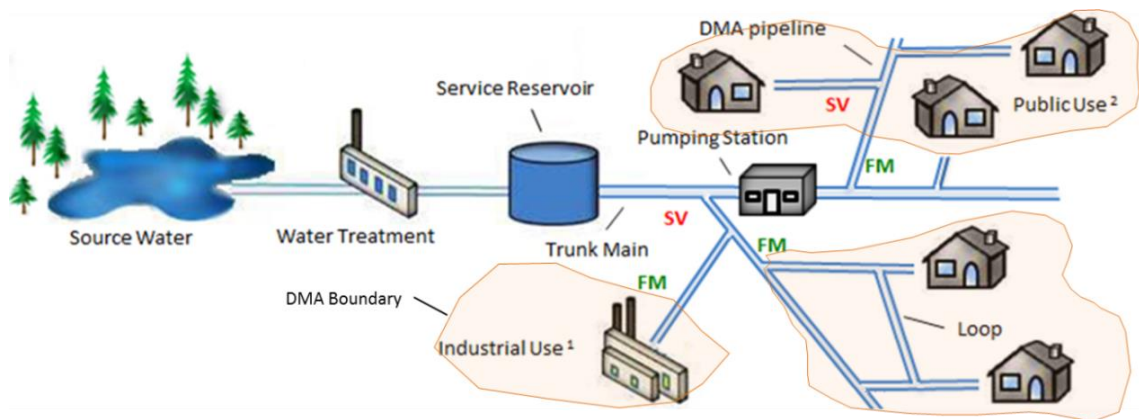


Figure 1.1 Schematic example of a drinking water system. Source water may be surface or ground, specific treatment processes vary. Treated water is generally pumped to a service reservoir from which it is distributed to consumers via the DWDS. ¹ Industrial Use: Some industries can be supplied with grey water, others require microbial free water; ² Public Use: residential use (with domestic plumbing), public recreation, street cleaning; SV – Service Valve; FM – Flow Meter; DMA – District Management Area.

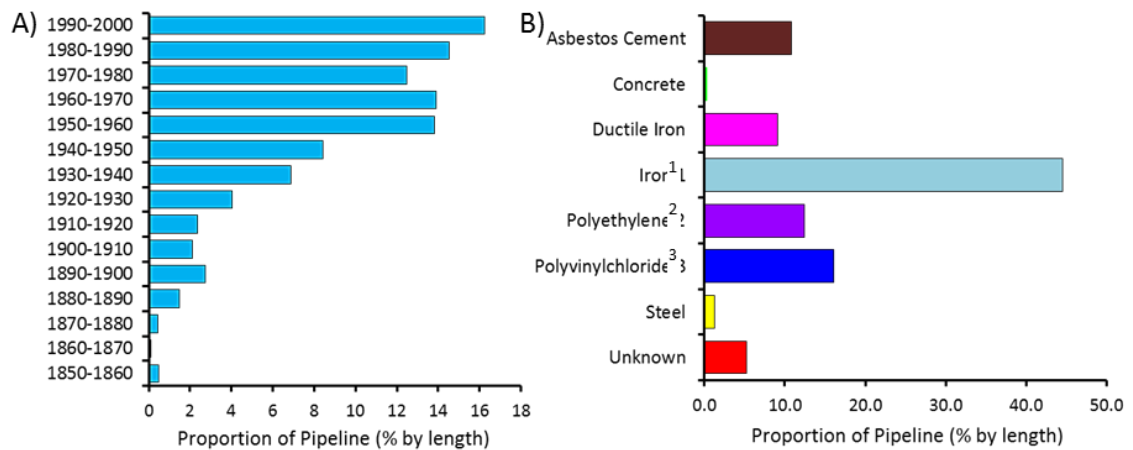


Figure 1.2 Diversity of ages and materials of pipelines within the DWDS. A) Dates (in years) between which pipeline was laid, 1860-1870 constitute a proportion of 0.11%; B) Materials comprising the pipelines, ¹Iron includes cast, galvanised, spun and grey, ²Polyethylene and ³Polyvinylchloride contain various sub groups. Copper, glass reinforced plastic and lead each accounted for 0.017%, 0.089% and 0.001% respectively, they are not included in the plot as no data points were visible due to x-axis scale. Values plotted are percentages, taken from UKWIR (2003)

1.3.2 Hydrodynamics

Demands within the DWDS vary temporally. Diurnal demands differ between weekends and weekdays where, generally, the domestic peak period is 7-9am, with a second small peak in the early evening (Figure 1.3) and an overnight stagnation or low flow period. Seasonal variation also occurs, during dryer months there will be an increased demand for watering gardens for instance (Ratnayaka *et al.*, 2009). The average flow rate observed in the UK is 0.4 l s^{-1} (for pipes of 75-100 mm internal diameter: ID) but fluctuating demands lead to varied flow rates (Figure 1.3), velocity, shear stress (Husband *et al.*, 2008) and residence times, i.e. the time taken for water to reach the consumer from the treatment plant (Kerneis *et al.*, 1995; Tinker *et al.*, 2009).

Hydrodynamics also vary spatially; at a small scale, water flow is less turbulent in the centre of a pipeline, nearer the pipe surface diverse velocities are observed and these produce more turbulent flow in the region adjacent to the wall, this is the boundary layer (Ratnayaka *et al.*, 2009). Variation in flow rates subsequently alters the boundary layer hydraulics. At a larger scale, low flows tend to occur in distant sections of the network, dead ends or looped pipelines (Figure 1.1), which result in a volume of water being “trapped” at a certain point (Walski, 2003; Ratnayaka *et al.*, 2009). Lower flows mean a greater residence so consumers receive older water, the quality of which is likely to have deteriorated somewhat (Kerneis *et al.*, 1995; AWWA, 2002; Machell *et al.*, 2009).

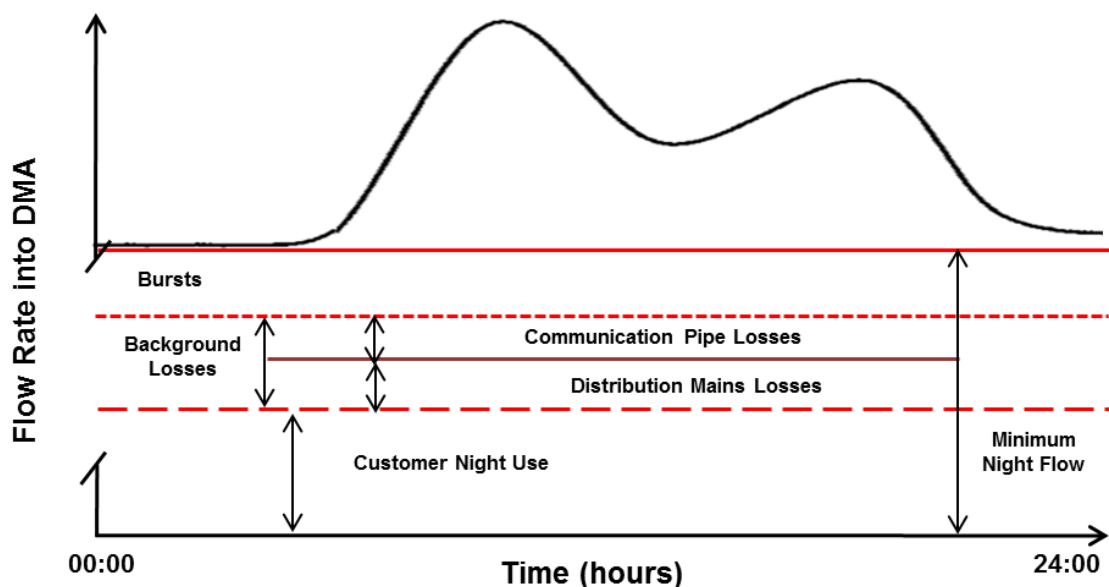


Figure 1.3 Schematic example of diurnal variation in flow rate. Not all the water transmitted is delivered to the consumer due to unavoidable background losses or periodic bursts. N.B. vertical scale is exaggerated.

1.3.3 Water quality: organics/inorganics

No treatment currently exists that can completely remove all organic matter and chemical particles from potable water, which is an unrealistic and, arguably, unnecessary demand. Even with modern engineering and purification techniques, there is no way of controlling all of the variables that govern the fate of water composition as it passes through a water treatment works and the subsequent DWDS (Ratnayaka *et al.*, 2009). The exact composition of drinking water varies on a global, local and temporal scale (e.g. Figure 1.4). Hence water quality is impacted by the source water origin (which may be surface or ground), treatment processes (in terms of both the removal and addition of organisms or particles), residence times and abiotic and biotic factors of the distribution pipelines (Covert *et al.*, 1999; Boxall *et al.*, 2007; Machell *et al.*, 2009; Ratnayaka *et al.*, 2009).

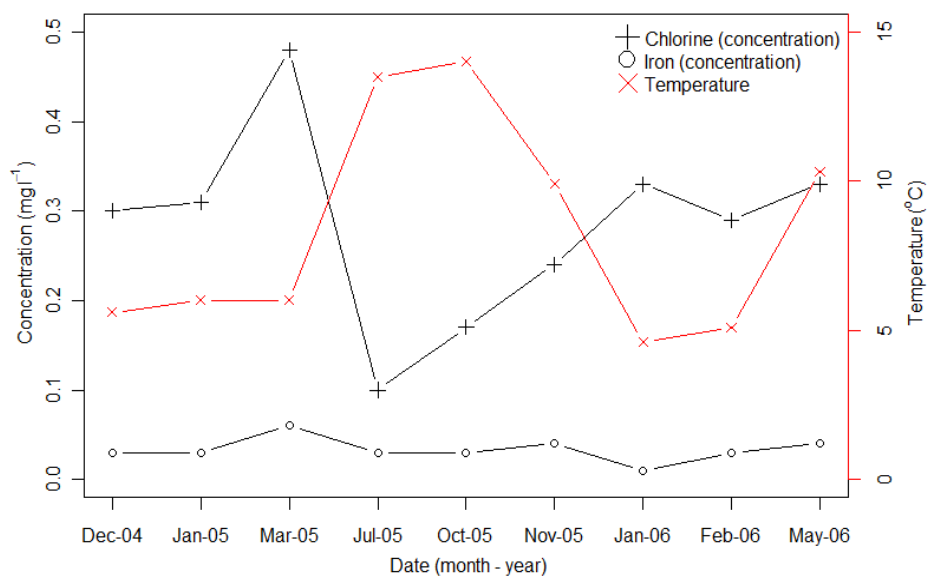


Figure 1.4 An example of temporal variation in water quality properties. (Based on data presented in Husband *et al.*, 2008).

Water treatment does reduce the amount of suspended material (both organics and inorganics) but safe, clean drinking water is not strictly “pure”; it contains very low concentrations of soluble and particulate material including organic matter, minerals such as iron and manganese, disinfectant residuals and microbial cells (Doggett, 2000; Hoefel *et al.*, 2003; Rinta-Kanto *et al.*, 2004; Machell *et al.*, 2009). A certain concentration of these water constituents (and thus some variation in water composition and quality) is tolerated as long as this does not cause a risk to the consumer (Ratnayaka *et al.*, 2009). Consequently, legislation regarding the acceptable concentrations of inorganic and organic compounds, in addition to microbiological parameters, have been established by governing bodies such as the World

Health Organisation (WHO), European Union (EU), UK Drinking Water Inspectorate (DWI) and US Environmental Protection Agency (EPA), in order to control the quality of distributed water (EU, 1998; DWI, 2008; Ratnayaka *et al.*, 2009). An example of some of the drinking water quality controls as stated by these different governing agencies is provided in Table 1.1.

It is noteworthy that the guidelines, particularly the microbiological guidelines, and the methods employed to enforce them, have substantial limitations; primarily there is no international consensus on the site of or frequency of sample collection and variation exists in the quality standards which must be met (Table 1.1). Additionally, the monitoring of microbiological parameters remains heavily reliant on culture-based enumeration of planktonic bacteria (often specifically limited to indicator organisms), which greatly underestimates cell concentrations (Chung *et al.*, 1998; Berney *et al.*, 2008; Hammes, *et al.*, 2008), sometimes by an order of magnitude (“the great plate count anomaly”; Staley & Konopka, 1985). Furthermore, this approach gives no regard to the biofilm microbial communities (Williams & Braun-Howland 2003; Kormas *et al.*, 2010) and yet the degradation of water quality during transmission through DWDS is thought to be caused, in part, by microbial activity at the pipe-bulk water interface, i.e. by biofilms (Menaia & Mesquita, 2004; Husband *et al.*, 2008).

The microbially accessible organics in the DWDS are collectively termed biodegradable organic matter (BOM), generally represented by the assimilable organic carbon (AOC) and the bioavailable dissolved organic carbon (BDOC; Batté *et al.*, 2003). AOC is utilised by microbes and has been reported at levels of 3-500 $\mu\text{g l}^{-1}$, ordinarily comprising 0.1-9% of the total organic carbon (TOC) in drinking water (Camper *et al.*, 1991; van der Kooij, 1992; Vaerewijck *et al.*, 2005). Organics in DWDS may be influenced by source water and treatment train, the microbial load of the network (cells contribute carbon) and the production of disinfectant by products (DBPs) which provide a proportion of AOC (LeChevallier *et al.*, 1991; van der Kooij, 1992; Escobar *et al.*, 2001). It should also be recognised that DBPs have been documented to present a potential health risk to consumers in some instances (Abdullah *et al.*, 2009; Ristoiu *et al.*, 2009; Wei *et al.*, 2010).

Table 1.1 Examples of drinking water guidelines stated by various governing bodies. Data collated from EU ,1998; WHO, 2004; 2011; DWI 2007; 2008; US EPA, 2009; Ratnayaka *et al.*, 2009.

Parameter	WHO Guidelines, 3 rd & 4 th Editions, (2004 & 2011)	EC Directive, 1998	UK Water Supply	US EPA Regulations under Safe Drinking Water Act 1996.
Arsenic (As)	0.01 mg l ⁻¹	5 µg l ⁻¹	5 µg l ⁻¹	0.006 mg l ⁻¹
Ammonia (NH ₄)	-	0.50 mg l ⁻¹	0.50 mg l ⁻¹	-
Chloramines (Cl ₂)	(max) 3 mg l ⁻¹	-	-	4 mg l ^{-1G}
Chlorate (ClO ₃)	0.7 mg l ⁻¹	-	0.7 mg l ⁻¹	- ^G
Chlorine (Cl ₂)	(max) 5 mg l ⁻¹	-	“detectable”	“detectable” - 4 mg l ⁻¹
Copper (Cu)	2 mg l ⁻¹	2 mg l ⁻¹	2 mg l ⁻¹	1.3 mg l ⁻¹
Fluoride (F)	1.5 mg l ⁻¹	1.5 mg l ⁻¹	1.5 mg l ⁻¹	4 mg l ⁻¹
Iron (Fe)	0.3 mg l ⁻¹	200 µg l ^{-1B}	200 µg l ⁻¹	0.3 mg l ^{-1H}
Lead	0.01 mg l ⁻¹	25 µg l ^{-1C}	25 µg l ^{-1C}	0.015 mg l ⁻¹
Manganese (Mn)	0.4 mg l ⁻¹	50 µg l ^{-1B}	50 µg l ⁻¹	0.05 mg l ^{-1H}
Nitrate	50 mg l ⁻¹ as NO ₃	50 mg l ⁻¹ as NO ₃	50 mg l ⁻¹ as NO ₃	10 mg l ⁻¹ as N
Nitrite	3 mg l ⁻¹ as NO ₂	0.5 mg l ⁻¹ as NO ₂	0.5 mg l ⁻¹ as NO ₂	1 mg l ⁻¹ as N
pH	-	≥ 6.5 and ≤9.5	6.5-9.5	6.5-8.5
Sodium (Na)	200 mg l ⁻¹	200 mg l ⁻¹	200 mg l ⁻¹	-
Sulphate	250 mg l ⁻¹	250 mg l ⁻¹	250 mg l ⁻¹	250 mg l ^{-1H}
Total Organic Carbon (TOC)	-	No abnormal change	No abnormal change	Varies with treatment technique
Turbidity	5 NTU	1-4 NTU ^D	1-4 NTU ^D	5 NTU ^I
Colonies/ml at 22°C ^A	-	No abnormal change ^E	No abnormal change ^E	Requirement for surface water <500 colonies/ml
Colonies/ml at 37°C ^A	-	-	No abnormal change ^E	
Total coliforms ^A	-	0/100 ml	0/100 ml ^F	Requirement for surface water, max contaminant level (MCL) <5%
<i>Escherichia coli</i> ^A	0/100 ml	0/100 ml	0/100 ml	

^A WHO and UK microbial guidelines are for water entering, within and leaving the DWDS, EC guidelines are for endpoint water (i.e. water emerging from taps), US EPA regulations are for representative sites along the DWDS; ^BAs stated in 1980 drinking water directive and now set as a national standard; ^C 10 µg l⁻¹ from 25th December 2013, EC states this concentration should be the weekly average; ^D Max values, water leaving a treatment plant must be ≤ 1 NTU, end point water ≤ 4 NTU; ^E Indicator parameter; ^F 95% of the last 50 samples taken must meet the standard; ^G Usually present as a DBP, therefore encompassed by the DBP rule in the US; ^HAs stated in the US EPA list of national secondary drinking water regulations, these are recommendations, they are not binding; ^I If direct filtering is used then turbidity must not exceed 1 NTU.

1.3.4 Microbial management

The efficiency of current microbial control strategies - namely disinfection and “flushing” (though air scouring, pigging, swabbing or scraping may also be employed) – in managing biofilm formation is uncertain, mainly because of a lack of understanding regarding the architecture and chemical properties of the biofilm (Abe *et al.*, 2012). Flushing programmes, which use high flow rates to force material off the pipe walls, are often applied, in conjunction

with high disinfection concentrations, to clean the DWDS network. However, these cleaning programmes are inefficient and disruptive – large volumes of water are used, the elevation of mobilised material may cause an increase in compliance failures and some biofilms remain attached regardless. In the Netherlands, a velocity with a daily peak of $\geq 0.4 \text{ ms}^{-1}$ ($\sim 2 \text{ ls}^{-1}$), irrespective of pipe diameter, is maintained with a view to preventing particles from settling and, therefore, “self-cleaning” the system (Vreeburg *et al.*, 2009). It has been suggested that this velocity is sufficient to resuspend material that may have accumulated during low flows and remove it before large quantities of material can accumulate. However, some biofilms are able to resist detachment and microorganisms can re-colonise a surface within a few hours, posing a potentially unrelenting risk to the water quality (Mackay *et al.*, 1998; Abe *et al.*, 2012) if they are able to resist these velocities.

Many DWDS supply chemically disinfected water, which retains residuals of a biocide agent; in the USA, Japan, the UK and various other European countries chlorine (Cl) or chloramines (NH_2Cl or NHCl_2) are generally retained in finished water (90% of the time; Euro Chlor, 2006) to limit regrowth and contamination risk during distribution (Ratnayaka *et al.*, 2009; Ohkouchi *et al.*, 2013). The current WHO guidelines for chlorine concentration recommended a biocide residual of no greater than 5 mg l^{-1} , although in reality most disinfected drinking waters have concentrations of $0.2\text{-}1 \text{ mg l}^{-1}$ (Table 1.1; DWI PR04a, 2004).

Physical disinfection such as ozonation or UV may be employed as an alternative to (or in conjunction with) chemical disinfection (Uhl *et al.*, 2001; Hageskal *et al.*, 2007). However, physical agents have no residual action, which can leave the DWDS susceptible to recolonisation (Hoefel *et al.*, 2003; Hammes, *et al.*, 2008). A number of utilities in countries such as Norway ($\sim 25\%$) and Germany ($\sim 50\%$) have no disinfection phase at all; those that do include disinfection tend to use UV radiation (Uhl *et al.*, 2001; Hageskal *et al.*, 2007). The Netherlands and Switzerland, aim towards producing high-quality drinking water via implementation of alternative methods to disinfection (Hammes, *et al.*, 2008) such as ultra-filtration or reverse osmosis (Kruithof *et al.*, 2001), which primarily control growth limiting substrates. This is in response to customers’ preference for drinking water without a chlorine residual, due to the taste and DBPs that can develop (Uhl *et al.*, 2001). The arguments for alternative treatments which would enhance the chemical quality of drinking water remain quite compelling, particularly as, irrespective of the disinfection process(es) applied, microorganisms prevail in DWDS (Hoefel *et al.*, 2003; Rinta-Kanto *et al.*, 2004; Hammes *et al.*, 2006; 2008; White *et al.*, 2011; and others).

1.3.5 Environmental parameters

Environmental parameters such as temperature, pH (Vroom *et al.*, 1999), turbidity (Lehtola *et al.*, 2007) and oxygen (Jacob *et al.*, 1998; Vaerewijck *et al.*, 2005) vary temporally and spatially throughout a network and between systems (LeChevallier *et al.*, 1996). Due to the complex interactions occurring within the DWDS, a change in one parameter can have a substantial effect on another. For instance, temperature or pH can impact the disinfection efficiency of chlorine. Keevil *et al.* (1990) report that biocide activity rapidly decreases in alkali conditions such that, at pH 8, a threefold increase in chlorine concentration is necessary to retain the disinfection activity seen at neutral conditions. The influences of temperature have been thought to be greatest in above ground water storage units, as buried pipes are surrounded by material which experiences little thermal variation, but the water temperature within DWDS has been shown to vary throughout the year. Husband *et al.* (2008) recorded a range of 4-14°C in UK systems (Figure 1.4) and ranges of 5-22°C were found in 90 US systems (LeChevallier *et al.*, 1996).

1.4 DWDS Microbiology and the Biofilm System

1.4.1 Microbiota of the pipeline

Imprecise water quality monitoring fuels the misconception that DWDS have low microbial loads with little diversity (Bartram *et al.*, 2004; Phe *et al.*, 2005; Berney *et al.*, 2008). In reality, microorganisms, comprising prokaryotes (bacteria and archaea) and eukaryotes (fungi and protozoa) remain autochthonous in drinking water (Vaerewijck *et al.*, 2005; Denkhaus *et al.*, 2007; White *et al.*, 2011). Several bacteria, fungi and protozoa have been identified in the course of DWDS microbial studies worldwide (see Table 1.2 for examples). Conversely, there is a paucity of research regarding archaea in DWDS which reflects the fact that researchers rarely seek to detect, identify or isolate these microbes post water treatment. Occasionally small invertebrates have even been found in drinking water supplies (both in iron and plastic pipelines and storage tanks), particularly where a ground water source is used and no chlorination has been employed (van Lieverloo *et al.*, 2004; Christensen *et al.*, 2011). It is thought that the microbial biofilms may serve as a nutrient supply for these larger organisms. Despite this diversity in the microbiota, water quality checks focus solely on bacteria (Otterholt & Charnock, 2011), with the exception of Swedish regulations which include fungi and state that concentrations must be ≤ 100 CFU per 100ml (Hageskal *et al.*, 2007).

Table 1.2 Examples of microorganisms isolated and identified in the course of drinking water research.

Domain	Kingdom	Phylum	Class/Order	Genus	Species	References
Bacteria	Bacteria	Proteobacteria	α- Proteobacteria	<i>Agrobacteria</i>	-	LeChevallier <i>et al.</i> , 1987; Kalmbach <i>et al.</i> , 1997; Flemming <i>et al.</i> , 2002; Lehtola <i>et al.</i> , 2004; Williams <i>et al.</i> , 2004; Berney <i>et al.</i> , 2008; Yu <i>et al.</i> , 2010; Revetta <i>et al.</i> , 2010; Moritz <i>et al.</i> , 2010; Kormas <i>et al.</i> , 2010; Wullings <i>et al.</i> , 2011; Gusman <i>et al.</i> , 2012; Park <i>et al.</i> , 2012; Zhang <i>et al.</i> , 2012; Liu <i>et al.</i> , 2012; Henne <i>et al.</i> , 2012; Farkas <i>et al.</i> , 2012; Pachepsky <i>et al.</i> , 2012; Lautenschlager <i>et al.</i> , 2013
				<i>Sphingamonas</i>	-	
			α- Proteobacteria/rhizobiales	-	-	
			β- Proteobacteria	<i>Alcaligenes</i>	-	
				<i>Burkholderia</i>	-	
				<i>Thiobacillus</i>	-	
			γ- Proteobacteria	<i>Pseudomonas</i>	<i>P. aeruginosa</i>	
				<i>Escherichia</i>	<i>E. coli</i>	
				<i>Salmonella</i>	<i>S. enterica</i>	
				<i>Shigella</i>	-	
			Epsilon- Proteobacteria	<i>Legionella</i>	<i>L. pneumophila</i>	
				<i>Campylobacter</i>	<i>C. jejuni</i> , <i>C. fetus</i> , <i>C. coli</i>	
			<i>Helicobacter</i>	<i>H. pylori</i>		
Actinobacteria	Actinomycetales	<i>Arthrobacter</i>	-			
		<i>Nocardia</i>	-			
<i>Mycobacteria</i>	<i>M. avium</i> , <i>M. gordonae</i> , <i>M. intracellulare</i>					
Bacteroidetes	Flavobacteriales	<i>Flavobacterium</i>	-	Williams <i>et al.</i> , 2004; Eichler <i>et al.</i> , 2006; Yu <i>et al.</i> , 2010		
Acidobacteria	-	-	-	Martiny <i>et al.</i> , 2003; 2005; Henne <i>et al.</i> , 2012		
Nitrospirae	Nitrospira	-	-			
Cyanobacteria ^A	-	-	-	Revetta <i>et al.</i> , 2010; Henne <i>et al.</i> , 2012		
Planctomycetes	-	-	-	Martiny <i>et al.</i> , 2003; 2005; Revetta <i>et al.</i> , 2010; Henne <i>et al.</i> , 2012		
Archaea	Archaea	Euryarchaeota	-	-	Ling & Liu, 2013	
		Crenarchaeota	-	-		

^A Photosynthetic but temporary survival is achieved anaerobically in dark conditions (Richardson & Castenholz, 1987).

Table 1.2 continued.

Domain	Kingdom	Phylum	Class/Order	Genus	Species	References			
Eukaryotes	Fungi	Basidiomycota	Spoidiales	<i>Cryptococcus</i>	-	Carson <i>et al.</i> , 1978; Arvanitidou <i>et al.</i> , 1999; Doggett, 2000; Zacheus <i>et al.</i> , 2001; Göttlich <i>et al.</i> , 2002; Gonçalves <i>et al.</i> , 2006; Hageskal <i>et al.</i> , 2007; Sammon <i>et al.</i> , 2010; Hageskal <i>et al.</i> , 2012; Liu <i>et al.</i> , 2012			
				<i>Rhodotorula</i>	-				
		Ascomycota	Saccharomycetes	Euroticiles	<i>Candida</i>		-		
					<i>Penicillium</i>		<i>P. spinulosum</i>		
			Hypocreales		<i>Aspergillus</i>		<i>A. calidoustus</i>		
					<i>Stachybotrys</i>		<i>S. chartarum</i>		
					<i>Fusarium</i>		<i>F. solani</i>		
					<i>Trichoderma</i>		<i>T. viride</i>		
		Chytridiomycota			<i>Acremonium</i>		-	Arvanitidou <i>et al.</i> , 1999; Zacheus <i>et al.</i> , 2001; Göttlich <i>et al.</i> , 2002; Gonçalves <i>et al.</i> , 2006	
					Chaetothyriales		<i>Phialophora</i>	<i>P. reptans</i>	Zacheus <i>et al.</i> , 2001; Göttlich <i>et al.</i> , 2002; Heinrichs <i>et al.</i> , 2013a
	<i>Exophiala</i>					<i>E. lecanii-corni</i> , <i>E. castellani</i>			
	Dothideomycetes						<i>Cladosporium</i>	<i>C. malorum</i> , <i>C. Cladosporioides</i>	Zacheus <i>et al.</i> 2001; Poitelon <i>et al.</i> , 2009; Sammon <i>et al.</i> , 2010; Heinrichs <i>et al.</i> , 2013a
							<i>Alternaria</i>	-	Heinrichs <i>et al.</i> 2013a
	Protists			Metamonada	Diplomonadida	<i>Giardia</i>	<i>G. lamblia</i>	Sibille <i>et al.</i> , 1998; Schwartz <i>et al.</i> , 1998; Helmi <i>et al.</i> , 2008; Valster <i>et al.</i> , 2009; Poitelon <i>et al.</i> , 2009; Liu <i>et al.</i> , 2012	
				Apicomplexa	Evococcidiorida	<i>Cryptosporidium</i>	<i>C. parvum</i>		
-				-	<i>Acanthamoeba</i>	<i>A. polyphaga</i>			
Ciliophora				-	-	-			
Cercozoa				-	-	-			
Amoebozoa				Tubulinida	<i>Hartmannella</i>	<i>H. verniformis</i>			

1.4.1.1 Bacteria

Internationally, bacteria are the only microorganisms monitored with respect to drinking water quality, as indicated in Table 1.1. Coliforms are a group of Gram-negative bacteria (including *E. coli*) that are used as indicator organisms in the water industry (EU, 1998; Hammes, *et al.*, 2008; DWI, 2008). They are easy to culture and, if detected, highlight the potential occurrence of faecal contamination, a major source of microbial pathogens in drinking water (Environment Agency, 2002). However, scientific studies have found that coliforms can be incorporated into biofilms where they persist for some time (Camper *et al.*, 1998; Zacheus *et al.*, 2001; Williams & Braun-Howland, 2003; Banning *et al.*, 2003). This is significant to the water industry as a breakthrough may be masked if the indicator organisms seek refuge in a biofilm and hence go undetected. The subsequent release of these microorganisms from the biofilm can simultaneously inoculate the biofilms downstream with potential pathogens and, incorrectly, suggest a recent contamination event (Williams & Braun-Howland, 2003).

A plethora of scientific studies have found bacteria to be the most common microorganisms in potable water, particularly *Pseudomonas spp.*, *Nocardia spp.*, and *Sphingomonas spp.* (Nagy & Olson, 1982; LeChevallier *et al.*, 1987; Lehtola *et al.*, 2004). Ultramicrocells, which are reduced (dwarf or starved) forms of bacteria, have also been isolated from drinking water and shown to be phylogenetically diverse but dominated by Proteobacteria and Actinobacteria (Silbaq, 2009). However, many of these studies provide a biased view of community composition due to their use of culture-based analysis methods and focus on the planktonic community. Many of the species in DWDS are not adapted to the constraints presented by synthetic media (Falkinham *et al.*, 2001; Connon & Giovannoni, 2002; Hoefel *et al.*, 2003). For instance, the environmental mycobacteria (EM), *Mycobacterium avium*, can grow in DWDS but is notoriously difficult to culture, hence it would not be detected and a false negative would be recorded (Covert *et al.*, 1999; Falkinham *et al.*, 2001). Consequently, many viable but not culturable (VBNC) cells potentially remain undetected in DWDS; a VBNC state may even be induced by the environmental conditions within the pipeline, as shown by Dwidjosiswojo *et al.*, (2011).

Research is being increasingly focused on the biofilm community, in conjunction with the planktonic population which, combined with the use of 16S rRNA genetic analysis or fluorescence microscopy, has overcome previous biases and is generating a more accurate identification of the microbial life in our pipelines (Santo Domingo *et al.*, 2003; Williams *et al.*, 2004; Tokajian *et al.*, 2005; Martiny *et al.*, 2005; Poitelon *et al.*, 2009; Revetta *et al.*, 2010; Yu

et al., 2010; Douterelo *et al.*, 2013). In line with culture based studies, those that utilise these new approaches also highlight the dominance of bacteria (Table 1.2) in DWDS. These studies present evidence of a much greater species diversity than was determined previously, the largest identifiable component of which is within the phylum Proteobacteria (Williams *et al.*, 2004; Vaerewijck *et al.*, 2005; Berney *et al.*, 2008; Zhang *et al.*, 2012; Park *et al.*, 2012; Lautenschlager *et al.*, 2013; Douterelo *et al.*, 2013), although other bacterial phyla such as Actinobacteria and Bacteroidetes have also commonly been found (Williams *et al.*, 2005; Eichler *et al.*, 2006; Revetta *et al.*, 2010; Yu *et al.*, 2010).

Proteobacteria have been found to dominate across a range of drinking water samples, states (planktonic or biofilm, the latter sampled from bench-top scale systems) and environments (Kalmbach *et al.*, 1997; Williams & Braun-Howland, 2003; Tokajian *et al.*, 2005; Kormas *et al.*, 2010), regardless of pipe material (Yu *et al.*, 2010), disinfection technique (Santo Domingo *et al.*, 2003; Williams *et al.*, 2005) or time of sampling (Revetta *et al.*, 2010). This is not to say that environmental variables do not influence the microbial community. Due to the heterogeneity of DWDS, the community composition and species diversity are unique to each system and vary throughout it (Kormas *et al.*, 2010). Generally Alpha (α) -, Beta (β) - and, or Gamma (γ) - proteobacteria are the most common bacterial classes found in drinking water (Williams *et al.*, 2004; Kormas *et al.*, 2010; Revetta *et al.*, 2010) and biofilm samples (Schwartz *et al.*, 1998; Tokajian *et al.*, 2005; Yu *et al.*, 2010; Douterelo *et al.*, 2013). Williams & Braun-Howland (2003) also isolated epsilon-proteobacteria from biofilm samples, whilst Poitelon *et al.* (2009) found high numbers of deltaproteobacteria in drinking water originating from three different treatment plants. While proteobacteria may tend to dominate in DWDS, there remains a wide variety of taxa present (Table 1.2) and the specific amalgamation of species differs (Poitelon *et al.*, 2009; Revetta *et al.*, 2010).

Bacteria such as *Mycobacteria gordonae*, non-pathogenic *Escherichia coli* and heterotrophic bacteria can degrade water quality aesthetics and affect DWDS operation (Fass *et al.*, 1996; Williams & Braun-Howland, 2003; Vaerewijck *et al.*, 2005). However, the majority of bacteria persisting in the DWDS pose no public health risk and most are harmless. Nevertheless, pathogenic bacteria such as *Helicobacter pylori*, *Pseudomonas aeruginosa*, *Campylobacter spp.* and *Legionella pneumophila* have been isolated from a number of potable samples (Bert *et al.*, 1998; Ferroni *et al.*, 1998; Mackay *et al.*, 1998; Mah & O'Toole, 2001; Park *et al.*, 2001). The presence of EM, which are emerging pathogens, is debated in the literature mainly due to the use of unsuitable isolation or detection techniques (Vaerewijck *et al.*, 2005). Several authors have, however, irrefutably illustrated the presence of EM (Schwartz *et al.*, 1998; Covert *et al.*,

1999; Falkinham *et al.*, 2001) and the role of the *M. avium* complex (MAC) as an active coloniser (Carson *et al.*, 1978; Falkinham *et al.*, 2001). Similarly, the bacterial pathogen *L. pneumophila* is difficult to isolate from water samples using culture methods so in the past its incidence has been disputed; however, it has since been accurately identified in samples via the use of molecular analyses (Fields, 1996; Williams *et al.*, 2004). These species have been shown to not only persist but proliferate in DWDS, contaminating drinking water in the process, hence, though rare, there are still incidences of waterborne illness (Ferroni, *et al.*, 1998; Mah & O’Toole, 2001). Nonetheless, it should be noted that pathogens are likely to be outcompeted by other cells within the biofilm and so represent a small proportion of the biofilm community; hence they are unlikely to be released in numbers sufficient to cause a disease outbreak (Wai *et al.*, 1998; Watnick & Kolter, 2000; Boe-Hansen *et al.*, 2002).

Interestingly, many of the studies using molecular techniques have revealed that a large number of drinking water isolates (over 57% in some instances) are “difficult to classify”. These sequences closely match other unclassified sequences originating from potable water, possibly indicating the existence of novel bacteria adapted to the oligotrophic nature of the DWDS (Williams *et al.*, 2004; Keinänen-Toivola *et al.*, 2006; Poitelon *et al.*, 2009; Revetta *et al.*, 2010). The fact that, even when equipped with the modern techniques, the majority of the microbial world remains unidentified, illustrates the extent of microbial diversity in these systems, the limitation of culture based analysis (Burtscher *et al.*, 2009) and the under representation of drinking water sequences in databases (Revetta *et al.*, 2010), which demonstrates the need for further research in this field. It is also important to appreciate that the majority of drinking water samples from which bacteria have been isolated or their communities studied, were obtained from laboratory based studies or the bulk water of DWDS (generally from taps), neither of which accurately represent the biofilms that develop within the pipeline.

1.4.1.2 Fungi

Research regarding fungi (eukaryotes encompassing moulds and yeasts) within DWDS has increased in the last decade and they are beginning to be accepted as part of the drinking water microbiota. Various fungal species have been detected (Table 1.2) in the biofilms and bulk water, regardless of differences in source water or treatment processes and, in some cases, little difference has been found between the community profiles of the raw and treated water (Doggett, 2000; Zacheus *et al.*, 2001; Poitelon *et al.*, 2009; Sammon *et al.*, 2010, 2011; Otterholt & Charnock, 2011; Liu *et al.*, 2012).

The contribution of fungi to DWDS microbial communities varies. Göttlich *et al.* (2002) reported that 7.5% of groundwater samples contained fungi, comparable with the proportion (8.3%) found by Poitelon *et al.* (2009) in samples from France, but significantly lower than results reported by Heinrichs *et al.* (2013a), who found that 98% of the surveyed German domestic pipelines contained fungi. This discrepancy could be attributed to different DWDS and water sources or, as the authors suggest, differences in methodological approaches and the limit of detection (LOD) between the studies (Göttlich *et al.*, 2002: LOD 1000 cfu l⁻¹; Poitelon *et al.*, 2009: assessed 18S rRNA gene occurrence not cell counts; Heinrichs *et al.*, 2013a: LOD 1 cfu l⁻¹). A study of tap water in Greece, by Arvanitidou *et al.* (1999), found that 82.5% of samples were positive for fungi, consistent with the high fungal occurrence reported by Heinrichs *et al.* (2013a).

Identified phyla or species (Table 1.2) include the filamentous fungi *Aspergillus spp.*, *Penicillium spp.*, *Cryptococcus spp.* (e.g. Nagy & Olson, 1982; Doggett 2000; Hageskal *et al.*, 2006; 2007; 2012) and the yeast species *Cladosporium malorum*, *Altemaria spp.* and *Exophiala castellanii* (Heinrichs *et al.*, 2013a). Hageskal *et al.* (2012) demonstrated that the most common species in Norwegian DWDS (as stated in Hageskal *et al.*, 2006) are those with an ability to survive the UV disinfection, primarily *P. spinulosum*, and *Trichoderma viride* which were also able to resist chlorination. It is thought that these species are less sensitive to UV due to their pigmentation and chlorination resistance may be conveyed via thick, melanised cell walls (Hageskal *et al.*, 2012). Research has shown that fungi are tolerant of bacterial disinfection regimes commonly used in DWDS and that the most effective treatment to inactivate fungi is ozonation (Hageskal *et al.*, 2012).

Not all fungi are able to reside in the DWDS for long periods (Göttlich *et al.*, 2002) and there is no consensus regarding the occurrence of filamentous fungi in the presence of bacteria, some authors have found a positive correlation (Sammon *et al.*, 2010) others a negative (Göttlich *et al.*, 2002; Gonçalves *et al.*, 2006). It is apparent though, that fungi, particularly filamentous fungi, are common in DWDS samples and are likely to play a role in water quality degradation, as well as acting as opportunistic pathogens that can cause systematic infections. Although research in this area is increasing, highlighting the diversity and spread of fungi, further research is required to demonstrate the role of fungi in DWDS microbial ecology (Niemi *et al.*, 1982; Kanzler *et al.*, 2007; Sammon *et al.*, 2011; Hageskal *et al.*, 2012). Moreover, as is the case for bacterial community research, many of the potable samples for which fungal communities are analysed have been developed within bench-top scale test facilities or isolated from end

point drinking water, neither environment accurately simulates that occurring within a DWDS pipeline and so the samples are not necessarily representative of the DWDS ecology.

1.4.1.3 Archaea

There are very few studies focusing on archaea within a DWDS context and their presence within the pipeline has yet to be definitively proven. A study in Sweden by Manz *et al.* (1993) detected no archaea in drinking water samples. Conversely, ammonia oxidising archaea (AOA) were isolated in drinking water from the Netherlands (Wielen *et al.*, 2009) and Euryarchaeota and Crenarchaeota were detected in ground water in Illinois, USA (Ling & Liu, 2013). However, in all cases it could be argued that the samples analysed do not accurately reflect the biofilms or water from the DWDS environment as Manz *et al.* (1993) used glass slides mounted within a Robbins device, Ling & Liu (2013) developed biofilm within a bioreactor and Wielen *et al.* (2009) collected water samples from household taps, rather than the distribution network.

1.4.1.4 Protozoa

Protozoa have been said to be unable to multiply in a DWDS as they require a host to do so (Quignon *et al.*, 1997), hence the protozoa that have been found tend to be recovered as inactive (oo)cysts (Karanis *et al.*, 1998; Schwartz *et al.*, 1998). However, Sibille *et al.* (1998) found protozoa actively predated the plethora of bacteria in biofilms of distribution systems. Free-living protozoa prey upon bacteria, fungi and organics within biofilms, which can impact upon the wider microbial community structure. In turn, the protozoan community composition is influenced by bacterial diversity and abundance which are impacted by water quality.

Protozoa have been found to be abundant in DWDS in the Netherlands, where disinfection use is limited (Otterholt & Charnock, 2011). Van Lieverloo *et al.* (2004) recorded a protozoan presence in 78% of water samples and Valster *et al.* (2009) found that ground water-fed systems exhibited diverse protozoan communities. More than 50% of the operational taxonomic units extracted matched protozoa species such as *Acanthamoeba polyphaga* which is an opportunistic pathogen and bacterial host (Valster *et al.*, 2009). A study of Parisian DWDS by Poitelon *et al.* (2009) also demonstrated a common detection of protozoa in water samples (50%) and Otterholt and Charnock (2011) detected protozoa in studies of samples from Norway. However, the use of genetic analyses in these studies may mean that some of these matches correspond to inactive or damaged cells, although the authors conclude that there is evidence for full, intact protozoa occurring in the water samples when assessed in conjunction

with other analysis. Despite the detection of protozoa in DWDS, little is known about the ecology of the microorganisms and the impact of the water quality or hydraulics upon them.

1.4.1.5 Viruses

A study of potable water in Wisconsin, USA, detected adenoviruses, enteroviruses and norovirus in samples exposed to UV treatment (Lambertini *et al.*, 2012). The concentration of viruses increased by 6.9 genomic copies (gc) l⁻¹ in samples downstream of the treatment compared to those taken immediately after, indicating that viruses were multiplying within the pipeline (Lambertini *et al.*, 2012). On rare occasions, Norwalk and Rotavirus have been isolated in DWDS, generally from within the biofilm matrix (Boyd & Chakrabarty, 1995; Quignon *et al.*, 1997; Mackay *et al.*, 1998), although (Lambertini *et al.*, 2012) detected Rotavirus in a single tap water sample (1/1452 samples). Helmi *et al.* (2008) spiked a rotating reactor fed with tap water with viable viruses and found that they became incorporated into the biofilm within an hour. However, this experimental system experienced a flow rate of 100 ml min⁻¹, which is much lower than the rates experienced in full scale DWDS.

1.4.2 Sources of contamination

Microorganisms can penetrate DWDS in a planktonic state from “external” sources, indirectly contaminating the pipe network due to poor practices or negative pressures (McCoy & Olson, 1986; Besner *et al.*, 2002; 2007). DWDS are pressurised to transport finished water from a treatment plant to customers, any change in this pressure can reverse the direction of the water flow, resulting in “external” contaminants, such as microorganisms from non-sterilised construction materials, being drawn into the pipeline via backflow (Kirmeyer & AWWA, 2000; US EPA, 2004). Göttlich *et al.* (2002) found that certain fungi were detected exclusively in regions of the DWDS where new pipes had been installed.

Many networks experience “internal” contamination; microbial cells indigenous to the source water may survive or avoid (if there is a break in purification) the treatment processes (particularly filtration and disinfection) and pass directly into the DWDS (Fass *et al.*, 1996; LeChevallier *et al.*, 1996; Besner *et al.*, 2002; Wright *et al.*, 2004; Keinanen *et al.*, 2004; US EPA, 2004). Vreeburg *et al.* (2008) suggests that the majority of particles within the DWDS originate from the source water but contamination from the treatment system (e.g. carbon particles, microflocs or coagulants) is not uncommon (Polychronopolous *et al.*, 2003). Microbial ingress in this way is feasible, as evasion of treatment is facilitated by the small size of microorganisms (bacteria 1-10 µm, protozoan cysts 4-6 µm, viruses 100 times smaller), which means that

extremely efficient filtration is necessary to prevent their infiltration into the DWDS (Quignon *et al.*, 1997). Furthermore, it is widely accepted that many microbial cells are able to withstand chlorination due to their complex cell walls, capsules, polysaccharide coatings (Mackay *et al.*, 1998) or by forming aggregates (as *Sphingomonas* does; Gauthier *et al.*, 1999) which offer a physical protection. In addition to aiding persistence of the cells through the treatment plant, such adaptations also convey protection from the disinfection residual within the water column.

1.4.3 Planktonic state vs. biofilm state

Planktonic cell counts of 10^3 - 10^4 cells ml⁻¹ (Hoefel *et al.*, 2003; Rinta-Kanto *et al.*, 2004; Hammes, *et al.*, 2008), have been reported in potable water. Some species such as *Arthrobacter spp.* (Gram-positive bacteria) experience higher growth rates in the water column and exhibit limited surface attachment (Murgel *et al.*, 1991; Manuel *et al.*, 2007; Park *et al.*, 2012). It should be noted that these studies used systems atypical of DWDS (different types of reactor), which do not accurately replicate the boundary layer hydraulics of full scale systems. On the other hand, a study by Srinivasan *et al.* (2008) used a model DWDS to show that biofilms may not dominate all pipelines, regions that have low chlorine concentrations may have a higher microbial load in the bulk water. The authors did however note that as chlorine concentrations increased microorganisms favoured the biofilm state. Many studies state that the majority of microorganisms survive and proliferate by forming or joining biofilms and so most of the DWDS microbiota occurs at the pipe surface (Lehtola, Miettinen, *et al.*, 2004) where organics/inorganics (including metals) also accumulate (Zacheus *et al.*, 2001). Even cells that have been inactivated during treatment will colonise the inner pipe surface or attach to existing biofilms, within which they can recover (LeChevallier *et al.*, 1996).

A biofilm consists of various elements (Table 1.3), the juxtaposition and spatial arrangement of these is referred to as the biofilm architecture, the specifics of which vary spatially and temporally with changing environmental conditions and microbial communities (Wimpenny *et al.*, 2000; Jenkinson and Lappin-Scott, 2001). The sessile assemblages comprise a complex mixed community (dominated by bacteria), with cell concentrations of 10^6 - 10^{11} cells cm² (Zacheus *et al.*, 2001; Morvay *et al.*, 2011; Abe *et al.*, 2012 – expressed concentration as cfu l⁻¹), which is hundreds or thousands of times greater than the concentrations in the water column and accounts for >90% of the biomass within the pipeline (LeChevallier *et al.*, 1983; 1987; 1988; Norton & LeChevallier, 2000; Besner *et al.*, 2002; Boe-Hansen *et al.*, 2002; Rompre *et al.*, 2002). Cells are present in a spectrum of states and experience biological fluidity, i.e. a

constant detachment and attachment of cells and architectural changes (van der Wende *et al.*, 1989; Menala *et al.*, 2003).

Table 1.3 Breakdown of biofilm features/components (adapted from Denkhaus *et al.*, 2007).

Biofilm Feature	Details of Composition
Extracellular polymeric substances (EPS)	<ul style="list-style-type: none"> • At a basic level: carbohydrates, proteins, phospholipids and extracellular DNA • Amino sugars and proteins (e.g. NH_3^+) are cationic groups • Uronic acids, proteins and nucleic acids (e.g. COO^- or HPO_4^-) are anionic groups • Apolar groups are present in proteins (such as in aromatic amino acids), phospholipids and humic substances
Microbial cells	<ul style="list-style-type: none"> • Multiple species – comprised of various taxa, dominated by bacteria • Live and dead cells will be present in a biofilm • Bacterial cells consist of: <ul style="list-style-type: none"> ○ Plasma membrane ○ Cytoplasm, containing DNA, mRNA and other cytoplasmic components ○ An outer membrane (gram-negative cells) ○ Other physical structures such as capsule, pili, flagella
Nutrients and Minerals	<ul style="list-style-type: none"> • Generally bound/incorporated into the EPS • Precipitates (sulphides, carbonates, phosphates, hydroxides) • Free and bound metals (e.g. iron, manganese, copper)
Environmentally relevant substances	<ul style="list-style-type: none"> • Organic contaminants (e.g. biocides, detergents, xenobiotics) • Inorganic pollutants (e.g. heavy metals)

The community compositions of the bulk water (planktonic cells) and pipe surface (biofilm cells) have been found to differ (Norton and LeChevallier, 2000; Zacheus *et al.*, 2001; Henne *et al.*, 2012). However, these states are dynamic; sessile cells will periodically be shed from the biofilm (actively or due to mechanical shear stresses) into the planktonic state as single cells or as aggregates which may reattach to an assemblage downstream (Costerton *et al.*, 1995; Vaerewijck *et al.*, 2005). The assorted adhesions produced by bacteria are regulated at a transcriptional level hence some microorganisms are able to switch between a sessile and nomadic lifestyle in response to different environmental influences (Ziebuhr *et al.*, 1999); in this way cells may actively detach from the biofilm and disperse (Telgmann *et al.*, 2004). For instance, *Pseudomonas aeruginosa* adheres to surfaces when a favourable nutrient concentration exists but can actively detach if nutrients decline at the interface (Costerton *et al.*, 1995). This vast population difference between planktonic and sessile populations suggests a survival advantage for biofilm cells, which is sacrificed by nomadic cells (Costerton, 1999; Lehtola *et al.*, 2007; Park *et al.*, 2001). Indeed, microorganisms in the biofilm encompass both morphological and metabolic specialisation, consequently showing fundamental differences to planktonic cells of the same species, which aid their survival (Wimpenny *et al.*, 2000; Sauer, 2003; Manuel *et al.*, 2007).

1.4.4 The biofilm cycle

The majority of drinking water biofilm research is based upon bench top scale systems, which tend to be run under idealised conditions. These set-ups do not replicate all of the environmental constraints placed upon microorganisms within a full scale system, which influence colonisation of a pipe surface and subsequent biofilm development (van der Wende, *et al.*, 1989; Rickard *et al.*, 2002; 2003; Menala *et al.*, 2003). However, the four basic steps which comprise biofilm formation (Figure 1.5) remain the same; primary adhesion (or docking), secondary adhesion (or locking), maturation (growth) and detachment (Stoodley *et al.*, 2001; Dunne, 2002; Vaerewijck *et al.*, 2005). Although the primary and secondary adhesion stages are necessary before the biofilm can evolve, detachment is not necessarily an “end stage”; it occurs continuously at various stages of biofilm formation and adds to the heterogeneity of the sessile community. The following section reviews the findings regarding biofilm development from all such idealised studies and other general biofilm research.

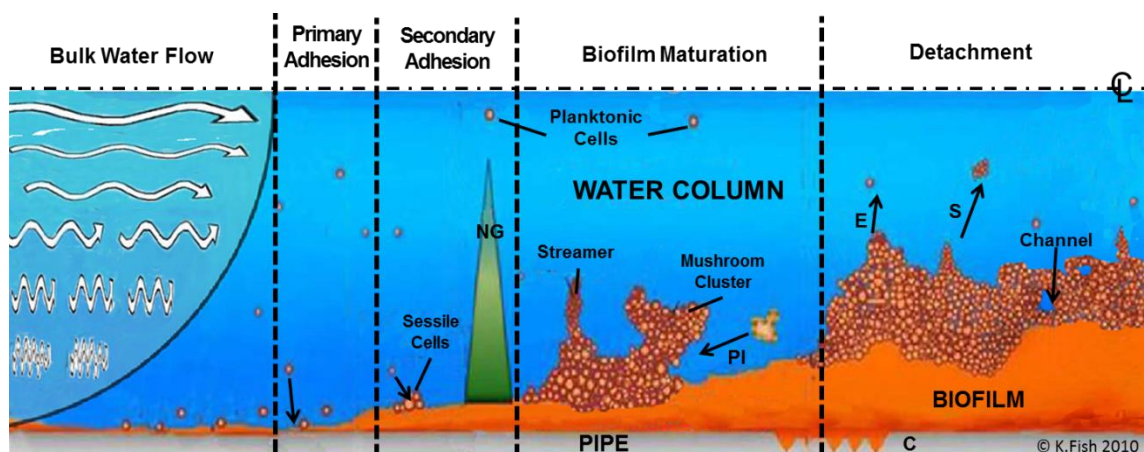


Figure 1.5 Processes involved in biofilm development ; growth stages, water flow within the pipe and some of the processes occurring within biofilms of the DWDS. As the distance from the wall increases flow becomes more laminar, NG – Nutrient Gradient, concentrates within the biofilm; PI – Protozoan Interactions; C – Corrosion of the pipe surface; E – Erosion; S – Sloughing; CL – centre line.

1.4.4.1 Primary adhesion (initial attachment)

The mechanism by which a cell recognises a surface is unclear (Prigent-Combaret *et al.*, 1999). However, it has been acknowledged that adhesion is dictated by various physical, chemical and biological aspects (Klein & Ziehr, 1990; Dunne, 2002). Primary adhesion, depicted in Figure 1.6A, refers to the serendipitous meeting and initial attachment of planktonic microorganisms with a surface, producing a community of initial colonisers, the diversity of which will likely be determined by the selection pressures of attachment (Martiny *et al.*, 2003). Attachment may be a random event driven by the bulk-water hydraulics or a direct result of cell motility and

chemo-taxis (Jenkinson & Lappin-Scott, 2001; Dunne, 2002). Consequently, attachment is facilitated in species that possess structures such as flagella, which enable mobility, aiding the positioning of a cell on the substratum (Mah & O'Toole, 2001; Vaerewijck *et al.*, 2005). When a microorganism reaches a close enough proximity (quoted as <1 nm in (Dunne, 2002) attraction and repulsion forces between the cell and surface come into play and, depending upon the sum of the forces (Allion *et al.*, 2011), single cell adhesion may occur (An *et al.*, 2000; Appenzeller *et al.*, 2002). Any repulsion from the surface may be overcome via molecular interactions mediated via external adhesions (Figure 1.6) such as pili (An *et al.*, 2000; Boland *et al.*, 2000).

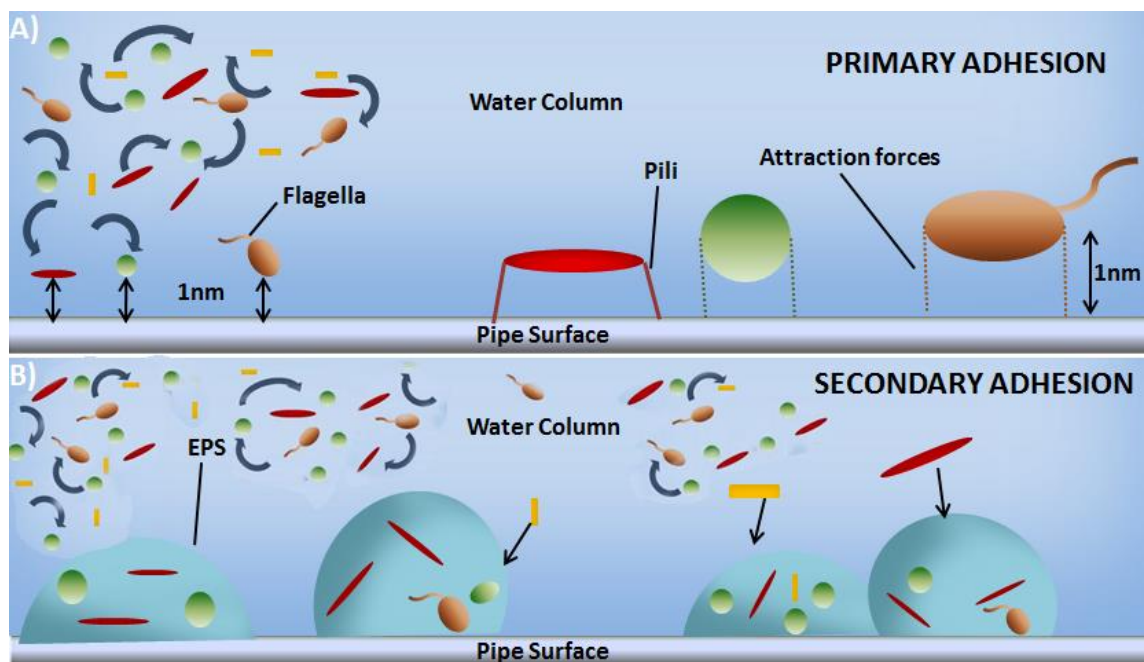


Figure 1.6 Schematic representation of biofilm adhesion. A) Primary Adhesion: Cell approaches surface by chance via hydrodynamic action or facilitated by flagella and loosely attaches if the net sum of attraction and repulsion forces is positive or by using adhesions such as pili, to overcome repulsion. B) Secondary Adhesion: EPS production begins and secondary colonisers begin to attach.

1.4.4.2 Secondary adhesion and mature biofilm development

Once attached, cells lock or anchor themselves in place (secondary adhesion) via the synthesis of EPS (Figure 1.6B), consolidating the binding between cell and surface (Danese *et al.*, 2000; Watnick & Kolter, 2000). Subsequently, other cells co-aggregate, attach, detach, grow and replicate (Figure 1.5), forming a complex mature biofilm with several components (Table 1.3) and a consortium of cells at different metabolic stages. The EPS matrix is the main constituent of biofilm; it becomes more extensive during development acting as a linking film between micro-colonies and the substratum. Additionally, EPS provides a microenvironment more suitable for secondary colonisers, such as fungi (Sammon *et al.*, 2011), that may be unable to

synthesise EPS themselves or require a more clement environment for attachment (van Loosdrecht *et al.*, 1990; Sutherland, 2001a, 2001b). In this way, the presence of one species can promote the binding of another (Dunne, 2002), leading to the growth of a diverse, mature biofilm as regards physical and community structure.

During secondary adhesion, cells have been reported to alter their phenotypes; as the biofilm matures various genes are transcribed, cell differentiation occurs and modifications in regulatory mechanisms are made via cell-cell signalling, termed quorum sensing (Davey & O'Toole, 2000). In brief, quorum sensing refers to the secretion and detection of signalling molecules such as the well characterized acylated homoserine lactone (AHL) employed by some Gram-negative bacteria (Davies *et al.*, 1998) and the less well studied peptides which are used by some Gram-positive cells (Dunny & Leonard, 1997). Following initial attachment, AHLs are used to activate transcription of specific genes such as *algL*, *algC* or *algD* in *Pseudomonas aeruginosa*, which control the production of essential anchor polymers, in this case alginate, ultimately controlling secondary adhesion (Boyd & Chakrabarty, 1995; Davies *et al.*, 1998; Stoodley *et al.*, 2001b; Mah & O'Toole, 2001; Sauer, 2003). It has been suggested that adhesion to a surface triggers the expression of sigma factors, proteins that manipulate gene regulation and are thought to cause the expression of biofilm specific phenotypes (Costerton *et al.*, 1995; Tolker-Nielsen & Molin, 2000; de Kievit *et al.*, 2001). Deretic *et al.* (1994) is often cited in support of sessile phenotypic differentiation, yet this research was based on analysis of single species cultures (*P. aeruginosa*) within the scope of Cystic Fibrosis biofilms. Although this bacterium is present in DWDS, research has yet to demonstrate it behaves in the same way in the pipe network. Prigent-Combaret *et al.* (1999) found that 38% of *E. coli* gene transcription and expression was affected following attachment, leading to cell function differentiation in the sessile cells. However, this study is nonspecific to DWDS as analysis was carried out on pure cultures grown in liquid media.

It should be noted that many of the current ideas and theories about drinking water biofilm colonisation are based on information acquired from studies that are not DWDS focused (Deretic *et al.*, 1994; Prigent-Combaret *et al.*, 1999; Mah & O'Toole., 2001) nor do they utilise relevant experimental set-ups (Vaerewijck *et al.*, 2005). Consequently, the observations and conclusions regarding these biofilms are not necessarily representative of the processes and patterns occurring within a DWDS; further research is necessary to confirm this.

1.4.4.3 Biofilm detachment

The balance between attachment and detachment determines the growth of biofilm; in a steady state biofilm the two are proportional (Telgmann *et al.*, 2004). This is rare in natural and engineered systems where low-level detachment, referred to as erosion, is continuously occurring. Detachment is thought to generally occur physically via disturbances such as sloughing or erosion (Figure 1.5) although some cells may actively detach (Quignon *et al.*, 1997; Piriou *et al.*, 1999; Falkinham *et al.*, 2001; Flemming *et al.*, 2002). A study of endpoint water by Stoodley *et al.* (2002) demonstrated that microorganisms are released from the biofilm in a diverse array of sizes. Cell cluster size has been reported to be inversely related to detachment frequency (Morton & Surman, 1994; Stoodley *et al.*, 2001a) and determines the scale of contamination (Stoodley *et al.*, 2002). Erosion refers to the continuous detachment of small aggregates, e.g. 1-10 cells, which rarely leads to a violation of microbiological quality guidelines (Quignon *et al.*, 1997; Mackay *et al.*, 1998; Stoodley *et al.*, 2001a) but is responsible for a slow-release of unknown microbial quantities leading to a low-level, persistent contamination of the water supply. Alternatively, sloughing may occur which refers to the sudden loss of large fractions of the biomass (Quignon *et al.*, 1997; Piriou *et al.*, 1999; Flemming *et al.*, 2002) in aggregates exceeding 1.5×10^3 cells (Stoodley *et al.*, 2001a), which can drastically alter the biofilm architecture (Vieira & Melo, 1999; Choi & Morgenroth, 2003; Horn *et al.*, 2003; Telgmann *et al.*, 2004). Larger aggregates have an increased chance of causing a microbiological failure or, potentially, a disease outbreak (Mackay *et al.*, 1998; Stoodley *et al.*, 2001a; Vaerewijck *et al.*, 2005).

Erosion and sloughing are affected by variations in disinfectant exposure and hydrodynamics (Camper *et al.*, 1991; Stoodley *et al.*, 2001a; 2002; Parsek & Singh, 2003). Ginige *et al.* (2011) demonstrated that an increase in disinfection residual or a change in temperature can lead to increased biofilm mobilization (detachment) due to a decrease in biofilm activity, the consequences of which were shown to be elevated turbidity in the bulk water. In order for the biofilm to be mobilised the external shear forces must overcome the internal cohesive forces; this may occur if the external force exceeds the inner, or if the internal forces are weakened, as has been documented to occur when biofilms age or nutrient concentrations decrease (Peyton and Characklis, 1993). Although it is known that environmental forces influence the structure and function of biofilms (Vieira *et al.*, 1993; Stoodley *et al.*, 1999; Pereira *et al.*, 2002) there have been limited studies regarding biofilm structure and stability (Ohashi & Harada, 1994; Ohashi *et al.*, 1999; Stoodley *et al.*, 1999; Korstgens *et al.*, 2001; Poppele & Hozalski, 2003; Simoes *et al.*, 2006; 2007) and detachment remains one of the least studied biofilm

processes despite being arguably one of the most important, particularly with respect to water quality management.

1.4.5 Biofilm architecture and composition

Established biofilms are highly hydrated assemblages, comprised predominantly of the EPS matrix which is reported to account for 50-90% of the biofilm organic content (Sutherland, 2001a, 2001b) and 65% of the mass (Lazarova & Manem, 1995). It is an essential element without which the biofilm would not exist (Flemming & Wingender, 2010). Biofilms were initially considered to be uniformly distributed assemblages with distinct basal and surface sub-communities, described by the continuum model (Bishop, 1997). In recent years the application of various advancing microscopic techniques and image analysis programs has produced much clearer, conclusive images, revealing the heterogeneity of biofilms and the extent of the EPS (van Loosdrecht *et al.*, 1990; Stewart *et al.*, 1995; Heydorn *et al.*, 2000; Wagner *et al.*, 2009). However, within the context of DWDS biofilms these insights have been limited to biofilms developed within reactors, such as in studies by Wagner *et al.* (2009) and Stewart *et al.* (1995) in which biofilms were seeded with wastewater sludge and a dual culture of *Pseudomonas aeruginosa* and *Klebsiella pneumonia*, respectively.

Biofilms are now commonly described as “coral-like”, 3D mushroom or streamer shaped assemblages (see schematic depiction in Figure 1.5) with a network of liquid filled channels (Menaia and Mesquita, 2004). A clear and thorough study tracking fluorescent beads through biofilms cultured within a reactor, has shown that the liquid in the channels is flowing (Stoodley *et al.*, 1994) and the use of microelectrodes has established that oxygen is circulated through the biofilm in this way (de Beer *et al.*, 1994). Although in some biofilms anoxic conditions have been detected in the deep layers (Wimpenny *et al.*, 2000), supporting a community of anaerobic bacteria (Santegoeds *et al.*, 1998). Further electrodes for the detection of pH, nitrification substrates, ammonia, sulphate reduction and sulphate oxidation have demonstrated that these are also circulated around wastewater (Kuhl & Jørgensen, 1992) and nutrient rich stream (Nielsen *et al.*, 1990) biofilms. However, these environments are a stark contrast to DWDS, thus the findings are not necessarily transferable to drinking water biofilms.

The communities within a mature biofilm are juxtaposed according to the constraints of the particular microenvironments (van Loosdrecht *et al.*, 1990; Marsh & Bradshaw, 1995; Moller *et al.*, 1998), as the environments alter so does the biofilm structure (Costerton *et al.*, 1987). It is

recognised that the architecture, composition and intensity of biofilms are mediated by multiple influences both intrinsically (by microorganisms) and externally (by environmental parameters; Ratto *et al.*, 2005; Denkhaus *et al.*, 2007). For example, Lawrence *et al.* (1991) used confocal laser scanning microscopy (CLSM) to demonstrate that the thickness, depth and cellular to non-cellular ratios of biofilms cultured within flow cells differ with species. Although all the biofilms were highly hydrated (73-98%), cell arrangement was found to differ between *P. aeruginosa* and *P. fluorescens* biofilms, where density was greatest at the surface-biofilm interface, and *Vibrio parahaemolyticus* biofilms, where the majority of cells were located at the periphery. This study is however limited in its representation of naturally occurring biofilms as single-species cultures were characterized.

1.4.5.1 The EPS matrix

All biofilms have a microbially produced EPS, composed of several biological macromolecules (Table 1.3); the characteristic elements are extracellular polysaccharides and proteins, although nucleic acids and lipids have also been identified (Weiner *et al.*, 1995; Sutherland, 2001a; 2001b; Ramasamy & Zhang, 2005). Exogenous substances may also become entrapped in the EPS leading to the accumulation of organic and inorganic particles such as iron or manganese (Denkhaus *et al.*, 2007). This may be particularly important within the context of DWDS, which presents an oligotrophic environment, therefore the concentration and entrapment of particles at the pipe surface, within a biofilm, could offer a survival advantage to the microorganisms residing at the pipe wall-bulk water interface. In combination, these molecules create the EPS matrix which forms and maintains the 3D space in which microbial cells are arranged, providing organisation, mechanical and chemical stability to the biofilm (Branda *et al.*, 2005).

Arguably the major role of the EPS framework is to anchor the cells and provide physical stability to the whole microbial assemblage (Wimpenny *et al.*, 2000; Sutherland, 2001a; 2001b; Jenkinson & Lappin-Scott, 2001; and others). Detachment of the biofilm requires a stronger shear force than that conditioning the biofilm in order for the EPS mechanical stability to be overcome (Stoodley *et al.*, 1999b; Korstgens *et al.*, 2001). This is in line with the “cohesive layer” theory of discolouration (section 1.2.2), although it has yet to be conclusively proven that biofilms developed under DWDS environmental constraints are conditioned to the hydraulics experienced during growth and cause discolouration due to detachment when this force is exceeded. However, it is known that diverse interactions exist between the EPS molecules (hydrogen bonds, electrostatic interactions, dispersion forces, van der Waals – see

An *et al.*, 2000, for a review), any combination of which are in force at any one time, which greatly enhances both adhesion and cohesion of the microcolonies to the surface and to each other (Neu & Marshall, 1990). In this way, EPS has an inherent internal tension which is in equilibrium with the external shear forces (Vieira & Melo, 1999; Beyenal & Lewandowski, 2002; Purevdorj *et al.*, 2002). It has been suggested that EPS is not exclusively found bound to the pipe wall - when cells are detached from the assemblage they may retain a coating of the EPS which could convey a level of protection from disinfectant residuals in the water column, which previously unbound cells do not have (Flemming *et al.*, 1999). A study of cultured *Pseudomonas fluorescens* found that the composition of EPS associated with planktonic cells differed from that associated with the biofilm, however, the authors acknowledge that improved polysaccharide extraction is necessary in order to more robustly differentiate between the two EPS types (Kives *et al.*, 2006).

Aside from a structural role, the EPS matrix has multiple functions associated with it: providing a nutrient reserve, absorbing heavy metals, reducing the penetration of disinfectant residuals, concentrating soluble particles (inorganic or organic) and acting as a buffer from the changing environmental conditions of the water column (Allison & Sutherland, 1987; Ophir & Gutnick, 1994; Sutherland, 2001a; 2001b; Hwang *et al.*, 2012). Extracellular enzymes and proteins used in quorum sensing (cell-cell signalling) are also thought to be regulated by the EPS, which aids the general functioning of the whole biofilm (Neu & Marshall, 1990; 1999; Visick & Fuqua, 2005).

Despite the multitude of vital roles of EPS, the interaction between differential synthesis of EPS (quantity, arrangement and composition), changing environmental conditions and the impact on biofilm matrix properties has received little attention in the literature. Commonly the focus is on variations in microbial community structure and diversity (e.g. Norton & LeChevallier, 2000; Williams *et al.*, 2005; Yu *et al.*, 2010; Revetta *et al.*, 2010). Where EPS is considered, the research tends to focus only on the carbohydrate fraction, particularly in studies using microscopic imaging analysis approaches such as Wagner *et al.* (1995) and Stewart *et al.* (2009). This is likely due to the difficulties in studying the EPS and associated components as no universal methods for investigation exist. Yet, as mechanical forces are often employed (in conjunction with chemical agents) to remove unwanted biofilms, it is surprising that there are limited studies regarding the mechanical stability of drinking water biofilms and even fewer that analyse EPS characteristics specifically.

1.4.5.2 Influence of detachment

Various studies have considered the effect of detachment upon biofilm characteristics and vice-versa. Detachment events have been found to be influenced not only by shear stress and biofilm mechanical strength, but also biofilm shape and growth rate. Under the same hydrodynamics and adhesive strengths, biofilms with increased growth rate have been modelled to incur an increase in detachment events (Piciooreanu *et al.*, 2001). It has often been reported that increased detachment results in a denser but thinner biofilm with increased roughness of the peripheral surface (Stoodley *et al.*, 1999b). Piciooreanu *et al.* (2001) used 2D mathematical modelling to show that erosion generates smoother biofilms, while sloughing off increases surface roughness. Morganroth and Wilderer (2000) also used mathematical models, specifically applied to a wastewater reactor scenario, to demonstrate that biofilm morphology is impacted by detachment and that different patterns of detachment lead to alternative microbial distributions.

A biofilm which has previously experienced sloughing off might potentially experience altered shear forces, at a local scale, to those experienced before mobilization due to the change in biofilm shape (Telgmann *et al.*, 2004). It has been suggested that the remaining biofilm may also detach if the architecture does not have enough mechanical pliability to resist the new stress imposed (Telgmann *et al.*, 2004). Consequently, Telgmann *et al.* (2004) speculate that a previously disturbed biofilm is more likely to experience subsequent spontaneous, large scale detachment events which can lead to a massive biofilm loss into the bulk water in a short period of time. Although detachment clearly impacts the morphology of biofilms and the extent of this material mobilization is dependent on the growth history of the biofilm, neither aspect (detachment or growth-history), is well monitored or understood and detachment is still commonly seen as a disruption in biofilm development rather than a process within it (Choi & Morgenroth, 2003; Telgmann *et al.*, 2004).

1.4.5.3 Sessile microbial community: interactions and processes

Successional development of the biofilm community has been found to result in distinct “young” and “old” compositions in model distribution systems (Martiny *et al.*, 2003) and syntrophic relationships, such as co-operative exchange of beneficial substrates, have been observed (Vroom *et al.*, 1999; Flemming *et al.*, 1999; Davey & O’Toole, 2000; Vaerewijck *et al.*, 2005). It has also been demonstrated that several bacteria (e.g. *Mycobacterium avium*, *Vibrio cholera*) are able to use protozoa, such as *Acanthamoeba castellanii*, as environmental hosts (Sibille *et al.*, 1998; Cirillo *et al.*, 1999). Vast numbers of pathogenic cells are protected from

the external environment in this manner; a single protozoan may be host to 120 *M. avium* cells and even greater numbers of *L. pneumophila* (Yee & Wadowsky, 1982). Although there is little research in this area, it is logical to suggest that, just as with populations of other organisms, the mature biofilm community also experiences competition between microcolonies whilst others may co-exist though not co-operate (Wimpenny *et al.*, 2000).

Various processes occur within the developed biofilm; metabolic cycling (Marsh & Bradshaw, 1995; Dunne, 2002), cell replication and growth, pipe surface interactions (bio-corrosion; Figure 1.5), interaction with the bulk water and quorum sensing. An important process employed by bacteria such as *Pseudomonas aeruginosa*, quorum sensing influences gene expression and ultimately coordinates: biofilm formation (adhesion), cell motility, cell aggregation with respect to local population density (Sauer, 2003) and has an impact on the biofilm architecture and cell detachment (Davies *et al.*, 1998; Stoodley, *et al.*, 1999c). It is due to intercellular communication that the microorganisms embedded in the EPS of a mature biofilm demonstrate a high degree of functional coordination, which facilitates interactions with the environment, whilst simultaneously limiting the exhaustion of biofilm resources, exemplifying the concept of microbial “multicellularity” (Shapiro, 1998; Oosthuizen *et al.*, 2002; Dunne, 2002; Sauer, 2003). The circulation of signalling molecules, in addition to organic substrates and minerals, throughout the biofilm represents a critical interrelationship between the biofilm structural form and its function (Kaiser & Losick, 1993; deBeer *et al.*, 1996; Wimpenny *et al.*, 2000).

Although there is a body of literature regarding biofilm architecture and impacts upon it, much of the research is focussed on the microbial communities, particularly bacteria, rather than differences in EPS production, quantity or composition, despite its central role to the biofilm structure. Many of the studies use cultured biofilms, which are often young assemblages (less than two weeks; Trulear & Characklis, 1982; Tolker-Nielsen & Molin, 2000) developed in experimental conditions and set-ups somewhat removed from natural and engineered systems. Consequently they may not be applicable to the complex environs of real life systems such as the DWDS, in which biofilms grow over months and years rather than days and experience a multitude of (often varying) environmental constraints.

1.5 Ecological/Engineering Effects and Biofilm Response

The physico-chemical characteristics of potable water (Williams *et al.*, 2004; Keinanen *et al.*, 2004; Roeder *et al.*, 2010), along with the environment within a DWDS (discussed in section

1.3), produce selective pressures influencing the diversity of species, which subsequently colonise the pipe network. As the selective pressures differ between systems, so do the native microorganisms within the bulk water and biofilms (Norton & LeChevallier, 2000; Yu *et al.*, 2010). Within the seemingly inhospitable environment of the DWDS microorganisms survive predominantly in biofilms, which act as a buffer against the ever-changing bulk water environment (Schulze-Röbbecke *et al.*, 1992; Rogers *et al.*, 1994; Costerton *et al.*, 1995). Thus biofilm bound cells are less affected by changes in the external environment than planktonic cells (Pedersen, 1990; Szewzyk *et al.*, 2000). Protection from the bulk water phase is conveyed in various ways but ultimately is due to the maintenance of a primitive homeostasis within the biofilm (Costerton *et al.*, 1995; Jenkinson & Lappin-Scott, 2001; Dunne, 2002). Interactions with the DWDS can influence the development and structure (both community structure and physical structure) of the assemblages. However, the environmental influences on the biofilms are not the only interactions at work in the DWDS ecosystem; biofilm bound cells interact with each other and modify the surrounding environment via metabolic activity and community processes, in this way microbes function as “ecosystem engineers”.

1.5.1 Pipeline surface

There is a known influence of both pipe inner surface and material on the growth of biofilm (Rogers *et al.*, 1994; Norton and LeChevallier, 2000). Both of these are factors which can influence the densities and compositions of attached microbial communities (Pedersen, 1990; Zacheus *et al.*, 2001; Yu *et al.*, 2010; Allion *et al.*, 2011). For instance, although genes control the synthesis of adhesive molecules, secondary adhesion occurs more quickly on hydrophobic, rougher surfaces (Denkhaus *et al.*, 2007), such as the internal surface of older pipes which commonly experience increased biofilm growth.

Biofilms are found worldwide, upon various materials associated with DWDS, including lead service lines in Illinois (White *et al.*, 2011), stainless steel taps in Romania (Morvay *et al.*, 2011), unplasticised PVC (uPVC) pipeline in the Netherlands (Wullings *et al.*, 2011) and asbestos cement distribution pipes in Australia (Sammon *et al.*, 2011). Many studies have shown a significant variation in the biofilm forming potential (BFP) of different materials, though many studies enumerated bacterial cells via culture based methods. Schwartz *et al.* (1998) reported that greater bacterial cell densities were found on HDPE and PVC than steel and that the community composition differed between the plastics and the metals. Conversely, a growing body of literature indicates that plastics (PVC, uPVC, HDPE/MDPE, polybutylene and polypropylene) support a reduced abundance and diversity of bacteria when

compared to steel (Zacheus *et al.*, 2001; Yu *et al.*, 2010), iron (Kerr *et al.*, 1999; Niquette *et al.*, 2000; Momba and Kaleni, 2002) or cement (Camper *et al.*, 2003). Kerr *et al.* (1999) found that the doubling times (exponential growth phase) for a heterotrophic bacterial population grown on cast iron and plastic (uPVC, MDPE) were 13.2 hours and 15.6 hours, respectively. A study by Boxall and Husband (2007) also demonstrated slower material accumulation upon plastics than on cast iron (4 years and 1.5 years respectively).

Kerr *et al.* (1999) reported a lag in biofilm development upon plastics, which resulted in a lower cell abundance than was seen on iron in both the short (21 days) and long (7 months) term experiments. This trend is particularly evident in studies using chlorinated water as an inoculum (Niquette *et al.*, 2000; Norton & LeChevallier, 2000; Hallam *et al.*, 2001). In non-chlorinated DWDS, the difference between plastics and other materials is less pronounced due to the release of biodegradable organic compounds, which in the absence of a disinfectant agent, have an increased positive influence on biofilm development. Hallam *et al.* (2001) found that the effect of pipe material on microbial occurrence is less significant than the impact of chlorine; hence material composition may be more influential in non-chlorinated systems or in areas of the network that experience reduced residuals (Norton and LeChevallier, 2000; Hallam *et al.*, 2001). Similarly, Henne *et al.* (2012) established that although initial colonisation may be surface specific, over time, biofilms demonstrate increased similarity to their neighbouring biofilms. Henne *et al.* (2012) investigated the bacterial communities of biofilms from real networks and found that the community fingerprints from a looped fire main grouped together in a single cluster, despite growing on different materials, hence location within the network had a more significant influence than material.

Copper is known to have a low BFP in comparison to plastics, as shown by Schwartz *et al.* (1998) and Yu *et al.* (2010). It is also known that the corrosion of copper produces inhibitory substances that have a toxic effect on most microorganisms. A few bacteria can however survive in this environment and continue to form biofilms (Percival *et al.*, 1998) albeit at an understandably reduced rate than those upon polyethylene (PE) as reported by Lehtola *et al.* (2004b). The initial lag in the rate of biofilm formation on surfaces, such as copper compared to plastics, is less evident with prolonged development time, demonstrating that each biofilm reaches a plateau or constant phase, though the rate at which this is achieved depends on the substratum (Lehtola *et al.*, 2004b). A study by Yu *et al.* (2010) found that polybutylene and PE had greater BFP and bacterial diversity than copper but that PVC had significantly lower BFP than the other plastics and was more comparable with the copper. There is currently no

definitive consensus in the literature as to which plastic has the lowest BFP, some studies have found there to be no difference between those tested (Schwartz *et al.*, 1998; Zacheus *et al.*, 2001), others have found that PVC has the lowest cell densities (Camper *et al.*, 2003; Yu *et al.*, 2010) or polypropylene (Tsvetanova & Dimitrov, 2012). Overall materials employed in DWDS construction are more likely to support biofilm accumulation if they leach nutrients when exposed to biological activity, thus standards are put in place to maintain high material quality and ensure that new materials have lower BFP than those currently in use (Kerr *et al.*, 1999; BS 6920).

Biofilm activity can lead to infrastructure deterioration via biocorrosion of the pipe surface, subsequently increasing the nutrient concentration at the solid-liquid interface and forming by-products that alter the pipe surface roughness or porosity (Niquette *et al.*, 2000; Norton & LeChevallier, 2000). For example, iron oxidising bacteria (e.g. *Shewanella* and *Pseudomonas* spp.) corrode iron and the by-products accumulate forming tubercles of Fe^{3+} , which increase surface roughness, further promoting biofilm development (LeChevallier *et al.*, 1993). Such biofilm promotion is considered to be due to the provision of a greater surface area for adhesion (Schwartz *et al.*, 1998), more niches for colonisation (Morton & Surman, 1994) and decreased detachment by offering protection from shear forces and disinfection (Pedersen, 1990; Gauthier *et al.*, 1999; Norton & LeChevallier, 2000). Biofilms can thus influence the DWDS hydrodynamics as a rougher pipe leads to energy losses which may not be accounted for in the standard roughness co-efficient used in modelling the DWDS (Bryers & Characklis, 1981; Stoodley *et al.*, 1999a). Unlike studies which used sludge (Rogers *et al.*, 1994) or cultures as the inoculum for the experimental system, Pederson (1990) used a reactor system fed with potable water and established that matt steel accumulates 1.44 times more biofilm than electro polished steel. Percival *et al.* (1998) also found a positive correlation between roughness and microbial density, using different grades of steel. Interestingly though, after 12 months there was no longer a significant difference between the steel surfaces. These findings demonstrate that initial biofilm development is promoted by a rough surface but that once a surface is stabilised with a mature biofilm, the substratum roughness or porosity has little influence upon the sessile community. Percival *et al.* (1998) also analysed EPS carbohydrate content showing a linear quantity increase with time and little variation between steel grades, suggesting that whilst pipe surface may influence cell attachment, EPS carbohydrate synthesis was not affected.

Although this body of data is very useful it should be noted that the laboratory set-ups commonly used do not replicate the dynamic conditions of the DWDS within which the surface

or material effects are not occurring in isolation. Hence the impact of pipe surface in a full scale network is likely to be different to those perceived in the lab. Furthermore the biofilms of DWDS are products of an old system; past working practices, prior microbial contamination and previous pipelines all influence the microbiology of the network. Future research should be directed towards understanding the interaction of pipe material with other parameters such as chlorine, as was investigated by Camper *et al.* (2003).

1.5.2 Hydraulic conditions

The hydraulics (in combination with pipe diameter) within a DWDS influence water residence times, boundary layer hydraulics, shear stress and the exchange of trace nutrients, disinfectants, oxygen and heat at the pipe wall-bulk water interface (Vieira *et al.*, 1993; de Beer *et al.*, 1994; 1996; Wijeyekoon *et al.*, 2000; Beyenal & Lewandowski, 2002). In this way, a change in the hydraulics may affect biofilm processes such as growth rate, pattern of development and detachment, and can provide inorganic or organic matter for use by biofilms (Peyton & Characklis, 1993; Vieira *et al.*, 1993). For instance, sudden changes in pressure, which alter the DWDS hydraulics, have been found to detach biofilm and simultaneously increase the concentrations of iron, copper and phosphorous in the bulk water, which were then available to biofilms downstream (Lehtola *et al.*, 2006). Turbidity was also found to be elevated but no change was found in AOC concentrations and only a slight increase (0.05 – 0.10 mg l⁻¹) in TOC was measured (Lehtola *et al.*, 2006).

A prolonged residence time increases exposure to the fabric of the network and a decline in disinfectant residuals as the water ages (Machell *et al.*, 2009), both of which increase the propensity for cell transfer between the planktonic and sessile states, influencing biofilm colonisation (Vieira *et al.*, 1993; Wijeyekoon *et al.*, 2000; Holzman, 2002). Not all microbial species can form biofilms readily but stagnant periods may facilitate the growth of such species, for instance the fungi *Exophiala lecanii-corni* and *Ochroconis mirabilis*, which were able to attach to and dominate in biofilms during static periods (Heinrichs *et al.*, 2013a). Vieira and Melo (1999) showed that lower velocities of bulk water (range tested in this study was 0.28 – 1.00 ms⁻¹) result in depleted penetration of substrate into *Pseudomonas fluorescens* biofilms, which formed protuberant, less dense structures than those grown under turbulent conditions.

The shear forces acting on a biofilm may not be solely dependent on the hydrodynamics of the bulk water; the morphology of the biofilm itself has also been stated to have an impact

(Telgmann *et al.*, 2004). Telgmann *et al.* (2004) state that a smoother biofilm will have a lower local shear force than a rougher assemblage, which will also experience heightened localised shear stresses. However, measuring the shear stress at the local scale of the pipe-wall and biofilm interface of a DWDS environment is implausible and so this theory has yet to be conclusively proven. Liu & Tay (2001) found that increased shear stress also invokes a change in metabolic activity (measured via growth yield and dehydrogenase activity) in order to balance the effects of detachment with consumption of energy (see Liu & Tay, 2001 for more details). Therefore, Liu & Tay (2001) hypothesise that detachment may lead to proton translocation across cell membranes, which favours the formation of a stronger biofilm.

In contrast to many biofilm constraints, the impacts of shear stress and flow velocity on physical structure rather than solely on the community structure have begun to be addressed, although rarely within the context of DWDS (Vieira & Melo, 1999; Wijeyekoon *et al.*, 2000; and others). Shear stress and flow dynamics have been reported by several authors to shape the density, thickness, structure, strength and erosion of developing and mature biofilms developed in bioreactors (Vieira & Melo, 1999; Beyenal & Lewandowski, 2002; Menaia & Mesquita, 2004; Abe *et al.*, 2012). Changes in the biofilm under different shear stresses are thought to be due to differential requirements in the mechanical stability required to resist the external forces and avoid detachment (Vieira & Melo, 1999; Beyenal & Lewandowski, 2002; Purevdorj *et al.*, 2002). It is the adhesive forces of the EPS matrix molecules which provide mechanical stability to the biofilm (Neu & Lawrence, 2009) yet very few studies have addressed the impact of shear stress upon EPS characteristics specifically. Moreover, many of the studies do not explore any effects of nutrient supply upon the EPS as an effect of changing hydraulics and most investigate only steady state (i.e. constant) flow rates with no daily pattern as is seen in real DWDS.

Wijeyekoon *et al.* (2000) hypothesised that flows exist at which initial colonisation is promoted but little or no erosion occurs from the biofilm. In this way the hydraulics of the DWDS, which vary spatially and temporally, may provide a complex conditioning force during biofilm development which significantly impacts biofilm structure and stability. Under laminar flow conditions, biofilms have been described to have a flat surface with reoccurring mound shaped colonies (Wijeyekoon *et al.*, 2000; Purevdorj *et al.*, 2002). Martiny *et al.* (2003) found biofilms developed under steady flows of 0.07 ms^{-1} within a model distribution system were present from day 1, decreasing in both coverage and diversity initially before increasing again temporally. A maximum thickness of $30\mu\text{m}$ was reported after 600 days though the maximum

coverage (95.2%) occurred at 1093 days. However, the system in this study was fed with drinking water with no disinfection so extrapolation to disinfected systems would be unwise.

Hydrodynamics have been documented to aid biofilm formation and resistance to detachment by influencing the internal cohesive strength of biofilms (Holzman, 2002). Conversely to laminar flow structures, during turbulent flow biofilms are reported to be elongated and patchy with a “ripple” structure that has been stated to follow the water flow (Wijeyekoon *et al.*, 2000; Purevdorj *et al.*, 2002). However, under turbulent conditions the water flow is extremely chaotic and varies with time and so it seems unlikely that the consistent ripple pattern observed is following the water flow. Under certain turbulent flow regimes the migration of biofilms downstream may even occur (Stoodley *et al.*, 1999b). Several authors have reported that compared to laminar flows, turbulent flows, which impose elevated shear stress, lead to increased biofilm density and cohesion but reduced thickness, possibly due to compression as suggested by Paul *et al.* (2012), which seem to convey heightened stability via stronger attachment in order to resist sloughing (Percival *et al.*, 1999; Ohashi *et al.*, 1999; Manuel *et al.*, 2007 and others). Interestingly, Abe *et al.* (2012) found the reverse to be true – young biofilms (up to 10^7 cells cm^2) had a greater cohesive strength when formed under lower shear stress. Atomic force microscopy (AFM) demonstrated that an 8 week old biofilm that experienced a shear stress of 0.120 Pa (0.120 Nm^{-2}) required 80 kPa (more than 100,000 times the conditioning force) to be removed, whereas biofilm exposed to 0.230 Pa (0.230 Nm^{-2}) shear stress during development was removed with 20 kPa, more than 10,000 times that of the conditioning force (Abe *et al.*, 2012). However, if these forces are correct then not only were the conditioning shear stresses below that of an average DWDS (Husband, *et al.*, 2008 state an average flow rate of 0.4 ls^{-1} in 75-100 mm diameter pipes, which relates to a shear stress of $\sim 0.30 \text{ Nm}^{-2}$), but the detachment forces were far greater than would be seen under normal operating conditions. Nonetheless, within the constraints of this study, an unusual pattern was observed, which Abe *et al.* (2012) suggest could be due to differences in the matrix structure. Indeed, previous research has also concluded that variations in biofilm stability may be due to the alignment of polysaccharides, proteins, ionic concentrations and hydration of the EPS matrix (Jenkinson & Lappin-Scott, 2001) but research has yet to conclusively demonstrate this.

Simoes *et al.* (2003; 2005) cultured biofilms of *Pseudomonas fluorescens* and *Bacillus cereus* within a bioreactor and determined their stability by increasing the shear stress imposed, measuring biomass before and after the increase. The results demonstrated that biofilms developed under turbulent flow had a greater protein mass (261 mg) than laminar flow

biofilms (128 mg), although these had higher polysaccharide mass (laminar: 1986 mg vs. turbulent: 151 mg; Simoes *et al.*, 2003). However, in Simoes *et al.* (2003) no separate EPS extraction is reported to have been applied, therefore these values may not reflect EPS compositional variations; rather they may demonstrate a difference in the total concentration of each fraction in the whole biofilm sample, which could be heavily influenced by cellular components. Conversely, a later paper by the same authors (Simoes *et al.*, 2007) did specify the inclusion of EPS extraction and found that *B. cereus* (a Gram-positive bacterium) produced a smaller content of EPS than *P. fluorescens* (Gram-negative bacterium), but experienced less biofilm loss suggesting it forms a more stable biofilm. These speculative and inconclusive links regarding specific EPS profiles and biofilm stability require further investigation before clear conclusions can be made.

Abe *et al.* (2012) determined that the shear stress required to detach biofilm decreases with increasing biofilm volume, i.e. larger biofilm clumps will be more readily detached. In contrast to these findings, Lehtola *et al.* (2006) found that large clumps (> 25µm) were more strongly adhered than small particles as they required more energy to be detached. It is established, however, that adhesive forces are not uniform throughout a biofilm, various studies provide evidence of biofilm stratification where layers possess different strengths and detach at different rates (Zhang & Bishop, 1994; Ohashi & Harada, 1994; Peyton, 1996; Paul *et al.*, 2012). It has been demonstrated that a strongly adhered base biofilm layer is consistently present, the depth of which may be influenced by carbon concentrations (Park *et al.*, 2012). Abe *et al.* (2012) found that biofilm developed within a disk reactor under three shear stresses (0.120, 0.175 and 0.230 Pa) was removed in layers when subjected to increasing shear stresses but that the maximum force in the AFM was unable to remove all the material. Some regions maintained a constant height which Abe *et al.* (2012) hypothesised was due to areas where rigid material, such as inorganic deposits (e.g. iron, manganese, corrosion products), were present among the softer organic deposits. However, as these biofilms were grown upon glass coupons within a tap water fed reactor it seems unlikely that such rigid material could form. Nevertheless, results from studies such as these could have important consequences upon the management of biofilm within the DWDS, especially as cleaning strategies rely heavily upon the use of elevated shear stress to remove biofilms during flushing programmes. However, research has yet to efficiently demonstrate the influence of conditioning hydraulics relevant to live DWDS upon the biofilm microbial community and conclusively determine the influence on physical structure stability. Future research should particularly focus on understanding the variation in the EPS matrix, which has an integral role in biofilm stability.

As with many studies into the DWDS environment, often cultured, single species biofilms (e.g. Vieira & Melo, 1999; Purevdorj *et al.*, 2002), or an artificially mixed community with two or three investigator-selected species (e.g. de Beer *et al.*, 1996; Stoodley *et al.*, 2002) are studied. The use of reactors and bench-top scale experimental systems (deBeer *et al.*, 1996; Chen & Huang, 2000; Liu & Tay, 2001), generally run at constant flow rates atypical of the DWDS, mean that the studied biofilms are exposed to pipe boundary hydraulic regimes different from those that occur in a full scale distribution network. The extent to which results from laboratory and pilot rig experimental systems, which use a constant flow rate, can be used to inform the dynamics of biofilms in DWDS is limited. Biofilms grown in this way experience only constant erosion, rather than the fluctuations in shear stress which are known to occur within a real network. Additionally, the constant flows do not accurately simulate the supply of nutrients to biofilms as would occur in a full scale DWDS with changing, turbulent flow patterns. Yet obtaining biofilms from a real DWDS has various issues associated with it, namely the access to field sites on a regular basis due to the nature of the DWDS as an operational system. Future research requires increased accuracy in simulating the DWDS environment from both an infrastructure and biofilm viewpoint, and needs to address the interrelationships between the impacts of shear stress on the sessile microbial community, the variation in the biofilm structure they produce and the stability of these. As it has been stated that biofilms and any associated material can only be mobilised if the external shear stress exceeds the internal cohesion between the EPS molecules (Stoodley *et al.*, 2001a; 2002), a greater understanding of the hydraulic impacts upon EPS should be sought. Achieving this in an increased realistic DWDS environment will allow more parallels to be drawn to the biofilms in full scale DWDS.

1.5.3 Biodegradable matter and inorganic nutrients

Nutrients (e.g. phosphate, nitrate, ammonia) and energy (i.e. a carbon source) are crucial for biological growth, particularly carbon, phosphorus and nitrogen, which are required in an approximate ratio of 100:10:1 respectively (Volk & LeChevallier, 1999; Chandy & Angles, 2001). Traces of these are found at oligotrophic levels in the DWDS water column (Camper *et al.*, 1991; Volk & LeChevallier, 1999; Keinanen *et al.*, 2004), following a gradient towards the pipe wall-bulk water interface (Gauthier *et al.*, 2001; Dunne, 2002), driven by the level of turbulence in the water column. Due to their low concentrations ($\mu\text{g l}^{-1}$) and difficulties in identifying them, few DBPs are monitored in practice also presenting an uncalculated energy source which can support microbial cell growth – the opposite intent of the initial disinfectant agent (Hammes *et al.*, 2006; Richardson *et al.*, 2007).

Some genera such as *Mycobacteria* (Falkinham *et al.*, 2001) and *Aeromonas* are able to grow and proliferate on the low nutrient and carbon concentrations of $\leq 0.1\mu\text{g l}^{-1}$ which are inevitably present in potable water (Carson *et al.*, 1978), but for many taxa the water column presents an inhospitable environment. In contrast, the biofilm presents a richer nutrient and carbon habitat where non-oligotrophs are able to thrive (Vroom *et al.*, 1999; Volk & LeChevallier, 1999) as trace substrates become trapped in the EPS (Morton & Surman, 1994) concentrating and providing a major carbon and nutrient source within the network. This gradient is elevated further as microorganisms within the biofilm, for example the bacterium *Gallionella*, metabolise disinfectant residuals and corrode pipe surfaces leaching substrates such as phosphorus and iron that are then available to the community (Mathieu *et al.*, 1992; Morton & Surman, 1994; van der Kooij *et al.*, 1999). Different pipe materials can leach diverse organic or chemical compounds and have distinct impacts on the degradation of disinfectants (Morton & Surman, 1994; Hallam *et al.* 2001; Lehtola, Miettinen *et al.* 2004), which in turn alters the organics and inorganics available.

Microorganisms within the biofilm may be autotrophic (synthesise organic molecules from inorganics) or heterotrophic (utilise organics and nutrients already within the ecosystem). Amongst the autotrophs of the DWDS are the nitrifiers, or ammonia oxidising bacteria (AOB), such as the beta proteobacteria *Nitrosomonas* which have been identified in both biofilm and bulk water (Regan *et al.*, 2002; 2003; Wielen *et al.*, 2009). AOA have also been identified, found in DWDS in the Netherlands (Wielen *et al.*, 2009); currently this identification has only been carried out on planktonic samples but, though research has yet to prove it, there is a possibility that archaea may also be present in drinking water biofilms. The use of chloramines as a disinfectant promotes the growth of AOB (or potentially AOA) because ammonia is introduced as a residual from the synthesis of chloramines and as a by-product from their decay (Regan *et al.*, 2002). The by-products produced by AOB (namely nitrite) can cause taste and other water quality issues, as well as potentially sustaining the growth of nitrite-oxidising-bacteria (e.g. *Nitrobacter* spp.) and heterotrophs (Regan *et al.*, 2002; 2003). Hence, unsurprisingly, an increase in ammonia has been found to increase total biofilm biomass and growth rate (Okabe *et al.*, 1999; Menaia & Mesquita, 2004).

The nitrogen cycle is one example of substrates being recycled between cells in the biofilm (Yee & Wadowsky, 1982). Synotrophic (mutually dependent) relationships readily arise in the sessile community as microorganisms (primarily bacteria) with different metabolic capabilities depend on each other for metabolites they would otherwise be unable to obtain (Davey & O'Toole, 2000). For example, *Flavobacterium* spp. releases cysteine which is a carbon source

for *Legionella pneumophila* (Yee & Wadowsky, 1982). Such cooperation of bacteria with diverse metabolisms is an important biofilm-specific function that aids microbial growth in the DWDS and provides an ideal environment within the attached assemblage compared to that of the bulk water (Vroom *et al.*, 1999).

Iron and manganese are two metals often detected in DWDS and linked to discolouration (Zacheus *et al.*, 2001; US EPA, 2004; Morton *et al.*, 2005; Husband *et al.*, 2008) both of which have been found to facilitate the accumulation of biofilm. Ginige *et al.* (2011) also found them to be positively correlated with biofilm activity. However, Hoefel *et al.* (2003) found a negative correlation between iron and manganese concentration and AOA abundance. This is logical as AOA require ammonium (NH_4^+) as an energy source and their growth would be limited if this was not readily available. Additionally, AOA may be outcompeted by autotrophs able to utilise the abundant iron and manganese particles. In line with this Zacheus *et al.* (2001) found heterotrophic bacteria to be less abundant in the presence of high manganese levels; as these heterotrophs require organics for growth they too may be outcompeted. These interactions are speculative though and have yet to be thoroughly investigated within the DWDS. Iron-oxidisers including Gram-negative bacteria such as *Pseudomonas spp.* and *Escherichia coli*, are capable of oxidising iron as part of their metabolic processes, hence their abundance may increase with increasing iron availability (LeChevallier *et al.*, 1993; Hersman *et al.*, 2001). Torvinen *et al.* (2007) found mycobacterium populations increased as iron increased but suggested that this correlation was not reflective of a causative relationship as the distal areas of the DWDS also experienced dramatically decreased chlorine concentrations. Hence microbial growth may indirectly benefit from high iron concentrations as oxides produced from corrosion react with chlorine in place of cells (Vaerewijck *et al.*, 2005) and can alter organic matter to a bio-available state (Camper *et al.*, 2003).

Manganese tends to be leached into the biofilm following the biocorrosion of PVC pipes (Cerrato *et al.*, 2006) and, like iron, can be used as an energy source by bacteria such as *Leptothrix* which are able to oxidise it (Kielemoes *et al.*, 2002) or may react with chlorine residuals forming manganese deposits which accumulate on the pipe surface (Cerrato *et al.*, 2006). Heavy metal resistant bacteria have also been found in DWDS biofilms, including species which are able to release nutrients from copper pipes leading to an increased copper concentration in the bulk water (causing blue water) due to their metabolic activity (LeChevallier *et al.*, 1987; Dutkiewicz & Fallowfield, 1998; Critchley & Fallowfield, 2001; Critchley *et al.*, 2004). Conversely, there also exist species which are thought to be able to

reduce the copper content of water by sorbing copper ions into their EPS matrix (Mittelman & Geesey, 1985; White *et al.*, 1996).

Phosphorus is an essential component of bio-molecules such as nucleic acids and phospholipids, and plays a crucial role in many cell functions. Normally microbially available phosphorus (MAP) is found in DWDS at concentrations of $\leq 10 \mu\text{g l}^{-1}$ (Batte *et al.*, 2003), though this may increase following upstream detachment events (Lehtola *et al.*, 2006). Several studies have cited phosphorus, rather than carbon, as the limiting substrate within the DWDS (Miettinen *et al.*, 1997; Lehtola *et al.*, 2002). An increase in phosphorus has been found to not only promote biofilm biomass (Appenzeller *et al.*, 2002; Lehtola *et al.*, 2002), particularly of Gram-negative proteobacteria (Batte *et al.*, 2003), but also deplete it (Keinanen *et al.*, 2002). The lack of consensus regarding the effect of phosphorus on microbial community composition is perhaps because the test water is not phosphorus-limited (Appenzeller *et al.*, 2002) or because many studies do not account for sources of phosphorus other than the bulk water, for example corroded iron (Morton *et al.*, 2005) or microbially-driven leaching from plastic pipe which can contribute phosphorous and nitrogen to the DWDS (Brocca *et al.*, 2002; Lehtola *et al.*, 2004b).

The presence of BOM, particularly the AOC fraction, has a great influence on microbial diversity, especially the heterotrophic bacteria which require a carbon source for growth (van der Kooij, 1992; Volk & LeChevallier, 1999; Norton & LeChevallier, 2000; and others). Organic carbon may be obtained from the bulk water, disinfection degradation or from cells within the biofilm. The concentration of AOC can have a significant impact upon growth, with various studies reporting concentrations of $\leq 10 - 100 \mu\text{g l}^{-1}$ as a limiting factor (Hammes *et al.*, 2011; Ohkouchi *et al.*, 2013). Falkinham *et al.* (2001) confirmed the limiting action of AOC, but did not provide a concentration at which cell growth was prevented. The exact limiting concentration will be different between DWDS and is impacted by other water quality parameters such as disinfection or temperature (Ohkouchi *et al.*, 2013). Joret *et al.* (1991) found that BDOC is also influential on the microbiota; *E. coli*, *Klebsiella pneumophila* and *Enterobacter* could not regrow in potable water with BDOCs of $\leq 0.1 \text{ mg l}^{-1}$. Consequently carbon is often considered the limiting factor of microbial growth in DWDS (Joret *et al.*, 1991; LeChevallier *et al.*, 1991; Chandy & Angles, 2001).

Cell growth is limited by nutrient concentration (Dunne, 2002), which can lead to alterations in the diversity, density and 3D structure of biofilms (Szewzyk & Schink, 1988; Stoodley *et al.*,

2001a; 2001b). Microscopy-based studies of cell movement have indicated that increases in carbon and nitrogen alter a thin, filamentous biofilm with protruding “streamers” to a structure supporting mushroom cell clusters (Stoodley *et al.*, 2001b). Variations in resource availability in combination with shear stress were found to affect the coverage of the substrate by a biofilm in a reactor system (van Loosdrecht *et al.*, 1990). Beyenal and Lewandowski (2002) identified the diffusivity at several locations within biofilms developed under different velocities. The authors found that more dense structures with decreased diffusion ability formed under higher velocities, two hypotheses regarding these adjustments in architecture were suggested as a result. Firstly, that architectural modification is undertaken to control the nutrient transport when resources are restricted and, secondly, that structural changes are made to control mechanical pliability. Of these two goals it has been stated that microbial assemblages place a higher priority on the latter and will increase their mechanical stability at the expense of nutrient availability and diffusion to the lower biofilm layers (Beyenal & Lewandowski, 2002).

While a plethora of studies exist regarding the use of nutrients within biofilms and their impact upon bacterial community composition, there is a paucity of research focusing on other microorganisms or the impacts upon biofilm physical structure.

1.5.4 Disinfection

Not all DWDS use disinfectants, countries such as the Netherlands and Switzerland aim towards producing high quality potable water via alternatives such as ultra-filtration or reverse osmosis (Kruithof *et al.*, 2001; Hammes, *et al.*, 2008), which primarily control growth limiting substrates (van der Kooij *et al.*, 2002; Hammes, *et al.*, 2008). However chemical disinfection application (typically chlorine or chloramines) is the most widespread strategy to limit regrowth and contamination during distribution. Hallam *et al.* (2001) found chlorine to have the strongest disinfection action across all investigated experimental permutations involving different disinfectants, temperatures and pipe materials, a conclusion supported by various other studies (Clark and Sivaganesan, 1999; Menaia and Mesquita, 2004). However, chloramines are less reactive than chlorine, thus they produce fewer DBPs and degrade less quickly upon contact with the biofilm, which has led to the suggestion that they penetrate the biofilm more deeply achieving a greater inhibitory effect (LeChevallier *et al.*, 1993; Chandy & Angles, 2001). Stewart *et al.* (2000) supports this conclusion demonstrating that free chlorine is less efficient than chloramines, at penetrating alginate beads, coated with bacterial cells. While this study provides useful evidence that goes some way to addressing the action of

disinfectants, the experimental set-up is significantly different to the DWDS environment, hence it is unrealistic to draw parallels between these findings and the dynamics of disinfection in a real network. Similarly, Hosni *et al.* (2011) demonstrated that chlorine dioxide is more efficient at reducing the activity of *Bacillus globigii* than free chlorine. However, Wang *et al.* (2013) demonstrated that a greater number of bacteria and protozoa were found in a chloraminated simulated distribution system than in a chlorinated system. Other authors also argue that chlorine is a stronger, faster biocide than chloramines (LeChevallier, 1988; deBeer *et al.*, 1994a).

It is important to note that the efficiency of a disinfectant does not rest on penetration alone, it is dependent on hydrodynamics, water chemistry, biofilm biomass and biocide action (deBeer *et al.*, 1994a). During transport through the DWDS water ages and residuals decay as they react with organic and mineral matter, producing DBPs (Mathieu *et al.*, 1992; Richardson, *et al.* 2007) and consequently promoting microbial activity, which can adversely impact taste and odour (Chandy and Angles, 2001) while increasing the microbial load of both the DWDS biofilms and the finished water (Rossman *et al.*, 1994). The ubiquitous formation of biofilm can in turn impact the efficiency of disinfection during distribution and may place a higher disinfection demand on the system. This results in increased biocide application, leading to a subsequent rise in DBPs and elevated operating costs (Chandy and Angles, 2001).

Ultimately, disinfectant residuals may injure or kill planktonic cells but they do not prevent biofilm development (Chandy and Angles, 2001; Williams and Braun-Howland, 2003, White *et al.*, 2011); at best they slow biological activity and growth (Hallam *et al.*, 2001). For example, Ginige *et al.* (2011) found that previously non-chlorinated biofilms decreased in activity from 55.12 ng cm⁻² ATP to 4.10 ng cm⁻² ATP within two days of chlorine application; simultaneously the turbidity of the bulk water increased from 2.4 NTU to 10.9 NTU. The biofilms in this study were developed using a glass reactor inoculated with biomass from surface waters in Western Australia, so although the inoculant is relevant to real DWDS the use of a material and hydraulics not used in live networks may introduce or remove interactions which are significant in governing the efficiency and action of chlorine in full scale systems.

Chlorination has also been documented to alter microbial community compositions; for example, *Campylobacter spp.* (a genus of *Proteobacteria*) are extremely sensitive to chlorine and thus are restricted to environments where chlorine can be eluded, such as networks employing alternative disinfection methods, those with low residuals facilitating the evasion of chlorine and allowing cells to seek refuge in a biofilm, or networks experiencing a mechanical

failure at the treatment works (Jacob *et al.*, 1998). Conversely, unpigmented morphs of *Mycobacteria avium* and *M. intracellulare* have been demonstrated to be particularly chlorine resistant, hence they are more likely to be abundant throughout various DWDS (Falkinham *et al.*, 2001). In the presence of chlorine, heterotrophic bacteria have been found to increase in abundance while AOB decreased; upon switching to chloramines the reverse was true (Santo Domingo *et al.*, 2003), this is likely due to the different organics supplied to the system. Chlorination has also been shown to cause bacterial population shifts towards Gram-positive species (LeChevallier *et al.*, 1998). As chlorine reacts with the cytoplasmic membrane of Gram-negative bacteria, oxidising cell structures and resulting in a cell lesion, it may be that the thicker cell wall of Gram-positive bacteria provides a survival advantage; alternatively Gram-positive species may be less able to attach to assemblages.

Regardless of the specific disinfectant agent(s) utilized, biofilm bound bacteria and fungi tend to be more resistant to residuals and tolerate higher concentration of disinfection than their planktonic counterparts (Costerton *et al.*, 1987; LeChevallier *et al.*, 1988a; Wingender *et al.*, 1999; Hageskal *et al.*, 2012). Santo-Domingo *et al.* (2003) found AOB to be more resilient when sessile than planktonic, therefore, once attached to the biofilm they are difficult to eradicate from the community. It has been stated that biofilms are 500 times more resistant to disinfection than planktonic cells (Costerton *et al.*, 1995), although some planktonic cells may form aggregates in the water column and those that have recently detached from the biofilm may retain a coating of the EPS matrix which affords a degree more protection (Crozes & Cushing, 2000). Despite being perhaps the most notable advantage of biofilm life, the mechanisms behind increased disinfectant resistance have caused controversy in the literature (Mackay *et al.*, 1998; Park *et al.*, 2001; Menaia & Mesquita, 2004). Generally it is accepted that the EPS provides physical protection in the form of a barrier which the disinfectant agents cannot penetrate (Morton & Surman, 1994; deBeer *et al.*, 1994b; Neu & Lawrence, 2009), either because they bind to and are neutralised by the EPS rather than reacting with the cells (Chen & Stewart, 1996; Menaia & Mesquita, 2004) or because enzymes in the matrix degrade the residuals (Costerton, 1999; Mah & O'Toole, 2001). Wingender *et al.* (1999) clearly demonstrated the crucial role of an alginate-based EPS matrix in limiting the action of chlorine and conveying protection to *Pseudomonas aeruginosa* cells. However, the alginate layer provided no protection against hydrogen peroxide, demonstrating that this is not a general resistance mechanism to all biocides; instead other EPS components or changes in the biofilm are likely to be associated with disinfection protection. Xue *et al.* (2013) investigated the reaction of EPS, produced by *P. aeruginosa*, with chlorine (0.5 mg l⁻¹), ammonium chloride (0.2

mM) and sodium hypochlorite (5.65 – 6%), concluding that EPS reduced the permeability of cell membranes, hence limiting the effect of the disinfectant residuals.

A further theory is that the sessile assemblage has an abundance of “persistor” cells with disabled “programmed cell death” (Lewis, 2000; 2001). Ordinarily, cells have an automatic function that cause them to lyse when injured or stressed, persistor cells do not have this programmed response. As there are more “persistor” cells than mutants in the biofilm this theory has been argued as more feasible than that of biofilm specific phenotypes (Lewis, 2001). Alternatively, biofilm cells may be less susceptible to disinfection due to biochemical changes (e.g. alterations in membrane composition), slow growth or phenotypic differences from the free-living cells (Lewis, 2000; 2001; Mah & O’Toole, 2001; Menaia & Mesquita, 2004). As it has been established that many biocide agents are more effective at lysing or injuring fast growing cells, this theory is feasible. Spoering and Lewis (2001) found evidence for a biofilm specific phenotype in cultures of *P. aeruginosa*. It is known that multispecies biofilms occur in DWDS and exhibit greater resistance when compared to single species assemblages (Berry *et al.*, 2006), yet the studies outlined here and many others (e.g. deBeer *et al.*, 1994a; Stewart *et al.*, 2000) are based on single species biofilms. Therefore their findings present only the first step towards understanding the biofilm-chlorine dynamics in DWDS.

Although there is a body of research regarding the action of disinfectants in biofilms, many of the studies are concerned with changes in microbial community structure or biocide decay; whilst the impact of disinfection on the biofilm structure in its entirety (i.e. the cells, EPS and their arrangement) is rarely addressed. Ling and Liu (2013) investigated the selective pressures of chloramination and found that as disinfection concentration and contact time increased, biofilms became thinner and more compact, but were still detectable. However, this study investigated laboratory grown biofilms and only stained the cells of the biofilm so, while providing some insight into the distribution of cells post chloramination, no conclusions can be made regarding the EPS. Wang *et al.* (2012) provides a rare study which does give consideration to the interactions between EPS and disinfection agents. Cultures of *P. aeruginosa*, which produces carbohydrate based EPS, and *P. putida*, which produces protein based EPS, were exposed to chlorine and the DBPs that were produced as a consequence were monitored. The results showed a positive correlation between the EPS volume and DBP formation and also showed that the chemical composition of the EPS influenced the type of DBPs: *P. putida* produced double the amount of nitrogenous DBPs as *P. aeruginosa*.

The conclusions from these studies provide a useful base of information about biofilm microbial composition but cannot be directly applied to the DWDS as most experimental set-ups comprise unrealistic simulations of the environment (LeChevallier *et al.*, 1988b; Chandy & Angles, 2001; Williams & Braun-Howland, 2003) with assessment of disinfectant agents that are not used in DWDS (Spoering and Lewis, 2001, used antibiotics; Stewart *et al.*, 2000, employed hydrogen peroxide), the impacts of which are often measured in biofilms that are unrepresentative of the microbiota occurring in a DWDS (de Beer, 1994; Stewart *et al.*, 2000; Kuhn *et al.*, 2002). Many studies also disregard the complex abiotic and biotic interactions (such as nutrient concentrations, temperature, biofilms comprising mixed-uncultured species) that are acting at any one time in tandem with the disinfection within the pipeline and are likely to play a part in shaping the degree of sensitivity that a biofilm has to disinfection.

1.5.5 Environmental parameters

As in all biological systems, temperature regulates reaction rates within DWDS (Menaia & Mesquita, 2004; Silhan *et al.*, 2006), particularly in those supplying non-disinfected water (Bagh *et al.*, 2002; Hallam *et al.*, 2001; Rogers *et al.*, 1994). Bacteriological issues are more common in warmer months, likely because microbial growth is accelerated (Tsvetanova & Dimitrov, 2012); various studies have shown a significant increase in bacteria (including coliforms) at temperatures ≥ 15 °C (LeChevallier *et al.*, 1996; Dukan *et al.*, 1996; Hallam *et al.*, 2001). LeChevallier *et al.* (1996) established that naturally cooler waters experienced a peak in coliforms at a slightly lower temperature of 10 °C. Research by Sharpe (2012), in which biofilms were developed under different temperatures and hydraulic regimes before being exposed to a flushing period, confirmed that temperature impacts the accumulation of cells at the pipe wall, with greater cell coverage occurring at 16 °C than at 8 °C. Furthermore, this study showed that under steady state flows temperature had a larger influence over the accumulation of cells and the subsequent mobilization of material than was observed under varied flow conditions. The turbidity, iron and manganese concentrations which were recorded during the mobilization of material previously accumulated under steady state flows at 8 °C were significantly different from those recorded during the mobilization of material accumulated under steady state flows at 16 °C. Conversely, there was little difference between the material mobilised from biofilms developed under varied flows at 8 °C and 16 °C.

Studies by Bagh *et al.* (2002, 2004) demonstrated that the diversity of bacteria in warm waters exceeds that within cool waters, yet recent research by Revetta *et al.* (2010) failed to confirm such an increase in diversity. This inconsistency is likely due to differences in diversity

assessment and species identification methods (Yee & Wadowsky, 1982; LeChevallier, 1999; Revetta *et al.*, 2010). Seasonal variation in temperature has been suggested to also influence the microbial community in source water and subsequently affect the abundance and diversity of microbes inoculating the DWDS (Vaerewijck *et al.*, 2005; Tsvetanova & Dimitrov, 2012). The study of temperature effects is seemingly restricted to pathogenic microorganisms or whole community assessment such as via fingerprinting, with limited study of the impacts on other elements of the biofilm, such as EPS (Bagh *et al.*, 2002).

The impact of pH and oxygen availability on microbial life within DWDS remains somewhat unexplored (Torvinen *et al.*, 2007). A very limited number of studies addressing pH variation in DWDS exist. This may be because the pH of water rarely deviates vastly from neutral, and suppliers would not distribute it if it did, therefore there is less interest in its effects. However, Meckes *et al.* (1999) did provide an (extreme) insight into the consequences of pH variation upon DWDS. Biofilms were developed in five identical test loops for 2 weeks, followed by three weeks of monitored growth under four different pH conditions (pH 5.0, pH 6.0, pH 9.0 and pH 10.0 ± 0.3 , one loop was left unaltered as the control). The greatest HPC were found in the alkali conditions with acidic conditions significantly inhibiting growth (at pH 5, cell abundance was $1.27 \log_{10}$ times lower than in the control). However, correlation does not imply causation and it could be that the pH change was affecting the pipe material or nutrient cycling rather than directly limiting growth, further research would be needed to draw conclusions on the impact of pH on microbial abundance. Generally, in biofilms from a wide range of environments, the basal layer experiences anaerobic conditions but the influences of restricted oxygen have not been thoroughly explored. A study by Paul *et al.* (2012) did provide a rare insight into the changes in physical appearance and established that anaerobic conditions resulted in denser, thicker biofilms than were seen under aerobic conditions.

1.6 Investigating DWDS Biofilms: A Methodological Aside

Each DWDS and each pipe within it, present a unique heterogeneous environment with many variables which are not easily replicated and no universal method of study exists to investigate biofilm physical characteristics. Previous studies have used culture based methods to analyse biofilm community structure, with known drawbacks (“great plate anomaly”). Hence alternative methods have been applied to bridge this gap, including microscopic techniques (fluorescent staining and imaging), energy quantification (ATP) and molecular analysis (e.g. community fingerprinting and gene sequencing) to study microbial cells across a range of environments (Hoefel *et al.*, 2003; Phe *et al.*, 2005). Flow cytometry is becoming an

increasingly used tool, particularly when coupled with fluorescent dyes (Porter *et al.*, 1996, 1997; Hoefel *et al.*, 2003; Hammes *et al.*, 2008), as it can rapidly analyse bacterial quantity (measuring in excess of 1000 cells s⁻¹). Similarly, DNA fingerprinting methods (e.g. terminal-restriction fragment length polymorphism, T-RFLP; denaturing-gradient gel electrophoresis, DGGE) allow simultaneous, rapid (and relatively cheap) profiling of microbial communities from multiple samples, in order to investigate structural or functional diversity. However, fingerprinting techniques do not provide direct taxonomic identification; rather they are used to investigate changes in or differences between microbial communities. Although fingerprinting techniques may underestimate community diversity due to a detection limit of microorganisms that account for $\sim \geq 1\%$ of the community, they nevertheless produce a robust index of community diversity (Osborn *et al.*, 2000), which correlates well with results from clone libraries (Fierer & Jackson, 2006). High throughput sequencing (i.e. next generation sequencing approaches such as 454 pyrosequencing or Illumina) is an increasingly used approach for community structure analysis, as it can rapidly determine the sequence of vast numbers of different DNA strands, in a single experiment (Rogers & Vetner, 2005). By extending the sequencing process in a massively parallel fashion (see Hert *et al.*, 2008 for a methodological overview) large numbers of sequences are produced, which increases the depth and detection level of sample analysis. This enables species level identification and the detection of rare microorganisms which may not be detected via fingerprinting techniques due to their low abundance. However, *a priori* sequence information for organisms within the samples is required to obtain species level information during the (often laborious) bioinformatic data analysis. Although technological advances are leading to reductions in the cost of high throughput analysis, this approach remains costly; therefore it is often employed alongside fingerprinting approaches (e.g. Hwang *et al.*, 2012), to enable the targeted use of the next generation sequencing to samples of notable interest, based upon community profiles.

It is noteworthy that, many of these techniques have been designed to test water samples rather than biofilms samples and therefore application to the sessile assemblages may not be accurate (Lazarova & Manem, 1995). As such, enumeration of microorganisms may differ depending upon the technique(s) used (Vaerewijck *et al.*, 2005; Lehtola *et al.*, 2007). Consequently the choice of experimental design and sample analysis presents an influential parameter of data collection, so comparison between papers should be interpreted with care.

1.6.1 DWDS simulation and biofilm samples

Empirical data is difficult to obtain from the field due to the nature of DWDS as sealed, working systems. Access to sampling sites on a regular basis is rare, hence replication is often

impossible. Unrepresentative sampling is likely as sites are not selected randomly but often allocated with regard to ease of access and limited disruption to consumers. Furthermore, environmental variables cannot be controlled and the removal of biofilms can be difficult and expensive (Hallam *et al.*, 2001). Therefore, bench-top systems such as flow cells, reactors or small scale pilot pipe systems (Table 1.4) have often been used for studying pipeline biofilms. Although studies have attempted to simulate real networks in this way, these experimental set-ups are often inaccurate representations of the real DWDS environment (Smith *et al.*, 1999).

The majority of previous studies used small areas of substrate such as glass (van der Kooij *et al.*, 1995) or beads (Stewart *et al.*, 2000) to develop biofilm; a setup which is drastically different from the length of plastic, metal or concrete pipe found in full scale DWDS. Some test systems are constructed of DWDS relevant materials, but these have two main drawbacks: the internal environment of these simulations is somewhat removed from the complex interaction of parameters occurring in a full-scale DWDS and the biofilms grown within them are not representative of those forming naturally. There are a range of environmental parameters within DWDS, as has been demonstrated in this review, which are not static or mutually exclusive, but experimental systems are generally designed to investigate a single parameter and so generally do not accurately mimic the diverse conditions that microorganisms (both planktonic and sessile) experience in a DWDS (Pedersen, 1990; Ohashi & Harada, 1994; deBeer *et al.*, 1994b; 1996; Percival *et al.*, 1998; Chen & Huang, 2000; Liu & Tay, 2001). Of particular importance is the flow regime, which alters the forces imposed upon a biofilm, the distribution of disinfection residuals and the nutrient supply. Additionally, many studies consider only a steady state, low flow rate scenario, drastically removed from the varied flow regime known to occur in real, operational DWDS and do not accurately replicate the boundary layer hydraulics (LeChevallier *et al.*, 1988a; Chandy & Angles, 2001; Williams & Braun-Howland, 2003).

Many studies inoculate the experimental systems with wastewater (Kuhl & Jørgensen, 1992; Rogers *et al.*, 1994; deBeer *et al.*, 1994a; Wimpenny *et al.*, 2000) or a liquid medium containing a single species (Vieira *et al.* 1993; Prigent-Combaret *et al.*, 1999; Stewart *et al.*, 2000; Purevdorj *et al.*, 2002; Beyenal & Lewandowski, 2002; Simoes *et al.*, 2003; 2005; 2007) or an artificially mixed group of species selected by the authors (Stoodley *et al.*, 2002; deBeer *et al.*, 1996). In reality, drinking water biofilms are composed of a consortium of species with an interplay of diverse metabolisms (Shapiro, 1998; Davey & O'Toole, 2000). Biofilms at the pipe wall are inoculated with planktonic cells in the water column, which is a significantly diluted microbial concentration than is enforced by inoculating a system with liquid media. Additionally, biofilms are heterogenic and change over time but many studies are carried out

Table 1.4 Examples of experimental systems used in studying pipeline biofilms

Research Focus	Experimental System		References
	Bench-top scale	Simulation Pipe Rig	
Bacterial growth (cellular)	-	Two stainless steel loops with removable plugs	Boe-Hansen <i>et al.</i> , 2002
Cell quantification, imaging of cells, community analysis	-	90 m coiled HPPE loop with removable coupons that fit to the curvature of the inner pipe surface	Deines <i>et al.</i> , 2010
Water treatment impact on biofilm growth	-	Reclaimed pipe length from DWDS, 9 m MDPE and 9 m cast iron	Holden <i>et al.</i> , 1995
Metabolic responses of cells to shear stress	PVC Annular reactor	-	Liu & Tay, 2001
Hydraulics and cell signalling of <i>P. aeruginosa</i>	Cultured inoculation of glass flow cells	-	Purevdorj <i>et al.</i> , 2002
Cell and EPS measurement	Polycarbonate slides, sludge reactor	-	Staudt <i>et al.</i> , 2004
Adhesion of <i>P. fluorescens</i>	Fermenter and test cell	-	Vieira <i>et al.</i> , 1993
Nutrient level impact on bacterial water quality	Drinking water annular reactor	-	Volk & LeChevallier, 1999
Pipe material impact upon microbial community	Pipe coupons (3 cm diameter) of six materials in reactor	-	Yu <i>et al.</i> , 2010
Mechanical stability of biofilms	Chemostat bioreactor	-	Simoes <i>et al.</i> , 2003; 2005; 2007
Iron and manganese accumulation in biofilms	Glass reactor, 60 cm long, 19.5mm diameter, flow 0.28 lmin ⁻¹ inoculated with biomass from surface waters	-	Ginige <i>et al.</i> , 2011
Material impacts upon biofilm	-	Storage tanks connected with four loops (dimensions not reported), supplied with modified drinking water and run for two years	Allion <i>et al.</i> , 2011
Succession of drinking water biofilm structure and diversity	-	12.2 m looped reactor, 2 hours retention time, flow 0.07 ms ⁻¹ , fed with non-disinfected groundwater from water works	Martiny <i>et al.</i> 2003
Biofilm formation on stainless steel	-	2 m long stainless steel pipes (different grades), both 20 mm in diameter, connected with brass compression joints	Percival <i>et al.</i> , 1998
Biofilm development upon stainless steel and PVC	Seven biofilm reactors connected in series, fed with municipal drinking water at a flow of 10 cm s ⁻¹	-	Pedersen, 1990
Cohesion of young water biofilms	Glass coupons in a rotating reactor (0.01 RPM-3500 RPM), 24 hour residence time, inoculated with tap water	-	Abe <i>et al.</i> 2012

on young biofilms (a few weeks to a month old), which are unlikely to have reached a “steady state” and are likely to have a different diversity and structure to those in the DWDS (Menala *et al.*, 2003; Telgmann *et al.*, 2004). Also, these short timescales may not be sufficient for a change in the microbiota, as a response to an environmental change, to be observed (Volk & LeChevallier, 1999). However, unlike field sampling, laboratory scale research allows the control of environmental parameters which may influence development and the experimental systems are designed to facilitate the removal of biofilm samples (Jones & Bradshaw, 1996; Deines *et al.*, 2010; Sharpe, 2012; Douterelo *et al.*, 2013). Removing the biofilm itself from the surface to which it is attached may be a delicate procedure, particularly if cell lysis needs to be avoided; this can be one of the limiting stages of biofilm study (Geesey & White, 1990).

The limitations discussed in this section apply to all of the literature considered throughout this review. Although the insights from these studies may not accurately reflect the biofilm characteristics (activity and functioning in an engineered system such as the DWDS tend to be focussed upon specific influences rather than an interaction between various parameters), they can nonetheless be used to inform and target future research.

1.7 Conclusions

A large body of research has demonstrated the role of DWDS as biological and chemical reactors, interacting with the water they transport leading to temporal and spatial variation in water quality. The interactions between biofilms and drinking water quality, beyond a consideration of pathogens, have begun to receive more research attention in recent decades. While the association between discolouration and biofilms is uncertain, it seems logical. For instance, leading discolouration research PODDS is based on the, now globally validated, model first put forward by Boxall *et al.* (2001), which assumes that discolouration material (organic and inorganic) developed upon the pipe surface in cohesive layers; biofilms are known to exhibit cohesive properties via their EPS matrix. The PODDS model further assumes that these cohesive layers are conditioned by the network hydrodynamics, with mobilization occurring following an increase in flow that elevates shear stress at the pipe boundary. The release of material is analogous to the observed erosion and sloughing behaviour of cultured and idealised biofilms. Consequently, it is likely that the mobilization of biofilm contributes to discolouration and may also cause microbiological quality failures and potentially engender a public health risk if pathogenic organisms are released. As part of the drive to improve DWDS operation, maintenance and management strategies, so as to improve drinking water quality in general, and increase the predictability of discolouration events, it is desirable to gain an

understanding of biofilm structure, in particular the interaction of structure, stability and environmental parameters.

There is a significant body of literature investigating environmental effects on biofilms but these have several overarching drawbacks. Firstly that, in part due to the complications associated with sampling live networks, the majority of knowledge we have regarding the development, architecture and composition of drinking water biofilms is extrapolated from biofilm studies in alternative environments or based on laboratory studies. DWDS microbiological research has commonly been based on bench-top reactor systems, flow through cells or small scale pilot rig systems. Although these studies have provided invaluable datasets, offering initial insights into biofilms that may occur within idealised potable water distribution systems, these experimental set-ups are often inaccurate representations of the real environment of DWDS, particularly with regard to replicating DWDS hydraulics and the physiochemical environment of the pipelines. Secondly, research often focuses on bacterial community analysis of cultured biofilms of investigator selected species, which are critically different and likely unrepresentative of the complex, naturally occurring, multi-species communities producing EPS and forming biofilm in DWDS. Despite the multitude of roles that EPS has within biofilms, in particular the crucial role of biofilm adhesion, very few studies consider the impact of environmental parameters upon EPS quantity, composition and distribution, and any subsequent impacts that variations in these have upon drinking water biofilm stability. Additionally, despite the diverse microbiota associated with drinking water, community analysis rarely incorporates microorganisms other than bacteria.

Knowledge regarding the structure and stability of drinking water biofilms, as well as the impact of DWDS environmental parameters on these, particularly hydraulics and chlorination which are used as current biofilm management techniques, is paramount to further understanding of the dynamics and functioning of DWDS biofilms in order to better predict and manage their behaviour. Research should be targeted towards investigating the impacts of hydraulic regime and disinfection upon EPS in particular, rather than just the cells, as the EPS is central to both the formation and detachment of these assemblages. Combining this with a wider consideration of the microorganisms present, and increased accuracy in the replication of the DWDS environment, will enable us to challenge the current biofilm “toleration” mindset to one of more understanding into how biofilms interact with the DWDS. Consequently, there is a need for future research agendas to address drinking water biofilm research via multidisciplinary approaches, in order to fully appreciate both the microbial and engineering details of these complex but crucial DWDS.

Chapter 2: Aims and Objectives

From the literature review (Chapter 1), it is clear that further research is required regarding the interactions between drinking water biofilm ecology and hydraulic conditions, relevant to full scale DWDS, with a wider microbial consideration than solely bacteria. This information is required to aid understanding of the biofilm structures that develop within DWDS pipelines under different hydraulic conditions and also to appreciate the effects upon the ability of the biofilm to resist detachment (and hence the risk it poses to water quality).

The aim of this research was to determine the effects of different hydraulic conditions upon the physical and community structure, and the stability of microbial biofilms forming within a drinking water pipeline. It was theorised that, compared to biofilms that have developed under a low shear stress, those which have experienced high shear stresses during development will express different characteristics as regards microbial community composition and biofilm architecture. It was thought that these characteristics would make the biofilms more stable. In particular, it was hypothesised that EPS characteristics exist (quantities or compositions) which promote biofilm cohesion and resistance to detachment. It was thought that diversity in these EPS characteristics would be seen in biofilms developed under one of three different hydraulic conditions, which could be responsible for changes in biofilm structure and stability, leading to the discolouration behaviour seen through the empirical PODDs model.

Using a simulated DWDS facility with flow, pressure and temperature control, constructed from high density polyethylene (HDPE) used in the water industry, this study set out to combine the advantages of laboratory control with an environment accurately mimicking the boundary layer hydraulics, nutrient supply and microbial inoculation occurring in live DWDS. In this way, information was generated that was directly relevant to the processes occurring in full scale DWDS.

This study had four main objectives:

1. To determine a reliable and repeatable methodology with which to visualise and quantitatively characterize the biofilm physical structure, with regard to both the EPS (proteins and carbohydrates) and cells.

2. To describe the physical and community structure of microbial biofilms within a steady state DWDS after 28 days of development.
3. To determine the influence of low varied and high varied flow patterns upon the physical and community structures of microbial biofilms within DWDS after 28 days, in comparison to biofilms that develop under steady state conditions.
4. To characterize the effect of elevated shear stress (i.e. “flushing”) upon the structure of biofilms that remain attached. Furthermore, to determine if there is a relationship between the hydraulics experienced during development and the response during flushing, with respect to the biofilm retained at the pipe surface and any changes observed in bulk water quality parameters.

In all instances the term biofilm “community structure” encompasses the assessment of bacterial, fungal and archaeal abundance and diversity. Biofilm “physical structure” refers to the qualitative and quantitative analysis of biofilm appearance and composition. A particular focus is on biofilm distribution and the quantity and composition of the EPS matrix (protein and carbohydrate content) in which the cells are embedded. The development and optimisation of a robust EPS analysis method is explained in Chapter 4, which addresses the first objective listed above. The subsequent results chapters (5, 6 and 7) present the data appropriate to the latter three objectives (2, 3 and 4 respectively) outlined above. Some of the data presented in these chapters was presented at international conferences and research symposia (see Appendix 1). In particular, conference papers were presented at the IWA Biofilms 2011 (Fish *et al.*, 2011) and WDSA 2012 conferences (Fish *et al.*, 2012; see Appendix A1.2 for details).

Chapter 3: Methodology

3.1 Experimental System

The majority of research investigating environmental effects acting upon biofilms has been based on bench-top reactor systems, flow through cells or small scale pilot rig systems (e.g. Boe-Hansen *et al.*, 2002; Deines *et al.*, 2010; Ginige *et al.*, 2011; Abe *et al.*, 2012), all of which allow fine-scale control of variables and replication. These studies have provided invaluable datasets, offering initial insights into biofilms that may occur within idealised DWDS. However, the experimental set-ups are often inaccurate representations of the real environment of DWDS, particularly with regard to replicating hydraulic conditions, natural variation in water chemistry and the physicochemical environment of the pipelines. Of particular importance are the hydraulic conditions, which alter the shear stresses imposed upon a biofilm, the distribution of disinfection residuals and the nutrient supply. Yet many studies consider only a steady state flow rate scenario (LeChevallier, *et al.*, 1988; Chandy & Angles, 2001; Williams & Braun-Howland, 2003), differing markedly from the varied flow regime known to occur in full scale DWDS.

Empirical data is difficult to obtain from the field due to pipe networks being sealed, working systems. Consequently, access to sampling sites on a regular basis is rare, hence replication is often impossible and unrepresentative sampling is likely as sites are not selected randomly, but often allocated with regard to ease of access and limited disruption to consumers. Even with access to field sites, the removal of biofilms from the pipe internal surface can be both difficult and expensive and environmental variables cannot be controlled (see section 1.6).

To bridge the gaps between these approaches, biofilm investigations were carried out within a full-scale experimental pipe facility (Figure 3.1), fed with water from the local distribution system and set within a temperature controlled room at The University of Sheffield. This internationally unique experimental facility allowed environmental manipulation, experimental replication and biofilm sampling, while accurately simulating the environmental conditions of DWDS, including: hydraulic regimes (including diurnal patterns in flow rate), bulk water quality and chemistry, and the exchange mechanisms between the bulk water and the pipe wall.

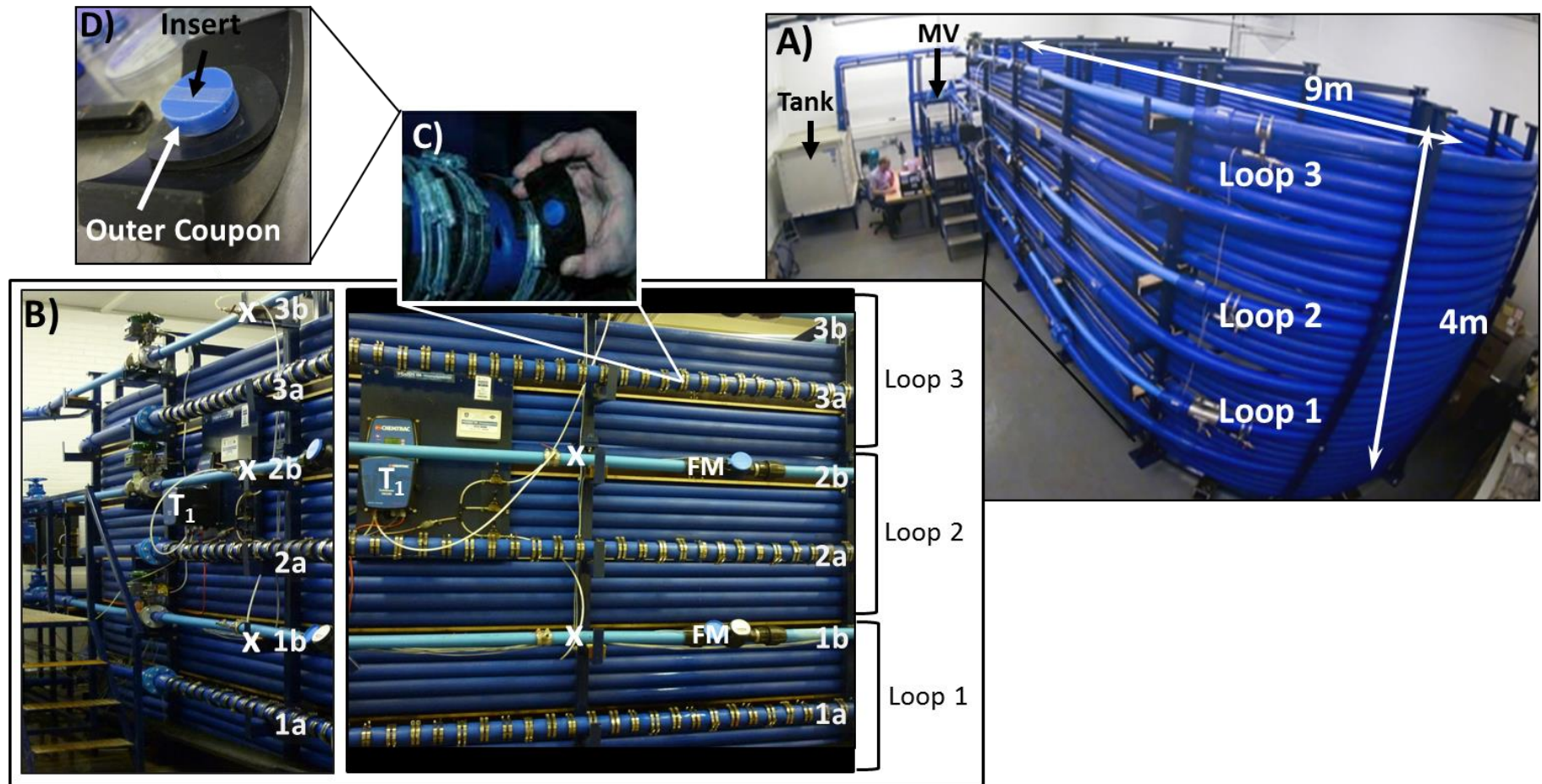


Figure 3.1 Drinking Water Distribution System (DWDS) simulation pipe rig. A) Main experimental facility, MV = manual valve, total water volume of 4.5 m³; B) Detail of loop arrangement as seen from two angles, showing the protrusion of the 5th coil of each loop (1a, 2a, 3a) into which coupons (27 per loop, 81 in total) were inserted, the 50 mm diameter pipeline at the end of each loop (1b, 2b, 3b) where flow meters (FM) were positioned. The outlet turbidity meter (T₁) was connected to tapping points “X”; C) Coupons inserted into the pipe and secured with brackets; D) HDPE coupon (PWG design).

3.1.1 DWDS experimental facility

The simulation facility (Figure 3.1; Figure 3.2) was comprised of three 203 m long, HDPE pipe loops, which were isolated via a series of valves and run as three replicates. HDPE was selected as it is now the most commonly used material in the repair and implementation of modern DWDS (Momba *et al.*, 2000; Husband *et al.*, 2008). The system was fed with drinking water from the local DWDS, which has an upland peat runoff surface water source and is treated using rapid gravity filtration, the Sirofloc colour and turbidity removal process technology, manganese contactor filters and inoculation with chlorine. Following treatment, the water was distributed via a cast iron trunk main direct into the building that housed the DWDS experimental facility (i.e. no local DMA was in place). Drinking water was re-circulated around the system from an enclosed, 1.34 m³ reservoir tank, via a variable speed pump. The water was trickle fed into the tank with a system retention time of 24 hours, preserving a baseline nutrient supply and disinfection residual, among other water quality parameters. Pipe loop retention time was a function of the chosen flow regime.

The flow rate and hence shear stress were regulated by a LabVIEW (version 8.2, National Instrument Corporation, UK) program developed during a previous research project (Sharpe, 2012). In brief, the program enabled the calculation and modification of hydraulic regimes to the desired flows by adjusting the controlled valves (Figure 3.2) at the end of each loop and/or the pump speed. The temperature of the whole system was controlled by a cooling unit (ICS Group) with a range of 4 °C to 21 °C, accurate to +/- 1 °C.

Each loop was comprised of nine and a half HDPE coils, each 21.4 m long and 79.3 mm in internal diameter, with the exception of a final 50 mm internal diameter section ~9 m in length, into which flow meters and the loop outlet turbidity meter were connected (Figure 3.1; Figure 3.2). The straight section (~2.67 m long) of the mid (5th) coil of each loop had 27 apertures into which removable coupons were inserted (Figure 3.1C). The mid coil was positioned to be proud from the other coils in order to enable coupons to be easily secured and accessed (Figure 3.1B).

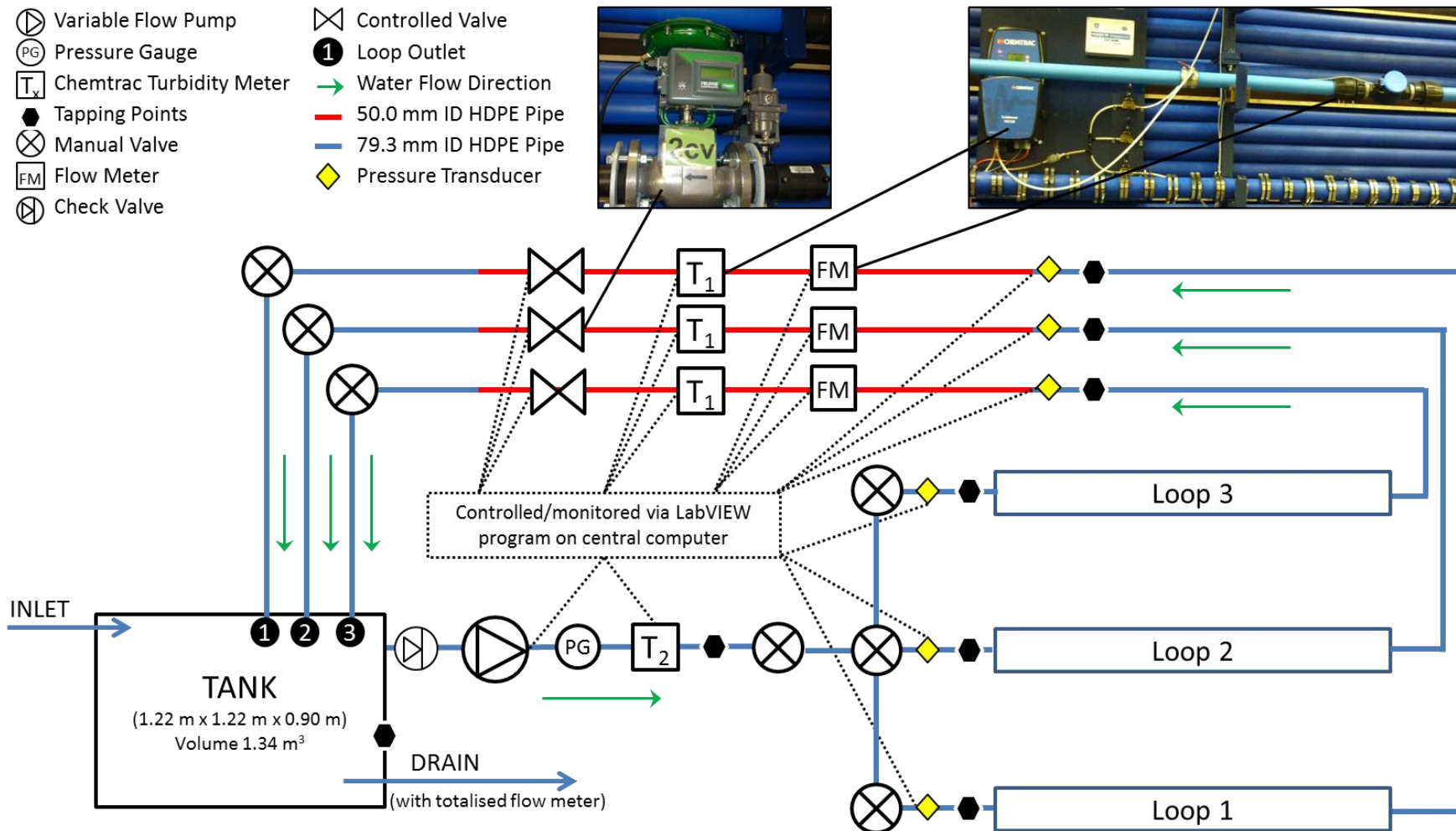


Figure 3.2 Schematic diagram of the DWDS experimental facility (not to scale). T_2 is connected to a tapping point at the loop inlet; T_1 is connected to a tapping point in the loop 2 outlet during the development phase and during the mobilization phase to the tapping point of the loop being flushed. ID: Internal diameter. See Figure 3.1 for more detail of the loops. Central computer refers to the main computer that controls all the rig functions.

3.1.2 Coupons

Previous studies investigating the biofilms of DWDS have used approaches such as the Robbins device (Kerr *et al.*, 1999), flow through cells (e.g. Manz *et al.*, 2003), “plugs” of various materials (e.g. Boe-Hansen *et al.*, 2002) or glass coupons/slides (e.g. Abe *et al.*, 2012), which either inaccurately replicate the boundary layer hydraulics of a DWDS pipeline or distort it due to intrusion into the bulk water from the surface. As boundary layer dynamics drive the shear stress, nutrient gradients and interactions at the bulk water-pipe wall interface, all of which impact biofilm formation, it is essential they are replicated. Consequently, the Pennine Water Group (PWG) coupon was implemented in this study as it was designed to fit exactly into the apertures of a pipe and to follow the internal pipe curvature, hence limiting the distortion of boundary layer hydraulics as described in Deines *et al.* (2010).

The PWG coupons (Figure 3.1D; Figure 3.3A) are made from HDPE and comprise a curved outer section (to enable DNA-based analysis of biofilm community structure) as well as a flat, removable insert, designed to allow non-destructive microscopy analysis (Deines *et al.*, 2010). The insert had a minimal width (top surface 4.5 mm) to minimise deviation from the pipe curvature and was specially manufactured so the surface finish closely matched that of the main pipeline and the outer coupon (Sharpe, 2012). Each coupon was secured to a backing piece with a circular rubber gasket in between to ensure a watertight fit when inserted into the DWDS experimental facility. Coupons were arranged around the pipeline in the sequence: bottom (invert), middle and top (crown), repeated nine times along the pipe length, as shown in Figure 3.3B, which enabled investigation into biofilms around the entire pipe to determine if position influences the attached microbial assemblages.

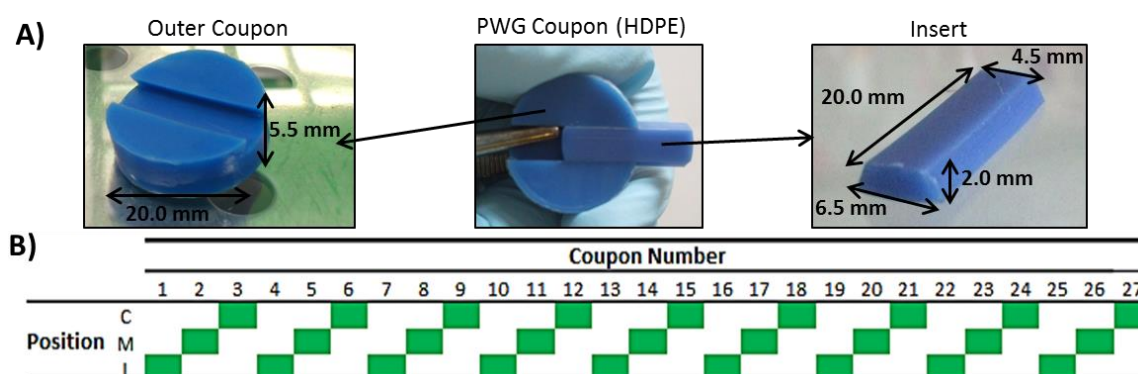


Figure 3.3 PWG Coupon dimensions (A) and positions (B) around each loop. Location around the pipe indicated by C=Crown, M=Middle, I=Invert. Numbers indicate the coupon placement along the pipe and were used for sample identification, along with the loop number from which the sample was obtained, e.g. sample “110” was taken from position 10 in loop 1.

3.1.3 Online instrumentation

A series of turbidity meters (Chemtrac, USA see Table 3.1), pressure transducers (Gems™ Sensors and Controls) and flow meters (Flownetix, UK, see Table 3.1) were located within the DWDS experimental facility (Figure 3.2) and provided continuous measurements for the duration of each experiment. This data was recorded using a LabVIEW programme which was independent of the control algorithm and was also developed in a previous research project (Sharpe, 2012).

Two Flownetix Ultrasonic flow meters, with different levels of accuracy were used during the course of each experiment; one for the growth phase and one for the mobilization phase (Table 3.1). Flow rates were recorded via the aforementioned LabVIEW program and also checked manually.

The drawbacks to measuring turbidity (a measurement of water “clarity” by determining the degree of light scatter due to suspended material) are well documented (Russell, 1994). The main difficulty is accurate quantification, because light scatter is based upon the interaction of various processes (e.g. diffraction, reflection and refraction) and may be easily influenced by disturbance in water flow such as air bubbles or dust particles (Russell, 1994; Boxall & Saul, 2005). Nevertheless, turbidity remains a commonly monitored water quality parameter as an indicator of discolouration in both live water distribution systems (see section 1.2.2) and in research scenarios (e.g. Boxall & Saul, 2005; Vreeburg *et al.*, 2008; Husband, *et al.*, 2008; Husband & Boxall, 2010; Sharpe, 2012;).

The DWDS experimental facility, was fitted with two Chemtrac TM2200 turbidity meters (Table 3.1), positioned at the loop inlet (T_2 in Figure 3.2) and outlets (T_1 in Figure 3.1; Figure 3.2). Both turbidity meters were calibrated using a dilution series (0.0, 2.5, 5.0, 10.0, 20.0 NTU) of formazin turbidity standards (Hach, USA) and distilled, deionised water. For each experimental trial, the LabVIEW recorded value for each of the standard turbidity solutions was noted and a calibration curve was plotted (see Figure 3.4 for an example), to enable the data generated to be related back to actual NTU units.

Table 3.1. Specifications of online instrumentation.

Instrument	Manufacturer	Range	Resolution	Accuracy
Flownetix Ultrasonic Water-Meter, Model 350 ^A	Flownetix, Birmingham, U.K.	0.04-8.33 ls ⁻¹	1 pulse = 10 litres	± 3.0% of reading
Flownetix Ultrasonic Water-Meter, Model 350 ^B	Flownetix, Birmingham, U.K.	0.04-8.33 ls ⁻¹	1000 pulses = 10 litres	± 3.0% of reading
Chemtrac TM2200 Turbidity Meter	Chemtrac Inc., U.S.A.	0-100 NTU	0.0001 for ≤ 2.0000 NTU 0.001 from 2.001 to 9.999 0.01 for > 9.99 NTU	± 1.0% of reading or ± 0.002 NTU

^A Used during the mobilization phase; ^B Used during the growth phase.

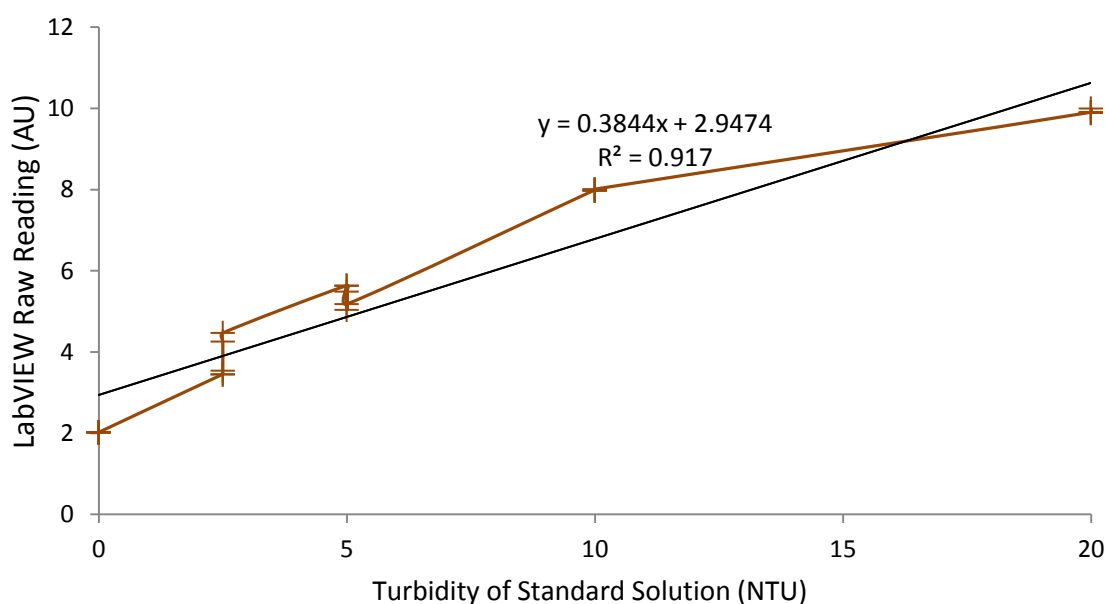


Figure 3.4 Calibration curve of turbidity standard solutions. Replication of n=5, regression analysis was performed in Excel to generate the calibration equation, data in this example is from the T₁ calibration at the start of the Steady State trial.

3.2 Experimental Programme and Sampling Regime

The experimental programme involved three consecutive month long experiments, during which biofilm development under different hydraulic regimes was investigated during a “growth” phase, and biofilm response to increasing shear stress under controlled increases in flow rate was assessed during a “mobilization” phase. These experiments ran between July and October 2011, the exact dates of each are summarised in Table 3.2.

Before each experiment, the whole system was disinfected for 24 hours with a 20 mg l⁻¹ concentration of Rodolite-H (RODOL Ltd, Liverpool, UK); a sodium hypochlorite solution (< 16% free chlorine), which was re-circulated within the system at a maximum flow rate of 4.5 ls⁻¹. After the 24 hour period, the whole system was flushed repeatedly at the maximum flow rate,

with fresh water from the local distribution system, until chlorine levels decreased to those of the inlet water. Before use, the PWG coupons were sterilised via sonication with a 2% (w/v) sodium dodecyl sulfate (SDS) solution for 45 minutes, then sonicated in distilled deionised water for a further 15 minutes before being autoclaved (Backhus *et al.*, 1997; Buss *et al.*, 2003).

Table 3.2 Overview of the hydraulic regime experiments completed in the DWDS experimental facility.

Experiment	Abbreviation	Dates		
		Whole experiment ^A	Growth	Mobilization
Steady State	SS	13/7/2011 – 12/8/2011	Day 0: 14/7/11 Day 28: 11/8/11	Flush loop 1: 11/8/11 Flush loop 2: 11/8/11 Flush loop 3: 12/8/11
Low Varied Flow	LVF	14/8/2011 – 13/9/2011	Day 0: 15/8/11 Day 28: 12/9/11	Flush loop 1: 13/9/11 Flush loop 2: 13/9/11 Flush loop 3: 13/9/11
High Varied Flow	HVF	14/9/2011 – 14/10/2011	Day 0: 15/9/11 Day 28: 13/10/11	Flush loop 1: 14/10/11 Flush loop 2: 14/10/11 Flush loop 3: 14/10/11

^ATime frame includes the cleaning period.

3.2.1 Growth phase

3.2.1.1 Duration

When investigating biofilms a range of experimental longevity is found in the literature, from tests spanning days (e.g. Purevdorj *et al.*, 2002; Simoes *et al.*, 2005;2007) to months or years (e.g. Yu *et al.*, 2010; Ginige *et al.*, 2011; Abe *et al.*, 2012). While Martiny *et al.* (2003) rightly argue that short term studies do not reflect the effects of the longer developmental time seen in live DWDS, it should be appreciated that biofilms in real networks are the product of decades of growth, which is still continuing, subsequently laboratory based tests will never fully converge with the real system.

Previous trials in the University of Sheffield experimental facility have observed measurable accumulation of material after only 7 days (Husband, *et al.*, 2008) and 28 days (Sharpe *et al.*, 2010; Douterelo, *et al.*, 2013). The experiments carried out within the scope of this thesis comprised a 28 day growth phase. This timeframe provides an insight into the initial development of biofilm within “new” pipes and allowed triplicate biofilm samples to be taken weekly (sampling of biofilm was limited by the 27 coupons).

3.2.1.2 Hydraulic regimes and environmental conditions

Drinking water biofilms were accumulated naturally (i.e. no cultures or inoculations were added to the drinking water) for 28 days under one of three conditioning hydraulic regimes: Steady State (SS), Low Varied Flow (LVF) or High Varied Flow (HVF), which are illustrated in Figure 3.5.

A SS conditioning flow rate of 0.4 ls^{-1} (shear stress 0.30 Nm^{-2}) was chosen as this was the average flow rate in 75-100 mm diameter pipes within UK DWDS, as stated by Husband *et al.* (2008). Although SS flows very rarely occur in live DWDS, this condition provided us with a baseline of biofilm development under undisturbed conditioning flow conditions, to use as a frame of reference and facilitate comparisons with data from previous research using idealised bench top set-ups. Drinking water biofilms actually experience diurnal and seasonal variations in flow, which are likely to impact upon their structure and stability; a biofilm will need to be more strongly attached to the pipe wall in order to remain in place during the increased flow rates (and shear stresses) observed during times of peak water demand. It is also important to recognise that, during night time periods, DWDS experience low flow rates or even stagnation, which may also be responsible for conditioning the biofilm. Hence two varied flow regimes were designed, which have been used in previous experiments (Sharpe *et al.*, 2010; 2012), both of which are based on the double peaked typical daily profiles from UK networks (Husband *et al.*, 2008) and both have the same night time flow rate (Figure 3.5). The LVF regime represents a typical daily profile, with two peaks and a period of night-time flow; HVF represents a daily profile in which the peak flow rates achieved are greater than at LVF. The average flow rate of each of the varied regimes remains 0.4 ls^{-1} and both regimes simulate the trends in real DWDS data as presented in Husband *et al.* (2008). This facilitated the testing of the hypotheses that biofilms may be conditioned to either the maximum flow rate (and shear stress) experienced during growth rather than the average flow rate, therefore would be more resistant to mobilization when developed under a HVF regime; or to the night time flow rate, in which case biofilms from LVF and HVF would be similar.

The same hydraulic regime was run in each loop of the facility (replication of $n=3$) and the three regimes were tested in consecutive experimental trials from July to October, 2011 (see Table 3.2 for specific dates). All the experiments were carried out at 16°C ($\pm 1^{\circ}\text{C}$), representative of the bulk water temperatures during summer in the UK, when microbiological activity is elevated. Room temperature was monitored via the online system provided for use with the cooling unit, checks were also made manually. The use of water from the local

distribution system accurately provided the natural variations in water chemistry and quality experienced by biofilms in live networks. However, such variation would likely occur not only during, but also between each of the experiments. Therefore, experiments were run in consecutive months to minimise any such variation. Bulk water samples were taken to monitor a range of water quality parameters during the growth phase of each test, in order to identify any significant changes in environmental conditions between experiments.

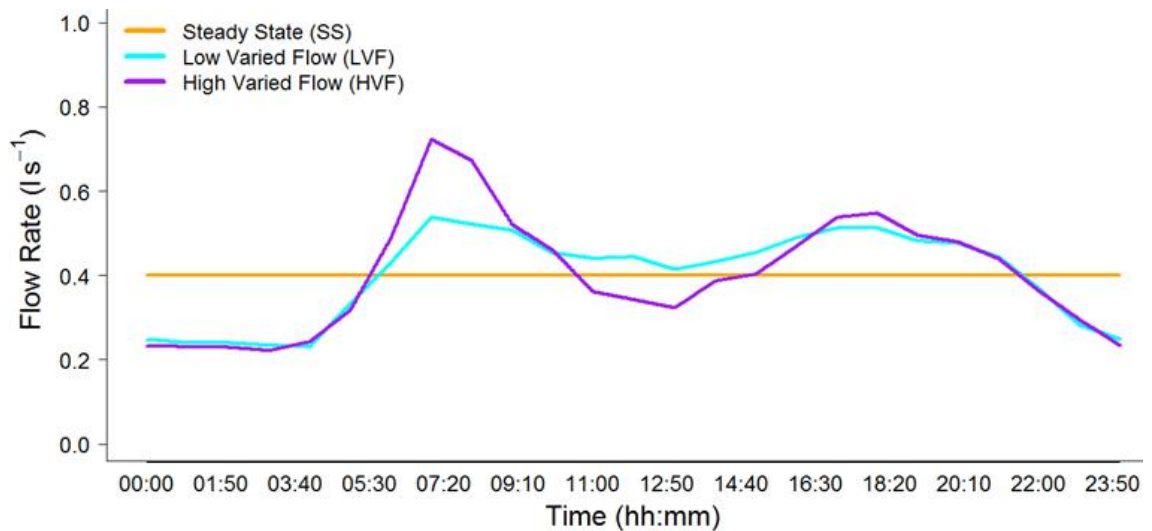


Figure 3.5 Daily flow patterns of the hydraulic regimes used in this study. Average night time flow was 0.23 l s^{-1} (0.25 Nm^{-2}) for both varied flow regimes, although this may be high with respect to live DWDS, it was the lowest flow that could be accurately achieved and monitored within the experimental facility. The peak for the LVF regime was 0.54 l s^{-1} (0.34 Nm^{-2}) and the peak in the HVF regime was 0.75 l s^{-1} (0.40 Nm^{-2}).

3.2.1.3 Sampling during the growth phase

Biofilms were randomly sampled in triplicate from each loop ($n=9$ in total) every 7 days – Days 0, 7, 14, 21 and 28. Each triplicate comprised a coupon from the crown, middle and invert of the pipe. However, it should be noted that only Day 0 (≤ 90 minutes within the experimental facility) and Day 28 biofilm samples were analysed within the scope of this thesis. In order for the biofilm samples to be removed, the pump was stopped and the valves closed; the system was not drained so the water remained within the loops, limiting the impact of sampling upon biofilm accumulation. Coupons taken as samples were replaced with sterile coupons and the location (1-27) noted so that no further samples were taken from that location.

Bulk water quality samples were taken in triplicate every 7 days from the tapping point in the reservoir tank and also from the inlet (Figure 3.2). Turbidity and flow rate were consistently recorded via the online instrumentation (section 3.1.3) throughout the growth phase.

3.2.2 Mobilization phase

3.2.2.1 Flushing steps

The cohesive layer theory as described in the PODDS model (see section 1.2.2) suggests that attached material (i.e. biofilm) expresses a defined, increasing strength profile which requires increasing shear stresses to be mobilised via flushing. The mobilization phase was thus designed to use a series of flushing steps, with increasing flow rate/shear stress (Figure 3.6), to investigate the removal of material from the pipe wall into the bulk water and simultaneously facilitate the evaluation of the structure of the developed biofilms remaining attached. Based upon previous work that used a range of shear stresses experienced in live networks (Husband, *et al.*, 2008; Sharpe, 2012), low (0.42 Nm^{-2}), medium (1.75 Nm^{-2}) and high (2.91 Nm^{-2}) shear stresses were selected; each one was run for three turnovers to provide enough time for the water to be mixed and turbidity to stabilise (Sharpe *et al.*, 2010; 2012). The mobilization phase was constrained to three flushing steps due to the number of available coupons (12 coupons per loop left undisturbed following the growth phase). Throughout the mobilization phase, the flow rate was monitored using online instrumentation (section 3.1.3), this was converted to boundary shear stress via a standard curve (Figure 3.7) based on fully calibrated data from a previous study using this experimental facility (Husband *et al.*, 2008).

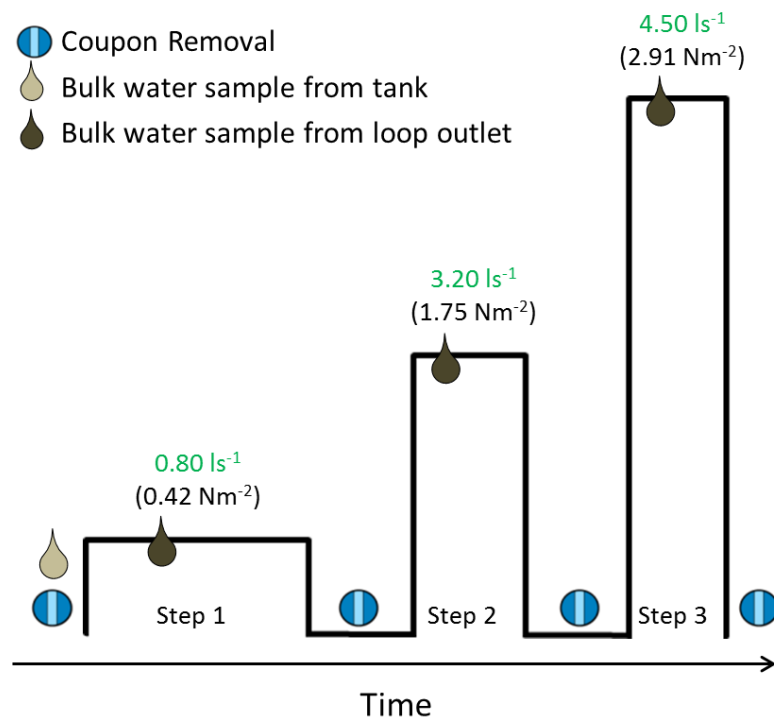


Figure 3.6 Mobilization phase schematic showing the flushing steps and sampling regime. Each step ran for 3 turnovers of the loop, the flow rate of each step is presented in green (ls^{-1}), the shear stress is presented in black (Nm^{-2}).

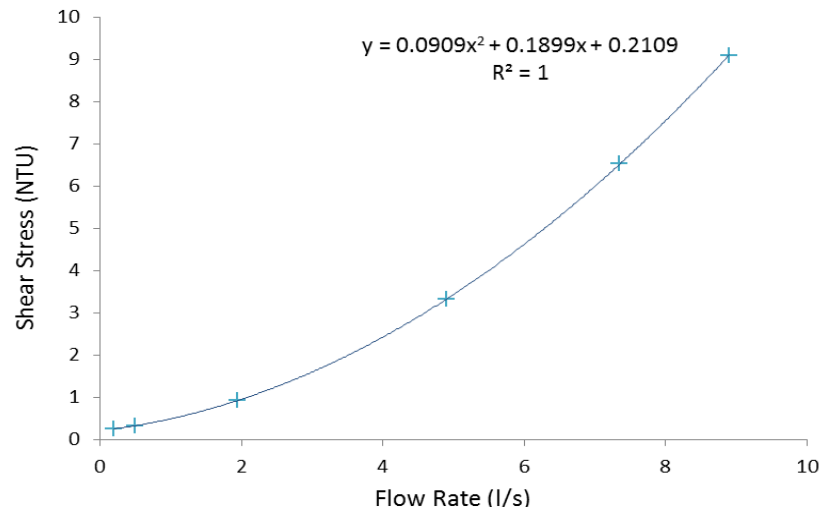


Figure 3.7 Standard curve used to determine boundary shear stress values. Graph plotted using data presented in Husband, *et al.* (2008).

Each of the shear stresses presented in Figure 3.7 were calculated by Husband *et al.* (2008) using the standard equation:

$$\tau = \rho g R_h S_o \quad \text{Equation 3.1}$$

where τ = boundary shear stress (N m^{-2}), ρ = density (Kg m^{-3}), g = gravity acceleration (m s^{-2}), R_h = hydraulic radius and S_o = hydraulic gradient.

3.2.2.2 Flushing protocol and sampling regime

As the three loops of the DWDS experimental facility shared a water tank, it was not possible to flush them simultaneously; rather, following the growth phase, each loop was isolated by manual closure of the valves and sequentially exposed to the series of flushing flow rates outlined in Figure 3.6. Furthermore, due to the length of the flushing experiments, it was not possible to flush all the loops on the same day as Day 28 sampling. Consequently, the loops experienced a staggered period of stagnation (≤ 24 hours). To account for any impact of this stagnation period “Pre-Flush” samples were collected as described below.

Before flushing, the flow from the growth phase was stopped and the bulk water sealed within each loop. The supply tank was emptied and refilled and the system sealed (i.e. no more inlet water added and the trickle turnover stopped). The fresh tank water was then combined with the water from one of the loops during a brief mixing phase at the average conditioning flow rate of 0.4 l s^{-1} , after which the flow was paused and “Pre-Flush” biofilm samples ($n=3$, comprising crown, middle and invert coupons) were taken - note that water was retained in the loop during sampling, as explained in section 3.2.1.3. Additionally, “Pre-Flush” bulk water samples were taken from the tank tapping point to provide an indication of the baseline water

quality parameters. The three flushing steps previously described (section 3.2.2.1) were then implemented – the flow, velocity and boundary shear stress at each stage are summarised in Table 3.3. Care was taken to elevate the shear stress smoothly between steps so as to avoid a transient dynamic effect and minimise the acceleration effect upon shear stress, which would alter the removal of material into the bulk water. Bulk water samples were taken after one turnover (indicated in Figure 3.6) from the loop outlet (indicated in Figure 3.2) in order to detect the initial mobilization of material into the water column before dilution (as described with respect to turbidity in Boxall & Husband, 2007). Turbidity was measured continuously throughout the mobilization phase, for all three turn overs of each flushing step. Biofilm samples (coupons) were taken after three turnovers of each flushing step (as illustrated in Figure 3.6), although it should be noted that only the coupons from the end of the mobilization phase (i.e. after flushing step 3) were analysed within the scope of this thesis. This process was then repeated for the other two loops.

Table 3.3 Flow rate, velocity and boundary shear stress at each of the flushing steps comprising the mobilization phase.

Flushing Step	Flow Rate ($l s^{-1}$)	Velocity (ms^{-1})	Boundary Shear Stress (Nm^{-2})
Mixing ^A	0.40	0.08	0.30
1	0.80	0.16	0.42
2	3.20	0.65	1.75
3	4.50	0.91	2.91

^A Mixing phase corresponds to the average conditioning flow rate during the growth phase of each trial.

3.3 Water Quality Samples

3.3.1 Physicochemical parameters and instrumentation

Water quality samples were taken throughout the growth and mobilization phases and a range of parameters were assessed using the instrumentation summarised in Table 3.4. Discolouration in drinking water has been found to be due to the suspension of fine particulate material, which previous studies have shown to be predominantly iron (Fe) and manganese (Mn), therefore the concentrations of these were monitored in addition to turbidity – the proxy for discolouration (see section 1.2.2). Other general water quality parameters were also monitored to ensure there were no significant differences in the bulk water during the growth phase and that any differences in biofilm were due to a hydraulic effect rather than a water quality effect.

All equipment was calibrated and maintained in accordance with the manufacturers' guidelines. Each of the parameters was monitored throughout the growth phase (samples taken from the tank) and the mobilization phase (initial samples taken from the tank, subsequent samples from the end of the loops). The total chlorine concentration and temperature of the inlet water were monitored during the growth phase. Additionally, when possible, water quality data (concentrations of chlorine, iron and manganese) from the treatment works supplying the local DWDS was monitored. Data is not presented due to confidentiality but, in brief, the chlorine concentration ranged from 0.45 – 0.85 mg l⁻¹, with an average of 0.63 mg l⁻¹, iron concentrations ranged from 6 – 57 µg l⁻¹ with an average of 31 µg l⁻¹ and only one manganese data point was available for the duration of these experiments (reported as 2200 µg l⁻¹).

Table 3.4 Bulk water quality parameters and the instrumentation used for their assessment.

Water Quality Parameter	Instrument/Analysis Method	Range	Resolution	Accuracy
Total Chlorine ^A	Hanna Chlorine Meter HI96711	0.00 to 5.00 mg l ⁻¹	0.01 mg l ⁻¹ for ≤ 3.50 mg l ⁻¹ 0.10 mg l ⁻¹ for > 3.50 mg l ⁻¹	± 0.03 mg l ⁻¹ or ± 3% of reading
TOC ^B	TC-IC ^E	1.0 – 50.0 mg l ⁻¹	0.10 mg l ⁻¹	-
Iron ^C	ICPOES ^F	LOD ^G : 9.47 µg l ⁻¹	-	9.50% at 200 ppb ^H
Manganese ^C		LOD ^G : 3.59 µg l ⁻¹	-	8.60% at 50 ppb ^H
Turbidity	Hach 2100Q portable Turbidimeter	0 to 1000 NTU	0.01 NTU	± 0.01 NTU or ± 1% of reading
pH	Hanna HI991003 portable multi-probe	-2.00 to 16.00 pH	0.01 pH	± 0.02 pH ^I
Temperature ^A		-5 to 105°C	0.1°C	± 0.5°C
ORP ^D		± 1999 mV	1mV	± 2mV ⁷

^A During growth these were measured at the inlet and from the tank tapping point; ^B Samples analysed by the Analytical Chemistry Laboratories, Krotto Research Institute, The University of Sheffield, UK; ^C Samples analysed by AlControl Laboratories, Rotherham, UK; ^D ORP – oxidising redox potential; ^E Total organic carbon determined by the “Total carbon-Inorganic carbon” method using a Shimadzu TOC-V CPH analyser; ^F Inductively Coupled Plasma Optical Emission Spectroscopy; ^G Limit of detection; ^H Uncertainty according to Shewhart charts; ^I Accuracy quoted from manufacturer is stated to be that when used at 20°C.

3.3.2 Water physicochemistry: methods

The majority of the water quality samples were analysed on site, all sample measurements were undertaken in accordance with the manufacturers' protocols and in all cases triplicate samples were taken (n=3). In addition to the continuous turbidity data from online instrumentation, discrete turbidity measurements (using a 15ml water sample) were taken using a Hach 2100Q portable turbidity meter. Total chlorine concentrations (using a 10ml water sample) were measured using the standard DPD (*n,n*-diethyl-*p*-phenylenediamine) spectrophotometric method (reagents from Hanna Instruments, Inc., USA).

Water samples and controls (20 ml) for TOC analysis were stored at -20 °C in 30 ml vials and sent for TC-IC analysis at the Analytical Chemistry Laboratories, Kroto Research Institute (The University of Sheffield, UK). The sampling vials initially provided were broken when the samples were defrosted for analysis; as a consequence the TOC data for the SS growth phase is considered to be unreliable. All subsequent TOC samples (from SS mobilization phase onwards) were collected in glass universals, which were a robust alternative. Water samples for iron and manganese analysis were taken in 125 ml sampling bottles, which contained 5 M nitric acid, stored at 4 °C and analysed to water industry standards via the ICPOES method (AlControl Laboratories, Rotherham, UK).

3.3.3 Water physicochemistry: data analysis

3.3.3.1 Turbidity

Due to the small sample volume (10 ml) and discrete nature of the manual turbidity samples, this data is best suited to capturing discolouration during the consistency of the growth phase and the “Pre-Flush” samples, rather than the mobilization phase where the variation between replicates is more greatly influenced by the time at which each water sample is taken. For this reason, continuous data is more appropriate for detecting discolouration events, as is simulated during the flushing in the mobilization phase.

During the mobilization phase each loop was flushed independently, with a tank of fresh water, which was combined with the growth phase water that was retained within the loop. Therefore the hand held turbidity data (and other parameters) of the “Pre-Flush” water samples was compared to demonstrate that there was little variation between loops at the start of the mobilization phase (Appendix Table A 2.1) and so no need to normalise the data.

The continuous raw data generated by LabVIEW from the Chemtrac meters was converted into “raw turbidity” values using the equations generated during the calibration described in section 3.1.3. It was noted before the experiments that the turbidity meters had an internal software option which automatically smoothed the data readings. However, no details were available to explain the algorithm behind this smoothing process; therefore it was deactivated. As a consequence, the “raw turbidity” data has a lot of “noise” associated with it (Figure 3.8), which is likely to be inherent to the instrument, hence the recommendation to use the pre-programmed smoothing. In order to remove some of the “noise”, the “raw turbidity” data was smoothed using Haar wavelet analysis which was previously ascertained by Sharpe (2012), as

the best approach when compared to the use of a rolling average, standard deviation outlier removal or high/low pass filters. The resulting “smoothed turbidity” data was generated via a MATLAB (v6.1, The MathWorks Inc., 2000) script using a wavelet decomposition level of 7, an example of the “smoothed turbidity” data output from the script is presented in Figure 3.8B.

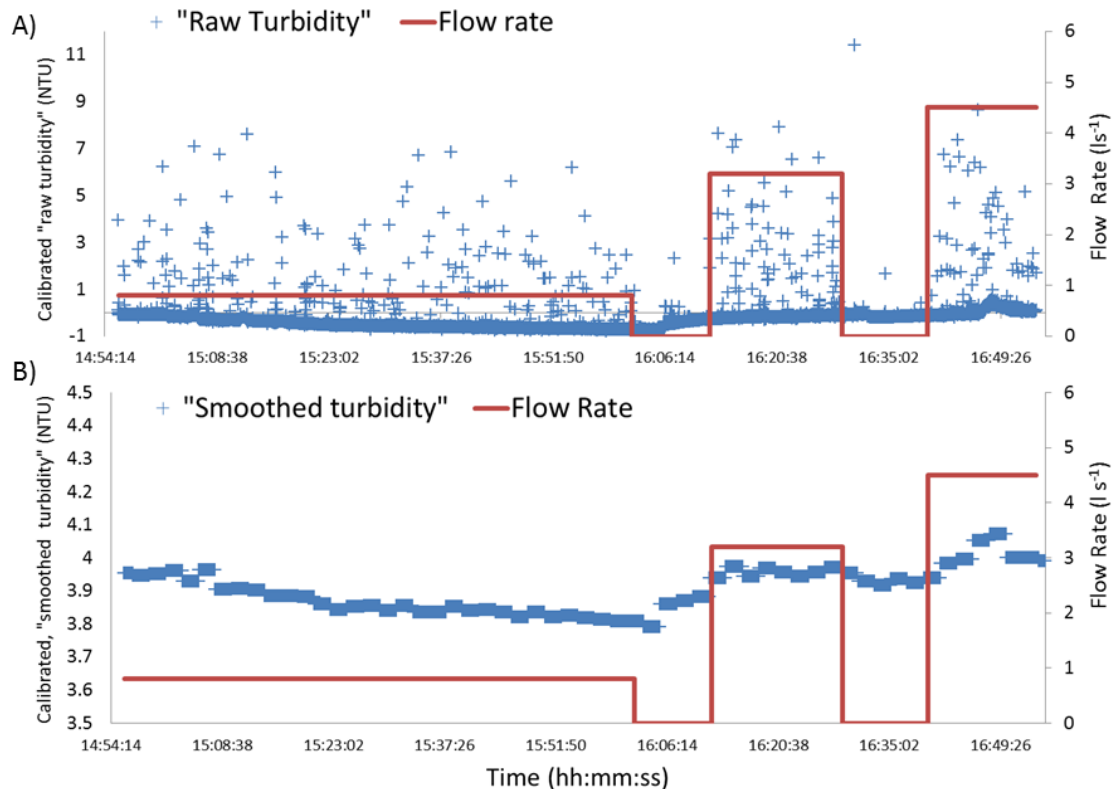


Figure 3.8 Turbidity data during the mobilization phase before and after wavelet analysis.

Data shown is from the T₁ Chemtrac during the mobilization phase of loop 1, during Steady State experiment. A) Calibrated unsmoothed data “raw turbidity” for each flushing step; B) “smoothed turbidity” data after the wavelet analysis. Red lines indicate the flow rate at each of the flushing steps as outlined in Figure 3.6.

Due to the “noise” in the data and the delay between the water flow in the loop and that passing through the Chemtrac turbidity meter (due to the built in de-bubbler), it was not always possible to detect an initial peak in turbidity at one turnover as was previously anticipated. This was particularly problematic at the final flushing step, where the turn over time was much shorter. Therefore, the average of the “smoothed turbidity” was calculated for the last turnover only, as this was the point at which: the water was most mixed, the turbidity was the most stable (hence data is most reliable) and no further material would be removed without increasing the flow, according to Boxall & Husband (2007).

The average “smoothed turbidity” (\pm one standard deviation) during the last turnover of each of the three flushing steps (Figure 3.6) was calculated for each loop and a general linear model (with regression analysis) was used to determine the relative change in turbidity as indicated

by the gradient in each case. All statistics and plots were carried out using the statistical package R version 2.15.1 (R Development Core Team, 2012), the significance level was $p < 0.05$.

Analysis of the Steady State results showed an increase in turbidity at each flushing step, as anticipated, for loops 1 and 2 (Figure 3.9) but the equipment failed during the flushing of loop 3 so no data was available. Unfortunately the issues with the Chemtrac instruments were unable to be completely resolved, leading to unreliability in the data that was collected during the subsequent LVF and HVF trials (Figure 3.9). For these reasons the only turbidity measurements that will be considered in the following sections are the discrete data from the growth phase. Given that discolouration is predominantly comprised of iron and manganese particles this data will be used as an indicator of material mobilization instead.

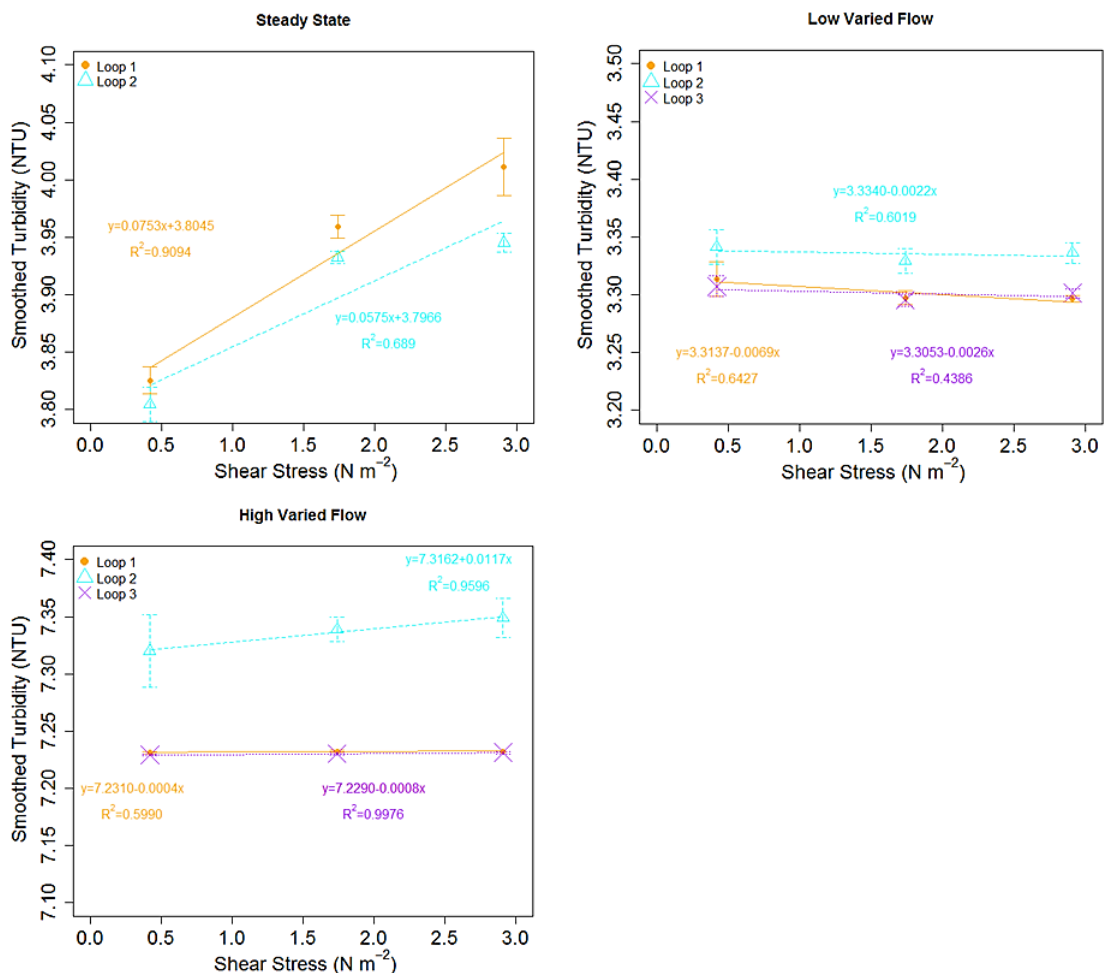


Figure 3.9 Turbidity response during the mobilization phase of each loop, for each experimental trial. Data shown is the average of the final turnover ± 1 standard deviation.

3.3.3.2 Discrete water quality samples

For each parameter measured (section 3.3.1), the range, median, mean and standard deviation were calculated for the growth phase. Normality of the data was tested via the Shapiro-Wilks test and parametric (ANOVA and Tukey) or non-parametric tests (Kruskal Wallis and two-

sample Wilcoxon) were applied, as appropriate, to identify any differences in water quality parameters between experiments (all statistical testing was carried out in R v2.15.1). In the statistical package R v2.15.1 the function “Wilcoxon” can be used to perform one- or two-sample Wilcoxon tests, the latter is also termed the “Mann-Whitney” test. There are some discrepancies in the literature regarding the exact definitions of Wilcoxon and Mann-Whitney tests, for clarity: throughout this thesis outputs presented from Wilcoxon tests relate to a two-sample test, unless otherwise stated.

In the case of TOC, before the above analysis was applied, the raw data was normalised based on the measurement of a standard solution (AQC control) of 10mg l⁻¹:

$$TOC_{normalised} = y \times \frac{10}{x} \quad \text{Equation 3.2}$$

where x is the recorded concentration of the AQC control and y is the recorded concentration of the sample.

The data collected during the mobilization phase was plotted (as an average \pm 1 standard deviation) against shear stress and a general linear model was applied (with regression analysis) to identify relative changes. Each loop was analysed separately, the R^2 and p values were used to assess the fit of the linear model to the data and the significance of the gradient, so as to determine which parameters responded significantly to the elevation in shear stress. All statistical analysis and graphical plots were produced in R v2.15.1 (R Core development Team, 2012) with a significance level of <0.05.

3.4 Biofilm Samples – Community Structure Analysis

The coupons taken during the growth and mobilization phases were carefully separated into their outer coupon and insert components; this was carried out in a laminar flow cabinet to prevent sample contamination. The inserts were fixed in 5% formaldehyde solution (Fisher Scientific, UK) for biofilm physical structure analysis as will be described in Chapter 4. Outer coupons were used to produce biofilm suspensions which were filtered to enable DNA extraction, PCR amplification and subsequent analysis of the microbial (bacteria, archaea and fungi) community structure via fingerprinting approaches, as is described in the following section. All the molecular analysis of samples was carried out at the NERC Biomolecular Analysis Facility at The University of Sheffield, UK (see Appendix A1.1 for grant details).

3.4.1 Biofilm removal and filtering

Outer coupons were analysed from Day 0, Day 28, Pre-flush and Post-flush sampling points (for each n=9), of the three experimental trials: SS, LVF and HVF (therefore 36 samples per experiment, 108 in total). Biofilm was removed from each coupon by immersing in 30 ml of sterile phosphate buffer solution (PBS; Appendix A3.1) and brushing the surface with a sterile toothbrush, using a standardised motion and number of strokes (30 horizontal and 30 vertical, rinsing the tooth brush in the solution after every 10 strokes). All tooth brushes were sterilised using the same protocol as for the coupons (sonication with 2% SDS and distilled deionised water and autoclaving). This 30 ml volume of biofilm suspension was transferred to a sterile falcon tube and stored at 4 °C for ≤ 30 minutes before filtering through a 47 mm diameter, 0.22 μm pore nitrocellulose filter (Millipore, MA, USA) using a Microstat membrane filtration unit (Sartorius, UK). Filters were then stored in sterile bags at -80 °C ready for DNA extraction.

Negative controls were carried out in triplicate for each set of samples (i.e. three negative controls for the SS samples, three negatives for the LVF samples and three negatives for the HVF samples). This involved the brushing of sterile coupons with sterile PBS, which was then filtered in the same way as the biofilm suspension. From here on these negative controls are referred to as “biofilm controls”.

3.4.2 DNA extraction

DNA was extracted from the nitrocellulose filters using the CTAB (hexadecyltrimethyl ammonium bromide) and Proteinase K chemical lysis method (Zhou *et al.*, 1996). Each filter was transferred into a sterile 15 ml tube to which 720 μl of SET buffer (see Appendix A3.2) and 90 μl of lysozyme 10 mgml^{-1} (Sigma Aldrich Co.,UK) were added. Samples were incubated at 37 °C for 30 minutes with rotation in a hybridization oven (Thermoscientific, UK). A 90 μl volume of 10% SDS (w/v) and 25 μl volume of Proteinase K (Applied Biosystems, Life Technologies Ltd., UK) were then added and the samples incubated for a further 2 hours (with rotation) at 55 °C. The lysate was transferred to a sterile tube to which 137 μl of 5 M NaCl and 115 μl of CTAB solution (Appendix A3.2) were added before incubation at 65 °C for 30 minutes (with rotation). Subsequently the top aqueous layer of the sample was removed and the supernatant extracted with an equal volume of chloroform, centrifuged at 13,000 RPM for 5 minutes.

DNA was precipitated at -20 °C, over a 12-14 hour period with 815 μl of 100% isopropanol before centrifugation at 13,000 RPM for 30 minutes. The supernatant was discarded and the

DNA pellet washed twice in 1 ml of 70% ethanol (centrifuge at 13,000 RPM for 10 minutes), dried and then eluted in 30 μ l of sterile nuclease free water (Ambion, Warrington, UK). DNA was visualised via gel electrophoresis and the quantity and quality of DNA was assessed with a Nanodrop ND-1000 spectrophotometer (Nanodrop, Wilmington, USA).

In addition to the samples, “biofilm control” filters were also exposed to the DNA extraction process and “DNA controls” were run: empty sterile tubes to which all the solutions were added and all the processes applied. Aliquots of the application ready stock DNA solution were made to limit the effects of freeze-thawing on DNA quality and were stored at -20 °C.

3.4.3 Gel electrophoresis

Gels (1%) were made up using 0.8-1.8 g of agarose (dependent on gel size), 1 x Tris acetate ethylenediaminetetraacetic acid (TAE) buffer (see Appendix A3.3) and 60-67 ng ml⁻¹ of SYBR®Safe Orange; 4 μ l of product (DNA or PCR) was run with 1 μ l of loading dye (Bioline, London, UK) alongside 5 μ l of Hyperladder I (Bioline, London, UK, range, according to supplier, 200 – 10,037 base pairs; bp). Samples were run on the gels at 90-120 V for 30-60 minutes (dependent on DNA fragment size) and visualized under UV light using a G:BOX gel imaging system and associated software GeneSnap v6.07 (Syngene, Cambridge, UK).

3.4.4 PCR amplification and purification

Three different PCR amplifications were carried out, using the DNA extract, to amplify specific genes from bacteria (16S rRNA), archaea (16S rRNA) and fungi (ITS region). The primer pairs used to amplify the regions of interest in each case are shown in Table 3.5. It should be noted that the forward primer used in each case was labelled with 6' carboxyfluorescein dye (6-FAM) to enable detection via fingerprint analysis.

To detect fungi, the 18S rRNA gene may be used, however this does not exclusively target fungi and may amplify other eukaryotes (Osborn & Smith, 2005). Alternatively, the internal transcribed spacer (ITS) regions of rDNA can be used to distinguish fungi (Martin & Rygiewicz, 2005). Commonly used in the literature are ITS1 and ITS4, which amplify the ITS region between the 18S and 28S rRNA genes (Ranjard *et al.*, 2001). Hageskal *et al.* (2006) previously used this primer combination to investigate drinking water samples; therefore they were selected for use within the context of the drinking water biofilm samples investigated in this project.

Table 3.5 Oligonucleotide primer pairs used to amplify 16S rRNA genes and ITS regions, PCR cycling conditions used in each case are indicated.

Microorganism (amplified gene)	Amplicon Size (nt)	Oligonucleotide Primers ^A		PCR Cycle Conditions			References ^B	
		Primer Pair	Primer Sequence (5' – 3')	PCR Stage	Temperature	Duration (mm:ss)		Cycles
Bacteria (16S rRNA)	~455	FAM-63F 518R	[6-FAM]-CAGGCCTAACACATGCAAGTC CGTATTACCGCGGCTGCTCG	Initial denaturation	94°C	2:00	x30	Girvan <i>et al.</i> , 2003
				Denaturation	94°C	0:30		
				Annealing	55°C	0:30		
				Elongation	72°C	0:45		
				Elongation stop	72°C	10:00		
Archaea (16S rRNA)	~849	FAM-Arch109F Arch958R	[6-FAM]-ACKGCTCAGTAACACGT YCCGGCGTTGAMTCCAATT	Initial denaturation	95°C	0:45	X35	DeLong, 1992
				Denaturation	95°C	0:45		
				Annealing	55°C	1:00		
				Elongation	72°C	1:30		
				Elongation stop	72°C	10:00		
Fungi (ITS region)	~200-1000	FAM-ITS1F ITS4	[6-FAM] -CTTGGTCATTTAGAGGAAGTAA TCCTCCGCTTATTGATATGC	Initial denaturation	95°C	5:00	X35	Hageskal <i>et al.</i> , 2006
				Denaturation	95°C	0:30		
				Annealing	55°C	0:30		
				Elongation	72°C	1:00		
				Elongation stop	72°C	10:00		

^A All oligonucleotide primers were sourced from Sigma, UK; ^B References that have used these primer combinations.

3.4.4.1 PCR reaction mixes and cycle conditions

The PCR for amplifying bacterial genes consisted of 12.5 µl of Sigma ReadyMix™ *Taq* solution (containing 1.5 U *Taq* DNA polymerase; 99% pure dNTPs and reaction buffer), 0.4 µM of each oligonucleotide primer (Table 3.5) and 2 µl of DNA template, made up to a volume of 25 µl with nuclease free water (provided with ReadyMix™ *Taq*). For all bacterial PCRs, positive (*Pseudomonas spp.* supplied by Dr. I. Douterelo) and negative controls (nuclease free water) were run.

An alternative PCR mixture was used to amplify archaea, which comprised 1 x reaction buffer, 100 µM dNTPs, 0.15 µM of each oligonucleotide primer (Table 3.5), 1.25 U of *Taq* DNA polymerase (Qiagen, Crawley, UK) and 1-2 µl of DNA template, made up to a 50 µl volume with 10 µl of Q-solution and nuclease free water. For each archaeal PCR two positive controls were run (unknown *spp.* supplied by Dr P.Deines) and a single negative (nuclease free water).

Fungal PCR mixtures contained 1 x reaction buffer, 1 mM MgCl₂, 50 µM dNTPs, 0.2 µM of each oligonucleotide primer (Table 3.5), 2.5 U of *Taq* DNA polymerase (Qiagen, Crawley, UK) and 1-2 µl of DNA template made up to 50 µl with nuclease free water. The initial fungi PCRs (a subset of samples from SS) were run with only a negative control; subsequently a Day 28 sample from SS was used as the positive control. It should be noted that due to the varied nature of the fungal ITS region, amplicons of different sizes are generated, which were visible on the agarose gels as multiple bands in some cases.

Each PCR was carried out on an AB 2720 thermal cycle following the conditions shown in Table 3.5. PCR products were visualized on a 1% agarose gel to check the amplicon presence and size (nt). Any samples for which the amplified product was weak or not detected were noted down and PCRs were repeated until either strong bands were visible, or there was a succession of weaker replicates of the sample which could be pooled together. If a sample was run through a successful PCR (i.e. the positive was visible on the gel) four times with no product visible, then it was declared to have no detectable DNA of the type for which the PCR was targeting.

3.4.4.2 PCR purification

All the PCR products were purified using the QIAquick® PCR purification kit (Qiagen, Crawley,UK) in order to remove excess primers and dNTPS. Where amplified products were weak, repeated PCRs of the same sample were pooled. Purification was carried out in

accordance with the manufacturer's guidelines and all samples were eluted in a final volume of 50 µl of the buffer EB (supplied in the Qiagen kit). Purified PCR products were visualized on a 1% agarose gel to check that the weaker samples had not been lost during the purification process.

3.4.5 Community fingerprinting

Two different fingerprinting techniques were used to assess the variation in microbial community structure between drinking water biofilm samples. Bacterial and archaeal communities were analysed using terminal-restriction fragment length polymorphism (T-RFLP; Liu *et al.*, 1997; Osborn *et al.*, 2000), in which PCR products (16S rRNA amplicons labelled with 6-FAM) were digested with a restriction enzyme that cut the products at a specific restriction site to produce terminal-restriction fragments (T-RFs), which vary in length. The size of each T-RF within a sample was determined via capillary electrophoresis using an ABI 3730 Genetic Analyzer (Applied Biosystems, Warrington, UK), which detected the fluorescently labelled T-RFs. Fungal communities were analysed using Automated Ribosomal Intergenic Spacer Analysis (ARISA; Ranjard *et al.*, 2001), which evaluates the variation in the size of the ITS regions via separation of fluorescently labelled amplicons using capillary electrophoresis.

3.4.5.1 T-RFLP: bacteria and archaea

Purified PCR products were digested using the restriction enzyme AluI (Roche, Germany) as preliminary tests showed AluI to be more discriminatory than CfoI. The digestion reaction contained 2-11.5 µl of purified PCR product (dependent upon the strength of the sample), 10 U of AluI and 1 x buffer solution (Roche, Germany) in a total volume of 15 µl. Samples were digested at 37 °C for 2 hours.

Aliquots of the digested samples (5 µl) were desalted via precipitation with 0.25 µl glycogen (20 mg ml⁻¹; Fermentas ThermoScientific, Loughborough, UK) and 0.53 µl of 3 M sodium acetate (pH 5.2) in 70% ethanol (ice cold). The solution was gently vortexed, to allow the DNA to precipitate, and centrifuged (13,000 RPM) at 4 °C for 20 minutes. The pellet was washed twice in 1 ml 70% ethanol (centrifuged at 13,000 PRM, 4 °C for 10 minutes), the supernatant was removed by inverting and centrifuging at 190 RCF for 30 seconds. Following the second wash, the pellet was air dried prior to re-suspension in 5 µl of nuclease free water (Ambion, Warrington, UK).

Desalted digests (0.5 µl, 1 µl, 1.5 µl or 2 µl dependent upon product strength) were denatured with 10 µl of hi-di formamide which contained 0.5% GeneScan™500 ROX™ internal size standard (Applied Biosystems, Warrington, UK). After denaturing at 94 °C for 3 minutes, the samples were cooled immediately on ice and were run on an ABI 3730 PRISM® capillary DNA analyser using POP7 (denaturing) polymer (Applied Biosystems, Warrington, UK), with injection times of 5, 10 or 20 seconds and an initial injection voltage of 2kV. Size standard controls (no sample added) were also run at these injection times (see Appendix A4.1 for the GS500 size standard profile obtained). All samples and controls were run a minimum of three times to ensure the profiles produced were representative.

3.4.5.2 ARISA: fungi

The purified fungal PCRs were desalted (5 µl volumes) using the protocol outlined in section 3.4.5.1; in brief precipitation using glycogen (20 mg ml⁻¹) and ethanol (70%), followed by two ethanol (70%) washes of the pellet and resuspension in nuclease free water. Desalted samples (1µl or 2µl) were combined with hi-di formamide containing 0.5% ROX™ GeneScan™2500 internal size standard (Applied Biosystems, Warrington, UK), in a total volume of 10µl. Samples were denatured at 94°C for 3 minutes, cooled immediately on ice and then run on an ABI 3730 PRISM® capillary DNA analyser using POP7 (denaturing) polymer (Applied Biosystems, Warrington, UK) at injection times of 5 or 10 seconds, with an initial injection voltage of 2kV. Internal size standard controls were run alongside the samples at the same injection times (see Appendix A4.2 for the GS2500 size standard profile obtained). All samples and controls were run a minimum of three times to ensure the profiles produced were representative.

3.4.6 Community composition data analysis

3.4.6.1 Electropherograms and alignment of profiles

All of the fingerprinting data obtained was analysed initially via GeneMapper® v3.7 (Applied Biosystems) in which the raw profiles were visualized via electropherograms and the size of each T-RF (50-500 nucleotides) or ITS fragment (94-827 nucleotides, see Appendix A4.2) was estimated using the Local Southern method (in comparison with the internal size standard). To remove any noise introduced during capillary electrophoresis, a threshold was applied so that only T-RF/ARISA peaks with a height greater than 50 fluorescent units were analysed. Furthermore, all bacterial profiles selected for further analysis had total peak areas of 11000-68000, archaeal profiles were within the range 12000-71500 and fungal ARISA profiles had total peak areas of 121000 – 959000.

A table was generated for each dataset, which included the T-RF/fragment size (nt), the peak area and the peak height. The total peak area of the profile for each sample was calculated and the electropherograms for each were visualized. Samples were re-run if either the size standard was too low to be accurately used or the total peak area was significantly lower or higher than the majority of profiles for other samples. The most representative profile for each sample was then selected for further data analysis.

Each fingerprint profile (from T-RFLP or ARISA) was expressed in terms of the peak area of each T-RF/ARISA fragment vs. T-RF/ARISA fragment size and aligned using the web based software T-align with a confidence interval of 0.5 nt (Smith *et al.*, 2005). T-RFs or fragments with a peak area $\leq 0.5\%$ of the total peak area were excluded from subsequent analysis. Two matrices of data were generated following alignment: 1) relative abundance of each T-RF expressed as a percentage of the total peak area and 2) the presence/absence of each T-RF expressed as a binary matrix.

3.4.6.2 Diversity indices and multivariate statistics

Aligned data (both relative abundance and presence/absence) was analysed using the software PRIMER-6 (v6.1.13, PRIMER-E Ltd, UK). In brief the data was square-root transformed and Bray-Curtis similarity matrices were generated (Clarke & Gorley, 2006). The “DIVERSITY” function was used to calculate: relative richness – defined as the total number of T-RFs or ARISA fragments per sample; relative diversity –determined using the Shannon index as calculated using Equation 3.3; and relative evenness – a measure of equitability determined using the Pielou index as calculated using Equation 3.4. It is important to note that due to the inherent issue of fingerprinting techniques detecting only the “dominant” microorganisms within a sample, application of diversity indices to these datasets produces values which are relative to the fingerprint community rather than representative of the true underlying community diversity, as addressed by Blackwood *et al.* (2007). The relative diversity indices were exported from PRIMER 6 and further analysed using R v2.15.1 (R Development Core Team, 2012) to determine similarities/differences (via T-tests or ANOVA).

$$H' = - \sum_{i=1}^s \rho_i \ln \rho_i \quad \text{Equation 3.3}$$

Where H' is the Shannon diversity index value, s is the total number of T-RFs/fragments and ρ_i is the relative abundance of each T-RF (i).

$$J' = H' / \ln s$$

Equation 3.4

Where J' is Pielou's evenness index value; H' is diversity according to the Shannon index and s is the total number of T-RFs/fragments.

Similarity between samples was also assessed using the multivariate approaches of non-parametric multidimensional scaling (nMDS) and hierarchical clustering with analyses of similarity (ANOSIM). All nMDS ordinations were plotted following 400 iterations of the data and the stress values for 2D and 3D plots were noted (stress < 0.05 = excellent representation of data, < 0.1 = good ordination, < 0.2 = potentially useful but check with cluster analysis, > 0.3 = weak representation, misleading, discard plot). Cluster analysis was run for 20,000 permutations and a dendrogram plotted with SIMPROF analysis (run with 20,000 permutations and simulations). SIMPROF analysis determines if two profiles can be statistically distinguished between, those profiles which cannot be separated are plotted with red links in the dendrogram, those which can are plotted with black links. ANOSIM analyses (one-way and two-way both run with a maximum of 400,000 permutations) detected the similarity between samples, expressed as the global R value (0-1, where 0 indicated no difference between samples and 1 indicated that samples are completely different) and determined if the difference/similarity was significant, via "significance levels". ANOSIM significance is expressed as a percentage, so a global R value with associated significance of $\leq 5\%$ (i.e. $p \leq 0.05$) is statistically significant. For the purposes of this thesis the significance levels (%) have been expressed in the format of traditional p values. SIMPER analysis was used to evaluate the similarity and dissimilarity between sample groups (expressed as %) and to identify the T-RFs or ARISA amplicons primarily responsible for the discrimination of sample clusters identified via nMDS or dendrograms.

3.5 Biofilm Samples - Scanning Electron Microscopy

Scanning electron microscopy (SEM) provided qualitative data on the biofilm physical structure and surface coverage, showing the HDPE surface, developed biofilm, single cells and inorganics (differentiated visually). In this study SEM was used to confirm and visualise the development of biofilm following the growth phase and visualise the biofilm remaining (if any) after the application of the flushing steps. All SEM sample preparation and imaging was carried out at the Biomedical Science Electron Microscopy Unit, The University of Sheffield.

3.5.1 SEM samples

The samples used for SEM analysis were the inserts taken from the PWG coupons that were used to fill the apertures in each loop, following the collection of Day 0 samples (n=9). These coupons were in place from 90 minutes into the start of each experiment. At Day 28, three of these Day 0 replaced coupons (one from each loop) were taken, the remaining six were left in place till the end of the flushing of each loop when three more (one from each loop) were removed.

3.5.2 SEM analysis method

Following an initial fixation step using 5% (v /v) formaldehyde, the HDPE inserts were secondarily fixed in 2% aqueous osmium tetroxide for an hour at room temperature. Samples underwent a series of 15 minute dehydrations, at room temperature, with ethanol in the sequence: 75% (once), 95% (once), 100% (twice) and 100% over anhydrous copper sulphate. The HDPE inserts were immersed in a 50/50% (v / v) solution of absolute ethanol and hexamethyldisilazane for 30 minutes and then transferred to 100% hexamethyldisilazane for a further 30 minutes. Samples were air dried overnight and then coated with ~25 nm of gold using S150B sputter coater (Edwards, UK). Images were obtained with an XL-20 scanning electron microscope (Philips, Cambridge, UK) at an accelerating voltage of 20 kV.

3.6 Summary of Samples

In Table 3.6 a summary is presented of the biofilm samples (coupons) and water physicochemistry (i.e. water quality) samples that were analysed within the scope of this thesis as explained throughout this chapter. Replication is indicated by the “n” values, for each sample point of each phase of each experimental trial: SS, LVF and HVF. The outer coupon was used for microbial community analyses as described in section 3.4, the insert was used for biofilm physical structure analysis, which is the focus of the following chapter.

Table 3.6 Summary of samples analysed across all experiments and the replication in each case.

Experiment ^A	Experimental Phase	Sample Point	Biofilm Samples		Water Quality Samples							
			Outer Coupon	Insert	Iron	Manganese	Chlorine ^C	TOC ^D	pH	Temperature ^E	ORP ^F	Turbidity ^G
SS	Growth	Day 0	n=9	n=9								
		Day 7										
		Day 14			n=15	n=15	n=15		n=15	n=15	n=15	n=15
		Day 21										
		Day 28	n=9 (+ n=3) ^H	n=9								
	Mobilization	Pre-flush	n=9	n=9	n=3	n=3	n=3	n=3	n=3	n=3	n=3	
	After Flush step 1			n=3	n=3	n=3	n=3	n=3	n=3	n=3		
	After Flush step 2			n=3	n=3	n=3	n=3	n=3	n=3	n=3		
	Post-flush ^B	n=9 (+ n=3) ^H	n=9	n=3	n=3	n=3	n=3	n=3	n=3	n=3		
LVF	Growth	Day 0	n=9	n=9								
		Day 7										
		Day 14			n=15	n=15	n=15	n=15	n=15	n=15	n=15	n=15
		Day 21										
		Day 28	n=9 (+ n=3) ^H	n=9								
	Mobilization	Pre-flush	n=9	n=9	n=3	n=3	n=3	n=3	n=3	n=3	n=3	
	After Flush step 1			n=3	n=3	n=3	n=3	n=3	n=3	n=3		
	After Flush step 2			n=3	n=3	n=3	n=3	n=3	n=3	n=3		
	Post-flush ^B	n=9 (+ n=3) ^H	n=9	n=3	n=3	n=3	n=3	n=3	n=3	n=3		
HVF	Growth	Day 0	n=9	n=9								
		Day 7										
		Day 14			n=15	n=15	n=15	n=15	n=15	n=15	n=15	n=9
		Day 21										
		Day 28	n=9 (+ n=3) ^H	n=9								
	Mobilization	Pre-flush	n=9	n=9	n=3	n=3	n=3	n=3	n=3	n=3	n=3	
	After Flush step 1			n=3	n=3	n=3	n=3	n=3	n=3	n=3		
	After Flush step 2			n=3	n=3	n=3	n=3	n=3	n=3	n=3		
	Post-flush ^B	n=9 (+ n=3) ^H	n=9	n=3	n=3	n=3	n=3	n=3	n=3	n=3		

^ACodes as outlined in Table 3.2; ^B Post-flush samples from the end of the mobilization phase i.e. after flush step 3; ^C Measured at the inlet and tank during growth, for SS inlet growth n=9; ^D TOC – total organic carbon; ^E Temperature in °C monitored at the inlet and tank during growth; ^F ORP – oxidising reduction potential; ^G Discrete turbidity, HVF growth n=9 due to bulb failure; ^H the “(+ n=3)” refers to the three samples taken for SEM.

Chapter 4: Evaluating Biofilm Physical Structure – Method Development

4.1 Introduction

Biofilm physical characteristics are attributed to the EPS matrix, which is synthesised by the attached microbial cells (section 1.4.5.1). The matrix has a complex composition of, primarily, carbohydrates and proteins, although lipids and extracellular DNA have also been identified (section 1.4.5.1). For the biofilm to be mobilised into the water column of the DWDS, the internal forces of the EPS must be overcome. Therefore, there is a need to understand the role of the matrix in shaping biofilm physical structure and promoting stability. However, there is limited research regarding the impact of environmental parameters on the distribution, composition and quantity of EPS. Moreover, most studies investigate biofilms that are not representative of those in a full scale DWDS. Additionally, there is currently no single accepted method for quantifying and/or visualising the cells and EPS (carbohydrates and proteins) of the biofilm (Denkhaus *et al.*, 2007; Neu and Lawrence, 2009; Wagner *et al.*, 2009).

Biofilm matrices may be studied via isolation of the EPS from the cellular fraction, prior to quantification or chemical characterisation. Various extraction techniques are commonly employed to extract, quantify and determine the biochemical composition of EPS (Appendix 5; Jahn & Nielsen, 1995; Sheng *et al.*, 2005; Denkhaus *et al.*, 2007). However, protocols are diverse as they are devised with respect to the particular experimental design of each study. Additionally, it is acknowledged that biofilm quantification, EPS yield and estimations of carbohydrate or protein content, are influenced by the particular chemical techniques employed (Jahn & Nielsen, 1995; Denkhaus *et al.*, 2007) so comparison between studies is often difficult. Several authors have compared different extraction techniques but no single method has been found to be consistently the most efficient, generally varying with the sample origin and methodology applied. There are few examples of EPS extraction from mixed species drinking water biofilms. A rare example is work by Michalowski *et al.* (2009; 2010) testing several EPS extraction techniques on drinking water biofilms grown in a reactor. The results established that all the tested methods successfully enabled isolation of EPS, but that a cation exchange resin (CER) Dowex based protocol was the most efficient (Michalowski *et al.*, 2009; 2010).

Extraction based processes in general offer the advantage that carbohydrates and proteins are isolated which, as well as enabling quantification, allows further chemical analysis using techniques such as PAGE gels and protein sequencing. A range of extraction, quantification and chemical assay methods were reviewed (Appendix 5) and those that were potentially the most suitable for use with the drinking water samples were selected for evaluation, as shown in Table 4.1.

Table 4.1 The EPS physical extraction, quantification and biochemical analysis techniques evaluated in this study.

Process	Method	References
Extraction of EPS from Biofilm	CER ^A	Jahn & Nielsen, 1995; Frolund <i>et al.</i> , 1996; McSwain <i>et al.</i> , 2005; Denkhaus <i>et al.</i> , 2007; Michalowski <i>et al.</i> , 2009
	EDTA ^B	Zhang <i>et al.</i> , 1999; Sheng <i>et al.</i> , 2005; Eboigbodin & Biggs, 2008
	FD+EtOH ^C	Hanlon <i>et al.</i> , 2006; Haynes <i>et al.</i> , 2007; Hofmann <i>et al.</i> , 2009
Protein Assay	Bradford Assay	Frolund <i>et al.</i> , 1996; Raunkjaer <i>et al.</i> , 1994; Berges <i>et al.</i> , 1993; Bradford, 1976
	RC DC ^D Assay	Lowry, 1951
Carbohydrate Assay	Phenol- Sulfuric Acid Assay	Dubois <i>et al.</i> , 1956; Raunkjaer <i>et al.</i> , 1994; Hanlon <i>et al.</i> , 2006; Haynes <i>et al.</i> , 2007; Hofmann <i>et al.</i> , 2009; Michalowski <i>et al.</i> , 2009
Cell Lysis Assay	G6PDH ^E Enzyme Assay	Lessie & van der Wijck, 1972; Jahn & Nielsen, 1995; Frolund <i>et al.</i> , 1996; McSwain <i>et al.</i> , 2005
Quantification of biofilm and EPS biomass	TOC ^F	Jahn & Nielsen, 1995; McSwain <i>et al.</i> , 2005
	Dry Weight (via Freeze-drying)	Hofmann <i>et al.</i> , 2009

^A Cation Exchange Resin; ^B Ethylenediaminetetraacetic acid; ^C Freeze-drying (ethanol precipitation) ^D Reducing Agent, Detergent Compatible; ^E Glucose-6-phosphate Dehydrogenase; ^F Total organic carbon.

In contrast to extraction techniques, staining and imaging allows visualization of the EPS distribution throughout the biofilm (Jahn & Nielsen, 1995; Neu & Lawrence, 2009). Fluorescent staining and CLSM have previously been successfully used to assess the EPS of flocs (Schmid *et al.*, 2003), granules (McSwain *et al.*, 2005) and single-species cultured biofilms (Shumi *et al.*, 2009), yet, no literature or evidence was available in which this technique was applied to multi-species biofilms within a DWDS environment. A multitude of fluorophores targeting various biofilm components are suggested in the literature, however, the focus is often limited to cells and carbohydrates, or identification of carbohydrates and proteins separately using different samples (Ivleva *et al.*, 2009). Evaluating the EPS in this way is limited to the combination of stains which are compatible and the laser availability at the given imaging facility. Also, this approach does not enable the detailed analysis of chemical-species (protein or carbohydrate) which is possible with the products from the extraction process. However, fluorescent staining and imaging techniques may be favoured over extraction techniques as they facilitate visual investigations of the 3D physical structure, as well as quantification of biofilm components via digital image analysis (DIA) and are more easily standardised, hence comparisons can be more readily made between studies. Raman microscopy (RM) has been

used to obtain detailed chemical composition data from cultured biofilms within a wastewater sludge seeded reactor (Ivleva *et al.*, 2009; Wagner *et al.*, 2009). However, this analysis was only successfully applied to samples older than a month, prior to this the biofilm coverage was too low to be detected (Wagner *et al.*, 2009). Given the low microbial content of drinking water in comparison to wastewater, it is unrealistic to expect biofilms developed for a month in the DWDS experimental facility to exhibit a greater coverage or biomass than the biofilms investigated by Wagner *et al.* (2009). For this reason, in addition to issues with the properties of the scaffold (the HDPE insert fluoresces), RM was deemed to be unsuitable for use with the drinking water biofilm samples analysed in this study.

4.2 Chapter Aim and Objectives

Using samples developed within a full scale pipe experimental facility (section 3.1), this chapter aimed to evaluate the use of physical extraction techniques for analysing EPS, in comparison with microscopy based techniques. Based on the results from this comparison, the subsequent intent of this research was to develop a reliable and robust method, compatible with drinking water biofilm samples, in order to quantify both the cells and EPS (carbohydrates and proteins).

A series of physical extraction experiments were run using standard carbohydrate and protein solutions in addition to preliminary biofilm samples. The main objectives of these preliminary trials were to:

- assess the accuracy of the techniques shown in Table 4.1;
- evaluate any influences of extraction techniques upon the subsequent chemical assays;
- determine which of the analyses (Table 4.1) were sufficiently sensitive for use with drinking water biofilm samples.

Additionally, a selection of fluorophores targeting cells, carbohydrates and proteins, were extensively tested via excitation/emission spectra analysis for their application to drinking water biofilms, in order to develop an optimised triple staining procedure to concurrently visualise the distribution of, and subsequently quantify, the matrix and cells of drinking water biofilms. The specific objectives of these tests were to:

- evaluate a range of stains targeting cells, carbohydrates and proteins when singularly applied to drinking water biofilms (upon the PWG coupon insert);

- test the stains in combination to determine those which are compatible with each other and the biofilm samples;
- identify the best triple stain combination (targeting cells, carbohydrates and proteins) appropriate for use with these samples;
- develop and optimise staining and imaging processes.

4.3 Preliminary Biofilm Samples

This study used preliminary biofilm samples obtained during a parallel test which used the facility described in section 3.1.1, as part of a complementary project to that presented in this thesis. The same experimental set-up was used as detailed in section 3.2 but with three constant flow regimes: 0.2 l s^{-1} , 0.4 l s^{-1} and 0.8 l s^{-1} , in loops 1, 2 and 3 respectively. Material was accumulated over 28 days, at $16 \text{ }^\circ\text{C}$. The presence of biofilm was confirmed using SEM analysis (see section 3.5 for methodology), as shown in Figure 4.1. The outer coupon was used to develop and optimise the extraction, quantification and chemical assay methods while the insert was used to develop and optimise the microscopy based approach.

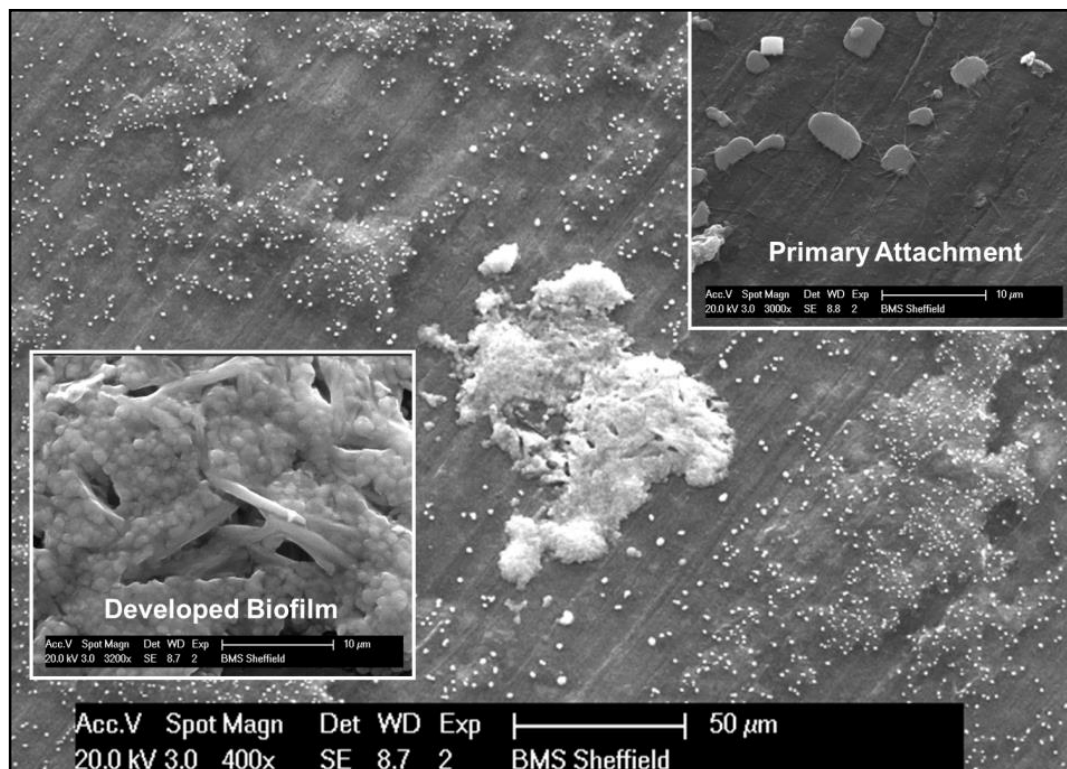


Figure 4.1 SEM image of a drinking water biofilm. Biofilm developed for 28 days under steady state conditions at $16 \text{ }^\circ\text{C}$. Scale bars are: main image $50 \text{ }\mu\text{m}$, inset images $10 \text{ }\mu\text{m}$.

4.4 Method Development and Optimisation: EPS Physical Extraction Analysis

4.4.1 Extraction techniques and associated methods

Three EPS extraction techniques were tested: CER dowex (Sigma Aldrich Co., UK), ethylenediaminetetraacetic acid (EDTA) and freeze-drying followed by precipitation with ethanol (FD+EtOH). Each technique was carried out according to standard protocols (see the references in Table 4.1) which were optimised during the course of the tests described in the following sections (see Appendix 6 for specific protocols). The G6PDH enzyme assay kit (BioVision, CA, USA) was carried out according to the supplier's guidelines as a proxy for cell lysis to ensure the EPS solution was not contaminated with cellular components, which are released if cells are damaged during the extraction process. Two methods for quantifying the volume of biofilm and EPS were applied: TOC analysis (methods detailed in section 3.3.2) and dry weight, obtained by freeze-drying samples in a Super Modulyo freeze-dryer (Thermo Scientific, UK).

Colorimetric spectroscopic analytical procedures were used to determine the carbohydrate and protein concentrations in aliquots of the EPS extraction solution. The phenol-sulfuric method (Dubois *et al.*, 1956) was selected to determine the carbohydrate concentrations and two protein assays were tested – the Bradford Assay (Bradford, 1976) and RC DC Assay (Bio Rad, Hertfordshire, UK). All assays were carried out according to standard protocols (Appendix 6) using a Jenway 6300 spectrophotometer (Jenway, Staffordshire, UK). Absorbance was recorded at a wavelength of 490 nm (for hexose sugars) and 480 nm (for pentose sugars) for the carbohydrate assay; 595 nm for the Bradford protein assay and 750 nm for the RC DC protein assay.

4.4.2 Extraction trials with standard solutions

4.4.2.1 Materials and methods

Standard curves for the Bradford and RC DC protein assays were generated using bovine serum albumin (BSA) concentrations of 0.000 – 0.050 mg ml⁻¹, made up in PBS (Appendix A3.1). Similarly, carbohydrate standards using glucose in PBS (Appendix A3.1) at concentrations of 0.000 – 0.150 mg ml⁻¹ were used to produce a standard curve for the phenol-sulfuric method (absorbance read just at 490 nm, the appropriate wavelength for hexose sugars such as

glucose). All the solutions were made up in triplicate and the data was plotted using the statistical package R v2.15 with regression analysis applied to determine the standard curve.

Following the establishment of standard curves, the quantification (TOC and dry weight) and extraction techniques (CER Dowex, EDTA and FD+EtOH) were applied to known concentrations of protein (BSA) solutions (0.001, 0.005 and 0.010 mg ml⁻¹) and carbohydrate (glucose) solutions (0.005, 0.010, 0.050 and 0.150 mg ml⁻¹). During this series of tests it became apparent that there was a high level of technical error introduced by freeze-drying small volumes, this was primarily due to the samples exploding during the pressure change. Consequently, a considerable number of samples were lost during the freeze-drying process, despite various modifications to the protocol. Therefore the techniques using freeze-drying, namely the EPS extraction technique FD+EtOH and the use of freeze drying to determine dry weights, were eliminated from all further method tests.

The accuracy of each of the assays following the use of the CER and EDTA extraction methods was established by using the standard curves to predict the concentrations of the known BSA (protein) and glucose (carbohydrate) standards. A control was also carried out using the known concentrations without any prior extraction process being applied, i.e. an “untreated” state. Confidence intervals of the predicted values were calculated using the equation:

$$X_B \pm \frac{tSy}{b} \sqrt{\frac{1}{m} + \frac{1}{n} + \frac{(y_B - \bar{y})^2}{b^2 \sum (x_i - \bar{x})^2}} \quad \text{Equation 4.1}$$

Where X_B is the unknown concentration, t is the t-statistic, Sy is the standard error, b is the gradient of the regression line, m is the number of replicates, n is the number of standards, x_i are the standard concentrations, \bar{x} is the mean of the concentrations, y is the standard absorbance and y_B is the absorbance of the unknown concentration. A Welch 2 Sample T-test was applied to determine any differences between the actual and predicted concentrations. All p values reported in association with these tests are from the T-test unless otherwise stated, the significance level was set at <0.05.

4.4.2.2 Results and discussion

The mean determined values (n=3) of each of the BSA solutions of known concentrations, established via the Bradford or RC DC assay, are presented in Table 4.2, together with the confidence interval in each case. When applied to the untreated solutions, both assays yielded concentrations which were not significantly different from the expected concentrations (RC DC, p=0.4306; Bradford p=0.4114), although the Bradford assay was more reliable as indicated

by the lower confidence interval. Both extraction methods (CER and EDTA) led to differences between the observed and expected protein concentrations when analysed via RC DC. Two thirds of the solutions were estimated to have negative protein quantities (denoted by “x” in Table 4.2) and, where a value was established, the RC DC assay overestimated the protein concentration by more than four times the expected value. In contrast, the Bradford assay produced consistently accurate quantifications of proteins, which were not significantly different from the expected concentrations (CER treated, $p=0.7887$; EDTA treated, $p=0.4834$). Therefore the Bradford assay was determined as the most reliable protein analysis to use in future tests. No difference ($p=0.7760$) was found between the determined concentrations following the CER and EDTA methods (using the Bradford assay) therefore when using BSA solutions neither extraction method is superior.

Mean determined values of carbohydrate concentration ($n=3$) are presented in Table 4.3. There was no difference between any of the observed and expected concentrations (untreated $p=0.9038$, CER $p=0.7986$, EDTA $p=0.7498$). Furthermore no significant difference existed between carbohydrate concentration values generated following CER or EDTA processing ($p=0.9770$). Therefore neither extraction technique significantly affected the efficiency of the subsequent carbohydrate assay, therefore both were taken forward to be tested with drinking water biofilm samples.

Table 4.2 Mean observed values of known protein concentrations generated by RC DC and Bradford assays (\pm confidence interval).

BSA Concentration (mg ml^{-1})	Predicted BSA Concentration (mg ml^{-1})					
	Controls (Untreated)		CER		EDTA	
	RC DC	Bradford	RC DC	Bradford	RC DC	Bradford
0.001	0.005 ± 0.009	0.005 ± 0.002	X	0.002 ± 0.002	X	0.004 ± 0.002
0.005	0.004 ± 0.009	0.008 ± 0.002	0.095 ± 0.009	0.003 ± 0.002	0.026 ± 0.009	0.007 ± 0.002
0.010	0.009 ± 0.009	0.012 ± 0.002	X	0.015 ± 0.002	X	0.014 ± 0.002

“X” denotes a negative concentration prediction.

Table 4.3 Mean observed values of known glucose concentrations generated using the phenol-sulfuric method (\pm confidence interval).

Glucose Concentration (mg ml^{-1})	Predicted Glucose Concentration (mg ml^{-1})		
	Untreated	CER	EDTA
0.005	0.001 ± 0.008	0.002 ± 0.008	0.004 ± 0.007
0.010	0.003 ± 0.008	0.006 ± 0.008	0.012 ± 0.007
0.050	0.031 ± 0.008	0.025 ± 0.008	0.050 ± 0.007
0.150	0.155 ± 0.008	0.133 ± 0.008	0.095 ± 0.007

4.4.3 Extraction trials with drinking water biofilms

4.4.3.1 Materials and methods

To determine the surface area (i.e. number of coupons) required to obtain detectable quantities of material, biofilm suspensions were generated (see section 3.4.1 for method) from different outer coupon surface areas, as detailed in Figure 4.2A, using preliminary biofilm samples (section 4.3). A sample area of 214.16 mm² was the equivalent of the surface area of a single outer coupon; this sample set consisted of nine biofilm suspensions from nine, single coupons. Three biofilm suspensions from a surface area of 642.48 mm² were created; each suspension was produced by pooling the biofilm removed from a set of three coupons. Similarly, three biofilm suspensions from a surface area of 1070.80 mm² were produced by pooling the biofilm removed from three sets of five coupons. Each set of samples included coupons from each of the loops except for the tests regarding a 1070.80 mm² surface area. In this instance, due to limited preliminary biofilm sample availability, each set comprised coupons from just one loop, i.e. a set of five from loop 1, five from loop 2 and five from loop 3. A series of sterile coupons were used to generate control suspensions.

All suspensions were processed as outlined in Figure 4.2. In brief, quantification was performed via TOC, cell lysis by G6PDH assay, both CER and EDTA were tested as extraction techniques and composition analysis was via protein and carbohydrate assays, using Bradford and phenol-sulfuric methods respectively. Standard curves were generated as explained in section 4.4.2.1 and used to determine the protein and carbohydrate concentrations within the biofilm. Background data from the control samples was subtracted from the biofilm suspension data prior to any further analysis. All quantities or concentrations were calculated back to the original 30 ml biofilm suspension volume and divided by the appropriate surface area.

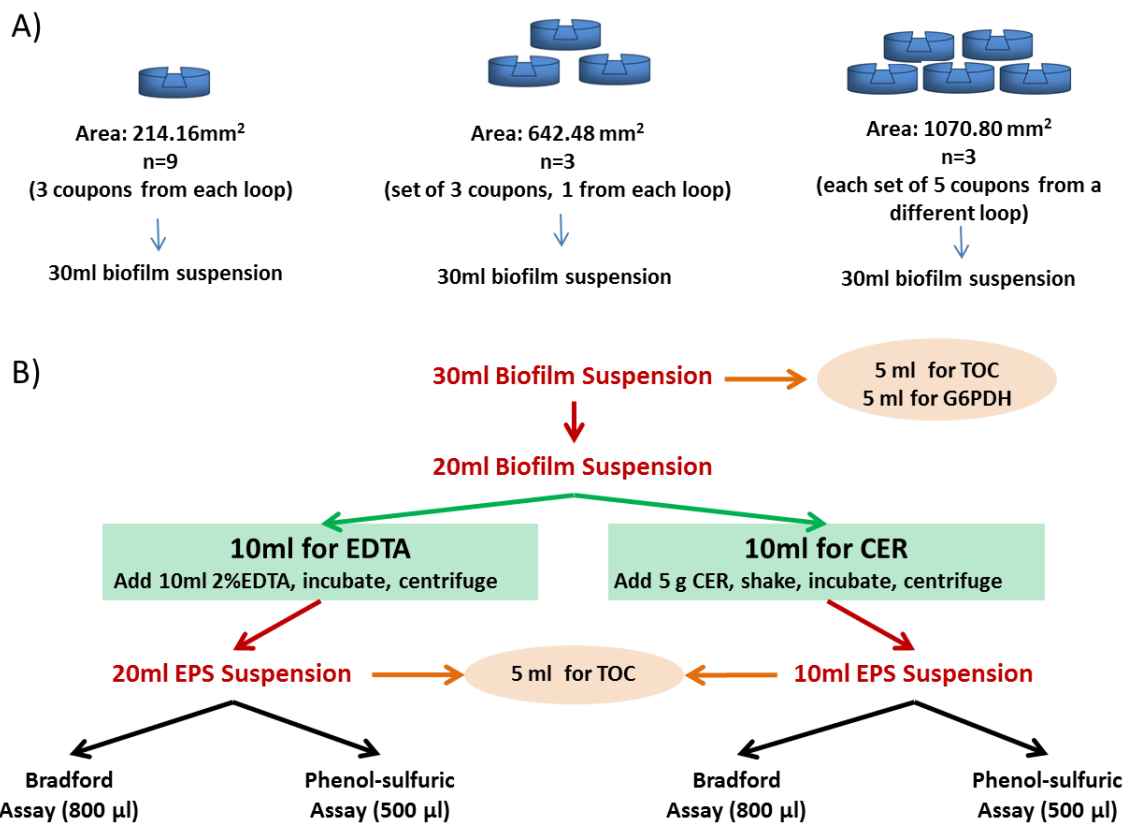


Figure 4.2 Experimental design for EPS analysis of drinking water biofilm samples. A) Sets of coupons from which biofilm suspensions were removed. B) Processes applied to the biofilm suspensions to test the different methods.

4.4.3.2 Results and discussion

Biofilm and EPS quantification was inconclusive using the extraction methods, as the majority of samples (10/15 biofilm suspensions, 14/15 CER extractions and 13/15 EDTA extractions) did not exceed the limit of detection (data not shown) for TOC analysis. Furthermore, all of the carbohydrate assay results were negative, therefore carbohydrate was deemed undetectable. Positive protein concentrations were only obtained for the EPS extracted from a surface area of 1070.80 mm² and were associated with large confidence intervals (Table 4.4). Although the average protein concentration was consistent between the extraction techniques, variation existed between replicates, which was likely partly due to the heterogenic nature of biofilms, rather than solely methodological problems.

In conclusion, the data collected clearly demonstrated that these methods did not have the degree of sensitivity necessary to detect the quantity of biofilm that was present. Therefore, for EPS to be studied in this way, a greater volume of biomass would need to be accumulated, either by extracting biofilm from a greater surface area, or by allowing the biofilm to develop for a longer period of time. However, to increase the surface area from which biofilm is extracted would require more or larger coupons. Previous experiments have demonstrated

that increasing the frequency of apertures within each loop, to allow for the insertion of more coupons, placed great stress on the pipe, causing it to distort and subsequently experience frequent leaks. Moreover, re-design of the coupons to enlarge the surface area was not possible due to the diameter of the pipelines within the experimental facility. Additionally, due to other studies requiring the use of the experimental facility, experiments much longer than a month would not currently be feasible and many further preliminary trials would be required to ascertain the time point at which biofilm quantities would be sufficient to enable detection.

Table 4.4 Concentration of protein in EPS extracted from 1070.80 mm² of drinking water biofilms using the CER and EDTA methods (\pm confidence interval).

Replicate	Protein Concentration ($\mu\text{g ml}^{-1}$)	
	CER	EDTA
1	0.027 \pm 0.028	0.072 \pm 0.028
2	0.056 \pm 0.028	0.037 \pm 0.028
3	0.033 \pm 0.028	0.009 \pm 0.028
<i>Mean</i>	<i>0.039</i>	<i>0.039</i>
<i>Standard Deviation</i>	<i>0.015</i>	<i>0.031</i>

4.5 Method Development and Optimisation: Fluorescent Microscopy Imaging of EPS

4.5.1 Fluorophores and biofilm staining protocols

Several fluorophores (Molecular Probes, Carlsbad, California, USA) with different target components (Table 4.5) were evaluated and subsequently selected on the basis of their previous application to microbial aggregates in the literature (e.g. McSwain *et al.*, 2005; Wagner *et al.*, 2009), their suitability for CLSM analysis and their distinct excitation/emission spectra (facilitating separation when applied in combination). To visualise cells, fluorophores targeting nucleic acids (DNA and RNA) were tested; Syto 9, BacLight Live-Dead and Syto 63. Although DAPI (4',6-diamidino-2-phenylindole) was used to visualise attached cells in a previous study using epifluorescent microscopy (Deines *et al.*, 2010; Sekar *et al.*, 2012), this fluorophore was not selected for use with CLSM analysis as no suitable single photon laser was available and the multiphoton laser damaged the sample (Appendix A7.1). It should be acknowledged that the fluorophores applied to target the cells, stain intracellular as well as extracellular DNA or RNA. However, extracellular DNA in the EPS has been reported at very low concentrations and, as is suggested in Ivleva *et al.* (2009), it is likely to be present in concentrations below the limit of detection of staining methods (if present at all). From here on, the nucleic acid stains and associated results are referred to in terms of cells.

The EPS was identified by targeting the two major components: carbohydrates and proteins. Proteins were stained with SyproOrange or fluorescein-5-isothiocyanate (FITC), which reacts with amines and has been successfully used in staining aerobic flocs and granular sludge (Schmid *et al.*, 2003; McSwain *et al.*, 2005). Before staining with FITC, samples were pre washed in 0.1 M sodium bicarbonate (as described in Chen *et al.*, 2007a), to retain the amines in non-protonated form. Two concanavalin A (Con A) lectin conjugates which bind to the carbohydrates of the EPS were evaluated – con A tetramethylrhodamine (Con A Rho) and Alexa Fluor 647. Single, paired and triple comparisons of these fluorophores were assessed for their application to drinking water biofilms.

The inserts taken from the preliminary biofilm samples (see section 4.3) were fixed in 5% formaldehyde for 48 hours at 4 °C, rinsed in PBS (3 x 1 minute washes) and then stored in PBS at 4 °C ready for staining (Pawley, 2006). Samples were stained using a 300 µl volume of the appropriate fluorophore solution before being incubated at room temperature (see Table 4.5 for concentration and incubation details). Sterile inserts (n=3) were stained with the same fluorophore combinations as samples to act as controls. Where combinations were tested, fluorophore application was in two or three stages, following the sequence: cell (nucleic acid) – protein – carbohydrate, with three intermediate washing stages of 1 minute, using sterile PBS, to remove excess stain. Once stained, the samples were left to air dry for 10 minutes and stored, in the dark, at 4 °C ready for CLSM imaging – all samples were imaged within 21 days of staining.

Table 4.5 Fluorophores (fluorescent stains) evaluated in this study, including the staining and imaging details.

Fluorophore	Target Component	Concentration Applied	Incubation Time (minutes) ^A	Excitation ^B (nm)	Emission ^C (nm)	Lambda Range ^D (nm)	Reference
Syto 9	Cells (DNA)	1 μ M	15	488	498	500.9-704.2	Lawrence <i>et. al.</i> , 2003
BacLight Live-Dead (Syto 9 / Propidium Iodide)	Cells (DNA)	As supplied	30	488	498/635	500.9-700.4/650.7-704.2	Dror-Ehre <i>et al.</i> , 2010; Ling & Liu, 2013
Syto 63	Cells (DNA and RNA)	20 μ M	30	633	673	650.7-704.2	McSwain <i>et al.</i> , 2005
SyproOrange	Protein	1:5000 ^E	15	488	570	500.9-704.2	Lawrence <i>et. al.</i> , 2003; Wagner <i>et. al.</i> , 2009
Fluorescein-5-isothiocyanate (FITC)	Protein (amines and amino-sugars)	0.1 mg ml ⁻¹	60	488	520	500.9-704.2	McSwain <i>et al.</i> , 2005
Concanavalin A tetramethylrhodamine (Con A Rho)	α -mannopyranosyl and α -glucopyranosyl sugars	0.1mg ml ⁻¹	30	543	580	554.4-704.2	McSwain <i>et.al.</i> , 2005; Chen <i>et. al.</i> , 2007a; 2007b; Shumi <i>et. al.</i> , 2009
Alex Fluor 647	α -mannopyranosyl and α -glucopyranosyl sugars	0.1 mg ml ⁻¹	30	633	668	650.7-704.2	Dror-Ehre <i>et al.</i> , 2010

^ADuring incubation samples were protected from light. ^BExcitation wavelength used in this study, 488 nm-argon laser, 543 nm and 633 nm-He/Ne lasers. ^CEmission maxima according to supplier(s); ^DLambda detection range used in this study; ^ESyproOrange provided at 5000x concentration, diluted 1:5000 using 7.5% acetic acid.

4.5.2 Confocal Laser Scanning Microscopy (CLSM) imaging methods

4.5.2.1 Optimising settings

A LSM510 meta upright confocal microscope and LSM510 software (Zeiss, Germany), within the Kroto Imaging Facility (The University of Sheffield, UK), were used to produce Z-stack and lambda-Z-stack images; a series of XY images (slices) taken at different optical depths (Z) and, for the lambda-Z-stacks, over a wavelength range (lambda) specific to each stain (see Table 4.5 for details). Three different single photon lasers were used: 488 nm - argon laser, 543 nm helium/neon laser and 633 nm helium/neon laser. During optimisation of the CLSM settings it became apparent that the air conditioning unit was causing a drift in the images. Thermal drift has also been reported to occur when imaging over long periods, so samples were removed from 4 °C storage and the air conditioning unit was turned off 30 minutes prior to imaging, to allow the room and sample temperatures to stabilise. Temperature was monitored throughout (average 24.6 °C ± 1 °C) using an EL-USB1 temperature logger (Lescar Ltd., Salsbury, UK).

All images were taken using a x20 EC Plan Neofluor objective (0.5 NA). Different objectives were tested but the x20 generated a frame size of 420 µm x 420 µm, which provided the best compromise between capturing the detail of the biofilm while also incorporating the heterogeneity of the biofilm coverage across the insert. A resolution of 832 pixels x 832 pixels was selected to facilitate detection of a single cell (1 pixel = 0.51 µm). The default optimal settings for the pin hole were for an optical slice of 4.7 µm, with an optimal optical interval of 2.35 µm and a 31.54 µs scan speed (time spent scanning each pixel). Z-stacks are advised to be taken in such a way that the slices are staggered so that each slice overlaps the previous by 50% - this is the optical interval. However, with the aim of imaging three stains, at seven fields of view (FOV) per sample, it was calculated that it would take almost 30 hours to image a single sample. Due to the study time constraints, it was necessary to optimise these settings to produce the best possible image within the most reasonable time frame. Therefore, a preliminary test (n=3, with three FOV) imaging a z-stack of 5 slices was conducted to investigate the impact of altering scan speed and optical slice thickness, upon total imaging time and image quality. Three optical thicknesses were assessed: 4.7 µm, 7.1 µm and 9.5 µm, at a scan speed of 31.54 µs. Three scan speeds: 31.54 µs, 15.77 µs and 7.89 µs were assessed at an optical thickness of 4.7 µm. Altering the optical thickness did not reduced the imaging time as much as altering the scan speed did (see Appendix A7.2). Also, altering the scan speed did not physically alter the Z-stack optimal proportions, rather it altered the exposure time,

which retained, to a greater degree, the level of detail and quality of the images produced using the optimised settings. Therefore, scan speed was chosen as the parameter to alter and, after further optimisation tests (Appendix A7.3), a specific speed of 3.94 μ s was selected for use with the optimal optical thickness of 4.7 μ m (pin hole adjusted accordingly for each stain).

4.5.2.2 Imaging and unmixing samples

Unstained biofilm samples and sterile inserts (n=3) were imaged, using the established optimal settings for each fluorophore, to control for autofluorescence of the HDPE scaffold and/or the unstained biofilm biomass. Each of the samples or controls was imaged at seven FOV to provide an accurate representation of the EPS distribution and composition, relative to that of the cells. Single slice images and multi-slice Z-stacks were taken using both single track and lambda mode with the appropriate excitation and emission wavelengths (see Table 4.5 for details) and the detector/amplifier offset settings for each stain were optimised so that pixels covered the range of under- to over-exposed.

In order to separate the fluorophores and autofluorescence, reference spectra were obtained for the unstained biofilm, unstained plastic and each individual fluorophore, when excited by each laser. Triplicate samples or controls were analysed in lambda mode and representative spectra were obtained for seven FOV for each sample (n=21). The emission spectra were analysed graphically and statistically (ANOVA) using R v2.15 (R development team, 2012). The similarity of emission spectra across the seven FOV of a sample was assessed, as was the similarity between the three replicates, before an “emission fingerprint” (reference spectra) was assigned to the fluorophore, unstained biofilm or unstained plastic, at each excitation. All the emission fingerprints were saved in a spectra database. Dual or triple stained samples were then imaged in lambda mode and the signals separated using the linear unmixing function of the LSM510 software combined with the predetermined reference spectra from the database.

Linear unmixing essentially separates the total emission signal of a pixel into weighted contributions of the stain and background autofluorescence based on the “emission fingerprints” of each, which are stored in the spectra database. This uses and compresses the lambda aspect of the images resulting in a Z-stack which contains “channels” for each of the “emission fingerprints” for which it was unmixed. For instance, imaging and unmixing a sample stained for the cells and carbohydrates would produce a Z-stack generated under the correct image settings for the cell stain, which would be unmixed into four channels: 1 -

autofluorescence of the biofilm; 2 – autofluorescence of the insert; 3 – fluorescence of the cell stain; 4 – any response of the carbohydrate stain to the cell stain image settings. A second Z-stack would be generated under the carbohydrate image settings, this would contain the same four channels as the first when unmixed but channel 3 would be the fluorescence of the carbohydrate stain and 4 would be the response (if any) of the cell stain at the carbohydrate stain image settings. In each case, channel 3 contained the stain specific images which are the images showing the cells and carbohydrates without the background autofluorescence.

4.5.3 Results and discussion: fluorophore combinations

4.5.3.1 Autofluorescence of controls

None of the fluorophores stained the sterile insert controls, however a signal was observed due to auto-fluorescence of the unstained plastic surface. Unstained biofilm samples also auto-fluoresced when exposed to each excitation wavelength (488 nm, 543 nm and 633 nm), see Figure 4.3A for an example. In order to remove this signal from the images, it was necessary to use lambda mode rather than single track mode. Therefore, emission spectra were obtained for seven FOV for each of the three unstained plastic and biofilm samples, at each wavelength, using each of the configurations optimised for each fluorophore. No significant difference was found between the seven FOV in each case (e.g. Figure 4.3B) so the median spectra was assigned to each unstained plastic or unstained biofilm replicate. These three spectra (one per replicate) were compared (e.g. Figure 4.3C) and, as there was no difference between them, the median emission spectra was selected as the reference signal in each case.

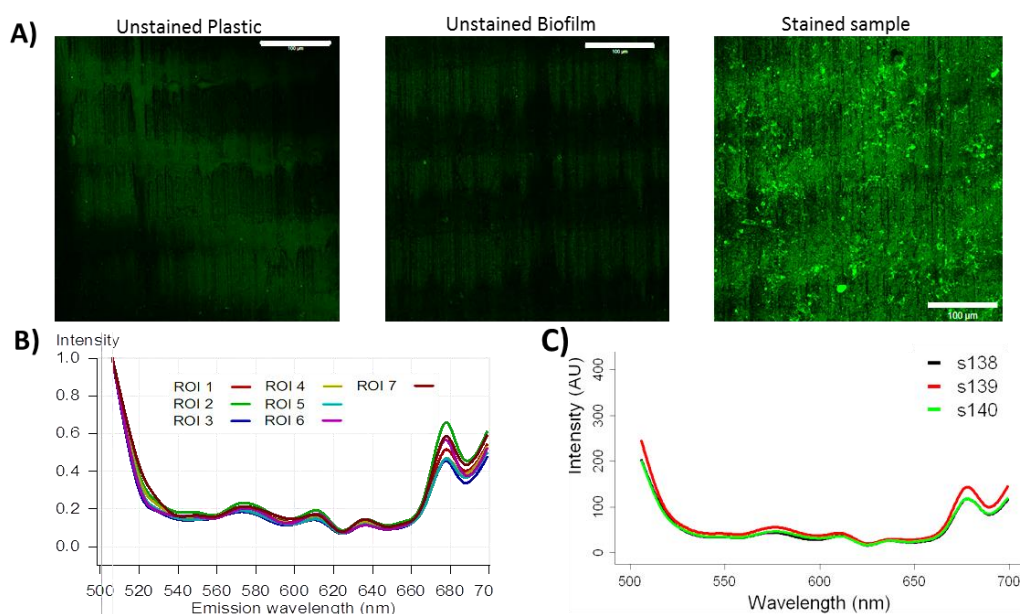


Figure 4.3 Auto-fluorescence of the unstained controls, imaged at 488 nm. A) Example of the unstained plastic and biofilm compared to a FITC stained sample, scale bar 100 µm; B) Unstained biofilm emission spectra from seven FOV, intensity units AU; C) Emission spectra for three unstained biofilm samples.

4.5.3.2 Individual fluorophores

Removal and separation of autofluorescence and fluorophore signals required lambda stack imaging, which allowed each component to be identified and isolated based on its emission spectra. For this separation process (termed linear unmixing) to be accurate a reference spectrum was required for each fluorophore (as well as the unstained controls) as explained in section 4.5.2.2. Consequently the emission spectrum of each fluorophore (Table 4.5) was determined via individual application to drinking water biofilm samples and lambda imaging. In all cases there was no significant difference between the signals produced by replicates ($n=21$) and so the median spectrum was assigned as the reference spectrum/emission fingerprint in each case.

4.5.3.3 Dual fluorophore combinations

Dual fluorophore combinations were analysed targeting: cells and carbohydrates, proteins and carbohydrates, cells and proteins (Table 4.6). For fluorophores to be successfully applied in conjunction and subsequently separated, each must have distinct excitation/emission spectra, criteria which were considered when selecting the combinations to test. The compatibility of stains was evaluated via dual application to biofilm samples and linear unmixing using the previously obtained reference spectra for each fluorophore, at all imaging configurations.

Some of the fluorophore combinations did not allow for clear spectral separation (Table 4.6) due to highly overlapping spectra in conjunction with large differences in fluorescence intensity. In particular, SyproOrange exhibited particularly high fluorescence intensities at each excitation wavelength (Figure 4.4A), masking any other signals produced. Furthermore, although SyproOrange should be excited only at 488 nm, spectra distinct from the autofluorescence controls were produced at 543 nm and 633 nm, which suggested that this stain had a broad excitation range. Although combination 6 (Table 4.6) has been successfully used previously to stain cells and proteins of biofilm from an annular reactor (Lawrence *et al.*, 2003), within the context of the drinking water biofilm samples in this study, these two stains could not be separated. Despite the broad excitation behaviour of SyproOrange, which was still excited at 633 nm (Figure 4.4), albeit at intensity less than at 543 nm, this stain was able to be separated from Alexa Fluor 647 which was also excited at 633 nm (Table 4.6).

In contrast to SyproOrange, FITC expressed a narrower excitation spectrum, only producing a distinct emission spectrum when excited at 488 nm (Figure 4.4). At 543 nm and 633 nm the FITC spectra were no different from the autofluorescence reference spectra (ANOVA, $p=0.7018$

and $p=0.7182$, respectively). Consequently FITC was successfully separated from, and used with, fluorophores emitting across the 554.4–704.2 nm and 650.7–704.2 nm wavelength ranges (Table 4.6, combinations 8 and 11) rather than being limited to separation from fluorophores with an emission at the far red wavelengths (650.7–704.2 nm), as was the case for SyproOrange.

Successful fluorophore pairs were established for staining cells and carbohydrates (combinations 1, 2 and 4), carbohydrates and proteins (combinations 10 and 11), or cells and proteins (combination 8; Table 4.6). By applying two pairs of complementary fluorophores which have a common target component between them, e.g. Syto 63 (cells)\Con A Rho (carbohydrates) and FITC (proteins)\Con A Rho (carbohydrates), it was then possible to stain the three desired biofilm elements but only on separate replicates of the same sample type.

Table 4.6 Fluorophore combinations applied to the biofilm samples in this study.

Target Biofilm Components	Combination Reference No	Fluorophore Combination ^A	Successful Separation ^B
Cells (nucleic acids) and Carbohydrates	1	Syto 9 and Con A Rho	✓
	2	Syto 9 and Alexa Fluor 647	✓
	3	BacLight Live-Dead and Con A Rho	X
	4	Syto 63 and Con A Rho	✓
	5	Syto 63 and Alexa Fluor 647	X ^C
Cells and Proteins	6	Syto 9 and SyproOrange	X
	7	Syto 9 and FITC	X ^C
	8	Syto 63 and FITC	✓
Proteins and Carbohydrates	9	SyproOrange and Con A Rho	X
	10	SyproOrange and Alexa Fluor 647	✓
	11	FITC and Con A Rho	✓
Cells, Proteins and Carbohydrates	12	Syto 63, FITC and Con A Rho	✓

^A See Table 4.5 for excitation/emission details of each individual fluorophore; ^B ✓ indicates emission spectra of the two fluorophores could be resolved, X indicates spectra could not be resolved; ^C Eliminated based on theoretical incompatible excitation/emission spectra rather than empirical evidence.

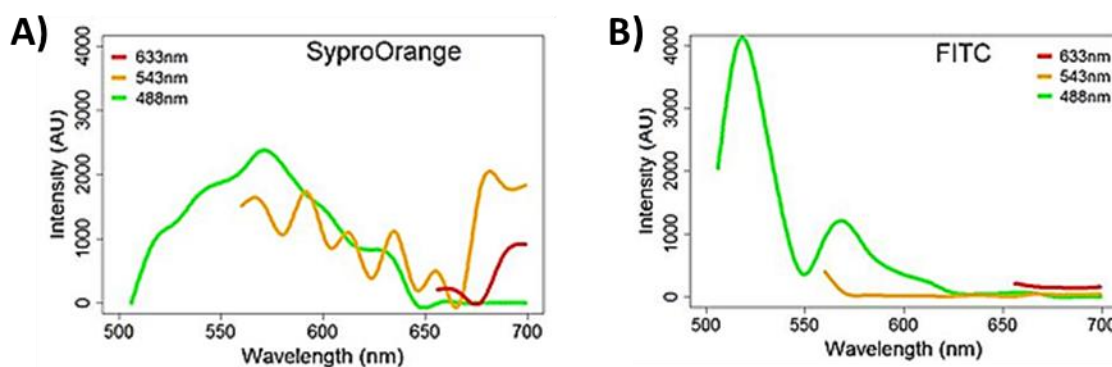


Figure 4.4 Emission spectra of protein fluorophores. A) SyproOrange; B) FITC. Image settings: 488 nm-fluorophore specific, 543 nm- as for Con A Rho, 633 nm-as for Syto 63. AU – Arbitrary Units.

4.5.3.4 Triple fluorophore combinations

In order to concurrently visualise biofilm cells and EPS (proteins and carbohydrates) *in situ* a triple fluorophore combination was required, which would subsequently allow the distribution of each element to be established in relation to the others, within the same sample. Based on the successful dual combinations 4, 8 and 11 (Table 4.6), the application of a triple staining combination (number 12) to drinking water biofilm was evaluated comprising Syto 63 (cells)\FITC (proteins)\Con A Rho (carbohydrates). This combination was used by Chen *et al.* (2007) and a similar combination, using Con A Texas Red rather than Con A Rho, was used by McSwain *et al.* (2005) to stain aerobic granules cultivated in accordance with a wastewater environment. However, no evidence was available documenting the application of this combination to drinking water biofilms.

4.5.3.5 Summary

Biofilm samples from the DWDS experimental facility were stained and successfully imaged in lambda mode using sequential excitation at 488 nm, 543 nm and 633 nm. The images were unmixed as described previously, to separate the autofluorescence and fluorophore; the emission fingerprints used in each instance (Figure 4.5) were representative spectra selected as explained in section 4.5.2.2; the fingerprints were not generated as an average emission pattern based upon spectra from all the samples. The successful application of this triple fluorophore combination demonstrated the compatibility of these stains and the ability of this approach to concurrently visualise the biofilm cells and EPS (proteins and carbohydrates).

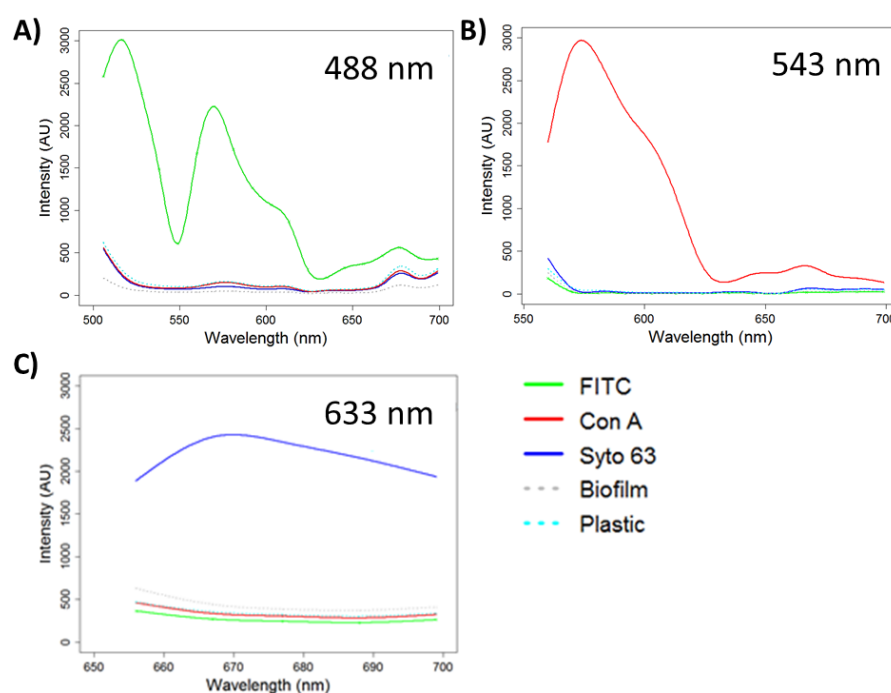


Figure 4.5 Reference spectra for the triple stain combination. A) Emission at 488 nm excitation, image settings for FITC; B) Emission at 543 nm excitation, image settings for Con A Rho; C) Emission at 633 nm excitation, image settings for Syto 63.

4.6 Digital Image Analysis (DIA) of Triple Stained Samples

Following the establishment and optimisation of a compatible triple staining and imaging approach (Fish *et al.*, 2011), a series of author written scripts (Fish *et al.*, 2012), were used to: reduce the image noise; generate a threshold; overlay, and render unmixed images; calculate various quantification parameters; and analyse the resultant data. A combination of the freely available programs Python and R2.15 were used during the DIA.

4.6.1 Median filters

When using the far red spectra (excitation 633 nm) images have greater random background noise associated with them. This was observed by McSwain *et al.* (2005) when imaging a sample stained with Syto 63 and it was also observed during the course of the research presented here. Noise is defined as discrete pixels which differ significantly in their fluorescence intensity from their neighbouring pixels. Several methods have been used to reduce noise in images across a range of disciplines, from microbial microscopy (Hanninen *et al.*, 1991; van Kempen & van Vliet, 2001) to astronomy (Privett, 2007). Where it is desirable to maintain a fine level of detail, non-linear filters are commonly used, particularly median filters (Privett, 2007). Median filters are advantageous as they highlight subtle features but do not over-process the image and provide a rigorous, repeatable technique for outlier control. Basically, a median filter examines a central pixel and compares it to neighbouring pixels to determine if the central pixel is spurious; if it is then it will be replaced with the most likely value generated from its neighbours. This process is repeated for every pixel in the image. Here a 3 x 3 median filter was applied to all slices of every unmixed Z-stack image series before quantification, thresholding or visualization was carried out.

4.6.2 Thresholding

Due to the weighting aspect of the linear unmixing, not all of the pixels within an image will be an exact match to a single emission fingerprint. Some pixels may express an element of similarity to the autofluorescence signals as well as to a particular stain and would, therefore, be assigned a reduced intensity of colour in comparison to those pixels with 100% affinity with the emission fingerprint of the stain. For this reason, it is necessary to determine a threshold in order to separate each stained image into two regions: a “particle region” in which everything is considered as the particular stained component (cells, carbohydrates or proteins) and a “background region”. For example, with the CLSM images presented in this study, a threshold

value of 1 would assign all of the pixels associated with a particular stain to the “particle region”, regardless of the weighting. Thus even a pixel with 0.1% affinity to the stain would be classed as being comprised entirely of the component of interest. In this study the possible threshold values ranged from 1 to 4001 (Figure 4.6A).

A specific threshold value was determined for each stain using area fraction data (explained in section 4.6.3) from all the imaged SS biofilm samples. As this study focuses on relative rather than absolute quantities, the data for each threshold was normalised by the maximum value and analysed graphically and statistically (Kruskal Wallis test) using R v2.15 (R Development Core Team, 2012) to determine the largest range of thresholds between which there was no significant difference in the normalised data (e.g. Figure 4.6B). The median of the range was then chosen as the threshold value for the particular stain: Syto 63 (DNA/cells) threshold 2401, Con A Rho (carbohydrates) threshold 1701, and FITC threshold 1701.

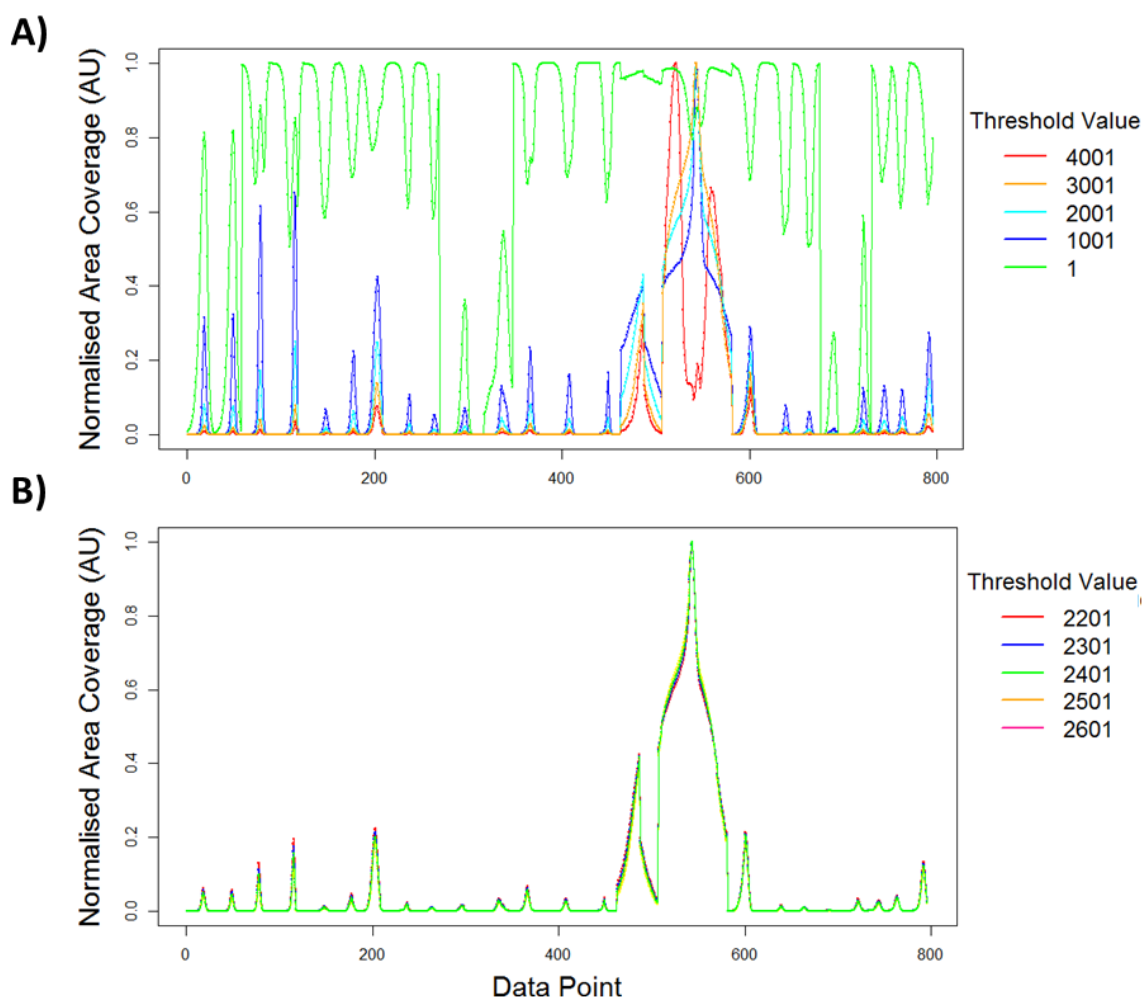


Figure 4.6 Example of the normalised data at different threshold values. A) Range from 1-4001 threshold values, showing the distinction between the extremes of 1 and 4001; B) Narrowed range of thresholds for which there was no difference. Dataset shown is the cell coverage (stained with Syto 63) from the pre-flush stage of the SS experiment.

The pitfalls of thresholding are well acknowledged (Yang *et al.*, 2001; Staudt *et al.*, 2004) but selecting a threshold in this way removes any investigator bias. Furthermore, it standardises the thresholding process maintaining a constant thresholding value between samples, removing any individual FOV influences, facilitating comparisons between datasets and providing reliable, replicable, relative data. It should be noted that due to the nature of any EPS analysis technique, either physical extraction or fluorescent staining, it is difficult to provide absolute data as the complete extraction or staining of particular components cannot be proven.

4.6.3 Biofilm physical structure: quantification analysis

A range of parameters were calculated to assist in characterising the biofilm physical structure, namely the distribution and volume of each stained component. All of the quantification measures use data from unmixed, median filtered and thresholded images. The example data provided in the following sections, to aid explanation of the different parameters, is not from the preliminary biofilm samples, but from the initial imaging of three SS, Day 28 biofilm samples – one from the middle position of each of the three loops of the experimental facility.

4.6.3.1 Calculating area fraction

Initially the area covered by each stain, per slice, for each z-stack (i.e. each FOV) for each sample (i.e. each insert) was expressed as a fraction, calculated by dividing the number of stain associated pixels (at the given threshold) by the total number of pixels in the image (832 x 832). These “area fractions” were generated for all the possible threshold values and were used to determine the thresholds for each stain as outlined in section 4.6.2. Subsequently, only the data for each of the selected thresholds (Syto 63 – 2401, Con a Rho – 1701 and FITC – 1701) was used.

4.6.3.2 Area distribution throughout the biofilm

Area fractions were calculated for each slice of each Z-stack (one Z-stack is one FOV). The slices of an individual Z-stack were numbered consecutively following the order in which the CLSM captured the images; hence “slice 1” refers to the image taken at the position deemed to be the top of the biofilm. However, because “slice 1” of each FOV is not comparable (the location of the top of the biofilm varies), the slices of each z-stack were normalised by alignment to the slice at which the maximum area fraction of cells (stained with Syto 63) occurred. The cells were chosen as the component to align to because they produce the EPS and, in physical

extraction EPS analysis, the EPS quantity is commonly related back to the cells. Alignment was achieved using the equation:

$$\text{Slice Number}_{\text{Aligned}} = \text{Slice Number}_{\text{raw}} - \text{Slice}_{\text{cellmax}} \quad \text{Equation 4.2}$$

Where $\text{Slice Number}_{\text{raw}}$ is the original placement of the slice in the Z-stack, and $\text{Slice}_{\text{cellmax}}$ is the number of the slice at which the maximum cell coverage is observed. So, for example, if the cell maximum area fraction occurred on “slice 12” of the original Z-stack, then “slice 1” would become “slice -11” in the aligned data, “slice 2” would become aligned “slice -10”, etc.

In order to quantitatively evaluate the distribution of each biofilm component, the area fraction covered by each stain was plotted against biofilm depth. Biofilm depth was determined by multiplying the aligned slice number by the thickness (4.7 μm) of each slice. An example of an “area distribution plot” is shown in Figure 4.7, which includes the cell, carbohydrate and protein data, as indicated, for the three replicates from SS, Day 28 biofilms. Each line represents a single FOV and the colour of each line indicates the biofilm sample from which the FOV was taken (see key for details). It should be noted that the x-axis scale is different for each of the stained biofilm components and the range in each case was selected to allow for consistency throughout this thesis, to facilitate comparison between results.

Due to the alignment process, the maximum area fraction of the cells always occurs at a biofilm depth of 0 μm , any slices above this point in the biofilm have a negative biofilm depth value and any slices below this point have a positive value. To reflect this, the y-axis runs from the largest positive value, through zero, to the most negative value; the values nearer the x-axis (positive values) correspond to the biofilm-plastic interface (i.e. the bottom of the biofilm), while the values furthest from the x-axis (negative values) correspond to the biofilm-bulk water interface (i.e. the top of the biofilm).

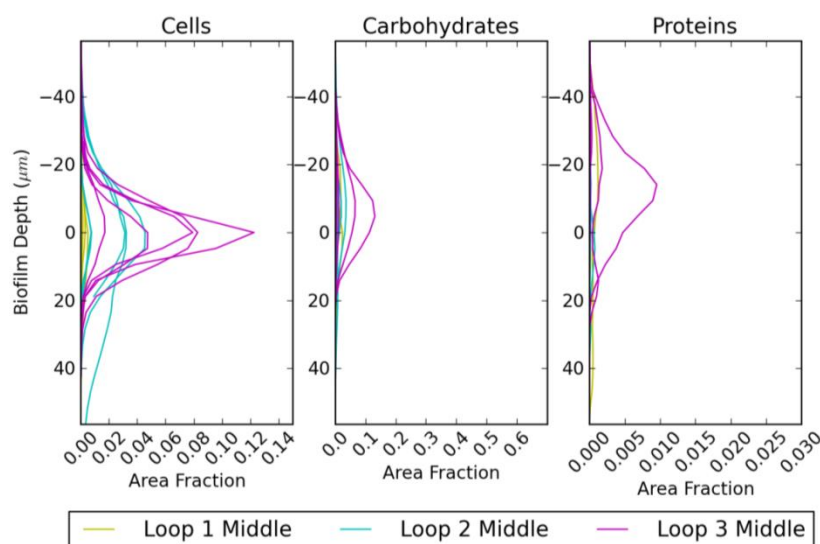


Figure 4.7 Area distribution of cells, carbohydrate and proteins throughout Day 28 biofilms developed under SS hydraulic conditions. Three replicates are shown, one from each loop. Note the difference in scale of the x-axis, for the different biofilm components.

4.6.3.3 Calculating relative volume

The relative volume (μm^3) of each of the targeted components (i.e. cells, carbohydrates and proteins) was generated using the equation:

$$\text{Relative Volume} = \frac{dZ}{2} \times \text{Image Area}_{\text{Total}} \times \sum_{i=a}^b \text{Area Fraction} \quad \text{Equation 4.3}$$

Where dZ is $4.7 \mu\text{m}$, $\text{Image Area}_{\text{Total}}$ is $420 \mu\text{m} \times 420 \mu\text{m}$, a is the first slice of the Z-stack, b is the last and Area Fraction (see 4.6.3.1 for details) is the proportion of the slice covered by the particular stain for which volume is being calculated. Additionally, using the relative volume, the total EPS and biofilm volumes were calculated and ratios of carbohydrate to protein, carbohydrate to cells and protein to cells were produced to allow quantitative analysis of the EPS composition. As the relative volume was calculated in the same way for each stained component, the results for cells, carbohydrates and proteins can be compared.

4.6.3.4 Calculating the spread

In order to establish the extent to which a component (i.e. cells, carbohydrates or proteins) occurs throughout the biofilm, without the bias introduced by using percentiles (which would require further thresholding but at an arbitrary number), a parameter termed “spread” was calculated, defined as:

$$\text{Spread} = \frac{\text{Relative Volume}}{\text{Area Fraction Peak}} \quad \text{Equation 4.4}$$

This enabled the distinction between differently shaped area distribution plots, as highlighted in Figure 4.8, where three distributions with different relative volumes and area fraction peaks, are shown to express different values of spread. In essence, the greater the spread value the greater the range of biofilm depth covered by the component in question.

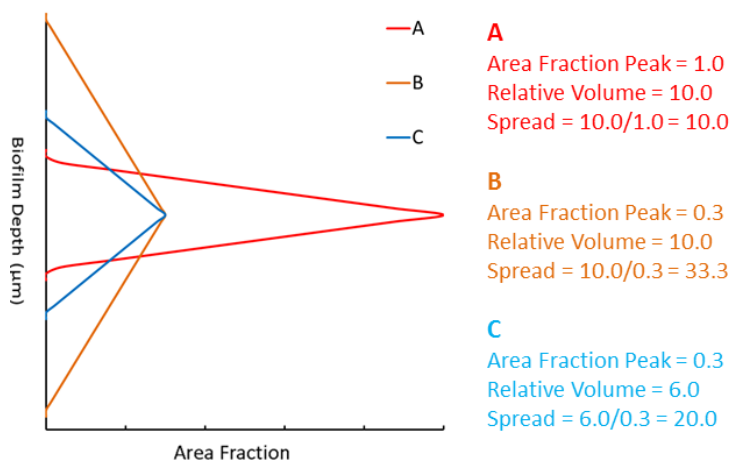


Figure 4.8 Schematic representation of three different hypothetical area distributions and their spread values calculated as indicated.

4.6.3.5 Analysis of peak location

The maximum area fraction, also termed the “peak” of the area distribution, was recorded for each stained component and the location at which this occurred was expressed in terms of the aligned slice number. As the cell datasets were used as the data to align to, the cell “peak location” was always zero, therefore analysis of the peak location was restricted to the carbohydrates and proteins.

4.6.3.6 Analysis summary of the physical structure parameters

The normality of the relative volume, spread and peak location data was assessed using the Shapiro Wilks test and in all cases the data was determined to be not normally distributed ($p < 0.05$). Therefore, non-parametric statistical tests (Kruskal Wallis and/or Wilcoxon) were used to determine any differences between samples. The raw data were plotted using a scatter plot and a box and whisker plot was overlaid, indicating the: total range, interquartile range and median.

4.6.3.7 Replication of three vs. five inserts

During the DIA of the initial biofilm samples, three middle biofilms from each of the three loops were imaged at seven FOV. Therefore, for the SS Day 28 sample point, the total number of FOV imaged was 21, with a total of 63 Z-stacks imaged overall because each stained component (i.e. cells, carbohydrates and proteins) had to be imaged separately. However, it

would be advantageous to also characterize biofilms from the crown and invert positions in order to determine if the biofilm physical structure is similar around the pipeline. Due to the laborious nature of generating lambda Z-stacks, the imaging time is a limiting factor with respect to the CLSM analysis. It was determined that the current study did not allow enough time to image a crown, middle and invert biofilm from each of the three loops (nine biofilm samples in total), each at seven FOV, which would be a total of 63 FOV, comprised of 189 Z-stacks. Consequently, a subset of five of the nine available biofilm samples was selected, which comprised the middle biofilm from each loop along with the crown and invert biofilms from loop 2. Each of these samples was imaged at seven and five FOV to determine the error associated in each case. The average relative volume of each stained component, per sample, as determined when imaged at seven or five FOV, is shown in Figure 4.9. The standard deviations at five FOV were not, however, significantly different from those at seven FOV (Wilcoxon, $p > 0.05$). Therefore, all subsequent samples were imaged at five FOV and a total of five biofilm samples (i.e. inserts) were characterized per sample point. In this way the effect of position on biofilm structure could be assessed along with the similarity between the loops, within the time constraints of this study, in order to generate a reliable and representative characterisation of the biofilm.

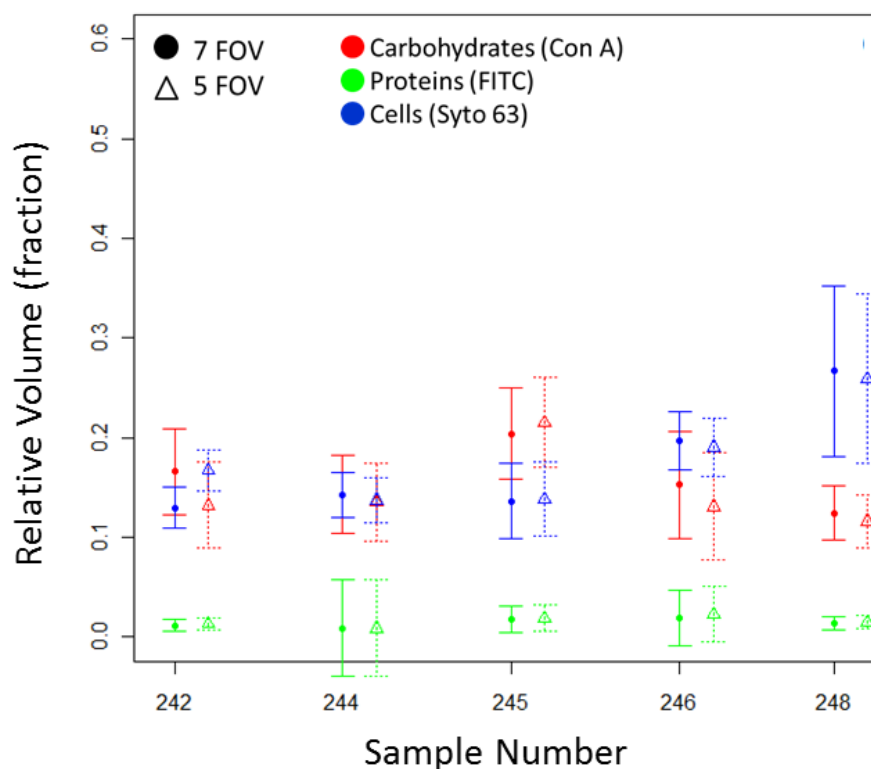


Figure 4.9 Relative volume of cells, carbohydrates and proteins from Day 28 biofilms when imaged at five and seven FOV. Note that relative volume is expressed in this instance as a fraction to enable each stained component to be assessed easily on the same plot. Means are plotted ± 1 standard deviation.

4.6.4 Biofilm physical structure: qualitative analysis

It was not possible to overlay the three z-stack galleries (one for each stain), which comprised a single FOV, using the LSM510 software (Zeiss, Germany) so a script was produced in Python to facilitate this. An advantage to overlaying the images in this way is that the median filtered data is used to produce the image and the threshold value can be set in exactly the same way as applied to the quantification analysis, thus the two sets of data are directly comparable. Each slice of the Z-stack can be visualised for each stain separately as well as overlaid, see Figure 4.10 for an example. Alternatively, a 2D Z-stack gallery can be used in which all the stains are overlaid for all of, or a specific subset of, slices (Figure 4.11). The FOV used in these images is an extreme example of a Day 28 biofilm; it does not necessarily reflect the trends seen across all the Day 28 biofilm samples. This FOV was chosen to optimise the imaging analysis process as it was the FOV with the most slices, therefore would require the most processing power. Thus settings that enabled the successful analysis of this FOV would be appropriate for all the other FOV.

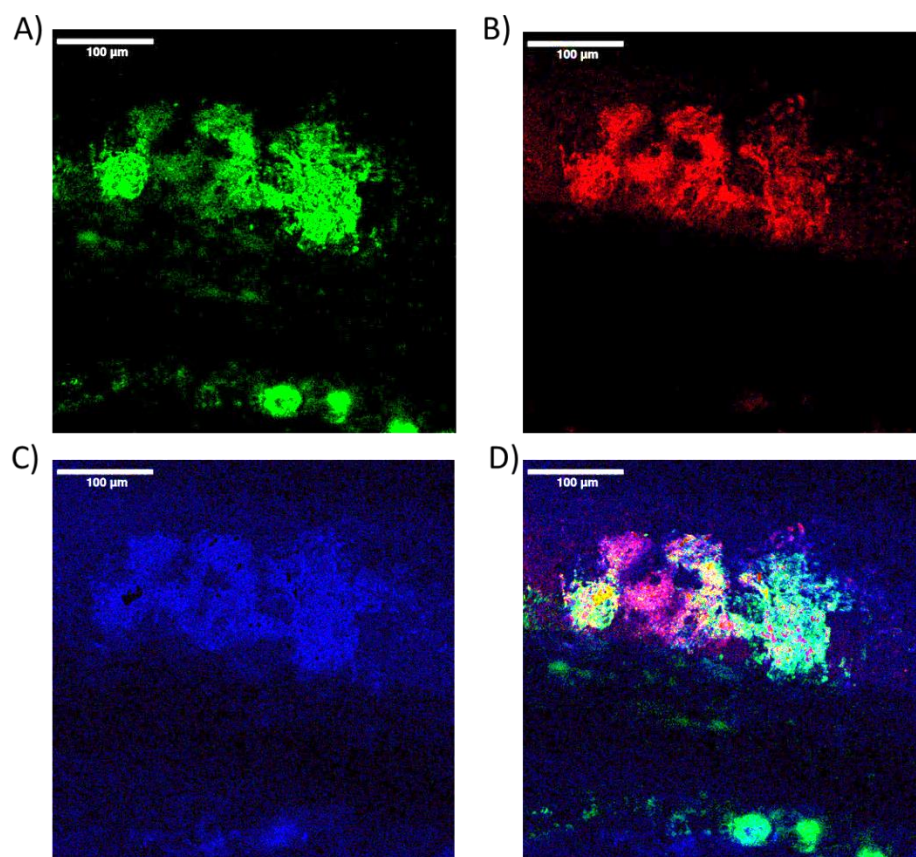


Figure 4.10 Unmixed and thresholded 2D images of a drinking water biofilm after 28 days of development at 16 °C, under the SS hydraulic regime. Image shown is a midslice of a Z-stack. A) Proteins, stained with FITC; B) Carbohydrates stained with Con A Rho; C) Cells (nucleic acids) stained with Syto 63; D) Combined image of the three components overlaid, proteins – green, carbohydrates-red, cells-blue, white areas – all three components present.

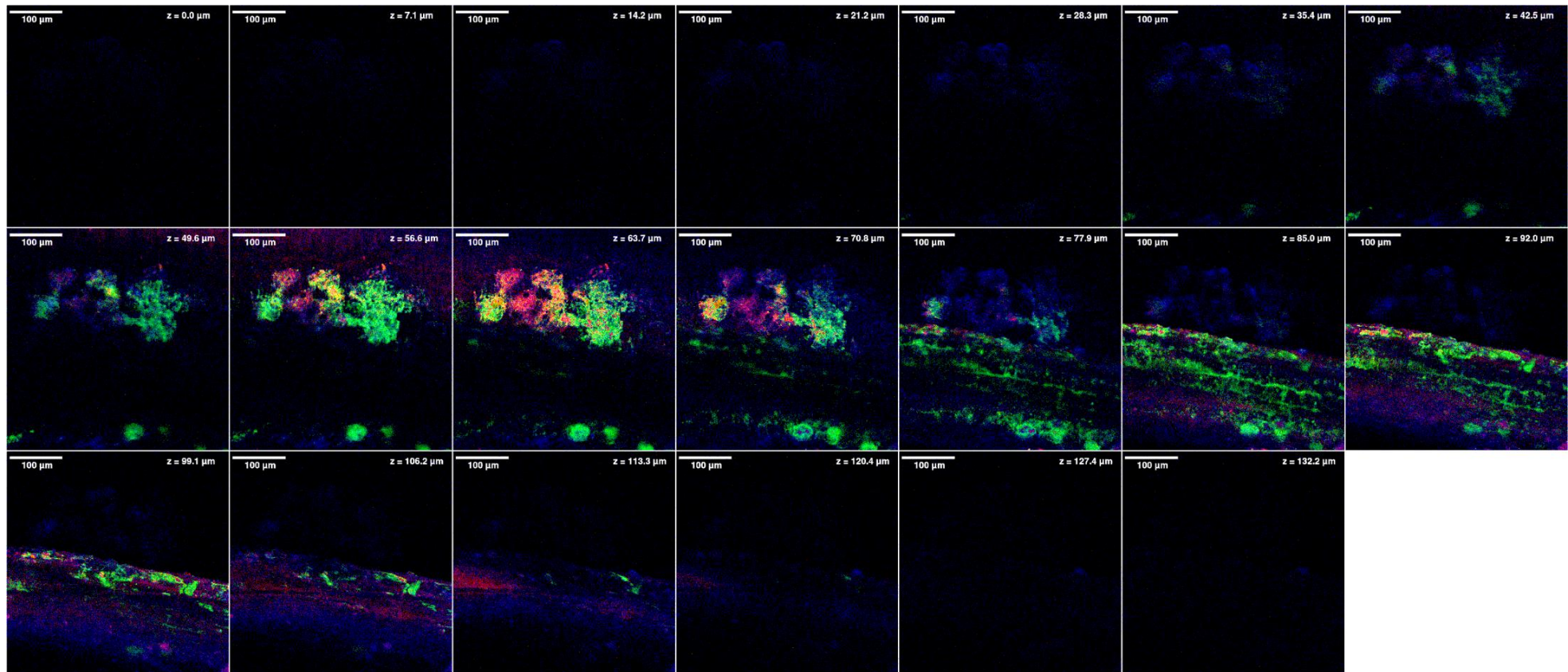


Figure 4.11 Z-stack gallery of a Day 28 biofilm using unmixed, combined images (i.e. cells, carbohydrates and proteins overlaid) for slices (XY) throughout the depth of the stack. Sample shown is a Day 28 sample developed at 16 °C under the SS hydraulic regime, every third slice of the z stack is shown, scale bar is 100 μm as indicated.

A 3D projection of each Z-stack was produced (e.g. Figure 4.12), using Para View (v.3.14.0), to show the arrangement of the stained components throughout the depth of the biofilm and in relation to each other. Each 3D image was generated using the median filtered data (section 4.6.1) from all the slices of a Z-stack. The colour of each stain was set to a 50% opacity level to enable the three components to be visualised more easily when they co-localised.

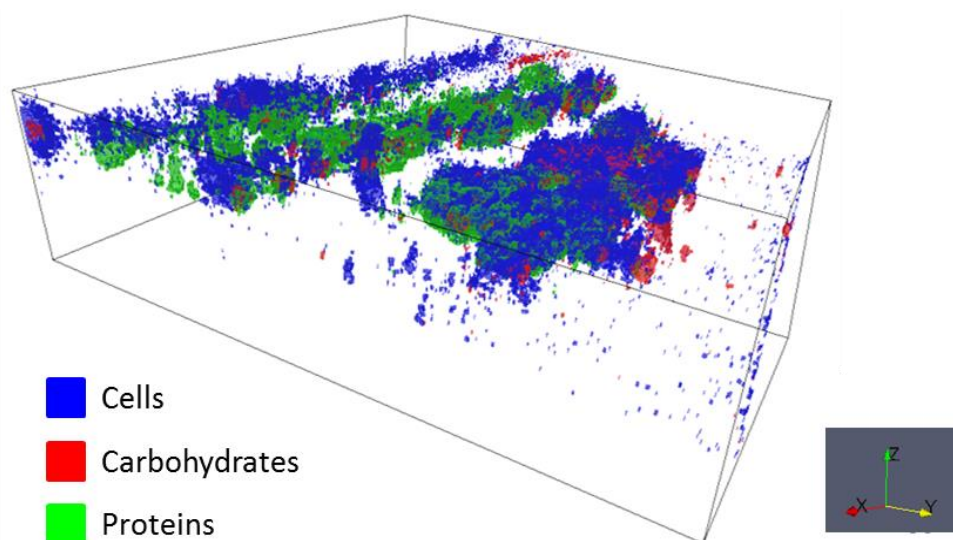


Figure 4.12 Example of a 3D projection of a Day 28 biofilm Z-stack. Sample shown is a Day 28 biofilm developed under the SS hydraulic regime at 16 °C. 3D plotting area shown by cube is 420 μm x 420 μm x 135.5 μm .

4.7 Conclusions and Outlook

The DWDS experimental facility offers a unique opportunity to study the physical structure of drinking water biofilm matrices, representative of those in real DWDS networks, with laboratory level control. After rigorous testing, it was established that the commonly used physical and chemical extraction procedures were not sensitive enough to be used to quantify the biofilm samples in this study. Following the evaluation of a range of fluorophores, with different excitation/emission properties, a triple stain combination was identified which was suitable for physical structure analysis of the drinking water biofilms, comprising Syto 63, Con A Rho and FITC to target cells, carbohydrates and proteins, respectively.

CLSM analysis has been used with bio aggregates in the past but has often been limited to cell\carbohydrate stain combinations; here fluorophores targeting proteins were also incorporated. The inclusion of proteins (stained by FITC) in a triple stain combination has previously been applied to aerobic flocs, or granular sludge, forming under physico-chemical conditions, representative of those occurring in a wastewater environment (McSwain *et al.*, 2005; Chen *et al.*, 2007a; 2007b). However, this research demonstrates the successful

application of this staining technique to the biofilms of a contrasting environment – drinking water.

Ultimately it is aimed to use this staining protocol in combination with lambda-z stacks to investigate the three-dimensional distribution of cells and EPS of biofilms grown under different hydraulic conditions, as will be presented in the following sections. Additionally, a robust and rigorous DIA was developed to: quantify the coverage of each biofilm component – area fractions; analyse its distribution – area distribution plots, peak location and spread; as well as determining the volume of each component and the biofilm composition with respect to ratios of cells, proteins and carbohydrates.

When coupled with CLSM and DIA, this triple staining approach allows concurrent visualization (qualitative analysis) and quantification to characterize the EPS matrix and cells of drinking water biofilms. In addition to providing a robust alternative tool to extraction and chemical assays, it is anticipated that the application of this triple staining approach will provide a novel insight into the matrix structure, composition and the architecture of DWDS biofilms. Furthermore this approach provides an opportunity to investigate biofilm architecture alongside community composition by using the insert from each sample for physical structure analysis and the outer coupon for biofilm community analysis.

4.7.1 Summary of the final EPS analysis method

Five replicates (inserts) from each sampling point (Day 0, Day 28, Pre-Flush and Post-flush) for each hydraulic experiment (SS, LVF, HVF) were used to investigate the biofilm physical structure. The five replicates consisted of the inserts of coupons from loop 2 (crown, middle and insert), loop 1, middle and loop 3, middle. Inserts were stained in randomly selected batches of five. Each insert was stained sequentially with Syto 63-FITC-Con A Rho (see Table 4.5 for concentrations and incubations). Samples were imaged within 21 days of staining.

A total of five FOV, selected at random (and blindly), were imaged per insert (n=5) to provide an accurate representation of the biofilm distribution at each time point (n=25). Lambda-z-stacks were taken at a bit depth of 12, using a x20 EC Plan Neofluor objective (0.5NA) and the settings shown in Table 4.7. The different stains were imaged sequentially (FITC, ConA Rho, Syto 63), this resulted in three lambda-Z-stacks (one per stain) for each FOV. Linear unmixing using reference spectra within a previously produced spectral database (Fish *et al.*, 2011;

Figure 4.5) was applied and a median filter was used to reduce the background noise. Previous unstained biofilm samples and sterile inserts were used as controls.

Table 4.7 Final details of the optimised image settings.

Image Parameter	Excitation wavelength		
	488 nm	543 nm	633 nm
Excited stain	FITC	Con A Rho	Syto 63
Laser	488 nm argon	543 nm He/Ne ^C	633 nm He/Ne ^C
Laser Power	12%	45%	54.4%
Optical Slice Thickness ^A	4.7 µm	4.7 µm	4.7 µm
Scan Speed	3.94µs	3.94µs	3.94µs
Amplifier Offset	-0.01	-0.085	-0.015
Detector Gain	800	805	790
HFT ^B	488/543/633	488/543/633	488/543/633
Lambda Range	500.9 – 704.2 nm	554.4 – 704.2 nm	650.7 - 704.2 nm
XY Frame Size	420µm x 420µm	420µm x 420µm	420µm x 420µm
XY Resolution	832 x 832 pixels	832 x 832 pixels	832 x 832 pixels
Time taken for 1 slice	2:55 minutes	1:57 minutes	0:59 minutes

^A Pin hole adjusted accordingly for each stain; ^B Main dichroic beam splitter; ^C He = helium, Ne = neon.

DIA image analysis was used to overlay the Z-stack images of each stain (either in 2D or 3D) for each FOV and generate data at thresholds of: 2401 for cells (Syto 63), 1701 for carbohydrates (Con A Rho) and 1701 for proteins (FITC). Biofilm physical structure was then characterized via analysis of:

- Distribution Parameters
 - Area distribution plots (aligned data)
 - Peak Location (aligned data)
 - Spread (aligned data)

- Relative Volume Parameters
 - Relative volume of each stain
 - Ratios of EPS-to-cells
 - Ratios of carbohydrates-to-cells, proteins-to-cells and carbohydrates-to-proteins

In combination the fluorescent staining and DIA approach outlined in this chapter provided a robust, reliable and replicable method of investigating the EPS matrix of drinking water biofilms developed under different hydraulic regimes as is presented in the following chapters.

Chapter 5: Characterising the Community and Physical Structure of a Steady State Biofilm

5.1 Introduction and Aims

Compliance with drinking water quality regulatory standards is high and measured failures are rare in the developed world but discolouration remains a common problem, accounting for many of the consumer contacts that water suppliers handle (DWI, 2007; Ginige *et al.*, 2011). Two general explanations for drinking water discolouration during distribution are provided in the literature: gravitational settling, sedimentation and subsequent mobilization of particles – the basis of the PSM model, or the “cohesive layer theory”, which suggests that interactions with the pipe wall lead to the attachment of particulate material in layers of different strengths which are detached when the shear stress exceeds that experienced during accumulation (1.2.2). Of these theories, the latter is most supported by the currently available discolouration research (1.2.2).

Following on from the “cohesive layer theory”, it is suggested that biofilms, which are known to attach to surfaces via an EPS matrix, may play a role in the accumulation of material at the pipe wall. However, much of the current understanding about biofilms in DWDS is based upon assumptions or extrapolations of findings from biofilm research in other areas or that use idealised laboratory studies, as addressed in section 1.6.1. Most prior EPS research (in general, not necessarily drinking water specific) has been based upon biofilms cultured within bench-top scale systems (e.g. Stoodley *et al.*, 2002; Simoes *et al.*, 2007), providing invaluable data for idealised systems and contributing to the development of EPS analysis techniques. Nonetheless, the resulting samples were unrepresentative of the complex, naturally occurring communities that produce and form biofilms under the various environmental pressures within a DWDS. Furthermore, the majority of studies focus only on the community structure (generally limited to bacteria) or the physical structure of biofilms, with little integration between the two. Yet the physical structure and cohesive properties of biofilms are attributed to the EPS matrix which consists primarily of carbohydrates and proteins, which are synthesised by the attached microbial community.

Characterisation of the EPS in drinking water biofilms is limited, partly due to the complications in obtaining biofilm samples and the limitations of techniques used to provide

information on the composition, quantity and distribution of the matrix and cells (as discussed in Chapter 4). Fluorescent microscopy based analysis has facilitated biofilm visualization, simultaneously enabling the collection of quantitative data also, but this analysis is often restricted to cells, occasionally with consideration for the carbohydrates of the matrix but rarely investigating proteins. Wagner *et al.* (2009) analysed the carbohydrates and proteins of biofilms developed upon a glass scaffold within a wastewater fed reactor, although these were not analysed simultaneously. CLSM was used with two dual combinations of fluorophores to target the glyco conjugates (carbohydrates)\cells of one sample, followed by the proteins\cells of another (Wagner *et al.*, 2009). In addition to visualising the biofilms, the samples were quantified via DIA of the CLSM images, but only with regard to the carbohydrates and cells (Wagner *et al.*, 2009). CLSM has also previously been successfully used to assess the protein and carbohydrate components of EPS in flocs, granules and in single-species cultured biofilms (Schmid *et al.*, 2003; McSwain *et al.*, 2005; Chen *et al.*, 2007; Shumi *et al.*, 2009). Yet, following an extensive literature review no references were found which applied this technique to concurrently assess both the carbohydrate and protein fractions of the EPS, along with the cellular volume, of multi-species biofilms within a full scale DWDS environment. Therefore, the overarching objective of this research was to visualise and quantify the cells and EPS (proteins as well as carbohydrates) of biofilms relevant to a full scale DWDS, while also characterising variation in the bacterial, archaeal and fungal community structures. A secondary objective was to determine any effect of position around the pipe (i.e. crown vs. middle vs. invert) upon biofilm structure, with a view to providing further evidence to distinguish between the PSM and cohesive layer theory. If the PSM holds true a difference would be seen between the biofilms from the invert (bottom) of the pipeline in comparison to those from the crown (top).

To address the above objectives drinking water biofilms were allowed to form upon PWG coupons, under Steady State (SS) hydraulic conditions, for 28 days within a full scale DWDS experimental facility (section 3.1). Biofilm samples were taken at Day 0 (n=9) and Day 28 (n=9) and the coupons separated into their insert and outer components. Biofilm physical structure was characterized (using five of the nine inserts from each sample point, see section 4.7.1) via the triple staining, CLSM and DIA protocol developed and optimised for use with these samples (section 4.7.1; Fish *et al.*, 2011; 2012). The nucleic acids (cells), carbohydrates and proteins of the samples were visualised and quantified with respect to their 3D arrangement, area fraction distribution, volume (and volume ratios), spread and peak location, as explained in section 4.6. Variation in the biofilm community structure was established via DNA fingerprinting techniques. T-RFLP analysis was used to assess the bacterial and archaeal communities and ARISA was used for characterisation of the fungal community (see section 3.4).

5.2 Results

5.2.1 Bulk water quality

Bulk water quality was monitored throughout the growth phase (see section 3.3 for methodology) to ensure no significant changes were observed. A summary of the measured parameters is presented in Table 5.1, all of which complied with the UK quality standards.

Table 5.1 Water quality of the bulk water during the formation of biofilms under SS conditions (n=15 unless otherwise stated).

Water Quality Parameter	Range (Min – Max)	Mean (St.Dev)	Median	UK Standards ^B
Total Chlorine – Inlet (mg l ⁻¹) ^A	0.08 - 0.49	0.22 (0.20)	0.11	Max 5.00
Total Chlorine – Tank (mg l ⁻¹)	0.00 - 0.47	0.23 (0.19)	0.26	Max 5.00
Turbidity (NTU)	0.11 - 0.82	0.39 (0.24)	0.30	1.00–4.00 ^C
Iron (µg l ⁻¹)	15.00 - 24.00	19.47 (2.85)	18.00	200.00
Manganese (µg l ⁻¹)	2.40- 3.10	2.70 (0.25)	2.70	50.00
pH	7.00-8.38	7.43 (0.54)	7.07	6.50 – 9.50
Oxidising Redox Potential (mV)	221 - 500	324 (102.46)	288	NONE
Temperature – Inlet (°C)	15.1 - 17.7	16.1 (1.00)	15.6	NONE
Temperature – Tank (°C)	15.6 - 17.6	16.4 (0.62)	16.3	NONE

^A n=9, data only for Day 7-Day 21; ^B Standards in place in the UK based on DWI or EU legislation, or in the case of chlorine WHO as DWI and EU do not provide a standard, see Table 1.1 for examples of standards provided by different governing bodies; ^C Max values, water leaving a treatment plant must be ≤ 1 NTU, end point water ≤ 4 NTU. N.B. Min = minimum, Max = maximum, St.Dev = standard deviation.

5.2.2 Biofilm physical structure

From each sampling point – Day 0 and Day 28 – five biofilm samples were stained and imaged in five FOV (n=25) using the protocol described in section 4.7.1. The five samples comprised: one insert from the middle position in loops 1, 2 and 3, in addition to one each from the crown and invert positions in loop 2. DIA was applied to quantitatively assess temporal differences in physical structure between Day 0 and Day 28 biofilms, along with any spatial variations, particularly between the invert and crown biofilms. In order to determine any effect of position upon biofilm structure the data was initially separated into a “position dataset”, which incorporated the biofilms from the invert, crown and middle positions of the pipeline (loop 2), and a “loop dataset”, which incorporated biofilms that developed within loops 1, 2 and 3 (middle position of the pipeline). It should be noted that the middle loop 2 biofilm sample was common to the two datasets. The samples within each of these datasets (n=15) were compared to identify any significant differences between biofilms from the different locations (position or loop). The two datasets were then compared with each other to determine if any differences seen within each of the datasets were actually a result of inherent differences between any three samples, due to the heterogenic nature of biofilms, rather than being

driven by a position (or loop) effect. Both datasets were then combined and analysed in their entirety (n=25) to accurately characterize the biofilm at each of the sample points and evaluate any variation between them.

The initial output from the DIA was the proportion, termed “area fraction” (see section 4.6.3.1), covered by each of the stained biofilm components - cells, carbohydrates and proteins –per slice of the biofilm. This data was qualitatively analysed via area distribution plots and 3D visualization of the biofilm. Additionally, this data was the basis for quantitative analysis of the biofilm physical structure evaluating the volume, peak location and spread of cells and EPS.

5.2.2.1 Visualization and qualitative analysis of area distribution

Area distribution plots, shown in Figure 5.1, illustrate the results from the “position dataset” and “loop datasets” for Day 0 and Day 28. Each line on the plots represents one FOV, the colour of the line indicates the biofilm sample from which it was obtained. The loop 2, middle biofilm sample (shown in light blue) is common to the two datasets. Each panel shows the results for cells (nucleic acids), carbohydrates or proteins as indicated. In all cases the plots show the area distribution of the aligned data (see section 4.6.3.2), therefore “0” is the biofilm depth (y-axis) at which the maximum cell area fraction coverage occurs for a particular Z-stack. The y-axis runs from positive values, which indicate the bottom of the biofilm in contact with the pipe surface, to negative values, which indicate the top of the biofilm in contact with the bulk water. Overall these plots demonstrated that, regardless of sample point, there was no single coupon location (position or loop) at which biofilm was consistently different from the others. There was often greater variation between the FOV of a particular sample (indicated by the different area distribution profiles of the same colour) than between different samples. Therefore, it was not appropriate to calculate and plot an average area distribution for each stained component. Instead, all of the FOV of each sample were plotted, for each biofilm component; as there was no effect of position or loop upon the physical structure it was unnecessary to retain the location information (i.e. position or loop) for each sample. The plots were subsequently coded to indicate the specific biofilm component (Figure 5.2A; C).

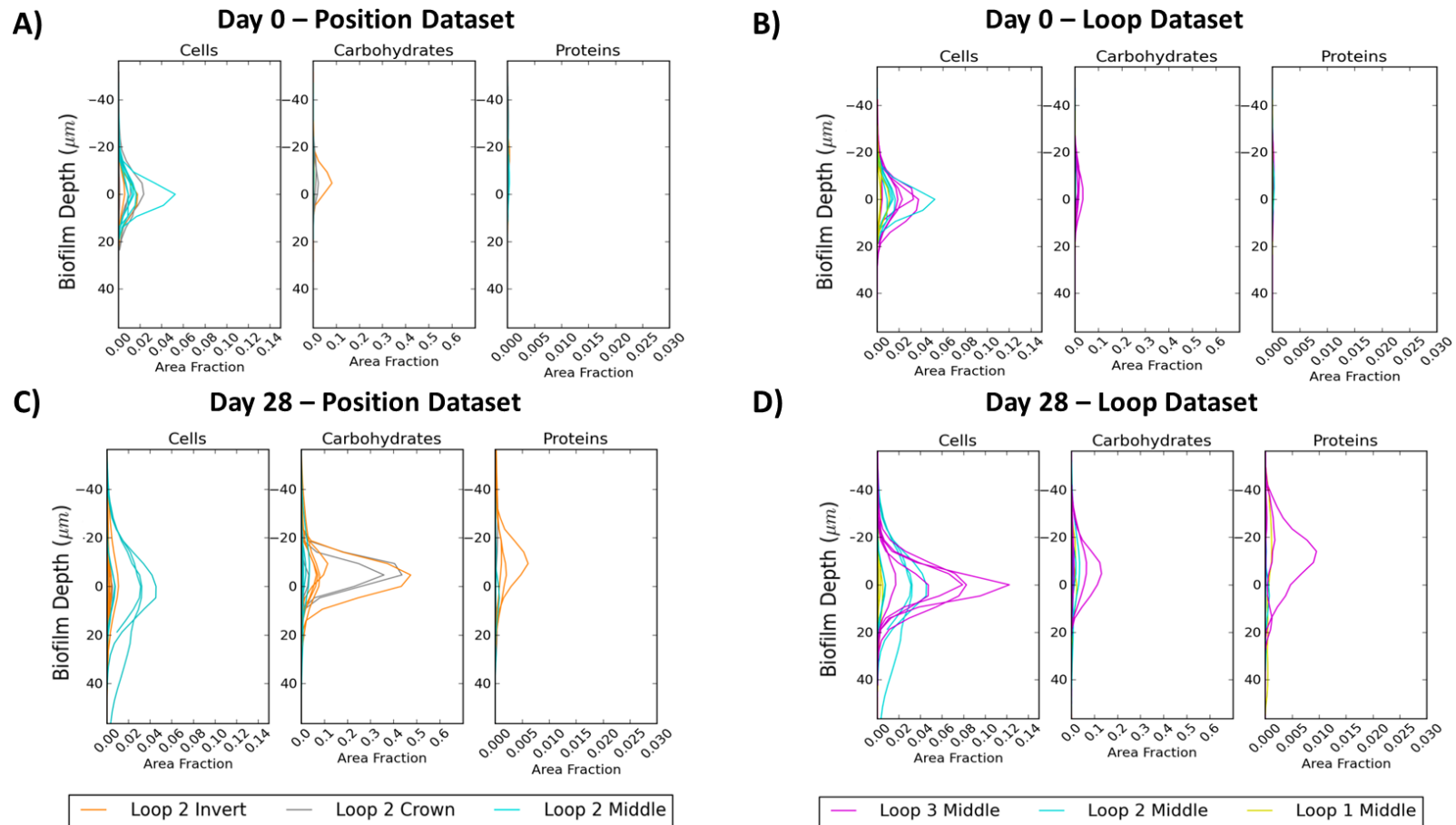


Figure 5.1 Area distribution plots for biofilms from Day 0 and Day 28 of the SS condition, showing the area fraction per slice of the Z-stack, which was covered by cells, carbohydrates or proteins for samples taken from different locations within the experimental facility. A) Day 0 area fractions from the “position dataset” i.e. biofilms from the invert, crown and middle positions (loop 2), colours as indicated in the key; B) Day 0 area fractions from the “loop dataset” i.e. biofilms from loops 1, 2 and 3 (middle position), colours as indicated in the key; C) Day 28 area fractions of “position dataset” biofilms; D) Day 28 area fractions of “loop dataset” biofilms. Note that the x-axis is different for each of the stained components: cells, carbohydrates, proteins. The y-axis runs from positive (indicating the biofilm-pipe surface interface) to negative (indicating the biofilm-bulk water interface); area fraction refers to the proportion of each XY image of the Z-stack covered by the particular component (see section 4.6.3.1).

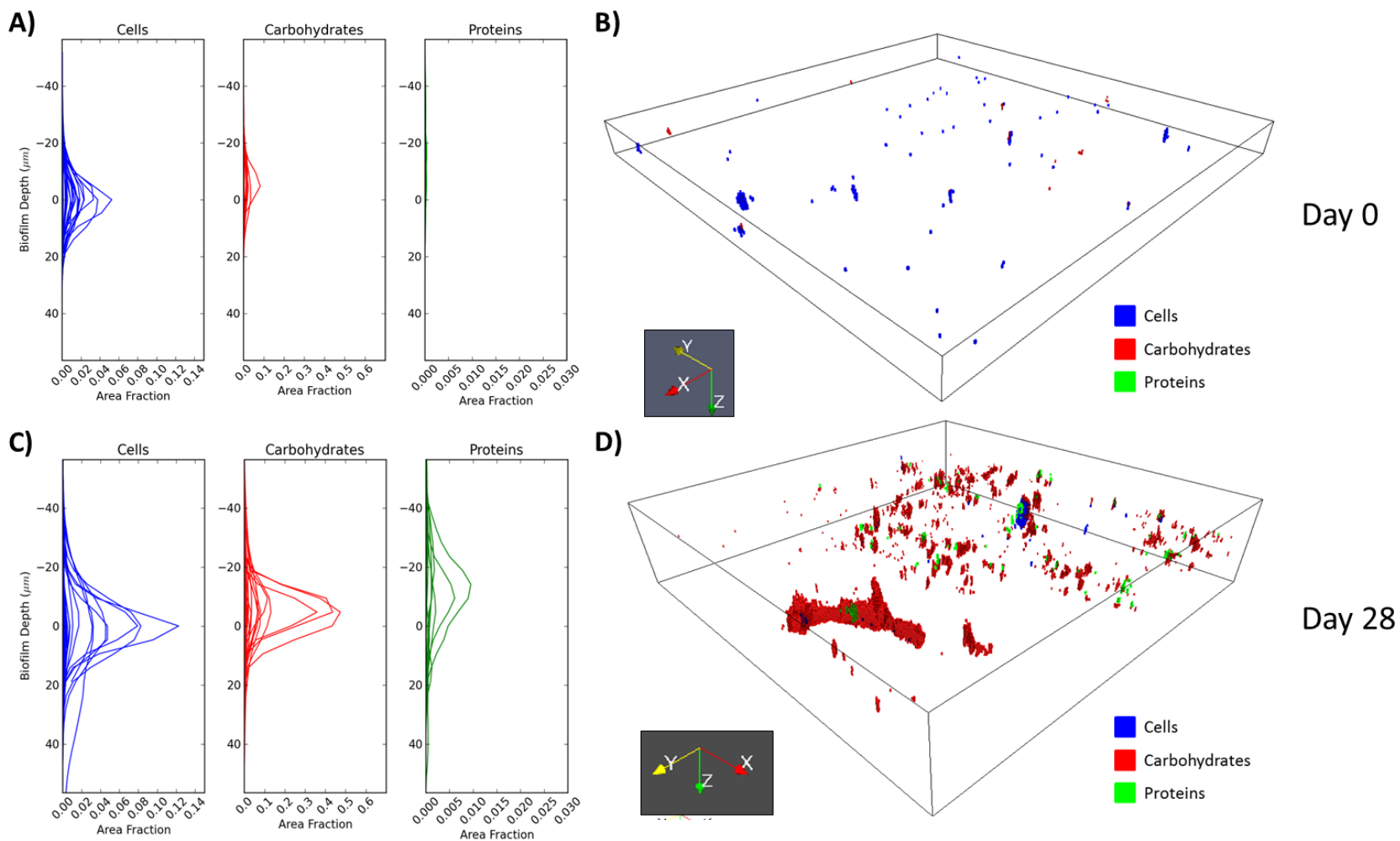


Figure 5.2 The area distribution and an example of the 3D arrangement of cells, carbohydrates and proteins of biofilms from Day 0 and Day 28 of the SS condition. A) Day 0 area fraction data ($n=25$); B) 3D projection of an example Day 0 biofilm, 3D plotting area shown by cube is $420 \mu\text{m} \times 420 \mu\text{m} \times 30.6 \mu\text{m}$; C) Day 28 area fraction data ($n=25$); D) 3D projection of an example Day 28 biofilm. 3D plotting area shown by cube is $420 \mu\text{m} \times 420 \mu\text{m} \times 94.4 \mu\text{m}$ of each component; note the different x-axis scales between components. Area fraction refers to the proportion of each XY image of the Z-stack covered by the particular component (see section 4.6.3.1).

Day 0 biofilm area distributions (Figure 5.2A) were generally constrained to a biofilm depth between -20 and 20 μm and had greater area fractions covered by cells than the EPS components. This trend was also evident in the 3D projection of a Day 0 biofilm, which highlighted the arrangement of the targeted biofilm components (cells, carbohydrates and proteins) in relation to each other. The cells, although sparse, were seen to be more common than the EPS (carbohydrates and proteins), proteins in particular were not visible in the example FOV shown in Figure 5.2B.

At Day 28 the area fractions (Figure 5.2C) covered by each of the biofilm components were greater than at Day 0, as was the depth of biofilm throughout which the components were distributed; -40 to 40 μm or more at Day 28, approximately double that at Day 0. The arrangement of the biofilm components throughout the depth at Day 28 was visualised via a 3D projection, shown in Figure 5.2D. In contrast to the Day 0 biofilm example, the Day 28 biofilm appeared to be dominated by the EPS and in particular by the carbohydrate fraction (Figure 5.2D). Complete co-localisation between the carbohydrates and the other two components was not observed, rather there were some areas across the FOV which appeared to consist solely of carbohydrates. Observing the matrix in this way showed that the proteins had a narrower XY distribution than was seen for the carbohydrates, with a reduced number of distinct protein only areas visible. At Day 28 the stain coverage was less sparse compared to that observed at Day 0 and any stained clusters were much greater in both depth and area, bearing very little resemblance to those samples obtained at the start of the growth phase.

A common trend across the area distribution plots for Day 0 and Day 28 was that the peak area fraction coverage of the carbohydrates and proteins generally occurred above that of the cells (i.e. closer to the bulk water); the peak location is addressed quantitatively in a subsequent section of this chapter.

5.2.2.2 Quantitative analysis of volume, spread and peak location

The majority of the data were not normally distributed (Shapiro Test, $p < 0.05$) and it was not appropriate to calculate the mean of the five FOV of each sample, which were shown to vary (Figure 5.1). Therefore, all quantification analysis was based upon the range (minimum to maximum), median and the application of non-parametric statistics (Kruskal Wallis or Wilcoxon test) to the raw data.

5.2.2.2.1 *Position effects*

The relative volume of cells, carbohydrates and proteins for biofilms within the “position dataset” and “loop dataset”, at both Day 0 and Day 28, are shown in Figure 5.3. Each data point represents the relative volume of a FOV and the colours indicate the position of the biofilm sample from which the FOV was obtained. Should two or more data points be likely to overlap, due to similar relative volumes (y-axis), each is shifted slightly along the x-axis to ensure they can be resolved. Therefore, it is the position of the points in relation to the y-axis which is of interest; the position on the x-axis is arbitrary, other than to indicate the dataset to which the point belongs. Box and whisker plots have been overlaid to show the total range (minimum to maximum), inter quartile range and median of each dataset.

Some differences in relative volume were found within the “position” and “loop” datasets, as indicated by p values <0.05 in Table 5.2 (highlighted in bold). At Day 0, no differences were found between the crown, middle and invert biofilms ($p>0.05$), with respect to any biofilm component and none were found between the protein relative volumes in biofilms from different loops. However, the relative cell volume of a Day 0 biofilm from loop 1 (middle) differed significantly from loop 2 and loop 3 ($p=0.0159$ in both cases) and the carbohydrate relative volume was significantly different between all three samples. At Day 28 there was no difference in the relative volume of carbohydrate or protein between the three positions ($p>0.05$) or the three loops ($p>0.05$). Conversely, the cell relative volume in the middle biofilm was significantly different from that in the crown ($p=0.0079$) or invert ($p=0.0159$) biofilms. Additionally, the loop 1 biofilm exhibited a significantly different relative cell volume than that in either loop 2 or 3 ($p=0.0079$ in both cases). However, it is likely that these differences are inherent differences between any three coupons rather than being driven by a particular position or loop. This was confirmed by the various comparisons of the “position dataset” to the “loop dataset”, between which no significant difference was found for any component at Day 0 or at Day 28, as demonstrated by the Wilcoxon test results, shown on each plot within Figure 5.3 ($p\geq 0.0590$ in all cases).

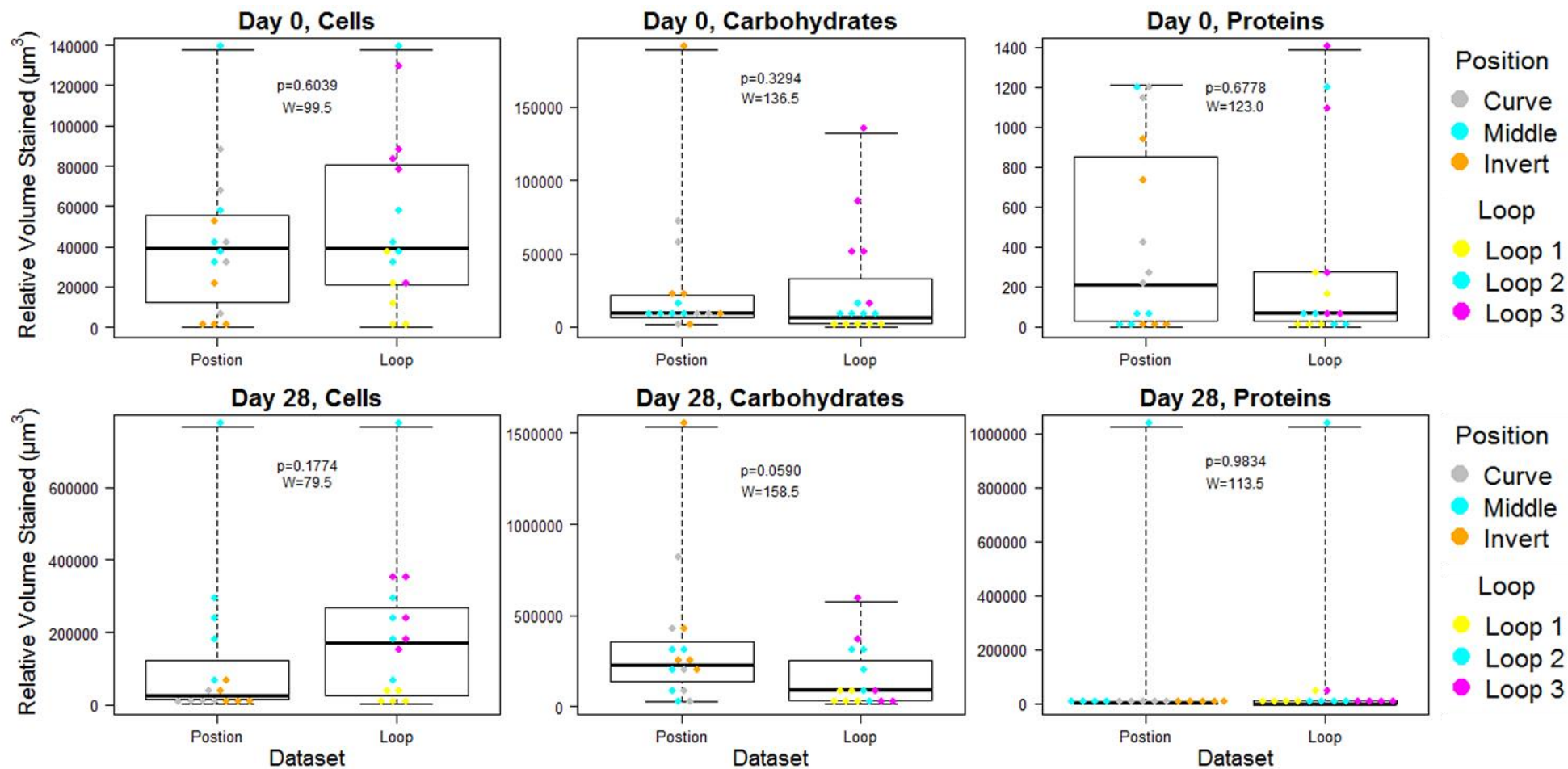


Figure 5.3 Relative volume of each of the stained biofilm components (cells, carbohydrates and proteins) for samples from Day 0 and Day 28. Colours indicate the biofilm sample location, each data point is a different FOV within that sample (n=5); box and whisker plots indicate the min, max, interquartile range and median (solid black line) of each dataset; p and W values are results from a Wilcoxon test between the two datasets; volume is relative to the threshold value (see section 4.6.3.3).

Table 5.2 Results from the Kruskal Wallis tests (and Wilcoxon if stated) to determine significant differences (in bold) between the samples within the position and loop datasets.

Sample Point	Biofilm Component	Position Dataset ^A	Loop Dataset ^B
Day 0	Cells	$\chi^2=5.04$, df=2, p=0.0805	$\chi^2=8.18$, df=2, p=0.0168 Wilcoxon: 1 vs. 2, W=1.0, p=0.0159 1 vs. 3, W=1.0, p=0.0159 2 vs. 3, W=16.0, p=0.5476
	Carbohydrates	$\chi^2=2.18$, df=2, p=0.3362	$\chi^2=12.02$, df=2, p=0.0025 Wilcoxon: 1 vs. 2, W=0.0, p=0.0079 1 vs. 3, W=0.0, p=0.0079 2 vs. 3, W=24.0, p=0.0159
	Proteins	$\chi^2=2.95$, df=2, p=0.2287	$\chi^2=3.46$, df=2, p=0.1772
Day 28	Cells	$\chi^2=9.14$, df=2, p=0.0104 Wilcoxon: C vs. M, W=25.0, p=0.0079 I vs. M, W=24.0, p=0.0159 C vs. I, W=17.0, p=0.4206	$\chi^2=9.38$, df=2, p=0.0092 Wilcoxon: 1 vs. 2, W=0.0, p=0.0079 1 vs. 3, W=0.0, p=0.0079 2 vs. 3, W=12.0, p>0.9999
	Carbohydrates	$\chi^2=1.82$, df=2, p=0.4025	$\chi^2=2.00$, df=2, p=0.3679
	Proteins	$\chi^2=1.52$, df=2, p=0.4677	$\chi^2=0.02$, df=2, p=0.9900

^A Includes biofilms from the crown (C), middle (M) and invert (I) of the loop 2 pipeline; ^B Includes biofilms from the middle position in each of the loops (1, 2, 3); N.B. Wilcoxon test is a pairwise analysis.

The spread (see section 4.6.3.4) and peak location (the aligned slice number at which the maximum area fraction occurs; see section 4.6.3.5) were also separated into position and loop datasets and the same analysis process applied as was used for the relative volume. At Day 0 no significant difference was found between the two datasets with respect to the spread of cells (Wilcoxon: W=122.5, p=0.6934) carbohydrates (Wilcoxon: W=125.5, p=0.6039) or proteins (Wilcoxon: W=96.5, p=0.5500). Similarly no differences in the spread of cells (Wilcoxon: W=119.5, p=0.7873), carbohydrates (Wilcoxon: W=78.5, p=0.1644) or proteins (Wilcoxon: W=103.5, p=0.7243) were found between the two datasets of Day 28 biofilms. As the Z-stacks were aligned using the cell stain (see section 4.6.3.2 for details) the peak location for the cells is always “0” and so this component is not included in the peak location data. No significant difference was found between the position and loop datasets with respect to the peak location of carbohydrates or proteins at Day 0 (Wilcoxon, carbohydrates: W=113.0, p>0.9999; proteins: W=88.5, p=0.3184) or Day 28 (Wilcoxon, carbohydrates: W=140.0, p=0.2161; proteins: W=152.5, p=0.0856) biofilms. Therefore all the biofilm samples from a given time point can be analysed together without requirement to account for differences in position (or loop). Note that the detailed plots and breakdown of statistical comparisons of samples within each dataset are not presented; they were shown for the relative volume data to assist in the explanation of the analysis and demonstrate the rigor behind the overall conclusions. From here onwards this level of detail will only be provided when differences were detected.

5.2.2.2.2 Day 0 vs. Day 28

Although some biofilm matter (the sum of the cells and EPS before averaging) was present at Day 0 (relative volume minimum=321 μm^3 , maximum=261128 μm^3 , median=50745 μm^3), there was a significant increase (Wilcoxon: $W=77.0$, $p<0.0001$) in the relative volume of stained biofilm at Day 28 (minimum= 31268 μm^3 , maximum=2085836 μm^3 , median=252325 μm^3). Each of the three stained components had a greater relative volume at Day 28 compared to Day 0 (Figure 5.4). However, this increase was only found to be significantly different for carbohydrates (Wilcoxon: $W=64.0$, $p<0.0001$) and proteins (Wilcoxon: $W=123.0$, $p=0.0002$), not cells (Wilcoxon: $W=258.0$, $p=0.2976$). Nevertheless, an increase in the range of cellular relative volume was clear – the minimum at Day 28 was more than 47 times the minimum at Day 0 (Table 5.3) and the Day 28 maximum was fivefold that at Day 0.

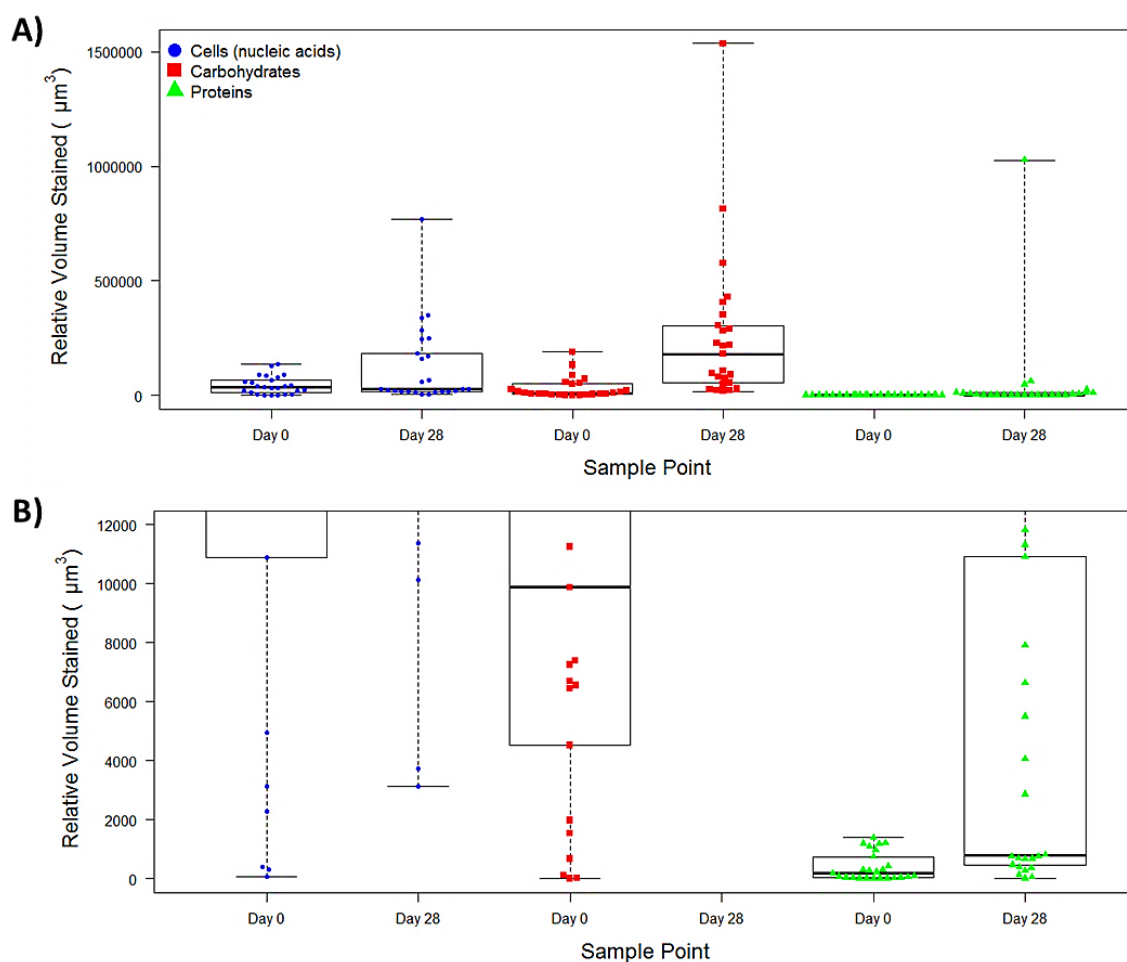


Figure 5.4 Relative volume of stained biofilm components within samples from Day 0 and Day 28. A) Y-axis scaled to the max data point; B) y-axis scaled to show protein data. Each data point represents a different FOV, $n=25$; box and whisker plots show the range, interquartile range and median – indicated by the solid black line; volume is relative to the threshold value (see section 4.6.3.3).

Table 5.3 Relative volumes of the stained biofilm components at Day 0 and Day 28.

Component	Range (Min – Max; μm^3)		Median (μm^3)	
	Day 0	Day 28	Day 0	Day 28
Cells	66 – 137860	3119 – 769191	35543	26099
Carbohydrates	1 – 189129	16257 – 1537181	9874	180802
Proteins	0 - 1387	6 – 1027266	177	800
EPS ^A	29 – 189132	16518 – 1545084	11059	184850

^A EPS = Carbohydrates + Proteins before averaging, data presented is therefore the min, max and median of the sums. N.B. Min = minimum, Max = maximum.

After 28 days, the young biofilm structure which developed had a greater relative volume of total EPS than was present at Day 0 (Wilcoxon: $W=60.0$, $p<0.0001$), see Table 5.3. Additionally, there was a significantly greater quantity of EPS per μm^3 of cells (Wilcoxon: $W=146.0$, $p=0.0010$), expressed as the EPS to cell ratio in Table 5.4. Other ratios indicated that between Day 0 and Day 28, there was a significant increase in the carbohydrate-to-cell (Wilcoxon: $W=151.0$, $p=0.0014$) and in the protein-to-cell ratio (Wilcoxon: $W=187.0$, $p=0.0153$). At Day 0 all the ratios with cells were <1.0 because the volume of cells was greater than that of the other biofilm components. However, by Day 28 the carbohydrate-to-cell ratio increased from a median of 0.31 to 4.80, indicating a shift from a greater volume of cells than carbohydrates at Day 0, to a much greater volume of carbohydrate than cells at Day 28. Conversely, despite an increase in the protein-to-cell ratio from Day 0 (median = 0.01) to Day 28 (median = 0.06), the cellular volume remained greater than that of the protein. This trend was also demonstrated clearly in Figure 5.4, in which, regardless of sample point, the proteins were shown to be the biofilm constituent with the lowest relative volume. Although the carbohydrates accounted for a greater proportion of both the EPS and total biofilm volume at Day 28, the carbohydrate-to-protein ratio was not significantly different (Wilcoxon: $W=249.0$, $p=0.5900$) between Day 0 (median = 46.81) and Day 28 (median = 62.31), which suggested no difference in the compositional makeup of the EPS.

Table 5.4 Range and median of various ratios of relative volumes of different components within biofilms from Day 0 and Day 28.

Ratios ^A	Range (Min – Max)		Median	
	Day 0	Day 28	Day 0	Day 28
EPS: Cells	0.02 -112.88	0.10 - 152.65	0.35	4.86
Carbohydrates: Cells	0.00 - 112.34	0.10 - 151.87	0.31	4.80
Proteins: Cells	0.00 - 0.54	0.00 - 2.54	0.01	0.06
Carbohydrates: Proteins	0.04 - 80480.50	0.28 - 36889.21	46.81	62.31

^A The first component is divided by the second, a value > 1 indicates a greater volume of the first component, a value <1 indicates a greater volume of the second, a value = 1 indicates an equal volume of each component. N.B. Min = minimum, Max = maximum.

An increase in spread was observed between Day 0 and Day 28 as shown in Figure 5.5. This increase was found to be significant for cells (Wilcoxon: $W=123.0$, $p=0.0001$), carbohydrates (Wilcoxon: $W=200.0$, $p=0.0288$) and proteins (Wilcoxon: $p<0.0001$, $W=82.0$). There was not, however, a significant difference in the peak location (Figure 5.6) of the EPS of a Day 0 biofilm compared to a Day 28 biofilm (Wilcoxon: carbohydrate, $W=233.5$, $p=0.1459$; protein, $W=323.0$, $p=0.5677$). The median peak location of carbohydrates at Day 0 and Day 28 was slice -1, indicating that the maximum area fraction was generally located above the cells at both sample points. At Day 28, there was one FOV for which the peak location of proteins occurred at slice 1, below the peak location of the cells, but generally the protein peak was above the cells with a median location of slice -2 and -3, at Day 0 and Day 28 respectively.

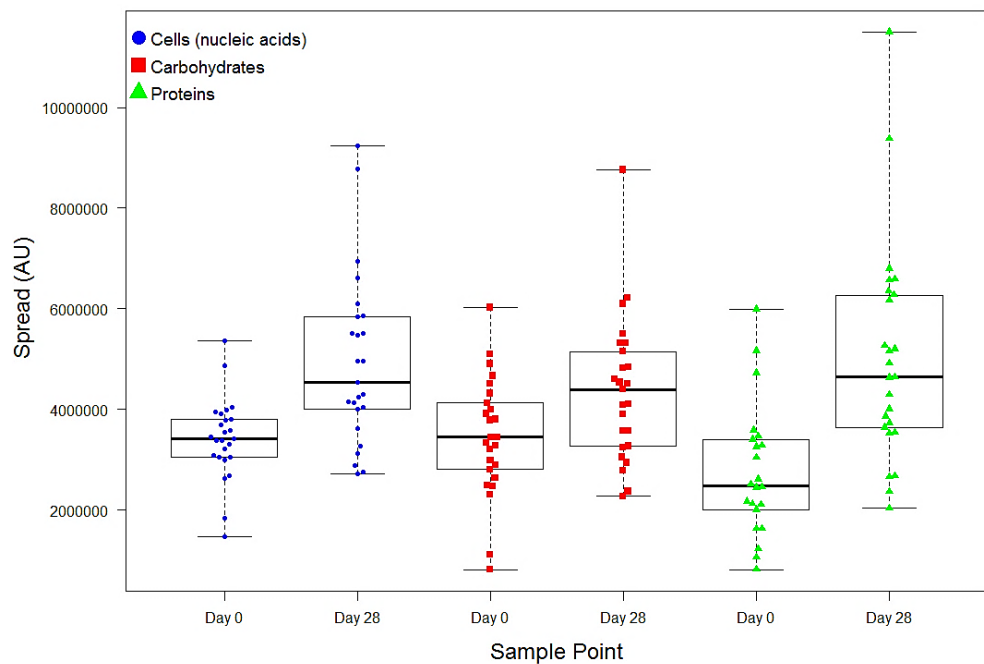


Figure 5.5 Spread of each of the stained biofilm components for Day 0 and Day 28 biofilms. Each data point represents a different FOV, $n=25$; box and whisker plots show the range, interquartile range and median - indicated by the solid black line; spread is calculated by the relative volume divided by the max area fraction (see section 4.6.3.4).

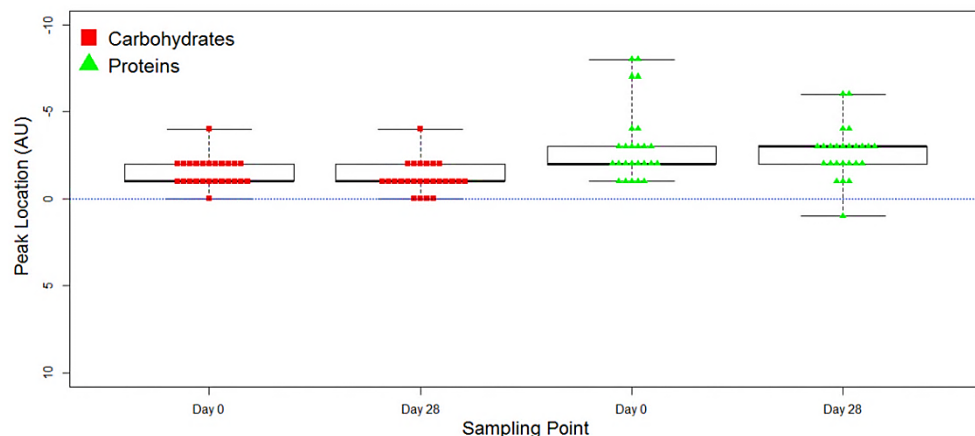


Figure 5.6 Carbohydrate and protein peak locations in relation to the cell peak location (indicated by the dotted line). Each data point represents a FOV, $n=25$; box and whisker plots show the range, interquartile range and median - indicated by the solid black line; peak location is the aligned slice number at which the maximum area fraction occurs (see section 4.6.3.5).

5.2.3 Biofilm community structure

5.2.3.1 PCR amplification of 16S rRNA genes and ITS regions

Bacterial and archaeal 16S rRNA genes and fungal ITS regions were amplified from nine DNA extractions per sample point (Day 0 and Day 28). However, not all of the nine DNA extractions contained detectable concentrations of each microbial type. For Day 0, PCR products were detected in 2/9 bacteria samples, 5/9 archaea samples and 5/9 fungi samples. By Day 28 bacterial, archaeal and fungal PCR products were detected in all nine DNA extractions, demonstrating the increased occurrence of biofilm at the end of the growth phase. Following purification some of the low concentration PCR products, namely the fungal PCR products at Day 0, were no longer visible when analysed on an agarose gel (Figure 5.7), however, when analysed via fingerprinting techniques DNA was detected in each of the samples.

All the archaeal products were of a similar concentration as shown by the similarity in band intensity, with little difference between the Day 0 and Day 28 products. However, the bacterial and fungal products varied within the sample groups as some of the replicates in each case had a stronger intensity than others. Generally, the Day 28 products had stronger band intensity than the Day 0 products, indicative of a greater number of bacteria or fungi in the Day 28 samples.

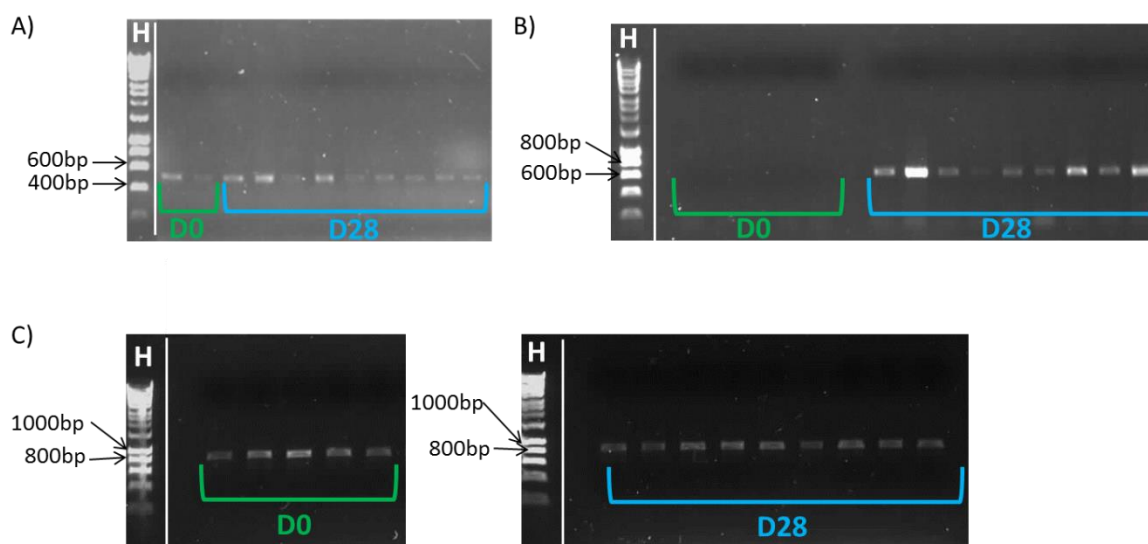


Figure 5.7 Agarose gel electrophoresis images of purified PCR products from Day 0 (D0) and Day 28 (D28) biofilms developed under SS conditioning flow rate. A) Bacterial purified PCRs; B) Fungal purified PCRs; C) Archaeal purified PCRs. In all cases gels are 1% agarose and Hyperladder I, (Bioline, London, UK), indicated by “H”, was used for sizing; bp = base pair.

5.2.3.2 Microbial community analysis

5.2.3.2.1 Variation in relative taxon richness, evenness and diversity

Electropherograms from T-RFLP and ARISA analysis showed similarities between replicates but distinct community fingerprints between Day 0 and Day 28 (Figure 5.8). The bacterial and fungal fingerprints were more complex at Day 28 than those at Day 0. Bacterial T-RFLPs at Day 0 comprised a total of 6 different T-RFs whereas 104 different T-RFs were found in total across the Day 28 replicates. The total number of different fungi ARISA amplicons ranged from 53 in the Day 0 replicates to 106 at Day 28. The range of bacterial T-RFs and fungal ARISA amplicons in individual profiles also increased from Day 0 to Day 28, as can be seen in Table 5.5, described as the minimum and maximum relative taxon richness. As bacteria were only detected in 2 samples from Day 0, an average of the various ecological indices could not be calculated and statistical comparison to Day 28 data was not plausible. However, comparisons of the minimum and maximum index values (Table 5.5) was possible and demonstrated an increase in relative taxon richness, Pielou's evenness index and Shannon's diversity index at Day 28. Each individual fungi ARISA profile was comprised of an average of 11 and 24 amplicons for Day 0 and Day 28 respectively, which demonstrated a significant increase in taxon richness (T-test: $df=11.61$, $p=0.0353$). However, there was no significant difference between Day 0 and Day 28 biofilms with respect to relative evenness, calculated using Pielou's Index (T-test: $df=11.75$, $p=0.8039$) or relative diversity, determined via Shannon's index (T-test: $df=9.03$, $p=0.0713$).

The archaeal profiles for the two sample points did not show as much complexity as was seen for the bacterial and fungal communities. Rather, the T-RFs occurring in each archaeal profile were similar between Day 0 and Day 28, dominated by a T-RF of size 104.76 nt. The total number of different T-RFs was 17 across the Day 0 replicates and 18 across the Day 28 replicates. Nevertheless the relative richness of the biofilm archaeal community increased significantly (T-test: $df=5.15$, $p=0.0441$) between Day 0 (average of 8 T-RFs per profile) and Day 28 (average of 11 T-RFs per profile). Relative evenness was found to be significantly lower at Day 28 than Day 0 (T-test: $df=6.50$, $p=0.0327$), which demonstrated a less even community in which one (or more) T-RFs were dominant, reflecting the pattern seen in the raw electropherograms (Figure 5.8). As with the bacterial and fungal communities, no difference was found in archaeal relative diversity between Day 0 and Day 28 (T-test: $df=4.68$, $p=0.1125$).

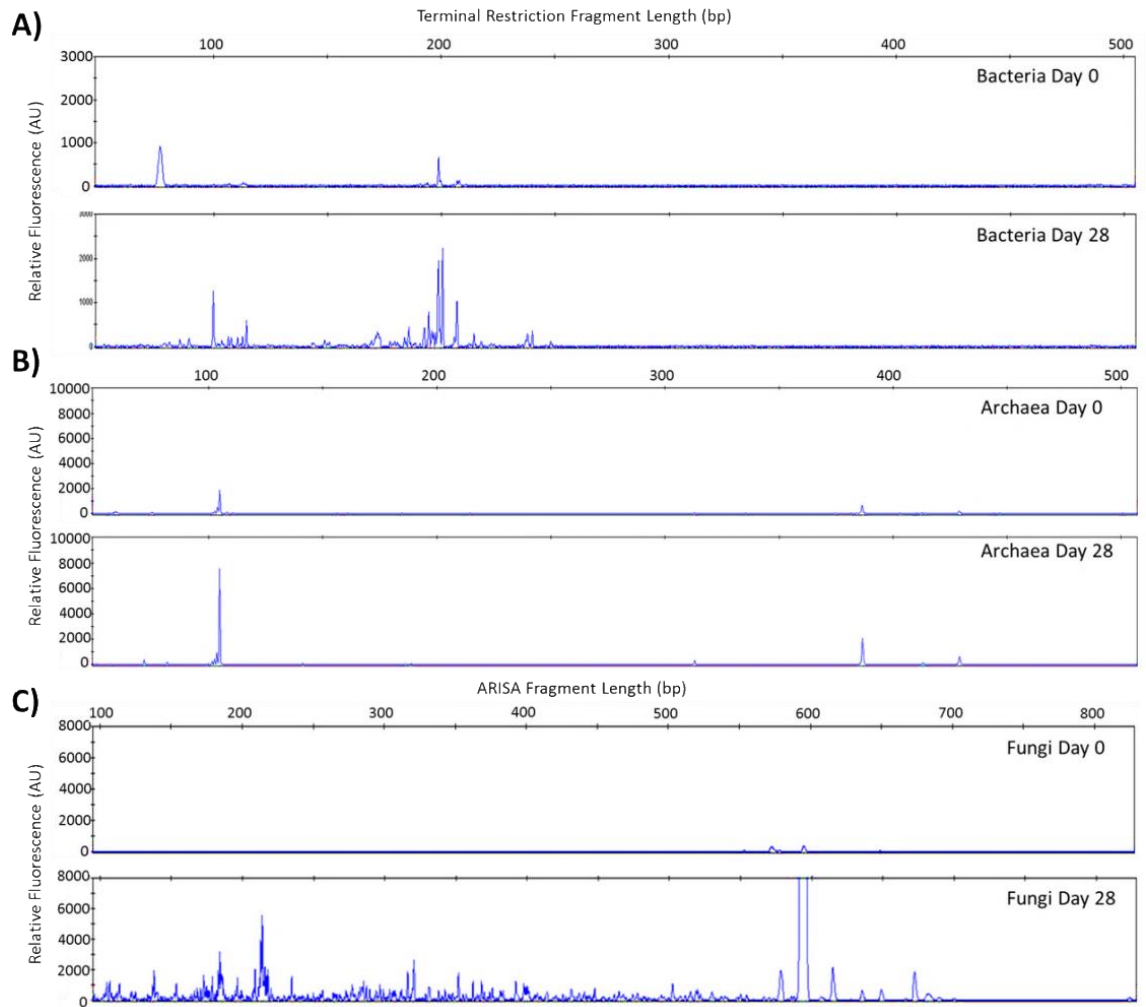


Figure 5.8 Representative T-RFLP or ARISA electropherograms of drinking water biofilm communities at Day 0 and Day 28, from the SS experiment. A) Bacterial communities (16S rRNA, T-RFLP); B) Archaeal communities (16S rRNA, T-RFLP); C) Fungal communities (ITS region, ARISA).

Table 5.5 Richness, evenness and diversity indices of the bacterial, archaeal and fungal communities from SS drinking water biofilm sampled at Day 0 and Day 28.

Sample Point	Microbial fingerprint	Relative Richness (number of T-RFs)			Relative Evenness (Pielou's Index)			Relative Diversity (Shannon's Index)		
		Min	Max	Mean (St.Dev)	Min	Max	Mean (St. Dev)	Min	Max	Mean (St. Dev)
Day 0	Bacteria ^A	3	5	-	0.89	0.95	-	1.04	1.43	-
	Archaea	5	11	8.20 (2.39)	0.90	0.95	0.92 (0.02)	1.45	2.16	1.90 (0.28)
	Fungi	3	18	11.2 (5.76)	0.88	0.94	0.91 (0.03)	1.04	2.65	2.05 (0.61)
Day 28	Bacteria	28	41	36.59 (4.59)	0.95	0.98	0.97 (0.01)	3.27	3.26	3.48 (0.13)
	Archaea	9	13	11.22 (1.20)	0.88	0.92	0.89 (0.01)	1.96	2.30	2.15 (0.11)
	Fungi	10	51	23.56 (13.51)	0.84	0.99	0.91 (0.06)	1.97	3.91	2.77 (0.67)

^A n=2 therefore no average could be calculated. N.B. Min = minimum, Max = maximum, St. Dev = standard deviation.

Day 28 SS biofilm archaea communities were less complex than the bacterial or fungal –this low diversity may be an accurate reflection of the community composition or may be due to a conserved region across different members of the archaea, which led to AluI cutting T-RFs of similar lengths across different species. A search was conducted against the current database (including sequences of known archaea species as well as “uncultured”) of the Ribosomal Database Project (RDP, 2013) to determine the T-RFs which would be generated using the primer Arch109F in combination with AluI. A total of 307 different sizes of T-RF were produced ranging from 2 nt to 500 nt. Of the 22,868 sequences found, the three most common T-RF lengths were 108 nt (5372 sequences, 23.4% of total), 4 nt (3355 sequences, 14.67% of total) and 144 nt (1939 sequences, 8.48% of total). It should be noted that a further 145 different T-RFs between 501 nt and 1018 nt in length were also reported but only those up to 500 nt in length are relevant to this study. Overall, many T-RF sizes are possible with the primer/enzyme combination used in this research, therefore the low diversity observed in the archaea samples is likely to be a true reflection of the small number of taxa which were present in the drinking water biofilms.

5.2.3.2.2 Variation in bacterial, archaeal and fungal community structure

Bacterial T-RFLP profiles from all of the biofilm samples were used to generate dendrograms based on the similarity of samples using the relative abundance or the presence/absence of T-RFs (Figure 5.9). Day 28 bacterial communities formed a distinct cluster from those at Day 0 when assessed with respect to T-RF relative abundance, shown in Figure 5.9A (ANOSIM: global $R=1.000$, $p=0.018$) or presence/absence, shown in Figure 5.9B (ANOSIM: global $R=1.000$, $p=0.018$). Day 0 replicates were 36.30% similar to each other (SIMPER test). Conversely, the replicates within Day 28 showed an average similarity of 52.83% (SIMPER test) but did exhibit a substructure, although most samples were unable to be distinguished from at least one other sample (Figure 5.9A; B). Another point to note is that there was a slight difference in the substructure of the Day 28 replicates when analysed using the T-RF relative abundance compared to the presence/absence data (Figure 5.9A; B). However, the same overall trends were observed, therefore, from this point forward only the relative abundance data will be presented, unless a different overall trend is observed in the presence/absence data. Bacterial community samples did not cluster by position (Figure 5.9C) or loop (Figure 5.9D) and no significant differences were found between samples from different loops (ANOSIM: relative abundance, global $R=-0.07$, $p=0.707$; presence/absence, global $R=-0.073$, $p=0.693$) or positions (ANOSIM: relative abundance, global $R=-0.050$, $p=0.626$; presence/absence, global $R=-0.122$, $p=0.857$).

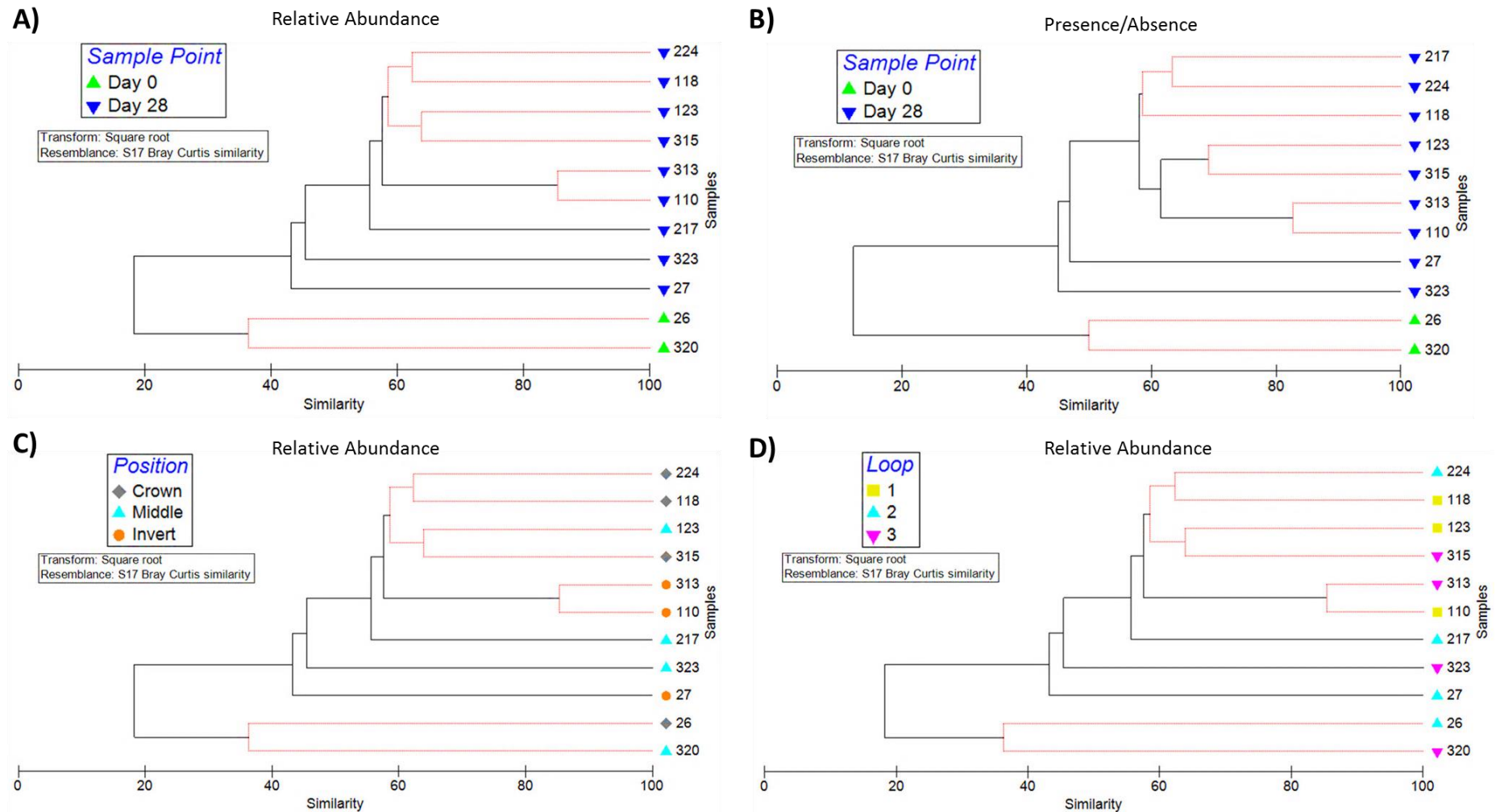


Figure 5.9 Cluster analysis using T-RFLP profiles to show the similarity between biofilm bacterial communities. A) Relative abundance of T-RFs, by sample time point; B) Presence/absence of T-RFs, by sample time point; C) Relative abundance of T-RFs, by coupon position; D) Relative abundance of T-RFs, by loop. Sample identification numbers are shown, in which the first number relates to the loop from which the sample was obtained, the second number(s) indicate the position from which the coupon was sampled, see Figure 3.3. Red lines indicate profiles not significantly dissimilar according to SIMPROF. Data was square root transformed and a resemblance matrix generated via a Bray-Curtis similarity test.

Cluster analysis of the archaeal T-RFLP and fungal ARISA profiles is shown via the nMDS plots in Figure 5.10. The 2D stress values were calculated for each nMDS, in each case this was <0.1 which indicated that a good representation of the data was provided (section 3.4.6.2). The Day 0 archaeal profiles were, on average, 66.54% similar to each other and the Day 28 profiles were an average of 85.80% similar to each other (SIMPER test), and therefore little variation existed between replicates from the same sample point. However, the Day 0 replicate 210 was found to be an outlier, distinct from all the other archaeal profiles (Figure 5.10A). As replicate 210 did not have a particularly low total peak area (30175, which is within the range of 12,000 -71,500; see section 3.4.6.1) or relative richness (the profile consisted of 7 T-RFs) compared to the other Day 0 samples, it can be concluded that the placement of this profile is a true reflection of the archaeal community composition it exhibits. Nevertheless, Day 0 archaeal profiles clustered independently from those of the Day 28 biofilms and were significantly very different from each other (ANOSIM: relative abundance, global R=0.822, p=0.0005; presence/absence, global R=0.826, p=0.0005). Therefore, although the number of T-RFs (relative richness) did not vary drastically between the sample points, the specific T-RFs which make up the profiles did.

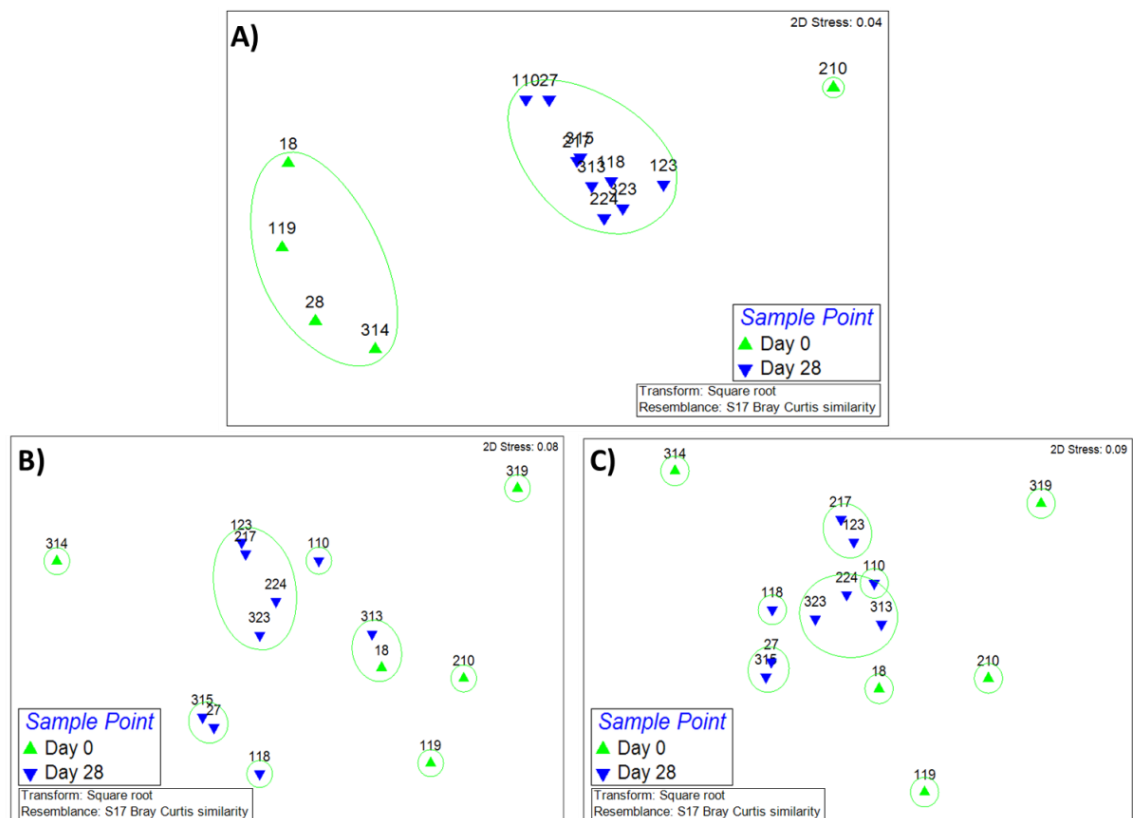


Figure 5.10 nMDS plots of archaeal and fungal community structures at Day 0 and Day 28. A) nMDS of archaea T-RF relative abundance data, the same pattern was seen in the presence/absence data; B) nMDS ARISA amplicons (fungi) relative abundance data; C) nMDS of ARISA amplicons presence/absence data. Green lines indicate clusters of: A) 75%, B) 40% and C) 40% similarity, based on group averages from hierarchical clustering analysis, and show the main groups which were highlighted in the dendrograms (not presented). Sample identification numbers are included

The fungal community at Day 0 was significantly different from that at Day 28 (ANOSIM: relative abundance, global $R=0.593$, $p=0.0005$; presence/absence, global $R=0.629$, $p=0.0005$). However, greater variation was observed between replicates than was seen in the archaeal or bacterial community analysis. The fungal Day 0 replicates were, on average, only 9.75% similar to each other (SIMPER test) and were clearly extremely divergent as demonstrated in the relative abundance nMDS and presence/absence nMDS (Figure 5.10B; C). Conversely, Day 28 replicates were more similar to each other as shown in the nMDS plots and by SIMPER analysis, which showed an average similarity between profiles of 25.83% (though this was much lower than the similarity between Day 28 replicates for both bacteria and archaea). The exception to this trend was the Day 28 replicate 313 which, when analysed by relative abundance was most similar to Day 0 replicate 18. However, this similarity was not seen when analysed by presence/absence, indicating that the same peaks were dominant between the samples but that there was a difference in the richness of ARISA fragments between the two samples.

Comparisons of microbial community structure between Day 0 and Day 28 via SIMPER analysis demonstrated that, although significantly different, the archaeal community profiles were the most similar between the two sample points, followed by the bacterial communities (Figure 5.11A). The fungal communities were the most different over time with an average similarity of just 7.35% between the Day 0 and Day 28 drinking water biofilms. The graphs in Figure 5.11B, C and D, show the T-RFs which accounted for the majority (60%) of the differentiation between the Day 0 and Day 28 bacterial, fungi and archaea communities, respectively. There were 16 bacterial T-RFs, 1 archaeal T-RF and 7 fungal ARISA amplicons which were only present at Day 28, therefore likely indicative of secondary colonisers. Equally, there were some T-RFs or amplicons (one bacterial, one archaeal and two fungal) which were only found at Day 0, indicating the presence of initial colonisers which were likely outcompeted by other species during the 28 day development phase.

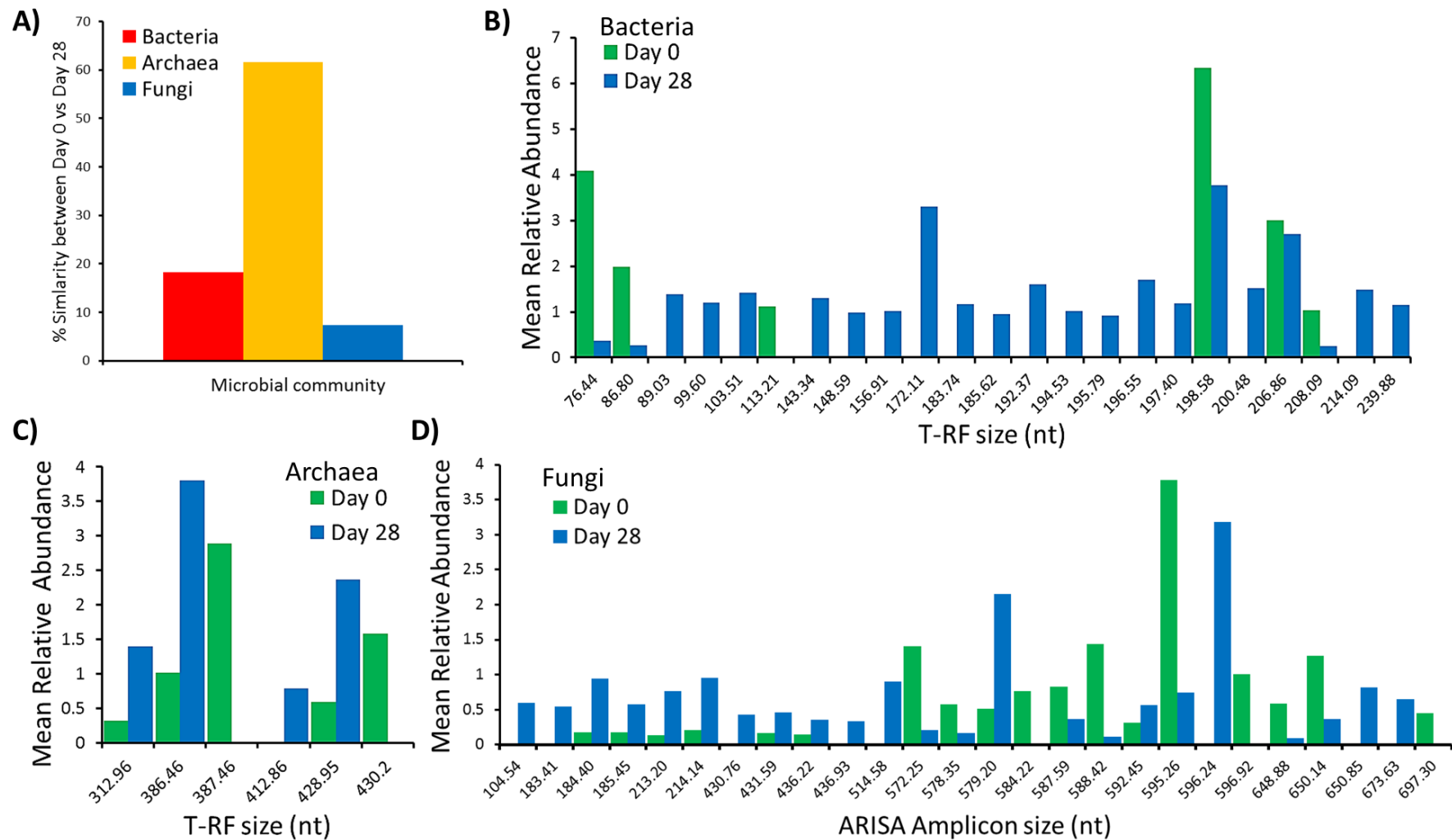


Figure 5.11 Results from SIMPER analysis comparison of microbial communities in drinking water biofilms at Day 0 and Day 28. A) Similarity of the microbial communities at Day 0 and Day 28 expressed as a %; the other plots show the size and mean relative abundance (AU) of the: B) Bacterial T-RFs (23); C) Archaeal T-RFs (6); D) Fungal ARISA amplicons (27), that explain 60% of the difference between Day 0 and Day 28 biofilm bacterial, fungal and archaeal communities respectively.

5.3 Discussion

The application of a newly developed triple staining protocol to biofilms from a full-scale DWDS environment, run under SS conditions is presented. This has provided a unique insight into the structure and composition of multi-species drinking water biofilms. The triple stain combination has previously been restricted to aerobic flocs or granular sludge forming under physico-chemical conditions representative of those occurring within a wastewater environment (McSwain *et al.*, 2005; Chen *et al.*, 2007). This study demonstrates, for the first time, the concurrent visualization of cells as well as the carbohydrates and proteins of the EPS, within drinking water biofilms. Even after a relatively short growth phase of 28 days, a quantifiable amount of biological matter was evident, which was able to be fluorescently labelled and assigned to one of the three identifiable biofilm components. Additionally, the biofilm community of these samples was also characterized, providing an evaluation of the variation of the bacterial, as well as fungal and archaeal community structures which comprised the cell volume.

After just 90 minutes within the pipeline, a small volume of biofilm material was detected upon the coupon surface; this was mainly comprised of cells with small areas of carbohydrate and protein. The cells of the Day 0 biofilms were predominantly fungal or archaeal, which were more commonly present in amounts detectable by the molecular analysis used in this study, than bacteria. Martiny *et al.* (2003) also demonstrated the presence of stained cells and detected bacterial DNA in samples at the beginning of a biofilm study, in this case within the first 24 hours, which highlights the rate at which primary attachment of microorganisms can occur.

By Day 28, the EPS volume was greater than that of the cells, which demonstrated the development of a more mature biofilm, producing an EPS matrix to adhere to the substrata, consistent with previous studies which identified EPS as the main component of the biofilm (e.g. Lazarova & Manem, 1995; Simoes *et al.*, 2007; Wagner *et al.*, 2009). Not only did the volume of EPS increase, the quantity per μm^3 of cells was also significantly greater at Day 28 compared to Day 0. This is in contrast to a study by Wagner *et al.* (2009), which showed that, within a wastewater inoculated biofilm, the volumes of carbohydrate and cells increased over 31 days but the ratio of EPS to cells did not significantly alter. A difference in the nutrient availability between the wastewater and drinking water may have promoted cellular growth in the study by Wagner *et al.* (2009), therefore maintaining the cell-to-carbohydrate ratio and

producing a trend different to that observed in the research presented in this study. Alternatively, the difference between the two studies may indicate an increased production of EPS in drinking water biofilms compared to the wastewater biofilms, which may be necessary to protect the embedded cells from the more extreme environment of the DWDS.

Although the quantity of the EPS increased, the composition did not significantly alter; it was consistently dominated by carbohydrates with small volumes of protein that accounted for a smaller proportion of the total stained biofilm volume than the cells. Past drinking water biofilm research has primarily focussed on the cells and carbohydrates so a comparison with proteins is rare, of the studies which did consider proteins the carbohydrate fraction was also reported to be dominant. There are a few examples of biofilms in other environments, such as activated sludge flocs, where proteins are the dominant EPS constituent (Schmid *et al.*, 2003). However, carbohydrates have been found to be the dominant component in biofilms cultured within reactors (Möhle *et al.*, 2007; Wagner *et al.*, 2009) and chemostats (Simoes *et al.*, 2005). In contrast to the results presented in this chapter, research by Wagner *et al.* (2009) was unable to determine the presence of proteins in biofilms aged up to 31 days, whether using CLSM or RM analysis. It should also be noted that Simoes *et al.* (2005) studied a single species biofilm via physical extraction techniques and different analytical methods were used to quantify the proteins and carbohydrates. Therefore, Simoes *et al.* (2005) state that comparison between the two EPS components should be undertaken with care as it may not be an accurate reflection of the true biofilm characteristics. The greater volumes of carbohydrates indicate that they are the primary EPS components which are developed in the earlier stages of biofilm development, perhaps as they play a greater role in biofilm structural stability (cohesion and adhesion) than proteins. Möhle *et al.* (2007) provide evidence for this theory as biofilms inoculated with activated sludge were found to contain particularly high amounts of carbohydrate in the basal layer, which was found to be more stable than the biofilm at the surface. However, this theory has yet to be investigated thoroughly in drinking water biofilms and more research is required before firm conclusions can be drawn.

Cells, carbohydrates and proteins were not uniformly distributed throughout the biofilm, nor did they completely co-localise. This study illustrated the extent of carbohydrate coverage throughout potable biofilms in contrast to the concentrated coverage of proteins and showed that there were some cell free areas where EPS was present. The differential location of nucleic acids and carbohydrates, including regions covered solely by the latter, was also highlighted by Stewart *et al.* (1995). While the presence of cell free areas where EPS is observed could be due to the cell volume being below the limit of detection, it seems more

likely that these EPS regions represent sites from which cells have migrated or been detached. The spread of each targeted biofilm component increased between Day 0 and Day 28, reflecting the occurrence of the biofilm throughout a greater depth but there was no change in the peak location of the EPS. The biofilm slice with the largest area fraction covered by carbohydrates and proteins was consistently found to be above the slice at which the maximum cell area fraction was detected. This may indicate that, whilst EPS exists below the cell peak location to adhere the biofilm to the pipe wall, there is a greater need for a larger volume of the matrix nearer the top of the biofilm to protect the cells from the environment in the bulk phase. The differential location of the majority of the EPS throughout the 3D structure of the biofilm, and in relation to the cells, has not been extensively considered in the literature. Wagner *et al.* (2009) noted that, in biofilms developed upon glass slides within a reactor, more cells were found nearer to the biofilm surface in contact with the bulk phase but no comment was made regarding the placement of the EPS components.

In addition to variation in physical structure between Day 0 and Day 28, the biofilms also experienced a shift in the microbial community structure. Fungal DNA was detected in more Day 0 samples (5/9) than bacteria (2/9) but at the end of the development phase both microbial groups were found in all nine biofilm samples. Previous drinking water studies in Germany (Heinrichs *et al.*, 2013a;2013b) and Greece (Arvanitidou *et al.*, 1999) also found fungi to be present in the majority of samples (> 80%). The relative richness of both communities increased between Day 0 and Day 28. The absence of some amplicons or T-RFs by Day 28 suggests the existence of initial colonising species which were outcompeted and replaced by secondary colonisers, indicated by the presence of amplicons or T-RFs unique to the biofilms at the end of the growth phase. However, it has yet to be conclusively established whether biofilm formation within DWDS involves the same primary and secondary colonisation as occurs in biofilm development within other environments. The successional integration of different bacterial species into a biofilm has been stated to be driven, at least in part, by co-aggregation – a process by which cells of different species attach to each other (Rickard *et al.*, 2003) . This phenomena has previously been observed in biofilms from dental plaque, which are known to experience primary and secondary colonisation (Kolenbrander, 2000) and it has also been reported in laboratory cultivated aquatic biofilms (Rickard *et al.*, 2002) and in bacteria extracted from a drinking water biofilm (Buswell *et al.*, 1997). In combination with the results presented in this chapter, it seems that bacterial successional colonisation in DWDS is plausible and fungal communities may experience this also, although more research is required within the context of drinking water biofilms to explicitly show this to be the case.

Within the SS drinking water biofilms the archaeal community was less complex than the bacterial or fungal communities. Although they have not often been compared to fungi, biofilm studies from other environments have also found archaea to be less diverse than bacteria. For example, Fernandez *et al.* (1999) showed bacterial diversity within a methanogenic reactor to be almost four times greater than that of the archaea. Aller & Kemp (2008) reviewed and analysed a range of studies investigating microbial communities from a variety of environments. The findings highlighted that reduced archaeal diversity is inherent across habitats; of the 173 libraries examined, only five expressed greater archaeal diversity than bacterial diversity. Archaea communities may be less diverse because they interact with the environment in a different way to bacteria, potentially expressing less physiological flexibility than bacterial cells. Interestingly, although less diverse, two thirds (on average) of the archaeal libraries assessed by Aller & Kemp (2008) consisted of rare phylotypes, the same proportion as seen in bacterial libraries. Although this suggests that research should be balanced with respect to investigating archaea and bacteria communities, the reality is that archaea are understudied. This is particularly true of the drinking water environment where bacteria are more studied than either archaea or fungi. Of those studies which have looked for archaea, some have concluded that they could not be detected (Manz *et al.*, 1993) while others have confirmed their presence (Wielen *et al.*, 2009; Ling & Liu, 2013). However, these studies have been based upon samples taken from benchtop systems or taps rather than from within the pipeline. The results from the research presented in this chapter show that archaea were detectable upon the pipesurface from Day 0 and that, although less diverse than the bacterial or fungal communities, the archaeal community developed over the growth phase resulting in detection in all Day 28 samples and a structure which was distinct from Day 0, with increased relative richness. The identification of several archaeal T-RFs demonstrates their role as an important, quantifiable part of the microbial community within biofilms of the DWDS, which should be given greater attention in future research.

No spatial variation, in relation to coupon location (position or loop), was found in biofilm physical or community structure at either Day 0 or Day 28. Although some variation between replicates was observed, this was not consistently explained by biofilms from a particular position or loop. Hence it can be concluded that the differences observed are due to the heterogenic nature of biofilms, and their stochastic development due to the way in which a cell randomly comes into contact with the pipe wall, both of which introduced uncontrollable variation into the samples. The evidence further suggests that the settling of particles is not the main driver for material concentration at the pipe wall, which is the basis of the PSM model. Biofilm was found around the whole circumference of pipe, therefore the “cohesive

layer theory” is a better explanation for the accumulation of material within the context of DWDS. This is in contrast to the processes occurring within wastewater distribution, where material does accumulate to a greater degree on the invert of the pipeline and the bacterial communities at the invert are distinct from those at the crown (Gomez-Alvare *et al.*, 2012).

5.3.1 Summary

The experimental system presented in this study provided a reliable and detailed approach to characterize the structure of drinking water biofilms and offered a unique insight into the EPS characteristics of multi-species drinking water biofilms. Overall a variation in biofilm physical and community structure characteristics was determined between Day 0 and Day 28 samples, the volume of each biofilm component increased as did the ratio of EPS to cells and all the microbial communities became more diverse. Furthermore this research presents a rare integration of physical and community structure assessment of biofilms which are representative of those within real DWDS networks. This study analysed samples from a full scale DWDS facility and thus the results are more relevant to real pipe networks. The biofilm samples were developed under SS flow rates, the same hydraulic approach as was taken in the majority of past research. While this has enabled comparison between the results presented in this chapter and the wider literature, constant steady flow rates rarely occur within real networks. Therefore, future work should be directed towards analysing the structure of biofilms developed under varied flow regimes, to the same level of detail as presented here.

Chapter 6: The Influence of Conditioning Hydraulic Regimes upon Biofilm Physical and Community Structure

6.1 Introduction and Aims

Biofilms within real DWDS are exposed to variations in flow rates and hence boundary layer hydraulics during their development. Typically a distribution pipeline will experience a double peaked diurnal hydraulic pattern with a low flow (or possibly stagnant) night time period (Figure 1.3). Variations in flow rate alter the conditioning shear stress imposed upon a biofilm in addition to the distribution of disinfectants, nutrients, inorganic particles and planktonic cells within the pipe. However, much of the previous research into drinking water biofilms has been based upon constant hydraulic conditions, where different flow rates may be tested but these are constant throughout the duration of the experiment. For example, Martiny *et al.* (2003) and Simoes *et al.* (2003; 2005) investigated the structure of biofilms developed under a velocity of 0.07 ms^{-1} and a flow rate of 1.7 lh^{-1} , respectively. Purevdorj *et al.* (2002) and Simoes *et al.* (2003) each grew biofilms under two different constant flow velocities within a reactor system: one laminar (0.033 ms^{-1} and 0.204 ms^{-1} , respectively) the other turbulent (1.000 ms^{-1} and 0.532 ms^{-1} , respectively). The interactions between shear stress, biofilm growth and the chemistry of the bulk phase within reactors are not representative of those occurring in real systems. Nevertheless, these studies provide an insight into how an increased velocity may affect a biofilm within an idealised system, but do not assess how a varied flow rate may condition the biofilms differently to a steady flow rate. For instance, it has yet to be established if the low night time period has the most influence upon biofilm accumulation and structure or if the main conditioning factor is the maximum flow rate reached. Moreover, although some of these studies have begun to investigate the impact of the hydraulics upon the biofilm physical structure rather than solely the bacterial structure, the majority remain limited to the cells and, in a few cases, the carbohydrates, of the biofilm.

The research presented within this chapter aimed to determine the impact of the varied flow hydraulic regimes LVF and HVF, described in section 3.2.1.2, upon biofilm structure and compare the biofilms that subsequently developed to those from the SS condition. In brief, the LVF and HVF hydraulic conditions were based upon field data from real DWDS but were designed to have the same average total daily flow rate (0.4 ls^{-1}) and shear stress (0.30 Nm^{-2})

as the SS condition. Therefore, if the important factor in biofilm conditioning was the average flow rate no difference would be seen between the hydraulic conditions. The LVF and HVF regimes each consisted of a 24 hour, double peaked pattern with flow rates of 0.23 - 0.54 ls^{-1} (shear stress 0.25 – 0.34 Nm^{-2}) and 0.23 – 0.75 ls^{-1} (0.25 – 0.40 Nm^{-2}) respectively (Figure 3.5). Each pattern had the same “night time” flow (0.23 ls^{-1} , 0.25 Nm^{-2}) but different maximum flow rates to provide an insight into the importance of the low flow and peak flow periods in influencing biofilm structure. If no differences were found between the biofilms from the LVF and HVF experiments, then it could be concluded that the night time steady flow period had a greater conditioning effect than the maximum flow rate. To achieve these aims three consecutive tests were run in the DWDS experimental facility during which biofilms were allowed to develop for 28 days under SS, LVF or HVF hydraulic conditions. Bulk water quality was monitored throughout the development phase of each experiment and biofilm samples were collected from Day 0 and Day 28. The presence of biofilm at the end of the development phase of each of the hydraulic tests was confirmed via SEM analysis (see section 3.5.2 for protocol). Figure 6.1 shows the clear distinction between the surfaces of a cleaned HDPE insert and Day 28 biofilm samples from each of the hydraulic conditions. The SEM images demonstrated the heterogenic presence of biofilm across the surface of the insert and enabled qualitative visual comparisons between the biofilms from each regime. For instance the microorganisms in the HVF biofilms appeared to be less embedded within EPS than those from SS or LVF. However, more detailed biofilm analysis was applied to further characterize the biofilms developed under each of the hydraulic regimes and facilitate comparisons between the three tests. The biofilm physical structure was analysed using the fluorescent staining, CLSM and DIA methods described in section 4.7.1 and DNA fingerprinting techniques (see section 3.4.5) were used to assess the biofilm bacterial, fungal and archaeal community structures.

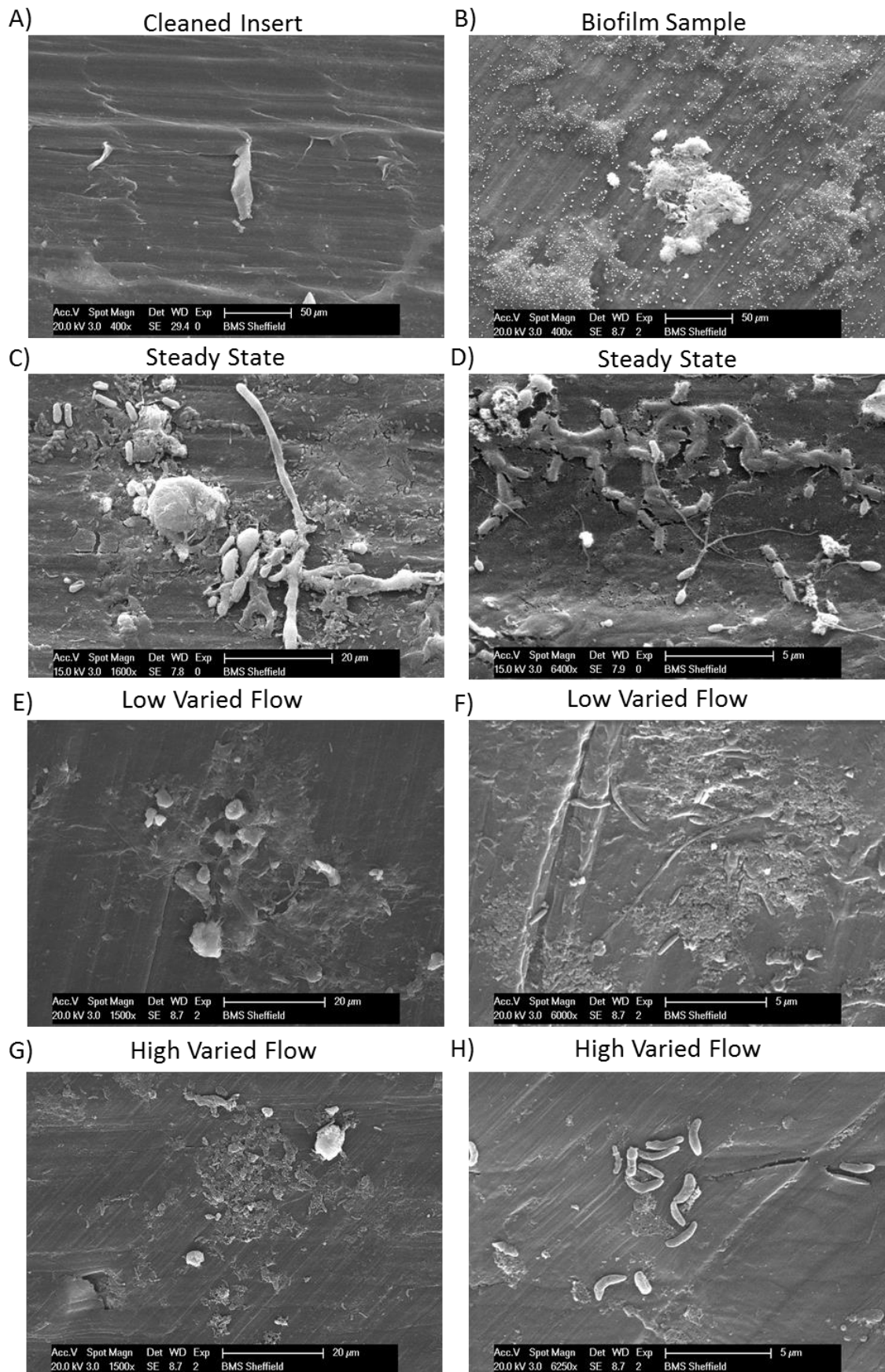


Figure 6.1 Representative SEM images of a cleaned insert (A) and Day 28 biofilm samples (B to H) developed under different hydraulic regimes. A) Surface of the HDPE insert when cleaned as described in section 3.2; B) SS biofilm sample imaged at the same magnification as the sterile insert; C to H) SS, LVF or HVF biofilms as indicated, imaged to two different scales as indicated by the scale bar on each image.

6.2 Results

6.2.1 Bulk water quality

The range, mean and median of each measured water quality parameter are shown in Table 6.1, for the development phase of each experiment – SS, LVF and HVF. Overall, there were no differences between the bulk water quality parameters during the growth phase of each trial (Kruskal Wallis and/or Wilcoxon, $p > 0.05$, see Appendix A8.1 for specific statistical outputs). An exception to this was the TOC concentration, which was significantly greater during the HVF test than the LVF test (Wilcoxon: $W=208.0$, $p < 0.0001$) by 2.85 mg l^{-1} (37.5%) if the means of the data were considered, or 3.04 mg l^{-1} (35.0%) if the medians were considered. The manganese concentration during HVF was found to be significantly greater than that at SS (Wilcoxon: $W=44.0$, $p=0.0045$) by an average of $0.43 \text{ } \mu\text{g l}^{-1}$ (based on mean, 16% increase) or $0.30 \text{ } \mu\text{g l}^{-1}$ (based on the median, 1.2% increase). Additionally, the ORP (oxidising redox potential) during HVF was significantly lower than SS (Wilcoxon: $W=171.0$, $p < 0.0001$) and LVF (Wilcoxon: $W=12.0$, $p < 0.0001$). The decrease in ORP observed between HVF and SS experiments was 129mV (39.8%) when calculated based on means and 107mV (37.2%) when based on medians. ORP was an average (mean) of 149mV (43.3%) or (median) 122mV (40.2%) lower during HVF compared to LVF. However, all the parameters fell within the UK standards; furthermore they fell within the low end of the acceptable range. Conversely, the hydraulic regimes that were imposed within each experiment were clearly distinct from each other and encompassed the whole range of hydraulic regimes seen in UK DWDS, as reported by Husband *et al.* (2008). It is, therefore, reasonable to state that the greatest variation between the three experiments was the hydraulic regime and any variation introduced by bulk water quality was minimal.

6.2.2 Biofilm physical structure

For each of the hydraulic conditions (SS, LVF and HVF), five biofilm samples from Day 0 and five from Day 28 were stained and imaged at five FOV. However, during the transfer of the HVF Z-stack images, a file (i.e. one FOV) from both Day 0 and Day 28 was corrupted and hence could not be unmixed and analysed. Therefore, $n=25$ for the SS and LVF samples and $n=24$ for the HVF samples. In all instances the data was not normally distributed (Shapiro Wilks: $p < 0.05$), therefore, quantification was based upon the range (minimum to maximum) and median. Statistical analysis was carried out using the non-parametric tests Kruskal Wallis (to compare the three hydraulic regimes) and Wilcoxon (used if Kruskal Wallis was significant, applied to a series of pairwise comparisons to see where the significant difference lay).

Table 6.1 Bulk water quality during the formation of biofilms during the SS, LVF and HVF experiments (n=15 unless otherwise stated).

Water Quality Parameter	Steady State (SS)			Low Varied Flow (LVF)			High Varied Flow (HVF)			UK Standards ^B
	Range (Min – Max)	Mean (St.Dev)	Median	Range (Min – Max)	Mean (St.Dev)	Median	Range (Min – Max)	Mean (St.Dev)	Median	
Total Chlorine –Inlet (mg l ⁻¹) ^A	0.08 - 0.49 ^A	0.22 (0.20) ^A	0.11 ^A	0.12 - 0.41	0.22 (0.08)	0.19	0.00 - 0.60	0.32 (0.20)	0.34	Max 5.00
Total Chlorine – Tank (mg l ⁻¹)	0.00 - 0.47	0.23 (0.19)	0.26	0.04 - 0.29	0.14 (0.08)	0.15	0.10 - 0.36	0.23 (0.08)	0.23	Max 5.00
Total Organic Carbon (mg l ⁻¹)				6.71 - 11.90	7.60 (1.72)	8.69	10.86 - 12.78	10.45 (1.09)	11.73	No abnormal change
Turbidity (NTU) ^B	0.11 - 0.82	0.39 (0.24)	0.30	0.10 - 0.81	0.35 (0.20)	0.34	0.11 - 0.30 ^B	0.20 (0.07) ^B	0.17 ^B	1.00 – 4.00 ^D
Iron (µg l ⁻¹)	15.00 - 24.00	19.47 (2.85)	18.00	13.00 - 28.00	19.40 (4.60)	19.00	16.00 - 30.00	19.73 (4.13)	18.00	200.00
Manganese (µg l ⁻¹)	2.40- 3.10	2.70 (0.25)	2.70	2.40 - 3.30	2.91 (0.31)	3.00	2.50 - 4.00	3.13 (0.48)	3.00	50.00
pH	7.00-8.38	7.43 (0.54)	7.07	6.51 - 7.70	7.27 (0.34)	7.29	6.77 - 7.92	7.23 (0.77)	7.10	6.50 – 9.50
Oxidising Redox Potential (mV)	221 - 500	324 (102.46)	288	200 - 572	344 (121.52)	303	174 - 261	195 (31.01)	181	NONE
Temperature – Inlet (°C)	15.1 - 17.7	16.1 (1.00)	15.6	15.5 - 17.1	16.4 (0.52)	16.5	16.2 - 18.1	16.9 (0.72)	16.6	NONE
Temperature – Tank (°C)	15.6 - 17.6	16.4 (0.62)	16.3	15.8 - 16.8	16.4 (0.34)	16.5	16.0 - 18.6	16.8 (0.95)	16.3	NONE

^A For SS, n=9, only have data for Day 7-Day 21; ^B For HVF n=9, only have data for Day 0-Day 14; ^C Standards in place in the UK based on DWI or EU legislation, or in the case of chlorine WHO as DWI and EU do not provide a standard, see Table 1.1 for examples of standards provided by different governing bodies; ^D Max values, water leaving a treatment plant must be ≤ 1 NTU, end point water ≤ 4 NTU. N.B. Min = minimum, Max = maximum, St.Dev = standard deviation.

As explained in section 5.2.1, the data was analysed to determine any effect of position (crown, middle or invert) or loop upon biofilm structure. Detailed results from this analysis can be found in section 5.2.1.3 for the SS samples and Appendix A9.1 for the LVF and HVF samples. To summarise, in all cases no difference was found between the “position dataset” and the “loop dataset” with respect to relative volume (Wilcoxon: SS, $W \geq 79.5$, $p \geq 0.0590$; LVF, $W \geq 106.5$, $p \geq 0.1692$; HVF, $W \geq 75.5$, $p \geq 0.1902$) or peak location (Wilcoxon: SS, $W \geq 88.5$, $p \geq 0.0856$; LVF, $W \geq 78.0$, $p \geq 0.1429$; HVF, $W \geq 61.5$, $p \geq 0.0576$). Generally there was also no difference in the spread of each of the stained components (Wilcoxon: SS, $W \geq 78.5$, $p \geq 0.1644$; LVF, $W \geq 41.0$, $p \geq 0.2633$; HVF, $W \geq 45.5$, $p \geq 0.3152$). The only exception being the spread of the cells within Day 0 biofilms of the HVF condition, for which a significant difference was found between the “position dataset” and the “loop dataset” (Wilcoxon: HVF, $W = 17.0$, $p = 0.0010$). This difference was likely due to the random initial contact of cells with the pipe wall because no single coupon from a particular position or loop was driving the difference, also by Day 28 no significant difference was found (Wilcoxon: HVF, $W = 107.5$, $p = 0.6790$). Therefore, there was no need to differentiate the samples based upon their location (position and loop) and subsequent analysis was applied to the whole dataset (i.e. $n = 25$ or $n = 24$) for each sample point of each hydraulic condition.

6.2.2.1 Visualization and qualitative analysis of area distribution

For each slice of a Z-stack the area fraction covered by each of the cells, carbohydrates or proteins was calculated and plotted to show the area distribution, as explained in section 4.6.3.2. In each plot “0” is the biofilm depth (y-axis) at which the maximum cell area coverage (expressed as a fraction) occurred for a particular Z-stack. Positive values on the y-axis indicate the biofilm nearer to the pipe surface; the negative values indicate the top of the biofilm, which is in contact with the bulk water.

At Day 0 the cells covered greater area fractions than the EPS components did, in biofilms from the SS (Figure 5.2), LVF and HVF conditions (Appendix A9.2). Regardless of hydraulic regime, all the area fractions were considerably less at Day 0 than at Day 28, indicating the development of biofilm material during the growth phase. Although the Day 0 area fractions were lower in the varied flow samples than the SS samples, there was less difference between the Day 0 area distribution plots from different hydraulic regimes than in the Day 28 area distribution plots for each hydraulic condition (Figure 6.2).

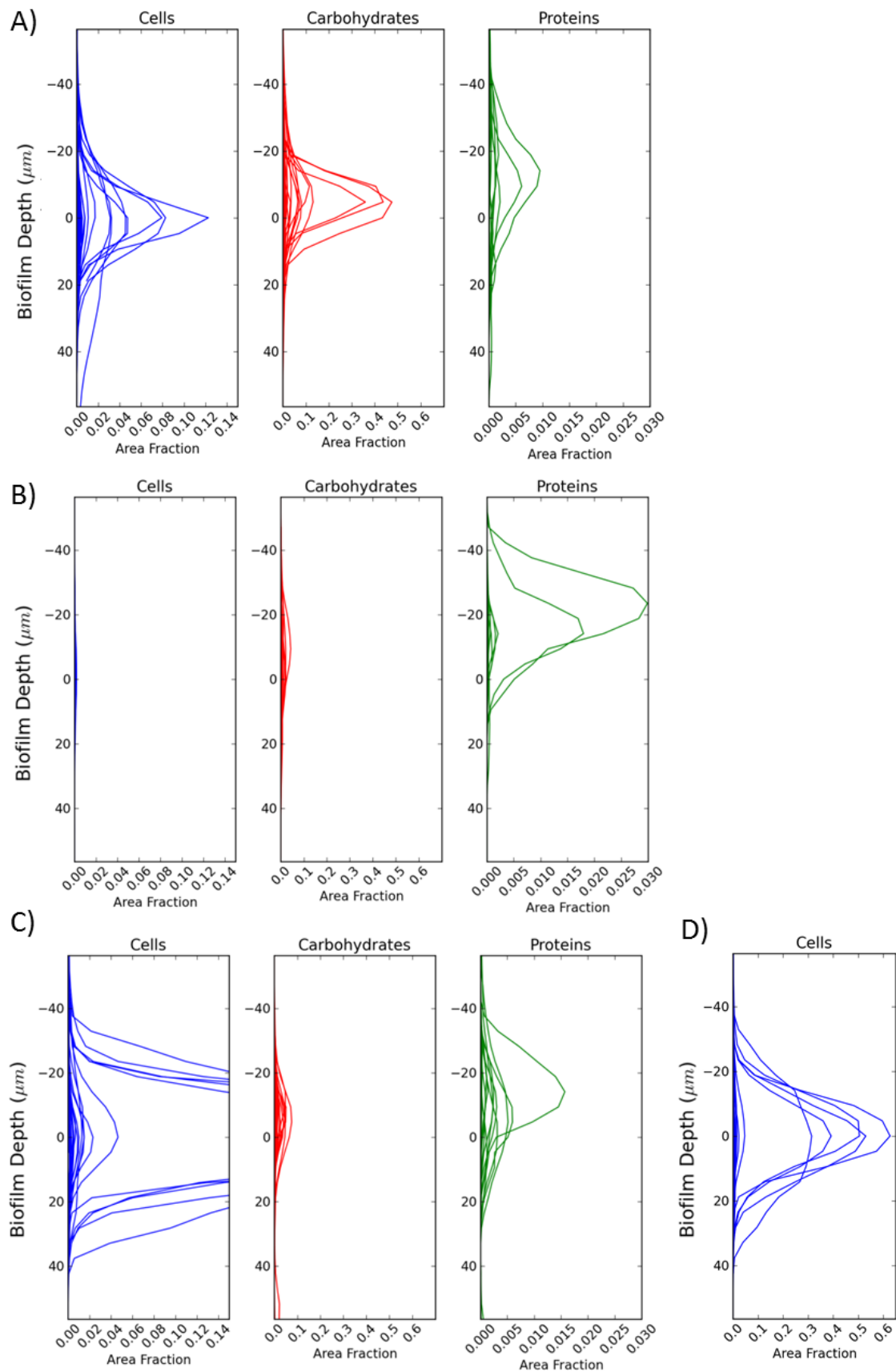


Figure 6.2 The area distribution of cells, carbohydrates and proteins within biofilms developed for 28 days under A) SS; B) LVF; C) HVF conditions. D) The cells of a Day 28 HVF biofilm plotted on an x-axis scale with a greater range. Each line represents one FOV (i.e. one Z-stack). SS, n=25; LVF, n=25; HVF, n=24. Area fraction refers to the proportion of each XY image of the Z-stack covered by the particular component (see section 4.6.3.1).

At Day 28 the biofilms from HVF and SS expressed a greater biofilm depth throughout which the cells were distributed (-40 to 40 μm or more) than was seen for LVF biofilms (a maximum of approximately -30 to 30 μm). However, the depth throughout which EPS (the carbohydrates and proteins) was distributed was -40 to 40 μm or greater for all Day 28 biofilms, regardless of flow regime. Additionally, in all the Day 28 biofilms, the peak area fraction of the carbohydrates and proteins was located above that of the cells. HVF biofilms had the greatest cell area fractions and LVF biofilms had the least. Five FOV from HVF biofilm samples had particularly high cell area fractions (Figure 6.2D), these all came from the loop 2 middle position coupon and were a true representation of the biofilm upon that insert. A greater coverage of cells in the HVF biofilm than in the SS or LVF biofilms was also observed in the 3D projections of an example biofilm developed under each flow regime (Figure 6.3). The 3D projections also illustrated that the LVF samples had a much sparser amount of total biofilm material than the HVF or SS samples; a trend which was also apparent in the LVF area distribution plots, which had the lowest area fractions of each biofilm component. Two FOV of the LVF biofilm samples did not follow this trend as they had large fractions of protein associated with them. One of these was from a loop 2 middle coupon, the other from a loop 2 invert coupon. None of the biofilms exhibited complete co-localisation of any of the stained components and in some instances there were areas of EPS which were cell free. In the HVF biofilms, although some of the cells were embedded within EPS, there was a greater occurrence of cell only areas (Figure 6.3C) than was seen in biofilms from SS and LVF (Figure 6.3A and B). Overall, while the HVF biofilms appeared to be dominated by cells, both the SS and LVF biofilms appeared to be dominated by EPS, particularly carbohydrates.

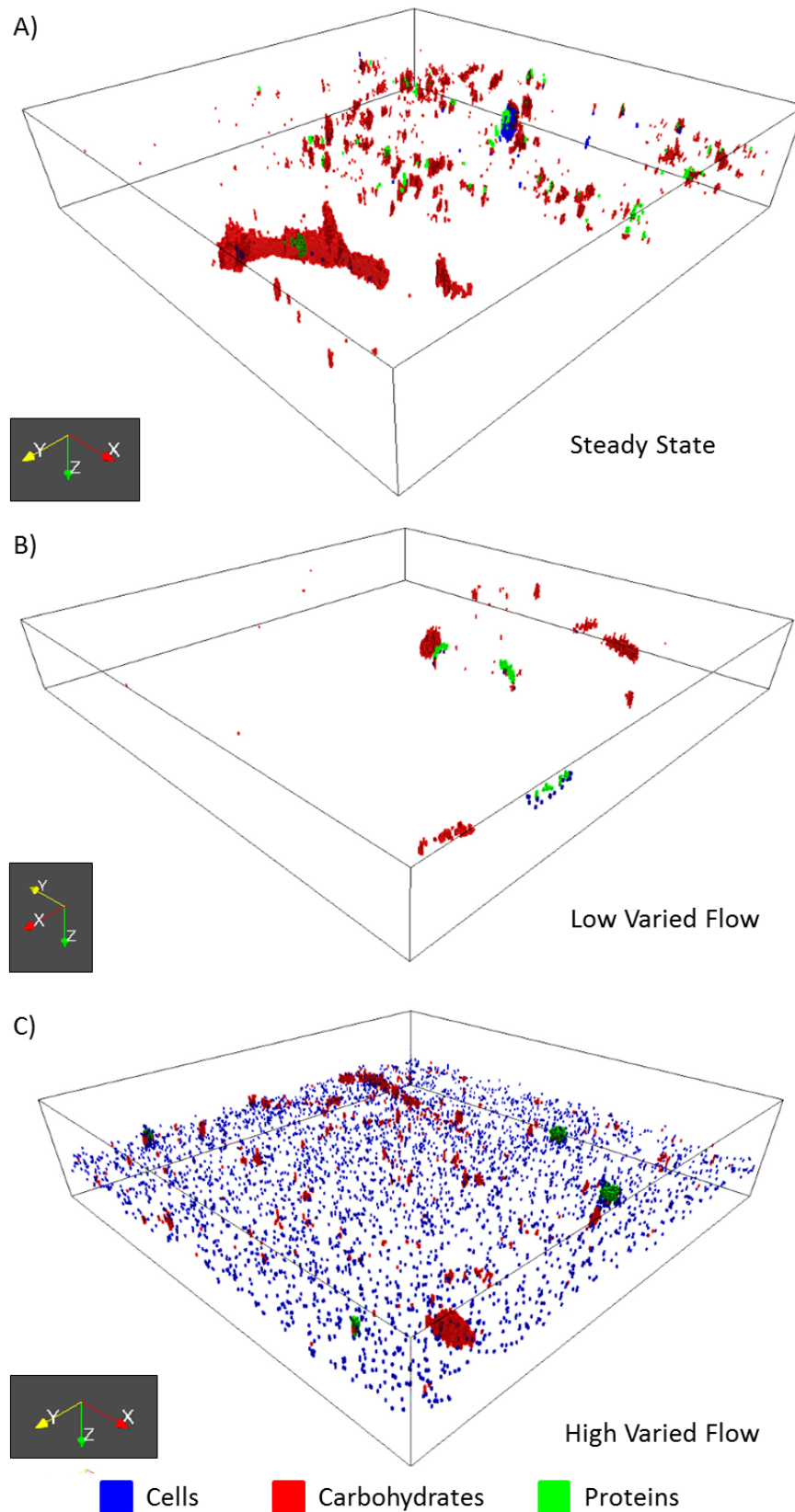


Figure 6.3 A representative example of the 3D arrangement of cells, carbohydrates and proteins within Day 28 biofilms developed under A) SS; B) LVF; C) HVF hydraulic conditions. Each 3D projection is within a plotting area shown by the cube which is $420\ \mu\text{m} \times 420\ \mu\text{m}$ (XY dimensions) in each case with a depth (Z) of: A) $94.4\ \mu\text{m}$; B) $63.5\ \mu\text{m}$ and C) $98.7\ \mu\text{m}$. N.B. the cells (blue) may be hard to distinguish from the carbohydrate (red) in some instances (particularly A), despite setting a mid-level opacity.

6.2.2.2 Quantitative analysis of volume, spread and peak location

Under SS conditions, the EPS-to-cell ratio, carbohydrate-to-protein ratio, relative volume and spread of each of the stained components were all greater at Day 28 than Day 0, but there was no significant difference in the peak location of carbohydrates or proteins (see section 5). The same analyse approaches used in section 5 were used to compare the LVF biofilms at Day 0 to those at Day 28, and the HVF Day 0 biofilms to Day 28 HVF biofilms. Under both LVF and HVF conditions, there was a significantly greater relative volume of biofilm at Day 28 in comparison to Day 0 (Wilcoxon: LVF, $W \leq 178.5$, $p \leq 0.0148$; HVF, $W \leq 89.0$, $p < 0.0001$), an increase in spread (Wilcoxon: LVF, $W \leq 206.0$, $p \leq 0.0368$; HVF, $W \leq 139.0$, $p \leq 0.0062$) and no difference in the peak location (Wilcoxon: LVF, $W \geq 311.0$, $p \geq 0.4638$; HVF, $W \geq 246.5$, $p \geq 0.3944$), see Appendix A9.3 for the specific statistical values for each stained component. Comparisons between Day 0 and Day 28 LVF biofilms showed a significant increase in the EPS-to-cell ratio (Wilcoxon: $W = 49.0$, $p < 0.0001$) from a median of 0.30 AU at Day 0 to 26.39 AU at Day 28. However, no significant difference was found between the carbohydrate-to-protein ratios (Wilcoxon: $W = 85.0$, $p = 0.2520$). Therefore, although the quantity of EPS per μm^3 of cells was greater at Day 28, the volume of carbohydrates and proteins (comprising the EPS) increased at the same rate because the compositional ratio of the EPS remained the same. Conversely, there was no difference in either the EPS-to-cell ratio (Wilcoxon: $W = 215.0$, $p = 0.1999$) or carbohydrate-to-protein ratio (Wilcoxon: $W = 148.0$, $p = 0.1433$) between Day 0 and Day 28 biofilms from HVF. This indicated that while the volume of each stained component increased over the 28 day development phase under HVF conditions, the proportion each contributed to the biofilm remained the same as was seen at Day 0. These results confirmed the development of biofilm material over the 28 day growth phase under each hydraulic condition; the data presented in the following sections evaluated any differences in the physical structure of the biofilms that had developed in each test, i.e. any effect of hydraulic regime.

6.2.2.2.1 Hydraulic effect (SS vs. LVF vs. HVF)

The relative volume of biofilm (cells and EPS) present at Day 0 differed between the three hydraulic regimes (Kruskal Wallis: $\chi^2 = 37.64$, $df = 2$, $p < 0.0001$; Wilcoxon: $W \leq 591.0$, $p \leq 0.0020$; see Appendix A9.4 for further details). LVF Day 0 biofilms had the lowest total biofilm relative volume (median = $1011 \mu\text{m}^3$), followed by HVF Day 0 biofilms (median = $3757 \mu\text{m}^3$) and SS Day 0 biofilms had the greatest (median = $50745 \mu\text{m}^3$). SS, Day 0 biofilms also had the greatest relative volume of each of the individually stained components and were significantly different from LVF and HVF Day 0 biofilms in all cases (see Appendix A9.4). The only relative volume comparisons which were not significantly different were the pairwise tests between LVF and

HVF biofilms with respect to carbohydrates (Wilcoxon: $W=369.0$, $p=0.1698$), proteins (Wilcoxon: $W=337.0$, $p=0.4575$) and, subsequently, total EPS (Wilcoxon: $W=364.5$, $p=0.2005$). In general, despite the slight differences in relative volume, there were no differences between the Day 0 biofilms from the different hydraulic regimes with respect to EPS-to-cell ratios (Kruskal Wallis: $\chi^2=0.26$, $df=2$, $p=0.8786$), all of which were less than 1, demonstrating the predominance of cells over EPS. There were also no differences in the carbohydrate-to-protein ratio (Kruskal Wallis: $\chi^2=5.57$, $df=2$, $p=0.0617$), the spread (Kruskal Wallis: $\chi^2 \geq 1.97$, $df=2$, $p \geq 0.1167$; see Appendix A9.4) or the peak location of carbohydrates (Kruskal Wallis: $\chi^2=5.83$, $df=2$, $p=0.0541$) and proteins (Kruskal Wallis: $\chi^2=0.02$, $df=2$, $p=0.9895$).

By Day 28 the biofilms developed under each of the hydraulic regimes were distinct in physical structure aspects other than relative volume. The relative volume of total biofilm increased by almost five times under the SS regime (Day 0 median= $50745 \mu\text{m}^3$, Day 28 median= $252325 \mu\text{m}^3$), an average of 36 times under the LVF regime (Day 0 median= $1011 \mu\text{m}^3$, Day 28 median= $31955 \mu\text{m}^3$) and an average of 45 times under the HVF regime (Day 0 median= $3757 \mu\text{m}^3$, Day 28 median= $171743 \mu\text{m}^3$). Although the LVF Day 28 biofilms experienced the second highest increase in relative volume (when compared to Day 0), these biofilms consistently had a significantly lower amount of stained material, whether considered with respect to each individually stained component, the EPS as a whole or the total biofilm relative volumes (Table 6.2; Figure 6.4). This reflected the trend seen in the area distribution plots and 3D projections which also highlighted the reduced occurrence of biofilm under the LVF regime (Figure 6.3). Consequently, the differences between the three regimes (shown by the Kruskal Wallis test), for each of the components presented in Table 6.2, were driven by the LVF biofilms, which were consistently significantly different from both SS and HVF biofilms. Conversely, SS and HVF biofilm relative volumes were not significantly different from each other in any respect other than the carbohydrates, which had a greater relative volume in biofilms developed under the SS conditions. The cell volume median for HVF biofilms was greater than SS biofilms, a trend illustrated in the example 3D biofilm projections and area distribution plots (Figure 6.3), however this difference was not statistically significant (Table 6.2).

Table 6.2 Comparison of the relative volumes of the stained biofilm components of Day 28 biofilms developed under SS, LVF and HVF conditions. Significant results are shown in bold. Data for the individual stained components is provided in (A) and for combinations, as indicated, in (B).

Component	Median Relative Volume (μm^3)			Kruskal Wallis	Wilcoxon Results	
	SS ^A	LVF ^A	HVF ^B	SS vs. LVF vs. HVF	Pairwise test	Result
(A) Individual						
Cells	26099	671	28859	$\chi^2=39.50$ df=2 p<0.0001	SS vs. LVF SS vs. HVF LVF vs. HVF	W=616.0, p<0.0001 W=296.0, p=0.9447 W=546.0, p<0.0001
Carbohydrates	180802	24969	74271	$\chi^2=22.87$ df=2 p<0.0001	SS vs. LVF SS vs. HVF LVF vs. HVF	W=535.0, p<0.0001 W=406.0, p=0.0340 W=468.0, p=0.0006
Proteins	800	466	2496	$\chi^2=9.9214$ df=2 p=0.0070	SS vs. LVF SS vs. HVF LVF vs. HVF	W=447.0, p=0.0093 W=285.0, p=0.7738 W=440.0, p=0.0052
(B) Combination						
EPS ^C	184850	29581	79271	$\chi^2=21.60$ df=2 p<0.0001	SS vs. LVF SS vs. HVF LVF vs. HVF	W=527.0, p<0.0001 W=403.0, p=0.0596 W=466.0, p=0.0007
All components ^D	252325	31955	141743	$\chi^2=33.93$ df=2 p<0.0001	SS vs. LVF SS vs. HVF LVF vs. HVF	W=583.0, p<0.0001 W=400.0, p=0.0916 W=528.0, p<0.0001

^A n=25; ^B n=24; ^C EPS = carbohydrates + proteins, before averaging, data presented is therefore the median of the sums; ^D All components = EPS + cells, before averaging, data presented is therefore the median of the sums.

The EPS-to-cell ratio, which describes the amount of EPS per μm^3 of cells, was less for the HVF biofilms (median=1.98) than those from SS (median=4.96), once again reflecting the trends seen in the 3D biofilm projections, but this difference was not statistically significant (Table 6.3). LVF biofilms expressed EPS-to-cell and carbohydrate-to-cell ratios that were more than five times greater than those for either SS or HVF; differences which were determined to be statistically significant (Table 6.3). Across all three flow regimes, the Day 28 biofilms contained carbohydrate volumes which were greater than the cell volume (see carbohydrate-to-cell ratio in Table 6.3). The protein volumes were less than the cell volume within the SS and HVF Day 28 biofilms but the LVF biofilms had, on average, the same volume of proteins as cells, which lead to significant differences between the LVF biofilm protein-to-cell ratio and those of the SS or HVF biofilms (Table 6.3). When biofilms from all three hydraulic conditions were compared no significant difference was found in the EPS compositional ratios (carbohydrate-to-protein ratio in Table 6.3). Yet, according to the pairwise tests, the carbohydrate-to-protein ratio of the LVF biofilms was significantly lower than in SS and indicated that the proteins contributed proportionally more to the LVF EPS matrices than they did in the EPS matrix of SS biofilms, which had the lowest proportion of proteins (indicated by the highest ratio value).

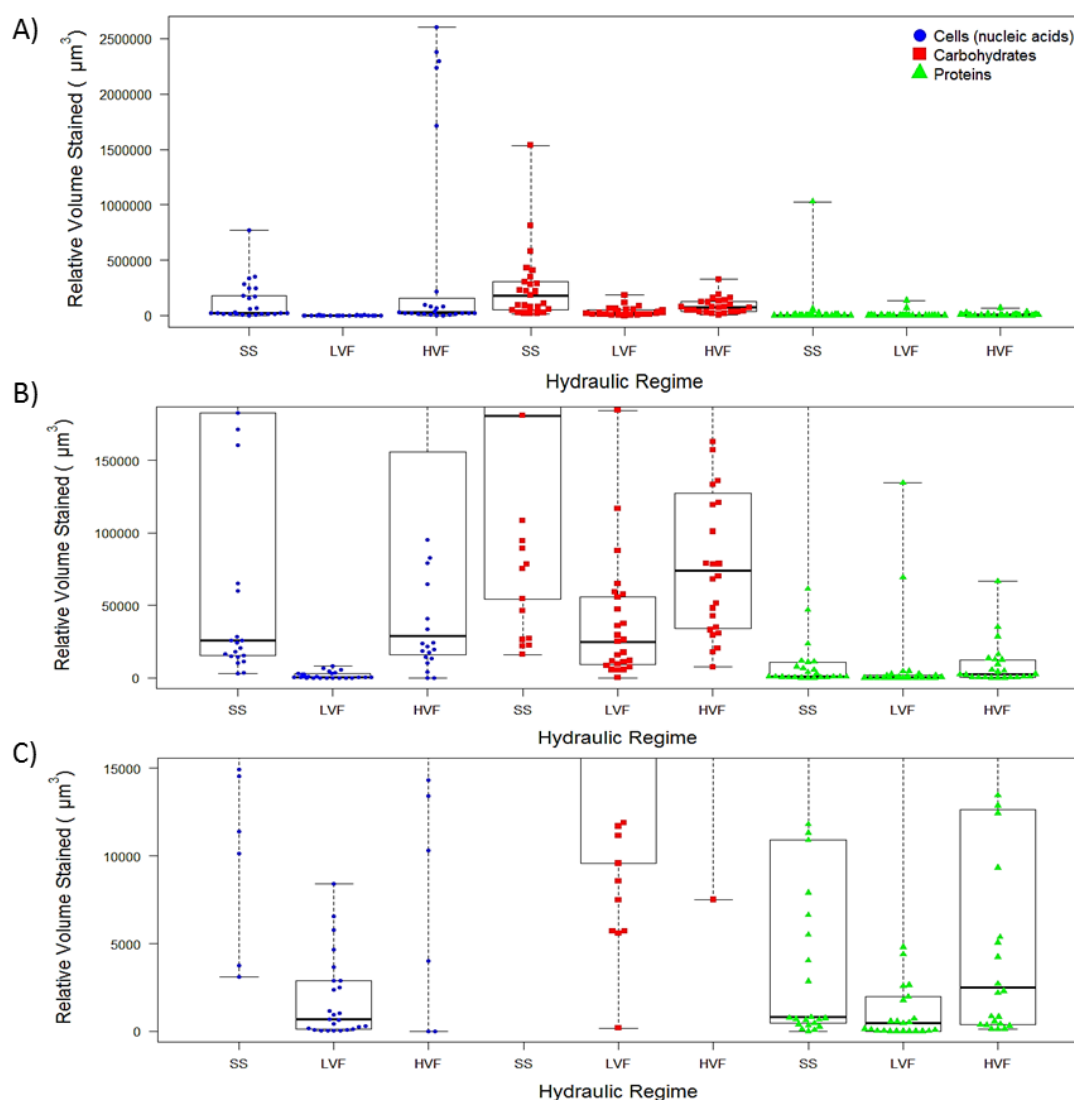


Figure 6.4 Relative volumes of stained biofilm components within Day 28 biofilms developed under SS, LVF or HVF hydraulic conditions. Y-axis scale is adjusted to: A) max data point; B) interquartile range of the cell data; C) interquartile range of the protein data. Each data point represents a different FOV, n=25 for SS and LVF, n=24 for HVF. Box and whisker plots show the range, interquartile range and median – indicated by the black solid line; volume is relative to the threshold value (see section 4.6.3.3).

Table 6.3 Comparison of relative volume ratios of different components within Day 28 biofilms from SS, LVF or HVF hydraulic conditions. Significant results are shown in bold.

Ratios ^A	Median Ratio Value			Kruskal Wallis SS vs. LVF vs. HVF	Wilcoxon Results	
	SS	LVF	HVF		Pairwise test	Result
EPS: Cells	4.86	26.39	1.98	$\chi^2=29.06$ df=2 p<0.0001	SS vs. LVF	W=105.0, p<0.0001
					SS vs. HVF	W=378.0, p=0.0629
					LVF vs. HVF	W=51.0, p<0.0001
Carbohydrates: Proteins	62.31	14.24	33.24	$\chi^2=4.16$ df=2 p=0.1249	SS vs. LVF	W=411.0, p=0.0285
					SS vs. HVF	W=354.0, p=0.2874
					LVF vs. HVF	W=359.0, p=0.2416
Carbohydrates: Cells	4.80	21.29	1.21	$\chi^2=26.04$ df=2 p<0.0001	SS vs. LVF	W=126.0, p=0.0002
					SS vs. HVF	W=401.0, p=0.0437
					LVF vs. HVF	W=66.0, p<0.0001
Proteins: Cells	0.19	1.00	0.06	$\chi^2=8.42$ df=2 p=0.0149	SS vs. LVF	W=106.5, p=0.0196
					SS vs. HVF	W=215.0, p=0.3184
					LVF vs. HVF	W=102.0, p=0.0135

^A The first component is divided by the second, a value > 1 indicates a greater volume of the first component, a value <1 indicates a greater volume of the second, a value =1 indicates equal volumes of each.

SS and HVF biofilms had similar cell, carbohydrate and protein spreads, as shown in Table 6.4. However, the cells and proteins of the LVF biofilms had a significantly reduced spread compared to that of the cells and proteins within the SS and HVF biofilms (Figure 6.5; Table 6.4). In contrast, the spread of the carbohydrates in the LVF biofilms was similar to the carbohydrate spread in SS biofilms and differed only from the HVF biofilms, which had the lowest carbohydrate spread of the three regimes. Within the SS Day 28 biofilms the cells, carbohydrates and proteins had similar spreads (Wilcoxon: $W \geq 251.0$, $p \geq 0.2389$), a trend which was also observed in the HVF biofilms (Wilcoxon: $W \geq 170.0$, $p \geq 0.1521$). However, within the LVF biofilms, the spread of the carbohydrates exceeded that of the cells (Wilcoxon: $W = 453.0$, $p = 0.0058$) and proteins (Wilcoxon: $W = 404.0$, $p < 0.0001$), which had a similar spread to each other (Wilcoxon: $W = 161.0$, $p = 0.0715$). Thus, the depth range of the carbohydrates exceeded that of the cells and proteins.

Despite the variations in spread and relative volume, there was no significant difference in the peak location of carbohydrates (Kruskal Wallis: $X^2 = 4.42$, $df = 2$, $p = 0.1099$; Wilcoxon: $W \geq 215.0$, $p \geq 0.0672$), which occurred (on average) at the aligned slice number -1 regardless of the flow regime under which the biofilm developed. An aligned slice of -1 indicated that the maximum area coverage of carbohydrates occurred above that of the cells, nearer to the top surface of the biofilm. There were however, three and four FOV of the LVF and HVF biofilms respectively, which had a carbohydrate peak location that occurred below that of the cells, nearer to the biofilm-pipe wall interface (Figure 6.6). There was no significant difference (Kruskal Wallis: $X^2 = 1.83$, $df = 2$, $p = 0.3998$; Wilcoxon: $W \geq 261.5$, $p \geq 0.1822$) in the peak location of proteins between the biofilms from SS (median: aligned slice -3), LVF (median: aligned slice -3) or HVF (median: aligned slice -2). Proteins were generally located above the peak location of the cells, and often a slice above the carbohydrates, though there were a few exceptions where the protein peak location was below the cell peak (see the data points below the dotted line in Figure 6.6).

Table 6.4 Statistical comparisons of the spread of the stained biofilm components in biofilms developed under SS, LVF or HVF conditions for 28 days. Significant results are shown in bold.

Biofilm Component	Median Spread Value (AU)			Kruskal Wallis SS vs. LVF vs. HVF	Wilcoxon Results	
	SS	LVF	HVF		Pairwise test	Result
Cells	4529622	3549221	4425734	$X^2=7.66$ $df=2$ $p=0.0217$	SS vs. LVF	$W=436.0, p=0.0161$
					SS vs. HVF	$W=294.0, p=0.9024$
					LVF vs. HVF	$W=402.0, p=0.0177$
Carbohydrates	4394548	4406852	3580180	$X^2=6.00$ $df=2$ $p=0.0498$	SS vs. LVF	$W=252.0, p=0.2467$
					SS vs. HVF	$W=352.0, p=0.3060$
					LVF vs. HVF	$W=172.0, p=0.0099$
Protein	4638752	2908246	3874705	$X^2=11.20$ $df=2$ $p=0.0037$	SS vs. LVF	$W=375.0, p=0.0008$
					SS vs. HVF	$W=377.0, p=0.1268$
					LVF vs. HVF	$W=310.0, p=0.0454$

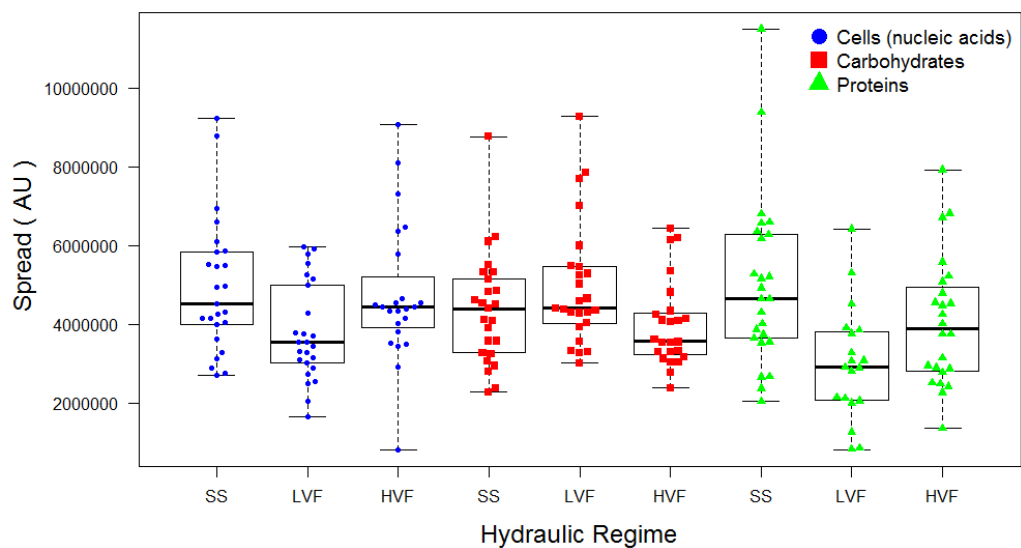


Figure 6.5 Spread of each of the stained biofilm components for Day 28 biofilms developed under SS, LVF or HVF regimes. Each data point represents a different FOV, n=25 for SS and LVF, n=24 for HVF. Box and whisker plots show the range, interquartile range and median – indicated by the black solid line; spread is calculated by the relative volume divided by the max area fraction (see section 4.6.3.4).

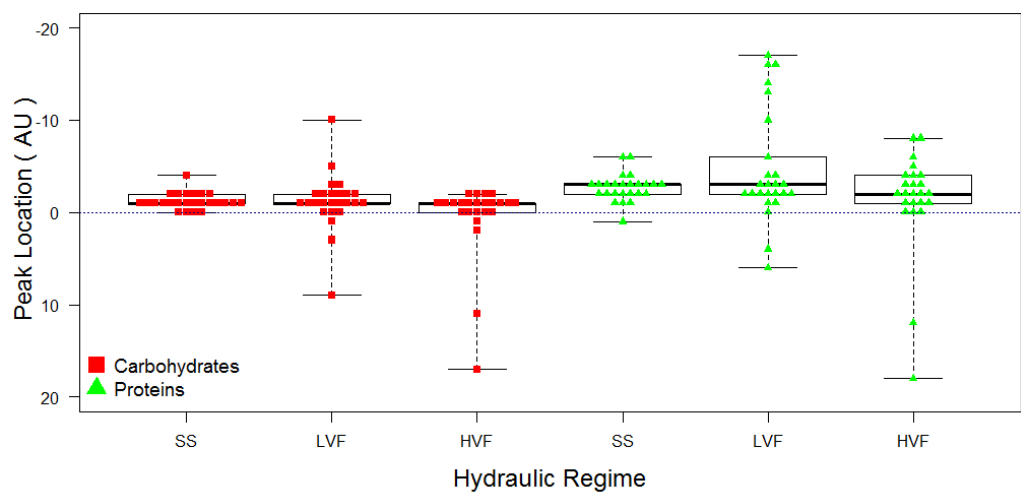


Figure 6.6 Peak location of carbohydrates and proteins, in relation to the cell peak location (indicated by the dotted line), for Day 28 biofilms from SS, LVF and HVF experiments. Each data point represents a different FOV, n=25 for SS and LVF, n=24 for HVF. Box and whisker plots show the range, interquartile range and median – indicated by the black solid line; peak location is the aligned slice number at which the max area fraction occurs (see section 4.6.3.5).

6.2.3 Biofilm community structure

6.2.3.1 PCR amplification of 16S rRNA genes and ITS regions

16S rRNA bacterial and archaeal genes and fungal ITS regions were amplified from nine DNA extractions per sample point (Day 0 and Day 28), for biofilms developed under SS, LVF and HVF hydraulic regimes. Detectable concentrations of bacterial DNA were more commonly found in the LVF (4/9) and HVF (5/9) Day 0 biofilms than they were in those from SS (2/9). By Day 28 bacterial DNA was detected in the majority of samples from each of the flow regimes, but was most commonly found in the SS biofilms (SS: 9/9; LVF: 8/9; HVF: 6/9). Even after just 90 minutes, fungi were detected upon the coupon surface of the SS samples (5/9), but were only found in one LVF replicate (1/9) and were not detected in any HVF biofilms. After 28 days of development fungal DNA was detected across all the SS replicates (9/9) but was restricted to 3/9 of the LVF replicates and a single HVF replicate. In all instances, when visualised on an agarose gel (not shown), the strength of the purified PCR products differed between replicates, but generally the Day 28 samples were observed to be more concentrated than Day 0.

No samples from either Day 0 or Day 28 of the HVF biofilms contained quantities of archaeal DNA detectable via the methods used in this study. Conversely, archaea were found in 5/9 of the Day 0 SS biofilms and all (9/9) of the Day 28 biofilms (detailed in Chapter 5). Unfortunately the LVF biofilm samples were contaminated with environmental archaea at the biofilm suspension stage (during which the biofilm is removed from the coupon), as was indicated by the strong bands visualised for the biofilm suspension controls following gel electrophoresis of the archaeal PCRs (Figure 6.7). As the negative control was clear the contamination was not due to the PCR process, furthermore, the replacement of PCR reagents did not remove the contamination. Bands of the same size and strength as those observed in the biofilm suspension controls were seen across all of the LVF biofilm samples, further indicating contamination at the biofilm suspension stage. Therefore the presence of archaea in the LVF samples remains undetermined.

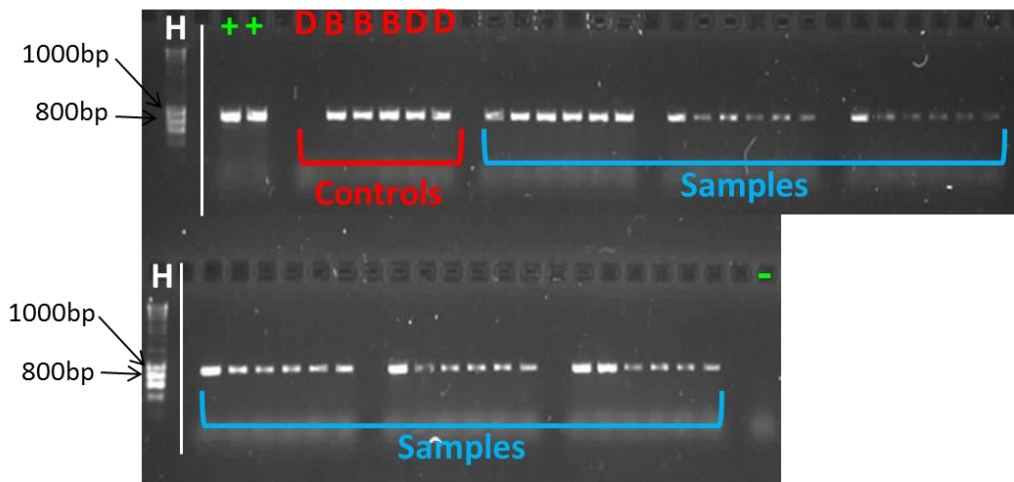


Figure 6.7 Agarose gel electrophoresis images of archaeal PCR products from biofilms developed under LVF conditions. Gel was 1% agarose, Hyperladder I (Bioline, London, UK), indicated by “H” was used for sizing, “+” indicates positive controls; “-” indicates the negative control. Samples shown are PCRs of the LVF DNA extractions at each sample point (Day 0, Day 28, Pre-flush, Post-flush) to demonstrate the extent of the contamination. The controls consist of biofilm suspension controls – “B” and DNA extraction controls “D”.

6.2.3.2 Microbial community analysis

A detailed comparison of the changes in microbial community between SS Day 0 and Day 28 biofilms is presented in Chapter 5, showing the distinction between the two sample points and illustrating that there was no effect of loop or position upon community structure. Analysis of the LVF Day 0 biofilms in comparison to Day 28 showed a significant difference in the bacterial community structures (ANOSIM: relative abundance, global $R=0.801$, $p=0.002$; presence/absence, global $R=0.805$, $p=0.002$); the relative richness (T-test: $df=9.35$, $p<0.0002$), and diversity (T-test: $df=6.10$, $p<0.001$) of the community was greater at Day 28, but there was no change in relative evenness (T-test: $df=2.10$, $p=0.06379$). Under HVF regimes the Day 0 biofilms were also significantly different from those at Day 28 (ANOSIM: relative abundance, global $R=1.000$, $p=0.002$; presence/absence, global $R=1.000$, $p=0.002$) and increases were seen in relative richness (T-test: $df=8.20$, $p<0.0001$), diversity (T-test: $df=6.66$, $p=0.0002$) and evenness (T-test: $df=3.92$, $p=0.0373$). There were no differences in biofilms from coupons from different loops or positions when samples were developed under LVF conditions (ANOSIM for position: relative abundance, global $R=0.254$, $p=0.062$; presence/absence, global $R=0.231$, $p=0.077$; ANOSIM for loop: relative abundance, global $R=-0.145$, $p=0.872$; presence/absence, global $R=-0.145$, $p=0.872$) or HVF conditions (ANOSIM for position: relative abundance, global $R=-0.069$, $p=0.644$; presence/absence, global $R=-0.085$, $p=0.697$; ANOSIM for loop: relative abundance, global $R=-0.132$, $p=0.804$; presence/absence, global $R=-0.135$, $p=0.814$).

The analysis above confirmed the increase in complexity of the biofilm communities over the 28 day development phase, regardless of the hydraulic regime imposed during this period. The subsequent data presented in this section demonstrates the similarities or differences between the communities that developed under each hydraulic condition (SS vs. LVF vs. HVF comparison). As archaea were restricted to SS samples, no comparison with LVF or HVF samples was possible and so the archaea were not considered in the community analysis results in the following sections. Additionally, fungal DNA was not detected in a sufficient number of LVF Day 0 samples (1/9) or HVF samples (not detect at Day 0 and 1/9 at Day 28) to enable an accurate comparison between the communities within biofilms from the three regimes. Three LVF Day 28 samples contained detectable amounts of fungal DNA so a pairwise comparison to the SS Day 28 fungal community was able to be made but should be interpreted with care due to the differences in replicates. Therefore, the community that could be compared across all three of the hydraulic conditions was that of the bacteria. However, statistical comparison between the ecological indices of the Day 0 bacterial community under each flow regime (data shown in Appendix A9.5) was not possible due to the limited number of samples for SS and so comparisons between Day 0 biofilms were restricted to the multivariate analysis of bacterial community similarities.

6.2.3.3 Effect of hydraulic regime upon relative taxon richness, evenness and diversity

The electropherograms from T-RFLP analysis demonstrated similarities between the bacterial communities developed under each hydraulic regime, as some peaks were conserved between the SS, LVF and HVF profiles, particularly around the 200 nt region (Figure 6.8A). However, the dominant peak for SS biofilms occurred at a T-RF of 198.57 nt in length, whereas for LVF and HVF the dominant peak was found at 199.72 nt. Bacterial T-RFLP profiles comprised a total of 103, 122 and 104 different T-RFs across the Day 28 biofilm replicates from SS (n=9), LVF (n=8) and HVF (n=6), respectively. Although the total number of different bacterial T-RFs was greatest in the LVF biofilms, the average number of T-RFs in individual profiles was lower than was observed in the SS or HVF biofilms (described as relative taxon richness in Table 6.5). However, the difference in relative taxon richness was only significant between the SS and LVF biofilms (ANOVA: df=2, p=0.0128; subsequent Tukey HSD test: SS vs. LVF, p=0.0109; SS vs. HVF, p=0.1417; LVF vs. HVF, p=0.5971). Similarly, the variation between the relative evenness and diversity indices was only statistically significant between the SS and LVF biofilms. The SS bacterial community was more even than that of the LVF biofilms (ANOVA: df=2, p=0.0055;

subsequent Tukey HSD test: SS vs. LVF $p=0.0056$) with greater diversity (ANOVA: $df=2$, $p=0.0081$; subsequent Tukey HSD test: SS vs. LVF $p=0.0067$).

Visual comparison between the fungi community fingerprints of SS and LVF biofilms (Figure 6.8B) highlighted the dominance of an ARISA amplicon at 595.11 nt within biofilms from both hydraulic conditions. Aside from the dominant amplicon, smaller peaks appeared to occur at similar ARISA amplicon lengths, with the exception of peaks between 600 and 700 nt, which were distinct within the SS profiles but less abundant within the LVF profiles. The total number of different ARISA amplicons was greater in the SS biofilms (106, $n=9$) than the LVF biofilms (78, $n=3$), which suggested that there was a greater diversity of fungi at SS. However, statistical comparison between the ecological indices (see Table 6.5 for range and average) of the SS and LVF biofilms found no differences in relative richness (T-test: $df=2.34$, $p=0.8647$), relative diversity (T-test: $df=2.47$, $p=0.9569$) or relative evenness (t-test: $df=2.49$, $p=0.8015$).

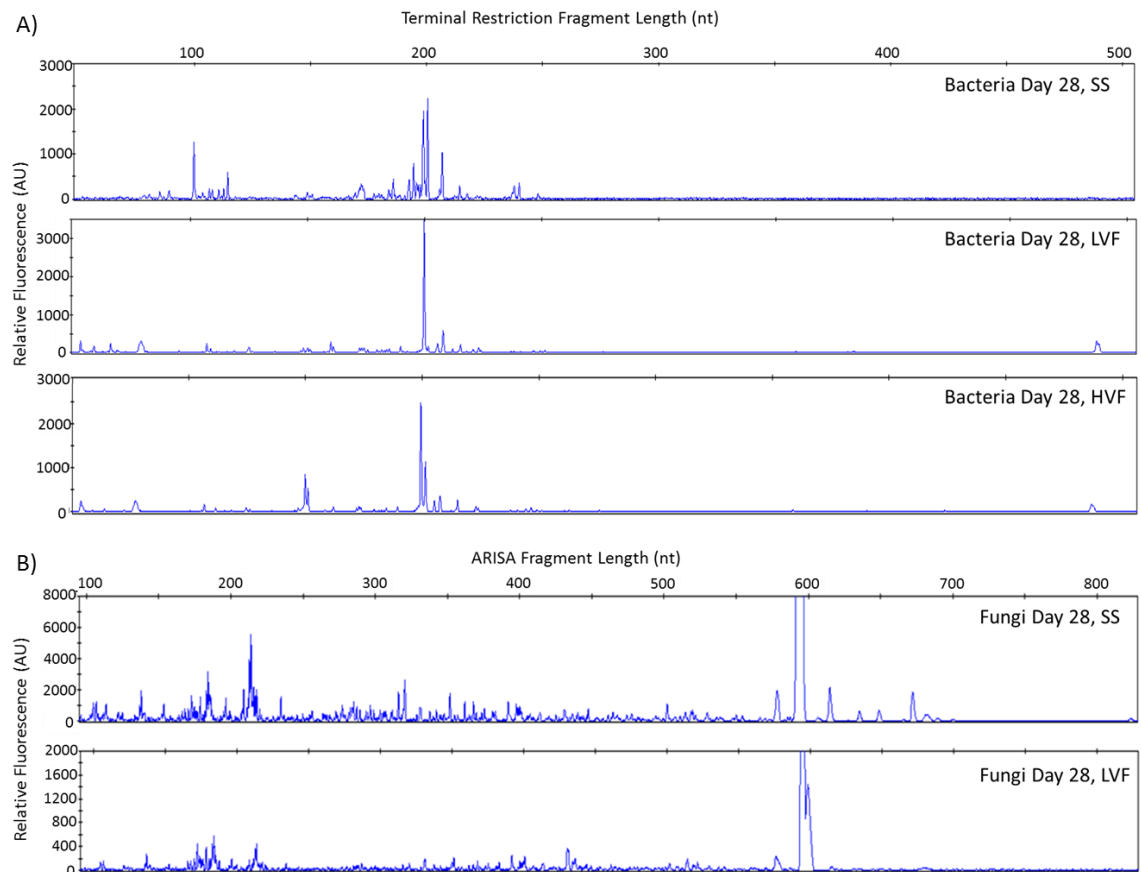


Figure 6.8 Representative T-RFLP or ARISA electropherograms of drinking water biofilm communities after 28 days of development under SS, LVF or HVF conditions. A) Bacterial communities (16S rRNA, T-RFLP analysis); B) Fungal communities (ITS region, ARISA analysis); N.B. fungi not detected in HVF biofilms.

Table 6.5 Relative richness, evenness and diversity indices of the bacterial and fungal communities from biofilms sampled at Day 28 from the SS, LVF or HVF condition.

Microbial fingerprint	Flow Regime	Relative Richness (number of T-RFs)			Relative Evenness (Pielou's Index)			Relative Diversity (Shannon's Index)		
		Min	Max	Mean (St.Dev)	Min	Max	Mean (St. Dev)	Min	Max	Mean (St. Dev)
Bacteria	SS	28	41	36.59 (4.59)	0.95	0.98	0.97 (0.01)	3.27	3.26	3.48 (0.13)
	LVF	15	38	26.38 (7.91)	0.89	0.96	0.94 (0.02)	2.41	3.48	3.04 (0.36)
	HVF	23	43	29.83 (7.14)	0.92	0.98	0.95 (0.02)	2.93	3.67	3.20 (0.27)
Fungi	SS	10	51	23.56 (13.51)	0.84	0.99	0.91 (0.06)	1.97	3.91	2.77 (0.67)
	LVF	8	58	26.67 (27.30)	0.81	1.00	0.92 (0.10)	2.00	4.05	2.73 (1.14)

N.B. Min = minimum, Max=maximum, St.Dev = standard deviation.

6.2.3.4 Effect of hydraulic regime upon bacterial and fungal community structure

Figure 6.9 provides a good representation of the bacterial community data (stress value <0.1), accurately showing that the Day 0 biofilms were predominantly no different between the hydraulic treatments; with the exception of a single outlier (sample 26, which had the lowest total peak area of all Day 0 samples) the Day 0 communities formed a single cluster. Conversely, Day 28 samples clustered into two distinct groups – SS and the varied flows. The SS Day 28 replicates were an average of 52.47% similar to each other (SIMPER analysis) and all fell within one cluster, whereas the biofilms from LVF (48.22% similar) and HVF (33.79% similar) experienced greater variation between replicates, with three LVF samples and one HVF sample clustering independently. The total peak area of each of the Day 28 outliers was within the accepted range of 11,000-68,000 (AU), therefore they did not cluster independently due to low fluorescence during T-RFLP analysis. The three LVF outliers (samples 122, 112 and 216) did not have particularly low relative richness and were not from one particular position or loop, therefore it can be concluded that the placement of these samples was a true reflection of a difference in community driven by the heterogenic nature of biofilm. Sample 36 was the HVF replicate with the greatest relative richness (45 T-RFs) with 13 more T-RFs than the next richest profiles; this is likely to be why this replicate does not cluster with the other HVF samples.

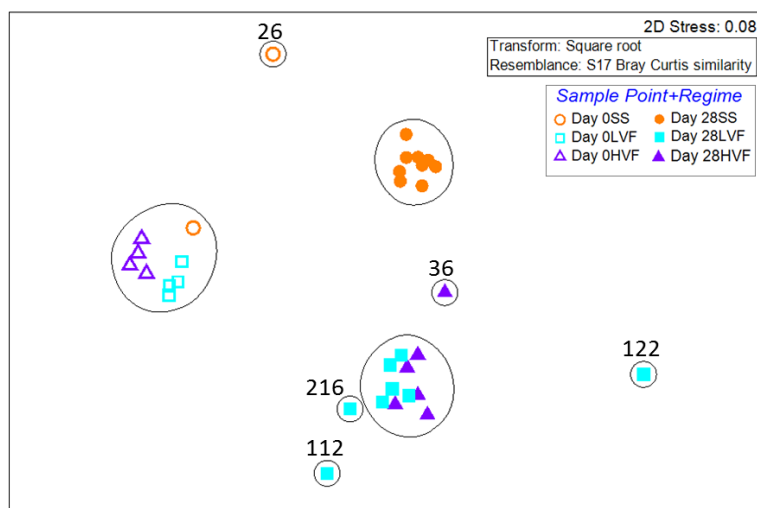


Figure 6.9 nMDS plot of bacterial community structures from biofilms developed under the SS, LVF or HVF hydraulic conditions for 28 days. nMDS shown was plotted using the relative abundance data, same pattern observed with the presence/absence data, black lines indicate clusters of at least 40% similarity, based on group averages from hierarchical clustering analysis and show the main groups which were highlighted in the dendrogram (not presented). Sample identification numbers are shown in some instances, in which the first number relates to the loop from which the sample was obtained and the second number(s) indicate the coupon which was sampled, see Figure 3.3.

Regardless of the outliers, the hydraulic regime imposed during the development phase had an effect upon the bacterial community (ANOSIM for SS vs. LVF vs. HVF: relative abundance, global $R=0.717$, $p<0.0001$; presence/absence, global $R=0.718$, $p<0.0001$). SS bacterial communities were, on average, 87.92% dissimilar (SIMPER test) from those within biofilms from LVF, which lead to a significant difference between the two hydraulic conditions (ANOSIM: relative abundance, global $R=0.865$, $p<0.0001$; presence/absence, global $R=0.855$, $p<0.0001$). The SS bacterial communities were also significantly different from those observed under HVF conditions (ANOSIM: relative abundance, global $R=0.998$, $p<0.0001$; presence/absence, global $R=0.979$, $p<0.0001$), with an average dissimilarity of 83.94%. The majority (60%) of the variation between the SS and LVF communities, and the SS and HVF communities was attributed to 37 and 33 T-RFs respectively (Figure 6.10A and B). LVF and HVF bacterial communities were not significantly different from each other (ANOSIM: relative abundance, global $R=0.069$, $p=0.1800$; presence/absence, global $R=0.110$, $p=0.1140$). Nonetheless, the samples from the two varied flow regimes were not exactly the same, SIMPER analysis demonstrated 63.05% dissimilarity between them, the majority of which was explained by the 33 T-RFs plotted in Figure 6.10C. Each graph in Figure 6.10 is plotted on an x-axis with the same T-RF lengths within the range 52 - 493 nt, so that comparisons between the pairwise tests can more easily be made. For a particular plot, if there is a T-RF which does not have any data associated with it, for example 52.87 nt in Figure 6.10A, then this T-RF was not accredited with discerning the bacterial communities from the two hydraulic regimes

compared, in this instance SS and LVF. However, it is important in differentiating between one or, as in this instance, between both of the other pairs of biofilms. That is not to say that the T-RF was necessarily absent from the SS and/or LVF communities, rather it indicates that this T-RF was not driving the variation between the two. Indeed, in this instance, the T-RF 52.87 nt was present in LVF bacterial communities as indicated in Figure 6.10C where this T-RF was one of those responsible for the differences between LVF and HVF bacterial communities. The absence of a particular T-RF from a particular bacterial community is indicated if data from only one of the samples sets being compared is associated with it. For example, of the 37 T-RFs that explained the majority of the differentiation between SS and LVF bacterial communities, 8 were found only in the LVF samples (only a blue bar was present) and 10 were exclusive to the SS samples (only an orange bar was present). The other 19 T-RFs were present in both bacterial communities but were found at critically different mean relative abundances. Of the 33 T-RFs that explained 60% of the difference between the SS and HVF bacterial communities, 7 were found only in SS, 7 solely in HVF and 19 were present in both communities but at different relative abundances. Contrastingly, of the 33 T-RFs driving the differences between LVF and HVF, 28 were found in both, 4 were exclusive to LVF and 1 was exclusive to HVF, which suggested that, rather than selecting for particularly different T-RFs, these two groups of biofilm had similar T-RFs present but at different abundances.

Although fungal communities could not be compared between all three regimes, a comparison was made between SS and LVF biofilms, though it is important to stress the difference in replication between the two ($n=9$ and $n=3$ respectively). Figure 6.11A shows a dendrogram of the SS and LVF fungi samples, with one large group which included all of the SS samples and one of the LVF biofilms (sample 216), which was not significantly different from four of the SS samples (indicated by the red lines). The other two LVF samples clustered independently from all the other samples. The SS replicates had a higher degree of similarity to each other (23.28%, SIMPER test) than the LVF replicates did (0.88%, SIMPER test) and the two sample sets were significantly different (ANOSIM: relative abundance, global $R=0.643$, $p=0.009$; presence/absence, global $R=0.620$, $p=0.027$) with just 7.8% similarity according to the SIMPER analysis. The majority (60%) of the variation between the fungal communities of SS and LVF biofilms was explained by 36 ARISA amplicons between 104 nt and 674 nt in length (Figure 6.11B), 11 of which were found solely in SS biofilms, 11 just in LVF biofilms and 14 of which were common between the two sample sets but were present at different abundances.

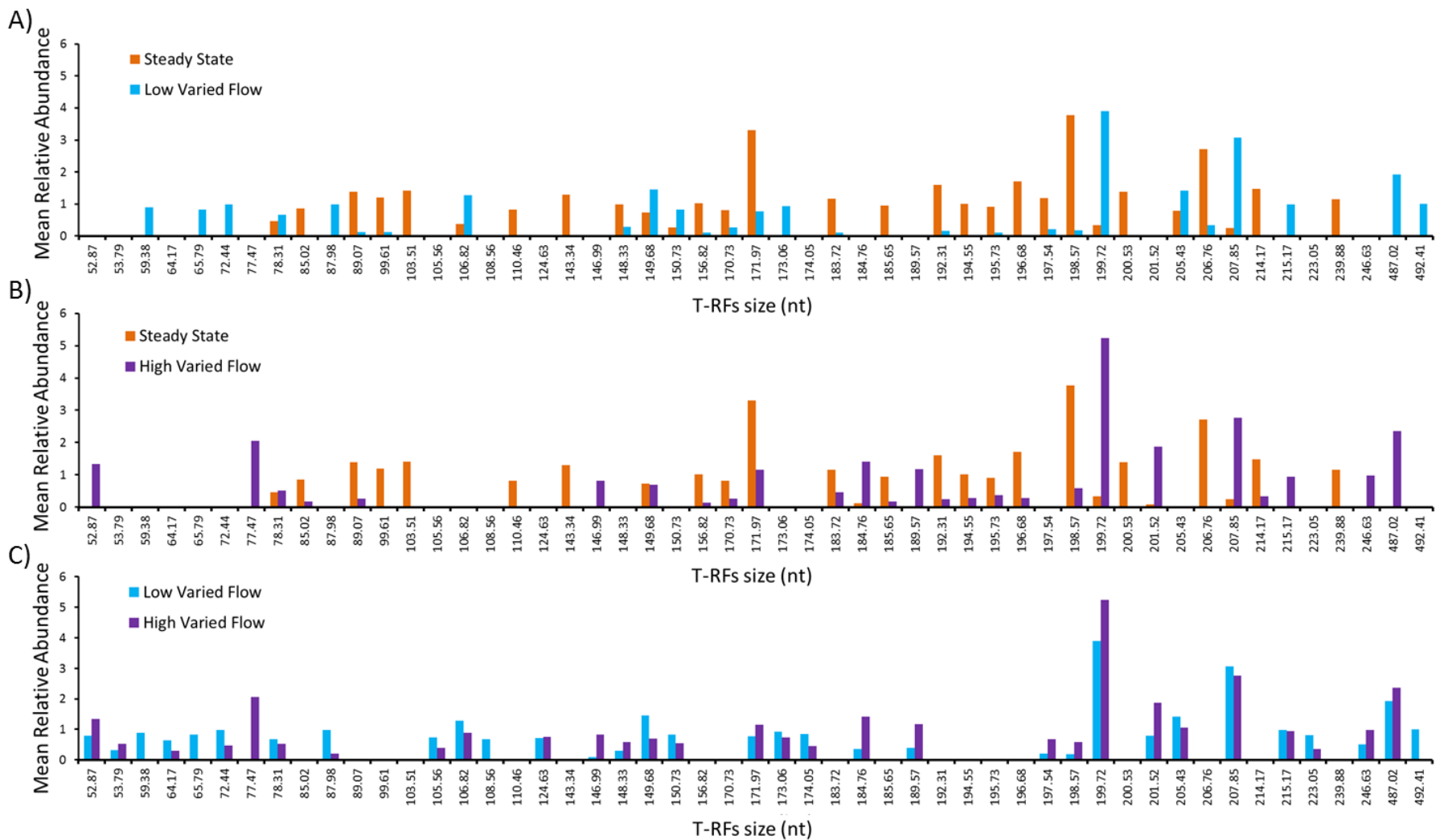


Figure 6.10 Results from SIMPER analysis comparison of bacterial communities sampled at Day 28 from different hydraulic regimes. Each graph shows the size and mean relative abundance (AU) of the bacterial T-RFs that explain 60% of the difference between biofilms from: A) SS vs. LVF; B) SS vs. HVF; C) LVF vs. HVF comparisons.

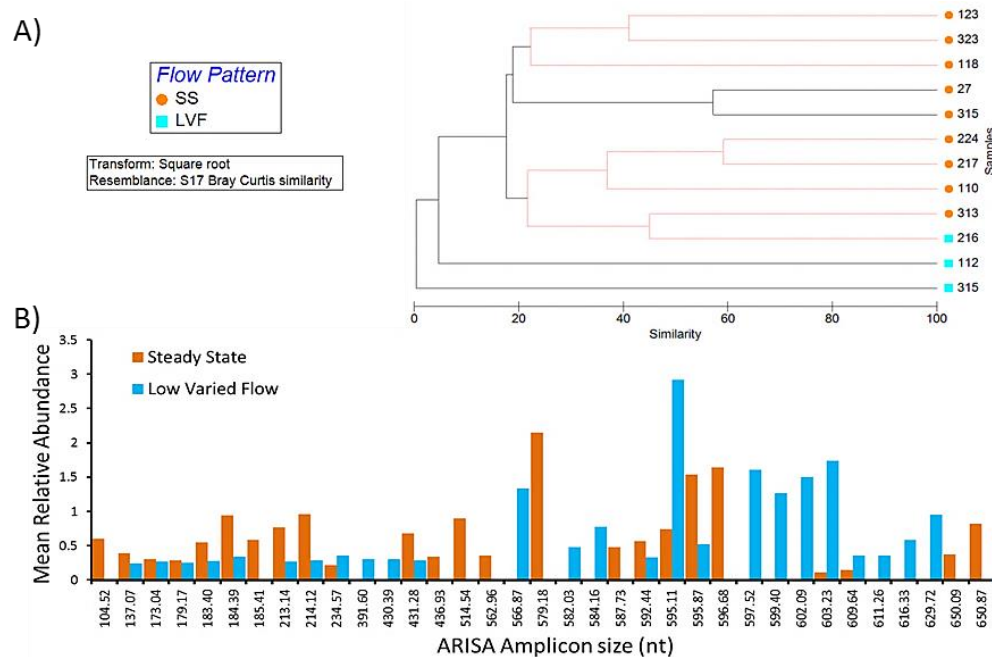


Figure 6.11 Comparison of the fungal communities within Day 28 biofilms from SS and LVF hydraulic conditions. A) Dendrogram showing the similarity between samples using the relative abundance data, the presence/absence data showed the same trends; red lines indicate profiles not significantly dissimilar according to SIMPROF. Sample identification numbers are shown; the first number relates to the loop, the second number(s) indicate the coupon position, see Figure 3.3. B) The ARISA amplicons which describe 60% of the variation between SS and LVF fungal communities.

6.3 Discussion

Within a full scale, temperature controlled DWDS experimental facility three experiments were conducted, during which biofilm was allowed to develop for 28 days, under one of three hydraulic conditions - SS, LVF or HVF. In each experiment the three loops of the experimental facility were run as replicates and fed with drinking water from the local system. TOC and manganese concentrations were slightly higher in the HVF test and ORP was slightly lower, however, the greatest variation between experiments was the hydraulic regime. Biofilm samples (taken using PWG coupons) were characterized with regard to physical (cells, carbohydrates and proteins) and community (bacteria, fungi and archaea) structures.

Samples taken at Day 0 showed no differences in bacterial community structure, EPS quantity or composition, the spread of the biofilm components, or the peak locations of carbohydrates and proteins, with respect to hydraulic regime. All the Day 0 biofilms were dominated by cells with little EPS. However, SS Day 0 biofilms had relative volumes of cells, carbohydrates and proteins significantly greater than was seen in LVF or HVF Day 0 biofilms, which were similar to each other. All Day 0 samples were in the facility for ≤ 90 minutes, at this point the LVF and HVF hydraulic regimes did not differ as they both started with a “low night time flow” period of 0.2 l s^{-1} , but the SS regime had a flow rate of 0.4 l s^{-1} . Therefore, as the only significant

difference between the Day 0 biofilms was the relative volume, with no significant difference in spread (the proxy for depth), it can be concluded that these differences were more likely due to variation in the XY biofilm coverage than the Z dimension, potentially due to the stochastic nature of the initial contact of planktonic cells with the pipe surface. It may be that the higher flow rate during the first 90 minutes of the SS experiment, compared to LVF or HVF, increased the chances of the initial contact of cells with the pipe wall due to a more turbulent water flow. This appears to be the first time a start point sample from different hydraulic conditions has been analysed in detail and so comparison to other studies is not possible.

Biofilm structure altered during the development phase of each hydraulic condition. Between Day 0 and Day 28, the relative volume and spread of each of the biofilm components increased and the quantity of EPS exceeded that of the cells, as the biofilms matured producing more EPS. This is a pattern which was also observed by Rochex *et al.* (2008) and Wagner *et al.* (2009). Biofilms from each regime included cell only areas, an observation which was also made with respect to wastewater biofilms developed within a reactor (Wagner *et al.* 2009). It is postulated that these were areas of more recent material accumulation where the biofilm was still in the primary adhesion stage. The biofilm communities also altered between Day 0 and Day 28, showing changes in the T-RFs or ARISA amplicons which were present, generally an increase in community complexity was observed. In all instances, biofilms were found upon coupons from each position around the pipe, with no obvious effect of gravitational settling and so location around the pipe had no influence upon biofilm structure.

The biofilms clearly developed and matured during the growth phase of each experiment, but the structures which occurred under each hydraulic condition were not identical. A summary of some of the similarities/differences is provided in Figure 6.12. Regardless of hydraulic condition, or the specific relative volumes, carbohydrates were the dominant component of the drinking water biofilms, a trend which has been reported previously for biofilms in general (e.g. Möhle *et al.*, 2007; Wagner *et al.*, 2009). Carbohydrates were particularly extensive in their depth throughout LVF biofilms, occurring across a greater spread than either the cells or proteins. Of the three regimes, the greatest proportional increase (in relation to the amount of material at Day 0) in biofilm relative volume was seen in the HVF biofilms, potentially due to a better penetration of nutrients into the biofilm because of the greater turbulence in the water column. Previous biofilm studies also found a greater amount of biofilm under higher flow rates, although these compared steady state conditions of different flow rates and shear stresses, rather than varied patterns. Rochex *et al.* (2008) found that after 21 days of growth within a reactor, biofilms inoculated with white water and nutrient growth medium had a

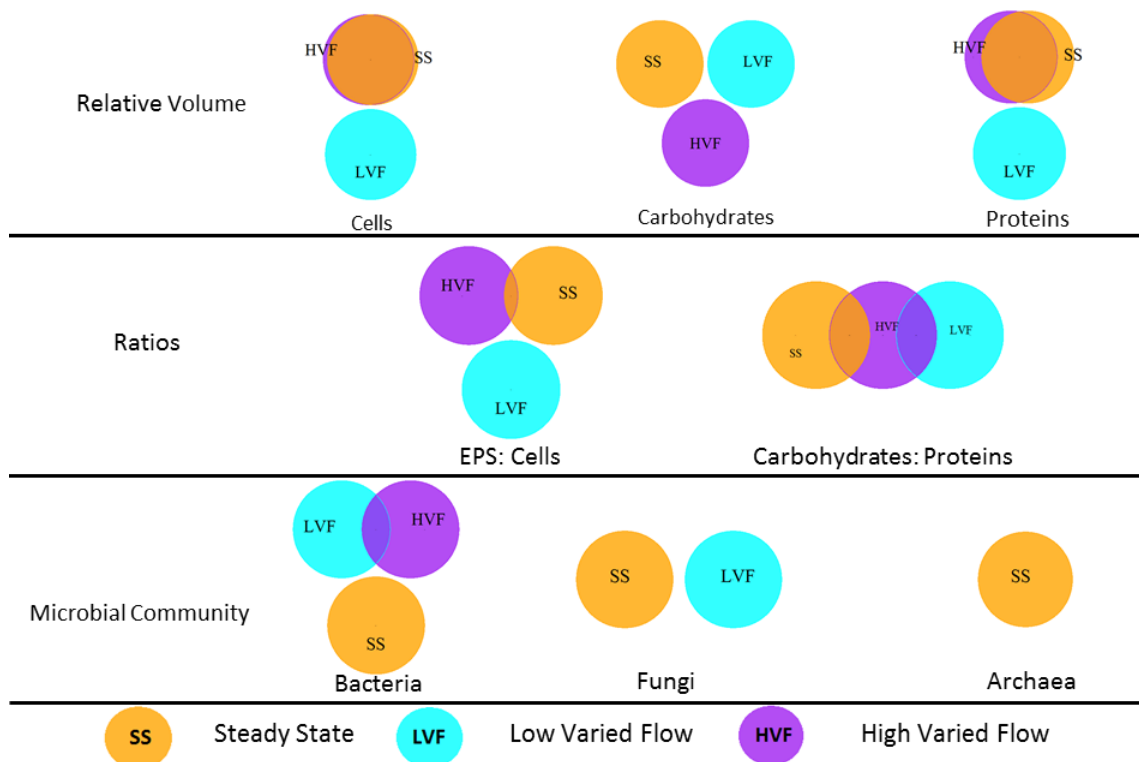


Figure 6.12 Summary of some of the patterns in biofilm structure parameters seen between the biofilms from SS, LVF and HVF conditions after 28 days of development. Diagram is a schematic representation of similarities and differences only, drawn in the statistical program R v2.15. Similarities are shown by the overlap of groups (not the order) which was determined by the p value associated with the relevant pairwise test such that $p > 0.9999$ would lead to a 100% overlap, $p=0.50$ would lead to a 50% overlap, etc. Where $p \leq 0.05$ the groups had no overlap. The physical structure parameters were based upon the Wilcoxon tests and microbial community patterns were based on the multivariate clustering analysis (i.e. the ANOSIM tests).

greater mass and thickness under a shear stress of 0.27 Nm^{-2} than 0.055 Nm^{-2} . Similarly, Dunsmore *et al.* (2002), Simoes *et al.* (2003) and Sly *et al.* (1988) reported greater material accumulation under greater velocities and more turbulent water flow. Sly *et al.* (1988) observed a greater TOC concentration on stubs from a Robbins device run at 0.5 ms^{-1} compared to 0.01 ms^{-1} , and also found higher concentrations of iron and manganese deposits upon the surface. In contrast, a study by Wagner *et al.* (2009), in which biofilms were inoculated with wastewater sludge and cultured under flow rates of 0.08 , 0.2 and 0.3 ls^{-1} , reported thinner more homogenous biofilms as the flow rates increased. Möhle *et al.* (2007) found that thicker biofilms formed within a rotating disc reactor, fed with activated sludge, when exposed to lower shear stresses (range tested was 0.007 , 0.020 and 0.037 Nm^{-2}). However, the authors simultaneously, altered shear stress and nutrient concentrations (by altering the glucose, urea and iron sulphate concentrations fed into the reactor), therefore it is not possible to determine the influence of these factors independently. The nutrients in the bulk phase of both Wagner *et al.* (2009) and Möhle *et al.* (2007) were in higher concentrations than those in drinking water. Consequently, it is possible that the mass transfer of nutrients,

driven by the bulk phase turbulence, was not a limiting factor in the reactor systems as it was in the DWDS experimental facility, hence the opposing trends in biofilm volume.

Despite a greater proportional increase in biofilm amount between Day 0 and Day 28 at HVF than LVF or SS, the relative biofilm volumes at Day 28 of the HVF were not different to those seen under SS conditions, except for the carbohydrates (Figure 6.12) of which there was a greater volume in SS. However, LVF biofilms had a significantly lower relative volume of carbohydrates, as well as cells and proteins, when compared to SS and HVF biofilms. Sharpe (2012) also provided evidence for less material accumulation under LVF, although this was limited to quantification of the cells. In Sharpe (2012), the SS, LVF and HVF regimes detailed in this thesis were run simultaneously, each in a different loop, for the same 28 day period. As the results presented in this chapter compliment the findings in Sharpe (2012), it can be concluded that this result was a true reflection of the influence of hydraulic regime and not an artefact of the month in which the LVF experiment was conducted. Interestingly though the greatest amount of EPS per μm^3 of cells was seen in the LVF biofilms, along with the greatest spread of carbohydrates and the greatest proportion of proteins. SS and HVF biofilms had, on average, less proteins than cells but, when developed under LVF conditions, the relative volume of biofilm proteins was (on average) equal to that of the cells. The impact of hydraulics upon protein production has not been fully explored, some studies show greater protein concentrations at lower flow rates (Wagner *et al.*, 2009) while others show a positive correlation between proteins and velocity (Simoes *et al.*, 2005). Within the context of the drinking water biofilms from this study, the differences in protein content led to subtle variations in EPS composition between the three conditions (see carbohydrate-to-protein ratio in Figure 6.12). No difference was found in the EPS-to-cell ratio or carbohydrate-to-protein ratio of SS and HVF biofilms, i.e. they had the same proportion of EPS, which was less than that within LVF biofilms and the same proportion of proteins within the EPS, which was also less than within LVF biofilms.

Although it is clear that hydraulic regime did influence biofilm physical structure characteristics, the processes driving the development of the different structures and the advantages they convey are complex. The findings contradict the theory that the HVF biofilms would have the greatest EPS proportion to enable them to remain adhered during the higher maximum flow rate experienced during the 24 hour flow profile. However, it has been suggested that an increase in shear stress alters biofilm dynamics, slowing down biofilm maturation and maintaining a younger biofilm (Rochex *et al.*, 2008). Potentially, the greater range of shear stresses the HVF biofilms were exposed to may have conditioned a more

immature biofilm with a less extensive EPS matrix than at LVF, but a greater volume of material due to the promotion of cell replication. An increase in the mass transfer rate at HVF may have improved the supply of trace organics and inorganics to the biofilm, thus promoting a higher cell growth rate. This theory is supported by Simoes *et al.* (2003; 2005) who found less carbohydrates per gram of biofilm, but greater respiratory activity (indicating more cellular activity via an increase in oxygen uptake) in samples grown under velocities of 0.532 ms^{-1} compared to samples from 0.204 ms^{-1} . While this reasoning explains the differences between LVF and HVF biofilms, it does not account for the similarity between SS and HVF biofilms or the differences between SS and LVF. Under SS conditions the biofilms were disturbed less than under LVF, therefore, compared to the LVF biofilms, they may have been able to grow and increase in volume more rapidly with less need for an extensive EPS matrix to keep them adhered to the pipe wall. Compared to LVF, the biofilms from HVF experienced a greater variation in flow rate; it is possible that they were more resistant to detachment as a result of this conditioning than those from LVF conditions. If both these theories are correct (that SS biofilms were undisturbed and HVF biofilms were more resistant to disturbance) this could account for the greater biofilm accumulation under these hydraulic patterns than LVF. As the LVF biofilms experienced greater disturbance than the SS samples, due to a greater peak daily force, it may be that they required greater volumes of EPS to remain attached and that under HVF conditions the greater differences in flow did not allow for a more expansive EPS framework to develop before it was removed, hence less EPS per cell. On the other hand, under LVF conditions, the biofilms may have had a reduced availability of nutrients compared to HVF, thus a more extensive EPS may have been required to entrap particles and aid recycling of nutrients between cells. This seems a less likely explanation as the two varied flow regimes have a similar flow rate (within 10% of each other) for 16.5 hours, which exceeds the duration of the varied period and the time-frame during which the HVF regime had a greater mixing potential was relatively short (approximately 3 hours). Moreover there is a period in the middle of the pattern during which time LVF has a greater flow rate than HVF. Therefore the two regimes likely experienced similar nutrient gradients.

Alternatively, the differences observed in the physical structure characteristics could be due to each regime imposing different selective pressures upon the biofilm community (which produced the EPS). The different regimes could have led to changes in microbial composition or different physiological adaptations of the same species. However, analysis of the biofilm community structures did not show the same patterns of similarity/differences between the hydraulic conditions as were seen in the physical structure analysis. Generally, SS and HVF samples were similar to each other in their physical structure but they were distinct from each

other in their community structure (Figure 6.12) and HVF communities were more similar to those from LVF. SS biofilms had the most diverse microflora, consistently comprised of bacteria, archaea and fungi. The fact that archaea were absent from, and fungi were less common in, LVF and HVF biofilms than SS, suggests that the varied flow regimes imposed selection pressures which adversely affected the integration of these organisms into the biofilm community. There is little information on the influence of hydraulic regimes upon biofilm communities, other than bacteria but Gonclaves *et al.* (2006) established that filamentous fungi require a longer growth time than bacteria. Therefore it is suggested that, in the research presented here, the fungi were removed from the biofilms during the varied flow regimes before they had chance to securely attach to the biofilm, whereas SS conditions were more suitable for long term colonization. There is a paucity of evidence regarding the influence of velocity upon fungi. Fungal populations were observed to experience no quantitative changes within biofilms exposed to different velocities of sea water within a water circulation loop (França and Cravo, 2000) but as this environment is considerably different from that of drinking water it is not feasible to draw parallels. Moreover, the fungal communities were evaluated using culture based techniques so it is possible that these were too crude to detect variation between the relatively small velocities which were investigated (3.6, 17.4, 20.0 and 34.8 cm s^{-1} ; França & Cravo, 2000). The literature regarding archaea in drinking water is restricted to studies identifying archaeal species in biofilms (see section 1.4.1.3), very little is known about their ecology and biofilm formation behaviour. Most archaeal based studies investigate aspects of the methanogens, specifically within reactor systems, and it is difficult to draw parallels between these studies and the results presented herein. As the presence of archaea follow a similar trend to that seen in the fungi, it is possible that they too are less able to attach securely under varied flow conditions and so are outcompeted by the sessile bacteria. Moissl-Eichinger & Huber (2011) present a review of current opinions of archaea, in which they state that the methanogens have the highest potential for a symbiotic lifestyle and are rare amongst archaea as they possess pili structures that have not been found in other archaeal groups. Methanogens are archaeal species which produce methane as a by-product when respiring under anoxic conditions, such as in wetlands or marine sediments. Although the DWDS presents a much greater oligotrophic environment than the common habitat of the methanogens it is possible that they would be found within biofilms as they are part of the Euryarchaeota, which have been detected in drinking water samples previously (see section 1.4.1.3). It is postulated that the presence of pili like structures within the methanogen species facilitates their attachment to biofilms but that this adhesion is weak and therefore negatively influenced by changes in shear stress.

Bacteria have been found to dominate biofilms in many studies (e.g. Nagy & Olson, 1982; LeChevallier *et al.*, 1987; Elvers *et al.*, 1998; Lehtola *et al.*, 2004b) from a range of environmental conditions and this was also the case for the SS, LVF and HVF drinking water biofilms characterized in this study. That is not to say that the communities were comprised of the same bacteria in each instance. Biofilms from freshwater (Rickard *et al.*, 2004) and industrial water systems (Rochex *et al.*, 2008) have been shown to have a less diverse bacterial community when developed under higher shear stresses. In contrast, a previous drinking water study, using the experimental facility described in this thesis, did not find differences between the bacterial communities of SS and varied flow conditioned biofilms (Douterelo *et al.*, 2013). However, the replication of that study was substantially less than the replication of this study (n=3 vs. n=9) and the operating conditions were different, both of which could account for the difference in trends between the two studies. In the current study detailed within this chapter, there were subtle differences in bacterial community relative richness, evenness and diversity indices which followed a pattern of SS > HVF > LVF, where only SS and LVF were significantly different. Furthermore, it was established that the SS biofilms were distinct from LVF and HVF in their bacterial community structure and contained a substantial number of T-RFs which were not found in the varied flow biofilms. Therefore, it can be concluded that the SS bacterial communities were the most complex, with the greatest variation in and most even distribution of T-RFs. Conversely, the varied flow regimes produced a greater selection pressure leading to biofilm communities dominated by particular bacterial T-RFs (e.g. 199.27 nt), which may correspond to species better adapted to resisting variations in flow than others. For example, Rickard *et al.* (2004) found that freshwater biofilms grown within a high shear stress environment contained more auto-aggregating than co-aggregating bacteria, the former of which have stronger interactions and are therefore more resistance to detachment. It could however, be argued that within the DWDS co-aggregating bacteria would have a better survival advantage as they would be more able to attach to an already developed assemblage and hence better resist removal than non-co-aggregating bacteria, which may be more likely to be removed with a change in shear stress. Interestingly, Elvers *et al.* (1998) established that more diverse populations produced thicker biofilms and, in the research presented in this chapter, the LVF biofilms were both the thinnest and least diverse, following this trend exactly.

6.3.1 Summary

Evidently, hydraulic regimes did condition the biofilms differently and the physical structure variations were not being driven by differences in the microbial communities. Overall, as the

biofilms did not all exhibit the same structure (physical or community) it can be said that the average flow rate is not the driving parameter influencing biofilm characteristics. The similarities between LVF and HVF community structure could indicate that it is the low flow period which drives the community structure development. However, the complex patterns in physical structure indicate that there is no simple, linear relationship between these and the attributes of the flow profiles. Although it seems unlikely that these differences in biofilm structure (particularly in EPS quantity and community structure) were purely correlative, within the context of the results within this chapter it is not possible to confirm what resistance to shear stress, if any, is conveyed by the different conditioned structures. It could be that the LVF biofilms with the greatest EPS proportion would be most stable to changes in shear stress or that the HVF biofilms, which have been conditioned to the highest flow rates, would be most stable. Further work would be needed to investigate any differences in the stability and hence potential discolouration or contamination risk of these biofilms when faced with changes in hydraulics.

Chapter 7: Assessing the Response of Biofilms Developed under Different Hydraulic Regimes to an Elevation in Shear Stress

7.1 Introduction and Aims

A few studies have investigated the influence of increasing shear stress upon the structure of biofilms developed within idealized systems (e.g. Percival *et al.*, 1999; Simoes *et al.* 2003; 2005; Lehtola *et al.*, 2006; Abe *et al.*, 2012). There are discrepancies in their findings as some studies conclude that biofilms which were developed under greater turbulent flows were more resistant to detachment (e.g. Percival *et al.*, 1999), while others have found the reverse to be true (e.g. Abe *et al.*, 2012). Not only were the sessile assemblages developed in environments far removed from those within a network pipeline (as discussed in previous chapters), but the shear stresses applied to remove the biofilms were rarely representative of those experienced in the DWDS. A complementary study to this thesis, which used the same DWDS experimental facility (section 3.1.1), showed a clear shift in bacterial biofilm community before and after exposure to increased shear stresses (Douterelo *et al.*, 2013). However, the effects of elevated shear stress upon fungal and archaeal communities have yet to be investigated and variations in the physical structure of drinking water biofilms have yet to be evaluated. Furthermore, the influence of the hydraulic regime experienced during development upon conditioning the biofilm structure to resist detachment has not yet been fully explored. Therefore the research presented herein aimed to evaluate the response of biofilms relevant to real DWDS, developed under the SS, LVF and HVF regimes, to elevated shear stresses, relevant to those occurring within real DWDS, and determine any differences/similarities between the biofilms remaining attached after exposure to these conditions (as set out in objective 4 in Chapter 2).

The previous work presented in this thesis established that drinking water biofilms had different physical and community structures when developed under different hydraulic regimes. In order to evaluate the stability of each of the different biofilm structures, and thereby assess the conditioning effect (if any) of the hydraulic regimes during growth, all the biofilms were exposed to a mobilization phase. A series of three shear stresses were applied during this mobilization phase (0.42, 1.75 and 2.91 Nm^{-2}) by flushing the loops at three increasing flow rates (0.80, 3.20, 4.50 ls^{-1}), see section 3.2.2.1 for more details. As previously explained (section 3.2.2.2), following the development phase of each hydraulic condition (SS,

LVF or HVF) each loop of the experimental facility was isolated and flushed independently with the same three incremental flow rates. Bulk water quality was monitored throughout each of the flushing stages and biofilm samples were taken at the Pre-flush and Post-flush sample points. Biofilm physical structure was characterized using the staining, imaging and DIA approaches outlined in section 4.7.1, bacterial, archaeal and fungal communities were analysed via DNA based fingerprinting techniques (section 3.4.5). Due to the logistics of the flushing period the loops were flushed sequentially and so experienced varying stagnation periods (no greater than 24 hours) between Day 28 and Pre-flush. Consequently, it was first necessary to determine if the different stagnation periods had an effect upon biofilm structure before investigating the aims set out above, so as to ensure that the comparison between biofilms before and after flushing was assessing the effect of elevated shear stress rather than a combined effect of stagnation and flushing.

7.2 Results of Hydraulic and Stagnation Effects upon Pre-flush Biofilms

Detailed analyses of the Day 28 samples and the effect of hydraulic regime upon the biofilm physical and community structures are provided in Chapter 6. The same analysis approaches were applied to the Pre-flush biofilms from each hydraulic condition and the results are presented (in brief) in the following sections. Additionally, within each hydraulic condition the Day 28 and Pre-flush samples were compared to evaluate any effect of stagnation.

7.2.1 Biofilm physical structure Pre-flush

Before comparing biofilm physical structure, it is important to note that the SS and LVF Pre-flush datasets contained a FOV unrepresentative of the biofilm sample; the corresponding area distribution data in each case is shown by the dotted lines in Figure 7.1B and D respectively (note that the x-axis of these two plots is greater than for other area distribution plots). The FOV from SS had an uncharacteristically large number of slices (119) and appeared to be covered by a fungal mass which was only seen in one area of the sample; subsequent molecular analysis detected a strong concentration of fungal DNA upon the outer coupon which corresponded to this insert. The FOV from LVF had a carbohydrate area distribution profile with a maximum peak area fraction of 1.00, which was not representative of the sample from which it was obtained. To prevent any skew in the results these FOV were excluded from further analysis, leaving n=24 for SS and LVF, the results of which are plotted in Figure 7.1A and C, respectively.

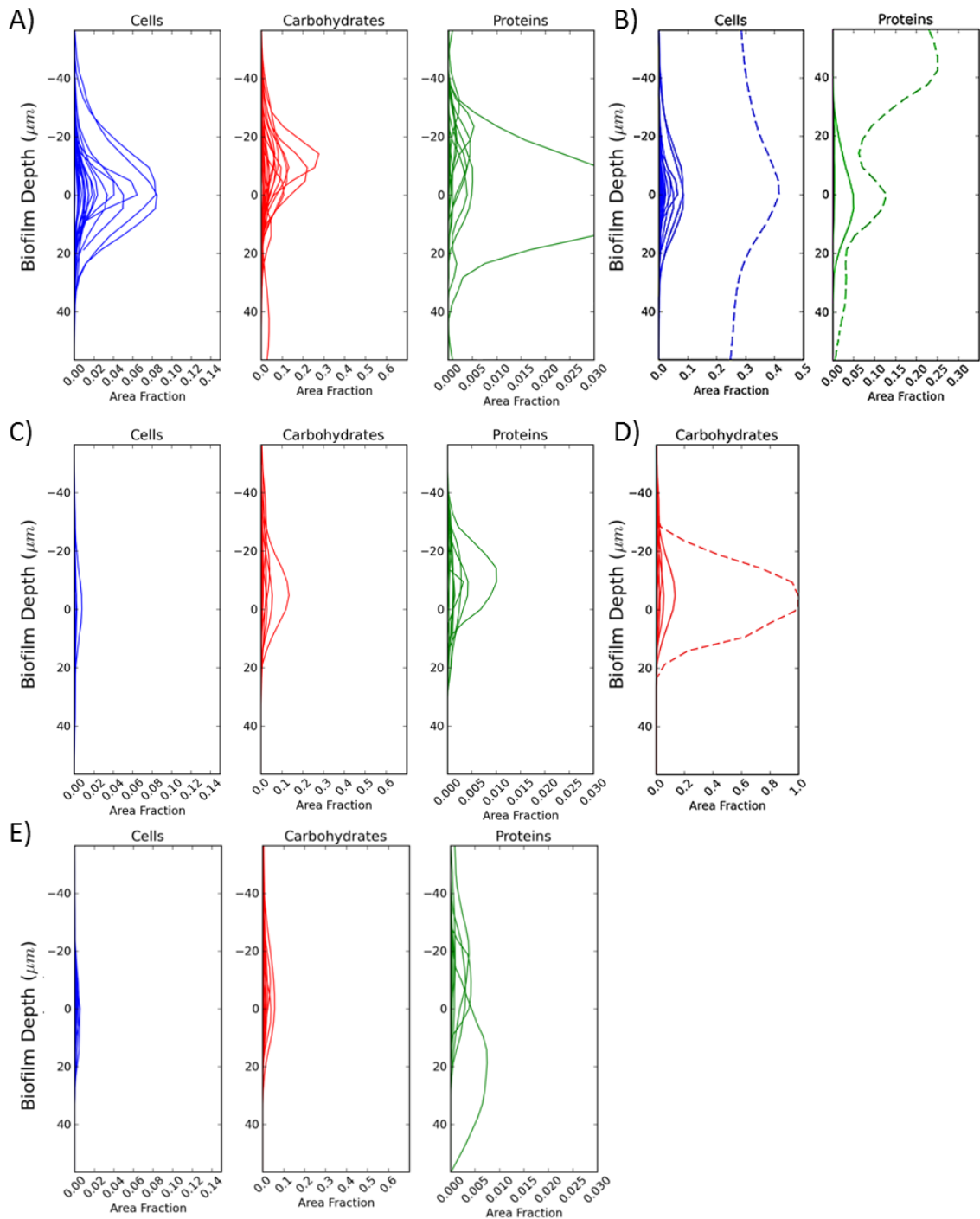


Figure 7.1 Area distribution of cells, carbohydrates and proteins within Pre-flush biofilms developed under SS, LVF and HVF conditions. A) SS samples (n=24); B) The cells and proteins of SS plotted on x axes with a greater range than that used in other area distribution plots (n=25); C) LVF samples (n=24); D) The carbohydrates of LVF plotted on an x-axis with a greater range than that used in other area distribution plots (n=25); E) HVF samples (n=25). Each line represents one FOV (i.e. one Z-stack); the dotted line shows any unrepresentative FOV. Area fraction refers to the proportion of each XY image of the Z-stack covered by the particular component (see section 4.6.3.1).

The SS, LVF and HVF datasets were analysed to determine any effect of position (i.e. crown, middle, invert) or loop upon biofilm structure using the approaches explained in previous chapters. No effect of coupon location was found upon any physical structure parameter of

Day 28 (see section 6.2.2) or Pre-flush (see Appendix 10 for details, overall Wilcoxon: $W \geq 39.5$, $p \geq 0.0767$) biofilms from any hydraulic condition. Consequently, there was no need to continue to differentiate the samples based upon their location (position and loop) and subsequent analysis was applied to the whole dataset at each sample point (i.e. $n=25$ or $n=24$). Moreover, the fact that there was no difference between the loops (which were flushed sequentially), i.e. no difference between Pre-flush replicates which had different lengths of stagnation, suggested that no effect of stagnation between Day 28 and Pre-flush would be detected.

7.2.1.1 Visualization and qualitative analysis of area distribution

Overall, the trends highlighted by the area distribution plots did not differ greatly between Day 28 (Figure 6.2) and Pre-flush (Figure 7.1) for biofilms developed under SS or LVF regimes. However, the area distributions of the HVF Pre-flush biofilm components (Figure 7.1E), particularly the cells, were greatly reduced compared to those of the Day 28 biofilms. Figure 7.1 also demonstrated that SS Pre-flush biofilms generally had greater cell, carbohydrate and protein area fractions than either the LVF or HVF biofilms; the latter two were more similar to each other. This is in contrast to the Day 28 samples where SS and HVF biofilm area distributions were most similar to each other and distinctly greater than those of the LVF biofilms. This difference in patterns of similarity was also observed in the 3D visualization of an example FOV from each hydraulic condition (Figure 7.2). At Pre-flush, the varied flow biofilm examples showed cells to be commonly associated with EPS but the SS biofilm example exhibited a considerable amount of cell only areas. This is opposite to the 3D visualisation of example Day 28 biofilms (Figure 6.3), which showed the greatest cell only coverage to occur under HVF conditions. Carbohydrates dominated the EPS of the each of the biofilms but the examples for LVF and SS also had a considerable protein presence. The biofilm components did not completely co-localise in any of the biofilm 3D projections, though they often were located in close proximity in micro colonies with considerable depth, the exception to this was the cells of the SS biofilm which appeared to have a more scattered, XY distribution. A common pattern across the three hydraulic treatments was that the peak area fraction coverage of the carbohydrates and proteins generally occurred closer to the bulk water than the peak area fraction of the cells (due to the alignment of the data this occurs at "0" in the area distribution plots), this trend was also seen in each of the previously analysed Day 28 biofilms.

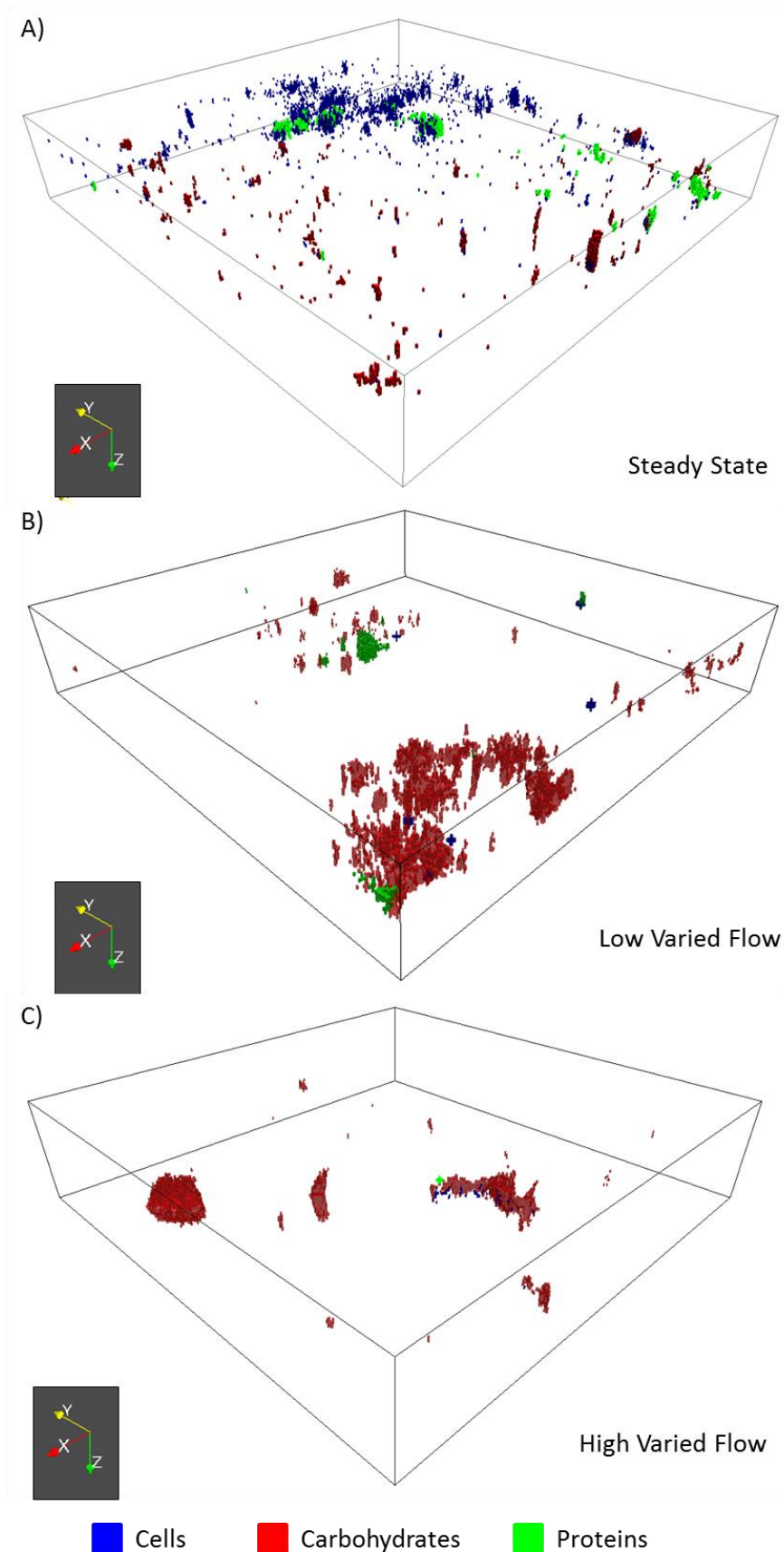


Figure 7.2 A representative example of the 3D arrangement of cells, carbohydrates and proteins within Pre-flush biofilms from A) SS; B) LVF and C) HVF conditions. Each 3D projection is within a plotting area shown by the cube which is 420 μm x 420 μm (XY dimensions) in each case with a depth (Z) of: A) 73.2 μm; B) 77.6 μm; C) 84.7 μm. N.B. the cells (blue) may be hard to distinguish from the carbohydrate (red) in some instances, despite setting a mid-level opacity.

7.2.1.2 Quantitative analysis of volume, spread and peak location

All the biofilm physical quantitative data was not normally distributed (Shapiro Wilks: $p < 0.05$), therefore, Kruskal Wallis tests were used to determine differences between the three hydraulic conditions and Wilcoxon tests were applied to detect any pairwise differences between Day 28 and Pre-flush biofilms.

As suggested by the area distribution plots, Day 28 and Pre-flush biofilms did not significantly differ in cell, carbohydrate or protein relative volume (see Table 7.1 for medians), when developed under SS (Wilcoxon: $W \geq 207.0$, $p \geq 0.3453$) or LVF (Wilcoxon: $W \geq 271.0$, $p \geq 0.4654$) conditions. Neither SS nor LVF biofilms experienced changes, between Day 28 and Pre-flush, in their proportional compositions (see relative volume ratios, Table 7.2; Wilcoxon: SS, $W \geq 202.0$, $p \geq 0.3556$; LVF, $W \geq 134.0$, $p \geq 0.2337$) or spread of cells, carbohydrates or proteins (see Table 7.3; Wilcoxon: SS, $W \geq 282.0$, $p \geq 0.0873$; LVF, $W \geq 154.0$, $p \geq 0.4527$). Conversely, HVF Pre-flush biofilms, in comparison to the Day 28 biofilms, had significantly lower relative volumes (Table 7.1) of cells (Wilcoxon: $W = 518.0$, $p < 0.0001$), carbohydrates (Wilcoxon: $W = 438.0$, $p = 0.0052$), proteins ($W = 430.0$, $p = 0.0092$) and, subsequently, lower volumes of EPS (Wilcoxon: $W = 146.0$, $p = 0.0046$) and all stained material in combination (Wilcoxon: $W = 223.0$, $p < 0.0001$). Despite occurring at lower volumes, the spread of carbohydrates (Wilcoxon: $W = 541.0$, $p = 0.2444$) and proteins (Wilcoxon: $W = 159.0$, $p = 0.7996$) did not alter, suggesting that the biofilms became less dense (less volume covering the same biofilm depth). There was, however, a significant reduction in the spread of cellular material between Day 28 and Pre-flush samples (Wilcoxon: $W = 401.0$, $p = 0.0187$). The decrease in the cellular fraction of the HVF biofilms, led to a significant increase in the proportion of EPS per μm^3 of cells (EPS-to-cell ratio, Table 7.2; Wilcoxon: $W = 461.0$, $p = 0.0004$) in Pre-flush biofilms. The protein-to-cell ratio was equally low in biofilms from both sample points (Wilcoxon: $W = 271.0$, $p = 0.7369$) but the carbohydrate-to-cell ratio increased significantly (Wilcoxon: $W = 446.0$, $p = 0.0011$) at Pre-flush. Nevertheless, the composition of the HVF biofilm matrices did not differ between Day 28 and Pre-flush (Wilcoxon: $W = 145.0$, $p = 0.5008$).

In spite of the decrease in relative volume of HVF biofilms during stagnation, the peak locations of the carbohydrates (Wilcoxon: $W = 309.0$, $p = 0.8566$) or proteins (Wilcoxon: $W = 425.5$, $p = 0.1190$), were consistently above that of the cells. Likewise, the SS and LVF biofilms did not exhibit variations in their carbohydrate (Wilcoxon: SS, $W = 341.0$, $p = 0.5726$; LVF, $W = 365.5$, $p = 0.1831$) or protein (Wilcoxon: SS, Wilcoxon: $W = 323.5$, $p = 0.8359$; LVF, $W = 335.5$, $p = 0.4800$) peak locations, which were also found above the cells in each case.

Table 7.1 Median relative volumes (μm^3) of the stained biofilm components in Day 28 and Pre-flush biofilms developed under SS, LVF and HVF conditions. Data for the individual stained components is provided in (A) and for combinations, as indicated, in (B)

Biofilm Component	SS (μm^3)		LVF (μm^3)		HVF (μm^3)	
	Day 28 ^C	Pre-flush ^D	Day 28 ^C	Pre-flush ^D	Day 28 ^D	Pre-flush ^C
(A) Individual						
Cells	26099	56220	671	713	28859	3019
Carbohydrates	180802	169187	24969	11571	74271	21022
Proteins	800	2512	466	60	2496	180
(B) Combinations						
EPS ^A	184850	182343	29581	13974	79271	24645
All material ^B	252325	270437	31955	23021	141743	26210

^A EPS = carbohydrates + proteins before averaging, before averaging, data presented is therefore the median of the sums; ^B Total biofilm = cells + EPS before averaging, before averaging, data presented is therefore the median of the sums; ^C n=25; ^D n=24.

Table 7.2 Median ratios of various different components within Day 28 and Pre-flush biofilms from SS, LVF and HVF conditions.

Ratios ^A	SS		LVF		HVF	
	Day 28 ^B	Pre-flush ^C	Day 28 ^B	Pre-flush ^C	Day 28 ^C	Pre-flush ^B
EPS: Cells	4.86	2.58	26.39	13.52	1.98	8.21
Carbohydrates: Proteins	62.31	42.38	14.24	10.56	33.24	7.59
Carbohydrates: Cells	4.80	2.56	21.29	11.23	1.21	8.21
Proteins: Cells	0.19	0.05	1.00	0.92	0.06	0.04

^A The first component is divided by the second, a value > 1 indicates a greater volume of the first component, a value <1 indicates a greater volume of the second, a value = 1 indicates an equal volume of each; ^B n=25; ^C n=24.

Table 7.3 Median spreads of the different components within Day 28 and Pre-flush biofilms from SS, LVF and HVF conditions.

Biofilm Component	SS (AU)		LVF (AU)		HVF (AU)	
	Day 28 ^A	Pre-flush ^B	Day 28 ^A	Pre-flush ^B	Day 28 ^B	Pre-flush ^A
Cells	4529622	4202254	3549221	3487013	4425734	3807066
Carbohydrates	4394548	4057783	4406852	4422862	3580180	4190004
Proteins	4638752	3742170	2908246	3431940	3874705	4387217

^A n=25; ^B n=24.

Comparison across the Pre-flush samples demonstrated a significantly higher relative volume of cells, carbohydrates and proteins in the SS biofilms than either LVF or HVF (Figure 7.3; Table 7.4). Consequently, the greatest volumes of EPS and all biofilm material (EPS + cells), at the Pre-flush stage, were found in SS biofilms, which had approximately ten times the overall biofilm volume of LVF or HVF Pre-flush biofilms. Proportionally though, LVF and HVF biofilms had a significantly greater EPS content (described as the EPS-to-cell ratio in Table 7.2; see Table 7.5 for the statistical tests) than SS. Biofilms from LVF and HVF conditions had similar relative volumes and EPS-to-cell ratios (Table 7.4; Table 7.5) but different EPS compositional ratios. The average (median) carbohydrate-to-protein ratio of LVF Pre-flush biofilms was 2.83 (Table 7.2), significantly lower than that of HVF and SS biofilms, both of which had a more

carbohydrate dominated matrix (Table 7.2; Table 7.5). Correspondingly, the SS and HVF biofilms had very low protein-to-cell ratios demonstrating the small proportion of proteins within the biofilms. LVF biofilms had a significantly higher protein-to-cell ratio, which, although still indicative of a greater cell than protein volume, was much closer to a one-to-one ratio than the protein-to-cell ratio found for SS or HVF biofilms (Table 7.2). The carbohydrate-to-cell ratio values were significantly different between all of the hydraulic conditions. The SS biofilms were observed to have the greatest carbohydrate relative volume across the three hydraulic conditions but, proportionally, these carbohydrates contributed less to the biofilm as a whole (indicated by the lowest ratio value; Table 7.2). However, regardless of flow regime, the drinking water biofilms comprised a greater proportion of carbohydrates than cells.

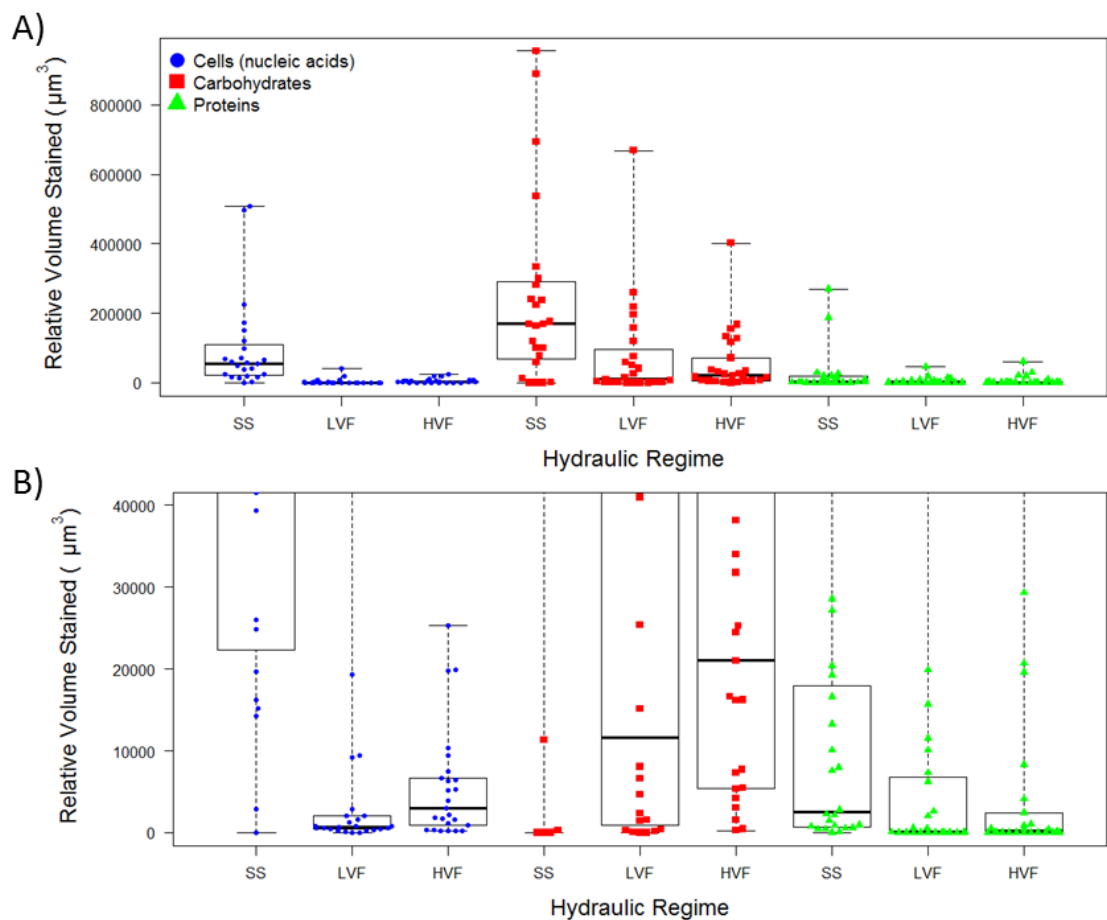


Figure 7.3 Relative volumes of stained biofilm components within Pre-flush biofilms developed under SS, LVF or HVF hydraulic conditions. Y-axis scale is adjusted to: A) max data point; B) interquartile range of the protein and cell data. Each data point represents a different FOV, n=24 for SS and LVF, n=25 for HVF. Box and whisker plots show the range, interquartile range and median – indicated by the black solid line; volume is relative to the threshold value (see section 4.6.3.3).

Table 7.4 Results from the statistical comparisons of the relative volume of the stained biofilm components within Pre-flush biofilms developed under SS, LVF and HVF conditions. Significant results shown in bold.

Biofilm Component	Kruskal Wallis	Wilcoxon Test		
	SS vs. LVF vs. HVF	SS vs. LVF	SS vs. HVF	LVF vs. HVF
Cells	$\chi^2=36.05$, df=2, p<0.0001	W=537.0, p<0.0001	W=549.0, p<0.0001	W=396.0, p=0.0556
Carbohydrates	$\chi^2=10.74$, df=2, p=0.0047	W=421.0, p=0.0063	W=444.0, p=0.0035	W=332.0, p=0.5287
Proteins	$\chi^2=11.71$, df=2, p=0.0029	W=426.0, p=0.0045	W=449.0, p=0.0028	W=269.0, p=0.5332
EPS ^D	$\chi^2=14.23$, df=2, p=0.0008	W=447.5, p=0.0033	W=465.0, p=0.0027	W=334.0, p=0.5063
All Material ^E	$\chi^2=23.77$, df=2, p<0.0001	W=509.5, p=0.0001	W=518.0, p<0.0001	W=343.0, p=0.5637

^A n=24; ^B n=25; ^C EPS = carbohydrates + protein, before averaging; ^D All Material = EPS + cells, before averaging.

Table 7.5 Results from the statistical comparisons of the various ratios of the stained biofilm components within Pre-flush biofilms developed under SS, LVF and HVF conditions. Significant results shown in bold.

Ratios ^A	Kruskal Wallis	Wilcoxon Test		
	SS vs. LVF vs. HVF	SS vs. LVF	SS vs. HVF	LVF vs. HVF
EPS: Cells	$\chi^2=9.66$, df=2, p=0.0080	W=118.0, p=0.0018	W=190.0, p=0.0453	W=202.0, p=0.0612
Carbohydrates: Proteins	$\chi^2=6.82$, df=2, p=0.0331	W=118.0, p=0.0018	W=154.0, p=0.7237	W=211.0, p=0.0394
Carbohydrates: Cells	$\chi^2=8.65$, df=2, p=0.0130	W=102.0, p=0.0004	W=200.0, p=0.0466	W=183.0, p=0.0407
Proteins: Cells	$\chi^2=9.21$, df=2, p=0.0100	W=116.0, p=0.0104	W=358.0, p=0.2457	W=120.0, p=0.0093

^A The first component is divided by the second, a value > 1 indicates a greater volume of the first component, a value <1 indicates a greater volume of the second, a value = 1 indicates an equal volume of each component.

Despite the differences in relative cell volume observed between SS and varied flow biofilms, there were no significant differences between the three conditions in terms of the spread (Table 7.3) of cells (Kruskal Wallis: $\chi^2=3.71$, df=2, p=0.1561), carbohydrates (Kruskal Wallis: $\chi^2=0.10$, df=2, p=0.9557) or proteins (Kruskal Wallis: $\chi^2=2.38$, df=2, p=0.3044). From these results it appeared that the density of the biofilms differed between regimes; SS samples contained a greater quantity of biofilm but within the same spread as LVF and HVF samples, therefore SS samples must have had a greater biofilm density. Although the median carbohydrate peak location in Pre-flush biofilms was -2 across all regimes, a statistical difference was found between the hydraulic conditions (Kruskal Wallis: $\chi^2=8.03$, df=2, p=0.0180), driven solely by a difference between LVF and HVF biofilms (Wilcoxon: W=439.0, p=0.0042; the other pairwise tests showed no significant differences, $W \geq 234.0$, $p \geq 0.1205$). The protein peak location was generally just above that of the carbohydrates and did not differ significantly between biofilms from each of the regimes (Kruskal Wallis: $\chi^2=3.34$, df=2, p=0.1885; Figure 7.4).

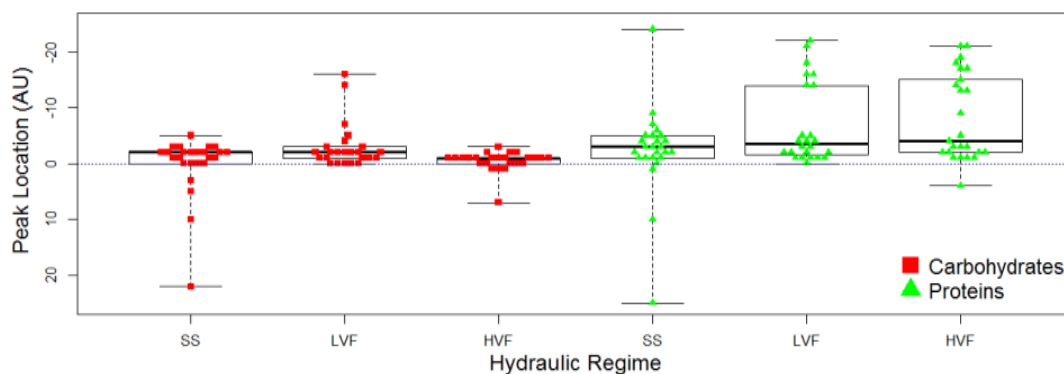


Figure 7.4 Carbohydrate and protein peak locations within Pre-flush biofilms from SS, LVF and HVF conditions. Peak locations are in relation to the cell peak location (indicated by the dotted line), each data point represents a FOV, n=24 for SS, n=25 for LVF and HVF; box and whisker plots show the range, interquartile range and median –indicated by the solid black line. Peak location is the aligned slice number at which the max area fraction occurs (see section 4.6.3.5).

7.2.2 Biofilm community structure Pre-flush

No effect of loop or position was found with respect to any of the Day 28 or Pre-flush microbial communities (ANOSIM: relative abundance or presence/absence data, global $R \leq 0.364$, $p \geq 0.150$), therefore the data presented in the following sections is based upon the datasets in their entirety. Bacterial 16S rRNA genes, archaeal 16S rRNA genes or fungal ITS regions were amplified from DNA extractions via PCR. The number of samples, from a maximum of 9, for which detectable concentrations of each microbial taxon were found are presented in Table 7.6. In some instances there were slight differences between the number of positive samples in Day 28 and Pre-flush samples but this may not be because of a stagnation effect, the differences could be due to the general heterogenic nature of biofilm development.

Due to the absence of archaeal DNA from LVF and HVF biofilms (see section 6.2.3.1) and the fact that no fungal DNA was detected in the HVF Pre-flush biofilms, only the bacterial community could be compared across all three hydraulic regimes (SS, n=9; LVF, n=8; HVF, n=8). The fungal community of SS (n=7) and LVF (n=3) biofilms were also compared but results should be interpreted with care due to the difference in replication.

Table 7.6 Number of DNA extractions for which bacteria, archaea or fungi were detected. DNA extractions were from biofilms conditioned under SS, LVF or HVF conditions as indicated, n=9.

Targeted Microorganism	SS		LVF		HVF	
	Day 28	Pre-flush	Day 28	Pre-flush	Day 28	Pre-flush
Bacteria	9/9	9/9	8/9	8/9	6/9	8/9
Archaea	9/9	8/9	Not determined ^A		0/9	0/9
Fungi	9/9	7/9	3/9	3/9	1/9	0/9

^A Presence of archaea within LVF samples was not determined due to contamination (see section 6.2.3.1).

7.2.2.1 Relative taxon richness, evenness and diversity

Electropherograms from T-RFLP analysis and ARISA showed similarities between Day 28 and Pre-flush biofilms from SS, LVF or HVF but variations between the Pre-flush biofilms from each hydraulic treatment (see Figure 6.8 for Day 28 and Figure 7.5 for Pre-flush example profiles).

The relative richness, evenness and diversity indices of bacterial and fungal communities at the Pre-flush stage are shown in Table 7.7, the same data for the Day 28 biofilms can be found in Table 6.5. Within each hydraulic condition, the Day 28 and Pre-flush bacterial communities did not differ in their relative richness (T-test for each regime, in summary $df \geq 10.78$, $p \geq 0.0684$), evenness (T-test for each regime, in summary $df \geq 10.14$, $p \geq 0.0982$) or diversity (T-test for each regime, in summary $df \geq 9.30$, $p \geq 0.0608$). Similarly, stagnation had no effect upon SS or LVF fungal communities, as regards relative richness (T-test: SS, $df=12.46$, $p=0.6517$; LVF, $df=2.03$, $p=0.3446$), evenness (T-test: SS, $df=13.04$, $p=0.874$; LVF, $df=3.88$, $p=0.3090$) or diversity (T-test: SS, $df=13.96$, $p=0.9351$; LVF, $df=2.21$, $p=0.2337$). The archaeal communities from SS Day 28 and Pre-flush also showed no differences with respect to: relative richness, the average of which was 11 T-RFs in each case (T-test: $df=9.74$, $p=0.6623$), relative evenness, the average of which was 0.89 in each case ($df=10.59$, $p=0.7410$) or relative diversity, the average of which was 2.15 and 2.11 for Day 28 and Pre-flush biofilms respectively (T-test: $df=10.44$, $p=0.5498$).

Visual comparison of the SS, LVF and HVF Pre-flush bacterial profiles showed similar peaks around the 170 nt – 210 nt range but the dominant T-RF in each case occurred at slightly different lengths (SS, 198.58 nt; LVF, 199.71 nt; HVF, 199.74 nt). Equally, profiles from each hydraulic regime showed a peak at the far end of the profile, which occurred at 485.77 nt in SS, 487.08 nt in LVF and 486.94 nt in HVF and was most pronounced in the HVF profiles. At Pre-flush, the total number of different bacterial T-RFs ranged from 92 in the HVF biofilms, to 98 and 103 in the SS and LVF biofilms respectively. However, there was no significant difference in the average number of T-RFs (Table 7.7) within an individual profile from each of the hydraulic regimes (ANOVA: $df=2$, $p=0.1240$). The bacterial communities from the different hydraulic regimes had equally high relative evenness (Table 7.7; ANOVA: $df=2$, $p=0.2050$) and diversity (ANOVA: $df=2$, $p=0.1110$). In contrast, the SS and LVF fungal communities yielded considerably different fingerprints (Figure 7.5B) with a greater total number of different ARISA amplicons present in the SS community (104) than the LVF (36). This pattern was reflected in the relative richness of each profile which was significantly greater in the SS communities (T-test: $df=1.00$, $p=0.0117$), leading to a significantly greater relative diversity than the LVF (T-test: $df=1.00$, $p=0.0060$). However, the SS and LVF communities had a similar relative evenness (T-test:

df=1.00, p=0.1360), so although there was a greater variety of ARISA amplicon size in the SS communities, these were as evenly distributed as those in the LVF community and no particular amplicon size was especially dominant.

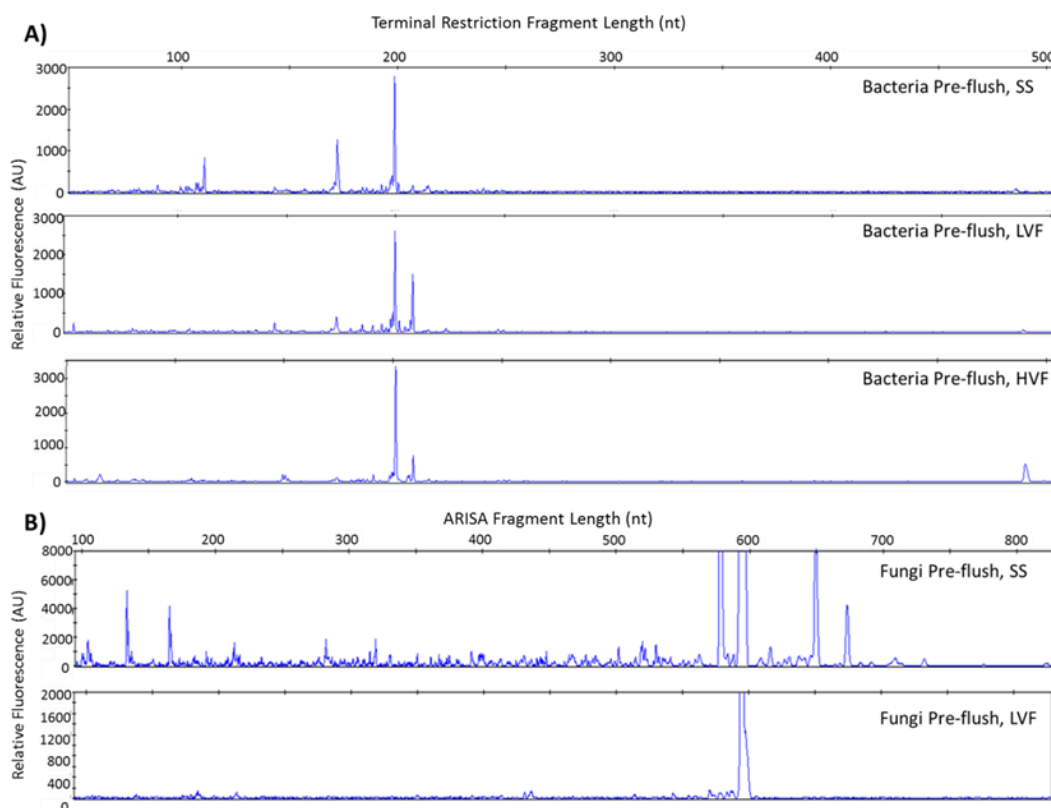


Figure 7.5 Representative T-RFLP or ARISA electropherograms of Pre-flush biofilm communities from the SS, LVF or HVF experiments. A) Bacterial communities (16S rRNA, T-RFLP); B) Fungal communities (ITS region, ARISA).

Table 7.7 Relative richness, evenness and diversity indices of the bacterial and fungal communities from Pre-flush biofilms sampled from the SS, LVF or HVF experiments.

Microbial fingerprint	Flow Regime	Relative Richness (number of T-RFs)			Relative Evenness (Pielou's Index)			Relative Diversity (Shannon's Index)		
		Min	Max	Mean (St.Dev)	Min	Max	Mean (St.Dev)	Min	Max	Mean (St.Dev)
Bacteria	SS	16	41	30(9)	0.92	0.98	0.96(0.02)	2.66	3.62	3.22 (0.34)
	LVF	16	35	24(6)	0.88	0.98	0.94 (0.03)	2.43	3.39	2.99 (0.28)
	HVF	11	39	22 (9)	0.88	0.96	0.94 (0.03)	2.12	3.52	2.85 (0.43)
Fungi	SS	10	31	21 (7)	0.79	0.96	0.91 (0.06)	1.82	3.27	2.75 (0.48)
	LVF	5	10	7 (3)	0.77	0.93	0.84 (0.08)	1.33	1.80	1.63 (0.26)

N.B. Min = minimum, Max=Maximum, St.Dev = standard deviation.

7.2.2.2 Microbial community structure

7.2.2.2.1 Stagnation effect on biofilm structure

Although there were no differences between any of the ecological indices for the bacterial, fungal or archaeal communities of Day 28 and Pre-flush biofilms, the specific T-RFs or ARISA amplicons within the communities could have been affected by the stagnation period. Therefore, the communities were analysed using hierarchical clustering, where samples were

labelled with respect to time since Day 28, i.e. stagnation time, in hours. Regardless of hydraulic regime the Day 28 samples were time “0”.

Following development under SS flow rates, each loop was flushed independently in the sequence: loop 2, loop1, loop 3, corresponding to 2, 6 and 23 hours after Day 28, respectively. The nMDS plots of each taxon (bacteria, archaea or fungi) had stress values ≥ 0.13 , which indicated that the data were best represented by dendrograms (Figure 7.6), which showed the same patterns when plotted using the relative abundance or presence/absence data. The only exception being that SIMPROF analysis found no definitive substructure between any of the archaeal samples when using the presence/absence data. ANOSIM analysis confirmed that there was no difference between the bacterial (relative abundance, global $R=0.184$, $p=0.119$; presence/absence, global $R=0.167$, $p=0.139$) or archaeal (relative abundance, global $R=-0.035$, $p=0.555$; presence/absence, global $R=0.065$, $p=0.334$) communities within the biofilms sampled at the different time points since Day 28. SS bacterial Day 28 and Pre-flush communities were an average of 48.93% similar to each other and the archaeal communities were an average of 86.45% similar to each other (SIMPER test). However, a slight effect of stagnation time upon the fungal communities was observed when the relative abundance of ARISA amplicons (ANOSIM: global $R=0.308$, $p=0.037$) was analysed. This effect was driven by a strong difference (global $R= 0.640$, $p=0.018$) between biofilms from 0 hours and 23 hours (ANOSIM analysis of all other pairwise combinations resulted in no significant differences: global $R\leq 0.267$, $p\geq 0.165$). Although the 0 hours and 23 hours samples were different, there were only two 23 hour samples which were just 2.44% similar to each other, but 8.71% similar to the Day 28 samples (SIMPER analysis). Moreover, no effect of stagnation time was found when the fungal communities were analysed with respect to the presence/absence of amplicons (ANOSIM: global $R=0.274$, $p=0.063$).

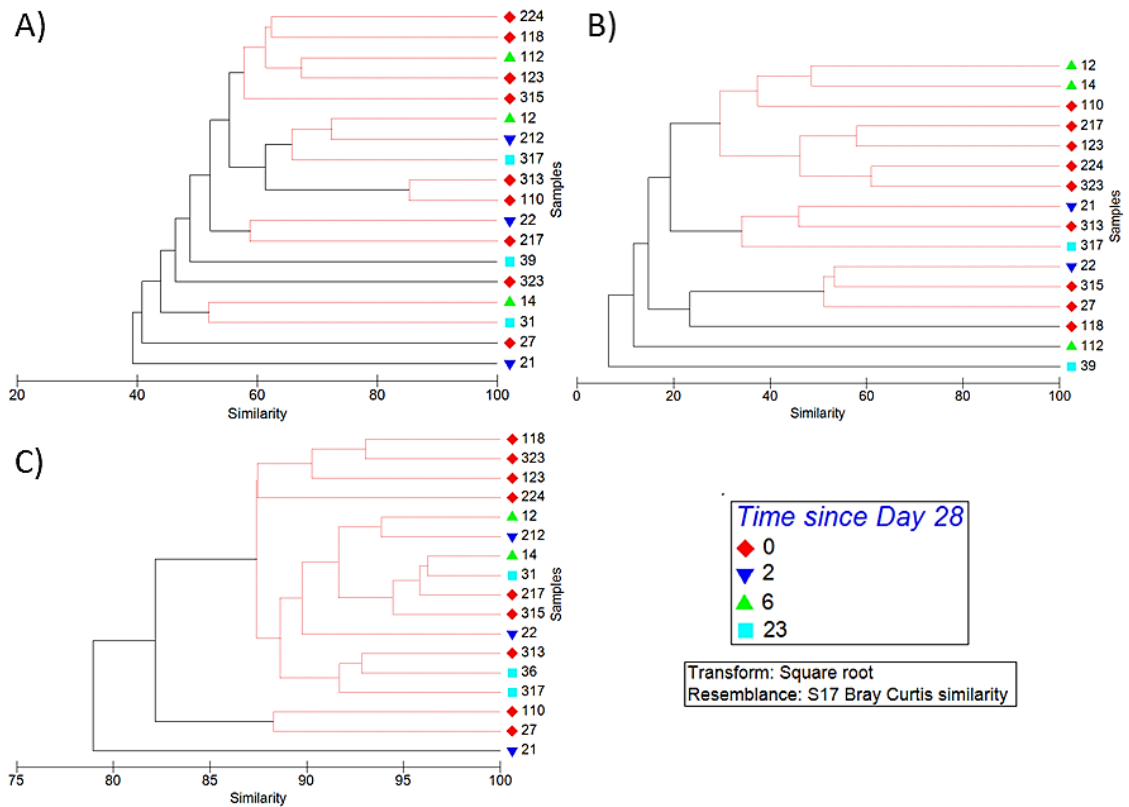


Figure 7.6 Dendrograms showing the similarity between biofilm communities from Day 28 and Pre-flush sample points of the SS condition. Samples labelled with respect to the time since Day 28 (hours) and sample identification number. A) Bacterial communities; B) Fungal communities; C) Archaeal communities. Dendrograms were plotted using the relative abundance data; red lines indicate profiles that were not significantly dissimilar (SIMPROF analysis). Data was square root transformed and a resemblance matrix was generated via a Bray-Curtis similarity test.

Pre-flush samples developed under the LVF regime were obtained 15 (loop 2), 20.5 (loop 3) and 24 (loop 1) hours after Day 28. The clustering of bacterial and fungal communities, with respect to stagnation time, is shown in Figure 7.7A and B respectively (nMDS plots had stress values of >0.1). No clustering by time since Day 28 was seen (the same trends were seen in the presence/absence data) for either bacteria or fungi. ANOSIM analysis confirmed that there was no effect of stagnation time upon the bacterial communities (relative abundance: global $R=0.007$, $p=0.487$; presence/absence: global $R=-0.045$, $p=0.593$), which were an average of 36.09% similar (SIMPER analysis) or the fungal communities (relative abundance: global $R=0.182$, $p=0.700$; presence/absence: global $R=-0.409$, $p=0.917$), which were an average of 18.14% similar (SIMPER analysis).

Pre-flush HVF samples were obtained 16 (loop 2), 19.5 (loop 3) and 22.5 (loop 1) hours after Day 28 samples were taken. There was no evidence of samples clustering by time since Day 28 (Figure 7.8; ANOSIM: relative abundance, global $R=0.149$, $p=0.159$; presence/absence, global $R=0.176$, $p=0.130$) and the Day 28 and Pre-flush bacterial communities were 33.87% similar to each other (SIMPER analysis).

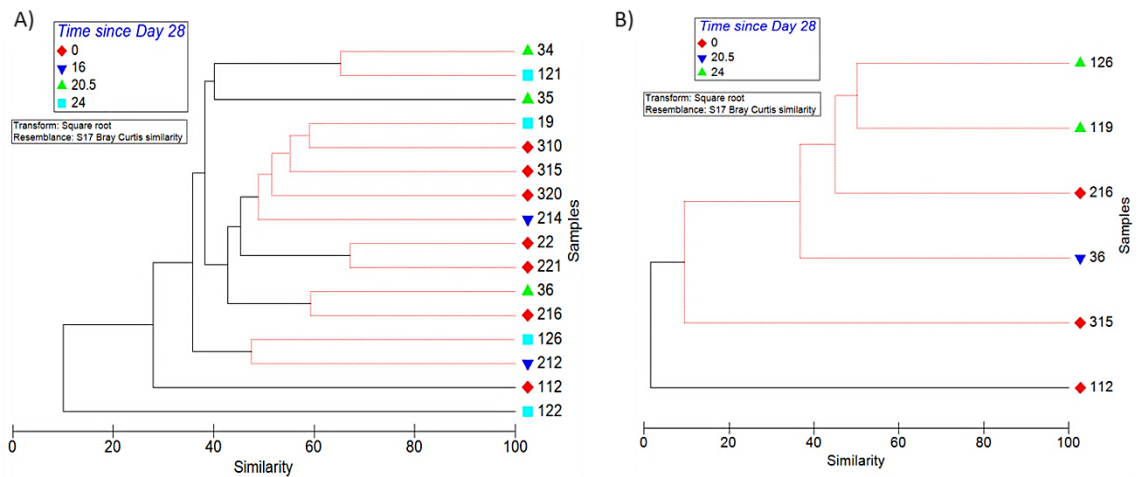


Figure 7.7 Dendrograms showing the similarity between biofilm communities from Day 28 and Pre-flush sample points of the LVF condition. Samples labelled with respect to the time since Day 28 (hours) and sample identification number. A) Bacterial communities; B) Fungal communities. Each dendrogram was plotted using the relative abundance data; red lines indicate profiles that were not significantly dissimilar (SIMPROF analysis). Data was square root transformed and a resemblance matrix was generated via a Bray-Curtis similarity test.

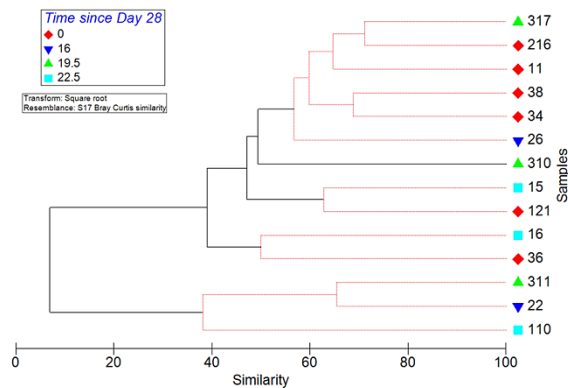


Figure 7.8 Dendrogram showing the similarity between bacterial biofilm communities from Day 28 and Pre-flush sample points of the HVF condition. Samples labelled with respect to the time since Day 28 (hours) and identification number; dendrogram was plotted using the relative abundance data; red lines indicate profiles that were not significantly dissimilar (SIMPROF analysis). Data was square root transformed and a resemblance matrix was generated via a Bray-Curtis similarity test.

7.2.2.2.2 Hydraulic effect on Pre-flush biofilm structure

Hierarchical clustering of the bacterial biofilm communities found the same trends with respect to hydraulic regime as were seen in the Day 28 communities; SS communities were different from those at LVF (ANOSIM: global $R=1.000$, $p<0.0001$) and HVF (ANOSIM: global $R=0.689$, $p<0.0001$) but LVF and HVF were very similar to each other (ANOSIM: global $R=0.084$, $p=0.147$). These relationships can be seen clearly in Figure 7.9A, with a single cluster of SS samples (an average of 46.52% similar to each other), a cluster containing all the LVF samples (an average of 40.41% similar to each other) along with five of the HVF samples and a final outlying cluster containing three HVF samples (these were each from a different loop and from

the invert or middle coupon positions), HVF samples were 25.37% similar to each other, on average.

The structure of the bacterial communities developed under SS and HVF were the least similar to each other (an average similarity of 9.65%), with 33 T-RFs explaining the majority of this differentiation, 8 of which were exclusive to the SS samples and five to the HVF profiles (Figure 7.9B). SS and LVF bacterial communities were 11.56% similar to each other, on average, with 30 T-RFs responsible for the distinction between them (Figure 7.9B), 14 of which were found in both communities but at significantly different mean relative abundances, 6 were found solely in LVF communities and 10 only in SS biofilms. Although there were no significant differences between LVF and HVF when analysed via ANOSIM, the community structures were not exactly the same, SIMPER analysis calculated an average similarity of 29.38%. The differences between LVF and HVF bacterial community structures were driven by 30 T-RFs (Figure 7.9B), most of which (26) were found in both communities, but at different relative abundances.

The SS fungal community structure was significantly different from that present under LVF conditions (ANOSIM: global $R=0.333$, $p=0.067$). Analysis of the similarity between the samples showed two main clusters of the fungal profiles (Figure 7.10A). One group contained the SS samples that were unable to be distinguished from each other, and the other contained the SS sample 21, which had the lowest relative richness and diversity indices of all the SS replicates and was most similar to the three LVF samples (which were 42.38% similar to each other and could not be distinguished from each other via SIMPROF analysis; Figure 7.10A). A total of 22 ARISA amplicons explained 60% of the difference between the SS and LVF samples, which were only 13.79% similar to each other. Only 7 amplicons were found in profiles from both regimes, 6 were exclusive to LVF biofilms and 9 were solely found in the more diverse SS biofilms.

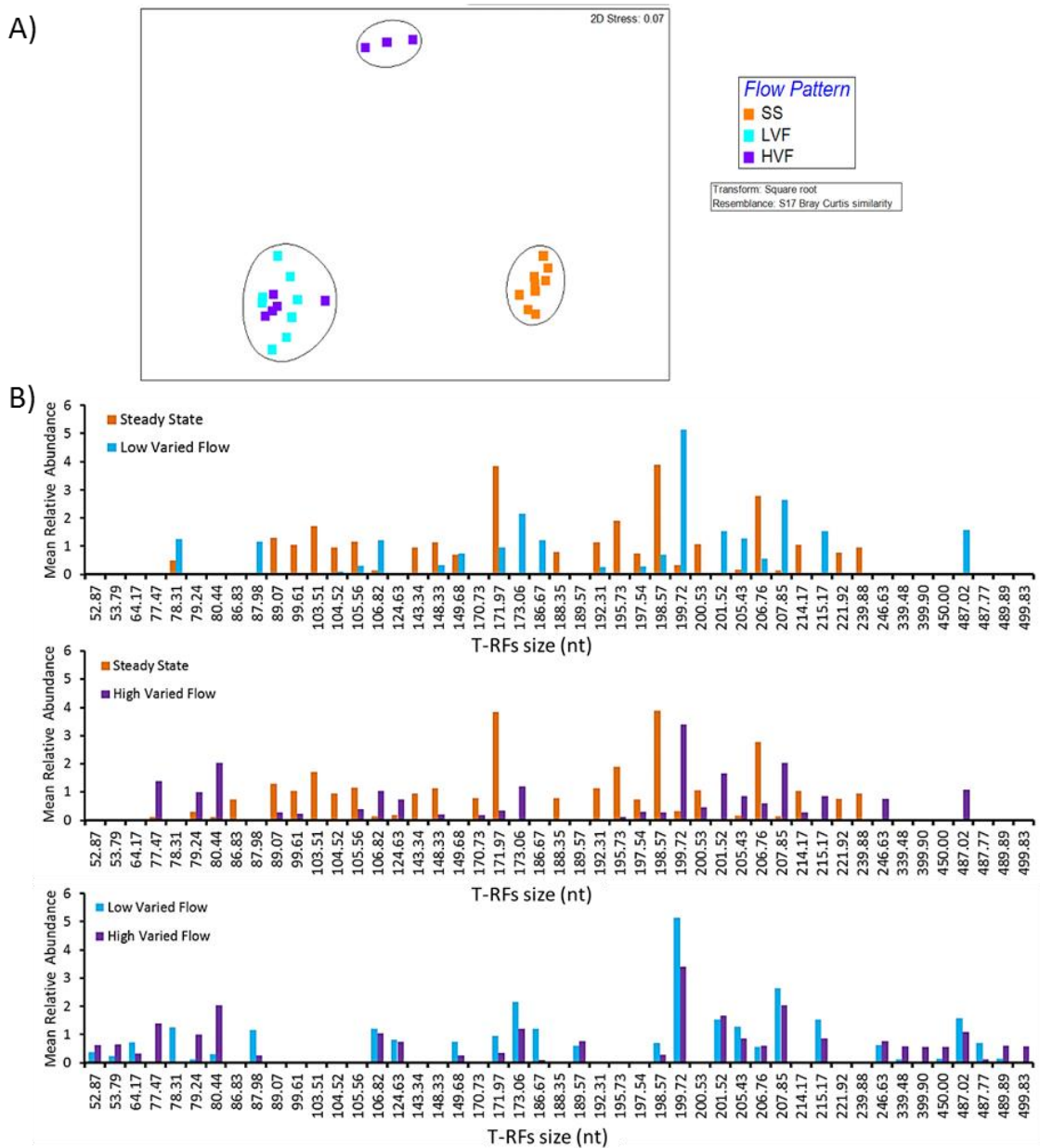


Figure 7.9 Comparison of bacterial community structures from Pre-flush biofilms developed under the SS, LVF and HVF hydraulic conditions . A) nMDS plotted using the relative abundance data, same pattern observed with the presence/absence data, black lines indicate clusters of at least 35% similarity and show the main groups which were highlighted in the dendrogram (not presented). B) SIMPER analysis showing the bacterial T-RFs that explain 60% of the difference between the biofilms from the two hydraulic regimes as indicated in the key of each plot.

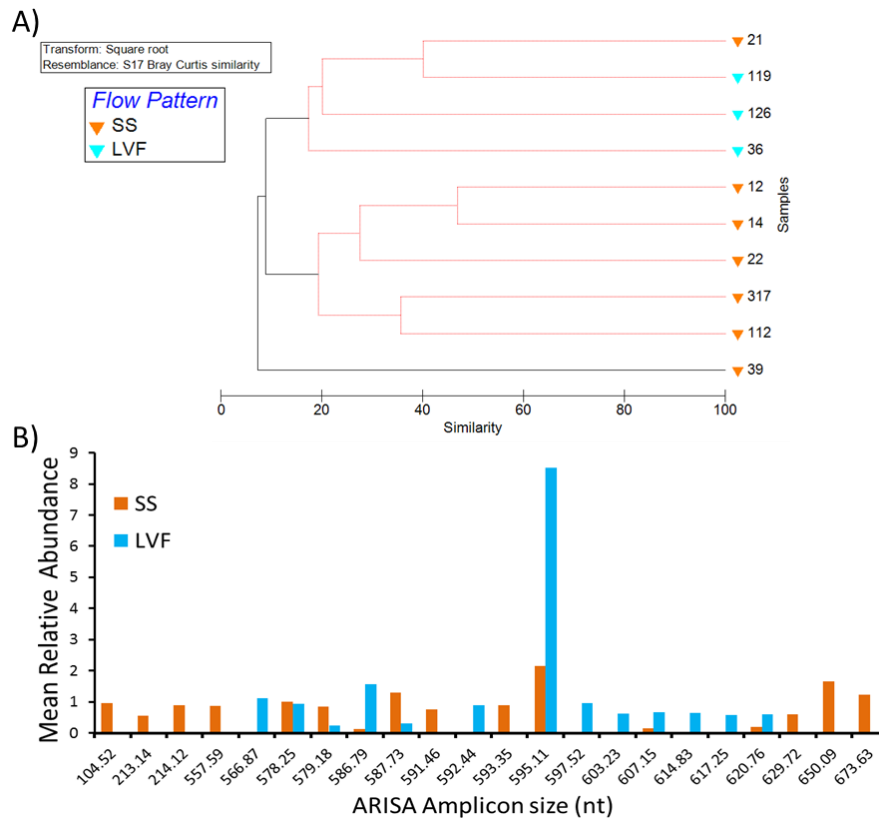


Figure 7.10 Comparison of the fungal community structure of Pre-flush biofilms from SS and LVF conditions. A) Dendrogram plotted using the relative abundance data; the same pattern observed with the presence/absence data, red lines shows those samples which could not be distinguished from each other (SIMPROF analysis); sample identification numbers are shown, in which the first number relates to the loop from which the sample was obtained and the second number(s) indicate the coupon which was sampled, see Figure 3.3. B) Size and mean relative abundance (AU) of the ARISA amplicons that explain 60% of the difference between SS and LVF.

7.2.3 Discussion

The quantifiable physical structure analysis supported the results from qualitative comparisons and microbial community structure analysis, confirming that only HVF biofilms experienced an effect of stagnation. Although the bacterial communities within SS samples taken after 23 hours of stagnation ($n=2$) were different, in terms of T-RF relative abundance, from those of Day 28 samples ($n=9$), they were more similar to the Day 28 biofilms than to each other. Consequently, there was no definitive effect of stagnation upon SS samples. Conversely, HVF Pre-flush biofilms had lower volumes and spread, but a greater proportion of EPS, than Day 28 biofilms. These differences were particularly driven by a decrease in cell volume and spread. During the stagnation period the biofilms were no longer exposed to a turbulent water flow, a change which was most pronounced following the HVF conditioning regime, and so the mass transfer of nutrients and other particles would likely be much reduced. This could have caused a considerable amount of cell death or led to the active detachment of cells (e.g. Telgmann *et al.*, 2004; section 1.4.3). Alternatively, the change observed could be an anomalous result, i.e. due to the HVF Pre-flush biofilms being left for approximately an hour after removal from the

experimental facility before initial processing (in all other instances samples were processed within 15 minutes or less of removal). As the HVF bacterial community did not alter between Day 28 and Pre-flush it seems unlikely that the differences in physical structure were due to cell lysis or active detachment, which would have altered some aspect of the community composition. Hence it is perhaps more likely that the physical structure of the samples was adversely impacted by the slightly longer exposure to the atmosphere.

7.2.4 Summary of stagnation and hydraulic effects Pre-flush

The similarities between SS, LVF and HVF Pre-flush biofilms are surmised in Figure 7.11. The patterns for the biofilm physical structure parameters were different at Pre-flush compared to Day 28 samples (Figure 6.12). Overall, SS and HVF biofilms were most similar at Day 28 but at Pre-flush the HVF biofilms were most similar to those from LVF. This change in similarity trends was primarily due to a reduction in cell relative volume between Day 28 and Pre-flush HVF biofilms, resulting in a structure at the latter time point more like that of the LVF biofilms.

Biofilms were dominated by carbohydrate, regardless of hydraulic regime or sample point, although the relationship between SS, LVF and HVF biofilms differed between Day 28 (each distinct) and Pre-flush (LVF and HVF were similar). The location of the greatest carbohydrate density occurred nearer to the bulk water in LVF biofilms than it did in SS or HVF biofilms. Essentially, the LVF and HVF biofilms had similar volumes of each stained component and similar proportions of EPS but the composition of their EPS was different. Compared to varied flow biofilms, SS samples had a greater volume of each component but a lower proportion of EPS, the composition of which was similar to that of HVF biofilms. The EPS matrices of Pre-flush biofilms developed under HVF and SS regimes were more heavily dominated by carbohydrate than the matrices of LVF biofilms. Interestingly the similarities/differences between the microbial community structures developed under each regime were the same at Day 28 as Pre-flush; namely that LVF and HVF had similar bacterial communities to each other and SS biofilms contained distinct bacterial, fungal and archaeal communities. Consequently, while stagnation only affected the HVF biofilm physical structure, these changes then altered the relationships between biofilms from all three hydraulic conditions. Therefore, to ensure the effect of flushing was characterized, rather than the effect of stagnation combined with flushing, the Pre-flush and Post-flush samples were compared to assess the biofilm response to elevated shear stresses. Due to the unexpected results at HVF Pre-flush, it was also appropriate to compare the Post-flush HVF samples with those from Day 28.

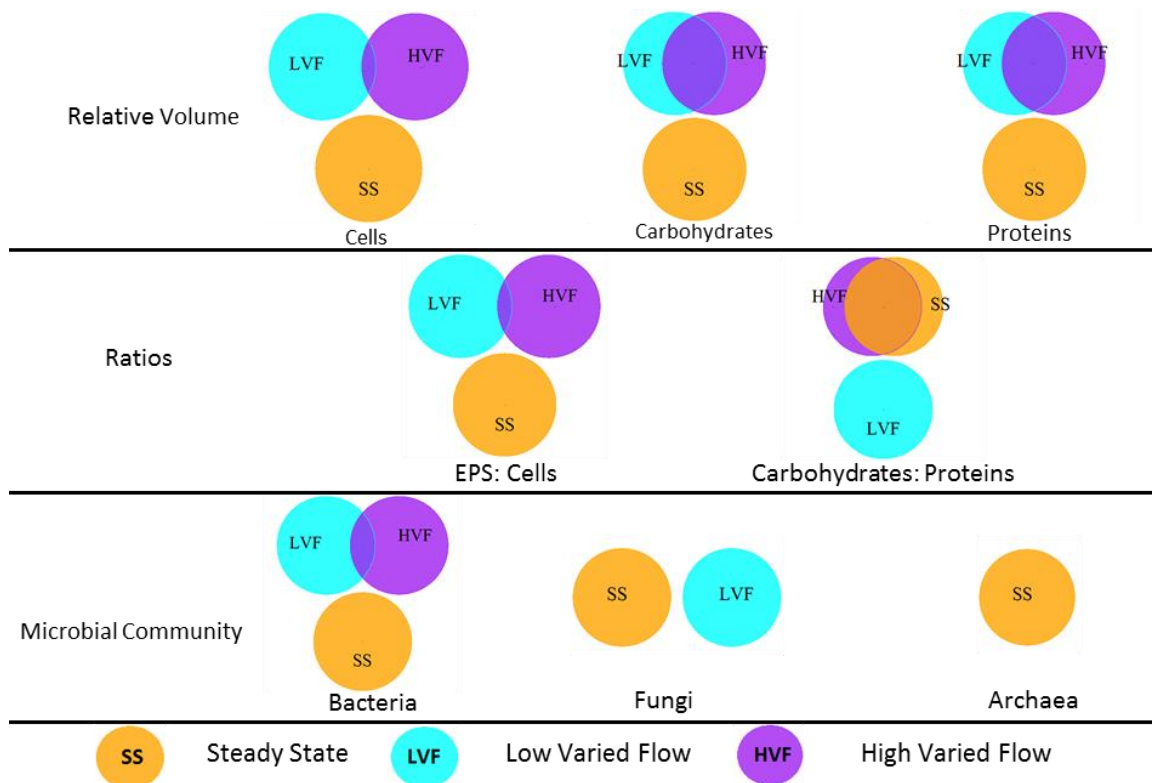


Figure 7.11 Summary of some of the patterns in biofilm structure parameters seen between the Pre-flush biofilms from SS, LVF and HVF conditions. Diagram is a schematic representation of similarities and differences only, drawn in the statistical program R v2.15. The overlap of groups was determined by the p value associated with the relevant pairwise test such that $p > 0.9999$ would lead to a 100% overlap of the groups, $p=0.50$ would lead to a 50% overlap, etc. Where $p \leq 0.05$ the groups had no overlap. The microbial community patterns are based on the multivariate clustering analysis (i.e. the ANOSIM tests).

7.3 Results Concerning the Effect of hydraulic regime upon Post-flush samples

Before exposure to elevated shear stress there was a definite presence of biofilm upon the pipe wall, regardless of the flow rate under which it had developed (Chapter 6, section 7.2). SEM was used to image the Post-flush samples, from each of the hydraulic tests (SS, LVF and HVF), after exposure to all three flushing steps (section 3.2.2). In all instances biofilm could still be visualized upon the coupon surface (Figure 7.12), in some cases the material remaining attached had a hole like appearance possibly where cells had been removed (e.g. Figure 7.12D), in others the biofilm appeared to still be intact but to have a flattened appearance (e.g. Figure 7.12B; F). In the LVF Post-flush samples stalked bacteria (identified visually) were particularly common (Figure 7.12E). Although the SEM analysis confirmed the presence of Post-flush biofilms, more detailed comparisons of biofilm structure were made to determine if the samples could still be differentiated based upon the hydraulic regime experienced during growth, the results from these analyses are presented in the following section

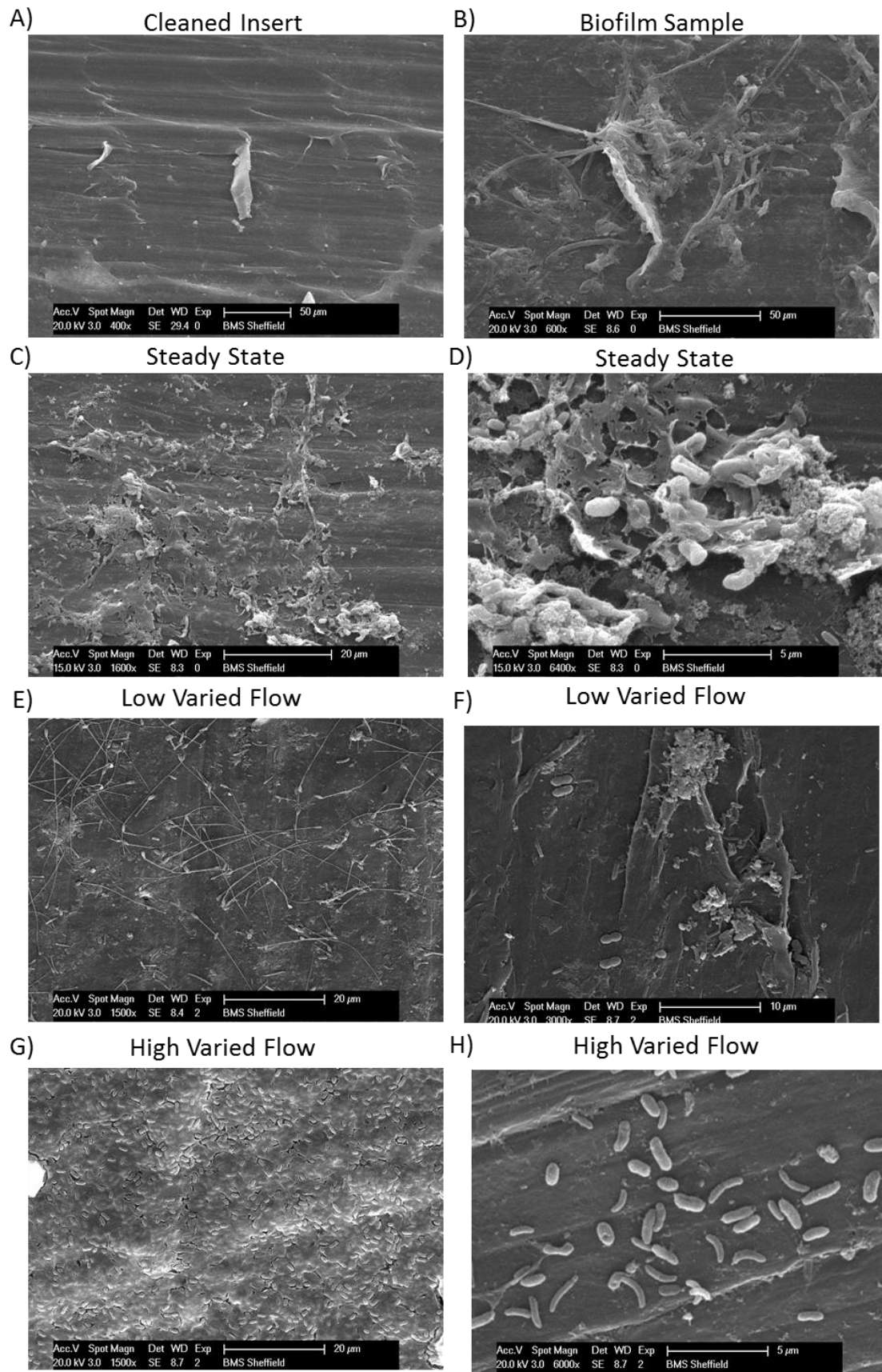


Figure 7.12 Representative SEM images of a cleaned insert (A) and Post-flush biofilm samples (B to H) developed under different hydraulic regimes. A) Surface of the HDPE insert when cleaned as described in section 3.2; B) SS biofilm sample imaged at the same magnification as the sterile insert; C to H) SS, LVF or HVF biofilms as indicated, imaged at different scales as indicated by the scale bar on each image.

7.3.1 Biofilm physical structure Post-flush

As with biofilms from the other samples points, five Post-flush biofilms from each of the hydraulic tests (SS, LVF and HVF) were imaged at five FOV (n=25). However, data for one of the FOV from a SS sample (loop 2, crown) was corrupted during the transfer of the images from the CLSM system, therefore the replication in this instance is n=24. There were generally no differences in the data due to location of biofilm samples (“position dataset” vs. “loop dataset”) with respect to relative volume (Wilcoxon: $W \geq 82.5$, $p \geq 0.1196$), spread (Wilcoxon: $W \geq 6.0$, $p \geq 0.1535$) or peak location (Wilcoxon: $W \geq 81.0$, $p \geq 0.1528$), see Appendix 10 for detailed statistical outputs. However, there was a significant difference between the position and loop datasets with regard to the relative volume of cells within SS biofilms (Wilcoxon: $W=164.5$, $p=0.0100$) and the relative volume of carbohydrates in SS (Wilcoxon: $W=51.5$, $p=0.0206$) and HVF (Wilcoxon: $W=34.5$, $p=0.0013$) biofilms. In these three instances the data was initially analysed in two groups: the “loop dataset” and “position dataset” before being analysed as a whole set with no differentiation in location. In each case the patterns seen within the data were the same and so, for clarity, only the results from the data analysed in its entirety (i.e. n=25 or n=24, with no differentiation between loop and positions) are presented in the following sections.

7.3.1.1 Visualization and qualitative analysis of area distribution

Irrespective of conditioning regime, after the flushing phase, the area distribution of carbohydrates was greater than that of the cells or proteins, the latter of which had the lowest area fractions and biofilm depth (Figure 7.13). Across the three regimes, the peak of the carbohydrates and proteins consistently occurred above that of the cells. Despite these similarities, the biofilms from the different conditions did have distinct area distributions. In particular, LVF biofilms had an obvious reduction in each biofilm component compared to SS or HVF biofilms, as indicated by the lower area fraction coverage throughout the biofilm (Figure 7.13) and the example 3D projection, which had much sparser biofilm coverage than that of the SS or HVF biofilms (Figure 7.14).

The area distributions of SS and HVF biofilms appear similar to each other, apart from, potentially, a greater variation between HVF replicates than SS replicates and a few of the HVF FOV containing greater cell area fractions than for SS. However, the 3D images of an example FOV from both SS and HVF did not show a distinct difference in cell coverage; rather, both were dominated by carbohydrates. The reason for this is that the five replicates with the greatest cell area fractions did not correspond to the five replicates with the greatest

carbohydrate fractions. Rather, the FOV with the greatest cell coverage had mid to low level carbohydrate coverage and vice-versa, therefore, the example HVF biofilm in Figure 7.14C is representative of one of the carbohydrate dominant FOV.

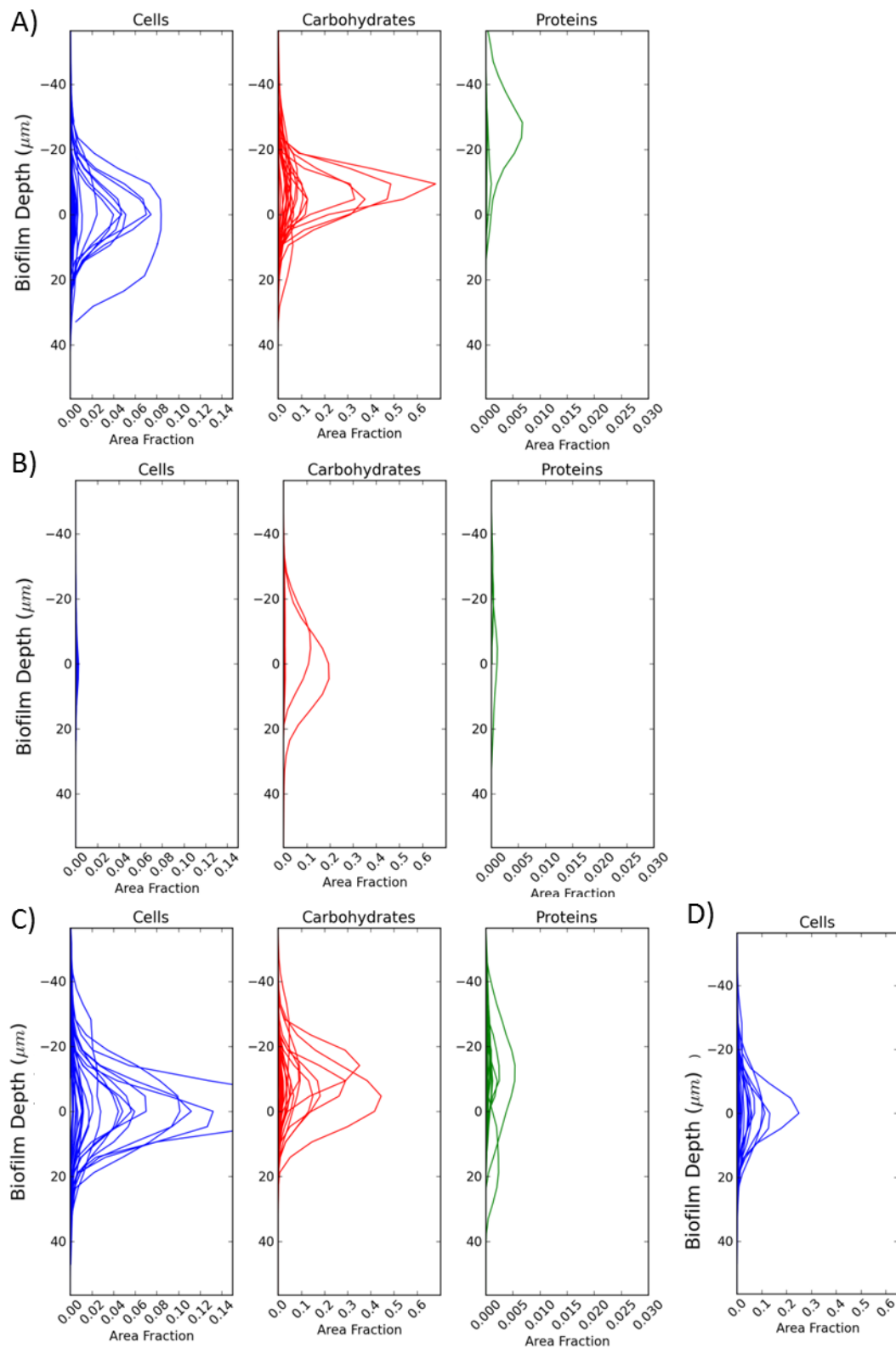


Figure 7.13 The area distribution of cells, carbohydrates and proteins within Post-flush biofilms previously developed under A) SS conditions (n=24); B) LVF conditions (n=25); C) HVF conditions (n=24). D) The cells of Post-flush HVF biofilm plotted on an x-axis scale with a greater range. Each line represents one FOV (i.e. one Z-stack). Area fraction refers to the proportion of each XY image of the Z-stack covered by the particular component (see section 4.6.3.1).

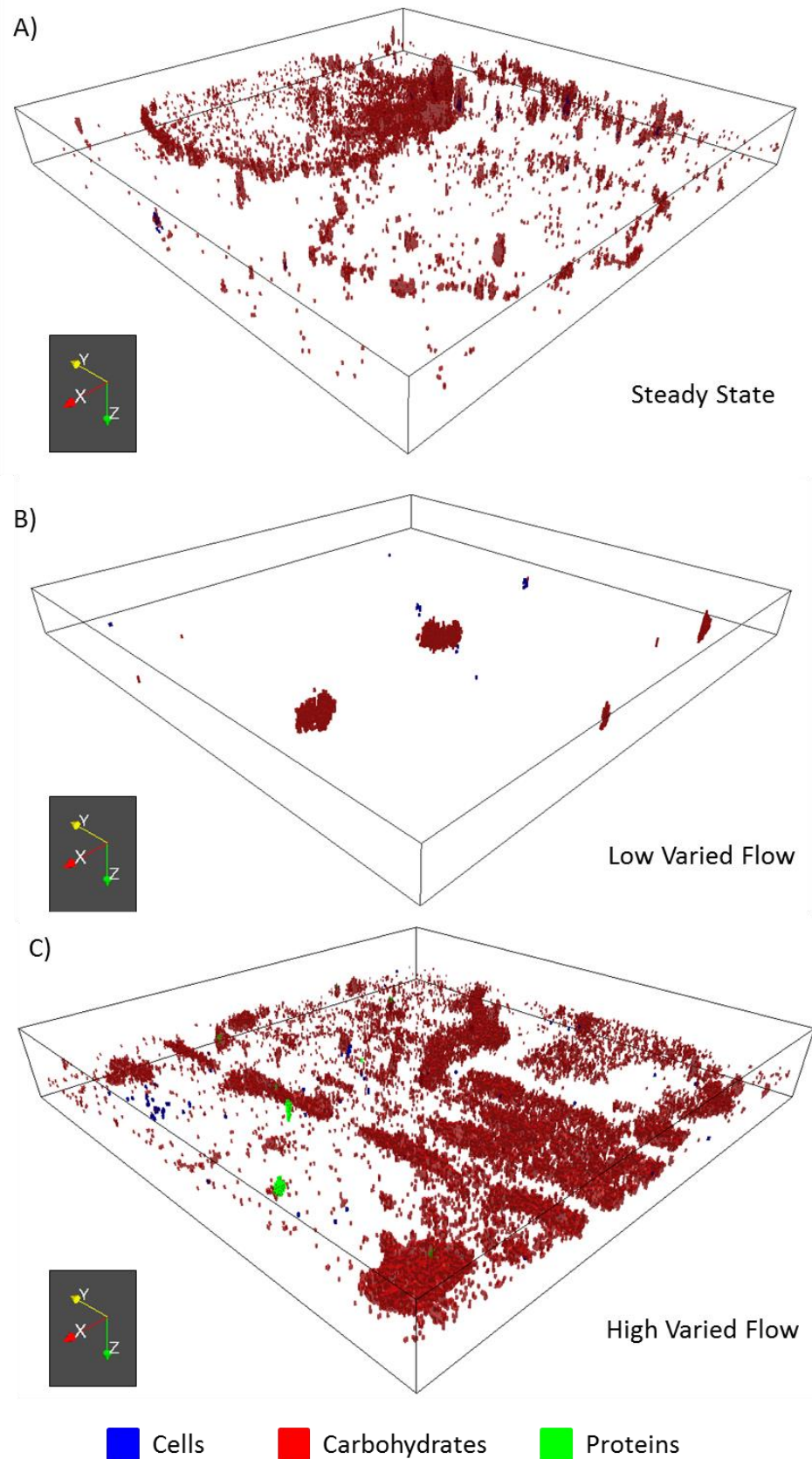


Figure 7.14 A representative example of the 3D arrangement of cells, carbohydrates and proteins within a Post-flush biofilm from A) SS; B) LVF; C) HVF conditions. Each 3D projection is within a plotting area shown by the cube which is 420 μm x 420 μm (XY dimensions) with a depth (Z) of: A) 47.0 μm; B) 37.6 μm and C) 61.1 μm. N.B. the cells (blue) may be hard to distinguish from the carbohydrate (red) in some instances, despite setting a mid-level opacity

7.3.1.2 Quantitative analysis of volume, spread and peak location

After flushing, LVF biofilms had significantly less total biofilm volume (and thus EPS) compared to SS or HVF biofilms. Carbohydrates dominated each biofilm regardless of conditioning regime but the relative volumes of cells, carbohydrates and proteins (Figure 7.15) were significantly greater in the biofilms from SS and HVF (which only differed from each other in protein content) than those from LVF (Table 7.8). This was particularly evident for the proteins, which were absent from many LVF samples, leading to a median protein-to-cell ratio of 0.00, despite a range of 0.00 – 30.00. Irrespective of flow regime, Post-flush biofilms had very low proportions of protein in comparison to cells and high proportions of carbohydrate (Table 7.9). The proportion of proteins to cells was significantly different between biofilms from all of the flow regimes, but the carbohydrate-to-cell ratios were similar between LVF and SS, in HVF the ratio value was significantly lower. Proportionally, EPS quantity did not differ between LVF and SS biofilms, however, HVF biofilms had significantly less (EPS-to-cell ratios in Table 7.9). The SS EPS was more dominated by carbohydrates than the matrices from LVF or HVF biofilms in which, though carbohydrate still dominated, proteins contributed to a greater extent.

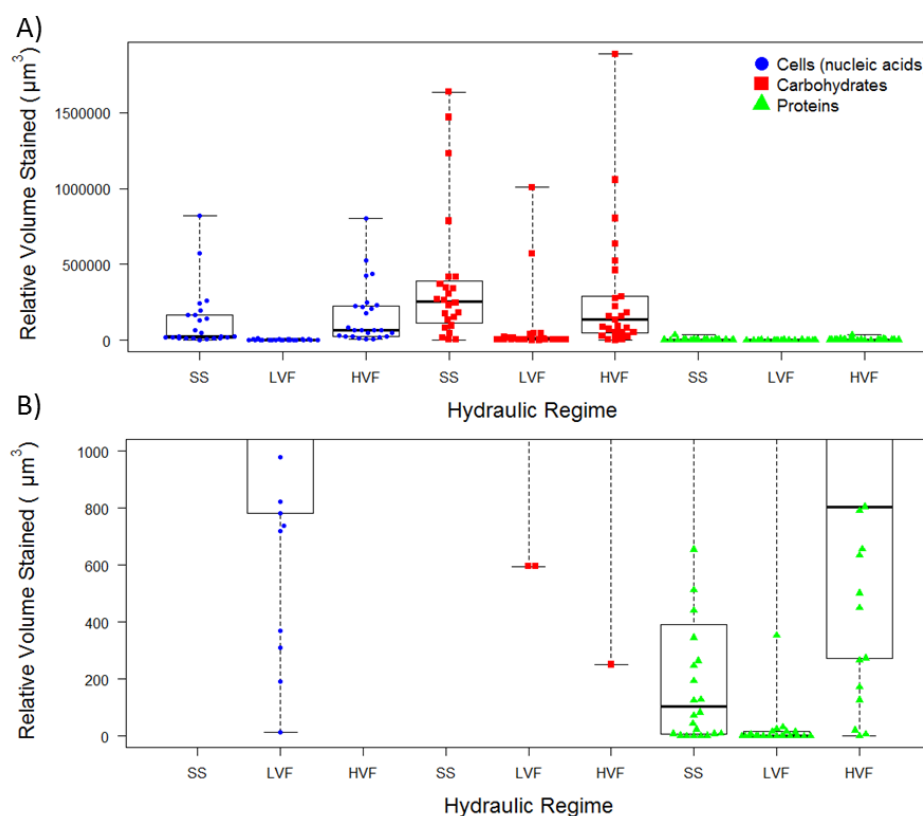


Figure 7.15 Relative volumes of stained biofilm components within Post-flush biofilms previously developed under SS, LVF or HVF conditions. Y-axis is scaled to A) max data point; B) protein data. Each data point represents a different FOV, n=24 for SS, n=25 for LVF and HVF. Box and whisker plots show the range, interquartile range and median – indicated by the black solid line; volume is relative to the threshold value (see section 4.6.3.3).

Table 7.8 Comparison of the relative volumes of the stained biofilm components of Post-flush biofilms, previously developed under SS, LVF or HVF conditions.

Component	Median Relative Volume (μm^3)			Kruskal Wallis	Wilcoxon Results	
	SS ^A	LVF ^B	HVF ^B	SS vs. LVF vs. HVF	Pairwise test	Result
Cells	22679	2190	67303	$X^2=210.37$ df=2 p<0.0001	SS vs. LVF SS vs. HVF LVF vs. HVF	W=588.0, p<0.0001 W=255.0, p=0.1372 W=623.0, p<0.0001
Carbohydrates	255601	5705	134539	$X^2=24.69$ df=2 p<0.0001	SS vs. LVF SS vs. HVF LVF vs. HVF	W=520.0, p<0.0001 W=365.0, p=0.1989 W=518.0, p<0.0001
Proteins	103	0	804	$X^2=212.74$ df=2 p<0.0001	SS vs. LVF SS vs. HVF LVF vs. HVF	W=466.0, p=0.0007 W=131.5, p=0.0008 W=560.0, p<0.0001
EPS ^C	259069	5705	139740	$X^2=26.48$ df=2 p<0.0001	SS vs. LVF SS vs. HVF LVF vs. HVF	W=520.0, p<0.0001 W=364.0, p=0.2061 W=536.0, p<0.0001
All Material ^D	357853	10913	306912	$X^2=35.93$ df=2 p<0.0001	SS vs. LVF SS vs. HVF LVF vs. HVF	W=561.0, p<0.0001 W=334.0, p=0.5063 W=574.0, p<0.0001

^A n=24; ^B n=25; ^C EPS = carbohydrates + proteins, before averaging, data presented is therefore the median of the sums; ^D All Material = EPS + cells, before averaging before averaging, data presented is therefore the median of the sums.

Table 7.9 Comparison of the values of the various ratios of relative volumes of different components within Post-flush biofilms from SS, LVF or HVF hydraulic conditions. Significant results are shown in bold.

Ratios ^A	Median Ratio Value			Kruskal Wallis	Wilcoxon Results	
	SS ^B	LVF ^C	HVF ^C	SS vs. LVF vs. HVF	Pairwise test	Result
EPS: Cells	11.37	4.40	1.06	$X^2=6.17$ df=2 p=0.0457	SS vs. LVF SS vs. HVF LVF vs. HVF	W=318.0, p=0.7287 W=395.0, p=0.0272 W=197.0, p=0.0396
Carbohydrates: Proteins	2977.61	286.62	62.46	$X^2=11.82$ df=2 p=0.0027	SS vs. LVF SS vs. HVF LVF vs. HVF	W=144.0, p=0.0246 W=410.0, p=0.0009 W=98.0, p=0.5910
Carbohydrates: Cells	11.37	3.47	1.06	$X^2=6.51$ df=2 p=0.0385	SS vs. LVF SS vs. HVF LVF vs. HVF	W=318.0, p=0.7287 W=397.0, p=0.0243 W=193.0, p=0.0323
Proteins: Cells	<0.00 ^D	0.00	0.01	$X^2=15.35$ df=2 p=0.0005	SS vs. LVF SS vs. HVF LVF vs. HVF	W=421.0, p=0.0130 W=129.5, p=0.0323 W=493.0, p=0.0004

^A The first component is divided by the second, a value > 1 indicates a greater volume of the first component, a value <1 indicates a greater volume of the second, a value = 1 indicates an equal volume of each component; ^B n=24; ^C n=25; ^D actual median ratio 0.004.

The spread of the cellular material (Table 7.10; Figure 7.16) was greater in the SS and HVF biofilms than LVF but, despite comprising a lower carbohydrate volume than SS or HVF, the spread of carbohydrates throughout LVF biofilms was not different from that in biofilms from the other regimes. This finding suggested that the LVF biofilms had a lower carbohydrate density than was seen for either SS or HVF regimes. Nonetheless, in biofilms from all regimes, the greatest XY coverage of carbohydrate occurred just above that of the cells (Kruskal Wallis: $X^2=2.00$, df=2, p=0.3688; median= -1 regardless of flow regime). As many of the replicates from LVF did not contain protein, the median spread of this component was 0 AU, however, where

protein was present, the spread ranged from 813363- 5196253 AU. Consequently, LVF biofilms had a significantly reduced protein spread compared to SS and HVF biofilms (Table 7.10). Where protein was found, the peak area fraction was a greater distance above that of the cells in LVF biofilms (median= -9) than was observed in either SS (median= -2; Wilcoxon: W=441.5, p=0.0045) or HVF (median=-3; Wilcoxon: W=476.0, p=0.0014) biofilms. Within each hydraulic regime, the proteins of the Post-flush biofilms occurred within a narrower biofilm depth than the cells or carbohydrates (Table 7.10). Across the hydraulic regimes, protein spread was similar between SS and HVF biofilms (Table 7.10) as was the peak location (Wilcoxon: W=266.0, p=0.4970), but both were distinct from LVF biofilms. The proteins within biofilms from each regime had an average protein peak location which was above that of the carbohydrates; this was most pronounced in LVF biofilms with a difference of 8 slices between the peak fractions of the two EPS components.

Table 7.10 Results from statistical comparisons of the spread of each of the stained biofilm components in Post-flush biofilms developed under SS, LVF or HVF conditions. Significant results are shown in bold.

Biofilm Component	Median Spread Value (AU)			Kruskal Wallis SS vs. LVF vs. HVF	Wilcoxon Results	
	SS	LVF	HVF		Pairwise test	Result
Cells	3783410	3290993	3921805	$X^2=10.18$ df=2 p=0.0062	SS vs. LVF	W=431.0, p=0.0082
					SS vs. HVF	W=288.0, p=0.8197
					LVF vs. HVF	W=460.0, p=0.0037
Carbohydrates	3848898	3741471	3652479	$X^2=0.08$ df=2 p=0.9598	SS vs. LVF	W=310.0, p=0.8493
					SS vs. HVF	W=314.0, p=0.7890
					LVF vs. HVF	W=309.0, p=0.9536
Protein	2929510	0	3182726	$X^2=25.95$ df=2 p<0.0001	SS vs. LVF	W=477.0, p=0.0003
					SS vs. HVF	W=214.0, p=0.0871
					LVF vs. HVF	W=556.0, p<0.0001

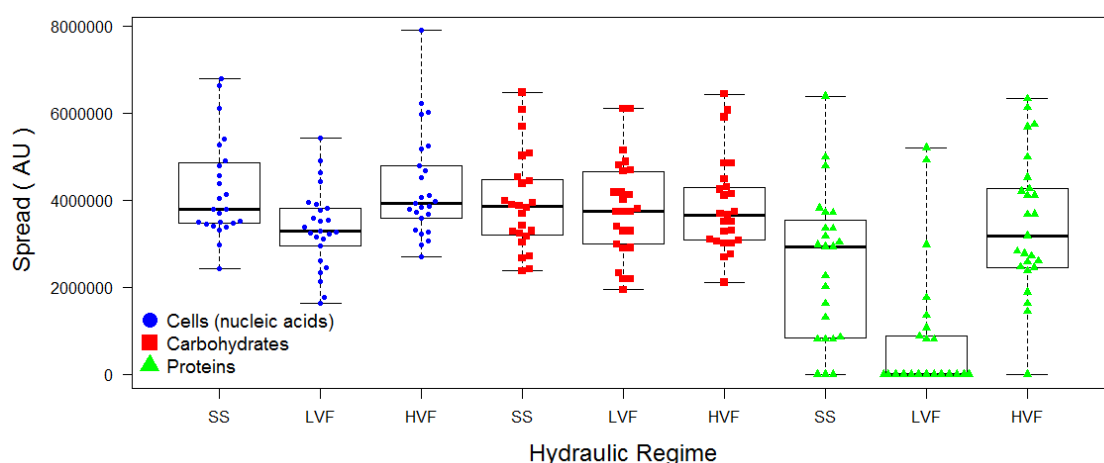


Figure 7.16 Spread of each of the stained biofilm components throughout Post-flush biofilms previously developed under SS, LVF or HVF regimes. Each data point represents a different FOV, n=24 for SS, n=25 for LVF and HVF; box and whisker plots show the range, interquartile range and median – indicated by the solid black line; spread is calculated by the relative volume divided by the max area fraction (see section 4.6.3.4).

7.3.2 Biofilm community structure Post-flush

7.3.2.1 PCR amplification of 16S rRNA genes and ITS regions

Amplification of 16S rRNA bacterial and archaeal genes and fungal ITS regions was applied to nine DNA extractions from each hydraulic regime. The strength of the amplified bacterial products differed between replicates when visualised on an agarose gel (not shown) but nevertheless detectable concentrations of bacterial 16S rRNA genes were found in the Post-flush biofilms from each hydraulic condition (SS: 9/9; LVF:9/9; HVF 8/9). Fungal amplicons were detected in all the SS Post-flush biofilms (9/9) but were far less common in the biofilms developed under varied flows (LVF: 1/9; HVF: 2/9), consequently statistical comparisons between the fungal communities from the three hydraulic conditions were not possible. However, though the difference in replication must be considered, qualitative comparisons between the HVF and SS fungal communities in terms of similarity could be made as the two HVF samples could potentially cluster with each other, as was seen with the two Day 0 bacterial communities from SS (see section 5.2.3.2.2). It was not appropriate to include the single LVF sample as the analysis arranges samples based upon their similarity to each other and, because of the lack of other LVF samples to potentially cluster with, this would force the LVF to be most similar to one of either the SS or HVF replicates, which would not be a true or representative result. Comparison between SS, LVF and HVF archaeal communities was also not possible as they were only found at detectable concentrations in the SS biofilms. Therefore the following sections present results for SS, LVF and HVF bacterial community comparisons and (tentative) comparison of the SS and HVF fungal communities.

7.3.2.2 Relative taxon richness, evenness and diversity

Visual comparisons between the bacterial community fingerprints (Figure 7.17A) of SS, LVF and HVF biofilms highlighted the similarity of some peaks, particularly the dominant peaks around 200 nt. It was also observed that smaller peaks, particularly at lengths <150 nt, differed between the regimes and appeared to be more diverse under SS conditions. The total number of different TR-Fs in all the SS profiles was 101, considerably greater than that of either of the varied flow biofilms (LVF: 36; HVF: 38). Individual SS profiles had significantly greater relative taxonomic richness than those of LVF or HVF biofilms (ANOVA: $df=2$, $p=0.0044$; subsequent Tukey HSD test: SS vs. LVF, $p=0.0039$; SS vs. HVF, $p=0.0493$). The relative evenness and diversity of SS communities were similar to those of HVF biofilms but significantly greater than those observed in LVF biofilms (Tukey HSD: relative evenness, SS vs. LVF, $p=0.0070$; SS vs. HVF $p=0.1024$; relative diversity, SS vs. LVF, $p=0.0022$; SS vs. HVF, $p=0.0809$). The bacterial

communities from LVF and HVF did not differ from each other in terms of relative richness (Tukey HSD: LVF vs. HVF, $p=0.5601$), evenness (Tukey HSD: $p=0.5027$) or diversity (Tukey HSD: $p=0.3213$).

Qualitative comparisons between the fungal communities of SS ($n=9$) and HVF ($n=2$) showed that the total number of different ARISA amplicons was similar in biofilms from both regimes (SS=56 amplicons; HVF=57 amplicons). Comparisons of the minimum and maximum ecological indices showed that, although fungi were less common in HVF biofilms than SS, where they were found, the communities tended to have greater relative richness, evenness and diversity than under SS. Visual comparisons of the ARISA electropherograms (Figure 7.17B) showed that the SS profile had a greater relative abundance of the ARISA amplicons than was seen at HVF, where diversity may be greater but each of the peaks was considerably smaller than in the SS profile (this is consistent with the HVF profiles being more even than SS).

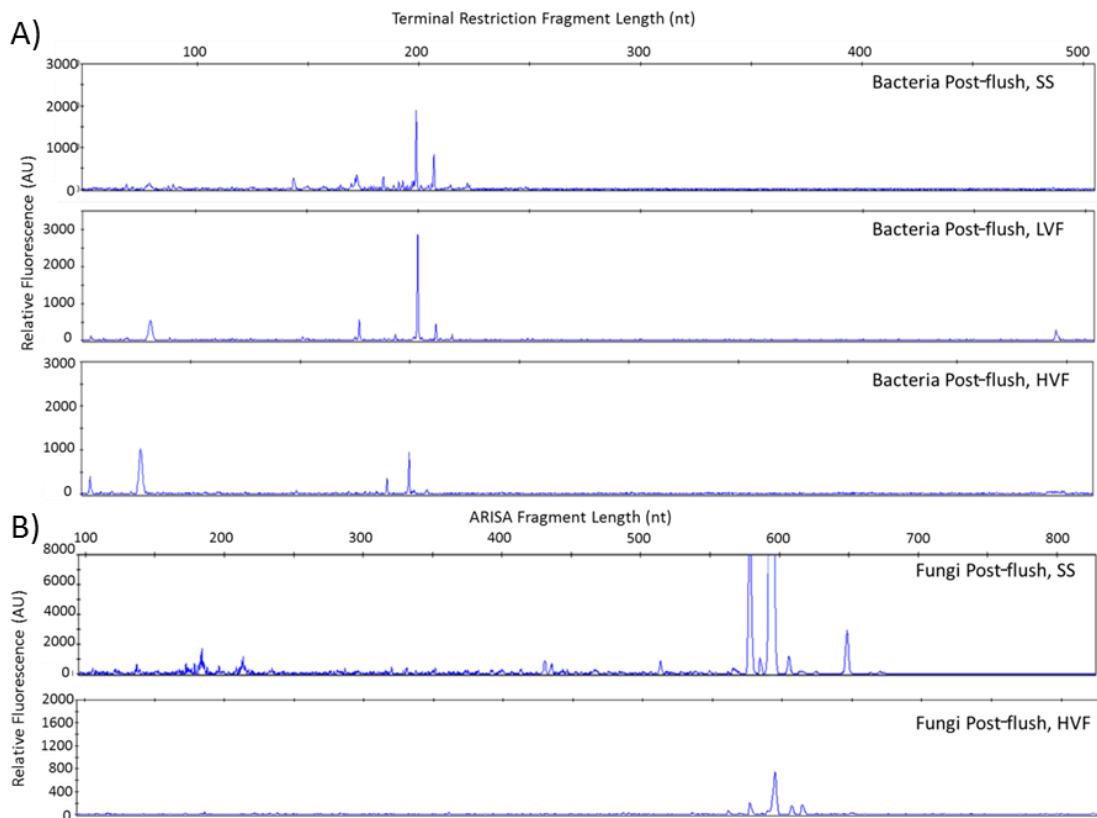


Figure 7.17 Representative T-RFLP or ARISA electropherograms of Post-flush biofilm communities from the SS, LVF or HVF experiments. A) Bacterial communities (16S rRNA, T-RFLP); B) Fungal communities (ITS region, ARISA). N.B. Fungi only found in a single LVF sample, the two HVF profiles were very similar to each other.

Table 7.11 Relative richness, evenness and diversity indices of the bacterial and fungal communities of Post-flush biofilms previously developed under SS, LVF or HVF conditions.

Microbial fingerprint	Flow Regime	Relative Richness (number of T-RFs)			Relative Evenness (Pielou's Index)			Relative Diversity (Shannon's Index)		
		Min	Max	Mean (St.Dev)	Min	Max	Mean (St.Dev)	Min	Max	Mean (St.Dev)
Bacteria	SS	10	33	19 (9)	0.94	0.99	0.96 (0.02)	2.24	3.36	2.76 (0.46)
	LVF	2	19	7 (6)	0.78	0.95	0.86 (0.07)	0.54	2.81	1.38 (0.88)
	HVF	3	18	10 (7)	0.77	0.97	0.90 (0.08)	0.85	2.77	1.92 (0.87)
Fungi	SS	6	21	11 (5)	0.71	0.94	0.86 (0.06)	1.27	2.86	2.01 (0.46)
	HVF ^A	33	39	-	0.67	0.83	-	2.35	3.03	-

^A n=2 therefore average could not be calculated. N.B. Min = minimum, Max= maximum, St.Dev = standard deviation.

7.3.2.3 Community structure

After flushing, the bacterial communities of SS, LVF and HVF biofilms were all different from each other (ANOSIM: relative abundance, global $R=0.536$, $p < 0.0001$; presence/absence global $R=0.542$, $p < 0.0001$). These differences were reflected in the nMDS plot (Figure 7.18A), which had a stress value of 0.12. Although previously where stress was >0.1 , a dendrogram was deemed a more accurate representation of the data, the nMDS plot in this instance showed the same patterns as were reflected in the dendrogram (Figure 7.18B) and so both are provided to aid interpretation of the data. Essentially four distinct groups existed – one comprised solely of SS samples (the majority of which could not be distinguished from each other), one primarily comprised of LVF samples and two clusters of the HVF samples (124, 125 and 327 were not distinguishable in Figure 7.18B). The SS samples were observed to be less divergent between replicates (an average of 40.84% similarity) than LVF (an average of 35.08% similarity) or HVF the latter of which had the greatest variation between replicate samples (an average of 20.38% similarity). SS bacterial communities were significantly different from LVF (ANOSIM: relative abundance, global $R=0.707$, $p < 0.0001$; presence/absence, global $R=0.702$, $p < 0.0001$) between which there was an average of 96.40% dissimilarity that was primarily explained by the 16 T-RFs in Figure 7.18C. Of the 16 T-RFs only 5 were found in both biofilm types, indicating that their differences were mainly due to the presence of different taxa. Similarly, SS samples differed significantly from HVF (ANOSIM: relative abundance, global $R=0.642$, $p < 0.0001$; presence/absence, global $R=0.656$, $p < 0.0001$) with which they had an average dissimilarity of 89.67%, explained by 20 T-RFs (Figure 7.18D), 10 of which were found in both communities but at different relative abundances. LVF and HVF datasets had outlying replicates clustering away from the main group, this placement was not driven by low total peak areas or coupon location; rather, in some instances, the outlier(s) were deemed to be more similar to a sample(s) from the alternative varied flow regime (e.g. sample 126 HVF was more similar to LVF samples). Nevertheless the bacterial communities from each regime were

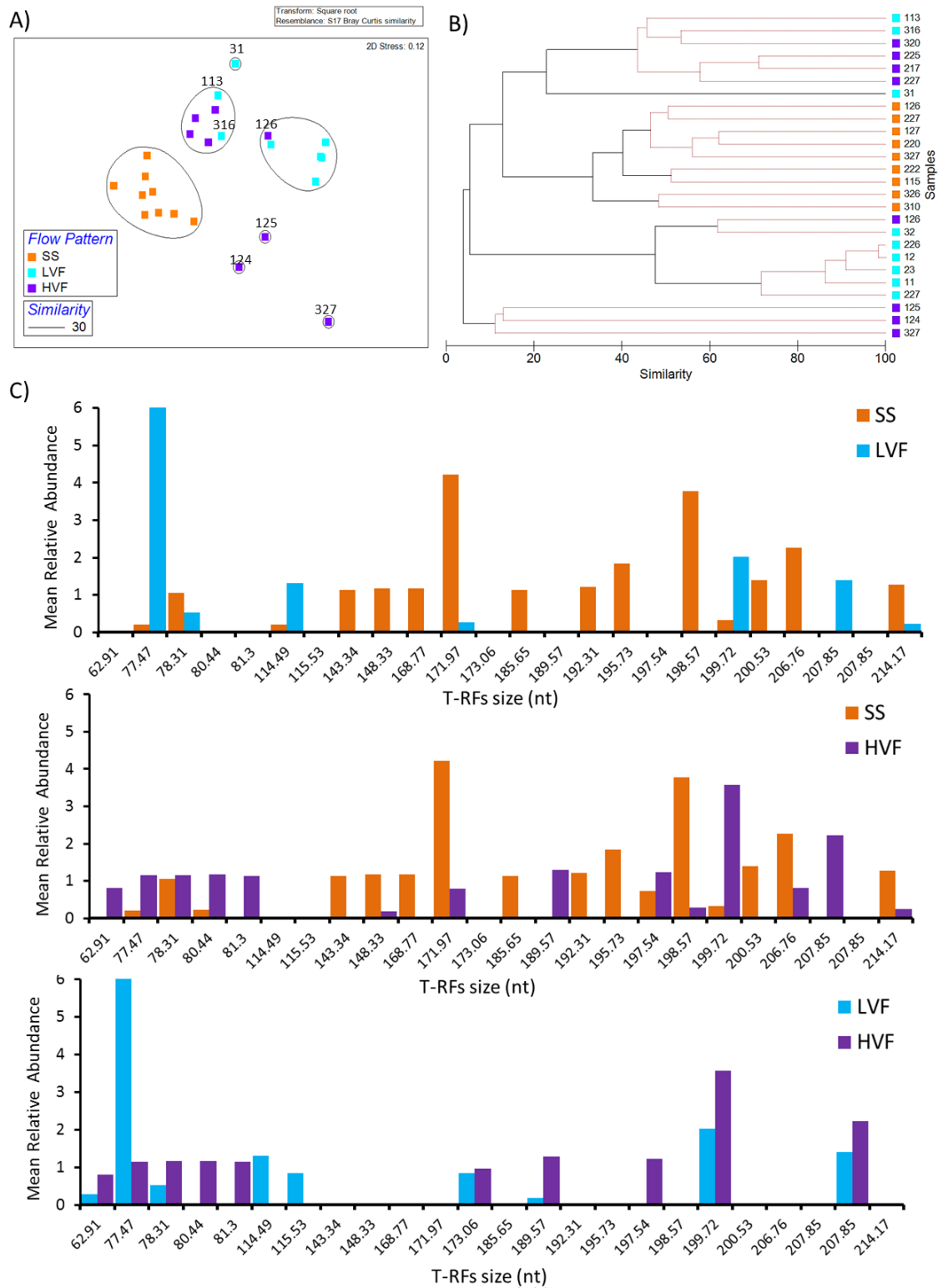


Figure 7.18 Comparison of the bacterial communities of Post-flush biofilms from SS, LVF or HVF conditions. A) nMDS plot using relative abundance data, black lines indicate clusters of at least 30% similarity, based on the group averages from hierarchical clustering; B) Dendrogram of the same data, red lines indicate profiles not significantly dissimilar according to SIMPROF. In both A) and B) sample identification numbers are shown, in which the first number relates to the loop from which the sample was obtained and the second number(s) indicate the coupon which was sampled, see Figure 3.3. Data was square root transformed and a Bray-Curtis similarity matrix was generated, the same patterns were observed in the presence/absence data. C) The size and mean relative abundance (AU) of the T-RFs which described 60% of the variation between the bacterial communities as indicated in the key.

significantly different from each other (ANOSIM: relative abundance, global $R=0.246$, $p=0.022$; presence/absence, global $R=0.236$, $p=0.025$) with 85.38% dissimilarity on average. The differences between LVF and HVF communities were driven by just 12 T-RFs (Figure 7.18E), 7 of which were common to both biofilm bacterial communities. A key difference between LVF and HVF or SS bacterial communities was the abundance of the T-RF 77.47 nt, which was present in biofilms from all regimes but had a much greater abundance under LVF.

The SS and HVF fungal communities were also distinct from each other (ANOSIM: relative abundance, global $R=0.441$, $p=0.0500$; presence/absence, global $R=0.710$, $p=0.018$), with an average dissimilarity of 91.45%, which clustered separately as seen in Figure 7.19A. The majority of the difference between the fungal communities was explained by the 28 ARISA amplicons in Figure 7.19B, 18 of which were exclusive to the more diverse HVF communities.

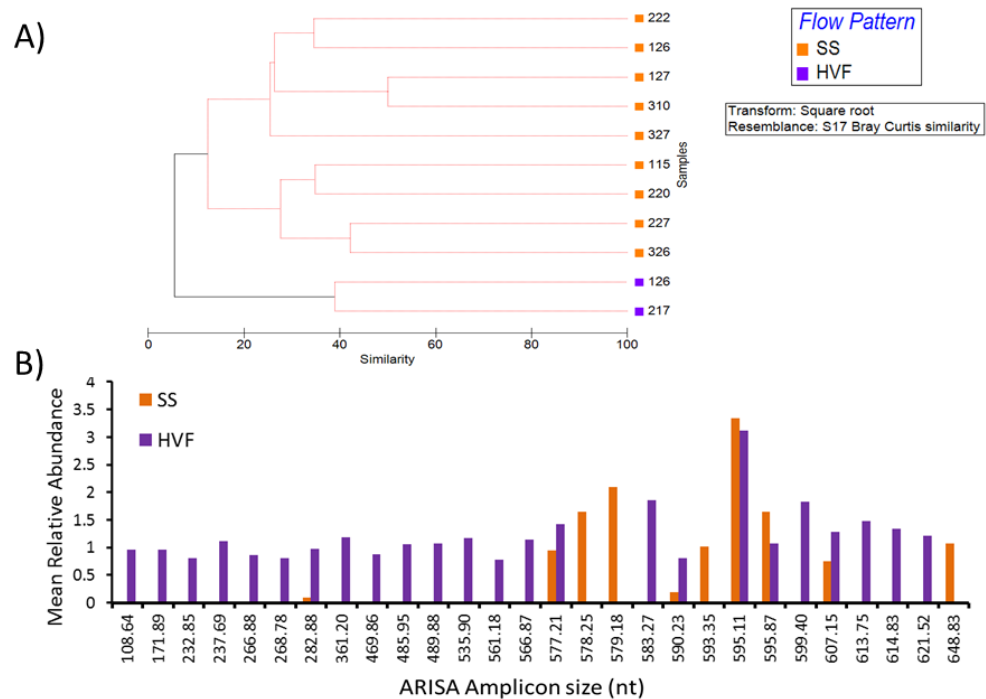


Figure 7.19 Comparison of the fungal communities within Post-flush biofilms from SS and HVF hydraulic conditions. A) Dendrogram showing the similarity between samples using the relative abundance data, the same trends were seen in the presence/absence data, red lines indicate profiles that were not significantly dissimilar according to SIMPROF; sample identification numbers are shown -the first number relates to the loop, the second number(s) the coupon position, see Figure 3.3. B) The ARISA amplicons which describe 60% of the variation between SS and HVF fungal communities.

7.3.3 Summary of hydraulic effects Post-flush

The flushing regime did not completely remove the biofilm, irrespective of the hydraulic regime to which it was conditioned. However, the biofilms which remained attached did not have the same structure across the conditioning regimes, nor were the relationships between the different hydraulic regimes at Post-flush (summarised in Figure 7.20) the same as those between the Pre-flush samples (summarised in Figure 7.11). Therefore, flushing did have an

effect upon biofilm structure but it appeared that each biofilm responded differently to the elevation in shear stress. For instance, the bacterial communities of LVF and HVF biofilms were similar before the flushing phase but different after, therefore they responded differently to the increase in shear stress, possibly due to the differences in their physical structure. Comparison between the Pre and Post biofilms was necessary to better determine if the conditioning hydraulic flow had an effect upon biofilm resistance to detachment during the mobilization phase.

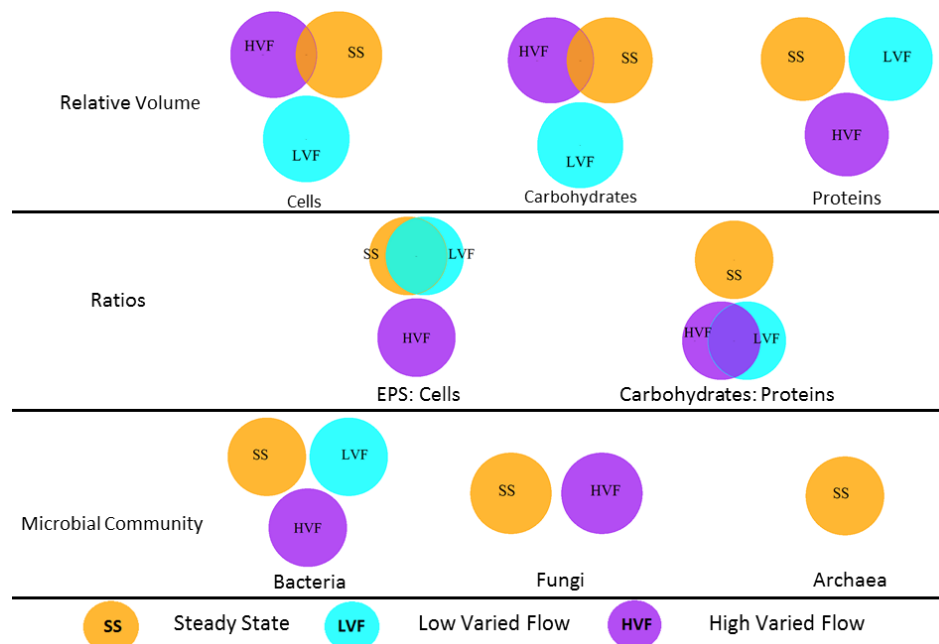


Figure 7.20 Summary of some of the patterns in biofilm structure parameters seen between the Post-flush biofilms from SS, LVF and HVF conditions. Diagram is a schematic representation of similarities and differences only, drawn in the statistical program R v2.15. The overlap of groups was determined by the p value associated with the relevant pairwise test such that $p > 0.9999$ would lead to a 100% overlap of the groups, $p=0.50$ would lead to a 50% overlap, etc. Where $p \leq 0.05$ the groups had no overlap. The microbial community patterns are based on the multivariate clustering analysis (i.e. the ANOSIM tests).

7.4 Results Concerning Variations in Water Quality and Biofilm Structure in Response to Elevated Shear Stress

A series of increasing flow rates were applied as explained in section 3.2.2, in order to determine the stability of the different biofilm structures observed in the Pre-flush samples from SS, LVF or HVF conditions. The response of biofilms developed under each of the three hydraulic conditions to an elevation in shear stress was subsequently characterized with respect to any variations in bulk water quality, biofilm physical structure or community structure between Pre-flush and Post-flush biofilms conditioned to SS, LVF or HVF hydraulic conditions. Due to the potentially anomalous HVF Pre-flush dataset, the HVF Post-flush samples were also compared to the Day 28 biofilms.

7.4.1 Bulk water quality

Various water quality parameters were monitored (n=3, taken after one turnover) throughout the flushing phase of each experiment (SS, LVF and HVF) in order to detect any response to the elevated shear stress occurring at the pipe wall. Across all of the experiments, no detectable significant changes were found in the bulk water TOC concentrations or temperature, and no consistent trends were observed in the pH or oxidising redox potential. However, the chlorine concentrations either remained constant or decreased slightly and variations in the iron and manganese concentrations were observed.

The response of iron and manganese during the flushing phase of each of the hydraulic tests is plotted in Figure 7.21 and showed that, although the concentration of manganese was less than iron, the same patterns in concentration with respect to loop and flushing step were seen between the two metals. Furthermore, the loops were generally good replicates of each other, the only exception being loop 1 in the SS experiment, which had a distinctly steeper gradient, indicating a greater change in concentration, than was observed for loops 2 and 3. Flushing of the LVF conditioned biofilms resulted in the lowest change in either of the metal concentrations within the bulk water (Figure 7.21). Regression analysis confirmed this finding as the gradients (indicating the rate of change) were consistently lower in the LVF samples than those from HVF or SS (Table 7.12). In some cases, the gradient was strongly positive but was not found to be significantly different from zero because the linear regression model was not a good fit to the data (see Table 7.12 for R^2 values). This occurred reasonably frequently and highlights the need for greater replication of the bulk water parameters in order to have increased confidence in the results. Nevertheless, a significant increase in iron and manganese was observed during the mobilization phase of SS conditioned biofilms in all three loops (see Table 7.12 for p values). This increase was greatest during the flushing of loop 1 where $100.33 \mu\text{g l}^{-1}$ of iron and $13.47 \mu\text{g l}^{-1}$ of manganese were incorporated into the bulk water. A significant increase of $15.33 \mu\text{g l}^{-1}$ and $8.67 \mu\text{g l}^{-1}$ of iron was observed during the mobilization phase of loops 2 and 3 of the LVF conditioned biofilms, respectively. Manganese concentrations during the mobilization of LVF biofilms only significantly altered in the flushing of loop 2 ($6.77 \mu\text{g l}^{-1}$ increase was observed). Flushing of the system following HVF conditioning also resulted in increases in the concentrations of metals in the bulk water, which were significant for loop 3 with respect to iron (corresponding to an increase of $34.00 \mu\text{g l}^{-1}$) and loops 2 and 3 with respect to manganese (corresponding to an increase of $10.00 \mu\text{g l}^{-1}$ and $9.00 \mu\text{g l}^{-1}$ respectively).

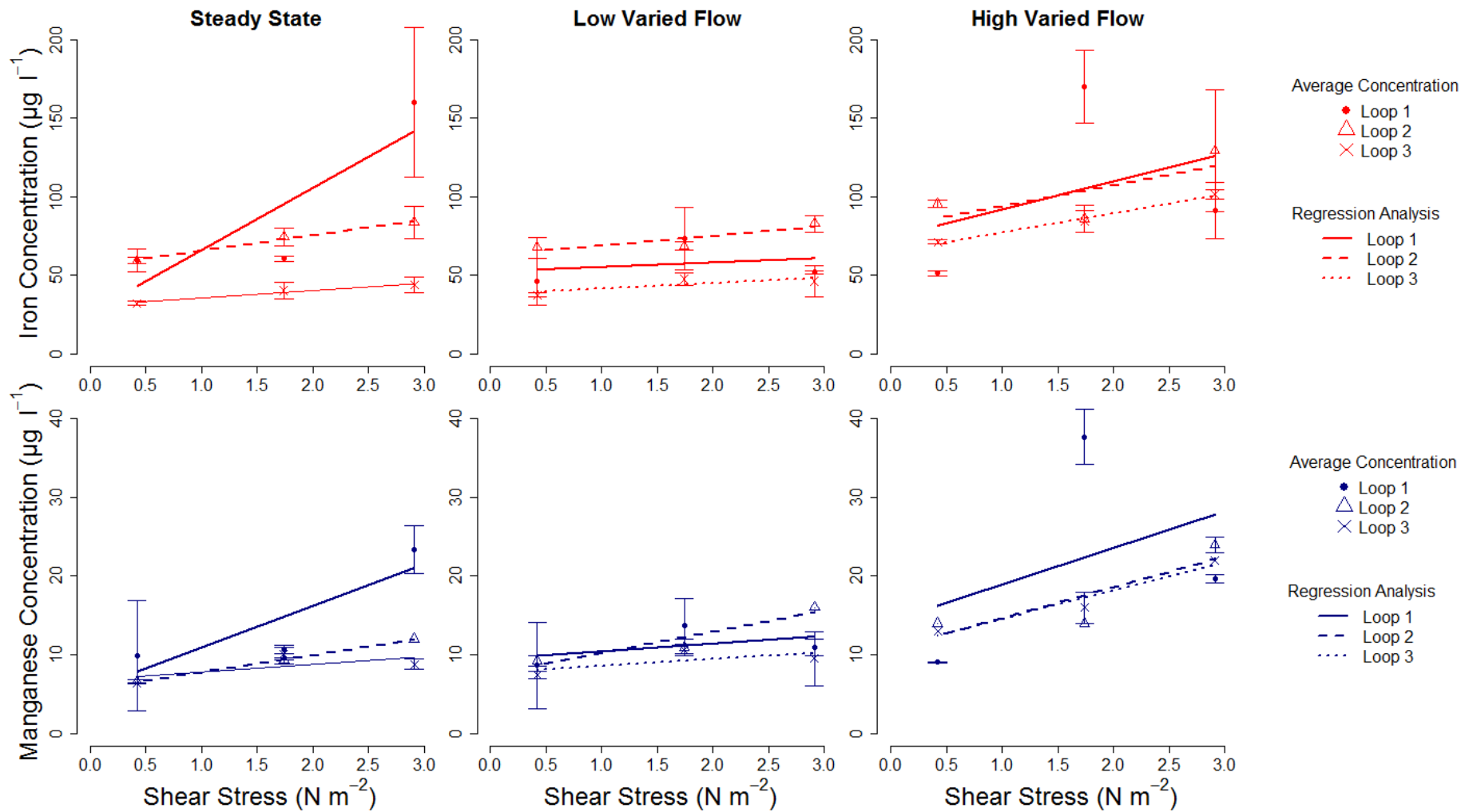


Figure 7.21 Concentrations of iron (in red) and manganese (in blue) during the flushing phase of biofilms developed under SS, LVF and HVF conditions. The average ($n=3$) concentrations (\pm one standard deviation) at the end of one turnover of each of the three flushing steps are plotted. As each loop had to be flushed separately, the data is plotted for each independently, the details of the regression analysis (e.g. gradient, R2 value) are presented in Table 7.12.

Table 7.12 Regression analysis results for iron and manganese during the flushing phase of each hydraulic experiment as indicated. Significant results are shown in bold.

Metal	Loop flushed	Steady State (SS)			Low Varied Flow (LVF)			High Varied Flow (HVF)		
		Gradient	R ^{2A}	p value ^B	Gradient	R ^{2A}	p value ^B	Gradient	R ^{2A}	p value ^B
Iron	1	39.45	0.7271	0.0157	2.80	0.0576	0.6603	17.63	0.1324	0.3551
	2	9.81	0.9869	0.0023	6.04	0.7701	0.0191	13.21	0.5210	0.1616
	3	4.72	0.9693	0.0095	3.57	0.6694	0.0120	12.13	0.9863	<0.0001
Manganese	1	5.30	0.7656	0.0189	0.99	0.2402	0.4839	4.64	0.1597	0.2921
	2	2.15	0.9980	<0.0001	2.69	0.9079	0.0002	3.93	0.7193	0.0042
	3	0.99	0.4283	0.0439	0.87	0.4607	0.2668	3.59	0.9503	0.0001

^A R² value indicates the goodness of fit of the linear regression model to the data, the closer to 1 the better the fit; ^B p value is one of the outputs from regression analysis in R v2.15, a significant p values indicates that the gradient is significantly different from 0.

7.4.2 Biofilm physical structure response

Visual comparisons of the example 3D images of Pre-flush and Post-flush biofilms (Figure 7.2; Figure 7.14) showed a loss of biofilm from the SS and LVF samples, with mainly carbohydrate remaining. However, the amount of HVF biofilm increased between these two sample points, further indicating that the Pre-flush data may be anomalous. Comparison of the HVF Day 28 3D sample projection (Figure 6.3) with the Post-flush sample (Figure 7.14) showed a decrease in cell coverage in the latter, but a greater coverage of carbohydrates.

7.4.2.1 Quantitative analysis of volume, spread and peak location

Between Pre-flush and Post-flush, the biofilms conditioned to the SS regime experienced a significant loss of protein (Figure 7.22), with a 2409 μm^3 difference in the median relative volume and a difference in the spread medians of 812660 AU. This resulted in a Post-flush EPS matrix which had a carbohydrate proportion more than 70 times greater than that of the Pre-flush (see carbohydrate-to-protein ratio Table 7.13). Despite the loss of the majority of the proteins there was no significant difference in the quantity of EPS per cells (Table 7.13) or the peak location of either EPS component in relation to that of the cells (Wilcoxon: carbohydrate, $W=269.5$, $p=0.5332$; protein, $W=313.0$, $p=0.8010$).

LVF biofilms from Pre-flush and Post-flush only differed in their protein content which decreased in relative volume (difference in medians was 60 μm^3), and in many FOV they were completely removed, which led to a median spread of 0 AU in the Post-flush samples (Figure 7.23). Despite the loss of proteins from many of the samples, the only significant difference in ratio values between Pre- and Post-flush was a decrease in the protein-to-cell ratio (Table 7.14) and there were no differences in the peak location of proteins (Wilcoxon: $W=343.5$, $p=0.3875$) or carbohydrates (Wilcoxon: $W=189.0$, $p=0.3875$).

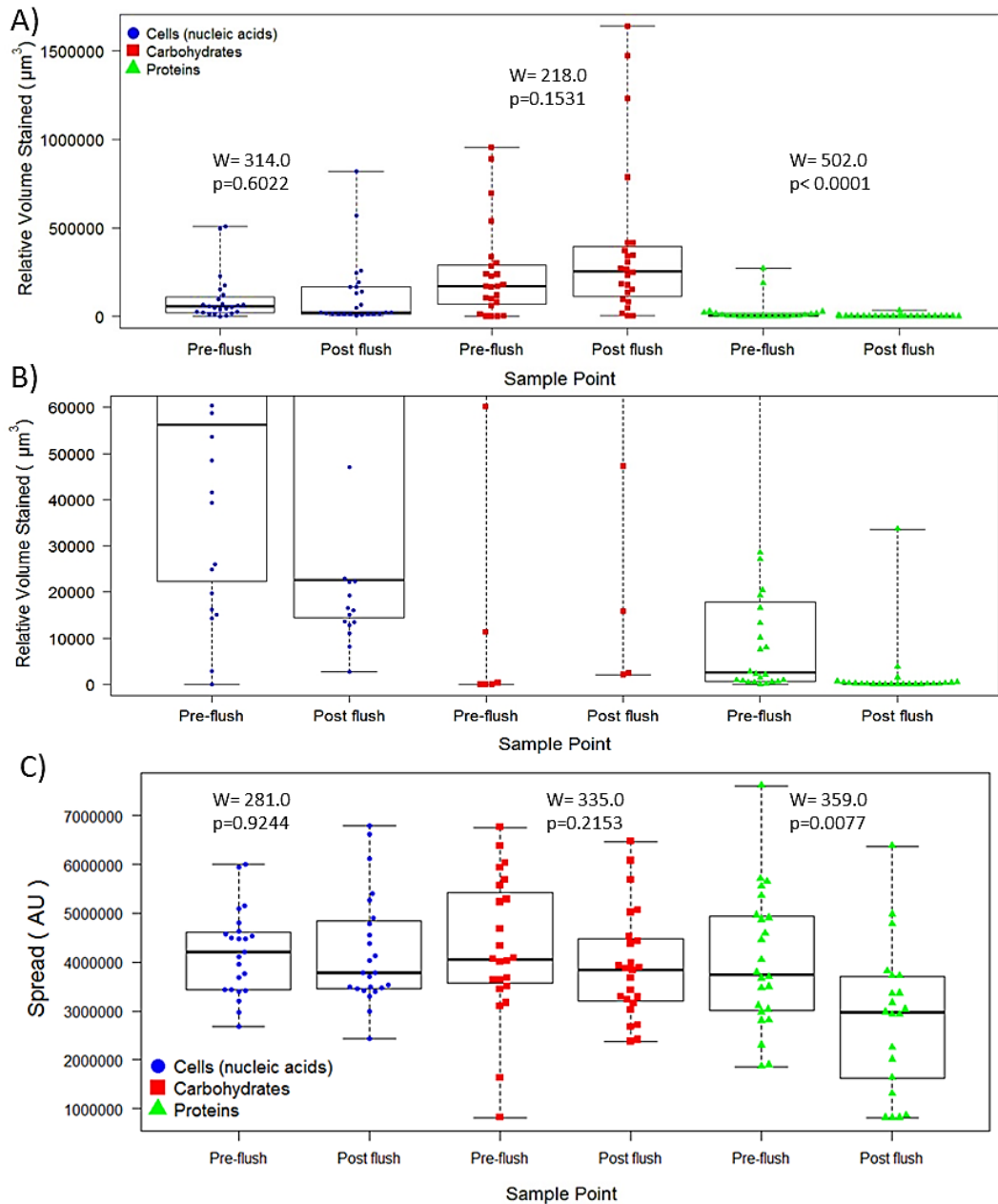


Figure 7.22 Comparison of the relative volume and spread of cells, carbohydrates and proteins in SS conditioned biofilms, Pre-flush and Post-flush. A) Relative volume, y-axis scale adjusted to max point; B) Relative volume, y-axis scale adjusted to show detail of cell and protein data; C) Spread of each component. Each data point represents a FOV, n=24. Box and whisker plots show the range, interquartile range and median – indicated by the solid black line; see section 4.6.3 for details of the relative volume and spread. Statistics shown are from Wilcoxon pairwise tests.

Table 7.13 Relative volume ratios of Pre-flush and Post-flush biofilms from SS. Significant results shown in bold.

Ratio ^A	Range (Min – Max)		Median		Difference in medians ^C	Wilcoxon Test
	Pre-flush	Post-flush	Pre-flush	Post-flush		
EPS: Cells	0.00 – 64.37	0.00 – 289.82	2.58	11.37	-8.79	W=228.0, p=0.2210
Carbohydrates: Proteins	0.00 – 11924.55	7.86 – 210068.00	42.38	2977.61	-2935.23	W=74.0, p<0.0001
Carbohydrates: Cells	0.00 – 57.77	0.00 – 289.73	2.56	11.37	-8.81	W=209.0, =0.1060
Proteins: Cells	0.00 – 7.54	0.00 – 0.26	0.05	<0.00 ^B	0.04	W=466.5, =0.0002

^A The first component is divided by the second, a value > 1 indicates a greater volume of the first component, a value <1 indicates a greater volume of the second, a value = 1 indicates an equal volume of each component; ^B actual median ratio 0.004; ^C Pre-flush median – Post-flush median. N.B. n= 24.

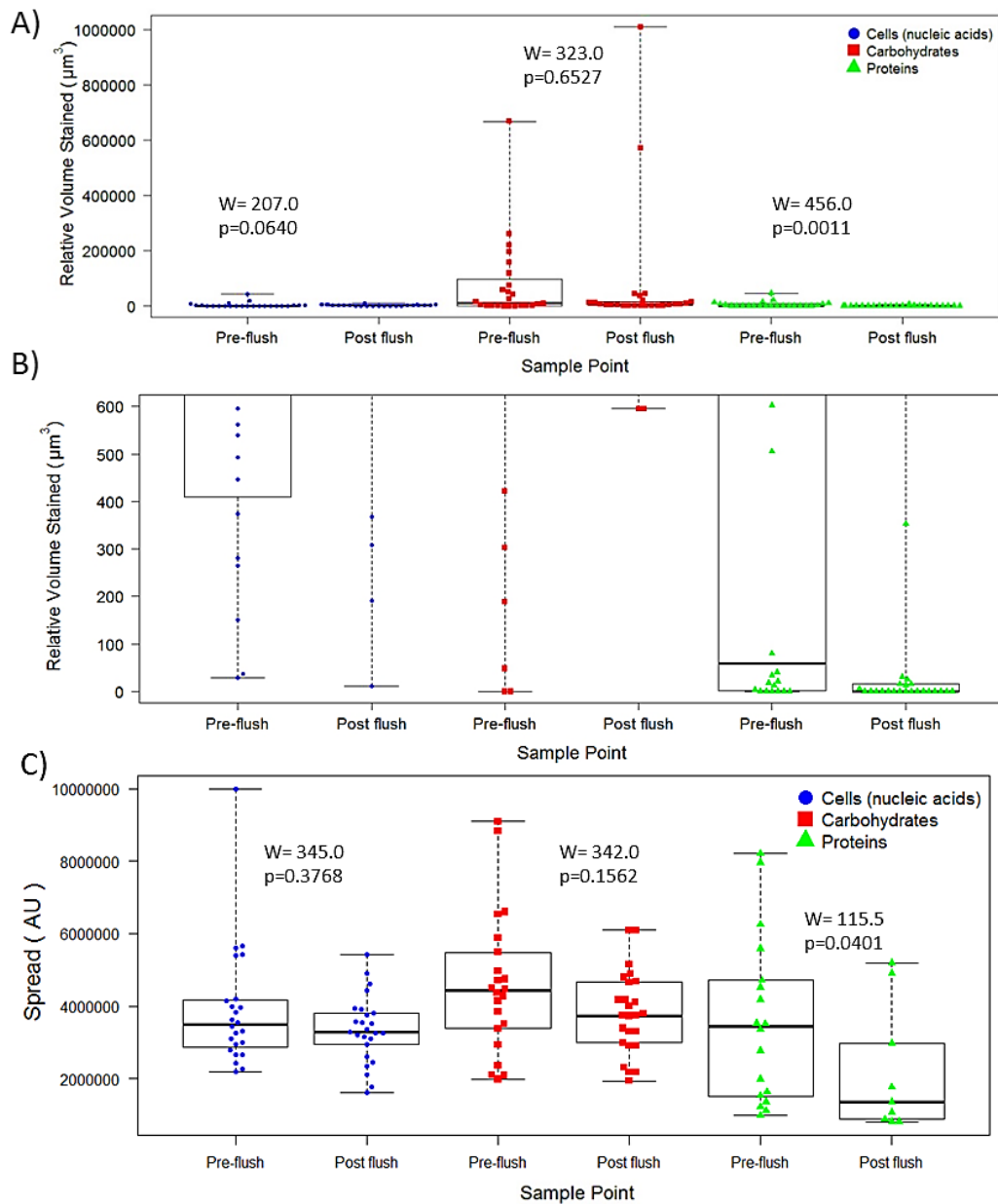


Figure 7.23 Comparison of the relative volume and spread of cells, carbohydrates and proteins in LVF conditioned biofilms, Pre-flush and Post-flush. A) Relative volume, y-axis scale adjusted to max point; B) Relative volume, y-axis scale adjusted to show detail of protein data; C) Spread of each component. Each data point represents a FOV, $n=24$ for Pre-flush and $n=25$ for Post-flush. Box and whisker plots show the range, interquartile range and median – indicated by the solid black line; see section 4.6.3 for details of the relative volume and spread. Statistics shown are from Wilcoxon pairwise tests.

Table 7.14 Relative volume ratios of Pre-flush and Post-flush biofilms from LVF. Significant results shown in bold.

Ratio ^A	Range (Min – Max)		Median		Difference in medians ^D	Wilcoxon Test
	Pre-flush ^B	Post-flush ^C	Pre-flush ^B	Post-flush ^C		
EPS: Cells	0.00 – 818.42	0.19 – 771.45	13.52	4.40	9.13	$W=377.0, p=0.0659$
Carbohydrates: Proteins	0.55 – 44533.67	3.68 – 2870.92	10.56	286.62	-276.06	$W=51.0, p=0.0907$
Carbohydrates: Cells	0.00 – 818.40	0.18 – 771.45	11.23	3.47	7.76	$W=364.0, p=0.0587$
Proteins: Cells	0.01 – 30.89	0.00 – 30.00	0.92	0.00	0.92	$W=410.0, p<0.0001$

^A The first component is divided by the second, a value > 1 indicates a greater volume of the first component, a value < 1 indicates a greater volume of the second, a value = 1 indicates an equal volume of each component; ^B $n=24$; ^C $n=25$; ^D Pre-flush median – Post-flush median.

The effect of flushing upon the HVF biofilms depended upon the sample point to which Post-flush samples were compared. Between Pre- and Post-flush there was a significant increase in the relative volume of cells and carbohydrates but no change in the proteins (Figure 7.24). Comparison of Day 28 and Post-flush samples found opposing results; no differences in the relative volume of cells and carbohydrates but a significant reduction in proteins (Figure 7.24), with a difference in the medians of 1692 μm^3 . The differences in spread due to flushing were also dependent upon the before flush sample point used for comparison; there were no significant changes in the spread of cells in either instance, carbohydrates or proteins had a similar spread between Day 28 and Post-flush, but both EPS components reduced in spread between Pre- and Post-flush (Figure 7.24). Analysis of the variation in relative volume ratios (Table 7.15A) between Pre- and Post-flush illustrated no change in the proportion of EPS within the biofilm but a significant increase in the carbohydrate content of the matrix of the Post-flush biofilms. There were also significant reductions in the carbohydrate-to-cell ratio, such that the Post-flush biofilms had an almost one-to-one ratio of these two components. The protein-to-cell ratio also decreased significantly, despite no significant change in protein relative volume. However, there were no differences in any of the relative ratios between Day 28 and Post-flush biofilms (Table 7.15B). In addition, the peak location of the carbohydrates did not differ between HVF Day 28 and Post-flush (Wilcoxon: $W=400.0$, $p=0.2840$) nor did that of the proteins (Wilcoxon: $W=321.0$, $p=0.6781$), with both occurring above that of the cells. Between Pre-flush and Post-flush the peak location of the carbohydrates did not differ (Wilcoxon: $W=410.5$, $p=0.36560$) but the peak of the proteins occurred nearer to the peak location of the cells in the Post-flush samples (median=-2) than those from Pre-flush (median=-4; Wilcoxon: $W=203.0$, $p=0.0330$).

Table 7.15 Relative volume ratios of HVF biofilms before and after flushing. A) Pre-flush (n=25) vs. Post flush (n=25), B) Day 28 (n=24) vs. Post-flush (n=25). Significant results shown in bold.

Ratio ^A	Range (Min – Max)		Median		Difference ^C in medians	Wilcoxon Test
	Before ^B	Post-flush	Before ^B	Post-flush		
A) Pre- vs. Post-flush						
EPS: Cells	0.29 – 216.60	0.02 – 41.66	8.21	1.06	7.15	$W=304.5, p=0.8835$
Carbohydrates: Proteins	0.00 – 523.57	0.19 – 17894.50	7.59	62.46	-54.87	$W=114.0, p=0.0002$
Carbohydrates: Cells	0.03 – 131.76	0.01 – 41.58	8.21	1.06	7.15	$W=129.0, p=0.0008$
Proteins: Cells	0.00 – 103.96	0.00 – 0.37	0.04	0.01	0.03	$W=489.0, p<0.0001$
B) Day 28 vs. Post-flush						
EPS: Cells	0.02-67117.63	0.02 – 41.66	1.98	1.06	0.92	$W=273.0, p=0.7726$
Carbohydrates: Proteins	0.22-1113.65	0.19 – 17894.50	33.24	62.46	-29.22	$W=228.0, p=0.2221$
Carbohydrates: Cells	0.01-66857.77	0.01 – 41.58	1.21	1.06	0.15	$W=264.0, p=0.6380$
Proteins: Cells	0.00-259.86	0.00 – 0.37	0.02	0.01	0.01	$W=334.0, p=0.3457$

^A The first component is divided by the second, a value > 1 indicates a greater volume of the first component, a value <1 indicates a greater volume of the second, a value = 1 indicates an equal volume of each; ^B Before refers to Pre-flush (A), n=24, or Day 28 (B), n=25; ^C Pre-flush (A) or Day 28 (B) median – Post flush median.

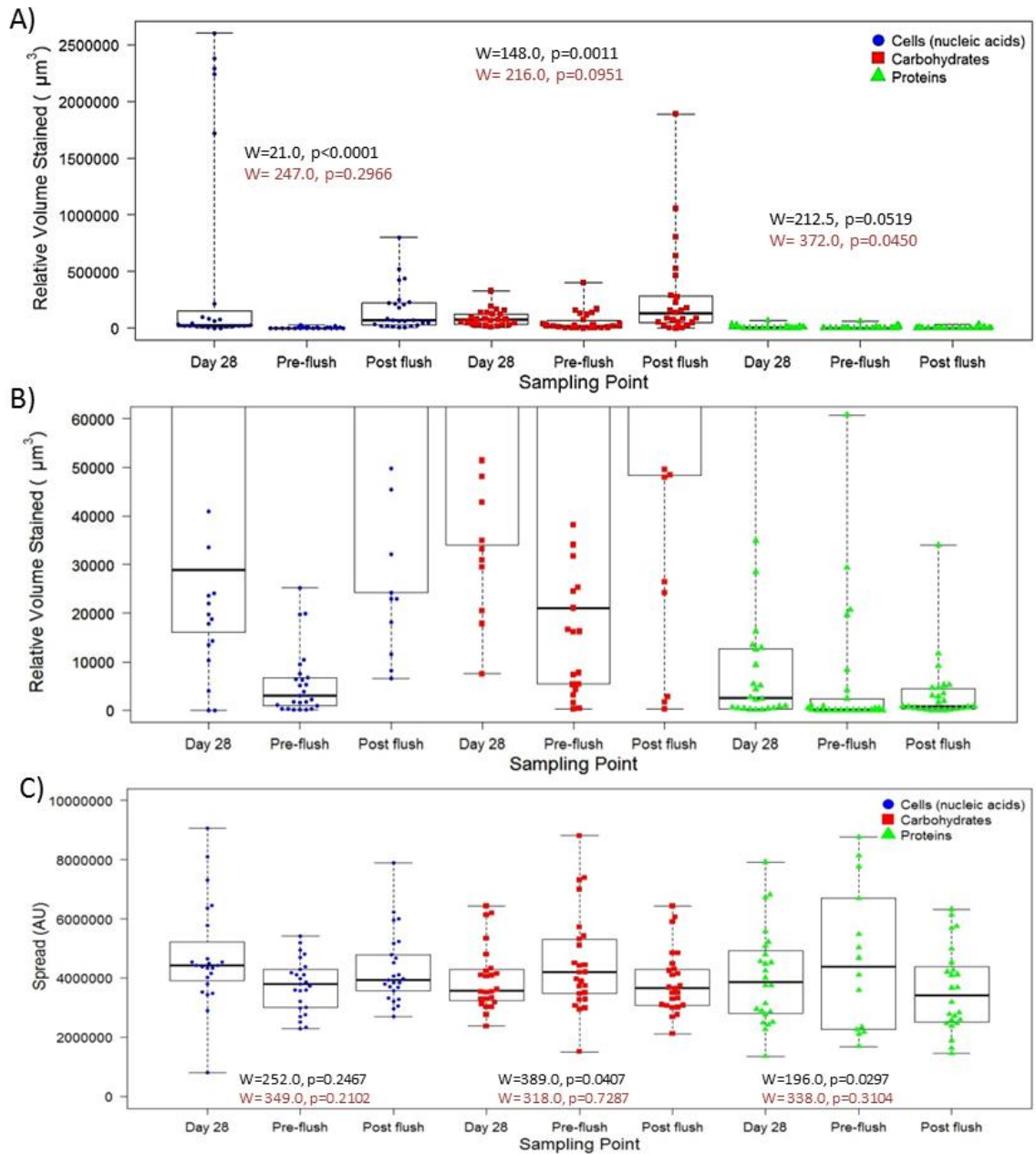


Figure 7.24 Comparison of the relative volume and spread of cells, carbohydrates and proteins in HVF conditioned biofilms, at Day 28, Pre-flush and Post-flush. A) Relative volume, y-axis scale adjusted to max point; B) Relative volume, y-axis scale adjusted to show detail of protein data; C) Spread of each component. Each data point represents a FOV, $n=25$. Box and whisker plots show the range, interquartile range and median – indicated by the solid black line; see section 4.6.3 for details of the relative volume and spread. Statistics shown are from Wilcoxon pairwise tests, the first results in black are from Pre-flush vs. Post-flush, the second results in brown are from Day 28 vs. Post-flush.

7.4.3 Community structure response

7.4.3.1 Variation in relative taxon richness, evenness and diversity

Within the SS biofilms, exposure to elevated shear stress led to a significant decrease in the relative richness (T-test: $df=16.00$, $p=0.0161$) and diversity (T-test: $df=14.85$, $p=0.0261$) of the bacterial community. On average over a third fewer T-RFs were present in Post-flush biofilms (average=19 T-RFs) than in Pre-flush (average=30 T-RFs). This shift did not significantly alter the relative evenness of the community (T-test: $df=15.97$, $p=0.7966$) which had an average of 0.96 in biofilms from both samples points. Similarly, the SS fungal communities experienced a significant decrease in taxon richness (T-test: $df=9.94$, $p=0.0073$) and diversity (T-test: $df=12.65$, $p=0.0087$) in response to the flushing phase. The average relative richness dropped by almost half, from an average of 21 ARISA amplicons in the biofilms Pre-flush to 11 Post-flush. However, as was observed in the bacterial communities, these changes in diversity did not affect the relative evenness of the fungal communities (T-test: $df=13.72$, $p=0.1195$). The same pattern was seen in the archaeal community response to the flushing phase in that the relative richness (T-test: $df=11.48$, $p=0.0002$) and diversity (T-test: $df=15.00$, $p<0.0001$) significantly decreased but relative evenness was not affected (T-test: $df=13.79$, $p=0.2505$). Archaeal communities had just over a third fewer T-RFs at Post-flush (average=7 T-RFs) than Pre-flush (average=11 T-RFs).

Biofilms conditioned to LVF were primarily comprised of bacteria both before and after the flushing phase. Although fungi were detected in a third of samples before flushing, the Post-flush biofilms contained only one sample with detectable concentrations. The bacterial communities of LVF biofilms experienced a significant reduction in relative richness (T-test: $df=14.99$, $p<0.0001$), exhibiting more than two thirds of a reduction in the average number of T-RFs within a profile (Pre-flush average=24, Post-flush average=7). Unsurprisingly, a significant reduction (T-test: $df=9.85$, $p=0.0004$) in the relative diversity index was observed (Pre-flush average=3.39; Post-flush average=2.81). Unlike the SS microbial communities, the LVF bacterial community also experienced a significant change in relative evenness (T-test: $df=11.38$, $p=0.0077$).

In HVF biofilms, at Pre-flush fungi could not be detected by PCR but two Post-flush biofilms were found to contain fungal DNA. The fungal communities of each of the samples were quite diverse as discussed in section 7.3.2.2, therefore it was likely that these were established communities that resisted detachment rather than a new incorporation of fungi into the

biofilm occurring during the mobilization phase. Bacteria were dominant in both Pre-flush and Post-flush biofilms with communities of similar relative evenness (T-test: $df=8.40$, $p=0.2159$) but significantly different diversity (T-test: $df=10.26$, $p=0.0228$) and richness (T-test: $df=13.10$, $p=0.0113$). Post-flush biofilms had, on average, a bacterial community comprised of less than half the richness of T-RFs seen before exposure to increasing shear stresses. Conversely the bacterial communities of Day 28 and Post-flush biofilms were no different in their relative richness (T-test: $df=10.78$, $p=0.1499$), diversity (T-test: $df=9.30$, $p=0.1082$) or evenness (T-test: $df=10.14$, $p=0.2973$).

7.4.3.2 Variation in microbial community structure

No difference was found between the SS bacterial communities Pre- and Post-flush, when analysed in terms of T-RF relative abundance (ANOSIM: global $R=0.091$, $p=0.114$; Figure 7.25 A). However, when analysed in terms of the presence/absence of T-RFs (Figure 7.25B) the communities from each sample point were slightly, but significantly different (ANOSIM: global $R=0.178$, $p=0.025$), which may indicate the removal of rarer T-RFs during the flushing phase as their loss would have little effect upon the relative abundance of the community profiles. Due to the high stress values of the nMDS (>0.2) the similarities between the communities were analysed using dendrograms. Figure 7.25B shows two main clusters; one comprising four Post-flush samples and two Pre-flush samples which could not be distinguished from each other (SIMPROF test), the other containing a more divergent set of samples, within which similarities between the biofilms from the two sample points were seen, but five of the Pre-flush samples were also observed to be most similar to each other. Pre-flush and Post-flush bacterial communities were found to be 57.82% dissimilar (average calculated by SIMPER); the majority of this difference was explained by the 27 T-RFs in Figure 7.25C. All but one (only present in Pre-flush samples) of the T-RFs were common to biofilms from both sample points, hence the biggest difference between the bacterial profiles was the variation in the contribution of the same T-RFs to the community Pre and Post-flush.

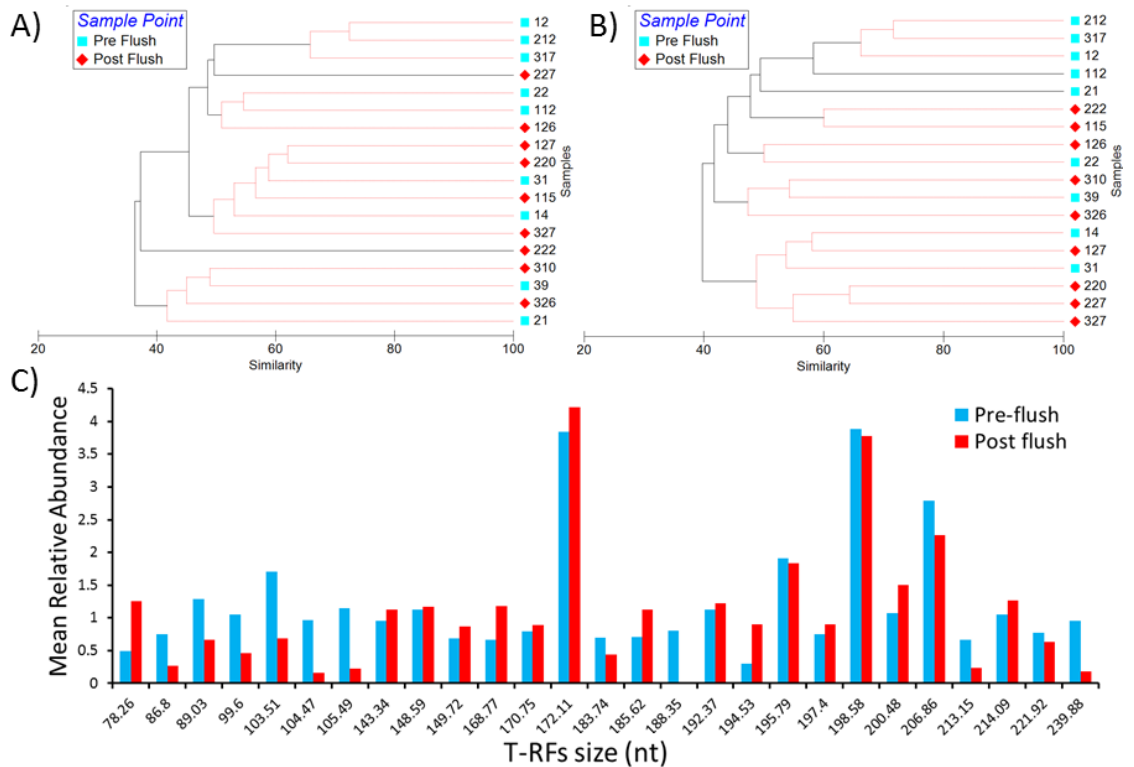


Figure 7.25 Comparison of the bacterial communities of Pre and Post-flush biofilms conditioned to the SS hydraulic regime. A) Dendrogram plotted using T-RF relative abundance; B) Dendrogram plotted using T-RF presence/absence. In both cases data was square root transformed and a Bray Curtis similarity matrix was generate; red lines indicate samples which were not statistically dissimilar (SIMPROF) and sample identification numbers are shown (first number indicates loop, second number(s) indicate coupon position, see Figure 3.3). C) The length and mean relative abundance (AU) of the T-RFs which account for 60% of the difference between the Pre-flush and Post-flush biofilms.

The pattern seen in the bacterial community was also observed in the fungal community; there was no significant difference in the community structure based upon the relative abundance of ARISA amplicons (ANOSIM: global $R=0.114$, $p=0.111$; Figure 7.26A) although differences were observed when analysis was based upon the presence/absence of amplicons (ANOSIM: global $R=0.227$, $p=0.024$; Figure 7.26B). The dendrogram of the similarities (nMDS stress values >0.17 , so not plotted) between fungal communities based upon presence/absence of ARISA amplicons (Figure 7.26B) showed two main clusters; one primarily containing the Pre-flush samples and the other predominantly containing those from Post-flush. Although there were a few replicates that were more similar to the communities in biofilms from the alternative sample point (Figure 7.26B e.g. sample 21 and 126), the two groups were an average of 83.45% dissimilar to each other. A total of 26 fungi ARISA amplicons (Figure 7.26C) were responsible for the differences between the communities, the majority of these were present in both Pre-flush and Post-flush biofilms. However, there were 3 amplicons which were present in the Pre-flush communities but absent in the Post-flush and, additionally, Post-flush

biofilms had 5 amplicons which were not detected Pre-flush. These could represent new fungal taxa which became incorporated into the biofilms during the flushing phase.

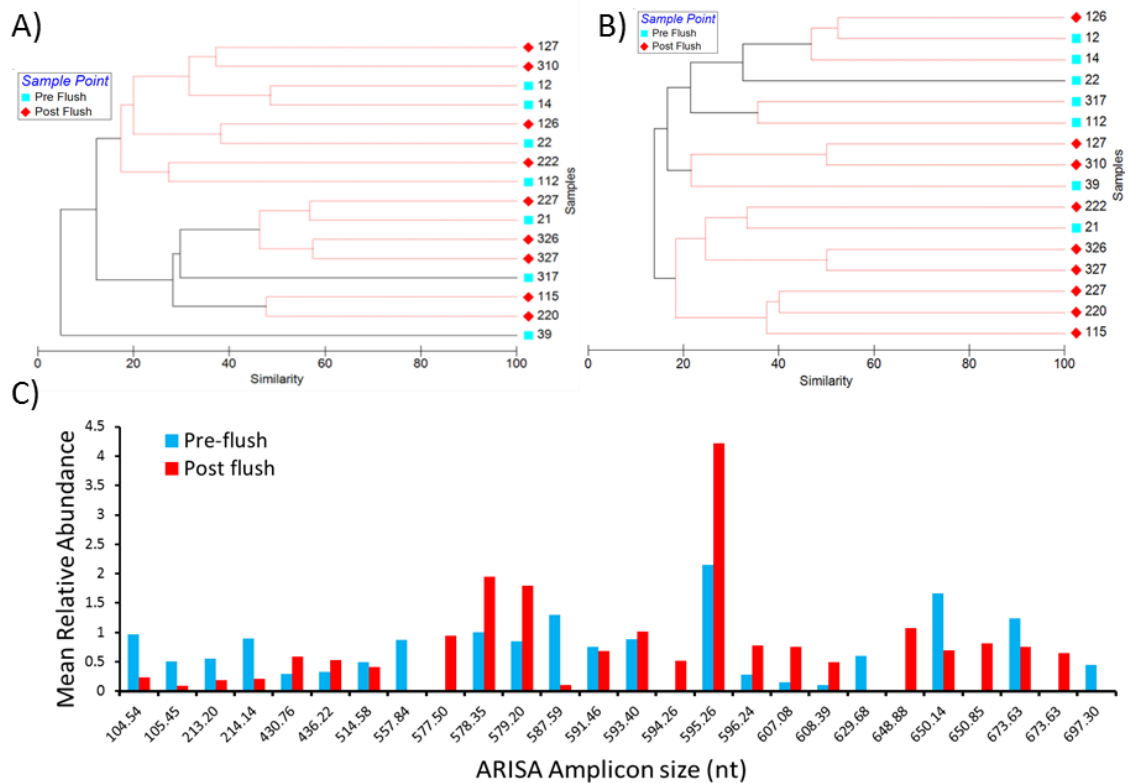


Figure 7.26 Comparison of the fungal communities of Pre and Post-flush biofilms conditioned to the SS hydraulic regime. A) Dendrogram plotted using ARISA amplicon relative abundance; B) Dendrogram plotted using ARISA amplicon presence/absence. In both A) and B) data was square root transformed and a Bray Curtis similarity matrix was generate; red lines indicate samples which were not statistically dissimilar (SIMPROF) and sample identification numbers are shown (first number indicates loop, second number(s) indicate coupon position, see Figure 3.3). C) The length and mean relative abundance (AU) of the ARISA amplicons which accounted for 60% of the difference between the Pre-flush and Post-flush biofilms.

The archaeal community altered during the flushing phase (ANOSIM: relative abundance, global $R=0.268$, $p=0.003$; presence/absence, global $R=0.332$, $p=0.0004$), with Pre-flush samples clustering together and Post-flush samples clustering distinct from these (Figure 7.27A). Greater variation was observed between the Post-flush replicates (an average of 69.57% similar to each other) than the Pre-flush replicates (an average of 87.32% similar to each other), indicative that the elevated shear stress increased the heterogeneity of the biofilms remaining attached. Pre and Post-flush archaeal communities were, on average, 27.44% dissimilar to each other with 8 T-RFs identified as driving this difference (Figure 7.27B).

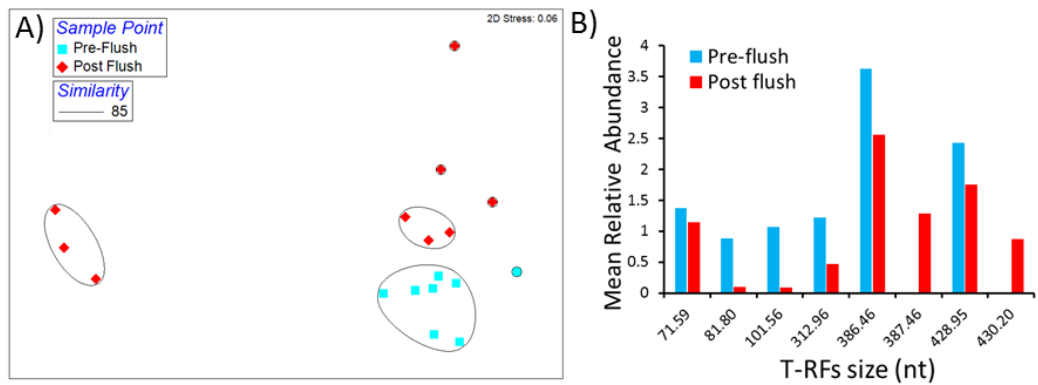


Figure 7.27 Comparison of the archaeal communities of Pre and Post-flush biofilms conditioned to the SS hydraulic regime. A) nMDS plotted using T-RF relative abundance (same pattern observed with T-RF presence/absence), black lines indicate clusters at least 85% similar; B) The length and mean relative abundance (AU) of the T-RFs which accounted for 60% of the difference between the Pre-flush and Post-flush biofilms.

The biofilms developed under the LVF hydraulic regime were dominated by bacteria but community compositions altered in response to the mobilization phase such that a considerable and significant difference was observed between Pre-flush and Post-flush communities (ANOSIM: relative abundance, global $R=0.535$, $p=0.002$; presence/absence: global $R=0.559$, $p=0.001$). The communities within the biofilms from the two sample points were 85.45% dissimilar and generally clustered independently (Figure 7.28A). A total of 18 T-RFs accounted for the differentiation of the communities before and after flushing (Figure 7.28B), 14 of which were common to biofilms from both sample points.

The structure of the bacterial communities within the HVF conditioned biofilms were unaffected by the mobilization phase. No significant differences were found between the Pre-flush and Post-flush samples (ANOSIM: relative abundance, global $R=0.052$, $p=0.202$; presence/absence, global $R=0.102$, $p=0.122$) nor were there differences between Day 28 and Post-flush (ANOSIM: relative abundance, global $R=0.064$, $p=0.176$; presence/absence, global $R=0.148$, $p=0.073$). When the data was plotted according to the similarity in community structure, most of the samples clustered with each other showing no distinction on the basis of sample point (Figure 7.29).

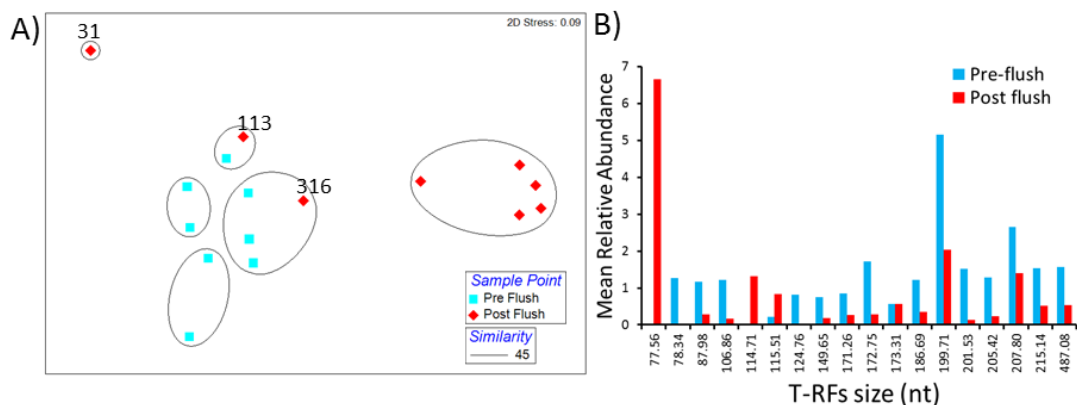


Figure 7.28 Comparison of the bacterial communities of Pre and Post-flush biofilms conditioned to the LVF hydraulic regime. A) nMDS plotted using T-RF relative abundance (same pattern observed with T-RF presence/absence), black lines indicate clusters at least 45% similar; in some instances sample identification numbers are shown – the first number indicates the loop, the second number(s) indicate the coupon position (see Figure 3.3). B) The length and mean relative abundance (AU) of the T-RFs which accounted for 60% of the difference between the Pre-flush and Post-flush biofilms.

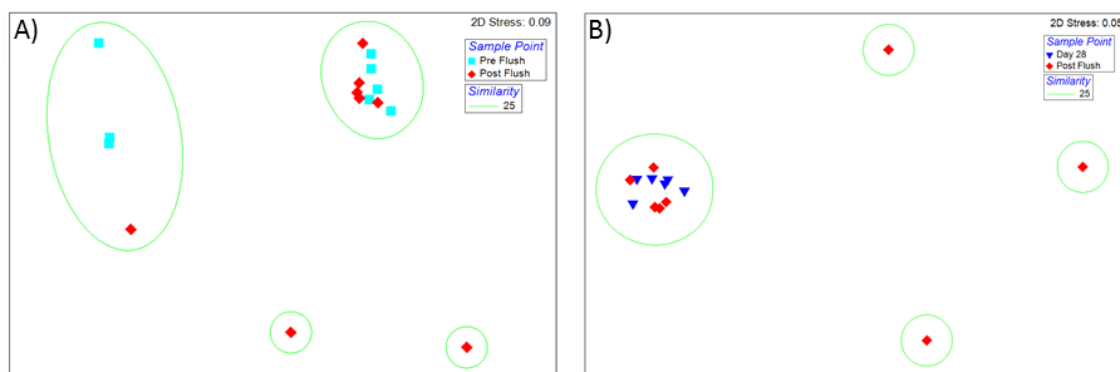


Figure 7.29 Comparison of the bacterial communities of Day 28, Pre and Post-flush biofilms conditioned to the HVF hydraulic regime. A) Pre and Post-flush biofilms; B) Day 28 and Post-flush biofilms. nMDS plotted using T-RF relative abundance (same pattern observed with T-RF presence/absence); green lines indicate clusters at least 25% similar.

7.4.4 Summary of responses to elevated shear stress

A summary of the patterns observed in the biofilms before and after flushing is presented in Figure 7.30. Both possible “before flush” sample points (Day 28 and Pre-flush) are shown for HVF, although after comprehensive analysis it was concluded that the Pre-flush sample set was anomalous. Not only were the HVF biofilms the only ones to be affected by the stagnation phase, it is also unlikely that biofilm material could be gained during the flushing phase, which was indicated in the Pre and Post-flush biofilm comparisons. Regardless of whether Day 28 or Pre-flush was used as the point of comparisons with Post-flush biofilms, no change in bacterial community structure was seen after the mobilization phase.

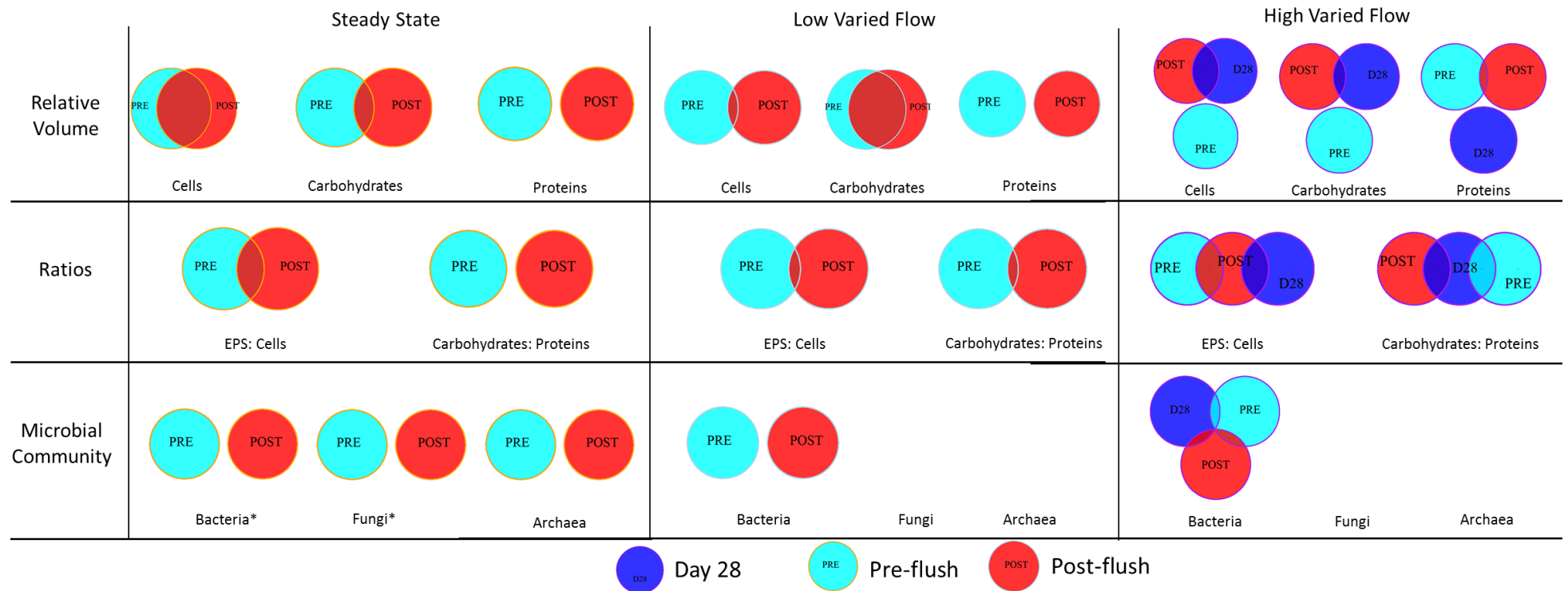


Figure 7.30 Summary of some of the patterns in biofilm physical and community structure between Pre-flush and Post-flush biofilms previously developed under SS, LVF or HVF conditions. PRE = Pre-flush; POST = Post-flush; D28 = Day 28. Diagram is a schematic representation of similarities and differences only, drawn in the statistical program R v2.15. The overlap of groups was determined by the p value associated with the relevant pairwise test such that $p > 0.9999$ would lead to a 100% overlap of the groups, $p = 0.50$ would lead to a 50% overlap, etc. Where $p \leq 0.05$ the groups had no overlap. The microbial community patterns are based on the multivariate clustering analysis (i.e. the ANOSIM tests). * Communities were not different based upon multivariate clustering analysis of relative abundance data but were different based upon multivariate clustering of presence/absence data, relative richness indices and relative diversity therefore plotted as different. N.B. Archaea were not detected at LVF or HVF; Fungi were not found in enough LVF or HVF samples from Pre- or Post-flush and so a comparison was not possible.

Essentially, irrespective of the conditioning hydraulic regime, the only significant differences in physical structure, as a response to the flushing phase, were associated with a loss of protein. The amount of protein lost from the SS, LVF and HVF biofilms is shown in Table 7.16, expressed as the relative volume of biofilm lost and also as a percentage of the total biofilm volume detected at the Pre-flush sample point. It should be noted that these values are based upon the medians of data corresponding to the 420 μm x 420 μm FOV, which present a far smaller surface area (0.00000017 m^2) than that of the pipelines being flushed, which have an approximate surface area of 49.84 m^2 . Subsequently the volumes of biofilm (determined to be solely protein) that could potentially be mobilised from the whole surface of the pipeline into the bulk water are likely to be many magnitudes greater than the values presented in relation to the biofilm FOV.

Table 7.16 Loss of biofilm volume from SS, LVF and HVF biofilms as a response to elevated shear stress.

Hydraulic Regime	All Material Pre-flush ^B (μm^3)	Biofilm Lost ^C (μm^3)	Proportion of biofilm lost ^D (%)	Extrapolation to Pipeline scale ^E	
				(μm^3)	(mm^3)
SS	270437	2409	0.89	7.05×10^{10}	70.5
LVF	23021	60	0.26	1.75×10^9	1.75
HVF ^A	141743	1692	1.19	4.96×10^{10}	49.6

^A Calculations using Day 28 as the before flush sample point as the Pre-flush samples were erroneous; ^B Median of cell + carbohydrate + protein relative volumes before averaging; ^C Relative volume (median) of proteins lost as this was the only biofilm component to experience a significant difference between Pre and Post-flush; ^D Biofilm lost expressed as a proportion of the total biofilm at Pre-flush; ^E Pipeline surface area is approximately 29317647 times greater than that of a FOV, extrapolation value is therefore the relative volume of biofilm lost multiplied by this value.

7.5 Discussion

Before the flushing phase, all the biofilms experienced a period of stagnation as outlined in section 7.2. This did not affect SS or LVF biofilm structures but a difference in the physical structure of HVF biofilms was observed. However, after comprehensive analysis it was established that this was an anomalous result (discussed in section 7.2.3). Therefore, it was deemed more appropriate to use the Day 28 HVF data as the “before flushing” sample point, with which to compare HVF Post-flush samples and thus only this comparison will be considered in the following discussion.

Chapter 6 compares the biofilms that developed under the different hydraulic conditions and the patterns highlighted also apply to the SS and LVF Pre-flush samples, as stagnation had no effect upon biofilm structure. Therefore, only a brief summary of the patterns in biofilm structure between regimes before flushing is provided here, for a more detailed comparison

and discussion see section 6.3. Prior to flushing, SS and HVF samples were the most similar with respect to their physical structure. The lowest volume of material accumulated under LVF but the LVF biofilms had the greatest proportional quantity of EPS and the matrix had greater protein content than the matrices of HVF or SS biofilms, though in all cases the proteins contributed less than carbohydrates to the EPS composition. Regardless of conditioning regime, the greatest carbohydrate and protein densities (i.e. peak fraction) occurred above that of the cells, i.e. nearer to the bulk water (proteins were often located just above the carbohydrates). Bacterial communities that developed under the varied flow regimes were most similar to each other but less diverse, and therefore possibly more specialised, than those of the SS samples, which also had archaea and fungi within their microbial community.

During the flushing, the bulk water iron and manganese concentrations increased more in the SS and HVF experiments than in LVF, either due to less material accumulation at LVF, or the development of a biofilm more resistant to detachment. It is also possible that iron and manganese were more readily incorporated into the SS or HVF biofilms than LVF biofilms, for instance Sly *et al.* (1988) found a greater iron and manganese coverage within a Robbins device following velocities of 0.5 ms^{-1} , than were seen at 0.01 ms^{-1} . As inorganics were only assessed visually, via SEM, it is not possible to quantify this theory within the scope of this research. In contrast to these findings, Sharpe (2012) demonstrated that the increases in iron, manganese and turbidity, during flushing, were no different between SS, LVF or HVF experiments, when conducted at $16 \text{ }^{\circ}\text{C}$. At $8 \text{ }^{\circ}\text{C}$, the response was greater during mobilisation of the SS conditioned material, than was observed in either LVF or HVF regimes (Sharpe, 2012). Douterelo *et al.* (2013) observed an increase in turbidity during the flushing phase of SS and LVF experiments, but a smaller increase during the flushing of the HVF experiment (all tests conducted at $16 \text{ }^{\circ}\text{C}$). The differences between these studies and the research presented in this chapter, are likely due to differences in the experimental set-ups and sampling points: Sharpe (2012) and Douterelo *et al.* (2013) applied a different series of flushing steps to those presented in this thesis, and simultaneously tested the three hydraulic conditions (one in each loop of the experimental facility with a common tank).

Flushing did not result in homogenous “end point” biofilms; the samples were able to be differentiated, based upon the previous conditioning hydraulics. The relationships (in terms of similarities and differences) between the Post-flush biofilms (Figure 7.20) from the different conditions were dissimilar to those seen at the Pre-flush (or Day 28) sample point (Figure 6.12; Figure 7.11), highlighting an effect of flushing upon structure rather than a continuation of the differences present prior to flushing. Within the investigations presented in this chapter there

were no significant, detectable differences in the physical characteristics of cells or carbohydrates Pre- and Post-flush within SS, LVF or HVF biofilms. For all of the biofilms the only significant physical changes were driven by a reduction in protein content. The greatest relative volume of protein removed was from SS biofilms, followed by HVF and LVF (which also accumulated the least biofilm volume during development). The SS tests also experienced the greatest increases in iron and manganese bulk water concentrations. Therefore, it is possible that these metals were bound to the proteins of the EPS and released when they were detached from the assemblage, as suggested by Lehtola *et al.* (2006) who reported increases in iron and manganese following biofilm mobilisation due to pressure shocks. Proportionally, with respect to the volume of biofilm present before flushing, the HVF biofilms were found to have lost the greatest percentage of material, followed by the SS and LVF samples, the latter of which was subsequently deemed the most physically stable. It is important to recognise that past drinking water biofilm research has not quantified the proteins in this way, which has significant implications when categorising a biofilm as “stable”. No significant change in cell or carbohydrate may be detected (such as in this study) leading to the conclusion that the assemblage was unaffected by the increased external forces, but in reality substantial quantities of protein may have been detached.

Proteins may have been more easily removed from the biofilms as their peak location occurred nearer to the bulk phase than that of the cells or carbohydrates, or because they were less strongly adhered within the biofilm. The material resisting detachment by mechanical forces was found to be predominantly carbohydrate based (Figure 7.15; Table 7.8), and the compositional ratios of the Post-flush EPS matrices were weighted more greatly towards carbohydrates than proteins than in the Pre-flush biofilms, therefore carbohydrates play a greater role in biofilm adhesion than proteins do. Further evidence for the persistence of a strongly adhered biofilm base layer has been provided within the context of mainly bench top scale systems, by Ohashi *et al.* (1999), Staudt *et al.* (2004); Simoes *et al.* (2007), Mohle *et al.* (2007), Paul *et al.* (2012) and Abe *et al.* (2012), some of whom also established that this layer had a high carbohydrate concentration. However, in many of the studies, proteins were not investigated and so it is not possible to ascertain if the carbohydrate content was greater. Not only do carbohydrates appear to stabilise the biofilm, their continued presence post flush provides an alternative surface for microbial attachment which may facilitate the incorporation of secondary colonisers into the biofilm and, furthermore, the molecules could provide an additional source of nutrients to the cells remaining attached.

HVF biofilms lost a greater proportion of proteins than LVF biofilms, which contradicts the theory that HVF assemblages would have stronger cohesive forces due to a higher daily peak shear stress during development. Moreover it is in contrast to many previous studies where growth under more turbulent conditions produced a stronger adhered biofilm (e.g. Percival *et al.*, 1999; Ohashi *et al.*, 1999; Paul *et al.*, 2012). However, Abe *et al.* (2012) also found that biofilms developed under a lower shear stress had a greater mechanical strength than those that experienced higher shear stress during growth. It is possible that these findings are related to a difference in EPS quantity, governed by the hydraulics during development. LVF biofilms, which were proportionally the most physically stable, had the greatest EPS-to-cell ratio and an extensive spread of carbohydrate throughout the sessile assemblage. As was suggested in section 6.3, HVF biofilms may be unable to develop an extensive EPS matrix due to a cyclical removal, driven by a daily peak flow which was greater than that in the LVF regime. Picuoreanou *et al.* (2009) found that biofilms with an increased growth rate were more susceptible to detachment events, which could be a consequence of a less extensive matrix due to microorganisms preferentially using energy in cell replication than EPS production. With consideration to the findings of Picuoreanou *et al.* (2009), it is possible that the HVF biofilms, which were previously shown to experience the highest growth rate of all the biofilms (see chapter 6), had a greater propensity to detach. Overall, a greater EPS-to-cell ratio, promoted by the LVF hydraulic regime resulted in a (proportionally) more stable biofilm.

Although there were no significant changes in the physical characteristics of the cellular fraction of the biofilm, all the microbial communities decreased in relative richness and diversity following the mobilisation phase, indicating the loss of taxa. Nevertheless, the SS biofilms remained the most microbially diverse Post-flush, with the archaeal community structure being less influenced by elevated shear stress than the fungi or bacteria were. This study presents the first assessment of the influence of elevated shear stress upon archaeal populations therefore comparisons with other drinking water biofilms are not possible. Bacterial community structure was most stable when conditioned under the HVF hydraulic regime, experiencing no significant changes in structure despite a reduction in relative richness and diversity, which was likely due to the loss of rarer T-RFs which had low relative abundance. A similar trend was highlighted by Möhle *et al.* (2007) who found very little change in the bacteria (and, interestingly, carbohydrate) contents of municipal wastewater biofilms developed under higher shear stress (0.037 Nm^{-2} within a rotating disc reactor) before and after gauging. In contrast, Douterelo *et al.* (2013) did detect differences in the HVF bacterial community Pre- and Post-flush, with a particular increase in Proteobacteria after flushing. These contradictory results could be due to the limited biological replication ($n=3$) in Douterelo

et al. (2013) causing high variability between the replicate samples, which might have masked similarities such as those presented in this chapter (where $n=9$). Also, in Douterelo *et al.* (2013) the three regimes (SS, LVF and HVF) had a common tank and therefore there was a greater chance of cross contamination between the regimes due to mixing of the water.

In contrast to the HVF bacterial community, those of the SS and LVF biofilms experienced a shift due to the flushing period. The majority of the differentiation between the Pre- and Post-flush bacterial communities was due to a reduction in the relative abundance of T-RFs rather than a considerable absence of T-RFs after flushing. However, in some instances T-RFs were present at Post-flush but absent prior to this. It could be that some planktonic bacteria were able to attach to the biofilm during the flushing phase, accounting for this “addition” to the biofilm. Alternatively, these T-RFs may have been present at abundances below the detection level in the Pre-flush samples but increased in abundance at Post-flush because they were better able to resist detachment and so contribute to a greater proportion of the Post-flush community. For instance, Douterelo *et al.* (2013) demonstrated that a shift in the bacterial communities of LVF biofilms occurred during the flushing phase and that the post flush biofilms were predominantly comprised of *Pseudomonas* (matched, on average, up to 65% of sequences).

Overall these results demonstrate that the hydraulics of the DWDS influences biofilm structure, but the relationships between the two are not linear. It is apparent that the average flow rate is not a conditioning factor in relation to biofilm structure because biofilms from the three regimes were different. The HVF regime produced a stable community structure and the LVF regime produced a physical structure more resilient to subsequent hydrodynamic changes. These findings are in contrast to the hypothesis that biofilm structure would be most stable when conditioned under HVF but in support of the role of certain EPS characteristics promoting biofilm adhesion strength. Essentially, regardless of the particular response of the differently conditioned biofilms, after flushing, biofilms were still detected upon coupons from SS, LVF and HVF conditions. This was despite mobilisation velocities exceeding 0.4 ms^{-1} (maximum flushing velocity applied in the work constituting this thesis was 0.91 ms^{-1}), which has been stated as the appropriate velocity for “self-cleaning” of networks in the Netherlands (Vreeburg *et al.*, 2009). Maintaining this velocity has been described to prevent the accumulation of material upon the pipe surface. However, if the system has previously experienced velocities below this level (during the growth phase velocities ranged from $0.04 - 0.14 \text{ ms}^{-1}$, dependent on regime) then biofilm may already have developed which is able to resist detachment at 0.4 ms^{-1} . In this sense, the “self-cleaning” may only be successful for pipes

which do not yet have biofilms present as, while it may limit accumulation, it does not remove biofilms that have already adhered and are producing EPS. Nevertheless, this “self-cleaning” approach has been found to be somewhat effective in the Netherlands, but the DWDS there are younger than the DWDS in many other countries where this approach may not be appropriate due to water being distributed through an older network, with (potentially) a high frequency of pre-established biofilms. While it may not be possible to prevent accumulation of material, and/or unrealistic to achieve a daily velocity of $\geq 0.4 \text{ ms}^{-1}$, within DWDS in countries other than the Netherlands, the results presented in this chapter indicated that different biofilm structures responded differently to elevations in shear stress, therefore it may be possible to use hydraulics to condition a biofilm which presents a lower risk to water quality.

Chapter 8: Concluding Comments

8.1 Summary of Findings

This thesis aimed to provide new knowledge about the structure of drinking water biofilms and in particular the impact of hydraulic regime upon their physical characteristics and community structure. Unusually, the biofilms investigated were relevant to real systems due to their natural accumulation under realistic hydraulic conditions, within an internationally unique, full scale, temperature controlled DWDS experimental facility. In order to investigate both the physical and community aspects of the biofilms, which have rarely been explored in combination, use was made of the innovative PWG coupons, which fit the inner curvature of the pipeline in order to limit distortion of the boundary layer hydraulics and include a removable insert designed specifically for microscopy based analysis.

A fluorescent microscopy and DIA protocol was developed and optimised (Chapter 4) which enabled the first characterisation of DWDS relevant biofilms, with regards to physical structure, concurrently visualising and quantifying not only the cells and carbohydrates, but also with the novel inclusion of proteins. Unique insights into the variations in the biofilm physical and community structures that developed under SS (Chapter 5) hydraulic conditions, in comparison to those conditioned to the LVF or HVF regimes (Chapter 6) were provided by application of the developed microscopy EPS analysis technique, in combination with molecular microbiology. The response of each of the different biofilm structures to elevated shear stress was subsequently evaluated (Chapter 7) via a series of flushing steps incorporating flow rates and shear stresses comparable to those reported in real DWDS. Discussions and overviews of the findings of this research are included within each of the previous chapters (see sections 4.7, 5.3, 6.3 7.5), and are summarised briefly below.

8.1.1 A robust EPS analysis approach was developed (Objective 1)

Physical extraction techniques and chemical assays were not sensitive enough for use in quantifying the carbohydrates, proteins and cells of drinking water biofilms from the experimental facility. In order to visualise and quantify all three targeted biofilm components a triple staining, CLSM imaging and DIA protocol, incorporating linear unmixing to remove autofluorescence, was developed and optimised for use with drinking water biofilms developed under conditions which were representative of a real DWDS. Previous fluorescent

microscopy based research into drinking water biofilms has been limited to cells and carbohydrates or two dual staining protocols targeting cells\carbohydrates of one sample and cells\proteins of another. For the first time, concurrent quantification and 3D visualization of the stained cells, carbohydrates and proteins of drinking water biofilms was possible due to the application of this analysis method, which facilitated the simultaneous analysis of the three components in relation to each other. Ultimately, this approach expedited the characterisation of the EPS, enabling a wider range of parameters to be measured in the matrices of biofilms than is possible via physical extraction methods.

8.1.2 Hydraulics influenced biofilm structure (Objectives 2 and 3)

Irrespective of hydraulic conditions, biofilm was found adhered upon coupons from all three positions (crown, middle, invert) around the circumference of the pipeline with no differences between the positions with respect to physical or community structure. Therefore, gravity driven effects were not observed to be acting upon biofilm formation, which opposes the gravitational settling and sedimentation based theories regarding the accumulation of material within DWDS, instead adding more weight to the “cohesive layer theory” (see section 1.2.2). A further trend common across each of the hydraulic conditions was that the greatest area density (assessed by peak area fraction and peak location) of the EPS components occurred above that of the cells (i.e. nearer to the bulk water); often the protein peak was just above the carbohydrates. This unique insight into the 3D arrangement of the biofilm components may indicate that a larger volume of EPS is necessary nearer to the top of the biofilm to protect the microorganisms from the bulk water environmental constraints.

Across the three hydraulic regimes microorganisms were found to rapidly attach to the pipe wall, as primary attachment (indicated by cell only areas at Day 0, with very few areas of carbohydrate or protein) was observed on all coupons even after just 90 minutes (or shorter) contact time with the bulk water. The initial coverage of cells across the pipe surface was slightly greater under SS conditions than LVF or HVF, which were similar to each other. Primary attachment in the first 90 minutes may have been promoted in SS due to a greater flow rate, leading to more turbulent conditions which may have increased the propensity for a planktonic cell to come into contact with the pipe wall. All other Day 0 physical and bacterial community characteristics were the same across the three regimes.

Previously, drinking water research has primarily focused upon planktonic or biofilm bacteria. Analysis of the wider microflora presented an advancement in the understanding of the

community structure of drinking water biofilms as archaea and fungi were investigated, alongside bacteria. Evidence was provided which, for the first time, conclusively demonstrated the incorporation of archaea into drinking water biofilms. Archaea have received little attention in biofilm research, not only within the context of drinking water, but across a range of environments. Prior to this study, the only detection or identification studies of archaea in DWDS were based upon water samples (e.g. Wielen *et al.*, 2009). Although the archaeal community was less diverse than that of bacteria or fungi, they may play key roles in biofilm function.

Microbial community structures experienced a shift between Day 0 and Day 28, although the successional integration of microorganisms in drinking water biofilms has yet to be fully explored these results are suggestive of initial colonisers being out-competed by secondary colonisers. The community composition of Day 28 biofilms was influenced by the hydraulic conditions experienced during development. SS biofilms had an extensive microflora including bacteria, fungi and archaea but in contrast archaea were not detected under either of the varied flow regimes and fungi became less common as the variation in flow rates increased. It is postulated that this was due to weaker adhesive forces in combination with slower development rates such that, under LVF and HVF regimes these organisms would not be afforded the contact times necessary from them to securely attach to the biofilm before a change in flow removed them from the pipe/biofilm surface. LVF and HVF biofilms had similar community structures, both were dominated by bacterial communities less diverse than those within SS, probably due to greater selection pressure imposed by the varied flows for a more specialised community.

Cells, carbohydrates and proteins had greater relative volume and spread at Day 28 than Day 0 but were not uniformly distributed or completely co-localised. Cell-only areas at Day 28 indicated the occurrence of biofilms in the primary adhesion stage, amongst the more mature biofilm. A trend which was observed in the SEM images (an example is shown in Figure 4.1) as well as across the CLSM based analysis. Under each regime, carbohydrate dominated both the EPS matrix and the biofilm as a whole; the next largest fraction was the cell content, followed by the protein content (although in LVF biofilms the median protein-to-cell ratio indicated equal volumes of each). However, the specific quantities, ratios and arrangement of these were different between hydraulic conditions. For example, carbohydrates had a greater spread in LVF biofilms than the cells or proteins, whereas all three components had similar spreads in SS and HVF biofilms. The greatest difference between Day 0 and Day 28 was observed under the HVF regime, demonstrating a higher growth rate, compared to LVF or SS, which may have

been promoted by an increased mass transfer of nutrients or an increased likelihood of planktonic cells coming into contact with the pipe wall, both due to increased turbulence in the water column. Although HVF biofilms experienced the highest growth rate, the relative volume of material present at Day 28 was greatest in SS conditioned biofilms. The LVF biofilms had the least biofilm volume but the proportion of EPS in relation to cells (expressed as a ratio) was far greater than that of SS or HVF samples. The EPS matrix composition was also shown to shift from one heavily dominated by carbohydrates at SS, to one with a greater protein content, although still predominantly carbohydrate based at LVF (HVF was between the two).

The first exploration of the influence of hydraulics upon EPS composition within biofilms of the DWDS has demonstrated that SS and HVF had similar physical structures with a lower proportional EPS content than was expressed in LVF biofilms. It is hypothesised that the SS biofilms did not develop a more extensive matrix as they did not experience a variation in shear stress and so stronger adhesion, a physical characteristic attributed the EPS (section 1.4.5.1), was unnecessary and not conditioned for. Conversely, the biofilms developing under HVF experienced substantial variation in shear stress at the pipe wall and it is theorised that exposure to the peak flow in this regime led to a consistent, diurnal removal of any EPS that developed, conditioning for a younger biofilm structure with a less well established matrix, as described to occur under high shear stress in industrial water fed biofilms (Rochex *et al.*, 2008). This theory is further supported by the similarity in the EPS-to-cell ratios of HVF Day 0 and Day 28 biofilms, which showed that at Day 28, although the relative volumes of each component had increased from Day 0, the proportion of EPS per cell (μm) did not. Conversely, the EPS-to-cell ratio of LVF biofilms increased significantly at Day 28, as would be anticipated during biofilm maturation. Although previous research has alluded to environmental impacts upon EPS, this is the first time that a link has been conclusively proven between hydraulics and characteristics of drinking water biofilm matrices.

There were clear differences between the biofilms developed under each of the hydraulic conditions, therefore it can be concluded that the average daily flow rate was not a driving conditioning factor, as if it were the biofilms would have been more homogenous. The similarities between LVF and HVF community structure implied that the biofilm microbial community was conditioned to the low flow period, which was an identical period of constant flow rate between the two regimes but different to the constant flow rate of the SS regime, under which communities developed that were distinct from those within varied flow biofilms. In contrast, the physical structure of the LVF and HVF communities was very different, which demonstrates that the membership of the microbial community has a lesser effect upon the

resulting biofilm physical structure than the environmental constraints to which the community is exposed.

Overall, under the SS regime a diverse community developed, promoted by the constant flow rate but with no conditioning force promoting EPS production. Under LVF regimes, the community was less diverse (conditioned by the low night flows), potentially containing organisms better adapted to a changeable environment, which produced a more extensive EPS matrix, the presence of which persisted due to less variation in flow rate and a lower daily peak than at HVF. The LVF conditions were found to be the most effective at limiting the accumulation of biofilm, potentially due to a combination of variations in shear stress greater than at SS, but less nutrient transfer or reduced likelihood of cells coming into contact with the pipe surface than occurred in the more varied HVF condition. Biofilms conditioned to the HVF regime potentially experienced a cyclical removal of EPS on a daily basis due to the peak flow; during the low night flow communities similar to those of LVF recolonised the surface beginning to produce EPS which was removed by the peak flow before it could consolidate. In this way it may be that the HVF regime will consistently “reset” the biofilm, promoting a younger physical structure.

8.1.3 Variation in biofilm structure leads to different responses to elevated shear stress (Objective 4)

A series of increasing shear stresses, relevant to the forces occurring within real DWDS, were applied to determine any difference in response to flushing between the conditioned multi-species biofilms. Regardless of the previously applied conditioning regime, a strongly adhered biofilm basal layer remained post-flush lending support to the “cohesive layer theory” as the weaker adhered layers, primarily protein, were removed. In all instances the biofilm remaining attached was predominantly carbohydrate with embedded cells, highlighting the importance of carbohydrate in biofilm adhesion and stability.

During mobilisation, concentrations of iron and manganese (indicative of discolouration) in the bulk water increased, possibly detached from the biofilms. At the pipe wall there was a reduction in biofilm protein content (relative volume and spread), the removal of which may have released metal particles which had been entrapped within the matrix. The microbial communities of each biofilm experienced a decrease in relative richness and diversity, likely indicative of a shift towards a more specialised community, better able to resist detachment. This observation demonstrates that cells were lost from the biofilm during the mobilisation

phase (otherwise no shift in community characteristics would have been observed), but at concentrations that were not found to be statistically significant with regards to the physical structure analysis. In SS and LVF biofilms the loss of taxa led to significant differences in community structure between the Pre- and Post-flush samples. However, the HVF bacterial community was not significantly different between the two sample points, therefore the taxa that were lost were likely representative of the rarer organisms. Interestingly, before flushing the bacterial communities of LVF and HVF biofilms were similar, afterwards they were significantly different. As the two biofilms expressed different physical structures, it is concluded that different physical characteristics, due to different hydraulic conditioning during development, caused the two communities to respond differently to elevated shear stress.

The LVF conditioned pipelines experienced the least discolouration response, in part due to the accumulation of a lower amount of material but also due to the biofilm being more physically resistant to detachment (a smaller proportion of the biofilm was removed). This suggests that LVF conditioning is the most effective for reducing discolouration risk and that biofilms with a greater EPS content, which comprise a more even carbohydrate-to-protein ratio are the most stable. In contrast, biofilms from SS and HVF presented a greater discolouration risk as more material accumulated and a greater proportion of that material was mobilised. It appears that the low variation between the night time flow and the daily peak flow, which characterised the LVF condition, promoted a more stable biofilm physical structure than the average flow (0.4 ls^{-1} , 0.30 Nm^{-2} across all the regimes) or the exposure to a higher peak daily flow (peak of LVF was 0.54 ls^{-1} , 0.34 Nm^{-2} , peak of HVF was 0.75 ls^{-1} , 0.40 Nm^{-2}), specifically promoting the production of a more extensive matrix as was discussed previously. Conversely, microbial community structure was the most stable in HVF conditioned biofilms which suggests that these biofilms may be able to recover quickly from a change in shear stress and present a consistent threat to drinking water quality in the long term. The key driver promoting this community stability appeared to be the range between the minimum and maximum daily flows within HVF, rather than just the peak, i.e. the community was developed under a high varied diurnal pattern rather than a high steady state flow, this selected for a community better adapted to changes in hydraulics rather than simply tolerant to high shear stresses. Evidence from Sharpe (2012) regarding discolouration response of differently conditioned systems, showed that a high steady state regime (0.8 ls^{-1}) had a discolouration response very similar to that of the SS regime (0.4 ls^{-1}), which was greater than, and hence distinct from, that of HVF. Therefore, though this data is based on the changes in the bulk water rather than at the pipe wall, it is plausible that it is the hydraulic variation which is driving material to be stable under HVF, not the daily peak flow. Overall, the SS biofilms

experienced the greatest and most consistent increase in discolouration (indicated by the largest increase in bulk water iron and manganese concentrations, which were significant for the flushing of each loop). Moreover, the greatest volume of proteins was detached from the SS biofilms (although proportionally this was less than the loss from HVF) and the microbial communities altered due to the loss of taxa, in this respect it could be argued that the SS biofilms experienced the greatest changes due to the flushing phase as both their physical and community structures were altered.

The fact that the most physically stable biofilm and the most stable community occurred under different flow conditions demonstrated that the environmental conditions of the pipeline had a greater impact upon the development of a stable physical structure than did the microbial community membership. It also demonstrates that biofilms with similar communities can respond in very different ways to flushing, likely due to their differences in physical structure. In this way it may be possible to manage the hydraulics of a pipeline to promote the development of a specific biofilm structure over another. For instance, maintenance of a LVF regime would convey less of a discolouration risk to the pipeline due to lower volumes of more strongly adhered biofilm forming. Alternatively, a HVF regime may be favoured as, while it presents a greater risk of discolouration if left unmonitored, the promotion of a younger biofilm with less EPS means that more material can be removed with targeted flushing, potentially leading to a cleaner pipeline. It could also be argued that promoting the presence of a younger biofilm may result in a biofilm structure more susceptible to disinfection agents as EPS is accredited with affording protection from disinfection. Therefore, as the HVF biofilms had lower EPS-to-cell content than LVF, biocides may have an increased efficiency in their action when applied to pipelines previously conditioned to this regime.

8.2 Future Work

The body of work presented within this thesis provides detailed evidence of the influence of hydraulic regime upon variations in biofilm structure, building on this foundation the following section includes recommendations and improvements for future investigations regarding DWDS biofilms.

8.2.1 Different environmental conditions

The methods used in this thesis are robust and replicable, which, if applied to other environmentally and microbially driven questions, will allow an accumulation and expansion in

the information available regarding microbial ecology and water quality. Of particular interest, based upon a review of the literature (Chapter 1), would be the effects of disinfection agent concentrations upon biofilm structure and subsequent stability, as these are commonly present within drinking water and are another of the currently used network cleaning approaches. Given that the DWDS experimental facility is fed with water from the local distribution system, chlorine would be the most appropriate disinfectant agent to test as the supply water is already chlorinated. The influence of nutrient concentrations upon biofilm development and stability has also been little explored within biofilms relevant to real DWDS. Given that it has been suggested that a decrease in nutrient concentrations can promote detachment (Peyton & Characklis, 1993) the possibility exists that this could be used as a way to manage the DWDS biofilms, however, a greater understanding of the behaviour of the physical structure and diversity of microbial assemblages would be required in order to accurately predict their response to changing nutrient availability.

In order to investigate these environmental parameters a greater integration of advanced water chemistry analysis would be required to ensure accuracy of initial dosing and maintenance of boosted disinfectant or nutrient concentration. A wider appreciation of water chemistry would undoubtedly offer new dimensions and insights into biological processes occurring within the DWDS and may aid explanation for the patterns of iron and manganese mobilisation observed in the current study. Therefore, future work should also aim to achieve a greater appreciation for the build-up of inorganics within the biofilms.

Furthermore, the analysis approaches described in this thesis, combined with the advantages of biofilm development within the DWDS experimental facility, lend themselves to evaluating the efficiency of different management techniques and the recovery of biofilms after exposure to these. In this sense, the established methods could be used to trial new management approaches that will likely emerge in the future as technological research in other fields advances, for instance the increasing use of nanobubbles as a disinfectant agent (e.g. Agarwal *et al.*, 2011), providing a stop gap between bench top tests and the risk of trialling such methods in a real system that supplies consumers.

8.2.2 Improvements to the DWDS experimental facility

The experimental facility successfully combines a full scale DWDS environment with laboratory level control. However, in order to investigate the impact of variations in bulk water quality upon microbial ecology, such as chlorine or nutrients, individual water tanks for each of the

three loops would be required, so that each could be dosed independently. This would also allow the mobilization phase of each loop to be staggered without the flow having to be stopped in the other loops, thereby avoiding periods of stagnation.

The results presented here are based upon young biofilms; it would be of interest to determine if the differences between the biofilm structures conditioned under the different regimes alter with an increased longevity of development. With respect to pipe material some authors found that over time the biofilms that develop upon different surfaces were less distinct from each other (Henne *et al.*, 2012). Establishing if this occurs with respect to hydraulics could have implications upon predicting the risk to water quality posed by biofilms within pipelines of particular ages. In order to achieve this it would be necessary to incorporate a greater number of coupons into the experimental facility, best achieved by the provision of a second coupon section per loop.

It is also strongly recommended that a greater number of bulk water quality sample replicates are taken and that turbidity analysis methods are improved. The inclusion of multiparameter probes for online continuous water quality data collection would also be beneficial.

8.2.3 Further analysis of the biofilm structure

This study presents a novel insight into the physical and community structures of drinking water biofilms, demonstrating the difference in microbial community diversity and EPS content and composition as response to different hydraulic conditions. However, fingerprinting techniques do not provide species level information of the organisms remaining attached post flush. In order to better characterise the remaining communities, species level information is necessary which may be obtained via the use of high throughput sequencing and metagenomics (e.g. Liu *et al.*, 2012; Douterelo *et al.*, 2013; Lautenschlager *et al.*, 2013). In a similar vein, advancement of the understanding of the microbial ecology of drinking water biofilms would benefit from mRNA analysis and investigations into the functionality of the species present, in combination with sequencing of not only bacteria but also archaea and fungi. Application of these tools would allow investigations to begin to determine if the less diverse LVF and HVF communities may be comprised of more specialist bacteria that are better EPS producers or better at coaggregating, for example, than those of the SS biofilms. It might also be the case that particular biofilm structures or conditioning forces promote the survival of pathogenic species as suggested by Holzman (2002).

It could be advantageous to adapt the microscopy based approach for use with alternative stains such as Live/Dead which has previously been applied to aquatic biofilms (e.g. Dwidjosiswojo *et al.*, 2011; Xue *et al.*, 2013). This could provide information on the proportion and location of cells which are alive within the biofilms, therefore actively shaping and producing the biofilms. The ratio of live to dead cells may also have an impact upon the physical stability of biofilms, potentially weakening the cohesive forces between EPS.

Future work could more accurately investigate the mechanical strength of the biofilms via techniques such as atomic force microscopy (Abe *et al.*, 2012), rather than solely inferring stability and cohesive strength of the biofilms by their response to elevated shear stress. However, maintaining forces relevant to real DWDS would be paramount to maintaining the application of resulting data to real life situations.

8.2.4 Improved characterisation of the bulk phase

A greater exploration of the change in planktonic microbial abundance and diversity post flush would aid in understanding the transfer of cells from the wall to the water column. Douterelo *et al.* (2013) began to address this using pyrosequencing and found that the planktonic and biofilm communities were significantly different from each other but that the planktonic communities did not significantly alter after the flushing phase. It is likely that this is due to the great dilution of any cells that do detach. An alternative way to investigate changes in the bulk phase would be the use of particle counters to determine if larger or smaller particles are present at different flushing steps. Not only would this provide potential insights into the way biofilm material is lost into the water column, it would also aid understanding of the transportation and distribution of particles, in which size plays an important role. The counting or sizing of planktonic aggregates may also be possible via flow cytometry (Hoefel *et al.*, 2003; Lautenschlager *et al.*, 2013), which would be particularly useful if it was installed inline to enable the collection of continuous data.

8.2.5 Field studies

The experimental facility provides invaluable knowledge of real drinking water biofilms due to its replication of the DWDS environment; it would however also be desirable to apply the approaches used successfully here, to samples from the field. This would allow for an assessment of the accuracy of the laboratory based results and assist in drawing parallels between the two systems (experimental and real DWDS). There are obvious complications in

achieving this as the sampling of biofilm from real systems has logistical and operational constraints but the incorporation of PWG style coupons into real networks would be particularly advantageous.

8.3 Outlook

The presence of complex multispecies biofilms, which developed naturally within the DWDS environment, emphasises the importance of moving away from conducting research in idealised systems with mono or dual specific cultured biofilms. Moreover, the clear differences between the community structure of SS conditioned biofilms and those from the LVF or HVF regimes highlights the need to consider a varied flow environment when investigating drinking water biofilms in order for the results to be relevant to real systems.

In combination, this research makes a substantial contribution to the fields of drinking water microbial ecology and discolouration research, providing a novel insight into the physical and community structure of drinking water biofilms and the effect of hydraulics upon these. The knowledge yielded is integral to stimulate a change in thinking of biofilms as something to be “tolerated” or completely removed (an impossible demand) to a more proactive mind-set of understanding how biofilms interact with the DWDS in order to better manage them, potentially even conditioning for “good” biofilms that have little impact upon water quality. In line with this, the findings presented here demonstrate that having knowledge of the history of the hydraulics of a pipeline will enable cleaning practices to be better prioritised and targeted due to better predictions of risk. This will be of use in the development of future maintenance strategies and facilitate a shift in management practises from reactive to pre-emptive.

This thesis has offered a greater understanding of drinking water biofilms and emphasised that microbial ecology is an important factor in determining water quality. The new knowledge generated regarding the impact of hydraulics upon biofilm structure and stability will be valuable in the future modelling of both biofilms and the DWDS, particularly in relation to discolouration events and may also aid the development of novel cleaning practices, for this to be achieved continued interdisciplinary research is essential.

Reference List

- Abdullah, M. P., Yee, L. F., Ata, S., Abdullah, A., Ishak, B. and Abidin, K. N. Z. (2009). The study of interrelationship between raw water quality parameters, chlorine demand and the formation of disinfection by-products, *Phys. Chem. Earth Parts A/B/C* 34(13–16): 806–811.
- Abe, Y., Skali-Lami, S., Block, J.-C. and Francius, G. (2012a). Cohesiveness and hydrodynamic properties of young drinking water biofilms, *Water Res* 46(4): 1155–1166.
- Agarwal, A., Ng, W. J. and Liu, Y. (2011). Principle and applications of microbubble and nanobubble technology for water treatment, *Chemosphere* 84(9): 1175–1180.
- Ainsworth, R. A. (2002). *Safe Piped Water: Managing Microbial Water Quality in Piped Distribution Systems*, IWA on behalf of the World Health Organisation.
- Aller, J. Y. and Kemp, P. F. (2008). Are Archaea inherently less diverse than Bacteria in the same environments?, *FEMS Microbiol. Ecol.* 65(1): 74–87.
- Allion, A., Lassiaz, S., Peguet, L., Boillot, P., Jacques, S., Peultier, J. and Bonnet, M.-C. (2011). A long term study on biofilm development in drinking water distribution system: comparison of stainless steel grades with commonly used materials, *Revue de Métallurgie* 108(4): 259–268.
- Allison, D. and Sutherland, I. (1987). The role of exopolysaccharides in adhesion of fresh-water bacteria, *J. Gen. Microbiol.* 133: 1319–1327.
- An, Y. H., Dickinson, R. B. and Doyle, R. J. (2000). Mechanisms of Bacterial Adhesion and Pathogenesis of Implant and Tissue Infections, In, *Handbook of Bacterial Adhesion*, Humana Press, pp. 1–27.
- Appenzeller, B. M. R., Duval, Y. B., Thomas, F. and Block, J.-C. (2002). Influence of Phosphate on Bacterial Adhesion onto Iron Oxyhydroxide in Drinking Water, *Environ. Sci. Technol.* 36(4): 646–652.
- Arvanitidou, M., Kanellou, K., Constantinides, T. C. and Katsouyannopoulos, V. (1999). The occurrence of fungi in hospital and community potable waters, *Lett. Appl. Microbiol.* 29(2): 81–84.
- AWWA, American Water Works Association. (2002). *Effects of water age on distribution system water quality*. Retrieved August 27, 2013, from: http://www.epa.gov/safewater/disinfection/tcr/pdfs/whitepaper_tcr_waterdistribution.pdf
- Backhus, D.A., Picardal, F.W., Johnson, J., Knowles, T., Collins, R., Radue, A. and Kim, S. (1997). Soil- and surfactant-enhanced reductive dechlorination of carbon tetrachloride in the presence of *Shewanella putrefaciens* 200. *J. Contam. Hydrol.* 28(4): 337–361.
- Bagh, L., Albrechtsen, H., Arvin, E. and Ovesen, K. (2002). Biofilm formation in a hot water system, *Water Sci. Technol.* 46(9): 95–101.
- Bagh, L., Albrechtsen, H., Arvin, E. and Ovesen, K. (2004). Distribution of bacteria in a domestic hot water system in a Danish apartment building, *Water Res* 38(1): 225–235.
- Banning, N., Toze, S. and Mee, B. J. (2003). Persistence of biofilm-associated *Escherichia coli* and *Pseudomonas aeruginosa* in groundwater and treated effluent in a laboratory model system, *Microbiology* 149(Pt 1): 47–55.

- Bartram, J., Cotruvo, J., Exner, M., Fricker, C. and Glasmacher, A. (2004). Heterotrophic plate count measurement in drinking water safety management - Report of an Expert Meeting Geneva, 24-25 April 2002, *Int. J. Food Microbiol.* 92(3): 241–247.
- Batte, M., Koudjonou, B., Laurent, P., Mathieu, L., Coallier, J. and Prevost, M. (2003). Biofilm responses to ageing and to a high phosphate load in a bench-scale drinking water system, *Water Res* 37(6): 1351–1361.
- Berges, J., Fisher, A. and Harrison, P. (1993). A comparison of lowry, bradford and smith protein assays using different protein standards and protein isolated from the marine diatom thalassiosira-pseudonana, *Mar. Biol.* 115(2): 187–193.
- Berney, M., Vital, M., Hulshoff, I., Weilenmann, H., Egli, T. and Hammes, F. (2008). Rapid, cultivation-independent assessment of microbial viability in drinking water, *Water Res* 42(14): 4010–4018.
- Berry, D., Xi, C. and Raskin, L. (2006). Microbial ecology of drinking water distribution systems, *Curr. Opin. Biotech.* 17: 297-302.
- Bert, F, Maubect, E, Bruneau, B, Berry, F and Lambert-Zechovsky, N. (1998). Multi-resistant *Pseudomonas aeruginosa* outbreak associated with contaminated tap water in a neurosurgery intensive care unit., *J. Hosp. Infect.* 39: 53–62.
- Besner, M., Gauthier, V., Servais, P. and Camper, A. (2002). Explaining the occurrence of coliforms in distribution systems, *J. Am. Water Works Ass.* 94(8): 95–109.
- Besner, M., Gauthier, V., Trepanier, M., Martel, K. and Prevost, M. (2007). Assessing the effect of distribution system O&M on water quality, *J. Am. Water Works Ass.* 99(11): 77–91.
- Beyenal, H. and Lewandowski, Z. (2002). Internal and external mass transfer in biofilms grown at various flow velocities, *Biotechnology Progress* 18(1): 55–61.
- Bishop, P. (1997). Biofilm structure and kinetics. *Water Sci. Technol.*, 36(1) 287-294
- Blackwood, C. B., Hudleston, D., Zak, D. R. and Buyer, J. S. (2007). Interpreting Ecological Diversity Indices Applied to Terminal Restriction Fragment Length Polymorphism Data: Insights from Simulated Microbial Communities, *Appl. Environ. Microb.* 73(16): 5276–5283.
- Boe-Hansen, R., Albrechtsen, H.-J., Arvin, E. and Jørgensen, C. (2002a). Bulk water phase and biofilm growth in drinking water at low nutrient conditions, *Water Res* 36(18): 4477–4486.
- Boland, T., Latour, R. A. and Stutzenberger, F. J. (2000). Molecular Basis of Bacterial Adhesion, In *Handbook of Bacterial Adhesion*, Humana Press, pp. 29–41. Retrieved from http://link.springer.com/chapter/10.1007/978-1-59259-224-1_2
- Boxall, J. B., Skipworth, P. J. and Saul, A. J. (2001). A novel approach to modelling sediment movement in distribution mains based on particle characteristics., In *Proceedings of the Computing and Control in the Water Industry Conference*, DeMonfort University, UK.
- Boxall, J. B., Skipworth, P. J. and Saul, A. (2003). Aggressive flushing for discolouration event mitigation in water distribution networks, *Wa. Sci. Technol.* 3(1-2): 179–186.
- Boxall, J. B. and Saul, A. J. (2005). Modeling Discoloration in Potable Water Distribution Systems, *J. Environ. Eng.* 131(5): 716–725.

- Boxall, J. B. and Husband, P. S. (2007). *PODDS II Final Report Part 1 Validation of PODDs Model and Practical Implications for Discolouration in Water distribution Systems*, UK: The Pennine Water Group, The University of Sheffield.
- Boxall, J., O'Hagan, A., Pooladsaz, S., Saul, A. and Unwin, D. (2007). Estimation of burst rates in water distribution mains, *Proceedings of the Institution of Civil Engineers-Water Management* 160(2): 73–82.
- Boyd, A. and Chakrabarty, A. (1995). *Pseudomonas-aeruginosa* biofilms - role of the alginate exopolysaccharide, *J. Ind. Microbiol.* 15(3): 162–168.
- BS 6920, British Standard, Suitability of non-metallic products for use in contact with water intended for human consumption with regard to their effect on the quality of water. Retrieved January 26, 2011, from: http://www.standardsdirect.org/standards/standards4/StandardsCatalogue24_view_5902.html [Accessed January 26, 2011].
- Bradford, M. (1976). Rapid and sensitive method for quantitation of microgram quantities of protein utilizing principle of protein-dye binding, *Anal. Biochem.* 72(1-2): 248–254.
- Branda, S., Vik, A., Friedman, L. and Kolter, R. (2005). Biofilms: the matrix revisited, *Trends Microbiol.* 13(1): 20–26.
- Bristol Water. (2008). *Drinking Water Quality - The Standards Explained*. Retrieved May 12, 2013, from <http://www.bristolwater.co.uk/pdf/environment/wqReport08.pdf>
- Brocca, D., Arvin, E. and Mosbaek, H. (2002). Identification of organic compounds migrating from polyethylene pipelines into drinking water, *Water Res.* 36(15): 3675–3680.
- Bryers, J. and Characklis, W. (1981). Early fouling biofilm formation in a turbulent flow system: Overall kinetics, *Water Res.* 15(4): 483–491.
- Burtscher, M. M., Zibuschka, F., Mach, R. L., Lindner, G. and Farnleitner, A. H. (2009). Heterotrophic plate count vs. in situ bacterial 16S rRNA gene amplicon profiles from drinking water reveal completely different communities with distinct spatial and temporal allocations in a distribution net, *Water SA* 35(4).
- Buss, H.L., Brantley, S.L. and Liermann, L.J., (2003). Nondestructive Methods for Removal of Bacteria from Silicate Surfaces. *Geomicrobiol. J.* 20(1): 25–42.
- Buswell, C. M., Herlihy, Y. M., Marsh, P. D., Keevil, C. W. and Leach, S. A. (1997). Coaggregation amongst aquatic biofilm bacteria, *J. Appl. Microbiol.* 83(4): 477–484.
- Camper, AK, Mcfeters, G. A., Characklis, W. G. and Jones, W. L. (1991). Growth kinetics of coliform bacteria under conditions relevant to drinking water distribution systems., *Appl. Environ. Microbiol.* 57: 2233–2239.
- Camper, A, Burr, M., Ellis, B., Butterfield, P. and Abernathy, C. (1998). Development and structure of drinking water biofilms and techniques for their study, *J. Appl. Microbiol.* 85 Suppl 1: 1S–12S.
- Camper, A. K., Brastrup, K., Sandvig, A., Clement, J., Spencer, C. and Capuzzi, A. J. (2003). Effect of distribution system materials on bacterial regrowth, *J. Am. Water Works Ass.* 95(7): 107–121.

- Carson, L.A; Petersen, N.J; Favero, M.S. and Agüero, S.M. (1978). Growth characteristics of atypical mycobacteria in water and their comparative resistance to disinfectants., *Appl. Environ. Microbiol.* 36: 839–846.
- Cerrato, J. M., Reyes, L. P., Alvarado, C. N. and Dietrich, A. M. (2006). Effect of PVC and iron materials on Mn(II) deposition in drinking water distribution systems, *Water Res.* 40(14): 2720–2726.
- Chandy, J. and Angles, M. (2001). Determination of nutrients limiting biofilm formation and the subsequent impact on disinfectant decay, *Water Res.* 35(11): 2677–2682.
- Chen, X. and Stewart, P. S. (1996). Chlorine penetration into artificial biofilm is limited by a reaction-diffusion interaction, *Environ. Sci. Technol.* 30(6): 2078–2083.
- Chen, S. Y. and Huang, S. Y. (2000). Shear stress effects on cell growth and L-DOPA production by suspension culture of *Stizolobium hassjoo* cells in an agitated bioreactor, *Bioprocess Eng.* 22(1): 5–12.
- Chen, M., Lee, D., Tay, J. and Show, K. (2007a). Staining of extracellular polymeric substances and cells in bioaggregates, *Appl. Microbiol. Biot.* 75(2): 467–474.
- Chen, M., Lee, D. & Tay, J. (2007b). Distribution of extracellular polymeric substances in aerobic granules. *Appl. Microbiol. Biot.*, 73(6), pp.1463–1469.
- Choi, Y. and Morgenroth, E. (2003). Monitoring biofilm detachment under dynamic changes in shear stress using laser-based particle size analysis and mass fractionation, *Water Sci. Technol.* 47(5): 69–76.
- Chung, E., Aldom, J. E., Chagla, A. H., Kostrzynska, M., Lee, H., Palmateer, G., Trevors, J., Unger, S. and De Grandis, S. (1998). Detection of *Cryptosporidium parvum* oocysts in municipal water samples by the polymerase chain reaction., *J Microbiol. Meth.* 33: 171–180.
- Cirillo, J.D; Cirillo, S.L.G; Yan, L; Bermudez, L.E; Falkow, S and Tompkins, L.S. (1999). Intracellular Growth in *Acanthamoeba castellanii* Affects monocyte entry mechanisms and enhances virulence of *Legionella pneumophila.*, *Infect. Inum.* 67: 4427–4434.
- Clarke, K.R. and Gorley, R.N. (2006). PRIMER v6: User Manual / Tutorial.
- Clark, R. M. and Sivaganesan, M. (1999). *Characterizing the Effect of Chlorine and Chloramines on the US EPA Office of Research and Development Formation of Biofilm in a Simulated Drinking Water Distribution system*, Cincinnati, OH: US EPA.
- Connon, S. and Giovannoni, S. (2002). High-throughput methods for culturing microorganisms in very-low-nutrient media yield diverse new marine isolates, *Appl. Environ. Microb.* 68(8): 3878–3885.
- Cook, D. M. (2007). *Discolouration material generation rates in live drinking water distribution systems*. Ph.D Thesis, The University of Sheffield, UK.
- Costerton, J., Cheng, K., Geesey, G., Ladd, T., Nickel, J., Dasgupta, M. and Marrie, T. (1987). Bacterial biofilms in nature and disease, *Annu. Rev. Microbiol.* 41: 435–464.
- Costerton, J., Lewandowski, Z., Caldwell, D., Korber, D. and Lappin-scott, H. (1995). Microbial biofilms, *Annu. Rev. Microbiol.* 49: 711–745.

- Costerton, J. (1999). The role of bacterial exopolysaccharides in nature and disease (Reprinted from *Developments in Industrial Microbiology*, vol 26, pg 249-261, 1985), *J. Ind. Microbiol. Biot.* 22(4-5): 551–563.
- Covert, T., Rodgers, M., Reyes, A. and Stelma, G. (1999). Occurrence of nontuberculous mycobacteria in environmental samples, *Appl. Environ. Microb.* 65(6): 2492–2496.
- Craun, G. F. and Calderon, R. (2001). Waterborne disease outbreaks caused by distribution system deficiencies, *J. Am. Water Works Ass.* 93(9): 64–75.
- Critchley, M. and Fallowfield, H. (2001). The effect of distribution system bacterial biofilms on copper concentrations in drinking water. Retrieved June 14, 2012, from <http://www.iwaponline.com.eresources.shef.ac.uk/ws/00104/ws001040247.htm>
- Critchley M.M., Pasetto R. and O’Halloran R.J. (2004). Microbiological influences in ‘blue water’ copper corrosion, *J. Appl. Microbiol.* 97(3): 590–597.
- Crozes, G. F. and Cushing, R. S. (2000). Evaluating Biological Regrowth in Distribution Systems, In *AWWA:Water Quality Technology Conference*, Denver,CO.
- Danese, P., Pratt, L. and Kolter, R. (2000). Exopolysaccharide production is required for development of *Escherichia coli* K-12 biofilm architecture, *J. Bacteriol.* 182(12): 3593–3596.
- Davey, M. E. and O’Toole, G. A. (2000). Microbial biofilms: from ecology to molecular genetics, *Microbiol. Mol. Bio. R.* 64(4): 847–867.
- Davies, D., Parsek, M., Pearson, J., Iglewski, B., Costerton, J. and Greenberg, E. (1998). The involvement of cell-to-cell signals in the development of a bacterial biofilm, *Science* 280(5361): 295–298.
- deBeer, D., Stoodley, P., Roe, F. and Lewandowski, Z. (1994a). Effects of biofilm structures on oxygen distribution and mass-transport, *Biotechnol. Bioeng.* 43(11): 1131–1138.
- deBeer, D., Srinivasan, R. and Stewart, P. (1994b). Direct measurement of chlorine penetration into biofilms during disinfection, *Appl. Environ. Microb.* 60(12): 4339–4344.
- deBeer, D., Stoodley, P. and Lewandowski, Z. (1996). Liquid flow and mass transport in heterogeneous biofilms, *Water Res.* 30(11): 2761–2765.
- Defra. (2011). Water for life. Retrieved February 16, 2013, from <http://www.defra.gov.uk/environment/quality/water/legislation/whitepaper/>
- Deines, P., Sekar, R., Husband, P., Boxall, J., Osborn, A. and Biggs, C. (2010). A new coupon design for simultaneous analysis of in situ microbial biofilm formation and community structure in drinking water distribution systems, *Appl. Microbiol. Biot.* 87(2): 749–756.
- de Kievit, T. R., Gillis, R., Marx, S., Brown, C. and Iglewski, B. H. (2001). Quorum-sensing genes in *Pseudomonas aeruginosa* biofilms: their role and expression patterns, *Appl. Environ. Microb.* 67(4): 1865–1873.
- DeLong, E. F. (1992). Archaea in coastal marine environments, *Proceedings of the National Academy of Sciences of the United States of America* 89(12): 5685–5689.
- Denkhaus, E., Meisen, S., Telgheder, U. and Wingender, J. (2007). Chemical and physical methods for characterisation of biofilms, *Microchimica Acta* 158(1-2): 1–27.

- Deretic, V., Schurr, M. J., Boucher, J. C. and Martin, D. W. (1994). Conversion of *Pseudomonas aeruginosa* to mucoidy in cystic fibrosis: environmental stress and regulation of bacterial virulence by alternative sigma factors., *J. Bacteriol.* 176(10): 2773–2780.
- Doggett, MS. (2000). Characterization of fungal biofilms within a municipal water distribution system., *Appl. Environ. Microbiol.* 66: 1249–1251.
- Douterelo, I., Sharpe, R. L. and Boxall, J. B. (2013). Influence of hydraulic regimes on bacterial community structure and composition in an experimental drinking water distribution system, *Water Res* 47(2): 503–516.
- Dror-Ehre, A., Adin, A., Markovich, G. and Mamane, H. (2010). Control of biofilm formation in water using molecularly capped silver nanoparticles, *Water Res* 44(8): 2601–2609.
- Dubois, M., Gilles, K., Hamilton, J., Rebers, P. and Smith, F. (1956). Colorimetric method for determination of sugars and related substances, *Anal. Chem.* 28(3): 350–356.
- Dukan, S., Levi, Y., Piriou, P., Guyon, F. and Villon, P. (1996). Dynamic modelling of bacterial growth in drinking water networks, *Water Res* 30(9): 1991–2002.
- Dunne, W. M. (2002). Bacterial Adhesion: Seen Any Good Biofilms Lately?, *Clin. Microbiol. Rev.* 15(2): 155–166.
- Dunny, G. and Leonard, B. (1997). Cell-cell communication in gram-positive bacteria, *Annu. Rev. Microbiol.* 51: 527–564.
- Dunsmore, B., Jacobsen, A., Hall-Stoodley, L., Bass, C., Lappin-Scott, H. and Stoodley, P. (2002). The influence of fluid shear on the structure and material properties of sulphate-reducing bacterial biofilms, *J. Ind. Microbiol. Biot.* 29(6): 347–353.
- Dutkiewicz, C. and Fallowfield, H. (1998). Assessment of microbial involvement in the elevation of copper levels in drinking water, *J. Appl. Microbiol.* 85(3): 597–602.
- DWI. (2001). Drinking Water 2001: Enquiries and Consumer Complaints. Retrieved December 12, 2012, from www.dwi.gov.uk/pdf/pdf01/150-153.pdf
- DWI. (2002). Information letter index page. Retrieved July 8, 2011, from <http://dwi.defra.gov.uk/stakeholders/information-letters/>
- DWI. (2005). *Drinking Water 2005, A report by the Chief Inspector and Drinking Water Inspectorate: Incidents in England and Wales*. Retrieved July 8, 2011 from www.dwi.gov.uk/pubs/annrep05/Incidents in England and Wales 2005.pdf
- DWI. (2007). *The Water Supply (Water Quality) Regulations 2000 (Amendment) Regulations 2007* (No. Statutory Instrument 2007. No. 2734).
- DWI. (2008). Drinking Water Inspectorate Guidelines and Water Safety. Retrieved May 12, 2012 from www.dwi.gov.uk/regs/pdf/micro.htm
- DWI PR04a. (2004). *Periodic Review of Water Price Limits 2004. 'Taste and Odour'*. Retrieved May 12, 2012, from www.dwi.gov.uk/Pr04/briefnotes/tasteso.htm
- Dwidjosiswojo, Z., Richard, J., Moritz, M. M., Dopp, E., Flemming, H.-C. and Wingender, J. (2011). Influence of copper ions on the viability and cytotoxicity of *Pseudomonas aeruginosa* under conditions relevant to drinking water environments, *Int. J. Hyg. Envir. Heal.* 214(6): 485–492.

- Eboigbodin, K.E., and Biggs, C.A. (2008). Characterisation of the Extracellular Polymeric Substances produced by *Escherichia coli* using Infra-Red Spectroscopic, Proteomic and Aggregation Studies *Biomacromolecules* 9:686-95.
- Eichler, S., Christen, R., Holtje, C., Westphal, P., Botel, J., Brettar, I., Mehling, A. and Hofle, M. (2006). Composition and dynamics of bacterial communities of a drinking water supply system as assessed by RNA- and DNA-based 16S rRNA gene fingerprinting, *Appl. Environ. Microb.* 72(3): 1858–1872.
- Elvers, K. T., Leeming, K., Moore, C. P. and Lappin-Scott, H. M. (1998). Bacterial-fungal biofilms in flowing water photo-processing tanks, *J. Appl. Microbiol.* 84(4): 607–618.
- Environment Agency. (2002). *The Microbiology of Drinking Water - Part 1 - Water Quality and Public Health*. Retrieved June 17, 2013, from <http://www.environment-agency.gov.uk/static/documents/Research/mdwpart1.pdf>
- Escobar, I., Randall, A. and Taylor, J. (2001). Bacterial growth in distribution systems: Effect of assimilable organic carbon and biodegradable dissolved organic carbon, *Environ. Sci. Technol.* 35(17): 3442–3447.
- Esrey, S. A., Potash, J. B., Roberts, L. and Shiff, C. (1991). Effects of improved water supply and sanitation on ascariasis, diarrhoea, dracunculiasis, hookworm infection, schistosomiasis, and trachoma, *Bulletin of the World Health Organization* 69(5): 609–621.
- EU. (1998). *98/83/EC of Council of 3rd November 1998 on the quality of water intended for human consumption*.
- Euro Chlor. (2006). *Chlorine: a vital water disinfectant*. Retrieved May 12, 2012, from www.eurochlor.org/index.asp?page=679
- Falkinham III, J.O, Norton, C.D and Lechevallier, M.W. (2001). Factors influencing numbers of *Mycobacterium avium*, *Mycobacterium intracellulare*, and other mycobacteria in drinking water distribution systems, *Appl. Environ. Microb.* 67: 1225–1231.
- Farkas, A., Dragan-Bularda, M., Ciataras, D., Bocos, B. and Tigan, S. (2012). Opportunistic pathogens and faecal indicators in drinking water associated biofilms in Cluj, Romania, *J. Water Health* 10(3): 471–483.
- Fass, S, Dincher, M.L, Reasoner, D.J, Gatel, D and Block, J.C. (1996). Fate of *Escherichia coli* experimentally injected in a drinking water distribution pilot system., *Water Res.* 30: 2215–2221.
- Fernandez, A., Huang, S., Seston, S., Xing, J., Hickey, R., Criddle, C. and Tiedje, J. (1999). How Stable Is Stable? Function versus Community Composition, *Appl. Environ. Microb.* 65(8): 3697–3704.
- Ferroni, A. et al. (1998). Outbreak of nosocomial urinary tract infections due to *Pseudomonas aeruginosa* in a paediatric surgical unit associated with tap-water contamination, *J. Hosp. Infect.* 39: 301 –307.
- Fields, B. (1996). The molecular ecology of legionellae, *Trends Microbiol.* 4(7): 286–290.
- Fierer, N., Jackson, R.B. (2006). The diversity and biogeography of soil bacterial communities. *Proc. Natl. Acad. Sci. USA.* 103:626–631.

- Fish, K. E., Sharpe, R. L., Green, N. H., Osborn, A. M. and Boxall, J. B. (2011). Visualising and Quantifying the Matrix of Drinking Water Biofilms, In *Proceedings of IWA Biofilm2011: Processes in Biofilms*, Shanghai, China.
- Fish, K. E., Collins, R. P., Sharpe, R. L., Osborn, A. M. and Boxall, J. B. (2012). The Structure and Stability of Drinking Water Biofilms, In *Proceedings of the 14th Water Distribution Systems Analysis*, Adelaide, Australia.
- Flemming, H., Wingender, J., Moritz, R., Borchard, W. and Mayer, C. (1999). Physico-chemical properties of biofilms - A short review, *Biofilms in the Aquatic Environment* (242): 1–12.
- Flemming, H., Percival, S. and Walker, J. (2002). Contamination potential of biofilms in water distribution systems, *Innovations in Conventional and Advanced Water Treatment Processes* 2(1): 271–280.
- Flemming, H. and Wingender, J. (2010). The biofilm matrix, *Nat. Rev. Microbiol.* 8(9): 623–633.
- França, F. P. de and Cravo, W. B. (2000). Variation in sessile microflora as function of flow velocity on coupons exposed to seawater, *World J. Microb. Biot.* 16(8-9): 811–814.
- Frolund, B., Palmgren, R., Keiding, K. and Nielsen, P. (1996). Extraction of extracellular polymers from activated sludge using a cation exchange resin, *Water Res* 30(8): 1749–1758.
- Gauthier, V., Barbeau, B., Milette, R., Block, J. C. and Prevost, M. (2001). Suspended particles in the drinking water of two distribution systems, *Wa Sci. Technol.* 1(4): 237–245.
- Gauthier, Vincent, Redercher, S. and Block, J.-C. (1999b). Chlorine Inactivation of *Sphingomonas* Cells Attached to Goethite Particles in Drinking Water, *Appl. Environ. Microbiol.* 65(1): 355–357.
- Geesey, G. and White, D. (1990). Determination of bacterial-growth and activity at solid-liquid interfaces, *Annu. Rev. Microbiol.* 44: 579–602.
- Ginige, M.P., Wylie, J. and Plumb, J. (2011). Influence of biofilms on iron and manganese deposition in drinking water distribution systems, *Biofouling* 27(2): 151–163.
- Girvan, M. S., Bullimore, J., Pretty, J. N., Osborn, A. M. and Ball, A. S. (2003). Soil type is the primary determinant of the composition of the total and active bacterial communities in arable soils, *Appl. Environ. Microb.* 69(3): 1800–1809.
- Gomez-Alvarez, V., Revetta, R. P. and Domingo, J. W. (2012). Metagenome analyses of corroded concrete wastewater pipe biofilms reveal a complex microbial system, *BMC Microbiol.* 12(1): 122.
- Gonçalves, A. B., Paterson, R. R. M. and Lima, N. (2006). Survey and significance of filamentous fungi from tap water, *Int. J. Hyg. Envir. Heal.* 209(3): 257–264.
- Göttlich, E., van der Lubbe, W., Lange, B., Fiedler, S., Melchert, I., Reifenrath, M., Flemming, H.-C. and de Hoog, S. (2002). Fungal flora in groundwater-derived public drinking water, *Int. J. Hyg. Envir. Heal.* 205(4): 269–279.
- Gusman, V., Medic, D., Jelesic, Z. and Mihajlovic-Ukropina, M. (2012). *Sphingomonas Paucimobilis* as a Biofilm Producer, *Arch. Biol. Sci.* 64(4): 1327–1331.
- Hageskal, G., Knutsen, A. K., Gaustad, P., De Hoog, G. S. and Skaar, I. (2006). Diversity and significance of mold species in Norwegian drinking water, *Appl. Environ. Microb.* 72(12): 7586–7593.

- Hageskal, G, Gaustad, P, Heier, B.T and Skaar, I. (2007). Occurrence of moulds in drinking water, *J. Appl. Microb.* 102: 774–780.
- Hageskal, Gunhild, Tryland, I., Liltved, H. and Skaar, I. (2012). No simple solution to waterborne fungi: various responses to water disinfection methods, *Wa. Sci. Technol.* 12(2): 220.
- Hallam, N., West, J., Forster, C. and Simms, J. (2001). The potential for biofilm growth in water distribution systems, *Water Res* 35(17): 4063–4071.
- Hammes, F, Salhi, E., Koster, O., Kaiser, H., Egli, T. and von Gunten, U. (2006). Mechanistic and kinetic evaluation of organic disinfection by-product and assimilable organic carbon (AOC) formation during the ozonation of drinking water, *Water Res* 40(12): 2275–2286.
- Hammes, F., Berney, M., Wang, Y., Vital, M., Koster, O. and Egli, T. (2008). Flow-cytometric total bacterial cell counts as a descriptive microbiological parameter for drinking water treatment processes., *Water Res* 42: 269–277.
- Hammes, Frederik, Boon, N., Vital, M., Ross, P., Magic-Knezev, A. and Dignum, M. (2011). Bacterial Colonization of Pellet Softening Reactors Used during Drinking Water Treatment, *Appl. Environ. Microb.* 77(3): 1041–1048.
- Hanlon, A., Bellinger, B., Haynes, K., Xiao, G., Hofmann, T., Gretz, M., Ball, A., Osborn, A. and Underwood, G. (2006). Dynamics of extracellular polymeric substance (EPS) production and loss in an estuarine, diatom-dominated, microalgal biofilm over a tidal emersion-immersion period, *Limnol. Oceanogr.* 51(1): 79–93.
- Hanninen, P., Stelzer, E. H. K. and Salo, J. (1991). Nonlinear filtering in Improving the Image Quality of Confocal Fluorescent Images, *Mach. Vision Appl.* 4: 243–253.
- Haynes, K., Hofmann, T., Smith, C., Ball, A., Underwood, G. and Osborn, A. (2007). Diatom-derived carbohydrates as factors affecting bacterial community composition in estuarine sediments, *Appl. Environ. Microb.* 73(19): 6112–6124.
- Heinrichs, G., Hübner, I., Schmidt, C. K., Hoog, G. S. and Haase, G. (2013a). Analysis of Black Fungal Biofilms Occurring at Domestic Water Taps (I): Compositional Analysis Using Tag-Encoded FLX Amplicon Pyrosequencing, *Mycopathologia* 175(5-6): 387–397.
- Heinrichs, G., Hübner, I., Schmidt, C. K., Hoog, G. S. de and Haase, G. (2013b). Analysis of Black Fungal Biofilms Occurring at Domestic Water Taps (II): Potential Routes of Entry, *Mycopathologia* 175(5-6): 399–412
- Helmi, K., Skraber, S., Gantzer, C., Willame, R., Hoffmann, L. and Cauchie, H. (2008). Interactions of *Cryptosporidium parvum*, *Giardia lamblia*, vaccinal poliovirus type 1, and bacteriophages phi X174 and MS2 with a drinking water biofilm and a wastewater biofilm, *Appl. Environ. Microb.* 74(7): 2079–2088.
- Henne, K., Kahlisch, L., Brettar, I. and Höfle, M. G. (2012). Analysis of Structure and Composition of Bacterial Core Communities in Mature Drinking Water Biofilms and Bulk Water of a Citywide Network in Germany, *Appl. Environ. Microb.* 78(10): 3530–3538.
- Hersman, L. E., Forsythe, J. H., Ticknor, L. O. and Maurice, P. A. (2001). Growth of *Pseudomonas mendocina* on Fe(III) (hydr)oxides, *Appl. Environ. Microb.* 67(10): 4448–4453.
- Hert, D.G., Fredlake, C.P. and Barron, A.E. (2008). Advantages and limitations of next-generation sequencing technologies: A comparison of electrophoresis and non-electrophoresis methods. *Electrophoresis.* 29: 4618 – 4626.

- Heydorn, A., Nielsen, A., Hentzer, M., Sternberg, C., Givskov, M., Ersboll, B. and Molin, S. (2000). Quantification of biofilm structures by the novel computer program COMSTAT, *Microbiol.-UK* 146: 2395–2407.
- Hoefel, D., Grooby, W., Monis, P., Andrews, S. and Saint, C. (2003). Enumeration of water-borne bacteria using viability assays and flow cytometry: a comparison to culture-based techniques, *J. Microbiol. Meth.* 55(3): 585–597.
- Hofmann, T., Hanlon, A., Taylor, J., Ball, A., Osborn, A. and Underwood, G. (2009). Dynamics and compositional changes in extracellular carbohydrates in estuarine sediments during degradation, *Mar. Ecol-Prog. Ser.* 379: 45–58.
- Holden, B., Greetham, M., Croll, B. T. and Scutt, J. (1995). The effect of changing inter process and final disinfection reagents on corrosion and biofilm growth in distribution pipes, *Water Sci. Technol.* 32(8): 213–220.
- Holzman, D. (2002). Shear forces might aid pathogens in quest for vulnerable sites, *ASM NEWS* 68(9): 420–421.
- Horn, H., Reiff, H. and Morgenroth, E. (2003). Simulation of growth and detachment in biofilm systems under defined hydrodynamic conditions, *Biotechnol. Bioeng.* 81(5): 607–617.
- Hosni, A. A., Szabo, J. G. and Bishop, P. L. (2011). Efficacy of Chlorine Dioxide as a Disinfectant for Bacillus Spores in Drinking-Water Biofilms, *J. Environ. Eng.* 137: 569.
- Hunter, P. R., Chalmers, R. M., Hughes, S. and Syed, Q. (2005). Self-Reported Diarrhea in a Control Group: A Strong Association with Reporting of Low-Pressure Events in Tap Water, *Clin. Infect. Dis.* 40(4): e32–e34.
- Hunter, N. (2011). Drinking water: Ensuring the future of US drinking water supplies, *Filtr. Separat.* 48(2): 28–31.
- Husband, P., Boxall, J. and Saul, A. (2008). Laboratory studies investigating the processes leading to discolouration in water distribution networks, *Water Res* 42(16): 4309–4318.
- Husband, S. and Boxall, J. B. (2010). Field Studies of Discoloration in Water Distribution Systems: Model Verification and Practical Implications, *J. Environ. Eng.* 136(1): 86–94.
- Hwang, C., Ling, F., Andersen, G. L., LeChevallier, M. W. and Liu, W.-T. (2012). Evaluation of Methods for the Extraction of DNA from Drinking Water Distribution System Biofilms, *Microbes Environ.* 27(1): 9–18.
- Ivleva, N., Wagner, M., Horn, H., Niessner, R. and Haisch, C. (2009). Towards a nondestructive chemical characterization of biofilm matrix by Raman microscopy, *Anal. Bioanal. Chem.* 393(1): 197–206.
- IWA. (2004). *The Bonn Charter For Safe Drinking Water*. Retrieved August 27, 2013, from http://www.iwahq.org/contentsuite/upload/iwa/all/The_Bonn_Charter_For_Safe_Drinking_Water.pdf
- Jacob, J., Woodward, D., Feuerpfeil, I. and Johnson, W. M. (1998). Isolation of *Arcobacter butzleri* in raw water and drinking water treatment plants in Germany, *Zentralblatt für Hygiene und Umweltmedizin, Int. J. Hyg. Environ. Med.* 201(2): 189–198.
- Jahn, A. and Nielsen, P. (1995). Extraction of extracellular polymeric substances (EPS) from biofilms using a cation exchange resin, *Water Sci. Technol.* 32(8): 157–164.

- Jenkinson, H. and Lappin-Scott, H. (2001). Biofilms adhere to stay, *Trends Microbiol.* 9(1): 9–10.
- Jones, K. and Bradshaw, S. (1996). Biofilm formation by the enterobacteriaceae: A comparison between *Salmonella enteritidis*, *Escherichia coli* and a nitrogen-fixing strain of *Klebsiella pneumoniae*, *J. Appl. Bacteriol.* 80(4): 458–464.
- Joret J.C, Levi, Y and Volk, C. (1991). Biodegradable dissolved organic carbon (BDOC) content of drinking water and potential regrowth of bacteria., *Water Sci. Technol.* 24: 95–101.
- Kaiser, D. and Losick, R. (1993). How And Why Bacteria Talk To Each Other, *Cell* 73(5): 873–885.
- Kalmbach, S., Manz, W. and Szewzyk, U. (1997). Isolation of new bacterial species from drinking water biofilms and proof of their in situ dominance with highly specific 16S rRNA probes, *Appl. Environ. Microb.* 63(11): 4164–4170.
- Kanzler, D., Buzina, W., Paulitsch, A., Haas, D., Platzer, S., Marth, E. and Mascher, F. (2007). Occurrence and hygienic relevance of fungi in drinking water, *Mycoses* 51(2): 165–169.
- Karanis, P., Schoenen, D. and Seitz, H. M. (1998). Distribution and removal of Giardia and Cryptosporidium in water supplies in Germany, *Water Sci. Technol.* 37(2): 9–18.
- Karanja, D., Elliott, S. J. and Gabizon, S. (2011). Community level research on water health and global change: Where have we been? Where are we going?, *Current Opinion. Environmental Sustainability* 3(6): 467–470.
- Keevil, C. W., Mackerness, C. W. and Colbourne, J. S. (1990). Biocide treatment of biofilms, *Int. Biodeterior.* 26(2–4): 169–179.
- Keinanen, M. M., Korhonen, L. K., Lehtola, M. J., Miettinen, I. T., Martikainen, P. J., Vartiainen, T. and Suutari, M. H. (2002). The Microbial Community Structure of Drinking Water Biofilms Can Be Affected by Phosphorus Availability, *Appl. Environ. Microb.* 68(1): 434–439.
- Keinanen, M., Martikainen, P. and Kontro, M. (2004). Microbial community structure and biomass in developing drinking water biofilms, *Can. J. Microbiol.* 50(3): 183–191.
- Keinänen-Toivola, M. M., Revetta, R. P. and Santo Domingo, J. W. (2006). Identification of active bacterial communities in a model drinking water biofilm system using 16S rRNA-based clone libraries, *FEMS Microbiol. Lett.* 257(2): 182–188.
- Kerneis, A., Nakache, F., Deguin, A. and Feinberg, M. (1995). The effects of water residence time on the biological quality in a distribution network, *Water Res.* 29(7): 1719–1727.
- Kerr, C., Osborn, K., Roboson, G. and Handley, P. (1999). The relationship between pipe material and biofilm formation in a laboratory model system, *J. Appl. Microbiol.* 85: 29S–38S.
- Kielemoes, J., Bultinck, I., Storms, H., Boon, N. and Verstraete, W. (2002). Occurrence of manganese-oxidizing microorganisms and manganese deposition during biofilm formation on stainless steel in a brackish surface water, *FEMS Microbiol. Ecol.* 39(1): 41–55.
- Kirmeyer, G. J. and AWWA. (2000). *Guidance Manual for Maintaining Distribution System Water Quality*, American Water Works Association.
- Kives, J., Orgaz, B. and SanJose, C. (2006). Polysaccharide differences between planktonic and biofilm-associated EPS from *Pseudomonas fluorescens* B52, *Colloid Surfaces B* 52(2): 123–127.

- Klein, J. And Ziehr, H. (1990). Immobilization of microbial-cells by adsorption, *J. Biotechnol.* 16(1-2): 1–16.
- Kolenbrander, P. E. (2000). Oral microbial communities: biofilms, interactions, and genetic systems, *Annu. Rev. Microbiol.* 54: 413–437.
- Kormas, K., Neofitou, C., Pachiadaki, M. and Koufostathi, E. (2010). Changes of the bacterial assemblages throughout an urban drinking water distribution system, *Environ. Monit. Assess.* 165(1): 27–38.
- Korstgens, V., Flemming, H., Wingender, J. and Borchard, W. (2001). Uniaxial compression measurement device for investigation of the mechanical stability of biofilms, *J. Microbiol. Meth.* 46(1): 9–17.
- Kruithof, J., Kamp, P., Folmer, H., Nederlof, M. and van Hoof, S. (2001). Development of a membrane integrity monitoring strategy for the UF/RO Heemskerk drinking water treatment plant, *Membranes in Drinking and Industrial Water Production II* 1(5 and 6): 261–271.
- Kuhl, M. and Jørgensen, B. B. (1992). Microsensor Measurements of Sulfate Reduction and Sulfide Oxidation in Compact Microbial Communities of Aerobic Biofilms, *Appl. Environ. Microb.* 58(4): 1164–1174.
- Kuhn, D., George, T., Chandra, J., Mukherjee, P. and Ghannoum, M. (2002). Antifungal susceptibility of *Candida* biofilms: Unique efficacy of amphotericin B lipid formulations and echinocandins, *Antimicrob. Agents Ch.* 46(6): 1773–1780.
- Lambertini, E., Borchardt, M. A., Kieke, B. A., Spencer, S. K. and Loge, F. J. (2012). Risk of Viral Acute Gastrointestinal Illness from Nondisinfected Drinking Water Distribution Systems, *Environ. Sci. Technol.* 46(17): 9299–9307.
- Lautenschlager, K., Hwang, C., Liu, W.-T., Boon, N., Köster, O., Vrouwenvelder, H., Egli, T. and Hammes, F. (2013). A microbiology-based multi-parametric approach towards assessing biological stability in drinking water distribution networks, *Water Res.* 47(9): 3015–3025.
- Lawrence, J. R., Korber, D. R., Hoyle, B. D., Costerton, J. W. and Caldwell, D. E. (1991). Optical sectioning of microbial biofilms, *J. Bacteriol.* 173(20): 6558–6567.
- Lawrence, J., Swerhone, G., Leppard, G., Araki, T., Zhang, X., West, M. and Hitchcock, A. (2003). Scanning transmission X-ray, laser scanning, and transmission electron microscopy mapping of the exopolymeric matrix of microbial biofilms, *Appl. Environ. Microb.* 69(9): 5543–5554.
- Lazarova, V. and Manem, J. (1995). Biofilm characterization and activity analysis in water and waste-water treatment, *Water Res.* 29(10): 2227–2245.
- Lechevallier, M., Cameron, S. And Mcfeters, G. (1983). New medium for improved recovery of coliform bacteria from drinking-water, *Appl. Environ. Microb.* 45(2): 484–492.
- LeChevallier, M., Babcock, T. and Lee, R. (1987). Examination and characterization of distribution-system biofilms, *Appl. Environ. Microb.* 53(12): 2714–2724.
- LeChevallier, M., Cawthon, C. and Lee, R. (1988a). Factors promoting survival of bacteria in chlorinated water-supplies, *Appl. Environ. Microb.* 54(3): 649–654.
- LeChevallier, M., Cawthon, C. and Lee, R. (1988b). Inactivation of biofilm bacteria, *Appl. Environ. Microb.* 54(10): 2492–2499.

- LeChevallier, M., Schulz, W. And Lee, R. (1991). Bacterial Nutrients In Drinking-Water, *Appl. Environ. Microb.* 57(3): 857–862.
- LeChevallier, M., Lowry, C., Lee, R. and Gibbon, D. (1993). Examining the relationship between iron corrosion and the disinfection of biofilm bacteria, *J. Am. Water Works Ass.* 85(7): 111–123.
- LeChevallier, M., Welch, N. and Smith, D. (1996). Full-scale studies of factors related to coliform regrowth in drinking water, *Appl. Environ. Microb.* 62(7): 2201–2211.
- LeChevallier, M. W. (1998). *Microbial impact of biological filtration*, American Water Works Association.
- LeChevallier, M. (1999). Biofilms in water distribution systems: Control and remediation, *Biofilms in the Aquatic Environment* (242): 220–230.
- Lehtola, M.J; Miettinen, I.T; Vartiainen, T. and Martikainen, P.J. (2002). Changes in content of microbially available phosphorus, assimilable organic carbon and microbial growth potential during drinking water treatment processes., *Water. Res.* 36: 3681–3690.
- Lehtola, M., Juhna, T., Miettinen, I., Vartiainen, T. and Martikainen, P. (2004a). Formation of biofilms in drinking water distribution networks, a case study in two cities in Finland and Latvia, *J. Ind. Microbiol. Biot.* 31(11): 489–494.
- Lehtola, M., Miettinen, K., Keinanen, M., Kekki, T., Laine, O., Hirvonen, A., Vartiainen, T. and Martikainen, P. (2004b). Microbiology, chemistry and biofilm development in a pilot drinking water distribution system with copper and plastic pipes, *Water Res.* 38(17): 3769–3779.
- Lehtola, M., Miettinen, I., Hirvonen, A., Vartiainen, T. and Martikainen, P. (2006). Resuspension of biofilms and sediments to water from pipelines as a result of pressure shocks in drinking water distribution system, In *IWA BiofilmSystems IV*, Amsterdam.
- Lehtola, M., Miettinen, I., Hirvonen, A., Vartiainen, T. and Martikainen, P. (2007). Estimates of microbial quality and concentration of copper in distributed drinking water are highly dependent on sampling strategy, *Int. J. Hyg. Envir. Heal.* 210(6): 725–732.
- Lessie, T. and Vanderwy.Jc. (1972). Multiple forms of *Pseudomonas-multivorans* glucose-6-phosphate and 6-phosphogluconate dehydrogenases - differences in size, pyridine-nucleotide specificity, and susceptibility to inhibition by adenosine 5'-triphosphate, *J. Bacteriol.* 110(3): 1107–&.
- Levy, D. A., Bens, M. S., Craun, G. F., Calderon, R. and Herwaldt, B. L. (1998). Surveillance for waterborne-disease outbreaks--United states, 1995-1996, *MMWR, Surveillance Summaries* 47(5): 1–34.
- Lewis, K. (2000). Programmed Death in Bacteria, *Microbiol. Mol. Biol. R.* 64(3): 503–514.
- Lewis, K. (2001). Riddle of biofilm resistance, *Antimicrob. Agents Ch.* 45(4): 999–1007.
- Ling, F. and Liu, W.-T. (2013). Impact of Chloramination on the Development of Laboratory-Grown Biofilms Fed with Filter-Pretreated Groundwater, *Microbes Environ.* 28(1): 50–57.
- Liu, W.T, Marsh, T.L, Cheng, H and Forney, L.J. (1997). Characterization of microbial diversity by determining terminal restriction fragment length polymorphisms of genes encoding 16S rRNA., *Appl. Environ. Microb.* 63: 4516–4522.

- Liu, R., Yu, Z., Zhang, H., Yang, M., Shi, B. and Liu, X. (2012). Diversity of bacteria and mycobacteria in biofilms of two urban drinking water distribution systems, *Can. J. Microbiol.* 58(3): 261–270.
- Liu, R., Yu, Z., Guo, H., Liu, M., Zhang, H. and Yang, M. (2012). Pyrosequencing analysis of eukaryotic and bacterial communities in faucet biofilms, *Science of The Total Environment* 435–436: 124–131
- Liu, H. & Fang, H., (2002). Extraction of extracellular polymeric substances (EPS) of sludges. *J. Biotech.*, 95(3), 249-256.
- Liu, Y. and Tay, J. (2001). Metabolic response of biofilm to shear stress in fixed-film culture, *J. Appl. Microbiol.* 90(3): 337–342.
- Lomborg, B. (2001). *The Skeptical Environmentalist.*, 1st ed., Cambridge University Press.
- Lowry, O., Rosebrough, N.J., Farr, A.L. and Randall, R.J. (1951). Protein measurement with the folin phenol reagent. *J. Biol. Chem.*, 193(1):265–275.
- Machell, J., Boxall, J., Saul, A. and Bramley, D. (2009). Improved Representation of Water Age in Distribution Networks to Inform Water Quality, *J. Water Res. Pl-Asce* 135(5): 382–391.
- Mackay, W.G; Gribbon, L.T; Barer, M.R and Reid, D.C. (1998). Biofilms in drinking water systems – a possible reservoir for *Helicobacter pylori*., *Water Sci. Technol.* 38(12): 181–185.
- MacKenzie, W. R., Schell, W. L., Blair, K. A., Addiss, D. G., Peterson, D. E., Hoxie, N. J., Kazmierczak, J. J. and Davis, J. P. (1995). Massive outbreak of waterborne cryptosporidium infection in Milwaukee, Wisconsin: recurrence of illness and risk of secondary transmission, *Clinical infectious diseases: an official publication of the Infectious Diseases Society of America* 21(1): 57–62.
- Mah, T.F.C. and O’Toole, G.A. (2001). Mechanisms of biofilm resistance to antimicrobial agents., *Trends Microbiol.* 9: 34–39.
- Mann, A. G., Tam, C. C., Higgins, C. D. and Rodrigues, L. C. (2007). The association between drinking water turbidity and gastrointestinal illness:a systematic review, *BMC Public Health* 7(1): 256.
- Manuel, C. M., Nunes, O. C. and Melo, L. F. (2007). Dynamics of drinking water biofilm in flow/non-flow conditions, *Water Res.* 41(3): 551–562.
- Manz, W., Szewzyk, U., Ericsson, P., Amann, R., Schleifer, K. H. and Stenström, T. A. (1993). In Situ Identification of Bacteria in Drinking Water and Adjoining Biofilms by Hybridization with 16S and 23S rRNA-Directed Fluorescent Oligonucleotide Probes., *Appl. Environ. Microb.* 59(7): 2293–2298.
- Manz, B., Volke, F., Goll, D. and Horn, H. (2003). Measuring local flow velocities and biofilm structure in biofilm systems with magnetic resonance imaging (MRI), *Biotechnol. Bioeng.* 84(4): 424–432.
- Marsh, P. and Bradshaw, D. (1995). Dental Plaque As A Biofilm, *J. Ind. Microbiol.* 15(3): 169–175.
- Martin, K. J. and Rygiewicz, P. T. (2005). Fungal-specific PCR primers developed for analysis of the ITS region of environmental DNA extracts, *BMC Microbiology* 5.

- Martiny, A. C., Jørgensen, T. M., Albrechtsen, H.-J., Arvin, E. and Molin, S. (2003). Long-Term Succession of Structure and Diversity of a Biofilm Formed in a Model Drinking Water Distribution System, *Appl. Environ. Microb.* 69(11): 6899–6907.
- Martiny, A., Albrechtsen, H., Arvin, E. and Molin, S. (2005). Identification of bacteria in biofilm and bulk water samples from a nonchlorinated model drinking water distribution system: Detection of a large nitrite-oxidizing population associated with *Nitrospira* spp., *Appl. Environ. Microb.* 71(12): 8611–8617.
- Mathieu, L., Paquin, J. L., Block, J. G., Randon, C., Maillard, J. and Reasoner, D. (1992). Parameters governing bacterial growth in water distribution systems., *Rev. Sci. Eau* 5(s): 91–112.
- McCoy, W. F. and Olson, B. H. (1986). Relationship among turbidity, particle counts and bacteriological quality within water distribution lines, *Water Res.* 20(8): 1023–1029.
- McSwain, B., Irvine, R., Hausner, M. and Wilderer, P. (2005). Composition and distribution of extracellular polymeric substances in aerobic flocs and granular sludge, *Appl. Environ. Microb.* 71(2): 1051–1057.
- Meckes, M. C., Haight, R., Dosani, M., CLARK, R. and Sivaganesan, M. (1999). Effect of pH adjustments on biofilm in a simulated water distribution system., In *Proceedings of the American Water Works Association Water Quality Technology Conference, AWWA*, Denver, CO.
- Menaia, J. and Mesquita, E. (2004). Drinking water pipe biofilm: present knowledge, concepts and significance, *Waterborne Pathogens* 4(2): 115–124.
- Menala, J., Alves, R., Sanches, S., Santos, G. and Mesquita, E. (2003). Monitoring the active sessile-colonisation of two drinking water distribution systems based on the protein contents in native biofilm samples, *Water Sci. Technol.* 47(5): 169–173.
- Michalowski, W., Flemming, H-C. and Wingender, J. (2009). Isolation and analysis of extracellular polymeric substances from drinking water biofilms. 5th ASM Conference on *Biofilms* 15-19th November, Cancun, Mexico
- Michalowski, W., Flemming, H-C. and Wingender, J. (2010). Isolation of extracellular polymeric substances from drinking water biofilms – a critical assessment of standard isolation methods. *Biofilms IV* 1-3rd September, Winchester, UK
- Miettinen, I., Vartiainen, T. and Martikainen, P. (1997). Changes in water microbial quality during bank filtration of lake water, *Can. J. Microbiol.* 43(12): 1126–1132.
- Mittelman, M. W. and Geesey, G. G. (1985). Copper-Binding Characteristics of Exopolymers from a Freshwater-Sediment Bacterium., *Appl. Environ. Microb.* 49(4): 846–851.
- Möhle, R., Langemann, T., Haesner, M., Augustin, W., Scholl, S., Neu, T., Hempel, D. and Horn, H. (2007). Structure and shear strength of microbial biofilms as determined with confocal laser scanning microscopy and fluid dynamic gauging using a novel rotating disc biofilm reactor, *Biotechnol. Bioeng.* 98(4): 747–755.
- Moissl-Eichinger, C. and Huber, H. (2011). Archaeal symbionts and parasites, *Curr. Opin. Microbiol.* 14(3): 364–370.
- Moller, S., Sternberg, C., Andersen, J., Christensen, B., Ramos, J., Givskov, M. and Molin, S. (1998). In situ gene expression in mixed-culture biofilms: Evidence of metabolic interactions between community members, *Appl. Environ. Microbiol.* 64(2): 721–732.

- Momba, M. and Kaleni, P. (2002). Regrowth and survival of indicator microorganisms on the surfaces of household containers used for the storage of drinking water in rural communities of South Africa, *Water Res.* 36(12): 3023–3028.
- Momba, M.N.B, Kfir, R, Venter, S.N and Loete, T.E.C. (2000). An overview of biofilm formation in distribution systems and its impact on the deterioration of water quality., *Water SA.* 26: 59–66.
- Morgenroth, E. and Wilderer, P. (2000). Influence of detachment mechanisms on competition in biofilms, *Water Res.* 34(2): 417–426.
- Moritz, M. M., Flemming, H.-C. and Wingender, J. (2010). Integration of *Pseudomonas aeruginosa* and *Legionella pneumophila* in drinking water biofilms grown on domestic plumbing materials, *Int. J. Hyg. Envir. Heal.* 213(3): 190–197.
- Morris, R. D., Naumova, E. N., Levin, R. and Munasinghe, R. L. (1996). Temporal variation in drinking water turbidity and diagnosed gastroenteritis in Milwaukee., *Am. J. Public Health* 86(2): 237–239.
- Morton, L. and Surman, S. (1994). Biofilms In Biodeterioration - A Review, *International Biodeterioration & Biodegradation* 34(3-4): 203–221.
- Morton, S., Zhang, Y. and Edwards, M. (2005). Implications of nutrient release from iron metal for microbial regrowth in water distribution systems, *Water Res.* 39(13): 2883–2892.
- Morvay, A. A., Decun, M., Scurtu, M., Sala, C., Morar, A. and Sarandan, M. (2011). Biofilm formation on materials commonly used in household drinking water systems, *Wa. Sci. Technol.* 11(2): 252.
- Murgel, G., Lion, L., Acheson, C., Shuler, M., Emerson, D. and Ghiorse, W. (1991). Experimental apparatus for selection of adherent microorganisms under stringent growth-conditions, *Appl. Environ. Microb.* 57(7): 1987–1996.
- Nagy, L. A. and Olson, B. H. (1982). The occurrence of filamentous fungi in drinking water distribution systems, *Can. J. Microbiol.* 28(6): 667–671.
- Neu, T. and Lawrence, J. (1999). Lectin-binding analysis in biofilm systems, *Biofilms* 310: 145–152.
- Neu, T. and Lawrence, J. (2009). Extracellular polymeric substances in microbial biofilms., In *Microbial Glycobiology: Structures, Relevance and Applications*, Elsevier, San Diego, pp. 735–758.
- Neu, T. R. and Marshall, K. C. (1990). Bacterial polymers: physicochemical aspects of their interactions at interfaces, *Journal of Biomaterials Applications* 5(2): 107–133.
- Nielsen, L. P., Christensen, P. B., Revsbech, N. P. and Sørensen, J. (1990). Denitrification and oxygen respiration in biofilms studied with a microsensor for nitrous oxide and oxygen, *Microb. Ecol.* 19(1): 63–72.
- Niemi, R. M., Knuth, S. and Lundström, K. (1982). Actinomycetes and Fungi in Surface Waters and in Potable Water, *Appl. Environ. Microb.* 43(2): 378–388.
- Niquette, P., Servais, P. and Savoie, R. (2000). Impacts of pipe materials on densities of fixed bacterial biomass in a drinking water distribution system, *Water Res.* 34(6): 1952–1956.

- Norton, C. D. and LeChevallier, M. L. W. (2000). A pilot study of bacteriological population changes through potable water treatment and distribution., *Appl. Environ. Microbiol.* 66: 268–276.
- Ohashi, A. and Harada, H. (1994). Adhesion strength of biofilm developed in an attached-growth reactor, *Water Sci. Technol.* 29(10-11): 281–288.
- Ohashi, A., Koyama, T., Syutsubo, K. and Harada, H. (1999). A novel method for evaluation of biofilm tensile strength resisting erosion, *Water Sci. Technol.* 39(7): 261–268.
- Ohkouchi, Y., Ly, B. T., Ishikawa, S., Kawano, Y. and Itoh, S. (2013). Determination of an acceptable assimilable organic carbon (AOC) level for biological stability in water distribution systems with minimized chlorine residual, *Environ. Monit. Assess.* 185(2): 1427–1436.
- Okabe, S., Satoh, H. and Watanabe, Y. (1999). In situ analysis of nitrifying biofilms as determined by in situ hybridization and the use of microelectrodes, *Appl. Environ. Microb.* 65(7): 3182–3191.
- Oosthuizen, M., Steyn, B., Theron, J., Cosette, P., Lindsay, D., von Holy, A. and Brozel, V. (2002). Proteomic analysis reveals differential protein expression by *Bacillus cereus* during biofilm formation, *Appl. Environ. Microb.* 68(6): 2770–2780.
- Ophir, T. and Gutnick, D. (1994). A Role For Exopolysaccharides In The Protection Of Microorganisms From Desiccation, *Appl. Environ. Microb.* 60(2): 740–745.
- Osborn, A. M. and Smith, C. J. (2005). *Molecular microbial ecology*, New York; Abingdon [England]: Taylor & Francis.
- Osborn, A.M, Moore, E.R.B and Timmis, K.N. (2000). An evaluation of terminal-restriction fragment length polymorphism (T-RFLP) analysis for the study of microbial community structure and dynamics., *Environ. Microb.* 2: 39–50.
- Otterholt, E. and Charnock, C. (2011). Identification and phylogeny of the small eukaryote population of raw and drinking waters, *Water Res.* 45(8): 2527–2538.
- Pachepsky, Y., Morrow, J., Guber, A., Shelton, D., Rowland, R. and Davies, G. (2012). Effect of biofilm in irrigation pipes on microbial quality of irrigation water, *Lett. Appl. Microbiol.* 54(3): 217–224.
- Park, S.R; Mackay, W.G and Reid, D.C. (2001). *Helicobacter* sp. recovered from drinking water biofilm sampled from a water distribution system., *Wat. Res.* 35: 1624–1626.
- Park, S.-K., Choi, J.-H. and Hu, J. Y. (2012). Assessing bacterial growth potential in a model distribution system receiving nanofiltration membrane treated water, *Desalination* 296(0): 7–15.
- Parsek, M.R and Singh, P.K. (2003). Bacterial Biofilms: An emerging link., *Annu. Rev. Microbiol.* 57: 677–701.
- Paul, E., Ochoa, J. C., Pechaud, Y., Liu, Y. and Liné, A. (2012). Effect of shear stress and growth conditions on detachment and physical properties of biofilms, *Water Res.* 46(17): 5499–5508.
- Pawley, J. (2006). *Handbook of Biological confocal Microscopy*, Springer.

- Payment, P. (1997). Epidemiology of endemic gastrointestinal and respiratory diseases: Incidence, fraction attributable to tap water and costs to society, *Water Sci. Technol.* 35(11-12): 7–10.
- Payment, P., Siemiatycki, J., Richardson, L., Renaud, G., Franco, E. and Prevost, M. (1997). A prospective epidemiological study of gastrointestinal health effects due to the consumption of drinking water, *Int. J. Hyg. Envir. Heal.* 7(1): 5–31.
- Pedersen, K. (1990). Biofilm development on stainless-steel and pvc surfaces in drinking-water, *Water Res.* 24(2): 239–243.
- Percival, S., Knapp, J., Edyvean, R. and Wales, D. (1998). Biofilm development on stainless steel in mains water, *Water Res.* 32(1): 243–253.
- Percival, S., Knapp, J., Wales, D. and Edyvean, R. (1999). The effect of turbulent flow and surface roughness on biofilm formation in drinking water, *J. Ind. Microbiol. Biot.* (22): 152–159.
- Pereira, M., Kuehn, M., Wuertz, S., Neu, T. and Melo, L. (2002). Effect of flow regime on the architecture of a *Pseudomonas fluorescens* biofilm, *Biotechnol. Bioeng.* 78(2): 164–171.
- Peyton, B. (1996). Effects of shear stress and substrate loading rate on *Pseudomonas aeruginosa* biofilm thickness and density, *Water Res.* 30(1): 29–36.
- Peyton, B. M. and Characklis, W. G. (1993). A statistical analysis of the effect of substrate utilization and shear stress on the kinetics of biofilm detachment, *Biotechnol. Bioeng.* 41(7): 728–735.
- Phe, M., Dossot, M., Guilloteau, H. and Block, J. (2005). Nucleic acid fluorochromes and flow cytometry prove useful in assessing the effect of chlorination on drinking water bacteria, *Water Res.* 39(15): 3618–3628.
- Picioreanu, C., van Loosdrecht, M. and Heijnen, J. (2001). Two-dimensional model of biofilm detachment caused by internal stress from liquid flow, *Biotechnol. Bioeng.* 72(2): 205–218.
- Piriou, P., Dukan, D. and Levi, Y. (1999). Modelling biofilm dynamics in drinking water distribution systems, *Biofilms in the Aquatic Environment* (242): 61–71.
- Poitelon, J., Joyeux, M., Welte, B., Duguet, J., Prestel, E., Lespinet, O. and Dubow, M. (2009). Assessment of phylogenetic diversity of bacterial microflora in drinking water using serial analysis of ribosomal sequence tags, *Water Res.* 43(17): 4197–4206.
- Poitelon, J.-B., Joyeux, M., Welté, B., Duguet, J.-P., Peplies, J. and DuBow, M. s. (2009). Identification and phylogeny of eukaryotic 18S rDNA phylotypes detected in chlorinated finished drinking water samples from three Parisian surface water treatment plants, *Lett. Appl. Microbiol.* 49(5): 589–595.
- Polychronopolous, M., Dudley, K., Ryan, G. and Hearn, J. (2003). Investigation of factors contributing to dirty water events in reticulation systems and evaluation of flushing methods to remove accumulated particles., *Wa Sci. Technol.* 3(1-2): 295–306.
- Poppele, E. and Hozalski, R. (2003). Micro-cantilever method for measuring the tensile strength of biofilms and microbial flocs, *J. Microbiol. Meth.* 55(3): 607–615.
- Porter, J., Deere, D., Pickup, R. and Edwards, C. (1996). Fluorescent probes and flow cytometry: New insights into environmental bacteriology, *Cytometry* 23(2): 91–96.

- Porter, J., Deere, D., Hardman, M., Edwards, C. and Pickup, R. (1997). Go with the flow - use of flow cytometry in environmental microbiology, *FEMS Microbiol. Ecol.* 24(2): 93–101.
- Prigent-Combaret, C., Vidal, O., Dorel, C. and Lejeune, P. (1999). Abiotic surface sensing and biofilm-dependent regulation of gene expression in *Escherichia coli*, *J. Bacteriol.* 181(19): 5993–6002.
- Privett, G. (2007). *Creating and Enhancing Digital Astro Images*, 1st ed., Springer-Verlag, London.
- Purevdorj, B., Costerton, J. and Stoodley, P. (2002). Influence of hydrodynamics and cell signaling on the structure and behavior of *Pseudomonas aeruginosa* biofilms, *Appl. Environ. Microb.* 68(9): 4457–4464.
- Quignon, F, L; Kiene, Y; Levi, M.S and Schwartzbrod, L. (1997). Virus behaviour within a distribution system, *Water Sci. Technol.* (35): 311–318.
- R Development Core Team (2012). R: A language and environment for statistical computing. *R Foundation for Statistical Computing, Vienna, Austria*. Downloaded from <http://www.R-project.org/>
- Ramasamy P and Zhang X. (2005). Effects of shear stress on the secretion of extracellular polymeric substances in biofilms, *Water Sci. Technol.* 52(7):217-223
- Ranjard, L., Poly, F., Mougel, C., Thioulouse, J. and Nazaret, S. (2001). Characterization of Bacterial and Fungal Soil communities by Automated Ribosomal Intergenic Spacer Analysis Fingerprints: Biological and Methodological Variability, *Appl. Environ. Microb.* 67(10): 4479–4487.
- Ratnayaka, D. D., Brandt, M. J. and Johnson, K. M. (2009). *Twort's Water Supply*, 6th ed., Great Britain: Butterworth-Heinemann.
- Ratto, M., Suihko, M. and Siika-aho, M. (2005). Polysaccharide-producing bacteria isolated from paper machine slime deposits, *J. Ind. Microbiol. Biot.* 32(3): 109–114.
- Raunkjaer, K., Hvitved-Jacobsen, T. And Nielsen, P. (1994). Measurement Of Pools Of Protein, Carbohydrate And Lipid In Domestic Waste-Water, *Water Res.* 28(2): 251–262.
- RDP. (2013). *Ribosomal Database Project*. Retrieved August 28, 2013 from <http://rdp.cme.msu.edu/>
- Regan, J., Harrington, G. and Noguera, D. (2002). Ammonia- and nitrite-oxidizing bacterial communities in a pilot-scale chloraminated drinking water distribution system, *Appl. Environ. Microb.* 68(1): 73–81.
- Regan, J. M., Harrington, G. W., Baribeau, H., Leon, R. D. and Noguera, D. R. (2003). Diversity of nitrifying bacteria in full-scale chloraminated distribution systems, *Water Res.* 37(1): 197–205.
- Revetta, R., Pemberton, A., Lamendella, R., Iker, B. and Domingo, J. (2010). Identification of bacterial populations in drinking water using 16S rRNA-based sequence analyses, *Water Res.* 44(5): 1353–1360.
- Richardson, L. and Castenholz, R. (1987). Enhanced Survival Of The Cyanobacterium *Oscillatoria-Terebriformis* In Darkness Under Anaerobic Conditions, *Appl. Environ. Microb.* 53(9): 2151–2158.

- Richardson, S. D., Plewa, M. J., Wagner, E. D., Schoeny, R. and DeMarini, D. M. (2007). Occurrence, genotoxicity, and carcinogenicity of regulated and emerging disinfection by-products in drinking water: a review and roadmap for research., *Mutat. Res-Rev. Mutat.* 636(1-3): 178–242.
- Rickard, A., Leach, S., Hall, L., Buswell, C., High, N. and Handley, P. (2002). Phylogenetic relationships and coaggregation ability of freshwater biofilm bacteria, *Appl. Environ. Microb.* 68(7): 3644–3650.
- Rickard, A., McBain, A., Ledder, R., Handley, P. and Gilbert, P. (2003a). Coaggregation between freshwater bacteria within biofilm and planktonic communities, *FEMS Microbiol. Lett.* 220(1): 133–140.
- Rickard, Alexander H, Gilbert, P., High, N. J., Kolenbrander, P. E. and Handley, P. S. (2003b). Bacterial coaggregation: an integral process in the development of multi-species biofilms, *Trends Microbiol.* 11(2): 94–100.
- Rickard, Alexander H., McBain, A. J., Stead, A. T. and Gilbert, P. (2004). Shear Rate Moderates Community Diversity in Freshwater Biofilms, *Appl. Environ. Microb.* 70(12): 7426–7435.
- Rinta-Kanto, J., Lehtola, M., Vartiainen, T. and Martikainen, P. (2004). Rapid enumeration of virus-like particles in drinking water samples using SYBR green I-staining, *Water Res.* 38(10): 2614–2618.
- Ristoiu, D., von Gunten, U., Mocan, A., Chira, R., Siegfried, B., Haydee Kovacs, M. and Vancea, S. (2009). Trihalomethane formation during water disinfection in four water supplies in the Somes river basin in Romania, *Environ. Sci. Pollut. R. (international)* 16 Suppl 1: S55–65.
- Roberts, J. A., Cumberland, P., Sockett, P. N., Wheeler, J., Rodrigues, L. C., Sethi, D., Roderick, P. J. and Infectious Intestinal Disease Study Executive. (2003). The study of infectious intestinal disease in England: socio-economic impact, *Epidemiol. Infect.* 130(1): 1–11.
- Rochex, A., Godon, J.-J., Bernet, N. and Escudié, R. (2008). Role of shear stress on composition, diversity and dynamics of biofilm bacterial communities, *Water Res.* 42(20): 4915–4922.
- Roeder, R., Lenz, J., Tarne, P., Gebel, J., Exner, M. and Szewzyk, U. (2010). Long-term effects of disinfectants on the community composition of drinking water biofilms, *Int. J. Hyg. Envir. Heal.* 213(3): 183–189.
- Rogers, J., Dowsett, A. B., Dennis, P. J., Lee, J. V. and Keevil, C. W. (1994). Influence of Plumbing Materials on Biofilm Formation and Growth of *Legionella pneumophila* in Potable Water Systems, *Appl. Environ. Microb.* 60(6): 1842–1851.
- Rogers, Y.H. and Venter, J.C. (2005). Massively parallel sequencing, *Nature.* 437:326-327
- Rompre, A., Servais, P., Baudart, J., de-Roubin, M. and Laurent, P. (2002). Detection and enumeration of coliforms in drinking water: current methods and emerging approaches, *J. Microbiol. Meth.* 49(1): 31–54.
- Rossmann, L. A., Clark, R. M. and Grayman, W. M. (1994). Modeling Chlorine Residuals in Drinking-Water Distribution Systems, *J. Environ. Eng.* 120(4): 803–820.
- Russell, S. (1994). *Turbidity: A guide to measurement in water applications*, WRc Instrument Handbooks.
- Sammon, N. B., Harrower, K. M., Fabbro, L. D. and Reed, R. H. (2010). Incidence and Distribution of Microfungi in a Treated Municipal Water Supply System in Sub-Tropical

- Australia, *International Journal of Environmental Research and Public Health* 7(4): 1597–1611.
- Sammon, N. B., Harrower, K. M., Fabbro, L. D. and Reed, R. H. (2011). Three Potential Sources of Microfungi in a Treated Municipal Water Supply System in Sub-Tropical Australia, *International Journal of Environmental Research and Public Health* 8(3): 713–732.
- Santegoeds, C., Muyzer, G. and de Beer, D. (1998). Biofilm dynamics studied with microsensors and molecular techniques, *Water Sci. Technol.* 37(4-5): 125–129.
- Santo Domingo, J. W., Meckes, M. C., Simpson, J. M., Sloss, B. and Reasoner, D. J. (2003). Molecular characterization of bacteria inhabiting a water distribution system simulator, *Water science and technology: a journal of the International Association on Water Pollution Research* 47(5): 149–154.
- Sauer, K. (2003). The genomics and proteomics of biofilm formation, *Genome Biol.* 4(6):219.0-219.5.
- Schmid, M., Thill, A., Purkhold, U., Walcher, M., Bottero, J. Y., Ginestet, P., Nielsen, P. H., Wuertz, S. and Wagner, M. (2003). Characterization of activated sludge flocs by confocal laser scanning microscopy and image analysis, *Water Res.* 37(9): 2043–2052.
- Schulze-Röbbecke, R., Janning, B. and Fischeder, R. (1992). Occurrence of mycobacteria in biofilm samples, *Tubercle and lung disease: the official journal of the International Union against Tuberculosis and Lung Disease* 73(3): 141–144.
- Schwartz, J., Levin, R. and Hodge, K. (1997). Drinking Water Turbidity and Pediatric Hospital Use for Gastrointestinal Illness in Philadelphia, *Epidemiology* 8(6): 615–620.
- Schwartz, T; Hoffman, S and Obst, U. (1998). Formation and bacterial composition of young, natural biofilms obtained from public bank-filtered drinking water systems., *Water Res.* 32: 2787–2797.
- Schwartz, J., Levin, R. and Goldstein, R. (2000). Drinking water turbidity and gastrointestinal illness in the elderly of Philadelphia, *J. Epidemiol. Com. H.* 54(1): 45–51.
- Scottish Executive, S. A. H. (2009). *Drinking Water Quality in Scotland 2008: Annual Report by the Drinking Water Quality Regulator* (Report), Retrieved June 5, 2013, from <http://www.scotland.gov.uk/Publications/2009/07/23170951/4>
- Sekar, R., Deines, P., Machell, J., Osborn, A. M., Biggs, C. A. and Boxall, J. B. (2012). Bacterial water quality and network hydraulic characteristics: a field study of a small, looped water distribution system using culture-independent molecular methods, *J. Appl. Microbiol.* 112(6): 1220–1234.
- Seth, A., Bachmann, R., Boxall, J., Saul, A. and Edyvean, R. (2003). Characterisation of Materials Causing Discolouration in Potable Water Systems, *Water Sci. Technol.* 49(2): 27–32.
- Shapiro, J. (1998). Thinking about bacterial populations as multicellular organisms, *Annu. Rev. Microbiol.* 52: 81–104.
- Sharpe, R. L., Smith, C. J., Biggs, C. A. and Boxall, J. B. (2010). Pilot scale laboratory investigations into the impact of steady state conditioning flow on potable water discolouration., *Water Distribution Systems Analysis Conference (13th WDSA). Tucson, Arizona, USA.*

- Sharpe, R. L. (2012). *Laboratory investigations into processes causing discoloured potable water*. Ph.D Thesis, The University of Sheffield, UK.
- Sheng, G., Yu, H. and Yu, Z. (2005). Extraction of extracellular polymeric substances from the photosynthetic bacterium *Rhodospseudomonas acidophila*, *Appl. Microbiol. Biot.* 67(1): 125–130.
- Shumi, W., Lim, J., Nam, S., Kim, S., Cho, K., Yoon, J. and Park, S. (2009). Fluorescence Imaging of the Spatial Distribution of Ferric Ions over Biofilms Formed by *Streptococcus mutans* under Microfluidic Conditions, *Biochip J.* 3(2): 119–124.
- Sibille, I., Sime-Ngando, T., Mathieu, L. and Block, J. (1998). Protozoan bacterivory and *Escherichia coli* survival in drinking water distribution systems, *Appl. Environ. Microb.* 64(1): 197–202.
- Silbaq, F. (2009). Viable ultramicrocells in drinking water, *J. Appl. Microbiol.* 106(1): 106–117.
- Silhan, J., Corfitzen, C. and Albrechtsen, H. (2006). Effect of temperature and pipe material on biofilm formation and survival of *Escherichia coli* in used drinking water pipes: a laboratory-based study, *Water Sci. Technol.* 54(3): 49–56.
- Simoës, M., Pereira, M. and Vieira, M. (2003). Monitoring the effects of biocide treatment of *Pseudomonas fluorescens* biofilms formed under different flow regimes, *Water Sci. Technol.* 47(5): 217–223.
- Simoës, M., Pereira, M. and Vieira, M. (2005). Effect of mechanical stress on biofilms challenged by different chemicals, *Water Res.* 39(20): 5142–5152.
- Simoës, L., Azevedo, N., Pacheco, A., Keevil, C. and Vieira, M. (2006). Drinking water biofilm assessment of total and culturable bacteria under different operating conditions, *Biofouling* 22(2): 91–99.
- Simoës, M., Cleto, S., Pereira, M. and Vieira, M. (2007). Influence of biofilm composition on the resistance to detachment, *Water Sci. Technol.* 55(8-9): 473–480.
- Sly, L., Hodgkinson, M. and Arunpairojana, V. (1988). Effect Of Water Velocity On The Early Development Of Manganese-Depositing Biofilm In A Drinking-Water Distribution-System, *FEMS Microbiol. Ecol.* 53(3-4): 175–186.
- Smith, S., Ta, T., Holt, D., Delanoue, A., Colbourne, J., Chamberlain, A. and Lloyd, B. (1999). A pipeline testing facility for the examination of pipe-wall deposits and red-water events in drinking water, *J. Chart. Inst. Water E.* 13(1): 7–15.
- Smith, C.J et al. (2005). T-Align, a web-based tool for comparison of multiple terminal restriction fragment length polymorphism profiles., *FEMS Microbiol. Ecol.* 54: 375–380.
- Spoering, A. and Lewis, K. (2001). Biofilms and planktonic cells of *Pseudomonas aeruginosa* have similar resistance to killing by antimicrobials, *J. Bacteriol.* 183(23): 6746–6751.
- Srinivasan, S., Harrington, G. W., Xagorarakis, I. and Goel, R. (2008). Factors affecting bulk to total bacteria ratio in drinking water distribution systems, *Water Res.* 42(13): 3393–3404.
- Staley, J. and Konopka, A. (1985). Measurement of insitu activities of nonphotosynthetic microorganisms in aquatic and terrestrial habitats, *Annu. Rev. Microbiol.* 39: 321–346.

- Staudt, C., Horn, H., Hempel, D. and Neu, T. (2004a). Volumetric measurements of bacterial cells and extracellular polymeric substance glycoconjugates in biofilms, *Biotechnol. Bioeng.* 88(5): 585–592.
- Stewart, P. S., Roe, F., Rayner, J., Elkins, J. G., Lewandowski, Z., Ochsner, U. A. and Hassett, D. J. (2000). Effect of Catalase on Hydrogen Peroxide Penetration into *Pseudomonas aeruginosa* Biofilms, *Appl. Environ. Microb.* 66(2): 836–838.
- Stewart, Philip S., Murga, R., Srinivasan, R. and de Beer, D. (1995). Biofilm structural heterogeneity visualized by three microscopic methods, *Water Res.* 29(8): 2006–2009.
- Stoodley, P., DEBeer, D. and Lewandowski, Z. (1994). Liquid flow in biofilm systems, *Appl. Environ. Microb.* 60(8): 2711–2716.
- Stoodley, P., Boyle, J., DeBeer, D. and Lappin-Scott, H. (1999a). Evolving perspectives of biofilm structure, *Biofouling* 14(1): 75-90.
- Stoodley, P., Dodds, I., Boyle, J. and Lappin-Scott, H. (1999b). Influence of hydrodynamics and nutrients on biofilm structure, *J. Appl. Microbiol.* 85: 19S–28S.
- Stoodley, P., Lewandowski, Z., Boyle, J. and Lappin-Scott, H. (1999c). Structural deformation of bacterial biofilms caused by short-term fluctuations in fluid shear: An in situ investigation of biofilm rheology, *Biotechnol. Bioeng.* 65(1): 83–92.
- Stoodley, P., Hall-Stoodley, L. and Lappin-Scott, H. (2001a). Detachment, surface migration, and other dynamic behavior in bacterial biofilms revealed by digital time-lapse imaging, *Microbial Growth in Biofilms, PT B* 337: 306–318.
- Stoodley, P., Jacobsen, A., Dunsmore, B., Purevdorj, B., Wilson, S., Lappin-Scott, H. and Costerton, J. (2001b). The influence of fluid shear and AlCl₃ on the material properties of *Pseudomonas aeruginosa* PAO1 and *Desulfovibrio* sp. EX265 biofilms, *Water Sci. Technol.* 43(6): 113–120.
- Stoodley, P; Cargo, R; Rupp, C.J; Wilson, S and Klapper, I. (2002). Biofilm material properties as related to shear-induced deformation and detachment phenomena., *J Ind. Microbiol. Biot.* 29: 361–367.
- Sutherland, I. W. (2001a). The biofilm matrix - an immobilized but dynamic microbial environment, *Trends Microbiol.* 9(5): 222–227.
- Sutherland, I. W. (2001b). Biofilm exopolysaccharides: a strong and sticky framework, *Microbiology* 147(1): 3–9.
- Szewzyk, Ulrich and Schink, B. (1988). Surface Colonization by and Life Cycle of *Pelobacter acidigallici* Studied in a Continuous-flow Microchamber, *J. Gen. Microbiol.* 134(1): 183–190.
- Szewzyk, U, Szewzyk, R., Manz, W. and Schleifer, K.-H. (2000). Microbiological Safety of Drinking Water., *Annu. Rev. Microbiol.* 54: 81–127.
- Telgmann, U., Horn, H. and Morgenroth, E. (2004). Influence of growth history on sloughing and erosion from biofilms, *Water Res.* 38(17): 3671–3684.
- Tinker, S., Moe, C., Klein, M., Flanders, W., Uber, J., Amirtharajah, A., Singer, P. and Tolbert, P. (2009). Drinking water residence time in distribution networks and emergency department visits for gastrointestinal illness in Metro Atlanta, Georgia, *J. Water Health* 7(2): 332–343.

- Tokajian, S., Hashwa, F., Hancock, I. and Zalloua, P. (2005). Phylogenetic assessment of heterotrophic bacteria from a water distribution system using 16S rDNA sequencing, *Can. J. Microbiol.* 51(4): 325–335.
- Tolker-Nielsen and Molin. (2000). Spatial Organization of Microbial Biofilm Communities, *Microb. Ecol.* 40(2): 75–84.
- Torvinen, E., Lehtola, M., Martikainen, P. and Miettinen, I. (2007). Survival of Mycobacterium avium in drinking water biofilms as affected by water flow velocity, availability of phosphorus, and temperature, *Appl. Environ. Microb.* 73(19): 6201–6207.
- Trulear, M. G. and Characklis, W. G. (1982). Dynamics of biofilm processes, *J. Water Pollut. Con. F.* : 1288–1301.
- Tsvetanova, Z. G. and Dimitrov, D. N. (2012). Biofilms and bacteriological water quality in a domestic installation model simulating daily drinking water consumption, *Wa. Sci. Technol.* 12(6): 720.
- Uhl, W., Schaule, G. and Gimbel, R. (2001). Preventing bacterial regrowth in old distribution systems without disinfection., *Water Supply 2*: 259–266.
- UKWIR. (2003). *National Database of Mains Failures 2003* (No. 23/3G/05/7).
- US EPA. (2004). Potential Contamination Due to Cross-Connection and Backflow and the Associated Health Risks. Retrieved June 17, 2013, from http://www.epa.gov/safewater/disinfection/tcr/pdfs/issuepaper_tcr_crossconnection-backflow.pdf
- US EPA. (2009). *2009 Edition of the Drinking Water Standards and Health Advisories*, Washington, DC.
- Vaerewijck, M. J. ., Huys, G., Palomino, J. C., Swings, J. and Portaels, F. (2005). Mycobacteria in drinking water distribution systems: ecology and significance for human health., *FEMS Microbio. Rev.* 29: 911–934.
- Valster, R. M., Wullings, B. A., Bakker, G., Smidt, H. and Kooij, D. van der. (2009). Free-Living Protozoa in Two Unchlorinated Drinking Water Supplies, Identified by Phylogenetic Analysis of 18S rRNA Gene Sequences, *Appl. Environ. Microb.* 75(14): 4736–4746.
- van der Kooij, D. (1992). Assimilable organic-carbon as an indicator of bacterial regrowth, *J. Am. Water Works Ass.* 84(2): 57–65.
- van der Kooij, D., Veenendaal, H., Baarslorist, C., Vanderklift, D. and Drost, Y. (1995). Biofilm formation on surfaces of glass and teflon exposed to treated water, *Water Res.* 29(7): 1655–1662.
- van der Kooij, D., van Lieverloo, J., Schellart, J. and Hiemstra, P. (1999). Distributing drinking water without disinfectant: highest achievement or height of folly?, *J. Water Serv. Res. Tec.* 48(1): 31–37.
- van der Kooij, D., Veenendaal, H., Slaats, N. P. G. and Vonk, D. (2002). Biofilm formation and multiplication of Legionella on synthetic pipe materials in contact with treated water under static and dynamic conditions, In *Biofilm Highlights*, Washington, DC: ASM, pp. 86–89.
- van der Wende, E., Characklis, W. and Smith, D. (1989). Biofilms and bacterial drinking-water quality, *Water Res.* 23(10): 1313–1322.

- van Kempen, G. M. P. and van Vliet, L. J. (2001). Prefiltering: Reducing the noise sensitivity of non-linear image restoration algorithms, *Fourth Quinquennial Review 1996* : 411–422.
- van Lieverloo, J. H. M., Bosboom, D. W., Bakker, G. L., Brouwer, A. J., Voogt, R. and De Roos, J. E. M. (2004). Sampling and quantifying invertebrates from drinking water distribution mains, *Water Res.* 38(5): 1101–1112.
- van Loosdrecht, M., Lyklema, J., Norde, W. and Zehnder, A. (1990). Influence of interfaces on microbial activity, *Microbiol. Rev.* 54(1): 75–87.
- Vieira, M. and Melo, L. (1999). Intrinsic kinetics of biofilms formed under turbulent flow and low substrate concentrations, *Bioprocess Eng.* 20(4): 369–375.
- Vieira, M., Oliveira, R., Melo, L., Pinheiro, M. and Martins, V. (1993). Effect of metallic-ions on the adhesion of biofilms formed by *Pseudomonas fluorescens*, *Colloid Surface B* 1(2): 119–124.
- Visick, K. and Fuqua, C. (2005). Decoding microbial chatter: Cell-cell communication in bacteria, *J. Bacteriol.* 187(16): 5507–5519.
- Volk, C. J. and LeChevallier, M. W. (1999). Impacts of the reduction of nutrient levels on bacterial water quality in distribution systems, *Appl. Environ. Microb.* 65(11): 4957–4966.
- Vreeburg, J. and Boxall, J. (2007). Discolouration in potable water distribution systems: A review, *Water Res.* 41(3): 519–529.
- Vreeburg, J. H. G., Schippers, D., Verberk, J. Q. J. C. and van Dijk, J. C. (2008). Impact of particles on sediment accumulation in a drinking water distribution system, *Water Res.* 42(16): 4233–4242.
- Vreeburg, J. H. G., Blokker, E. J. M., Horst, P. and van Dijk, J. C. (2009). Velocity-based self-cleaning residential drinking water distribution systems, *Wa. Sci. Technol.* 9(6): 635.
- Vroom, J., De Grauw, K., Gerritsen, H., Bradshaw, D., Marsh, P., Watson, G., Birmingham, J. and Allison, C. (1999). Depth penetration and detection of pH gradients in biofilms by two-photon excitation microscopy, *Appl. Environ. Microb.* 65(8): 3502–3511.
- Wagner, M., Ivleva, N. P., Haisch, C., Niessner, R. and Horn, H. (2009). Combined use of confocal laser scanning microscopy (CLSM) and Raman microscopy (RM): Investigations on EPS - Matrix, *Water Res.* 43(1): 63–76.
- Wai, S., Mizunoe, Y., Takade, A., Kawabata, S. and Yoshida, S. (1998). *Vibrio cholerae* O1 strain TSI-4 produces the exopolysaccharide materials that determine colony morphology, stress resistance, and biofilm formation, *Appl. Environ. Microb.* 64(10): 3648–3655.
- Walski, T. W. (2003). *Advanced water distribution modelling and management.*, Waterbury, Conn: Haestad Press.
- Wang, Z., Kim, J. and Seo, Y. (2012). Influence of Bacterial Extracellular Polymeric Substances on the Formation of Carbonaceous and Nitrogenous Disinfection Byproducts, *Environ. Sci. Technol.* 46(20): 11361–11369.
- Wang, H., Masters, S., Hong, Y., Stallings, J., Falkinham, J.O., Edwards, M.A. and Pruden, A. (2012). Effect of Disinfectant, Water Age, and Pipe Material on Occurrence and Persistence of *Legionella*, *Mycobacteria*, *Pseudomonas aeruginosa*, and Two Amoebas. *Environ. Sci. Technol.*, 46 (21):11566-11574.

- Watnick, P. and Kolter, R. (2000). Biofilm, city of microbes, *J. Bacteriol.* 182(10): 2675–2679.
- Wei, J., Ye, B., Wang, W., Yang, L., Tao, J. and Hang, Z. (2010). Spatial and temporal evaluations of disinfection by-products in drinking water distribution systems in Beijing, China, *The Science of the total environment* 408(20): 4600–4606.
- Weiner, R., Langille, S. and Quintero, E. (1995). Structure, function and immunochemistry of bacterial exopolysaccharides, *J. Ind. Microbiol.* 15(4): 339–346.
- Whiley, H., Keegan, A., Giglio, S. and Bentham, R. (2012). Mycobacterium avium complex – the role of potable water in disease transmission, *J. Appl. Microbiol.* 113(2)223-232.
- White, D. C., Sutton, S. D. and Ringelberg, D. B. (1996). The genus *Sphingomonas*: physiology and ecology, *Curr. Opin. Biot.* 7(3): 301–306.
- White, C., Tancos, M. and Lytle, D. A. (2011). Microbial Community Profile of a Lead Service Line Removed from a Drinking Water Distribution System, *Appl. Environ. Microbiol.* 77(15): 5557–5561.
- WHO. (2000). *The World Health Report: Making a difference*, Geneva.
- WHO. (2002). Water, Sanitation and Hygiene. Retrieved October 6, 2009, from http://www.who.int/water_sanitation_health/en/
- WHO. (2004). *Guidelines for Drinking-water Quality*, 3rd ed.
- WHO. (2011). *Guidelines for Drinking-water Quality*, 4th ed.
- WHO and OECD. (2003). *Assessing Microbial Safety of Drinking Water: Improving Approaches and Methods*, IWA.
- WHO and UNICEF. (2000). *Global water supply and sanitation assessment 2000 report*, USA. Retrieved May 12, 2012, from www.who.int/water_sanitation_health
- WHO and UNICEF. (2012). WHO | Progress on drinking water and sanitation, *WHO*. Retrieved June 5, 2013, from http://www.who.int/water_sanitation_health/publications/2012/jmp_report
- Wielen, V. D., J. P. W. J., Voost, S. and van der Kooij, D. (2009). Ammonia-Oxidizing Bacteria and Archaea in Groundwater Treatment and Drinking Water Distribution Systems, *Appl. Environ. Microb.* 75(14): 4687–4695.
- Wijeyekoon, S., Mino, T., Satoh, H. and Matsuo, T. (2000). Growth and novel structural features of tubular biofilms produced under different hydrodynamic conditions, *Water Sci. Technol.* 41(4-5): 129–138.
- Williams, M. and Braun-Howland, E. (2003). Growth of *Escherichia coli* in model distribution system biofilms exposed to hypochlorous acid or monochloramine, *Appl. Environ. Microb.* 69(9): 5463–5471.
- Williams, M., Domingo, J., Meckes, M., Kelty, C. and Rochon, H. (2004). Phylogenetic diversity of drinking water bacteria in a distribution system simulator, *J. Appl. Microbiol.* 96(5): 954–964.
- Williams, M., Domingo, J. and Meckes, M. (2005). Population diversity in model potable water biofilms receiving chlorine or chloramine residual, *Biofouling* 21(5-6): 279–288.
- Wimpenny, J., Manz, W. and Szewzyk, U. (2000). Heterogeneity in biofilms, *FEMS Microbiol. Rev.* 24(5): 661–671.

- Wingender, J., Grobe, S., Fiedler, S. and Flemming, H. (1999). The effect of extracellular polysaccharides on the resistance of *Pseudomonas aeruginosa* to chlorine and hydrogen peroxide, *Biofilms in the Aquatic Environment* (242): 93–100.
- Wright, J., Gundry, S. and Conroy, R. (2004). Household drinking water in developing countries: a systematic review of microbiological contamination between source and point-of-use., *Trop. Med. Int. Health* 9: 106–107.
- Wu, J., N. Noui-Mehidi, C. Grainger, B. Nguyen, P. Mathes, G. Ryan and A. Jayaratne (2003). Particles in Water Distribution System – 6th progress report. Particle sediment modelling: PSM software
- Wu, C.G.; Wu, Y.; Gao, J.L. and Zhao, Z.L. (2005) Research on water detention times in water supply network. *Journal of Harbin Institute of Technology*. 12(1):188-193
- Wullings, B. A., Bakker, G. and van der Kooij, D. (2011). Concentration and Diversity of Uncultured *Legionella* Spp. in Two Unchlorinated Drinking Water Supplies with Different Concentrations of Natural Organic Matter, *Appl. Environ. Microb.* 77(2): 634–641.
- Xue, Z., Hessler, C. M., Panmanee, W., Hassett, D. J. and Seo, Y. (2013). *Pseudomonas aeruginosa* inactivation mechanism is affected by capsular extracellular polymeric substances reactivity with chlorine and monochloramine, *FEMS Microbiol. Ecol.* 83(1): 101–111.
- Yang, X., Beyenal, H., Harkin, G. and Lewandowski, Z. (2001). Evaluation of biofilm image thresholding methods, *Water Res.* 35(5): 1149–1158.
- Yee, R. B. and Wadowsky, R. M. (1982). Multiplication of *Legionella pneumophila* in unsterilized tap water., *Appl. Environ. Microb.* 43(6): 1330–1334.
- Yu, J., Kim, D. and Lee, T. (2010). Microbial diversity in biofilms on water distribution pipes of different materials, *Water Sci. Technol.* 61(1): 163–171.
- Zacheus, O., Lehtola, M., Korhonen, L. and Martikainen, P. (2001). Soft deposits, the key site for microbial growth in drinking water distribution networks, *Water Res.* 35(7): 1757–1765.
- Zhang, M., Liu, W., Nie, X., Li, C., Gu, J. and Zhang, C. (2012). Molecular Analysis of Bacterial Communities in Biofilms of a Drinking Water Clearwell, *Microbes Environ.* 27(4): 443–448.
- Zhang, T. and Bishop, P. (1994). Structure, activity and composition of biofilms, *Water Sci. Technol.* 29(7): 335–344.
- Zhang, X., Bishop, P. and Kinkle, B. (1999). Comparison of extraction methods for quantifying extracellular polymers in biofilms, *Water Sci. Technol.* 39(7): 211–218.
- Zhang, T. and Fang, H. (2001). Quantification of extracellular polymeric substances in biofilms by confocal laser scanning microscopy. *Biotech. Lett.* 23: 405–409.
- Zhou, J., Bruns, M. A. and Tiedje, J. M. (1996). DNA recovery from soils of diverse composition, *Appl. Environ. Microb.* 62(2): 316–322.
- Ziebuhr, W., Krimmer, V., Rachid, S., Lossner, I., Gotz, F. and Hacker, J. (1999). A novel mechanism of phase variation of virulence in *Staphylococcus epidermidis*: evidence for control of the polysaccharide intercellular adhesin synthesis by alternating insertion and excision of the insertion sequence element IS256, *Mol. Microbiol.* 32(2): 345–356.

Appendices

Appendix 1 Grant Bids, Scientific Dissemination and Awards

A1.1 Grants

NERC Biomolecular Analysis Facility (NBAF): Small Projects Competition

“NBAF569 – Microbial Communities in Biofilms of the Drinking Water Distribution System “

Applied for and awarded £2588 by NERC to carry out proposed molecular analysis work within the NERC Biomolecular Analysis Facility (NBAF), Sheffield. This grant was written by me as co-investigator, with input from Prof. Joby Boxall (named as the principal investigator) and Prof. Mark Osborn.

Conference attendance was financially assisted, in part, by the Society for General Microbiology:

SGM Student Travel Grant

Applied for and received £180 towards attendance at the SGM Spring Conference 2010, Edinburgh, U.K.

SGM Scientific Meetings Grant

Applied for and granted £500 towards travel in order to present at the IWA Biofilms Conference 2011, Shanghai, China.

A1.2 International Conferences

Fish, K.E., Sharpe, R.L., Green, N.H., Osborn, A.M. and Boxall, J.B. (2011)

Visualising and Quantifying the Matrix of Drinking Water Biofilms

Oral Presentation and Paper

Proceedings of IWA Biofilm2011: Processes in Biofilms

27th-30th October, Shanghai, China

Fish, K., Green, N., Collins, R., Osborn, A.M. and Boxall, J.B. (2012)

Imaging and Characterising the Matrix of Potable Water Biofilms

Poster Presentation

Society for General Microbiology Spring Conference 2012

26th-29th March, Dublin, Ireland

Fish, K.E., Douterelo, I., Osborn, A.M. and Boxall, J.B. (2012)

Characterising the Physical Structure and Microbial Community Structure of Drinking Water Biofilms

Poster Presentation

14th International Symposium on Microbial Ecology

19th-24th August, Copenhagen, Denmark

Fish, K., Collins, R., Sharpe, R.L., Osborn, A.M. and Boxall, J.B. (2012)

The Structure and Stability of Drinking Water Biofilms

Oral Presentation and Paper

Proceedings of the 14th Water Distribution Systems Analysis

24th-27th September, Adelaide, Australia

The SGM Spring Conference 2010, "Systems, Mechanisms and Micro-organisms" (Edinburgh, Scotland, UK) and the Biofilms 4th International Conference 2010 (Winchester, England, UK) were also attended.

A1.3 Research Symposiums and Meetings

Fish, K.E., Osborn, A.M and Boxall, J.B. (2010)

The Microbiology of Drinking Water Distribution Systems

Oral presentation at the PWG Conference

9th February, The University of Sheffield, UK

Fish, K.E., Osborn, A.M and Boxall, J.B. (2011)

Structure and Stability of Drinking Water Biofilms: The Matrix

Oral presentation at the PWG Conference

11th March, The University of Sheffield, UK

Fish, K.E. (2011)

Drinking Water Biofilms: Structure and Stability

Departmental Seminar, Civil and Structural Engineering

6th October, The University of Sheffield, UK

Fish, K.E. (2012)

The Journey to Safe Drinking Water

Seminar lecture for the Water Group within Engineers without Borders

24th April, Kroto Research Institute, UK

Fish, K.E., Osborn, A.M and Boxall, J.B. (2012)

The Structure of Drinking Water Biofilms

Oral presentation at PODDS Steering Meeting

24th April, The University of Sheffield, UK

Fish, K.E., Osborn, A.M and Boxall, J.B. (2012)

Characterising the Physical Structure of Drinking Water Biofilms

Oral presentation at the Pipe Dreams Conference Day

30th August, The University of Sheffield, UK

Fish, K.E., Osborn, A.M and Boxall, J.B. (2013)

The Impact of Hydraulic Regime upon Biofilm Structure

Oral presentation at the Pipe Dreams Conference Day

22nd July, The University of Sheffield, UK

Throughout this PhD progress and results have also presented at a series of research meetings as part of the Microbiology in Urban Water Systems (MUSE) and Pipe Dreams research groups. The diagram of biofilm development presented in this thesis (Figure 1.5) was copyrighted in 2010. SEM images from this research were used in the promotional Sheffield University Booklet “Water and Environment Sustainability Research” (unaccredited).

A1.4 Awards

14th WDSA Conference (Adelaide, Australia)

Awarded best paper presentation by the convenor of WDSA 2012 for the paper entitled “The Structure and Stability of Drinking Water Biofilms” (Fish *et al.*, 2012).

PWG Conference 2012 (Sheffield, UK)

Awarded best conference paper of the year by the PWG committee for the paper entitled “Visualising and Quantifying the Matrix of Drinking Water Biofilms” (Fish *et al.*, 2011).

Appendix 2 Supporting data for turbidity analysis

Water quality parameters of the fresh tank water introduced before the mobilization phase of each loop were compared to ensure that there were no differences between the "Pre-Flush" starting points of each loop. The turbidity, iron and manganese raw data is shown in Table A2.1 for the "Pre-Flush" of each loop during the SS trial.

Table A 2.1 Comparison of turbidity in "Pre-Flush" water samples during the mobilization phase of the SS experiment.

Loop	Turbidity (NTU) ^A				Iron ($\mu\text{g l}^{-1}$)				Manganese ($\mu\text{g l}^{-1}$)			
	A	B	C	Mean (StDev.)	A	B	C	Mean (StDev.)	A	B	C	Mean (StDev.)
1	0.64	0.51	0.54	0.56 (0.07)	45	43	45	44.33 (1.15)	6.2	5.8	6.1	6.03 (0.21)
2	0.66	0.61	0.70	0.66 (0.05)	56	54	60	56.67 (3.06)	5.8	5.8	18.0	9.87 (7.04)
3	0.43	0.58	0.81	0.61 (0.19)	48	36	36	40.00 (6.93)	10	11	11	10.67 (0.58)

^ATurbidity recorded for three replicates using the portable turbidimeter.

Appendix 3 Buffers and Solutions

A3.1 Phosphate Buffer Saline (PBS)

2 mM Na_3PO_4 (tri sodium phosphate); 4 mM NaH_2PO_4 (mono sodium phosphate); 9 mM NaCl (sodium chloride); 1 mM KCl (potassium chloride). Autoclaved and stored at room temperature.

A3.2 Reagents for DNA Extraction

SET Buffer

0.75 M sucrose , 40 mM EDTA (Ambion, Warrington, UK); 50 mM Tris-HCl, pH 9.0 (Sigma Aldrich Co.,UK. Autoclaved and stored at room temperature.

CTAB/NaCl solution

0.7 M NaCl; 1% (w/v) CTAB (Hexadecyltrimethyl ammonium bromide; Sigma Aldrich Co., UK) made up in distilled, deionised water.

A3.3 Tris acetate EDTA (TAE) buffer for gel electrophoresis

50x stock solution

2 M Tris; 0.05 M EDTA (pH 8.0); 1 M glacial acetic acid.

Appendix 4 Internal Size Standards

A4.1 GeneScan™ 500 ROX™ (GS500)

The GS500 ROX size standard is comprised of double stranded DNA sequences (of which only one strand was labelled) of a range of sizes, which produces an electropherogram (Figure A 4.1) of defined, single peaks of each size (following denaturation and capillary electrophoresis as detailed in section 3.4.5.1). The size of each peak is automatically assigned by GeneMapper® when the GS500 size standard is selected, although all the size standard profiles were also checked manually. Due to the fluorescent flare at the beginning of each T-RFLP profile only T-RFs within the range 50-500 nt were analysed.

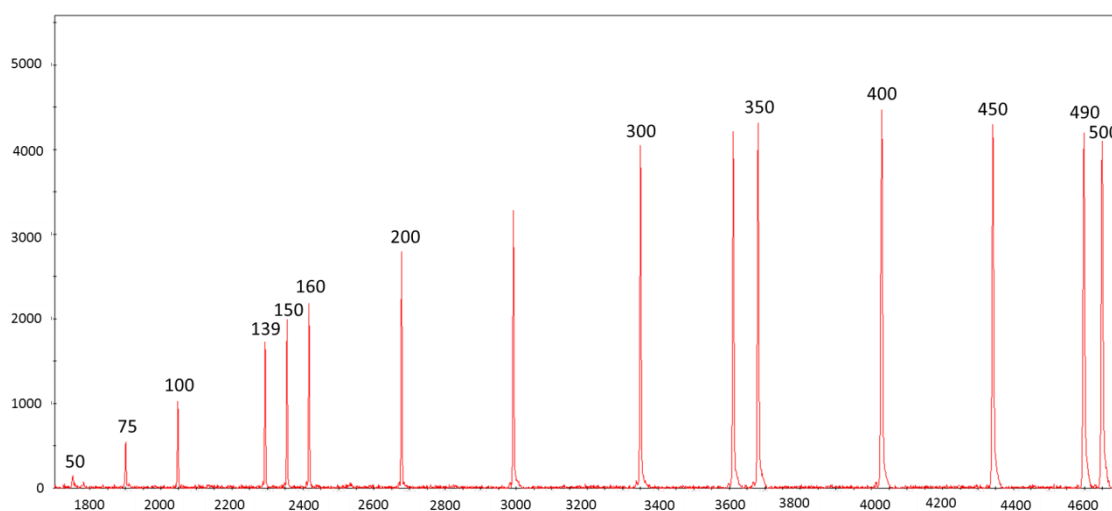


Figure A 4.1 Electropherogram of the ROX™ GeneScan™ 500 size standard. Numbers above the peaks refer to the size in nucleotides, although not labelled by GeneMapper® the x-axis represents the data points and the y-axis is the fluorescence intensity (AU).

A4.2 GeneScan™ 2500 ROX™ (GS2500)

The GS2500 size standard is comprised of a range of differently sized double stranded DNA sequences, with each strand being labelled. Therefore after denaturation (94 °C for 3 minutes) single DNA strands, each of which are labelled, are present for each DNA sequence. This led to the presence of double peaks of each sequence in the electropherogram (Fig A2.2) produced by capillary electrophoresis. GeneMapper® is unable to automatically assign sizes to these peaks, therefore every ARISA size standard profile was manually labelled to ensure consistency between samples. Although GS2500 theoretically sizes between 94 nt and 2500 nt, when samples are denatured the linear range of the size standard is reduced. Following correspondence with Applied Biosystems (UK) and liaison with the NBAF advisors it was decided that the most accurate way to assess the datasets was to limit the analysis to the last size marker reliably resolved, which was found to be 827 nt.

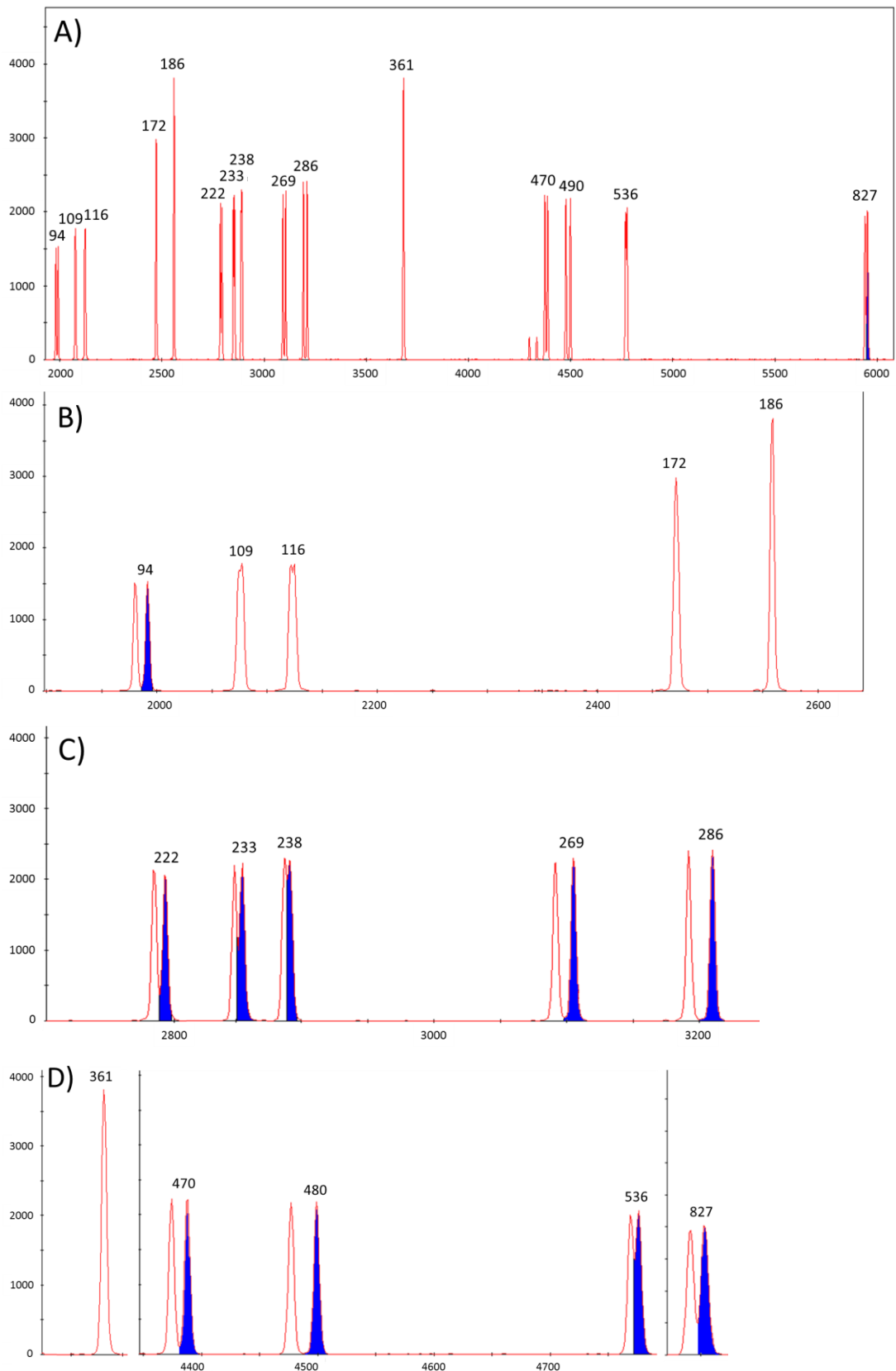


Figure A 4.2 Electropherograms showing the profile of ROX™ GeneScan™ 2500. Numbers above the peaks refer to the size in nucleotides, although not labelled by GeneMapper® the x-axis represents the data points and the y-axis is the fluorescence intensity (AU). Blue areas show when the peak could be split into two, in all cases the size was assigned to the right hand peak. A) The whole size standard profile; B) Close up of peaks between 94-186 nucleotides; C) Close up of peaks between 222-286 nucleotides; D) Close up of peaks between 361-827 nucleotides, x-axis not continuous in final panel.

Appendix 5 Review of extraction, quantification and chemical composition techniques

A range of techniques applied to analyse the EPS of biofilms were reviewed and summarised in Table A 5.1, the techniques which were likely to be the most suitable and feasible with the drinking water biofilm samples were selected for preliminary analysis, highlighted in bold in the table and outlined in section 4.4.

Table A 5.1 Summary of the extraction, quantification and chemical assay approaches used in the literature to study, analyse and quantify the cellular and biochemical composition of biofilms. Methods shown in bold were tested in this study.

Aim/Process	Method	Notes	References
Extraction of EPS From Biofilm	Cation Exchange Resin (CER)	Used in drinking water samples from a reactor; reported to increase extraction yield and quality from biofilms from a wide range of environments, although limited comparison with other methods	Jahn & Nielson, 1995; Frolund <i>et al.</i> , 1996; McSwain <i>et al.</i> , 2005; Denkhaus <i>et al.</i> , 2007; Michalowski <i>et al.</i> , 2009
	Freeze-drying (ethanol precipitation)	Used to assess EPS carbohydrates in estuarine sediments but no references of application in drinking water context	Hanlon <i>et al.</i> , 2006; Haynes <i>et al.</i> , 2007; Hofmann <i>et al.</i> , 2009
	Steaming	Best method for subsequent protein analysis, limited use in literature	Zhang <i>et al.</i> , 1999
	Ethylendiaminetetraacetic acid(EDTA)	Commonly used method but inhibits protein analysis; found to release the fewest nucleic acids in a study of <i>Rhodopseudomonas acidophila</i>	Zhang <i>et al.</i> , 1999; Sheng <i>et al.</i> , 2005; Eboigbodin & Biggs, 2008
	Formaldehyde	Stated as best method for subsequent carbohydrate analysis	Zhang <i>et al.</i> , 1999
	Formaldehyde with NaOH	Extracted a limited amount of EPS from activated sludge biofilms	Liu and Fang, 2002
Protein Assay	Bradford Assay	Commonly used, recommended due to: speed, simplicity and insensitivity to other compounds (compared to Lowry). Wide variability in sensitivity to different proteins	Bradford <i>et al.</i> , 1976; Raunkjaer <i>et al.</i> , 1994; Frolund <i>et al.</i> , 1995
	Lowry	Subject to interference; laborious ; slight variability in sensitivity to different proteins but distinguishes between molecules as small as dipeptides	Raunkjaer <i>et al.</i> , 1994; Jahn & Neilsen, 1995; Sheng <i>et al.</i> , 2005
	Modified Lowry	Used in drinking water, removes humic acids but adds to time and complexity of assay	Bradford <i>et al.</i> , 1976; Frolund <i>et al.</i> , 1995; Michalowski <i>et al.</i> , 2009
	RC DC Assay^A	Based on the commonly used Lowry method but modified so it is reducing agent- and detergent agent- compatible, should be compatible with EDTA	Lowry, 1951
Carbohydrate Assay	Phenol- Sulfuric Acid	Used with drinking water samples, commonly used in other biofilm studies. Reportedly more comprehensive than anthrone method, has high specificity for all carbohydrates, which undergo the colour change with the same intensity	Raunkjaer <i>et al.</i> , 1994; Hanlon <i>et al.</i> , 2006; Haynes <i>et al.</i> , 2007; Michalowski <i>et al.</i> , 2009; Hofmann <i>et al.</i> , 2009
	Anthrone	Commonly used; more complex than phenol-sulfuric method, not all carbohydrates produce colour of the same intensity – problem if protein composition is unknown	Raunkjaer <i>et al.</i> , 1994; Jahn & Neilsen, 1995; Frolund <i>et al.</i> , 1995

Table A5.1 Continued.

Aim/Process	Method	Notes	References
Cell Lysis	Nucleic Acid	Does not distinguish between free DNA already in EPS from natural cell lysis and that occurring due to damage during extraction	Wingender <i>et al.</i> , 1999; Michalowski <i>et al.</i> , 2009
	G6PDH Enzyme Assay ^B	G6PDH is strictly an intracellular enzyme; accurate indicator of cell lysis as it is not found naturally outside of cells, unlike extracellular DNA found in the EPS	Lessie & van der Wijck, 1972; Frolund <i>et al.</i> , 1995; McSwain <i>et al.</i> , 2005
	DAPI ^C	Cannot differentiate between DNA present in cells or EPS	Jahn & Neilsen, 1995; Frolund <i>et al.</i> , 1995
Quantification	CLSM and Staining	Allows visualization of EPS in biofilm along with live cells; CLSM 510, Zeiss LSM software; CLSM found to provide higher estimation of EPS quantity than extraction amounts	Zhang & Fang, 2001; Liu & Fang, 2002; McSwain <i>et al.</i> , 2005; Shumi <i>et al.</i> , 2009
	TOC ^D	Commonly used to assess biomass and EPS amount, relatively quick and reliable	Jahn & Neilsen, 1995; McSwain <i>et al.</i> , 2005
	TS or TSS or VSS ^E	Used to indicate biofilm or cell mass	Zhang <i>et al.</i> , 1999; Sheng <i>et al.</i> , 2005
	Dry Weight (via Freeze-drying)	Samples are freeze-dried and weighed before being resuspended in sterile water; provides a dry weight for quantification	Hofmann <i>et al.</i> , 2009

^A Reducing Agent Compatible, Detergent Agent Compatible; ^B Glucose-6-phosphate Dehydrogenase; ^C 4',6-diamidino-2-phenylindole; ^D total organic carbon; ^E TS – total solids; TSS – total suspended solids; VSS – volatile suspended solids.

Appendix 6 Optimised physical protocols for EPS analysis

A6.1 CER Dowex

5 g of washed (1 hour in PBS - see Appendix A3.1) CER Dowex (Marathon, sodium form, Sigma Aldrich Co., UK) was used per 10 ml volume of sample. The solution was agitated at 600 RPM for 1 hour at 4 °C prior to centrifugation at 16,000 g for 20 minutes. The supernatant was extracted and centrifuged at 3,777 g for 5 minutes to remove cells. The supernatant, now application ready for chemical assays, was transferred to a clean and stored at -20 °C.

A6.2 EDTA

A 10 ml volume of 2% EDTA was added to a 10 ml sample volume and incubated at 4 °C for 3 hours prior to centrifugation at 14,000 g for 20 minutes. The solution was filtered through a 49 mm diameter, 0.22 µm cellulose acetate membrane (Millipore, MA, USA) to remove cells. The resultant filtered solution was stored at -20 °C ready for further analysis (protein and carbohydrate assays).

A6.3 Freeze Drying and Ethanol Precipitation

Sample tubes were weighed before use and a hole was pierced in the lid of each. 1.5 ml aliquots of samples were transferred to the pre-prepared tubes and frozen at -80 °C for at least 24 hours. Samples were freeze dried using a Super Modulyo freeze-dryer (Thermo Scientific, UK) for 48 – 72 hours.

After freeze-drying, each sample was weighed. Each 10 mg of freeze dried sample was resuspended in 150 µl sterile distilled deionised water and incubated at room temperature for 30 minutes. The solution was centrifuged at 6750 RPM for 15 minutes. A 100 µl volume of the supernatant was removed and combined with 300 µl of 100% ethanol prior to incubation at 4 °C for 24 hours. The solution was centrifuged at 6750 RPM for 15 minutes, the supernatant was discarded and the pellet was resuspended in 1 ml of sterile distilled deionised water. The samples were then ready for further analysis.

A6.4 Phenol-sulfuric Assay

A 250 µl volume of 5% phenol solution and 1.25 ml of concentrated sulphuric acid was added rapidly and directly to the surface of a 500 µl volume of sample/standard/control. The solution was incubated at room temperature for 10 minutes, vortexed gently for 15 seconds and incubated at 27 °C for a further 15 minutes. Absorbance was measured at 490 nm and/or 480 nm within the hour.

A6.5 Bradford Assay

A 800µl volume of sample/standard/control was combined with 200µl of diluted coomassie blue dye; dilution of 4 parts sterile distilled deionised water to 1 part dye, filtered before use. Solution was vortexed gently for 5 seconds and incubated at room temperature for at 5 - 60 minutes. Absorbance was measured at 595 nm within the hour.

A6.6 RC DC Assay

A mastermix comprised of 2.5 µl of DC Reagent S and 125 µl DC Reagent A for each sample was prepared. A 25 µl volume of sample/standard/control was added to 125 µl RC Reagent I and 125 µl RC Reagent II. This solution was vortexed and incubated at room temperature for 1 minute prior to being centrifuged at 15,000 xg for 3-5 minutes. The supernatant was discarded and 127 µl of the mastermix was added to the pellet. This solution was vortexed gently and incubated for 5 minutes at room temperature; vortexed once more and combined with 1 ml of DC Reagent B. The final solution was vortexed gently and incubated at room temperature for 15 minutes, the absorbance was read at 750 nm within the hour.

Appendix 7 Supporting information for optimising the fluorescent staining and imaging method

A7.1 Biofilm staining issues with the multiphoton laser

Biofilm staining with DAPI was tested but no suitable single photon laser was available at the required excitation wavelength of 358 nm, therefore the available multiphoton laser was used. However, exposure to this laser was observed to damage the carbohydrates of the sample as was apparent by the distorted images when DAPI was tested in combination with Con A Rho (Figure A 7.1). Although the multiphoton was tested at different powers this effect was not able to be averted.

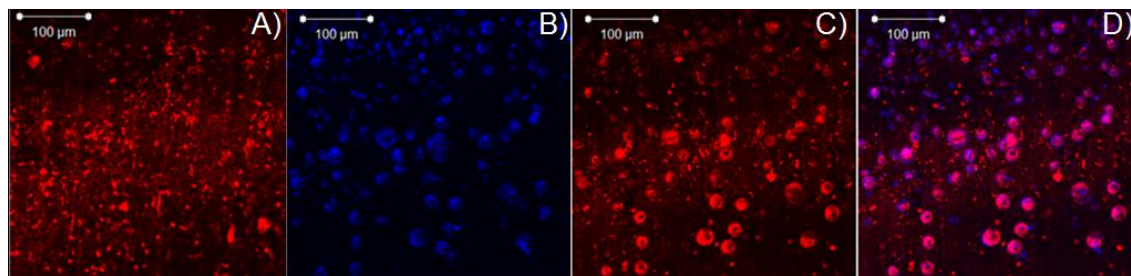


Figure A 7.1 CLSM image demonstrating the detrimental effect of the multiphoton laser on a dual stained sample. A) Visualization of the carbohydrates (stained with Con A Rho) before exposure to the multiphoton; B) Visualization of the cells (stained with DAPI); C) Visualization of of the carbohydrates after exposure to the multiphoton laser; D) Cell and carbohydrate images overlaid. Scale bar 100 µm as indicated.

A7.2 Optimising Z-stack imaging: Scan speed vs. Optical thickness

A total imaging time of over 27 hours would be required to image a single sample at seven FOV for the three stains (FITC - ~ 14 hours, Con A Rho - ~9 hours and Syto 63, ~ 4.5 hours). This does not include the time taken to: stabilise the room and sample temperature, position the sample and set up the image, save the files (can take up to 30 minutes) or unmix the image. Hence it was necessary to optimise the scan speed and/or optical slice thickness to generate the best possible image within a more realistic time frame. The results from the optimisation tests are shown in Table A 7.1 and led to the conclusion that the best parameter to alter was the scan speed.

Table A 7.1 Z-stack imaging times for different scan speeds and optical thicknesses.

Stain	Imaging time for a 5 slice Z-stack (minutes: seconds)					
	At scan speed (μs)			At optical thickness (μm)		
	31.54	15.77	7.89	4.7	7.1	9.3
FITC ^A	20:31	12:57	8:57	20:31	14:39	11:43
Con A Rho ^B	13:40	8:35	6:02	13:40	9:46	7:49
Syto 63	6:50	4:17	3:02	6:50	4:53	3:54
Total time	41:01	25:49	18:01	41:01	29:18	23:26

^A fluorescein-5-isothiocyanate; ^B concanavalin A tetramethylrhodamine.

A7.3 Optimising Z-stack imaging: Testing Different Scan Speeds

To determine the best scan speed to select all possible speeds were tested. Triplicate samples were imaged at three FOV (without air conditioning on) at scan speeds of: 31.54 μs , 15.77 μs , 7.89 μs , 3.94 μs , 1.58 μs and 0.99 μs . Optical thickness was kept at 4.7 μm , with an optimal interval of 2.35 μm . A Z-stack of 5 slices was produced in each case and the time taken was recorded (Table A 7.2).

The same pattern of “brightness” was observed with an increase up to and including 7.89 μs , a decline at 15.77 μs and an increase again at 31.54 μs (Figure A 7.2). This trend was observed for the raw, unmixed and thresholded images and so it is likely that the Zeiss software uses an undisclosed averaging algorithm, the application of which is triggered at scan speeds of 15.77 μs or greater. As this non-monotonic pattern was established to occur across all the images and all the settings, it was considered as a constant unknown and in order to avoid it, while simultaneously reducing imaging time to ~25% of the original time, a scan speed of 3.94 μs was selected.

Table A 7.2 Imaging times for 5 slice lambda-Z-stacks imaged under different scan speeds.

Scan Speed (μs)	Imaging time (minutes:seconds) for each stain		
	FITC ^A	Con A Rho ^B	Syto 63
31.54	14:39	09:46	04:53
15.77	09:12	06:08	03:06
7.89	06:23	04:15	02:07
3.94	03:11	02:07	01:03
1.58	01:19	00:53	00:28
0.99	00:48	00:32	00:18

^A fluorescein-5-isothiocyanate; ^B Concanavalin A tetramethylrhodamine.

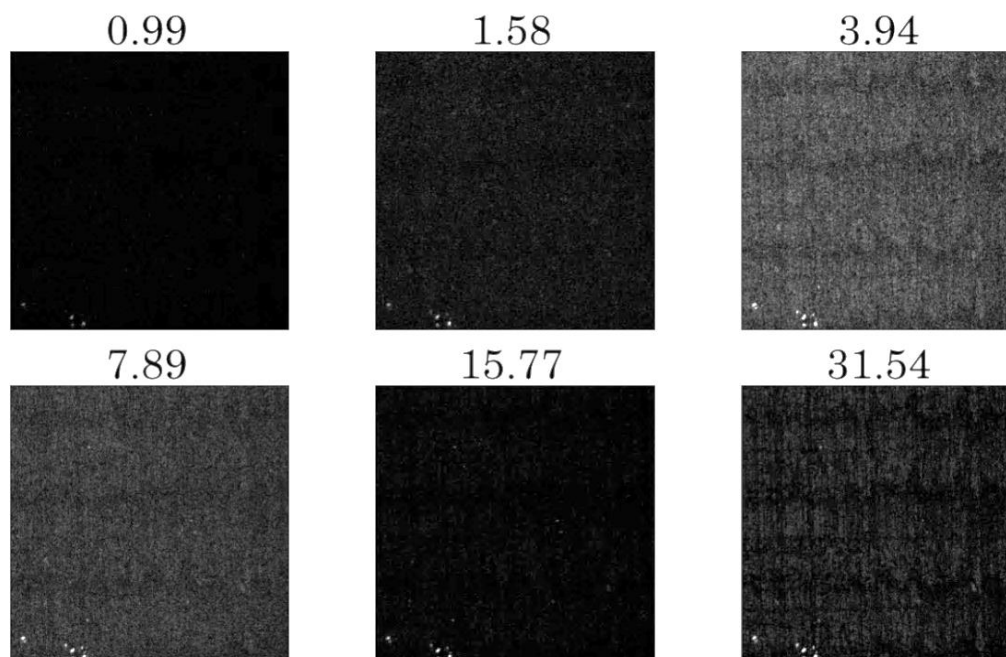


Figure A 7.2 Example of a single FOV imaged at the six scan speeds (μs) listed in Table A 7.2. FOV shown is from a SS Day 28 biofilm sample, stained with Concanavalin A tetra-rhodamine.

Appendix 8 Statistical Analysis of Bulk Water Quality

A8.1 Growth phase comparisons between experiments – p values

The majority of the water quality data was not normally distributed when tested using Shapiro-Wilks test, therefore the Kruskal Wallis test was applied to determine any differences in water quality parameters during the growth phase of each experiment, the p values are shown in Table A 8.1, a p value of <0.05 indicates a statistically significant difference. Where a difference was found, Wilcoxon pairwise tests were carried out to see where that difference lay.

Table A 8.1 Kruskal Wallis p values for water quality parameter comparisons between all three hydraulic experiments.

Water Quality Parameter	Kruskal Wallis Test (SS vs LVF vs HVF)
Total Chlorine –Inlet (mg l ⁻¹)	p=0.1550, $\chi^2=3.73$, df=2
Total Chlorine – Tank (mg l ⁻¹)	p=0.0705, $\chi^2=5.31$, df=2
Total Organic Carbon (TOC)	p<0.0001, W=208 (Wilcoxon) ^A
Turbidity (NTU) ^A	p=0.0733, $\chi^2=5.23$, df=2
Iron ($\mu\text{g l}^{-1}$)	p=0.9911, $\chi^2=0.02$, df=2
Manganese ($\mu\text{g l}^{-1}$)	p=0.0134, $\chi^2=8.63$, df=2 ^B
pH	p=0.1408, $\chi^2=3.92$, df=2
Oxidising Redox Potential (mV)	p<0.001, $\chi^2=22.71$, df=2 ^C
Temperature – Inlet (°C)	p=0.0805, $\chi^2=5.04$, df=2
Temperature – Tank (°C)	p=0.8381, $\chi^2=0.35$, df=2

^A No SS data available so Kruskal Wallis not feasible, Wilcoxon test used; ^B Wilcoxon pairwise tests: SS vs LVF, p=0.0545, W=66; SS vs HVF, p=0.0045, W=44; LVF vs HVF p=0.3686, W=134.5; ^C Wilcoxon pairwise tests: SS vs LVF, p=0.9029, W=87; SS vs HVF, p<0.001, W=171; LVF vs HVF, p<0.001, W=12.

Appendix 9 Supporting information for comparisons between biofilms from the growth phase of different hydraulic regimes

A9.1 Statistical analysis of position and loop effects

In order to determine any effect of position or loop upon LVF or HVF biofilm physical structure at Day 0 and Day 28, the data was initially split into the “position dataset” comprising the crown, middle and invert biofilm samples from loop 2 and the “loop dataset” comprising the middle biofilm samples from loops 1, 2 and 3. These datasets were analysed as explained in section 5.2.1.3. The statistical outputs from the comparisons between the two datasets, for Day 0 and Day 28 of LVF and HVF are shown with respect to the relative volume (Table A 9.1), the spread (Table A 2.1) or the peak location (Table A 9.3). A p value of <0.05 indicates a statistically significant difference. The details of the calculations of the relative volume, spread and peak location parameters are provided in section 4.6.

Table A 9.1 Results from the Wilcoxon test to determine any position or loop effect upon the relative volumes of the stained components of biofilms from the LVF or HVF regimes.

Sample Point	Biofilm Component	Position Dataset vs. Loop dataset	
		LVF	HVF
Day 0	Cells	W=131.5, p=0.4422	W=153.0, p=0.1220
	Carbohydrates	W=133.0, p=0.3950	W=76.5, p=0.3343
	Proteins	W=140.5, p=0.2448	W=75.5, p=0.3080
Day 28	Cells	W=124.5, p=0.6332	W=99.5, p=0.8272
	Carbohydrates	W=106.5, p=0.8194	W=135.5, p=0.1902
	Proteins	W=146.0, p=0.1692	W=93.5, p=0.6310

Table A 9.2 Results from the Wilcoxon test to determine any effect of position or loop upon the spread of the stained components of biofilms from the LVF or HVF regimes.

Sample Point	Biofilm Component	Position Dataset vs. Loop dataset	
		LVF	HVF
Day 0	Cells	W=93.5, p=0.6310	W=170.0, p=0.0010
	Carbohydrates	W=41.0, p=0.7802	W=91.5, p=0.7387
	Proteins	W=64.5, p=0.2683	W=45.5, p=0.5690
Day 28	Cells	W=106.5, p=0.8194	W=107.5, p=0.6790
	Carbohydrates	W=99.5, p=0.6039	W=128.5, p=0.3152
	Proteins	W=70.5, p>0.9999	W=119.5, p=0.5409

Table A 9.3 Results from the Wilcoxon test to determine any effect of position or loop upon the peak location of carbohydrates or proteins of biofilms from the LVF or HVF regimes.

Sample Point	Biofilm Component	Position Dataset vs. Loop dataset	
		LVF	HVF
Day 0	Carbohydrates	W=123.5, p=0.6612	W=76.5, p=0.2724
	Proteins	W=121.0, p=0.7371	W=66.0, p=0.1443
Day 28	Carbohydrates	W=78.0, p=0.1429	W=91.0, p=0.5280
	Proteins	W=158.0, p=0.0577	W=61.5, p=0.0576

A9.2 Area Distribution Plots of Day 0 Biofilms Developed Under LVF and HVF Conditions

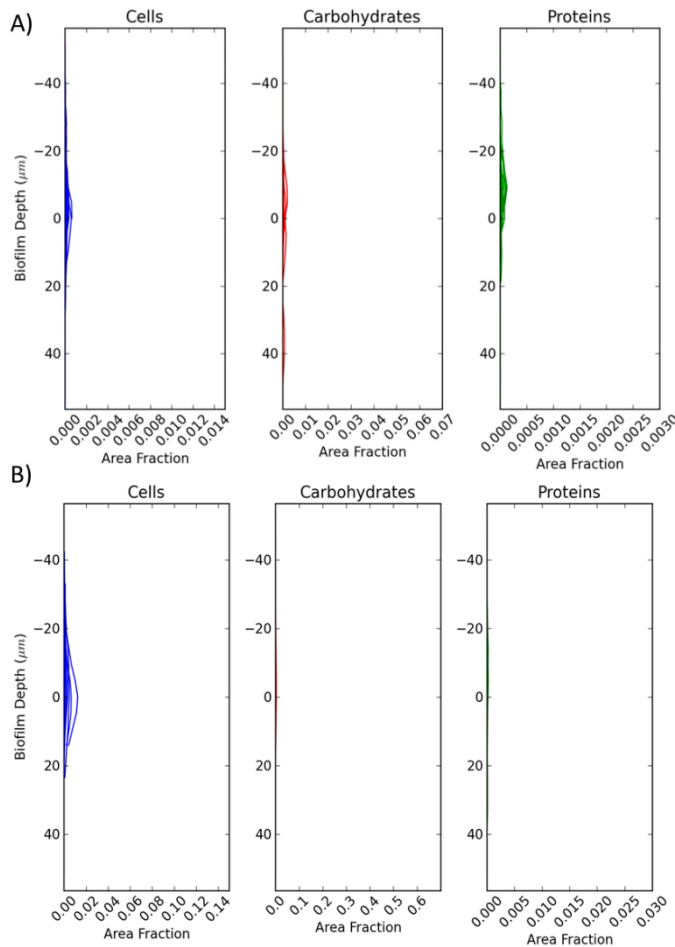


Figure A 9.1 The area distribution of cells, carbohydrates and proteins of A) LVF Day 0 biofilms (n=25) and B) HVF Day 0 biofilms (n=24). Note that the x-axis scale is a magnitude less in A) than the x-axis scales of B) and other area distribution plots. Each line represents one FOV (i.e. one Z-stack). Area fraction refers to the proportion of each XY image of the Z-stack covered by the particular component (see section 4.6.3.1).

A9.3 Comparison Statistics of LVF and HVF, Day 0 and Day 28 biofilms

In order to confirm that biofilm had developed under the LVF hydraulic conditions the Day 0 biofilms were compared to the Day 28 biofilms, in the same way as the SS biofilms from the growth phase were analysed in Chapter 5:. The same analysis was applied to compare the Day 0 and Day 28 biofilms from the HVF experiment. The results from the comparison of the relative volume of each stained biofilm component are shown in Table A 9.4, for the LVF samples and Table A 9.5 for the HVF samples. The results from the comparison of the spread of the cells, carbohydrates and proteins are shown in Table A 9.6 for the LVF samples and Table A 9.7 for the HVF samples. No difference was found in the peak location of carbohydrates (Wilcoxon: $W=311.0$, $p=0.9843$) or proteins (Wilcoxon: $W=350.0$, $p=0.4638$) between the Day 0 and Day 28 biofilms developed under the LVF conditions. Similarly, no significant differences were found between the carbohydrate (Wilcoxon: $W=282.0$, $p=0.9037$) and protein (Wilcoxon: $W=246.5$, $p=0.3944$) peak locations within the Day 0 and Day 28 biofilms from the HVF experiment.

Table A 9.4 Comparison of the relative volume of the stained components within Day 0 and Day 28 biofilms, developed under LVF conditions. Significant results are shown in bold.

Component	Range (Min – Max, μm^3)		Median (μm^3)		Wilcoxon Results
	Day 0	Day 28	Day 0	Day 28	
Cells	0 - 1845	25 - 8434	296	671	W=82.0, p=0.0148
Carbohydrates	0 - 6239	192 - 184549	152	24969	W=19.0, p<0.0001
Proteins	0 - 472	0 - 134577	14	466	W=178.5, p=0.0086

Table A 9.5 Comparison of the relative volume of the stained components within Day 0 and Day 28 biofilms, developed under HVF conditions. Significant results are shown in bold.

Component	Range (Min – Max, μm^3)		Median (μm^3)		Wilcoxon Results
	Day 0	Day 28	Day 0	Day 28	
Cells	5 - 50908	0 - 2608492	1434	28859	W=89.0, p<0.0001
Carbohydrates	0 - 18445	7512 - 327390	659	74271	W=2.0, p<0.0001
Proteins	0 - 1845	118 - 66593	296	2496	W=40.0, p<0.0001

Table A 9.6 Comparison of the spread of the stained biofilm components within Day 0 and Day 28 biofilms, developed under LVF conditions. Significant results are shown in bold.

Component	Range (Min – Max, AU)		Median (AU)		Wilcoxon Results
	Day 0	Day 28	Day 0	Day 28	
Cells	875930 – 6419519	1653839 – 5967084	3093272	3549221	W=206.0, p=0.0305
Carbohydrates	864198 – 5038226	3013141 – 9270172	2587974	4406852	W=139.0, p=0.0062
Proteins	813363 – 4671029	813363 – 6418663	1955012	2908246	W=97.5, p=0.0368

Table A 9.7 Comparison of the spread of the stained biofilm components within Day 0 and Day 28 biofilms, developed under HVF conditions. Significant results are shown in bold.

Component	Range (Min – Max, AU)		Median (AU)		Wilcoxon Results
	Day 0	Day 28	Day 0	Day 28	
Cells	1040038 – 6087343	813363 – 9067427	3537493	4425734	W=130.0, p=0.0015
Carbohydrates	929558 – 5029707	2373899 – 6429579	2875359	3580180	W=139.0, p=0.0062
Proteins	813363 – 3849919	1351188 – 7915235	2323895	3874705	W=75.0, p=0.0006

A9.4 Comparison of physical structure parameters of the Day 0 Biofilms from SS, LVF and HVF

The biofilm material which was present upon the coupon surface, even after ≤ 90 minutes within the experimental facility, was compared between the three hydraulic tests. Table A 9.8 shows the results from comparisons of the SS, LVF and HVF Day 0 biofilms with respect to relative volume of each of the stained components of the biofilm. Table A 9.9 shows the results from the comparisons of the spread of the cells, carbohydrates or proteins within the Day 0 biofilms from each hydraulic condition.

Table A 9.8 Comparison of the relative volumes of the stained biofilm components within Day 0 biofilms developed under SS, LVF or HVF conditions. Significant results are shown in bold.

Component	Median Relative Volume (μm^3)			Kruskal Wallis	Wilcoxon Results	
	SS ^A	LVF ^A	HVF ^B	SS vs. LVF vs. HVF	Pairwise test	Result
Cells	35543	296	1434	$\chi^2=34.44$ df=2 p<0.0001	SS vs LVF SS vs HVF LVF vs HVF	W=580.5, p<0.0001 W=492.0, p<0.0001 W=463.0, p=0.0012
Carbohydrates	9874	152	659	$\chi^2=26.49$ df=2 p<0.0001	SS vs LVF SS vs HVF LVF vs HVF	W=551.0, p<0.0001 W=501.0, p<0.0001 W=369.0, p=0.1698
Proteins	177	14	296	$\chi^2=9.38$ df=2 p=0.0092	SS vs LVF SS vs HVF LVF vs HVF	W=460.0, p=0.0041 W= 411.0, p=0.0265 W=337.0, p=0.4574
EPS ^C	11059	189	724	$\chi^2=27.86$ df=2 p<0.0001	SS vs LVF SS vs HVF LVF vs HVF	W=553.0, p<0.0001 W=502.0, p<0.0001 W=364.5, p=0.2005
All Material ^D	50745	1,011	3757	$\chi^2=37.64$ df=2 p<0.0001	SS vs LVF SS vs HVF LVF vs HVF	W=591.0, p<0.0001 W=571.0, p<0.0001 W=452.0, p=0.0020

^A n=25; ^B n=24; ^C EPS = carbohydrates + proteins, before averaging, data presented is therefore the median of the sums; ^D All Material = EPS + cells, before averaging, data presented is therefore the median of the sums.

Table A 9.9 Comparison of the spread of the stained biofilm components within Day 0 biofilms developed under SS, LVF or HVF conditions. Significant results are shown in bold.

Component	Median Spread (AU)			Kruskal Wallis	Wilcoxon Results	
	SS ^A	LVF ^A	HVF ^B	SS vs. LVF vs. HVF	Pairwise test	Result
Cells	3409865	3093272	3537493	$\chi^2=2.94$, df=2 p=0.2296	SS vs LVF SS vs HVF LVF vs HVF	W=328.5, p=0.1035 W=288.0, p=0.8197 W=353.0, p=0.1853
Carbohydrates	3443148	2587974	2875359	$\chi^2=4.30$ df=2 p=0.1167	SS vs LVF SS vs HVF LVF vs HVF	W=353.0, p=0.0056 W=342.0, p=0.1562 W=270.0, p=0.1137
Proteins	2483387	1955012	2323895	$\chi^2=1.97$ df=2 p=0.3737	SS vs LVF SS vs HVF LVF vs HVF	W=231.5, p=0.1035 W= 221.0, p=0.3426 W=158.0, p=0.4379

^A n=25; ^B n=24.

A9.5 Variation in bacterial community relative taxon richness, evenness and diversity between Day 0 biofilms from different hydraulic regimes

The ecological indices are shown in Table A 9.10 for Day 0 biofilms from the SS (n=2), LVF (n=4) or HVF (n=5) experiments, as indicated. The total number of different T-RFs constituting the bacterial community fingerprint at Day 0 was 6, 13 and 4, for SS, LVF and HVF biofilms, respectively.

Table A 9.10 Relative richness, evenness and diversity indices of the bacterial communities from Day 0 of the different hydraulic conditions.

Flow Regime	Relative Richness (number of T-RFs)			Relative Evenness (Pielou's Index)			Relative Diversity (Shannon's Index)		
	Min	Max	Mean (St.Dev)	Min	Max	Mean (St. Dev)	Min	Max	Mean (St. Dev)
Steady State ^A	3	5	-	0.89	0.95	-	1.04	1.43	-
Low Varied Flow	4	8	5.75 (1.71)	0.83	0.92	0.87 (0.04)	1.17	1.91	1.50 (0.32)
High Varied Flow	1	3	2.20 (1.10)	0.72	0.87	0.78 (0.08)	0.00	0.95	0.51 (0.47)

^A Not enough samples to calculate an average; N.B. Min = minimum, Max = maximum, St.Dev = standard deviation.

Appendix 10 Supporting information for comparisons between biofilms from the mobilization phase of different hydraulic regimes

Detailed statistical outputs from the comparisons between the “position” and “loop” datasets, for each of the stained components of Pre-flush (Table A 10.1) and Post-flush (Table A 10.2) from SS, LVF and HVF hydraulic conditions are shown in with respect to the relative volume, spread and peak location. The statistics presented in each table are the results of the Wilcoxon

test with a significance level set at $p < 0.05$, the details of the calculations of the relative volume, spread and peak location parameters are provided in section 4.6.3.

Table A 10.1 Statistical comparisons of biofilm physical structure parameters to determine any effect of position or loop upon the Pre-flush biofilms from the SS, LVF or HVF regimes.

Physical Structure Parameter	Biofilm Component	Position Dataset vs. Loop dataset (Wilcoxon test)		
		SS	LVF	HVF
Relative Volume	Cells	W=97.0, P=0.9817	W=73.5, p=0.1758	W=84.5, p=0.2538
	Carbohydrates	W=59.0, P=0.0767	W=47.5, p=0.1280	W=101.5, p=0.6630
	Proteins	W=117, P=0.3950	W=71.0, p=0.1408	W=96.5, p=0.5023
Spread	Cells	W=114.0, p=0.2746	W=109.5, p=0.8163	W=131.5, p=0.4426
	Carbohydrates	W=85.0, p=0.7894	W=61.5, p=0.1590	W=115.5, p=0.9174
	Proteins	W=100.0, p=0.9450	W=43.0, p=0.2761	W=39.5, p=0.6457
Peak Location	Carbohydrates	W=129.0, p=0.1528	W=102.5, p=0.9289	W=109.5, p=0.9131
	Proteins	W=123.5, p=0.2477	W=75.0, p=0.1949	W=91.5, p=0.3929

Table A 10.2 Statistical comparisons of biofilm physical structure parameters to determine any effect of position or loop upon the Post-flush biofilms from the SS, LVF or HVF regimes.

Physical Structure Parameter	Biofilm Component	Position Dataset vs. Loop dataset		
		SS	LVF	HVF
Relative Volume	Cells	W=164.5, P=0.0100	W=125.2, p=0.6039	W=82.5, p=0.2208
	Carbohydrates	W=51.5, P=0.0206	W=94.5, p=0.4674	W=34.5, p=0.0013
	Proteins	W=102.5, P=0.9303	W=131.0, p=0.3873	W=150.5, p=0.1196
Spread	Cells	W=94.5, p=0.6623	W=116.5, p=0.8845	W=95.5, p=0.4935
	Carbohydrates	W=107.5, p=0.9304	W=117.0, p=0.8681	W=116.5, p=0.8845
	Proteins	W=89.5, p=0.7966	W=6.0, p=0.1535	W=135.5, p=0.1902
Peak Location	Carbohydrates	W=81.0, p=0.2575	W=90.0, p=0.3180	W=123.5, p=0.6017
	Proteins	W=129.0, p=0.1528	W=134.0, p=0.3811	W=124.5, p=0.6275